ISSN: 2153-1196 Vol. 7, No. 10, June 2016

Scientific Research Publishing

Journal of Modern Physics

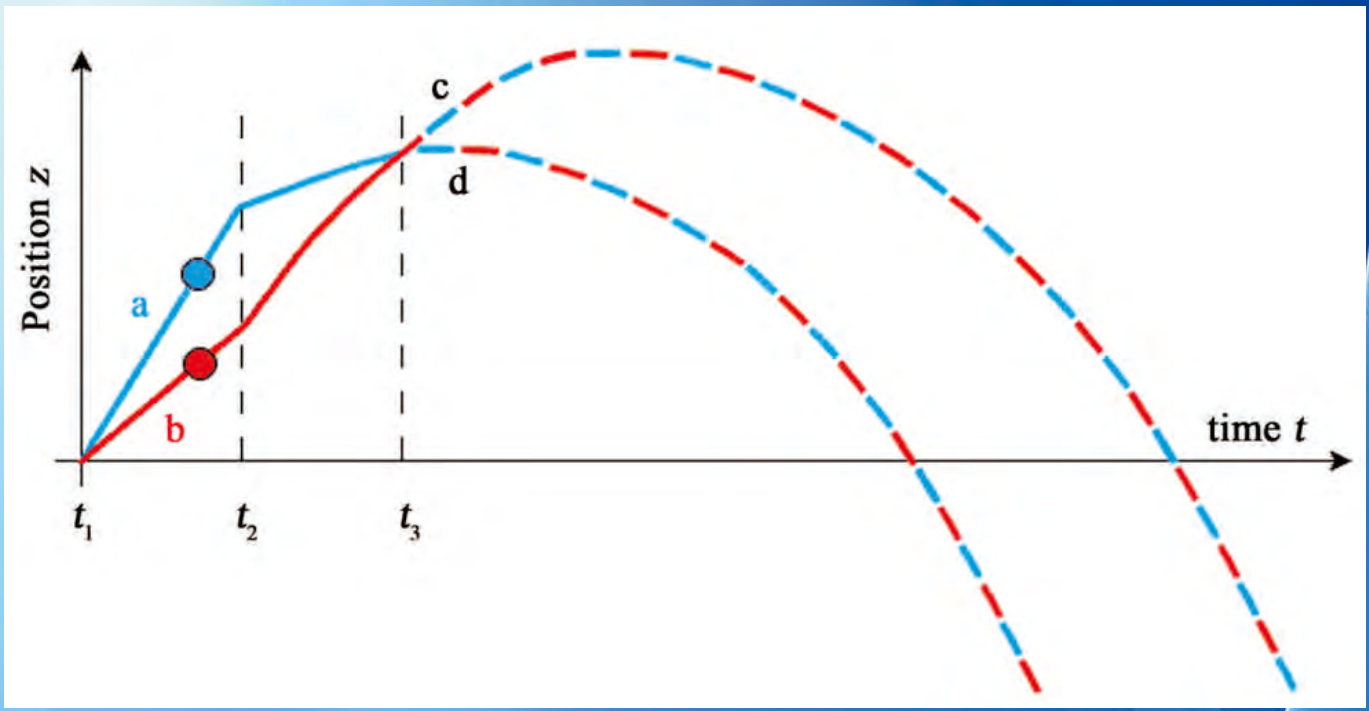

ISSN: 2153-1196

www.scirp.org/journal/jmp

Journal Editorial Board

ISSN: 2153-1196 (Print) ISSN: 2153-120X (Online)
http://www.scirp.org/journal/jmp

Journal of Modern Physics, 2016, 7, 1045-1295
Published Online June 2016 in SciRes. http://www.scirp.org/journal/jmp

Scientific Research Publishing

Table of Contents

Volume 7 Number 10 June 2016

Journal of Modern Physics, 2016, 7, 1045-1295
Published Online June 2016 in SciRes. http://www.scirp.org/journal/jmp

The figure on the front cover is from the article published in Journal of Modern Physics, 2016, Vol. 7, No. 10, pp. 1091-1097 by Sofia Wechsler.

Journal of Modern Physics (JMP)

Journal Information

SUBSCRIPTIONS

The *Journal of Modern Physics* (Online at Scientific Research Publishing, www.SciRP.org) is published monthly by Scientific Research Publishing, Inc., USA.

Subscription rates:

Print: $89 per issue.
To subscribe, please contact Journals Subscriptions Department, E-mail: sub@scirp.org

SERVICES

Advertisements
Advertisement Sales Department, E-mail: service@scirp.org

Reprints (minimum quantity 100 copies)
Reprints Co-ordinator, Scientific Research Publishing, Inc., USA.
E-mail: sub@scirp.org

COPYRIGHT

PRODUCTION INFORMATION

For manuscripts that have been accepted for publication, please contact:
E-mail: jmp@scirp.org

Journal of Modern Physics, 2016, 7, 1045-1048
Published Online June 2016 in SciRes. http://www.scirp.org/journal/jmp
http://dx.doi.org/10.4236/jmp.2016.710093

The Problem on Stationary States in Self Gravitational Field

Stanislav Fisenko

"Rusthermosinthes" JSC, Moscow, Russia
Email: StanislavFisenko@yandex.ru

Received 25 April 2016; accepted 3 June 2016; published 8 June 2016

Abstract

To follow is the problem on stationary states of an electron in its own gravitational field where the boundary conditions earlier described in [1] are made specific. The simplest approximation provides an assessment of the energy spectrum of stationary states only. Nevertheless, this is enough to confirm the existence of such stationary states and to further elaborate a detailed solution of the problem on stationary states including determination of all the quantum numbers' spectra and corresponding wave functions. No other matters are discussed here. The case in hand is a purely mathematical problem, further physical interpretation of which is of a fundamental value.

Keywords

Gravity, Electron, Irremovable Space-Time Curvature, Spectrum

1. Introduction

The physical nature of the problem under consideration hereinafter can be briefly summarized as follows [1]. Generally covariant relativistic form of the equations of Einstein's theory of gravitation, as we know, has the following form:

$$R_{ik} - \frac{1}{2} g_{ik} R - \Lambda g_{ik} = \chi T_{ik} \tag{1}$$

In these equations χ is a constant that relates to the geometrical properties of space-time distribution of physical matter, so that the origin of the equations is not associated with the numerical restriction of the values. Only the requirements of compliance with the Newton's law of universal gravitation leads to numerical values $\Lambda = 0, \chi = 8\pi G/c^4$, where G is the Newton's gravitational constant. Equation with certain constants determined in this way is the equations of the Einstein's theory of general relativity. Equation (1) is a common mathematical

How to cite this paper: Fisenko, S. (2016) The Problem on Stationary States in Self Gravitational Field. *Journal of Modern Physics*, **7**, 1045-1048. http://dx.doi.org/10.4236/jmp.2016.710093

form of the gravitational field equations corresponding to the principle of equivalence and the postulate of general covariance. The equations of the form (1) are obtained simultaneously by Einstein and independently by Gilbert [2]. At the same time, we refer to A. Salam [3], as he is the one of the first who drew attention to the discrepancy between the quantum level of the numerical value and the Newtonian gravitational constant. It is he who proposed the concept of "strong" gravity, which was based on the assumption of the existence of f-mesons of spin-2 generating SU (3) multiplet (described by Pauli-Fierz equation). It is shown that the possibility of another link constant along with the Newtonian is not inconsistent with the observed effects [3]. This approach was not further developed due to a number of reasons. It is clear now that the numerical value of the "strong" gravity constant should be used in Equation (1) with $\Lambda \neq 0$. By the way, when $\Lambda \neq 0$ there are stationary solutions of general Einstein's equations as it was stated by Einstein himself, but after the discovery of non-sta- tionary solutions with $\Lambda = 0$ by A. Friedman [4], finally the general theory of relativity was formed as it is now known. The decisive argument in general relativity for equating Λ-member to zero is the need to correct limiting transition to Newton's theory of gravitation.

2. Mathematical Model

Starting from the 70 s it became evident [3] that in the quantum domain numerical value of G is not compatible with the principles of quantum mechanics. A number of studies [3] have shown that in the quantum domain acceptable is constant K, wherein $K \approx 10^{40} G$. This marked the problem of generalization of the relativistic equations for the quantum level: this generalization should join the numerical values of the constants in quantum and classical fields.

In the development of these results as an approximation to the micro level of the field equations of Einstein, a model based on the following assumptions is proposed:

The gravitational field in the region of localization of elementary particles with mass m_0 is characterized by the values of the gravitational constant K and constant Λ, which lead to the stationary states of a particle in its own gravitational field, and stationary states of the particles themselves are the source of the gravitational field with the Newtonian gravitational constant G.

The complexity of solving this problem forced to turn to the simplest approximation, namely the calculation of the energy spectrum only in the approximation of the fine structure due to relativism

The problem on the stationary states of an elementary source in its own gravitational field is reduced to the solution of the eigenvalue problem $K_n = E_n/\hbar c$ and eigenfunctions of the radial wave function f (describing the states with definite energy E and orbital moment l: indices El are omitted) of boundary value problem:

$$f'' + \left(\frac{\nu' - \lambda'}{2} + \frac{2}{r}\right) f' + \mathrm{e}^{\lambda}\left(K_n^2 \mathrm{e}^{-\nu} - K_0^2 - \frac{l(l+1)}{r^2}\right) f = 0 \tag{2}$$

$f\left(\sqrt{\Lambda^{-1}}\right) = 0$ Left bo und (3)

$f(r_n) = 0$ Right boun d (4)

$\int_{\sqrt{\Lambda^{-1}}}^{r_n} f^2 r^2 \mathrm{d}r = 1$ Normalization r equirement (5)

Equation (2) is complemented by the equations:

$$-\mathrm{e}^{-\lambda}\left(\frac{1}{r^2} - \frac{\lambda'}{r}\right) + \frac{1}{r^2} + \Lambda = \beta(2l+1)\left\{f^2\left[\mathrm{e}^{-\lambda}K_n^2 + K_0^2 + \frac{l(l+1)}{r^2}\right] + f'^2\mathrm{e}^{-\lambda}\right\} \tag{6}$$

$$-\mathrm{e}^{-\lambda}\left(\frac{1}{r^2} + \frac{\nu'}{r}\right) + \frac{1}{r^2} + \Lambda = \beta(2l+1)\left\{f^2\left[K_0^2 - K_n^2\mathrm{e}^{-\nu} + \frac{l(l+1)}{r^2}\right] - \mathrm{e}^{\lambda}f'^2\right\} \tag{7}$$

With boundary conditions

$$R\left(\sqrt{\Lambda^{-1}}\right) = \Lambda \tag{8}$$

$$\left\{-\frac{1}{2}\left(\nu''+\nu'^2\right)-\left(\nu'+\lambda'\right)\left(\frac{\nu'}{4}+\frac{1}{r}\right)+\frac{1}{r^2}\left(1+\mathrm{e}^{\lambda}\right)\right\}_{r=r_n}=0 \tag{9}$$

Scalar curvature R in the condition (8) is given by the same expression that is written in the left side of the condition (9).

Equations (2) and (6)-(7) follow from Equations (10)-(11)

$$\left\{-g^{\mu\nu}\frac{\partial}{\partial x_\mu}\frac{\partial}{\partial x_\nu}+g^{\mu\nu}\Gamma^{\alpha}_{\mu\nu}\frac{\partial}{\partial x_\alpha}-K_0^2\right\}\Psi=0 \tag{10}$$

$$R_{\mu\nu}-\frac{1}{2}g_{\mu\nu}R=-\kappa\left(T_{\mu\nu}-\mu g_{\mu\nu}\right) \tag{11}$$

after the substitution of Ψ in the form of $\Psi=f_{El}(r)Y_{lm}(\theta,\varphi)\exp\left(\frac{-iEt}{\hbar}\right)$ into them and specific computations in the central-symmetry field metric with the interval defined by the expression [5]

$$\mathrm{d}S^2=c^2\mathrm{e}^{\nu}\mathrm{d}t^2-r^2\left(\mathrm{d}\theta^2+\sin^2\theta\mathrm{d}\varphi^2\right)-\mathrm{e}^{\lambda}\mathrm{d}r^2 \tag{12}$$

Above indicated: f_{El} is radial wave function describing the state with a definite energy E and the orbital angular momentum l (hereinafter indexes El are omitted), $Y_{lm}(\theta,\varphi)$ are spherical functions, $K_n=E_n/\hbar c$, $K_0=cm_0/\hbar$, $\beta=(\kappa/4\pi)(\hbar/m_0)$, $\kappa=8\pi K/c^4$.

Right-hand sides of Equations (6)-(7) are calculated from the general expression for the energy-momentum tensor of a complex scalar field:

$$T_{\mu\nu}=\Psi^{+}_{,\mu}\Psi_{,\nu}+\Psi^{+}_{,\nu}\Psi_{,\mu}-\left(\Psi^{+}_{,\mu}\Psi^{,\mu}-K_0^2\Psi^{+}\Psi\right)g_{\mu\nu} \tag{13}$$

The respective components $T_{\mu\nu}$ are obtained summing by index m using specific identities for the spherical functions [6] after the substitution in (13) $\Psi=f(r)Y_{lm}(\theta,\varphi)\exp\left(\frac{-iEt}{\hbar}\right)$.

3. Energy Spectrum

In the simplest (in terms of initial mathematical evaluations) approximation, the problem for stationary states in its gravitational field (with the constants K and Λ) was solved in [7]. From the solution of this problem it should be:

1) If the numerical values of $K\approx 5.1\times10^{31}$ N·m^2·kg^{-2} and $\Lambda=4.4\times10^{29}$ m^{-2}, there is a spectrum of stationary states of the electron in its own gravitational field (0.511 MeV ··· 0.681 MeV). The main state is the observed electron rest energy 0.511 MeV. *This numerical value of Λ has important physical meaning: an introduction to the Lagrangian density permanent member, not dependent on the state of the field. This implies the existence of irremovable space-time curvature, not affiliated with any matter, nor with the gravitational field.*

2) These steady states are the sources of the gravitational field with constant G.

3) Transitions between the stationary states of the electron in its own gravitational field lead to gravitational radiation, which is characterized by a constant K that gravitational radiation is the emission of the same level as electromagnetic (electric charge e, gravitational charge) $m\sqrt{K}$. In this regard, it makes no sense to say that the gravitational effects in the quantum region are characterized by the constant G. This constant applies only to the macroscopic field and it cannot be transferred to the quantum level (which, by the way, we remind, show negative results for the detection of gravitational waves with the constant G, and they cannot be). It is considered that according to General Relativity (GR), gravitational radiation can generate only system with variable quadrupole or higher multipole moments. Under this assumption, the corresponding power of gravitational radiation is determined by the relationship:

$$L=\frac{1}{5}\frac{G}{c^5}\left\langle\frac{\mathrm{d}^3Q_{ij}}{\mathrm{d}t^3}\frac{\mathrm{d}^3Q^{ij}}{\mathrm{d}t^3}\right\rangle,$$

where Q_{ij} is a quadrupole moment tensor of the mass distribution of the radiating system, and the constant in this relationship defines the order of magnitude of the radiation power. Wrongfulness of this formula, as follows from the above, is not to use the quadrupole approximation, but in the scheme calculation. The presence of stationary states in the own gravitational field allows the correct calculation of gravitational radiation in the strict quantum approach based on the spectrum of transitions to stationary states already with constant K. It is permissible to use not only quadrupole, but also dipole quantum approach, which is quite obvious. Gravitational waves with the constant G do not exist. *That is evidenced by the negative results of the detection of gravitational waves*, *based on the assumption of a completely illegitimate assumption of gravitational wave generation by any mass distribution with variable multipole* (*starting with quadrupole*) *moments.*

4) The presence of the stationary states of the electron in its own gravitational field is in full compliance with the special theory of relativity. According to STR, relativistic relation between energy and momentum is broken, if we assume that the total energy of the electron is determined only by the Lorentz electromagnetic energy [8].

This means that the total energy of an electron at rest is 4/3 of its Lorentz electromagnetic energy. That corresponds to the numerical data on the spectrum of stationary states of the electron in its own gravitational field. In the Standard Model the relativistic relation between the energy and momentum of the electron is broken, as it is assumed that the total energy of the electron is determined only by the Lorentz electromagnetic energy. This follows from the fact that the gravitational interaction at the quantum level in the Standard Model is not considered.

It should immediately be noted that the numerical evaluation of the spectrum is approximate. The greatest uncertainty is the estimation of the numerical value of the first steady state, as more and more accurate as you approach $E_\infty = 171\,\text{keV}$.

5) Estimate of the numerical value of K can be obtained with the help of Kerr-Newman metric using the following formula:

$$K = \frac{r^2}{\left(mcr^2/L - L/mc\right)\left(m/rc^2 - e^2/r^2c^4\right)}; \tag{14}$$

where r, m, e, L, c are the classical electron radius, mass, charge, orbital angular momentum, the speed of light, correspondingly. The numerical value of the orbital angular momentum was taken equal to the spin of the electron.

Thus, we can assume that the physical nature of spin is possible that this value is the orbital angular momentum of the particles in their own gravitational field. This gives ground to consider that the use of Klein-Gordon equation is not so easy.

The distance at which the gravitational field with the constant K is localized is less than the Compton wavelength, and for the electron, for example, this value is of the order of its classical radius. At distances larger than this one, the gravitational field is characterized by the constant G, *i.e.*, correct transition to Classical GR holds.

References

[1] Fisenko, S.I. and Fisenko, I.S. (2015) *Journal of Physics*: *Conference Series*, **574**, 012157. http://dx.doi.org/10.1088/1742-6596/574/1/012157

[2] Hilbert, D. (1915) Grundlagen der Physik, 1 Mitt. Gött. Nachr., 1915, math.-nat. Kl., S. 395.

[3] Siravam, C. and Sinha, K. (1979) *Physics Reports*, **51**, 112-123.

[4] Friedmann, A. (1922) *Zeitschrift für Physik*, **10**, 377-386. http://dx.doi.org/10.1007/BF01332580

[5] Landau, L.D. and Lifshitz, E.M. (1976) Field Theory. Publishing House «Nauka», Moscow.

[6] Warshalovich, D.A., *et al*. (1975) Quantum Theory of Angular Momentum. Publishing House «Nauka», Leningrad, 282-285.

[7] Fisenko, S.I. and Fisenko, I.S. (2009) *The Old and New Concepts of Physics*, **6**, 495-452.

[8] Pauli, W. (1958) Theory of Relativity. Pergamon Press, Oxford.

Journal of Modern Physics, 2016, 7, 1049-1067
Published Online June 2016 in SciRes. http://www.scirp.org/journal/jmp
http://dx.doi.org/10.4236/jmp.2016.710094

Scientific Research Publishing

Energy Conversion Mechanics for Photon Emission per Non-Local Hidden-Variable Theory

Dirk J. Pons[1*], Arion D. Pons[2], Aiden J. Pons[3]

[1]Department of Mechanical Engineering, University of Canterbury, Christchurch, New Zealand
[2]University of Cambridge, Cambridge, UK
[3]Rangiora New Life School, Rangiora, New Zealand
Email: *dirk.pons@canterbury.ac.nz

Received 27 April 2016; accepted 3 June 2016; published 8 June 2016

Abstract

Problem-Energy conversion processes in optical phenomena are incompletely explained by wave theory or quantum mechanics. There is a need for ontologically rich explanations at the level of individual particles. Purpose: This paper reports on the application of a non-local hidden-variable solution called the Cordus theory to this problem. The method is directed to the systematic development of a conceptual framework of proposed causal mechanisms. Findings: It has long been known that the bonding commitments of the electron affect its energy behaviour but the mechanisms for this have been elusive. We show how the degree of bonding constraint on the electron determines how it processes excess energy. A key concept is that the span and frequency of the electron are inversely proportional. This explains why energy changes cause positional distress for the electron. Natural explanations are given for multiple emission phenomena: Absorbance; Saturation; Beer-Lambert law; Colour; Quantum energy states; Directional emission; Photoelectric effect; Emission of polarised photons from crystals; Refraction effects; Reflection; Transparency; Birefringence; Cherenkov radiation; Bremsstrahlung and Synchrotron radiation; Phase change at reflection; Force impulse at reflection and radiation pressure; Simulated emission (Laser). Originality: The paper elucidates a mechanism for how the electron responds to combinations of bonding constraint and pumped energy. The crucial insight is that the electron size and position(s) are coupled attributes of its frequency and energy, where the coupling is achieved via physical substructures. The theory is able to provide a logically coherent explanation for a wide variety of energy conversion phenomena.

*Corresponding author.

How to cite this paper: Pons, D.J., Pons, A.D. and Pons, A.J. (2016) Energy Conversion Mechanics for Photon Emission per Non-Local Hidden-Variable Theory. *Journal of Modern Physics*, **7**, 1049-1067. http://dx.doi.org/10.4236/jmp.2016.710094

Keywords

Photon, Light, Electron, Emission, Cordus Conjecture, Physical Interpretation

1. Introduction

Many optical phenomena have ontologically poor explanations at the level of individual photon particles, despite satisfactory mathematical representations. Examples are the processes of photon emission, photon absorption, phase change at reflection, and laser emissions. These are adequately described by the classical electromagnetic wave theory of light, but that applies to waves and is difficult to extend to individual particles. Quantum theory better represents the behaviour of individual particles, but its ontological power of explanation is weak, *i.e.* it can quantify many phenomena but its explanations are difficult to ground in physical realism. This paper reports on the application of a non-local hidden-variable (NLHV) solution called the Cordus theory to explain several optical phenomena involving energy conversion.

1.1. Need for Richer Explanations

Quantum Mechanics (QM) is built on the premise that particles comprise zero-dimensional (0D) points. This assumption results in a mathematically tractable representation of the photon, but has the detriment that key empirically observable variables, such as spin and polarisation, are denied a physical basis. They are instead treated as merely intrinsic variables, and this causes incongruence relative to physical realism. QM is able to show via Feynman diagrams that photon processes occur, and is able to quantify the output channels, but is unable to explain how input particles are transformed into the outputs. QM is unable to explain in an ontologically sufficient manner how the 0D point of the photon is absorbed into the 0D point of the electron, or how a 0D photon separates into an electron and antielectron (pair production), or how matter and antimatter annihilate back to photons. The latter two processes represent mass-energy equivalence, and thus even this foundational principle lacks an ontologically satisfactory explanation. Some interpretations of QM, such as the Copenhagen, do not see this as a problem, since the quantitative formulation of QM is adequate for most practical purposes. In contrast others expect to see fundamental physics grounded on physical realism. Thus the unnaturalness of QM's explanations is, from this perspective, an artefact of its 0D premise.

1.2. Hidden-Variable Solutions

Since the 0D point premise is at the root of this problem it follows that theories of physics that describe the internal structure of photons and matter may have a better chance of providing explanations. These are the hidden-variable designs. There was a time in the early development of quantum theory when these were believed to be the way forward, at least for explaining entanglement [1], but subsequent work in the form of the Bell-type inequalities [2]-[4] invalidated all *local* hidden-variable designs and some classes of *non-local* designs too. However, non-local hidden-variable (NLHV) designs have not been totally eliminated: this is not contentious. The greater problem has been the scarcity of candidate solutions to evaluate. The first theory of substance was the de Broglie-Bohn pilot-wave theory [5] [6], but this has progressed only slowly. A subsequent development was the Cordus theory which proposed that particles had a specific internal structure comprising two reactive ends, connected but some distance apart [7]. This structure explains wave-particle duality in the double-slit device, and provides a quantitative derivation of optical laws for reflection, refraction, and Brewster's angle [7]. Other applications of the theory include photon emission from the electron [8], pair production [9], and asymmetrical genesis [10].

Thus the NLHV sector is able to qualitatively and quantitatively explain several energy phenomena. This is a promising start, but there is a need to explain other energy phenomena too. The area under examination in the present paper is the need to explain one category of energy conversion effects, namely the interaction between photons and matter.

2. Methodology

The purpose of this paper is to develop a conceptual theory for photon emission and absorption, using the Cor-

dus theory.

The methodology used is logical inference in a gedanken (thought) experiment. This method starts with an initial set of lemmas, which are the principles of physics accepted at the outset. These could be based on any theory of physics such as thermodynamics, quantum mechanics, M/string theory, NLHV theory, etc. The starting theory here was the Cordus theory. The next stage in the methodology is to determine the logical consequences if those lemmas were true. The result of this is an extension to the theory, sometimes with the addition of new lemmas. The logical extension continues until explanations are available for existing physical phenomena, which allow a checking and validation of the theory.

This means that the method is potentially able to predicting the underlying mechanisms of physical causality for phenomena not originally encompassed by the founding lemmas. It also has the potential, shown here, of providing entirely new and original explanations for existing physical phenomena, *i.e.* provides a new conceptual framework. This is a particularly useful feature of the methodology, especially when prospecting for access ways into possible new physics. The progressive nature of this process of theory development results in a theory with high internal consistency or congruence, and this is an attractive feature of the method. However the resulting theory tends to be qualitative if the starting premises are qualitative, and hence it is not always practicable to construct quantitative formalisms this way, which is sometimes a disadvantage. In the present case we are primarily interested in providing ontologically rich explanations for a variety of phenomena, and the lack of a formalism is not an issue.

The approach applies this systematic methodology to the existing Cordus theory to infer the photon mechanics within this framework. Prior work [8] has proposed the mechanics whereby an electron emits a photon. The present work extracts the underlying assumptions, and then infers a proposed physical causality. These principles are then applied to explain other optical phenomena. As will be shown, the theory is able to provide a logically coherent explanation for a wide variety of optical energy conversion phenomena.

The method is directed to the systematic development of a conceptual framework of proposed causal mechanisms. It is an abstract method and results in a conceptual formulation of the system, as opposed to the mathematical formalism or quantitative models of other methods. The proposed physical causality is represented using integration definition zero (IDEF0) systems engineering flowchart notation [11].

3. Results

3.1. Relevant Principles of the Cordus Theory

3.1.1. Structure of the Cordus Particule

The Cordus theory proposes that a particle consist not of a 0D point but rather two reactive ends that are some distance apart and connected by a fibril. The ends are energised in turn at the de Broglie frequency, during which time they emit discrete forces in three orthogonal directions [7]. These discrete forces are connected in a flux tube and the inward/outward direction of propagation determines the charge, and the handedness of the energisation sequence determines the matter-antimatter attribute [12]. The Cordus literature calls this a particule to differentiate it from the 0D point construct of QM. The photon structure is shown in **Figure 1**, and the electron in **Figure 2**.

The internal structures of the proton [15], neutron [16], and neutrino-species [17] have likewise been determined for this theory. Further details may be found in the references.

Importantly, the Cordus theory requires that the span of the matter particules be inversely proportional to the frequency. Thus the span of the electron becomes smaller as its frequency (hence also energy) increases. This is important in what follows regarding emission and absorption.

3.1.2. Remanufacture of Particule Identities at Photon Emission

Previous work in the Cordus theory [8] has proposed a physical process whereby an electron emits a photon. This is given as set of geometric transformations of structure, hence the explanation is based on physical realism. The theory also explains why it should be that the bonds imposed on an electron would constrain the energy of the photon it emitted. The work proposed that emission was an escapement mechanism "whereby matter particles that are over-prescribed in position can get rid of that energy" by emitting a photon. Hence the underlying causes of emission are proposed to be constraints on geometric position of reactive ends. The process is summarised as follows, see also **Figure 3**.

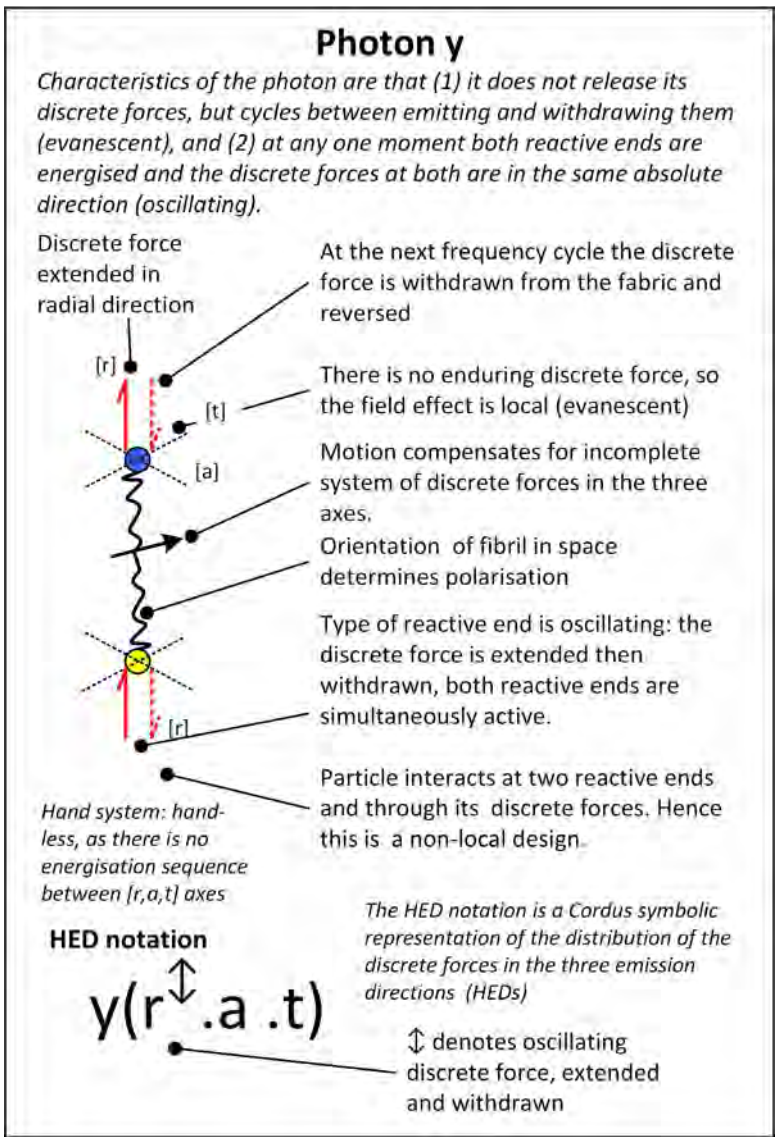

Figure 1. Cordus theory for the internal structure of the photon, and its discrete field arrangements. The photon is proposed to have a pump that shuttles energy outwards into the fabric. Then at the next frequency cycle it draws the energy out of that field, instantaneously transmits it across the fibril, and expels it at the opposite reactive end. From [13] reproduced under CC-BY-4.0.

1) An energetic electron, one that has absorbed energy via a prior process, requires higher frequency and also shorter span. However the change in frequency and span are resisted by bonding commitments with other particules. These commitments fix the frequency (for synchronous emission of discrete forces) and co-location of reactive ends. This is a consequence of the synchronous interaction (strong force) [15] [18].

2) If the electron is unable, due to its bond commitments to change frequency and span, then it needs to discard its excess energy. One of those routes is photon emission, which discards the energy into the fabric. The fabric is the surrounding skein of discrete forces emitted by all the other particules in the accessible universe [19]. The electron does this by creating an independent pair of discrete forces, one at each reactive end. These are created simultaneously at both ends-this is achieved by the superluminal communication across the fibril. For charge conservation, one of the new reactive ends has a negative charge (outward direction of discrete force) and the other a positive charge (inward direction). The new photon discrete forces are in the [r] directions, since that is the dimension in which the positional constraint exists, *i.e.* in the span direction.

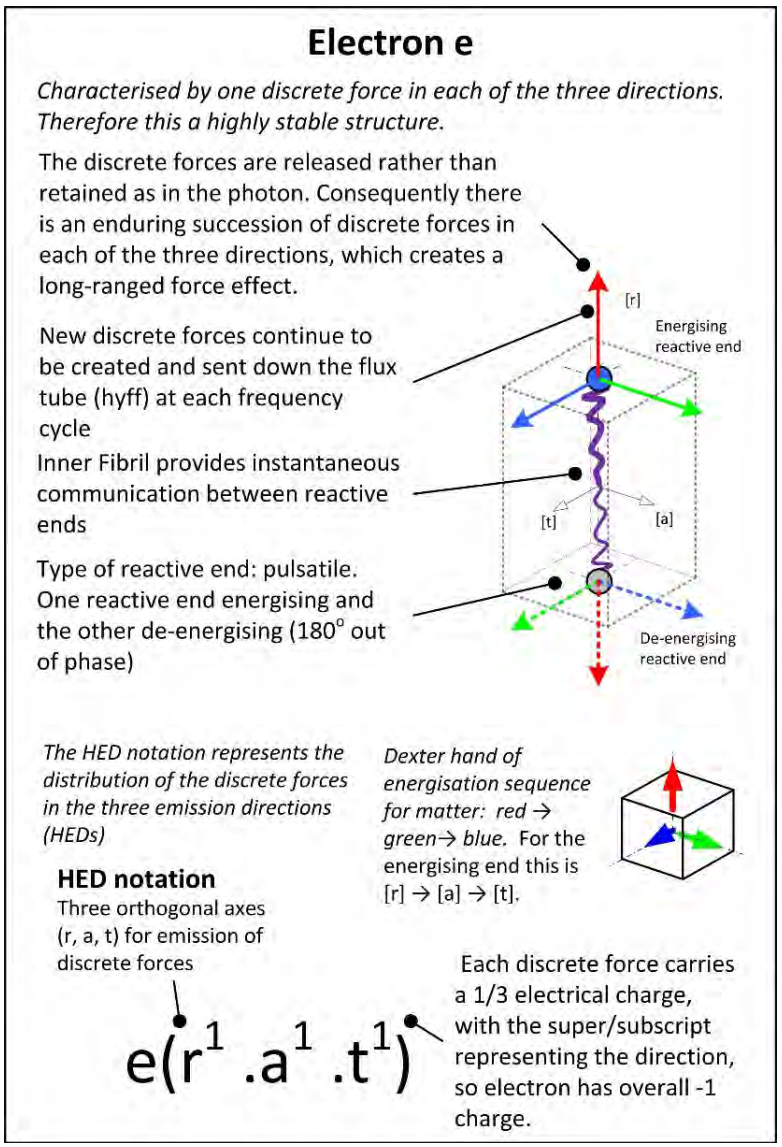

Figure 2. The representation of the electron's internal and external structures. It is proposed that the particle has three orthogonal discrete forces, energised in turn at each reactive end. Image source [14] reproduced under CC-BY-4.0.

3) The new discrete forces are accompanied by new reactive ends which are the termination points. These emerge from the electron structures and are briefly co-incident with them. In this theory particule identity is determined by the discrete force structure [17], and this type of structure with one discrete force at each reactive end, and a directional flow of energy (in at one reactive end, out at the other) defines the photon. The photon basically polarised the fabric to store energy, but the storage is dynamic. This external polarisation then reverses, causing the directions of the discrete forces to also reverse, hence the oscillating nature of the photon. The greater the energy to be stored in volumetric strain, the quicker the renewal, hence proportionately higher frequency of the fibril: this is consistent with the observation that higher energy is linearly related to higher frequency via the de Broglie relation.

4) The photon moves away from the assembly. The theory predicts that the motion is perpendicular to the [r] axis of the common assembly. The need for movement of the photon arises to compensate for the photon only having discrete forces in the [r] direction. A similar mechanism also explains the motility of the neutrino species [17]. The span of the photon is initially that of the electron that released it, but is predicted to be flexible, such

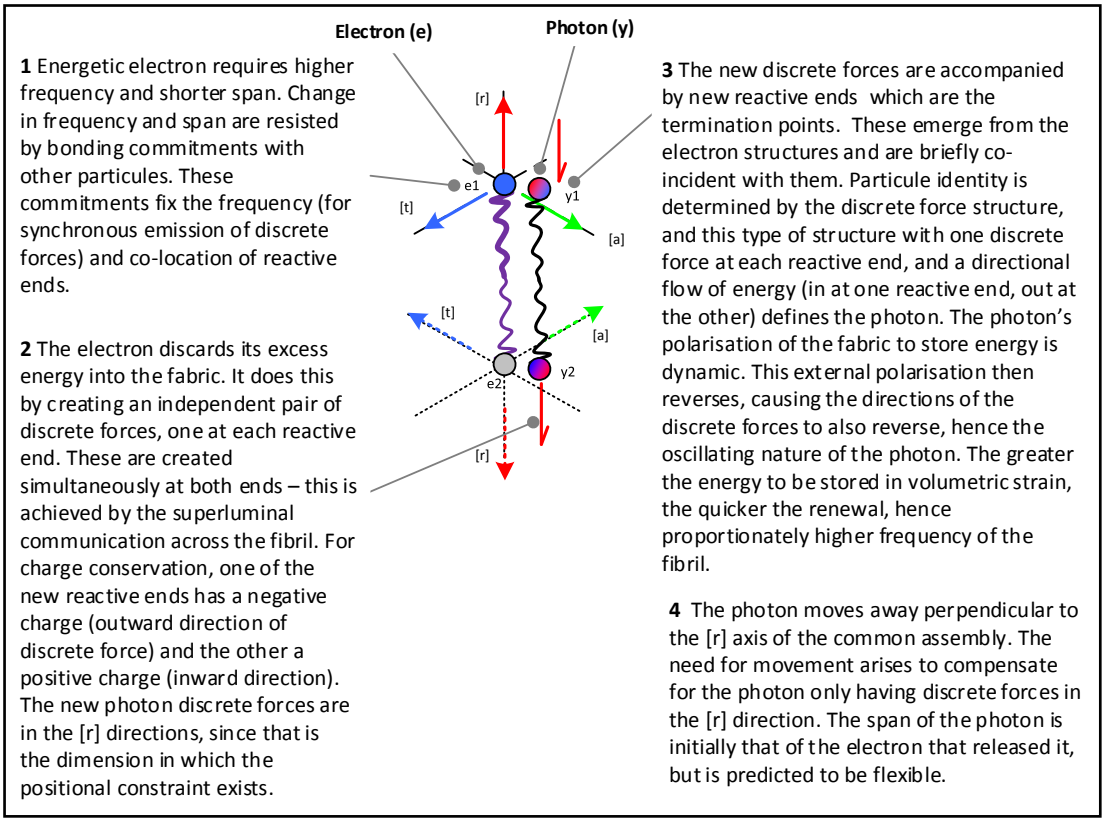

Figure 3. Proposed process of photon emission from an electron. Shown here is only one stage in the larger process, where the photon structures (reactive ends and discrete forces) start to emerge from the electron structures. It is proposed that the photon is emitted because the bonding constraints on the electron cause the locations of its reactive ends to be fixed at a greater span than is congruent with the electron's internal energy. Image adapted from [8].

that it follows the paths presented to it by the fabric (e.g. wave guides).

The significance of this finding is that it explains why nature of the chemical bonding of the electron in the substrate affects optical phenomena (reflection, transmission), and laser frequency among other effect. These "bonding constraints affect geometric span of the particule, which affects frequency [and] this constrains the energy that the electron can contain, and explains why the emitted photon has a specific quantum of energy" [8] (p. 14). That prior work contained a set of diagrams showing how the field structure of the photon particule emerged from the electron. The Cordus theory has elsewhere shown how particule identities arise from the discrete field structures, and how changes to these structures result in new particule identities. This has been applied to explain the decay processes [16] [17] [20], annihilation [12] [21], pair production [9], and the genesis production sequence that culminated in asymmetrical baryogenesis [10].

These papers established the principles whereby discrete field structures may be remanufactured and change the particule identities. There are a number of conservation principles involved, and at the detailed level it is necessary to keep track of the number and types of discrete fields. The present paper takes a higher level approach by examining the processes as a whole rather than the detailed transformations.

3.2. A System Model for Optical Energy Conversion

We start with what is already known about the reasons for photon emission. The basic process is that external energy is pushed into the electron as explained in [8]. The electron then responds in one of several ways to that energy. One of those ways is photon emission. Note that the situation under examination is electron-photon interactions, but the principles are expected to be applicable to photon interactions with other particules. This section proposes the situational constraints that cause those responses, with a particular focus on the causal pathway

for photon emission.

3.2.1. Energy Mechanics inside the Particule

It is proposed that, under this NLHV theory, the energy mechanics adhere to the following principles, see **Figure 4**. The numbers in the following text correspond to functional blocks in the diagram. We start with a case where external energy is pushed into the particule (1). The next effect is a conflict within the particule between its energy and its constraints (2) (elaborated below). This results in the particule responding to the excess internal energy (3). Several outcomes are possible (elaborated below), one set of which lead to the electron emitting a photon (3). The process is described for the electron case, but the principles apply to any photon emission. The emission process itself has been described in detail elsewhere [8].

3.2.2. External Energy Pushed into Particule

The external energy may arise from a number of sources. These include: Movement (frequency, phase, or location) of the host atom or neighbouring electron/atom; Absorption of an incident photon; Interaction with fields and fabric discrete forces including electro-magneto-gravitational forces of remote particules, and the acceleration of the particule itself; Disturbance from a transient in the fabric, *i.e.* a localised dynamic increase in density of discrete forces such as an energetic photon that passes nearby; Energy transferred from other atoms (phonons),

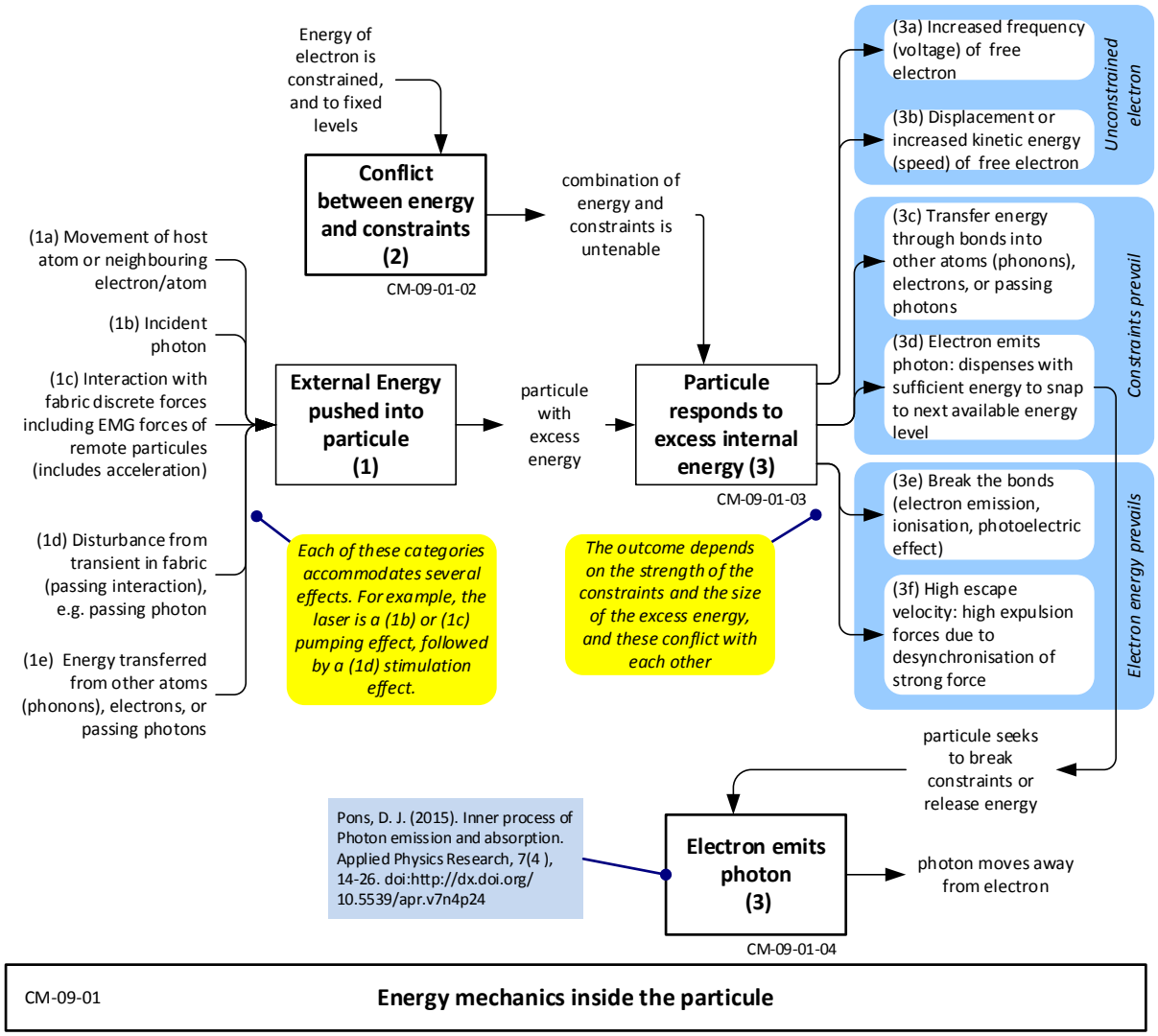

Figure 4. The proposed energy mechanics occurring inside the particule.

electrons, or passing photons. Each of these categories accommodates several effects. For example, the laser is proposed to be a (1b) or (1c) pumping effect, followed by a (1d) stimulation effect.

In the Cordus theory all energy transfers occur exclusively through the discrete force (field) system, and more specifically the constraints that external discrete forces impose on the position, and emissions of the recipient reactive end.

3.2.3. Conflict between Energy and Constraints

The next step is to explain how and why the electron is geometrically constrained at its reactive ends, see **Figure 5**. The primary components of the constraint model are that the electron has two reactive ends (1), of which one is typically bonded to a nucleus (2), and the other is bonded to the electron in another atom or is a free valence

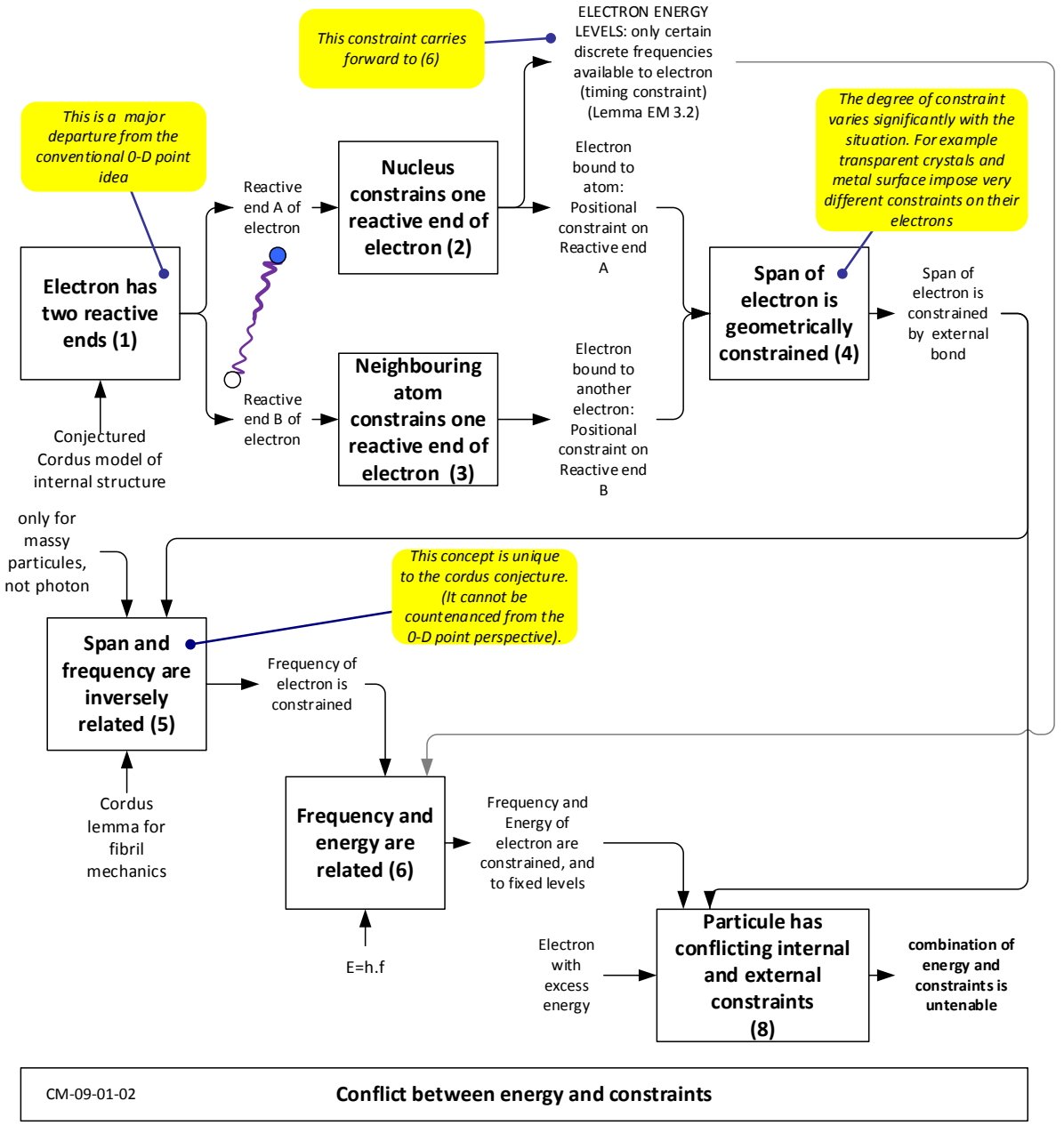

Figure 5. The particule has conflicting internal and external constraints. This diagram represents several of the underlying principles of the Cordus theory (see text for elaboration) that give rise to these constraints.

end (3). Thus the span of the electron is geometrically constrained (4). Consequently, according to the Cordus theory, the frequency of the electron is also constrained by its bonding arrangements (5), and therefore its energy too (6). These constraints depend on the strength of the bonding obligations. Thus the particule has conflicting internal and external constraints (8).

3.2.4. Particule Responds to Excess Internal Energy

The particule responds to excess internal energy in several ways. The outcome depends on the strength of the constraints and the size of the excess energy, and these conflict with each other. We propose a categorisation of responses based on the constraints: unconstrained electrons; constrained electrons; and situations where the electron breaks the constraints.

1) *Unconstrained electron*

The first category of events is where the situation involves a free electron, e.g. in an electron gas. In this case the electron is free to change its frequency and span to suit its situation. For example, if the electron receives energy, then it can increase its frequency and reduce its span, hence the two reactive ends will become closer together. Since the reactive ends have no bonding commitments, this is not problematic. Consequently the system responses are (3a) Increased frequency (voltage) of the free electron, or (3b) Displacement or increased kinetic energy (speed) of the free electron.

2) *Constrained electron*

In the situation where the electron has bonds with other particules then the situation is more complex. This is because the nature of bonding, according to the Cordus theory, is that bonded particules co-locate one reactive end from each particule, and then synchronise their emission of discrete forces. Hence the bonding occurs via synchronisation of emissions rather than charge per se, and this "synchronous interaction" [15] is proposed as the explanation for the strong nuclear force. This novel reconceptualisation of the strong force also yields an explanation of nuclear structures [18] [22].

The complexity arises because frequency and span are coupled variables in this theory. Thus the electron that gains energy needs to increase its frequency, but must also decrease its span. This has two problems for a bonded electron. First, the change in frequency perturbs the frequency synchronisation with the other particule. If the electron is to be allowed to increase its frequency, then the chain of other particules to which it is bonded will also have to increase theirs. Second, the spatial location of the electron's reactive ends needs to change to accommodate the shortened span, but the assembly of other particules resists this. The assembly, e.g. of the atom, is an extensive polymer of Cordus particules each of which is rod-like, so the assembly has physical volume and high stiffness. These two constraints on the particule, frequency and span, are coupled. The electron in the atom is bonded into an extensive assembly of other particules, all of which are bonded by one synchronous interaction (with harmonics). That atom has similar though more remote bonds with other atoms. Consequently the energetic electron has difficulty changing the frequency of that whole assembly to accommodate its own frequency needs. The assembly imposes a frequency on the electron, and while the electron stays in the assembly it must energise at that frequency, because bonding occurs via synchronicity. This imposed frequency is a constraint on the electron, and if this constraint prevails then the electron stays in the assembly but disperses its surplus energy into the assembly via phonons and heat.

Hence the second category of response is where the electron is bonded (is not free) but the synchronicity constraints of the bonds prevail. In which case the electron's options are: (3c) Transfer energy through bonds into other atoms (phonons), electrons, or passing photons; or (3d) Electron emits photon: dispenses with sufficient energy to access the next available energy level. The 3d outcome leads to photon emission, whereas the other routes do not. Multiple routes 3a-f may apply sequentially, so photons may be emitted in later processes.

3) *Electron energy prevails*

Alternatively a sufficiently energetic electron may disregard the bonding constraints, and change its frequency and span. In doing so it disqualifies itself for ongoing membership of the larger assembly of particules (e.g. atom, molecule) because it has desynchronised itself. The process of desynchronisation exposes both subcomponents, the electron and the rest of the atom, to the repulsive effect of each others' discrete forces, *i.e.* both the attractive and repulsive characteristics of the strong force are due to synchronicity effects. As the electron is the lighter subcomponent, it tends to be forcefully ejected. Hence the third category of responses is for the electron energy to prevail over the bond constraints, and this results in: (3e) electron breaks its bonds with the atom, resulting in electron emission, ionisation, and the photoelectric effect; and/or (3f) High escape velocity of the electron, from

the high expulsion forces due to desynchronisation of the strong force.

Note that although the presentation has been in terms of an electron, the principles apply to any massy particule or assembly thereof.

To help make sense of the various ways the electron responds to excess energy, we represent the relationship as two independent variables: the degree of constraint on the electron vs. the extent of the excess energy in the electron. Thus external vs. internal variables, see **Figure 6**.

The electron responses 3 a-f are located on the figure, and proposed to be limited to certain regions. Thus ionisation (3e) requires that the electron receive greater energy than the constraints (bonding energy). On the other side, if the electron's excess energy is much less than the constraints, then it disperses the energy into the atoms to which it is connected (3c).

Both scales of this diagram are energy units, but the present purpose is not so much to quantify the relationships as understand the causality. In that regard, it is useful to categorise the response surface into three regions.

- The region above the diagonal contains electron mobility responses, *i.e.* the electron does the moving. By implication higher escape velocities at (3f) require stronger mismatch between the constraints and the energy.
- The region below the diagonal is an internal thermal response, *i.e.* the electron discharges the energy into neighbouring atoms, hence heat.
- The diagonal itself corresponds to photon emission responses, *i.e.* the electron emits a photon. Thus emission is widely available across a range of bonding situations and input energies. This also explains the very wide range of frequencies that an emitted photon can take. The details of the photo emission process itself, and how the photon structures emerge from those of the electron, are already described [8].

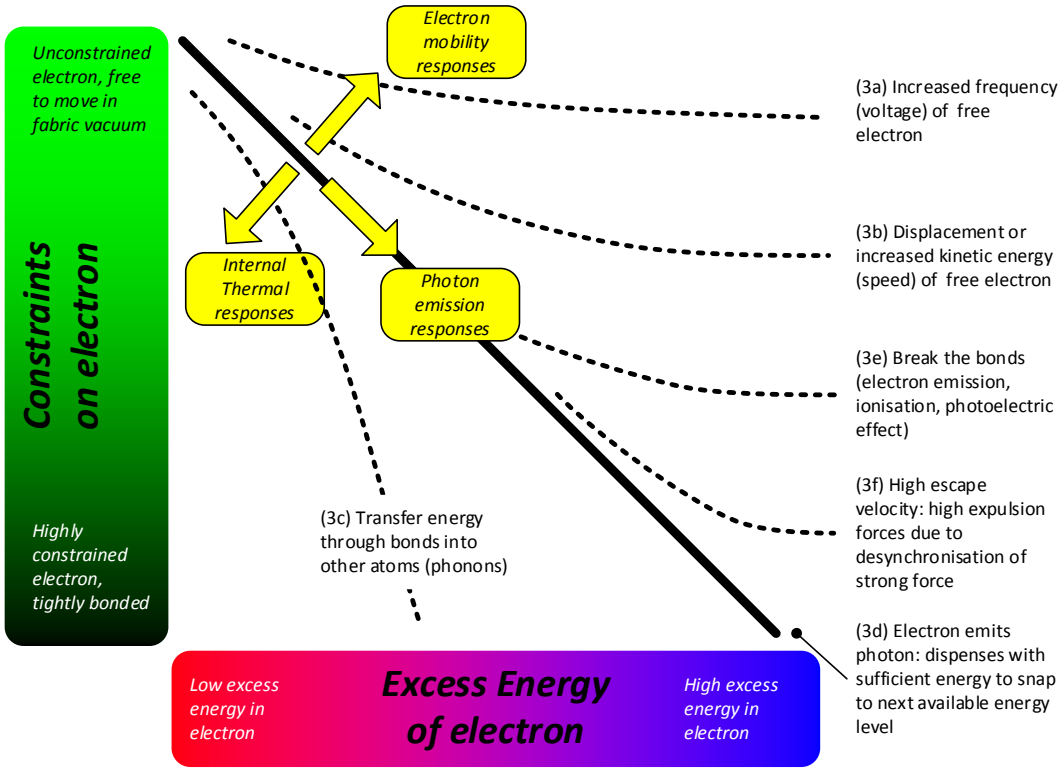

CM-09-01-03B	**Particule responds to excess internal energy**

Figure 6. Representation of the proposed relationships showing how the electron responds to combinations of bonding constraint and pumped energy.

Key to this theory is the concept that the span and frequency (hence energy) of the electron are inversely proportional. This explains why energy changes cause geometric spatial distress for the electron. This makes it much easier to explain how bonding affects the behaviour of photons. By comparison the concept of frequency is merely abstract in the conventional QM photon emission model that assumes 0D points, and there is no concept of span, nor any dependency between frequency and span.

Summarising this part:

1) The photon emission/absorption processes have been identified for the Cordus theory, based on behaviours of the discrete field elements and internal structures.

2) The functional implications of this have been identified. The two main variables are identified as *bonding* and *input energy*.

3) A conceptual theory has been created for how those variables interact to determine what the electron does with its excess energy.

Therefore the first output of the present work is a process model for the energy mechanics within the electron. This is valuable, despite being qualitative, as it provides a means to represent the causality under various contingencies, *i.e.* it shows how various factors cause the different energy conversion outcomes to arise. The next section applies this theory to explain a number of optical energy related phenomena.

3.3. Application to a Variety of Phenomena

This theory is now applied to a variety of known photon emission phenomena. The objective is to check the internal construct validity of the theory by seeing whether it gives logically consistent explanations for these diverse phenomena. The focus is primarily on photon emission and absorption phenomena.

3.3.1. Absorbance

High-energy photons like X-rays tend not to be absorbed by materials but instead pass through. If they are absorbed, they tend to break chemical bonds and release electrons. Our explanation is that these photons have too high a frequency to readily engage with the electron, and therefore the necessary match cannot be achieved for absorption. When it does, the energy absorbed by the electron forces it to adopt a shorter span (hence also higher frequency) and this severs its bonds with the atom. Thus the positional constraint to energise at a shorter span is stronger than the constraint to bond at a certain location. Hence the electron breaks free from its bond, and ionisation occurs in this situation (8e response).

3.3.2. Saturation

Absorption can be saturated by the intensity of light. The usual explanation is that electrons are so excited that they cannot absorb further energy or emit photons fast enough. Our explanation is that saturation occurs because the electron, having absorbed one photon, is attempting to move to a shorter span (also higher frequency). To the extent to which it achieves this, it becomes less receptive to absorbing further photons of the original frequency. So the electron does not absorb electrons indefinitely, hence saturation. This also means that the energy is not cumulative: the energy of many low frequency photons cannot be concentrated within the electron all at one time. If the electron is to be stripped away (ionisation), it requires one photon of sufficient energy rather than many of lesser energy. This also applies to the photo-electric effect (see below).

3.3.3. Beer-Lambert Law

Absorbance of light into a material does not happen entirely at the surface layer but progressively into the material. The transmissivity is $T = \exp(-\alpha' s)$ where α' is the absorption coefficient and s is the distance into the material (Beer-Lambert law). Our explanation is that 1) only a certain proportion of electrons have their fibril orientation (spin) suitably aligned to engage with the incoming photon stream, and 2) those electrons that have already absorbed a photon are in a higher energy state and prefer to re-emit the energy than absorb more. Therefore some photons get deeper into the material before meeting an appropriate electron. The transmissivity is expressed in terms of an inverse exponential of distance travelled, which is consistent with the idea that a constant proportion of the incoming photons are absorbed at any one layer of electrons into the substrate. The absorption coefficient may thus be given a physical interpretation as representing the density of suitable electrons in the substrate.

3.3.4. Colour of Materials

Materials may selectively absorb light of certain frequencies, and transmit other frequencies. Our explanation is that absorption requires compatible frequencies between the incoming photon and the electron. In turn, frequency is linked to electron span, and span to the bonding commitments of the electron. Thus chemical composition and bonding arrangements determine electron span. Consequently the material preferentially absorbs certain frequencies and reflects others, hence colour of materials.

3.3.5. Transparency

The evidence is that transparent bodies tend to comprise electrically non-conductive materials. Our explanation is that transparent materials such as glass have chemical structures that more tightly constrain the mobility and span-length of the electron. This fixation is also results in low electrical and thermal conductivity. Thus these materials have selective absorption of certain frequencies that match the span constraints of the electrons. Photons with very different frequencies cannot engage with these electrons and therefore pass through, hence high transmissivity.

3.3.6. Quantum Energy States

The Cordus theory qualitatively recovers the quantum energy emission of bound electrons. Photons emitted in these cases have a fixed energy, hence frequency, in discrete though unequal increments, corresponding to the difference in energy states for the electron. Our explanation is that the electron is constrained by its bonding commitments to the nucleus and external electrons to certain geometric configurations and hence frequencies or harmonics thereof. Since the electron can only energise at these specific frequencies, thus the emitted photon will also have an energy determined by the gap between these frequencies.

3.3.7. Direction of Photon-Emission

It is not possible to explain the direction of photon-emission using a quantum theory based on 0D particles with spin being merely a mathematical property. In contrast the concept of fibril orientation in the Cordus theory explains why an emitted photon would have a preferred direction of travel, see [8] for details.

3.3.8. Photoelectric Effect

In the photoelectric effect the photon ejects an electron from the metal substrate. Importantly, this effect depends on the frequency of the light, not its intensity. There is a minimum threshold frequency, which varies with the metal, below which the effect does not occur. Our explanation is that the metal creates a basal level of bonding between the nuclei and the electrons, which depends on the elements and chemical composition. The electron has freedom to move, hence electrical conductivity. For the electron to escape, it needs to absorb sufficient energy to break those bonds entirely. It does this by absorbing an energetic photon, which increases the frequency and decreases the span of the electron. This conflicts with the bonding constraint which seeks to maintain location of the reactive ends within the matrix of nuclei. If the energy is sufficient, then the electron severs those bonds and escapes. If the input photon has more than enough energy to liberate the electron, then it creates a large mismatch in the bonding constraints and thus high ejection forces, hence kinetic energy of the electron.

From the Cordus theory the reason this does not depend on the number of photons, *i.e.* light intensity, is that the electron absorbs one photon at a time, and if this is insufficiently energetic to break the bond, then there is no ejection. The electron, having absorbed one photon, becomes saturated against receiving further photons of similar frequency. This because its frequency increases slightly, hence receptivity decreases. The insufficiently energised electron then transfers its slight energy surplus into the substrate, via the unbroken bond. This corresponds to the 8c response above, and occurs in the form of phonons (internal vibrations). Hence temperature of the substrate rises. Thereafter the electron reverts to its former span and is ready to receive another photon. In this regard the explanation is similar to that for saturation above.

3.3.9. Emission of Polarised Photons from Crystals

The Cordus theory is consistent with the known behaviour that crystals produce highly polarised photons. Our explanation is that the crystal structure imposes tight positional constraints on the electrons, since the electrons provide the bonding between atoms. Hence also the orientation of the span of the electrons is controlled. Consequently the emitted photons also have an orientation, hence the polarisation. Polarised light is thus explained

as photons with common orientation.

3.3.10. Refraction Effects

The Cordus theory has previously been used to explain reflection and refraction [7]. However that explanation was mainly in terms of a Cordus photon interacting with a homogenous substrate. Adding the electron side of the theory allows a fuller description of a number of refraction effects. Thus dispersion and chromatic aberration, where refractive index varies with frequency, may now be explained as a consequence of higher frequency photons having less interaction with electrons.

3.3.11. Reflection

The electrons in metals have a high degree of freedom, which gives them freedom to change the orientation and length (hence energy) of their span. Thus such electrons have a high receptivity to engage with incoming photons of various orientations and frequencies. However engagement does not mean absorption, because the mobility of the electrons also means they have freedom to move in the surface plane of the substrate instead of absorbing the energy. Consequently the incident photon is momentarily captured by an electron. The electron quickly re-emits the photon, hence emission of a reflected electron. The electron moves in the plane during this interaction. Where the plane of the reflective surface is made very small, then the mobility of the electron is impeded and the angle of reflection is also changed. This is consistent with the observation that optical surfaces comprising small ridges behave differently to flat surfaces.

3.3.12. Birefringence

Crystals may have two refractive indices, and this is associated with different molecular lattice-spacing in different directions. There can also be a frequency dependence of absorption for polarisation, or pleochroism. Birefringence also arises where transparent materials have differential internal strain (photoelasticity). Our explanation is that the different geometric spacing of the crystal lattice causes the respective bonding electrons to have different orientations of their fibrils, and in the case of pleochroism also different span (hence frequency). Consequently the incoming photons interact according to their orientation relative to that of the electron spans, though in this case they are not absorbed but merely re-directed hence refracted. The electrons, being fixed in location, emit discrete fields that are also fixed in direction. The spans of the transmitted photons are re-oriented to align with these fields, and hence the photons become preferentially polarised along one of the available orientations. This explanation also accommodates the known effects whereby birefringence arises from strain. The effect is evident whether the strain is induced mechanically as in the freezing of plastic, and photoelasticity, or by electric field (Pockels effect), or magnetic field (Faraday effect). In all these cases we propose there is a change in the alignment of the electron spans in the principal strain directions, and hence two preferred orientations for photon transmission. Hence the polarisation of the transmitted light is correlated to the strain.

Similarly the chromatic effects may be explained by frequency considerations. The chemical composition determines atomic spacing, which controls electron span, which determines electron frequency, and hence frequency (colour) of emitted light. Hence materials may absorb light differently and show different colours depending on the wavelength of light, such that they change colour when the polarisation of the light changes plane (pleochroism).

Explaining birefringence as geometric alignment is not difficult when the electron and photon are permitted to have a Cordus structure. By comparison the orthodox particle perspective labours with abstract concepts, since polarisation and spin have no physical representation for 0D points. Electromagnetic wave theory is thus the usual means of explaining optical effects, but is limited to light en-masse rather than single photons. The Cordus theory makes the original contribution of being able to conceptually explain optical effects at the level of single photons.

3.3.13. Cherenkov Radiation

Charged particles are known to radiate photons when moving with physical speed faster than the speed of light in the dielectric medium. The conventional explanation is that the particle polarises the local molecules, or disturbs the bonds, which then release the energy along a shock front due to interference. The effect only occurs with charged particles (not neutral ones), and in dielectric media (not conductive ones).

The Cordus explanation is that the energetic charged particle has an emission problem: the forward emission of discrete forces by the reactive end is resisted due to the inability to make an emission at the local speed of

light. Consequently the emission directions are reoriented away from the forward direction. The discrete forces of the moving particle interact with the electrons in the medium, with two consequences. First, the electron span in the medium is locally realigned to be complementary to the emission direction imposed by the moving particle. Second, the moving particle transfers via the discrete forces, its excess energy to the stationary electrons in the medium. However these electrons cannot move freely to escape their bonding commitments, since it is the nature of a dielectric medium to permit electrical polarisation but not electron mobility. Therefore the electrons re-emit the energy as photons. This sets up the angular alignment for the emitted photon.

3.3.14. Bremsstrahlung and Synchrotron Radiation

In bremsstrahlung the deceleration of an electron (or any charged particle) produces radiation in the form of photons. This typically happens to high-speed electrons that are arrested in matter. In synchrotron radiation it is the acceleration of the particle in a curved path by magnets that produces photons. This typically happens to fast-moving electrons in a synchrotron, hence the name. The emission occurs in the vacuum. The light is strongly polarised. Lighter particles such as electrons, lose more energy than heavier ones. In both cases the radiation has a continuous frequency spectrum, and higher-speed electrons produce higher frequency radiation. The radiation is only significant at ultrarelativistic speeds. The conventional explanation is incomplete. One of the difficulties with the classical model of the atom is that if an electron orbits round the nucleus, then it should emit a photon (synchrotron radiation) and collapse into the nucleus. Quantum mechanics partly solves this by providing orbitals in which there is only a probability of the electron appearing. However this is an incomplete solution as it does not explain how the electron gets from one location to another, and why it should not emit a photon while doing so.

The Cordus explanation is that any change in speed of the electron, whether acceleration or deceleration, causes the electron's span to change its alignment relative to the direction of motion. The theory is that as the speed increases so the span orientation becomes progressively perpendicular to the velocity. Hence there is an alignment of spin and self-polarisation of spin as velocity increases. This provides the mechanism for the directionality of the emitted photons. This also explains the Sokolov-Ternov effect. As regards the energy of the photons, the process of acceleration or deceleration of the electron necessarily involves the interaction of the electron's discrete fields with those of other particules. In the synchrotron case there is an external magnetic field operating, which is created by the discrete force emissions of other moving charges in a coil. These discrete forces exist through the vacuum. In the case of bremsstrahlung the deceleration is caused by the impact of the electron into other matter particules. The latter also emit discrete forces. In both cases the interactions seek to change the position of the reactive ends of the moving electron, hence change its frequency and span. However the same external interaction also constrains the positions of those reactive ends, so the electron cannot accommodate the energy internally and has to instead emit it as a photon. This theory asserts that even for electrons being braked by a plasma (free-free radiation), there are still constraints created by the interaction of externally imposed discrete fields, so the particules are not really 'free'. The effect is not frictional but rather reactive interference between the discrete force emissions of the moving electron and the external discrete forces.

For slower electrons it is known that the frequency of radiation drops, as does the intensity. The Cordus explanation is that for slower electrons there is more time to relax the opposing constraints of the electron and the medium, so a degree of accommodation disperses some of the energy as frictional losses. Thus the electron is partly relieved of the need to eject the energy as a photon. From this perspective, the electron's emission of a photon is an energy escapement mechanism due to over-constraint on the location of its reactive ends. Such constraints also affect its span-length, fibril orientation, frequency of emissions, and orientation of emissions [8].

3.3.15. Phase-Change Effects

The interaction of a photon and electron is known to result in a phase change in certain situations, particularly when photons are reflected. There is also the curious case of the annihilation of orthopositronium, which can also be interpreted as phase effect. As shown below, the Cordus theory proposes that an electron retards its energisation by half a frequency cycle when emitting a photon, and this is proposed as the common mechanism in all the effects listed below.

3.3.16. Phase Change at Reflection

In the case of reflection, it is the reflected photon that changes phase, *i.e.* changes polarity. This only occurs for

light reflecting off a denser material (higher refractive index), e.g. air to glass. For reflection off a less dense material, e.g. internal reflection glass to air, then the polarity stays the same.

The earlier Cordus explanation for this [23] was that reflection delays the renewal of the reactive end, but only when the photon has to pass into a denser material. The term *transdermis* was used to describe the material *beyond* the interface plane. Thus the nature of the volume beyond the interface plane is important in the reflection effect, even if the reflection itself nominally occurs in the plane. There is no delay in the glass-to-air case, because the *cisdermis* is the denser material and the delay has already occurred in the form of the refractive index, though this is progressive and does not need a frequency cycle.

We now add another level of explanation. The photon is not so much bounced off the reflection interface as a rigid intact particule, but is instead elastically mangled by its interaction with the electron. That mangling causes the phase change. The extreme interpretation of this, which is easier to represent, is that the photon is totally absorbed and a new one emitted. In which case the process is as follows: the incident photon is wholly, semi-instantly and neatly absorbed into an electron → that electron is free to move in the interface plane → the electron temporarily accepts the component of the photon's energy that is in the plane of the interface → the electron is not free to move deeper into the transdermis (perpendicular to the interface plane) because of the electrons already there → the electron therefore cannot cope with that component of the photon's energy that was perpendicular to the interface plane → the electron thus has to elastically return that component → this energy is used at the electron's *next frequency cycle* to create a one-time force impulse (per photon) on a neighbouring electron or atom (force in the Cordus model is a constraint on the location of re-energisation) → the in-plane component of energy is also recovered → a new photon is emitted → however that photon is spooled out of the electron half a frequency cycle later (the electron has had the use of the energy in the intervening period) → this corresponds to a phase shift or change in polarisation of the reflected photon. This explanation is likely to be a simplification of a more geometrically complex and dynamic transformation of the incident photon into the reflected one.

3.3.17. Force Impulse at Reflection, and Radiation Pressure

A mirror surface receives an impulse of up to $p = 2E/c = 2hf/c$ (with photon energy E, Planck constant h, frequency of light f, speed of light c). The Cordus explanation is that the electron uses the energy to create an impulse, and then returns it to the photon. This explanation also accommodates radiation pressure, where photons are not reflected but instead absorbed by a body. The in-plane and perpendicular components of incident energy cause the absorbing electron (or other structure) to exert a positional constraint on its neighbours, in those directions. Thus the Cordus model suggests a mechanism for transforming energy into discrete force impulses, and thus into momentum of the body as a whole. The phase change at reflection allows the electron to have the use of the photon's energy for a moment of time, during which it uses that energy to create a momentary force impulse. Thereafter the photon returns the energy back to the photon. So this provides an answer to the question of how a photon can cause reaction forces in the substrate, and momentum thereof, while still exiting with its same original energy. There is a time delay, wherein the electron is taking energy from the future: the photon arrives half a frequency cycle later at its eventual destination.

The phase change of the photon at reflection off a denser material is a known effect. The Cordus theory suggests that this form of reflection uses a different mechanism to internal reflection. In the former the electron at least partially absorbs the photon and re-emits it after a delay, whereas in the latter the photon stays intact but its locus is bent by the imbalance in the evanescent fields at the interface.

3.3.18. Number of Photons at Positronium Annihilation

The other case for phase change is in the annihilation process. The known annihilation behaviour of positronium is that it produces two photons when the electron and positron have antiparallel spins (parapositronium), and three photons for parallel spins (orthopositronium). Conventional explanations are lacking.

The Cordus theory for annihilation [21] explains why parapositronium produces two photons of equal energy, and orthopositronium three. In the orthopositronium case two photons have the same energy, but the third has a different energy, and the theory explains this too. The Cordus theory readily explains particules taking parallel or antiparallel states with respect to each other, since this corresponds to cis or transphasic frequency coordination. The theory explains why the transphasic (antiparallel) state is necessary for the annihilation process. For orthopositronium either the electron or the antielectron must first emit a photon so as to change the phase of its

frequency and hence enter the transphasic state. The process of emitting a photon is thought to always changes the phase of the electron by half a frequency cycle, corresponding to changing its phase by 180˚ [8]. In the language of QM this corresponds to flipping the "spin". So for orthopositronium one photon is emitted to change the assembly into the parapositronium state, and then the annihilation process itself liberates two photons. In this way the new theory can explain the spin requirement, and the direction thereof. It also accommodates the fact that one of the photons in the case of orthopositronium may be of a different energy. Note that in the annihilation case it is the electron or antielectron that makes the phase adjustment, not the photon.

The theory requires that generally an electron will change its phase by half a frequency cycle (change its spin) when it emits a photon, and the photon will be likewise offset in phase. This requirement arises at [8] (**Figure 5** therein, note 2.6). We are not yet sure whether the electron has this phase change at every emission, or only when it is over-constrained, being accelerated (includes deceleration), or forced to change its orientation (spin). We tentatively expect the former interpretation and note this as an open question.

3.3.19. Simulated Emission (Laser)

The main features of the laser that differentiate it from conventional incandescent light sources are: a single frequency is produced, the photons are all in phase, and the photons all move in the same direction. The conventional explanation is that the electron in the gain medium is pumped with energy (electrical or optical). Since the electron is bonded to a nucleus, therefore it cannot take any energy level but can only take one of the specific quantum levels available. Having absorbed the energy, the electron therefore moves to an orbital which accommodates higher energy. However the electron is not fully stable in that excited state, and will eventually decay back to a lower energy level, and in the process it emits a photon with the energy difference. That emission can be spontaneous (random), or in the case of the laser, it is stimulated by another photon of the same energy. The laser is designed to maximise the chances for this to happen, typically by having mirrors that reflect the light many times. In this way the initial emission of photons recruits the other atoms to also emit photons. The new photons are emitted in the same direction as the stimulating photon, and with the same frequency and phase. However it is difficult to explain emission direction or the recruitment process.

The Cordus explanation is similar to the above but permits further clarification of the processes. The first photon triggers an electron to drop an energy level and emit another photon, and the original photon survives because it engages with the electron only in passing [24], *i.e.* is not absorbed. We can now expand that explanation with insights from the later Cordus work. It is important in what follows to note that in this theory the interactions between the photon and electron occur between the discrete forces of the particules, and this occurs *before* the particules are touching, per the principle of Wider Locality. So particules respond to what is happening in space around them, before they are spatially coincident. By comparison the conventional perspective, including of quantum mechanics, is that particles are only affected by fields at that one infinitesimally small point where the particle exists. A second important Cordus concept is that the reactive end of the electron energises at a characteristic frequency related to its energy. Third, the reactive end is only available to interact with the discrete forces of other particules when it is energising and generating discrete forces itself. Consequently there are timing windows in which interaction events can occur. When these interactions do occur, the particules have a tendency to become aligned and synchronised, which corresponds to phase, spin, or polarisation depending on the situation.

So the Cordus explanation for the stimulated emission is as follows: An initial trigger photon arises and travels down the barrel of the laser cavity → the discrete forces of this photon interact with the discrete forces of an electron of compatible frequency → their energy systems start to (briefly) connect via the discrete forces → the electron was previously pumped hence already needing to dispose of a photon → the interaction between the discrete forces of the electron and photon applies a positional constraint on the electron → being fully laden with energy the electron cannot accommodate this constraint and instead dumps the energy by emitting its own photon → this emitted photon is in the same phase as the trigger photon because of the synchronous interlock of discrete forces → the trigger photon also survives though it might be slightly reduced or increased in energy (hence small changes in frequency) → the two photons propagate and disturb electrons in other atoms → a cascade emission of photons occurs as a spatial progression through the laser body.

Explaining the common frequency of the multiple photons emitted in the laser process is straightforward: the electron is ready to emit a photon of that frequency, and only needs to be triggered to do so. It is to be expected that a small energy transfer occurs between the two particules, hence the observed slight spread in output fre-

quencies.

The common phase is explained as arising from the electron emitting its photon at the same point in the frequency cycle as its engagement with the incident photon. Practical lasers do not always emit in a single polarisation, and since polarisation corresponds to the orientation of a Cordus fibril, we therefore infer that the electron Cordus as a whole does not have to be perfectly aligned with the polarisation of the photons for the synchronous emission to occur. From the Cordus perspective, the incident photon does not have to be totally co-located with the electron to stimulate it, just as long as their discrete forces affect each other. Thus we predict that the emitted photon may be laterally offset from the incident one. It may also be axially offset, and this is consistent with the finite size of the laser bunches.

Also, the theory predicts that the light is not so much amplified as additional photons are recruited from the electrons. This also explains why the power increases exponentially when the device starts to lase: one photon recruits several more from the next layer of atoms, and those again. So there is a growing tree of recruitment, with a constant proportional increase in recruitment at each stage, hence exponential. The gain can therefore be interpreted as a measure of the efficacy of recruitment of electrons.

4. Discussion

4.1. What Has Been Achieved?

This paper makes a number of original contributions. The first is the provision of a conceptual theory whereby the bonding constraints on the electron may be related to the way that it deals with excess energy. This permits a broad-ranging theory to be constructed for how the electron responds to combinations of bonding constraint and pumped energy, and how it emits a photon, summarised in **Figure 5**. This diagram is novel in providing a compact representation of a wide range of phenomena. The crucial insight is the way the electron reactive ends are constrained by bonding commitments. These constraints apply to the reactive ends' spatial position, frequency, and phase. Hence these become coupled attributes, where the coupling is achieved via physical substructures. In contrast quantum theory treats these as merely independent intrinsic (disembodied) variables, and hence has no mechanism to relate these together.

The second contribution is being able to explain how bonding, hence chemistry, affects photon emission phenomena. Different types of materials, e.g. electron gas, metals, dielectrics, ceramics, crystals, have different chemical bonding arrangements. These bonds are mediated by electrons, hence binding chemistry directly affects electron constraints and hence photon emission phenomena. The key component to making this theory work is the idea of the Cordus particule, with its two reactive ends, their energisation frequency, and the inverse relationship between span and frequency. This gives naturally representation for spin and phase. Such constructs are not available to other theories based on 0D point particles or continuum materials.

A third contribution is providing qualitative explanations for a range of emission phenomena: Absorbance; Saturation; Beer-Lambert law; Colour of materials; Quantum energy states; Direction of photon-emission; Photoelectric effect; Emission of polarised photons from crystals; Refraction effects; Reflection; Transparency; Birefringence; Cherenkov radiation; Bremsstrahlung and Synchrotron radiation; Phase change at reflection; Force impulse at reflection, and radiation pressure; Number of photons at positronium annihilation; Simulated emission (Laser). This is original because a comprehensive set of ontologically rich explanations has not previously been provided by other theories of physics. This also moves the hidden-variable sector forward. The explanations are grounded in assumptions of physical realism, which cannot be said of all theories.

4.2. Implications

This theory provides insights into the role of the photon in the cosmos. As the theory previously identified, the photon provides an energy escapement mechanism for a massy particule [8]. This is possible because of the (a) the difference in the discrete force emissions of the massy and photon particules, (b) the span of particules, separating two reactive ends, (c) the fabric of discrete forces external to the particule.

The massy particules release their discrete forces into the void, thereby colonising it and creating a relativistic fabric and also the vacuum of free space. These particules also interact with other massy particules via synchronisation of discrete emissions, hence the synchronous interaction (strong force) and strong bonding. However the synchronous interaction only applies to massy particules in coherent assembly. In the more general case of

decoherent (non-synchronised) interactions, particules affect each other via the electro-magneto-gravitational fields they create. The photon interactions are a third case, where the massy particule discards its extra energy (or absorbs energy). In emitting a photon the particule transfers its energy problem elsewhere in space. By dumping the energy into the fabric, and leaving it to travel there until it intersects another reactive end, the energy is taken out of the present and transferred to the future. There are two important implications of this. One is that the fabric separation creates the macroscopic perception of time [25]. The second is that the emission of photons adds considerably to the number of particules in the universe, and this and the different time delay before each is reabsorbed adds greatly to the number of states for the universe, hence to entropy.

The photon is an astonishingly beautiful and useful feature in the universe: "*The photon transfers spare energy around the place. It is an escapement mechanism whereby particules that are over-prescribed in terms of positional constraints on re-energisation can get rid of that energy. The free photon is not quantised, but flexible in its ability to contain whatever energy it is given: like an expandable container. Yet it is sufficiently like a matter particule to be able to interact with matter. Further, it has no hand and is therefore predicted to be able to freely interact with, and transfer energy between, both matter and antimatter*" [26].

Another profound implication is the role of the photon in inverse problem, which is the formation of the matter universe at genesis. Other work in the Cordus theory has proposed a detail processes for the conversion of a pair of photons into matter (pair production) [9], and a baryogenesis theory for how these products could be asymmetrically transformed into matter [10].

A further implication is that we now have a plausible theory, based on physical realism, for explaining how photons interact with matter to give rise to contextual measurement. Hence the photons used to interrogate a system may cause it to change state as in the Zeno effect. This means it is also possible to explain why electromagnetic radiation should affect the decay rates of nuclides and unstable particules [27].

4.3. Limitations and Implications for Further Research

The principal limitation of this work is its conjectural foundation. The idea that particules are not 0D points but instead have two reactive ends is a radical one and frequently met with disbelief and an expectation of extraordinary proof. However it is not possible to prove this lemma, and it remains a potential limitation. Neither has this paper, which is a conceptual work, presented a mathematical formalism. This is only available for optics [7] and nuclear stability [18]. This is left to future work now that the energy framework has been sketched out.

A more specific limitation, and an area of possible future research, concerns the phase-change effects predicted by the theory. Do all electrons fully change their phase when they emit a photon? We are not fully satisfied with the explanations so far, and we suspect there may be deeper concepts that need elucidating.

5. Conclusion

This paper has developed a conceptual theory for photon emission and absorption using the Cordus theory. We propose an energy mechanics whereby the electron (or other particule) has multiple mechanisms for dealing with any excess energy that it might have. It has long been known that the bonding commitments of the electron affect its energy behaviour but the mechanisms for this have been elusive. The present theory offers an explanation based on the supposition that particles have internal structure. The causal mechanisms have been inferred, and three main categories have been identified whereby the electron responds to excess internal energy. Collectively these responses encompass energetic free electrons, transferral of energy to other massy particles, photon emission, and electron escape. This is valuable as it provides a means to represent the causality under various contingencies, *i.e.* it shows how various factors cause the different energy conversion outcomes to arise. The theory is able to provide a logically coherent explanation for a wide variety of optical energy conversion phenomena. These include the direction of photon-emission, photoelectric effect, absorbance and the Beer-Lambert law, emission of polarised photons form crystals, refraction, birefringence, bremsstrahlung & synchrotron radiation, and simulated emission (lasers).

Author Contributions

All authors contributed to the creation of the underlying concept, DP developed the functional models, DP and AJP formulated the underlying concepts for simulated emission, and all authors contributed to the development

of the ideas and editing of the paper.

Conflict of Interest Statement

The authors declare that there is no conflict of interests regarding the publication of this article. The research was conducted without personal financial benefit from any third party funding body, nor did any such body influence the execution of the work.

References

[1] Einstein, A., Podolsky, B. and Rosen, N. (1935) *Physical Review*, **47**, 777. http://dx.doi.org/10.1103/PhysRev.47.777

[2] Bell, J.S. (1964) *Physics*, **1**, 195-200.

[3] Leggett, A. (2003) *Foundations of Physics*, **33**, 1469-1493. http://dx.doi.org/10.1023/A:1026096313729

[4] Groblacher, S., Paterek, T., Kaltenbaek, R., Brukner, C., Zukowski, M., Aspelmeyer, M. and Zeilinger, A. (2007) *Nature*, **446**, 871-875. http://dx.doi.org/10.1038/nature05677

[5] de Broglie, L. (1925) *Annales de Physique*, **3**(10).

[6] Bohm, D. and Bub, J. (1966) *Reviews of Modern Physics*, **38**, 453-469. http://dx.doi.org/10.1103/RevModPhys.38.453

[7] Pons, D.J., Pons, A.D., Pons, A.M. and Pons, A.J. (2012) *Physics Essays*, **25**, 132-140. http://dx.doi.org/10.4006/0836-1398-25.1.132

[8] Pons, D.J. (2015) *Applied Physics Research*, **7**, 14-26. http://dx.doi.org/10.5539/apr.v7n4p24

[9] Pons, D.J., Pons, A.D. and Pons, A.J. (2015) *Journal of Nuclear and Particle Physics*, **5**, 58-69.

[10] Pons, D.J., Pons, A.D. and Pons, A.J. (2014) *Journal of Modern Physics*, **5**, 1980-1994. http://dx.doi.org/10.4236/jmp.2014.517193

[11] NIST (1993) Integration Definition for Function Modeling (IDEF0). http://www.itl.nist.gov/fipspubs/idef02.doc

[12] Pons, D.J., Pons, A.D. and Pons, A.J. (2014) *Physics Essays*, **27**, 26-35. http://dx.doi.org/10.4006/0836-1398-27.1.26

[13] Pons, D.J. (2015) Internal Structure of the Photon (Image License Creative Commons Attribution 4.0). Wikimedia Commons.

[14] Pons, D.J. (2015) Internal Structure of the Electron (Image License Creative Commons Attribution 4.0). Wikimedia Commons.

[15] Pons, D.J., Pons, A.D. and Pons, A.J. (2013) *Applied Physics Research*, **5**, 107-126.

[16] Pons, D.J., Pons, A.D. and Pons, A.J. (2015) *Applied Physics Research*, **7**, 1-11.

[17] Pons, D.J., Pons, A.D. and Pons, A.J. (2014) *Applied Physics Research*, **6**, 50-63. http://dx.doi.org/10.5539/apr.v6n3p50

[18] Pons, D.J., Pons, A.D. and Pons, A.J. (2015) *Physics Research International*, **2015**, Article ID: 651361. http://dx.doi.org/10.1155/2015/651361

[19] Pons, D.J. and Pons, A.D. (2013) *The Open Astronomy Journal*, **6**, 77-89.

[20] Pons, D.J., Pons, A.D. and Pons, A.J. (2015) *Applied Physics Research*, **7**, 1-13.

[21] Pons, D.J., Pons, A.D. and Pons, A.J. (2014) *Applied Physics Research*, **6**, 28-46. http://dx.doi.org/10.5539/apr.v6n2p28

[22] Pons, D.J., Pons, A.D. and Pons, A.J. (2013) *Applied Physics Research*, **5**, 145-174. http://dx.doi.org/10.5539/apr.v5n6p145

[23] Pons, D.J., Pons, A.D., Pons, A.M. and Pons, A.J. (2011) Cordus Optics: Part 2.2 Reflection. http://vixra.org/pdf/1104.0020v1.pdf

[24] Pons, D.J., Pons, A.D., Pons, A.M. and Pons, A.J. (2011) Cordus Matter: Part 3.3 Energy Cycles within Matter. http://vixra.org/pdf/1104.0024v1.pdf

[25] Pons, D.J., Pons, A.D. and Pons, A.J. (2013) *Applied Physics Research*, **5**, 23-47. http://dx.doi.org/10.5539/apr.v5n6p23

[26] Pons, D.J. (2011) Contrasting Internal Structures: Photon and Electron. http://vixra.org/pdf/1109.0045v1.pdf

[27] Pons, D.J., Pons, A.D. and Pons, A.J. (2015) *Applied Physics Research*, **7**, 18-29.

Journal of Modern Physics, 2016, 7, 1068-1081
Published Online June 2016 in SciRes. http://www.scirp.org/journal/jmp
http://dx.doi.org/10.4236/jmp.2016.710095

An Experimental Study of Microstructure through SEM and AFM by Interaction from High Power Femtosecond Laser Wave with $BaTiO_3$

Shivani Saxena[1], Sanjay Dixit[1], Sanjay Srivastava[2]

[1]Department of Physics, Government Motilal Vigyan Mahavidyalaya College, Barkatullah University, Bhopal, India
[2]Department of Material Science & Metallurgical Engineering, Maulana Azad National Institute of Technology, Bhopal, India
Email: sxn_shvn@yahoo.co.in, sanjay_007dixit@rocketmail.com, s.srivastava.msme@gmail.com

Received 2 March 2016; accepted 5 June 2016; published 8 June 2016

Abstract

This paper deals with the interaction of femtosecond laser with strain dependent high dielectric material. For this investigation, ferroelectric material like $BaTiO_3$ has been chosen because of centrosymmetric structure. Due to irradiation of laser light, the micro-structure of $BaTiO_3$ is found to change along the direction of heat propagation. SEM and AFM tools have been used to detect the morphology and roughness of the femotosecond laser treated $BaTiO_3$. The change of morphology and surface behavior depends upon the laser fluence and intensity of laser light. The maximum change in morphology has been observed at a higher laser fluence.

Keywords

$BaTiO_3$, Femtosecond Laser, Laser Fluence, Ablated Areas

1. Introduction

The interactions of light with matter are described theoretically by Maxwell's Equations [1] [2]. Experimentally, light's interaction with matter can be understood as an input signal (light) delivered to a system (matter) which acts upon the signal and returns an output. In our daily life, however, we are surrounded by nonlinear systems. The characteristics of a $p-n$ junction, the distortion of an acoustic signal in a speaker, and ferromagnetic permeability are all manifestations of nonlinear systems [3]. Yet, nonlinear optical systems remain uncommon in

How to cite this paper: Saxena, S., Dixit, S. and Srivastava, S. (2016) An Experimental Study of Microstructure through SEM and AFM by Interaction from High Power Femtosecond Laser Wave with $BaTiO_3$. *Journal of Modern Physics*, **7**, 1068-1081.
http://dx.doi.org/10.4236/jmp.2016.710095

daily life. Nonlinear phenomena in the optical frequency range became easily accessible, only after the invention of the laser in 1960 [4]. Understanding the propagation of femtosecond light pulses is of great value for both scientific and technological applications. The short pulse duration provides scientists with the possibility to explore physical phenomena with unprecedented time resolution, chemical reactions can be studied at the atomic level, and ultrafast changes in material properties can be measured. The high intensity levels achieved with ultra short laser pulses create strong nonlinear light-matter interactions, which have led to new optical phenomena, such as the formation of spatio-temporal solitons [5] [6]. Several methods have been implemented to visualize the propagation of femto second pulses. If temporal resolution is not required, one can measure a trace left in a material after a pulse has gone through and reconstruct the time-integrated spatial profile of the beam. For example, for pulse propagation through solids, if there is permanent damage in the material the beam profile can be inferred from the damage tracks. In the case of fluids, the trace can be visualized by dissolving a fluorescent dye in the material and capturing a side view of the fluorescence [7] or by imaging the light emission from plasma generated by the pulse. The femtosecond laser pulse appears as an emerging and promising tool for processing wide band gap dielectric material for a variety of applications. The conventional view of laser-material interaction with wavelength between near IR and UR includes the transfer of electromagnetic energy to electronic excitation, followed by electron lattice interaction that converts energy into heat. However, the processes of material response following intense femtosecond pulse irradiation are far more complex, particularly wide range band gap dielectrics. When a high dielectric material is subjected to femtosecond Laser irradiation, the refractive index of the material may become intensity dependent and a large amount of electrons are generated by the infrared pulses in transparent dielectrics. Relation channels of electronic excitation in the wide band material may produce intrinsic defects, leading to photo induced damages in otherwise defect free medium. These fundamentally non linear processes have stimulated substantial efforts in both the understanding of the complexity of femtosecond laser interaction with dielectric and the application of the microscopic mechanism to innovate material fabrication [8] [9]. In the case of femtosecond laser-pulse interaction, the absorption of laser radiation occurs on a time scale of the pulse duration before any significant hydrodynamicmotion ablation can occur. Such hydrodynamic response of the target surface has characteristically been observed on the time scale of tens of picoseconds. [10]. A simple semianalytical model of femtosecond electron heating and resultant optical absorption is developed to describe the time dependence and integral reflectivity covering the range from cold metal response to the hot plasma response. The model is in good agreement with experimental ultrafast reflectivity measurements over the intensity range studied [11].

The terahertz (THz) power radiated by the femtosecond laser excited semiconductor surfaces was measured by the Golay cell. Intrinsic InSb crystals as well as n-type and p-type InAs were investigated by using three different wavelengths −780, 1030, 1550 nm, femtosecind lasers [12].

In this paper, the high dielectric material like $BaTiO_3$ has been used to examine the morphology of the sample after treatment of femtosecond laser light. For the surface behavior, Ti: sapphire oscillator-amplifier laser system of 100 - 300 fs pulse laser is used to investigate the change in morphology of $BaTiO_3$. SEM and AFM are the basic tool to investigate the morphology after the interaction of the laser light with the rotating $BaTiO_3$.

2. Experimental Details

Highly oriented thin file of BTO was deposited on a Cu-substrate by using PECVD method. The prepared samples of BTO were used in a plasma chamber as target materials which were directly opted from the market. The Cu-substrate was placed on a substrate holder tray that can hold six samples at one time, of dimension 1 × 1 × 1 inch. The reason for selecting the Cu-substrate is its better conductivity; it conducts heat easily at the time of irradiation with high laser intense. The substrate tray can easily slide in the deposition chamber for better and uniform deposition of $BaTiO_3$. The disposition was controlled by controlling the bias voltage and current. The prepared sample was annealed at 750˚C for 2 hr. The prepared film of thickness more than 68 nm was irradiated in air at atmospheric pressure by Ti: sapphire oscillator-amplifier laser system of 100 - 300 fs pulse laser. The frequency modulation through nonlinear interaction was evaluated by the fs laser pulse generation. *i.e.* $\omega \approx 2\omega_0 \approx 3\omega_0$. The delayed pulse reflected from the target surface after interaction with the first pulse and its detection of intensity change from the change in information tells about the processes which occurred on the surface. For microstructural examination, a scanning electron microscope (SEM) operating at 15 - 20 kV was used to see the morphology of the film before and after laser treatment and roughness of the sample was studied by the AFM investigation.

3. Experimental Results

Figure 1(a) and **Figure 1(b)** show the top view and the cross-section view of SEM micrograph of $BaTiO_3$ sample generated by four pulses of different fluencies from 55 and 430 J/cm^2. Due to laser heating, the microstructure of $BaTiO_3$ starts to change which depends upon the Fluency of the laser beam. The splash around the craters is mainly from the phase explosion. The diameter and depth of the craters increase with an increase in the laser fluence. The modification of the image depends upon the laser power. The laser power also modifies both the diameter and depth of the interaction. These views are taken at higher magnification. From this result, the spot are calculated from spot marker. The laser beam focus diameter obtained from these results was roughly 3.88 μm, which is close to the theoretical focus size at 4.436 (1.22 λ/NA, λ = 800 nm is the wave length used in laser ablation, NA = 0.22 is the numerical aperture).

The ablation threshold fluences of the Gaussian laser beam can be calculated by measuring the diameter of the ablated areas versus the pulse energy and extrapolating to zero. It is known that for a Gaussian spatial beam profile with a $1/e^2$-beam radius, ω_0, the maximum laser fluence, F_0, increases linearly with the laser pulse energy, E_p,

$$F_0 = \frac{2E_p}{\pi\omega_0^2} \tag{1}$$

where ω_0 is 11.5 μm taken in this experiment. The squared diameters, D^2, of the laser ablated craters are correlated with F_0 by $D_0^2 = 2\omega_0^2 \ln\left(\frac{F_0}{F_{th}}\right)$. Therefore, it is possible to determine the Gaussian beam spot size by measuring the diameters of the ablated area, D, versus the applied pulse energies, E_p. Due to the linearity between energy and maximum laser fluence, a $1/e^2$-beam radius of Gaussian beam, ω_0, can be determined by a linear least squares fit in the representation of D^2 as a function of $\ln(E_p)$. Bonse *et al.* [13] gave an empirical equation between the ablation threshold for N pulses ($F(N)$) and the ablation threshold for single pulse ($F(1)$)

$$F_{th}(N) = F_{th}(1) \cdot N^{\zeta-1} = 0.223\tau_L^{1/2} N^{\zeta-1} \tag{2}$$

where ξ is a material-dependent coefficient and is equal to 0.84 during Femto-second laser ablation of silicon obtained by burns *et al.* In our experiment, we obtain the LIPSS on the entire ablated area at $N \geq 25$.

$$D_0^2 = 2\omega_0^2 \ln\left(\frac{F_0}{0.223\tau_L^{1/2} N^{\zeta-1}}\right) \tag{3}$$

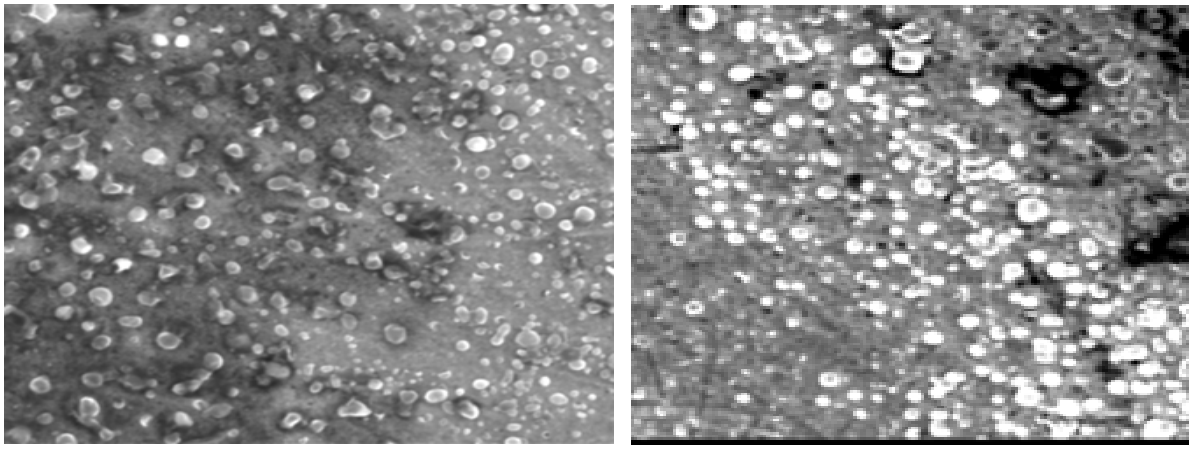

(a) (b)

Figure 1. Craters and their interaction profile at different fluence: (a) 55 and (b) 430 J·cm^2.

Figure 2 shows the results of D^2 versus with the applied laser fluence F_0, obtained from the ablation experiment. The threshold ϕ_{th} can be obtained from the extrapolating the linear fit to $D^2 = 0$ in the plot. It can be deduced that the threshold ablation is found at 0.455 J/cm^2 for a single pulse, and 0.865, 0.866, 0.455, −0.0911, and 0.455 J/cm^2 for 5, 10, 25, 50 and 100 pulses respectively with $BaTiO_3$ film in the air. Certainly, the slope of the linear fit lines can be calculated from the **Figure 3**, which is approximately equal to −82.49 μm^2. Therefore the measured 1/e^2—value of the beam radius ω_0 of 9.5 μm can be calculated.

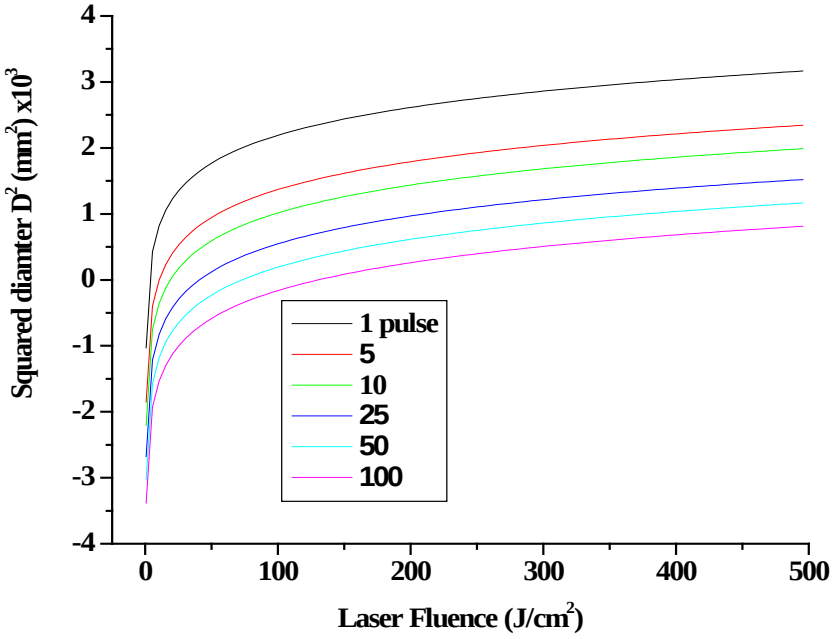

Figure 2. Relation between squared diameter of the ablated areas with laser fluence at different pulses on $BaTiO_3$ thin film in air (τ_L = 148 fs, λ = 800 nm).

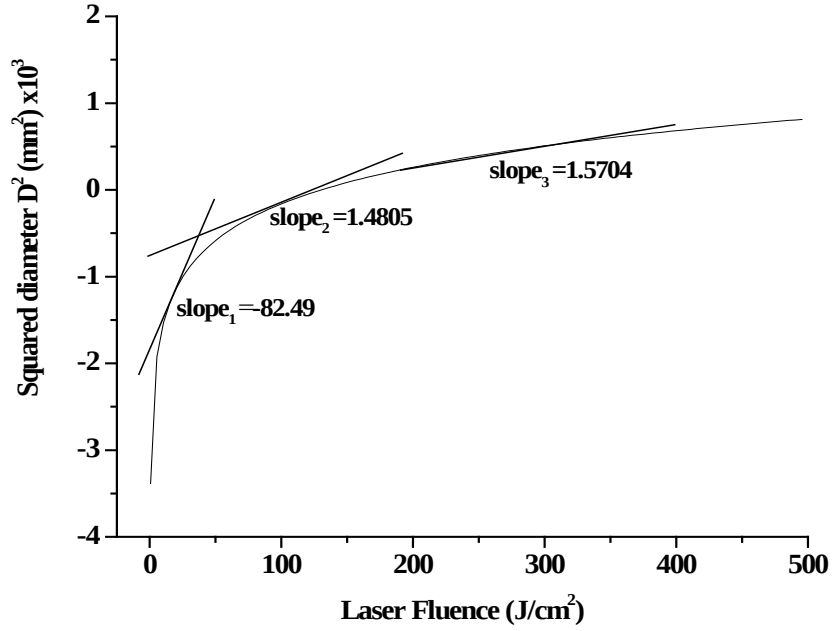

Figure 3. Calculation of slope of the ablated areas with laser fluence at 100 pulses on $BaTiO_3$ thin film in air (τ_L = 148 fs, λ= 800 nm).

Figure 4 shows the ablated diameter D depending on the number of laser pulses N with different laser fluence. The ablation diameter decreases with an increase in the number of laser pulses at different laser fluence, while the ablation diameter increases with an increase in the laser fluence at particular laser pulses. The energy of the laser pulse is applied in order to heat up the material to evaporation temperature and to overcome the latent heats of melting and evaporation. Material in a vapor state is ablated. The model assumes 100% energy absorption and neglects heat conduction effects as well as overheating of metal vapor:

$$m = \frac{N \cdot E_{\text{pulse}}}{c_p \cdot (T_v - T_0) + \Delta H_m + \Delta H_V} \tag{4}$$

Here m is the ablated mass, N the number of laser pulses, E_{pulse} the pulse energy, C_p the heat capacity, T_V evaporation temperature, T_0 ambient temperature, ΔH_m melting enthalpy and ΔH_v evaporation enthalpy.

Another way of using the multisport ablation threshold is the logarithmic dependence of the ablation rate χ on the laser fluence can be described by

$$\chi = \alpha_{eff}^{-1} \ln\left(\frac{F_0}{0.223\tau_L^{1/2} N^{\zeta-1}}\right) \tag{5}$$

Here α_{eff}^{-1} is defined as the "effective optical penetration depth" as expected from the Beer-Lambert Law. The depth of the ablated material after establishing the steady state material removal is given by

$$h_a = (N - N_{th}) \ln\left(\frac{F_0}{0.223\tau_L^{1/2} N^{\zeta-1}}\right) \tag{6}$$

Here, the number of incubation pulses N_{th} represent the minimum number of laser pulses to initiate ablation and its value depends on the laser fluence, close to the threshold N_{th} and well above the threshold $N_{th} = 0$. **Figure 5** shows this linear relationship between the multiple shot and the logarithm of laser fluence. The ablation rate increases with an increase in the laser fluence. Below 50 J/cm^2, the ablation rate increases sharply and between 50 to 500 J/cm^2, the ablation rate tries to attain the steady state. The difficulty arises in material removal from the deep crater due to the development of the plasma by the charged oscillation which reduces the ablation rate at the higher laser fluence in steady state conditions.

This phenomenon was studied by observing the change in microstructure through laser irradiation. **Figure 6**

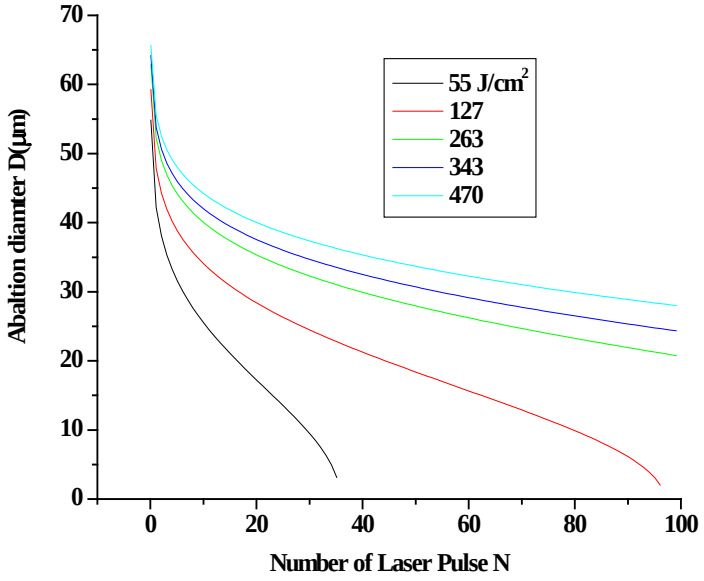

Figure 4. Ablation depth as a function of the pulse number at different laser fluencies.

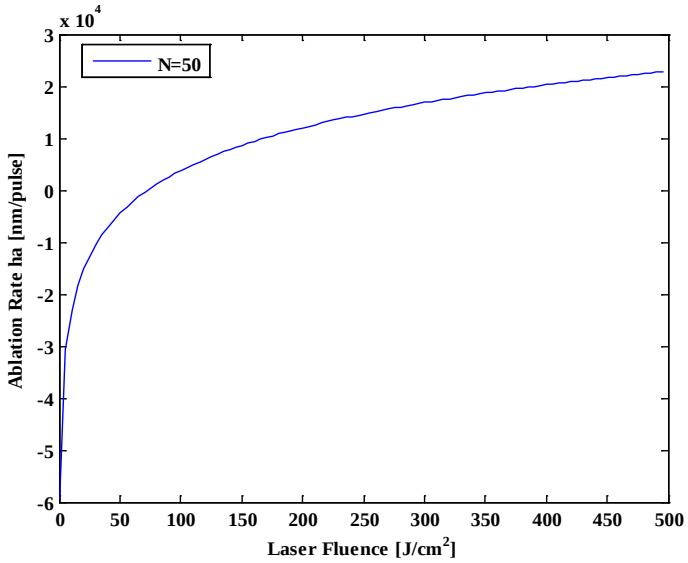

Figure 5. Variation of ablation rate with laser fluence at $N = 50$ pulse.

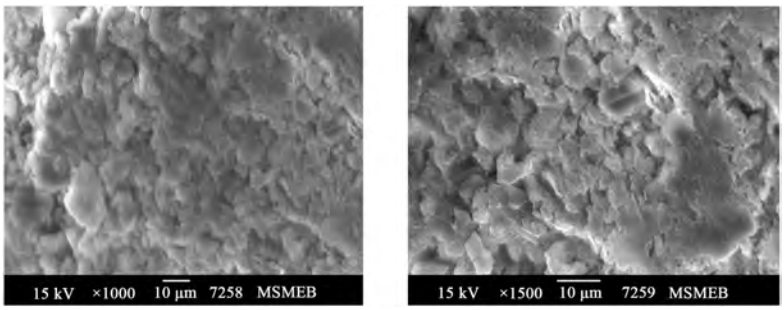

Figure 6. SEM morphology of $BaTiO_3$ without laser interaction.

shows the SEM micrograph of $BaTiO_3$ with laser ablation. It is evident from that only patch of single phase are seen in the micrograph. The same experiment has been also carried out by the irradiation of the laser with different laser fluence.

Figure 6 at different magnification shows the change in the microstructure of $BaTiO_3$ after the irradiation of laser with different fluence for 148 fs pulse duration. Due to the impact of laser with different fluence, the microstructure changes along the direction of the heat propagating zone. It can be observed that the present modifications in microstructure resulting from the single shot at very high fluence are about three to four times the average depth obtained from the SEM investigation. The surface of the sample was irradiated with different pulse energy. It is evident from the analysis of the results obtained from the AFM that the fluence of the laser spot affects the depth of the interaction with the surface but they don't disturb the spacing of the $BaTiO_3$. The spacing of the lattice is not altered by exposing the $BaTiO_3$ with a laser beam (**Figure 7**).

The AFM micrograph of $BaTiO_3$ after irradiation with different intensity laser beam is presented in **Figure 8** A & B at 55 J/cm^{-2} laser fluence. It shows that the depth of the ripples increase nonlinearly with the pulse energy. AFM is an important technique for studying the morphology of laser irradiated $BaTiO_3$. The irradiation of laser was applied at the sample by varying the laser fluency. Tapping mode AFM imaging was applied to study the femtosecond laser induce $BaTiO_3$. **Figure 8(A)** shows a typical medium-scale AFM image (0.9 µm × 0.9 µm) of the $BaTiO_3$ thin film supported on Cu whereas, **Figure 8(B)** presents a topographical view of the sample. The topographic maps revealed that the film was rich in the dents and irregularities on their surfaces. The rough surfaces provide a greater number of active sites and comparatively possess a greater surface area than smooth ones; such particles can play a better role in the field of catalysis. Results obtained with AFM identified that newly synthesized $BaTiO_3$ NPs grown on $BaTiO_3$ thin film, possessed an average size of 14 nm. The results acquired

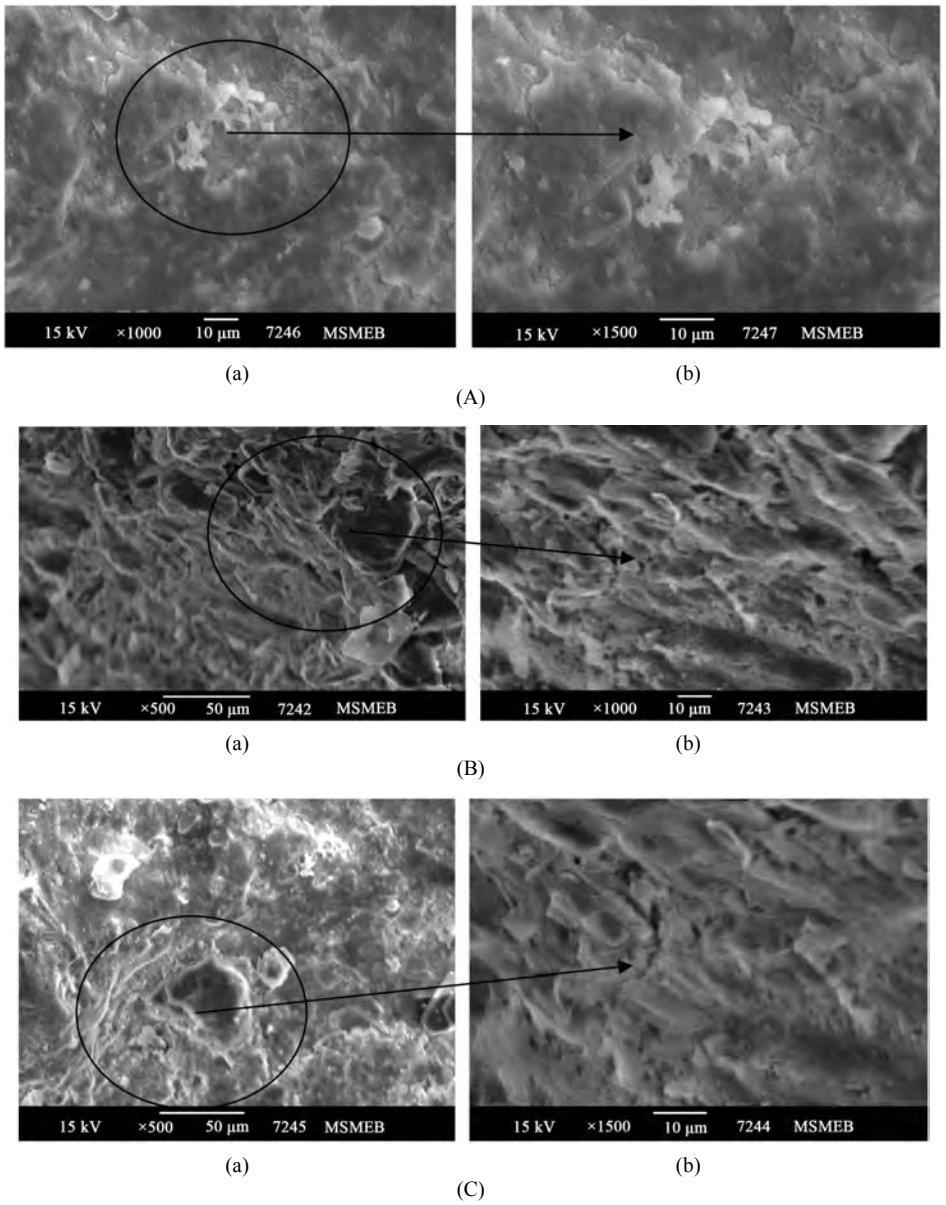

Figure 7. SEM morphology of $BaTiO_3$ with laser interaction at different laser irradiation (A) 55 (B) 127 (C) 263 in (a) & (b) photograph.

for size elucidation using AFM and TEM image analysis were in good agreement.

The interaction with laser light with the $BaTiO_3$ sample depends upon the laser fluence because the micro structure of the $BaTiO_3$ thin film supported by Cu plate is totally damaged by the irradiation of laser light with a higher fluence. The laser fluence changes the roughness of the sample after irradiation with Laser light. **Figures 9(A)-(D)** reveal the AFM images and distribution chart of $BaTiO_3$ NP film. AFM images prove that the grains are uniformly distributed within the scanning area (2000 × 2000 nm) with individual columnar grains extending upwards. This surface topography is important for many applications such as responsivity of photo-detector and catalysts. The $BaTiO_3$ NPs have spherical shaped with good dispensability and homogeneous grains aligned vertically. The duration of the interaction time with the $BaTiO_3$ sample is also important to judge the microstructural change by laser irradiation. **Figures 10(A)-(E)** show the AFM micrograph of $BaTiO_3$ irradiation with different time. The estimated values of root mean square (RMS) of surface roughness average and average grain size are calculated by using the AFM image. The images of the micrograph are plotted in terms of 2D and 3D views.

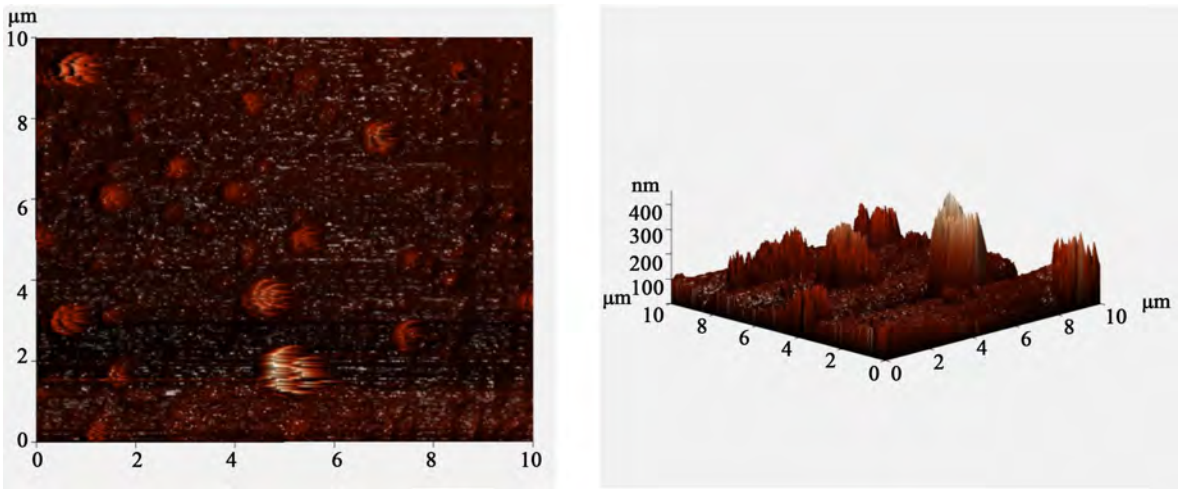

(A) (B)

Figure 8. AFM imgae of surface AFM images of surface after irradiation with laser of intensity of 55 J/cm^2.

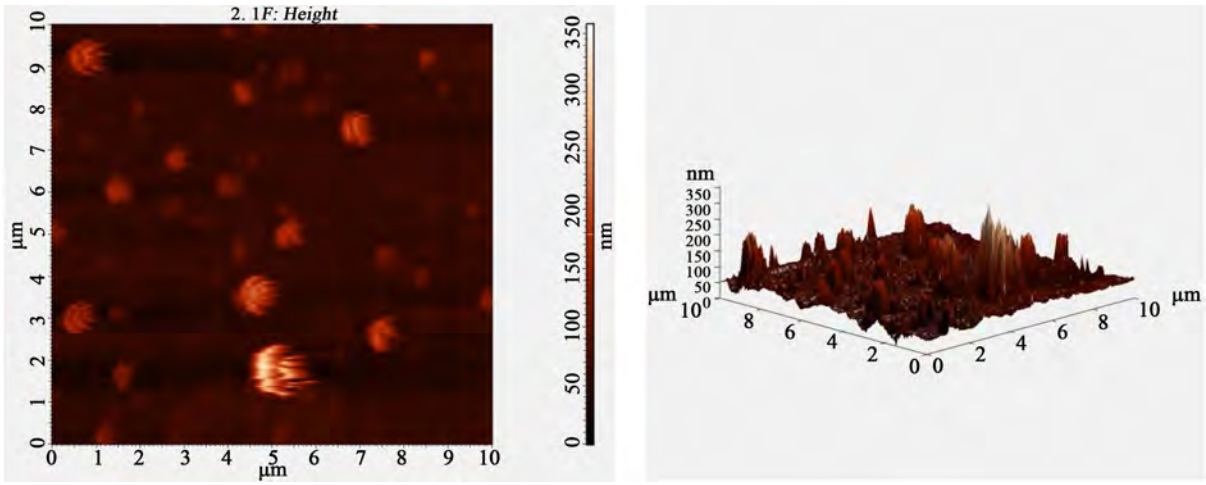

(a) (b)

(A)

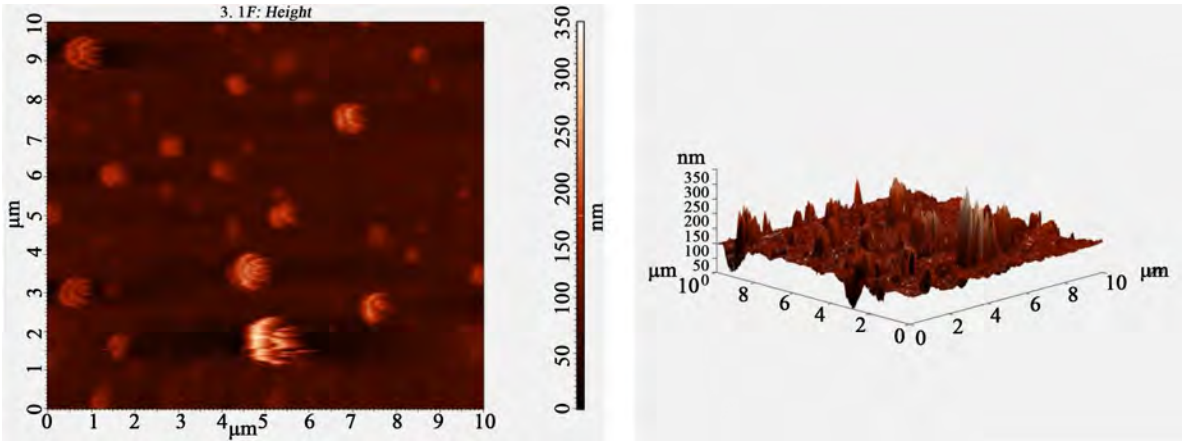

(a) (b)

(B)

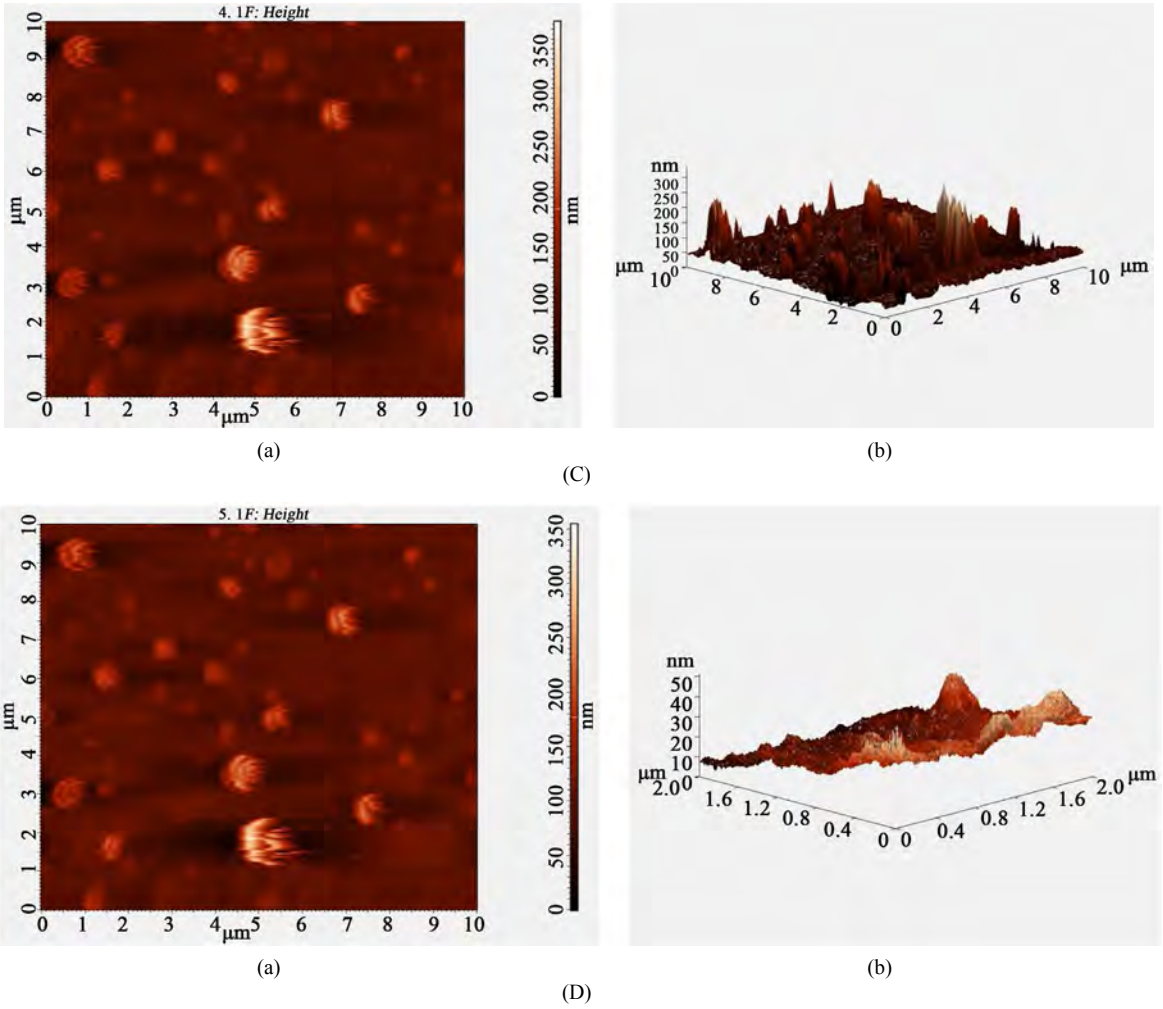

Figure 9. AFM images of surface after irradiation with laser of intensity of (A) 55 (B) 190 (C) 320 (D) 430 J/cc^2.

The roughness profile measured through AFM investigation is shown in **Figure 11**. From the interaction with femtosecond laser light, the roughness of the sample increase from 42% to 89% with increase the laser fluence. The depth of the interaction was analyzed from the analysis of the roughness through the AFM cross-section image and it was plotted in **Figure 12**.

Figure 13 shows the change in lattice parameter of the laser treated sample. It is evident from the figure that the maximum change in lattice parameter is found at 430 J/cm^2. This investigation has been carried out from the XRD analysis. The c/a ratio continuously increases with an increase in the laser fluence and the % elongation slowly decreases with an increase in the laser fluence. Initially, it shows the higher change in elongation but later it changes slowly with laser fluence. **Figure 14** shows the change in dielectric from 2328 to 7798 with the laser fluence. The increment is found along with the development of the strain in the dielectric material due to irradiation of the sample from the high intensity laser light. This change in the dielectric is due to change in morphology. This development is possible only from the rise in temperature in the ablated zones. From the large heating, the microstructure is completely changed, but crystal structure remains the same. This leads to developing the maximum strain in the material and their percentage with respect to laser fluence are presented in **Figure 14**. This strain is directly calculated from the unstained situation or before the laser irradiation. The strain factor (g) is calculated from the following factor:

$$\chi = \alpha_{eff}^{-1} \ln\left(\frac{F_0}{0.223\tau_L^{1/2} N^{\zeta-1}}\right) \tag{7}$$

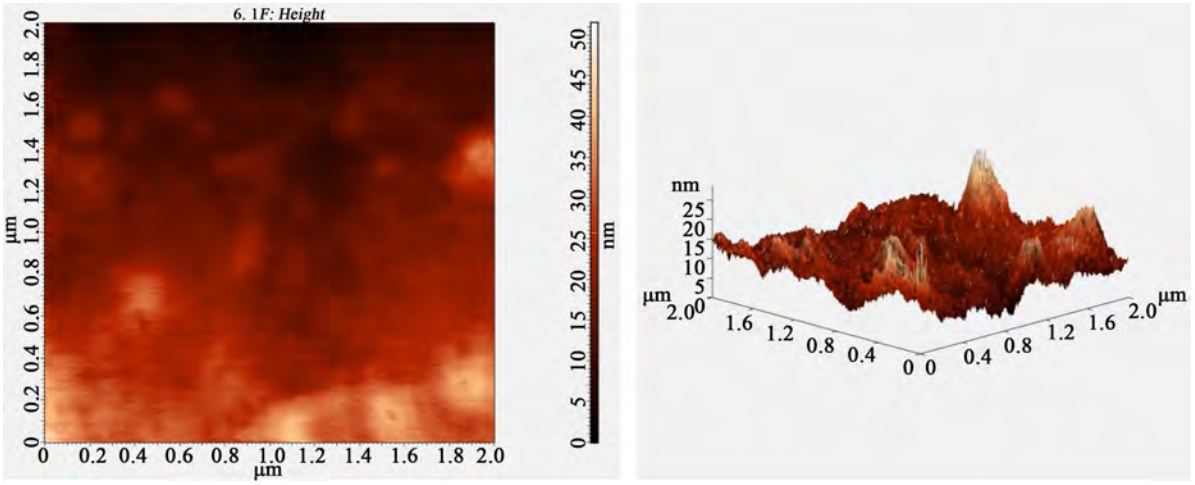
6. 1F: Height
µm
nm
0 0.2 0.4 0.6 0.8 1.0 1.2 1.4 1.6 1.8 2.0
0 5 10 15 20 25 30 35 40 45 50
nm
25
20
15
10
5
µm
2.0 1.6 1.2 0.8 0.4 0
0 0.4 0.8 1.2 1.6 2.0 µm

(a) (b)

(A)

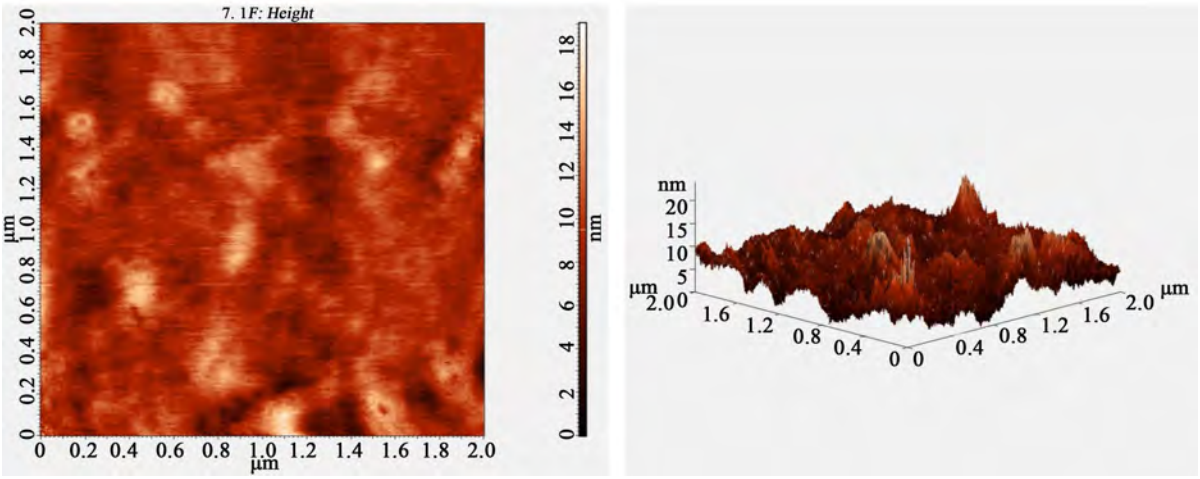
7. 1F: Height
µm
nm
0 0.2 0.4 0.6 0.8 1.0 1.2 1.4 1.6 1.8 2.0
0 2 4 6 8 10 12 14 16 18
nm
20
15
10
5
µm
2.0 1.6 1.2 0.8 0.4 0
0 0.4 0.8 1.2 1.6 2.0 µm

(a) (b)

(B)

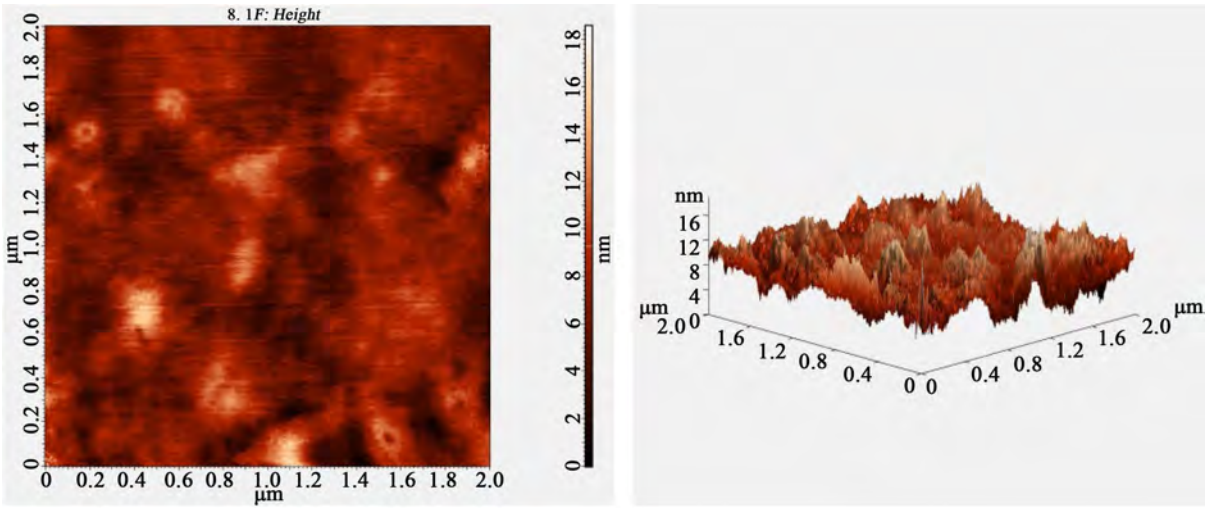
8. 1F: Height
µm
nm
0 0.2 0.4 0.6 0.8 1.0 1.2 1.4 1.6 1.8 2.0
0 2 4 6 8 10 12 14 16 18
nm
16
12
8
4
µm
2.0 1.6 1.2 0.8 0.4 0
0 0.4 0.8 1.2 1.6 2.0 µm

(a) (b)

(C)

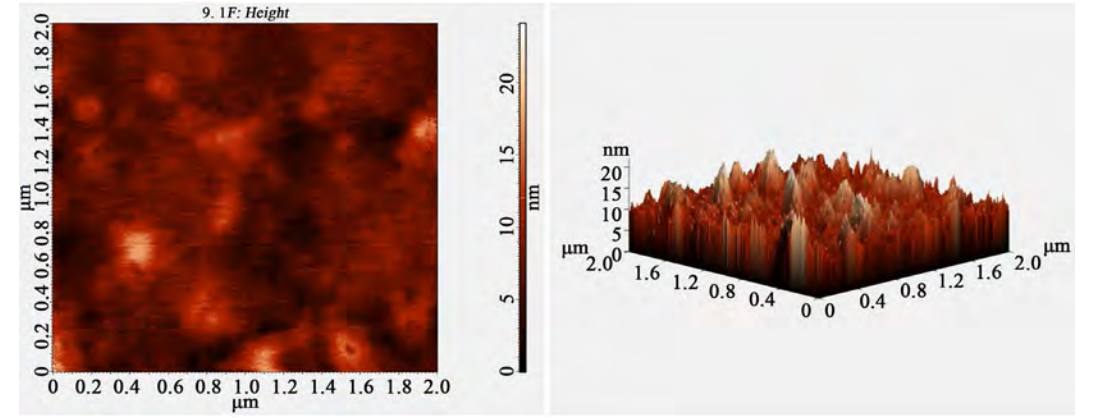

Figure 10. AFM images of surface after irradiation with laser of intensity of (A) 2 (B) 4 (C) 5 (D) 7 (E) 9 sec.

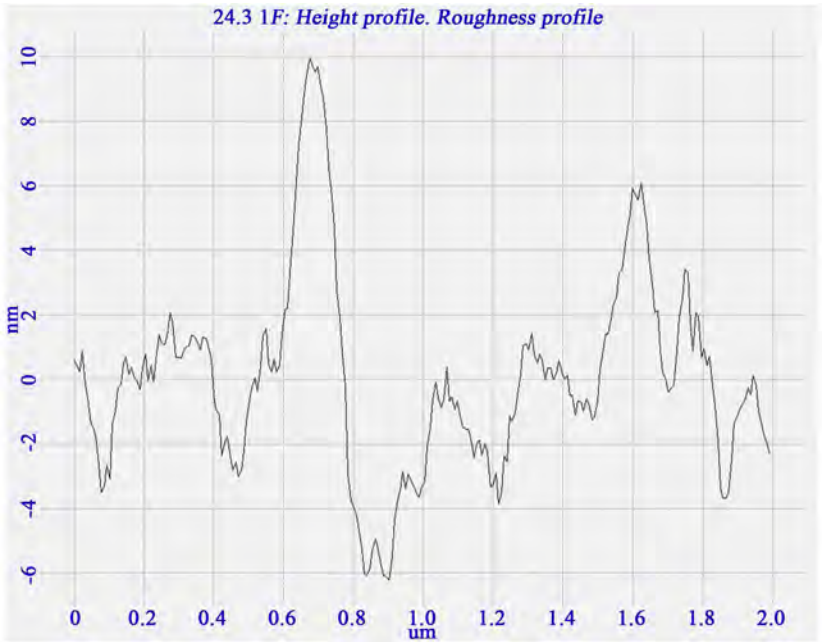

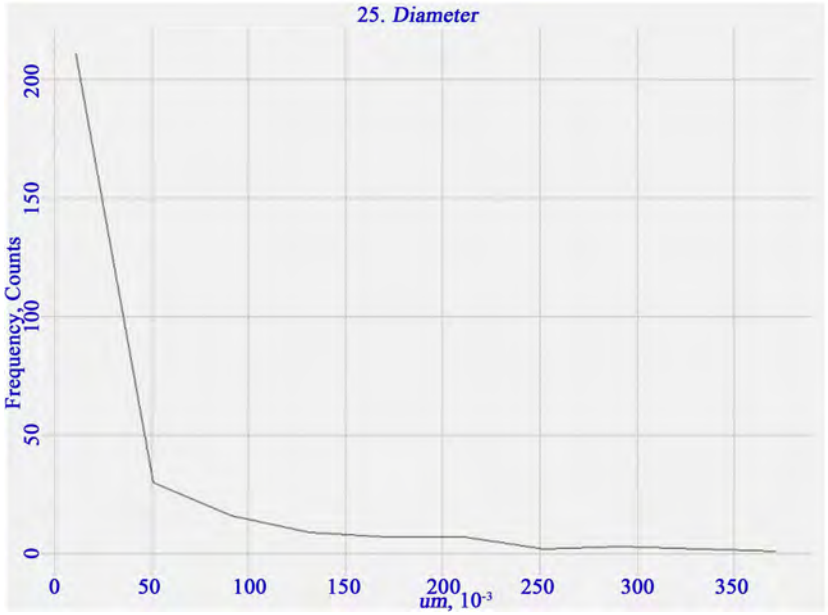

Figure 11. Surface roughness of the laser treated sample.

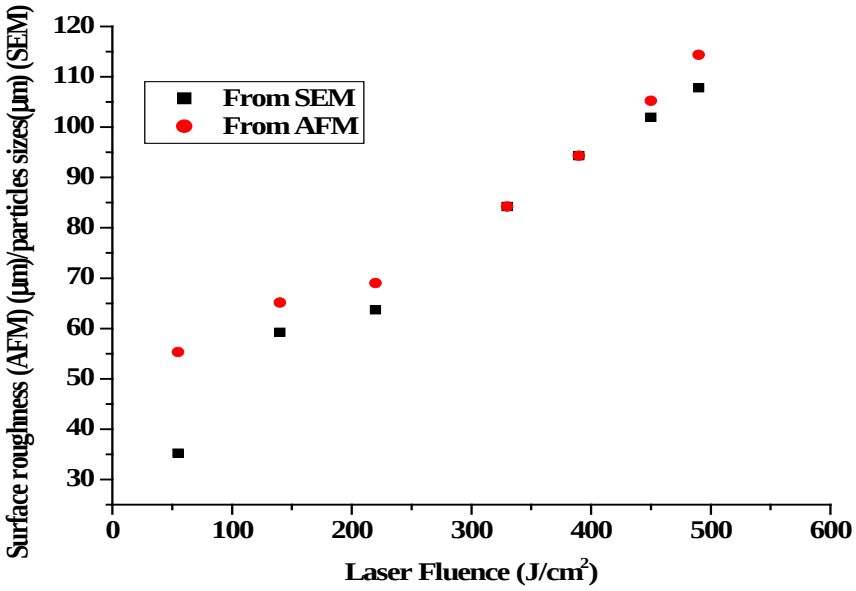

Figure 12. Surface roughness versus pulse intensity.

4. Conclusion

Based on the experimental research, a simple theory with the experimental results on the interaction of laser light with surface of high dielectric material has been proposed. This theory actually deals with the temperature dependent oscillation of the atoms and the maximum deflection of the amplitude at which an atom is separated from the lattice, depends upon the laser fluence. The maximum changes in morphology have been observed 430 J/cm^2 and also change the spot of the interacted zones. The squared diameter rapidly increases with increase the laser fluence and attains the steady state beyond 350 J/cm^2 whereas the size of the spot continuously decrease with an increase in the laser fluence because of a change in times of pulse interaction with rotating sample. Meanwhile the ablation rate from the interaction of the laser light increases with an increase in the laser light due to large changes in temperature from the localized heating of the sample. This shows the maximum impact

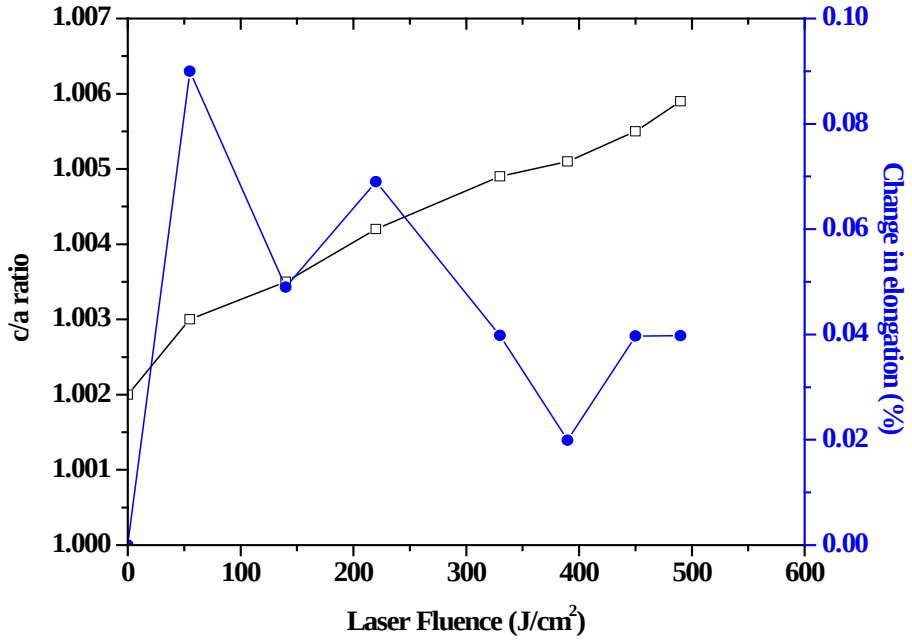

Figure 13. Variation of c/a ratio and change in elongation with laser fluence.

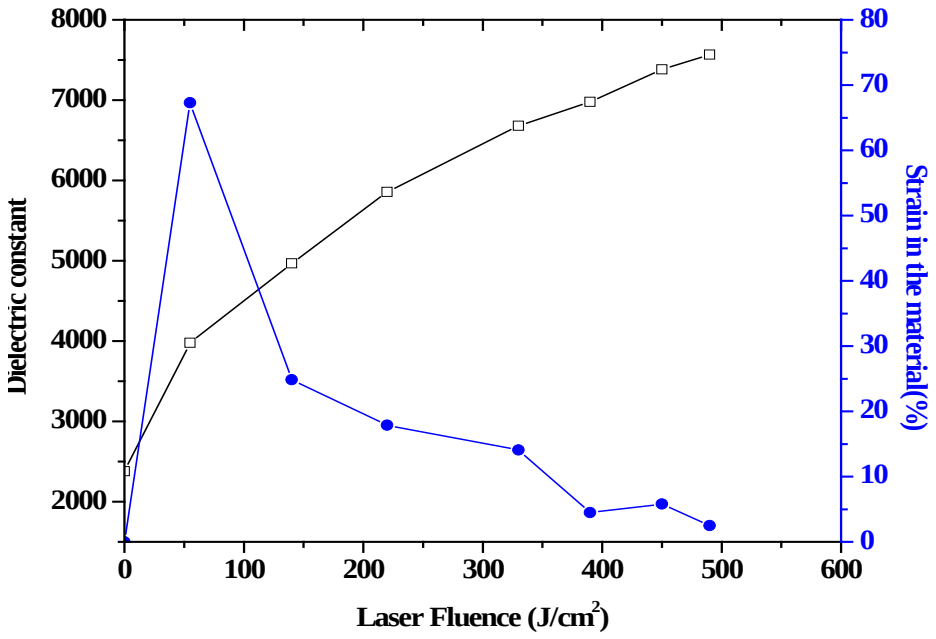

Figure 14. Change in dielectric constant and % strain produced in the material with laser fluence.

on change in morphology of the $BaTiO_3$, observed from the SEM and AFM investigation. The roughness of the sample also increases with an increase in the laser fluence. The roughness of the sample has been observed at 430 J/cm^2. At the higher laser fluence, the dimple features have been observed in morphology due to the maximum transport of the material from the melted region to the heat flow direction. At the last but not least, the maximum strain has been found in material at the higher laser fluence. This result has been observed from the measurement of dielectric constant at room temperature of the laser treated sample. The other important results are dielectric and the elongated lattice parameter of the laser treated material, which may increase with an increasing strain in the material.

Acknowledgements

The authors are very much thankful to Principal Govt. M. V. M. College and Material Science & Metallurgical Engineering Department MANIT for providing facilities.

References

[1] Maxwell, J.C. (1865) *Philosophical Transactions of the Royal Society of London*, **155**, 459-512. http://dx.doi.org/10.1098/rstl.1865.0008

[2] Heaviside, O. (1950) Electromagnetic Theory. Complete and Unabridged ed. of v.1, 2, 3 with a Critical and Historical Introduction by Ernst Weber. Dover, New York.

[3] Bloembergen, N. (2000) *IEEE Journal of Selected Topics in Quantum Electronics*, **6**, 876-880. http://dx.doi.org/10.1109/2944.902137

[4] Maiman, T.H. (1960) *Nature*, **187**, 493-494. http://dx.doi.org/10.1038/187493a0

[5] Rossi, F. and Kuhn, T. (2002) *Reviews of Modern Physics*, **74**, 895-950. http://dx.doi.org/10.1103/RevModPhys.74.895

[6] Sundaram, S.K. and Mazur, E. (2002) *Nature Materials*, **1**, 217. http://dx.doi.org/10.1038/nmat767

[7] Gordon, J.P. (1983) *Optics Letters*, **8**, 596. http://dx.doi.org/10.1364/OL.8.000596

[8] Stegeman, G.I. and Segev, M. (1999) *Science*, **286**, 1518. http://dx.doi.org/10.1126/science.286.5444.1518

[9] Schroeder, H. and Chin, S.L. (2002) *Optics Communication*, **234**, 399.

[10] von der Linde, D., Sokolowski-Tinten, K. and Bialkowski, J. (1997) *Applied Surface Science*, **109-110**, 1-10. http://dx.doi.org/10.1016/s0169-4332(96)00611-3

[11] Kirkwood, S.E., Tsui, Y.Y., Fedosejevs, R., Brantov, A.V. and Yu. Bychenkov, V. (2009) *Physical Review B*, **79**, 144120. http://dx.doi.org/10.1103/PhysRevB.79.144120

[12] Biciunas, A., Malevich, Y.V. and Krotkus, A. (2011) *Electronics Letters*, **47**, 1186. http://dx.doi.org/10.1049/el.2011.1925

[13] Bonse, J., Baudach, S., Krüger, J., Kautek, W. and Lenzner, M. (2002) *Applied Physics A*, **74**, 19-25. http://dx.doi.org/10.1007/s003390100893

Journal of Modern Physics, 2016, 7, 1082-1090
Published Online June 2016 in SciRes. http://www.scirp.org/journal/jmp
http://dx.doi.org/10.4236/jmp.2016.710096

On the Charges and Currents in the Quantum Field Theory

Daniel Sepunaru

RCQCE—Research Center for Quantum Communication, Holon Academic Institute of Technology, Holon, Israel
Email: danielsepunaru@walla.co.il

Received 7 January 2016; accepted 9 June 2016; published 14 June 2016

Abstract

This paper is concerned with the determination of currents and charges in hypercomplex extensions of the Feynman-Dyson derivation of the Maxwell-Faraday equations. We analyze the appearance of charges and currents in non-Abelian versions of that approach: SU(2), SU(3) and G2. The structure constants of G2 Lie algebra are computed explicitly. Finally, we suggest a seven-dimensional treatment of color.

Keywords

Gauge Charges, Structure Constants, Multiplication Tables, Color

1. Introduction

This paper is a continuation of the discussion on hypercomplex extensions of the Feynman-Dyson derivation of the Maxwell-Faraday equations. Usually mathematical proofs have only relatively minor value since for any set of mathematical arguments it is possible to present an equally valuable set of contra-arguments; in physics, by contrast, the ultimate verification of a statement is its confirmation by experiment and the solution is unique.

The specific topic of the present discussion is the determination of currents and charges in the suggested schemas [1]-[4]. As the defining model we consider the structure of the classical electrodynamics which consists of two parts: the first, the "inertial" fields produced by a moving source that is wrapped around the source, and the second, the radiated part that consist of the excessive field due to the accelerated motion of the source. Equivalently, the solutions may be viewed as a description of the motion of a source under the influence of an external field. The role of the inhomogeneous equations in all that is crucial. They define the electromagnetic parameters of the source: charge and current. This is not "merely" a definition, for it produces a drastic change in the physical content of the theory which leads to reconsideration of the structure of the space-time continuum (a change from Galilean to Lorentz group transformations that leave the equations invariant). It also introduces a

How to cite this paper: Sepunaru, D. (2016) On the Charges and Currents in the Quantum Field Theory. *Journal of Modern Physics*, **7**, 1082-1090. http://dx.doi.org/10.4236/jmp.2016.710096

new type of symmetry—internal local gauge symmetry.

Thus, charge and the current turn out to be newly conserved quantities. Note that the non-Abelian extension of the gauge fields proceeds through the steps described above [3]. Therefore a more detailed analysis of what has been done so far is required as well as an explanation of the reasoning behind it.

2. Mathematical Preliminary.

Mathematical background for our discussion is necessary.

Since we are interested in a theory with uniquely determined predictions, it is advisable to use a numeric system that allows that to occur: normed division algebras which include the real (1dimensional), complex (2 dimensional), quaternion (4 dimensional) and octonion (8 dimensional) algebras that satisfy the definition of quadratic composition algebras:

$$x^2 - Tr(x)x + N(x)1 = 0,\ \forall x = \text{real, complex, quaternion, octonion}$$

$$x + \bar{x} \equiv Tr(x)1,\ \ Tr(x) = \text{real}, \tag{1}$$

$$x\bar{x}\left(= \bar{x}x\right) \equiv N(x)1,\ \ N(x) = \text{real}.$$

Definitions of trace $Tr(x)$ and norm $N(x)$ are consistent with those of matrix calculus.

Note that in contrast with reals, complex and quaternions, octonions are non-associative (but still alternative) algebra and therefore can't be represented by matrices.

Now we need to introduce multidimensional numeric objects-vectors to extend the usual arithmetic operations-addition, multiplication by a constant number, and multiplication between them. In so doing, we now gain three types of multiplication:

1) scalar multiplication described by the Jordan product

$$\boldsymbol{A}\cdot\boldsymbol{B} \equiv \frac{1}{2}(\boldsymbol{AB} + \boldsymbol{BA})$$

which maps vector fields into scalars;

2) vector multiplication described by the Lie bracket product

$$\boldsymbol{A}\times\boldsymbol{B} \equiv \frac{1}{2}(\boldsymbol{AB} - \boldsymbol{BA})$$

which maps vector fields into vectors; and

3) tensor multiplication $\boldsymbol{A}\otimes\boldsymbol{B}$ which leads to the higher dimensional algebras.

Surprisingly, vector multiplication does not always satisfy the usually required properties [5] [6].

It realized consistently only in $n = 1$, $n = 3$ and $n = 7$ dimensional space according to [7] [8]:

$$n(n-1)(n-3)(n-7) = 0, \tag{2}$$

where n is the dimension of the underlined vector space.

Bearing in the mind the definition of charge in the following discussion, from now on, by the term multiplication we mean the Lie bracket product

$$e_a \times e_b = \frac{1}{2}(e_a e_b - e_b e_a). \tag{3}$$

For the quaternions ($n = 3$) the structure constants f_{abc} may be computed from

$$e_a \times e_b \equiv \frac{1}{2}[e_a, e_b] = f_{abc}e_c;\quad a,b,c = 1,2,3 \tag{4}$$

where $f_{abc} = \varepsilon_{abc}$, and ε_{abc} is totally antisymmetric Levi-Civita symbol with the only nonzero independent components $\varepsilon_{123} = 1$. Thus we get quaternion multiplication table (see **Figure 1**), where $e_a^2 = -1; a = 1,2,3$. From (1) it follows that e_a are the traceless, antihermition generators of quaternion algebra. We compute the quaternion and octonion multiplication tables in order to compare them with the corresponding commutation

e_a / e_b	e_1	e_2	e_3
e_1	0	e_3	e_2
e_2	e_3	0	e_1
e_3	e_2	e_1	0

Figure 1. Quaternion multiplication table.

relation tables and structure constants for the most popular in physical applications Lie algebras.

For the octonions ($n=7$) we get octonions multiplication table (see **Figure 2**), where $e_a^2 = -1; a = 1,2,\cdots,7$. From (1) it follows that e_a are the traceless, antihermition generators of octonian algebra. Then the structure constants f_{abc} may be computed from

$$e_a \times e_b \equiv \frac{1}{2}\left[e_a, e_b\right] = f_{abc} e_c; \quad a,b,c = 1,\cdots,7 \tag{5}$$

where $f_{abc} = \varepsilon_{abc}$, and ε_{abc} is the totally antisymmetric analog of the Levi-Civita symbol in seven-dimensional vector space with only nonzero independent components

$$f_{abc} = f_{123} = f_{246} = f_{435} = f_{651} = f_{572} = f_{714} = f_{367} = 1 \tag{6}$$

3. Internal (Local Gauge) Symmetries

Our knowledge of the physical system is expressed in terms of conserved measurable quantities. The Noether theorem provides the connection between them and the symmetry transformations which leave the equations of motion invariant.

Now let us consider the symmetries that play a major role in the description of the fundamental interactions. These are rank-one electromagnetic U(1) and its extension, the Weinberg-Salam-Glashow electroweak model SU(2) $\otimes$ U(1). Further, we use the second-rank extension of these-SU(3) of QCD and its close relative, G(2) [9]. In all the cases we have dealt with, the continuous Lie groups and algebras associate the transformations in the inner space of the particle with quantities measurable by macroscopic devices according to Noether theorem [10]. That connection is established by the universal relation

$$\left[T_a, T_b\right] = i f_{abc} T_c \tag{7}$$

where T_a are traceless, hermitian matrices, which we call gauge charges and f_{abc} are the structure constants that uniquely determine the symmetry group.

3.1. The Lie Algebra of the SU(2) Group

The group parameters form a three-dimensional vector space. As its base we choose standard Pauli matrices:

$$T_1 = \frac{1}{2}\begin{pmatrix} 0 & 1 \\ 1 & 0 \end{pmatrix}; \quad T_2 = \frac{1}{2}\begin{pmatrix} 0 & -i \\ i & 0 \end{pmatrix}; \quad T_3 = \frac{1}{2}\begin{pmatrix} 1 & 0 \\ 0 & -1 \end{pmatrix}. \tag{8}$$

Here and in the following we use the normalization:

$$Tr\left\{T_a T_b^{+}\right\} = \frac{1}{2}\delta_{ab}; \quad a,b = 1,2,3 \tag{9}$$

We use the common normalization convention in order to allow the comparison of vector spaces formed by consecutive Lie algebras. Then, structure constants f_{abc} are computed from (7). It is convenient to present the results in the form of a multiplication table (see **Figure 3**).

The $f_{abc} = \varepsilon_{abc}$ obtained is a totally anti-symmetric Levi-Civita symbol in three-dimensional vector space with only independent nonzero components $f_{123} = 1$.

e_a/e_b	e_1	e_2	e_3	e_4	e_5	e_6	e_7
e_1	0	e_3	e_2	e_7	e_6	e_5	e_4
e_2	e_3	0	e_1	e_6	e_7	e_4	e_5
$e_{\backslash 3}$	e_2	e_1	0	e_3	e_4	e_7	e_6
e_4	e_7	e_6	e_3	0	e_3	e_2	e_1
e_5	e_6	e_7	e_5	e_3	0	e_1	e_2
e_6	e_5	e_4	e_7	e_2	e_1	0	e_3
e_7	e_4	e_5	e_6	e_1	e_2	e_3	0

Figure 2. Octonions multiplication table.

T_a/T_b	T_1	T_2	T_3
T_1	0	T_3	T_2
T_2	T_3	0	T_1
T_3	T_2	T_1	0

Figure 3. Lie algebra and structure constants of SU(2).

3.2. The Lie Algebra of the SU(3) Group

Here we have to deal with eight group parameters. In order to maintain the connection with the Lie algebra of the SU(2) group we choose traceless, hermitian Gell-Mann matrices as the base of our vector space:

$$T_1=\frac{1}{2}\begin{pmatrix}0&1&0\\1&0&0\\0&0&0\end{pmatrix};\ T_2=\frac{1}{2}\begin{pmatrix}0&-i&0\\i&0&0\\0&0&0\end{pmatrix};\ T_3=\frac{1}{2}\begin{pmatrix}1&0&0\\0&-1&0\\0&0&0\end{pmatrix};\ T_4=\frac{1}{2}\begin{pmatrix}0&0&1\\0&0&0\\1&0&0\end{pmatrix};$$
$$T_5=\frac{1}{2}\begin{pmatrix}0&0&-i\\0&0&0\\i&0&0\end{pmatrix};\ T_6=\frac{1}{2}\begin{pmatrix}0&0&0\\0&0&1\\0&1&0\end{pmatrix};\ T_7=\frac{1}{2}\begin{pmatrix}0&0&0\\0&0&-i\\0&i&0\end{pmatrix};\ T_8=\frac{1}{2\sqrt{3}}\begin{pmatrix}1&0&0\\0&1&0\\0&0&-2\end{pmatrix}. \tag{10}$$

Now from (7) we calculate the structure constants and present the results as a multiplication table (see **Figure 4**).
where

$$f_{123}=1;\ f_{147}=f_{516}=f_{246}=f_{257}=f_{345}=f_{637}=\frac{1}{2};\ f_{458}=f_{678}=\frac{\sqrt{3}}{2} \tag{11}$$

are non-vanishing, totally anti-symmetric structure constants.

3.3. The Lie Algebra of the G2 Group

The general elements of the G2 Lie algebra are described by fourteen parameters. The standard base is given in terms of fourteen 7 × 7 traceless hermitian matrices [11]:

T_a/T_b	T_1	T_2	T_3	T_4	T_5	T_6	T_7	T_8
T_1	0	T_3	T_2	T_7	T_6	T_5	T_4	0
T_2	T_3	0	T_1	T_6	T_7	T_4	T_5	0
T_3	T_2	T_1	0	T_5	T_4	T_7	T_6	0
T_4	T_7	T_6	T_5	0	T_3	T_2	T_1	T_5
T_5	T_6	T_7	T_4	T_3	0	T_1	T_2	T_4
T_6	T_5	T_4	T_7	T_2	T_1	0	T_3/T_8	T_7
T_7	T_4	T_5	T_6	T_1	T_2	T_3/T_8	0	T_6
T_8	0	0	0	T_5	T_4	T_7	T_6	0

Figure 4. Lie algebra and structure constants of SU(3).

$$T_1=\frac{1}{2\sqrt{2}}\begin{pmatrix}0&1&0&0&0&0&0\\1&0&0&0&0&0&0\\0&0&0&0&0&0&0\\0&0&0&0&-1&0&0\\0&0&0&-1&0&0&0\\0&0&0&0&0&0&0\\0&0&0&0&0&0&0\end{pmatrix},\quad T_2=\frac{1}{2\sqrt{2}}\begin{pmatrix}0&-i&0&0&0&0&0\\i&0&0&0&0&0&0\\0&0&0&0&0&0&0\\0&0&0&0&-i&0&0\\0&0&0&i&0&0&0\\0&0&0&0&0&0&0\\0&0&0&0&0&0&0\end{pmatrix}$$

$$T_3=\frac{1}{2\sqrt{2}}\begin{pmatrix}1&0&0&0&0&0&0\\0&-1&0&0&0&0&0\\0&0&0&0&0&0&0\\0&0&0&-1&0&0&0\\0&0&0&0&1&0&0\\0&0&0&0&0&0&0\\0&0&0&0&0&0&0\end{pmatrix},\quad T_4=\frac{1}{2\sqrt{2}}\begin{pmatrix}0&0&1&0&0&0&0\\0&0&0&0&0&0&0\\1&0&0&0&0&0&0\\0&0&0&0&0&-1&0\\0&0&0&0&0&0&0\\0&0&0&-1&0&0&0\\0&0&0&0&0&0&0\end{pmatrix}$$

$$T_5=\frac{1}{2\sqrt{2}}\begin{pmatrix}0&0&-i&0&0&0&0\\0&0&0&0&0&0&0\\i&0&0&0&0&0&0\\0&0&0&0&0&-i&0\\0&0&0&0&0&0&0\\0&0&0&i&0&0&0\\0&0&0&0&0&0&0\end{pmatrix},\quad T_6=\frac{1}{2\sqrt{2}}\begin{pmatrix}0&0&0&0&0&0&0\\0&0&1&0&0&0&0\\0&1&0&0&0&0&0\\0&0&0&0&0&0&0\\0&0&0&0&0&-1&0\\0&0&0&0&-1&0&0\\0&0&0&0&0&0&0\end{pmatrix}$$

$$T_7=\frac{1}{2\sqrt{2}}\begin{pmatrix}0&0&0&0&0&0&0\\0&0&-i&0&0&0&0\\0&i&0&0&0&0&0\\0&0&0&0&0&0&0\\0&0&0&0&0&-i&0\\0&0&0&0&i&0&0\\0&0&0&0&0&0&0\end{pmatrix},\quad T_8=\frac{1}{2\sqrt{6}}\begin{pmatrix}1&0&0&0&0&0&0\\0&1&0&0&0&0&0\\0&0&-2&0&0&0&0\\0&0&0&-1&0&0&0\\0&0&0&0&-1&0&0\\0&0&0&0&0&2&0\\0&0&0&0&0&0&0\end{pmatrix}\tag{12}$$

$$T_9 = \frac{1}{2\sqrt{6}}\begin{pmatrix} 0 & 0 & 0 & 0 & 0 & 0 & \sqrt{2} \\ 0 & 0 & 0 & 0 & 0 & -1 & 0 \\ 0 & 0 & 0 & 0 & 1 & 0 & 0 \\ 0 & 0 & 0 & 0 & 0 & 0 & \sqrt{2} \\ 0 & 0 & 1 & 0 & 0 & 0 & 0 \\ 0 & -1 & 0 & 0 & 0 & 0 & 0 \\ \sqrt{2} & 0 & 0 & \sqrt{2} & 0 & 0 & 0 \end{pmatrix}, \quad T_{10} = \frac{1}{2\sqrt{6}}\begin{pmatrix} 0 & 0 & 0 & 0 & 0 & 0 & i\sqrt{2} \\ 0 & 0 & 0 & 0 & 0 & i & 0 \\ 0 & 0 & 0 & 0 & -i & 0 & 0 \\ 0 & 0 & 0 & 0 & 0 & 0 & -i\sqrt{2} \\ 0 & 0 & i & 0 & 0 & 0 & 0 \\ 0 & -i & 0 & 0 & 0 & 0 & 0 \\ -i\sqrt{2} & 0 & 0 & i\sqrt{2} & 0 & 0 & 0 \end{pmatrix}$$

$$T_{11} = \frac{1}{2\sqrt{6}}\begin{pmatrix} 0 & 0 & 0 & 0 & 0 & 1 & 0 \\ 0 & 0 & 0 & 0 & 0 & 0 & \sqrt{2} \\ 0 & 0 & 0 & -1 & 0 & 0 & 0 \\ 0 & 0 & -1 & 0 & 0 & 0 & 0 \\ 0 & 0 & 0 & 0 & 0 & 0 & \sqrt{2} \\ 1 & 0 & 0 & 0 & 0 & 0 & 0 \\ 0 & \sqrt{2} & 0 & 0 & \sqrt{2} & 0 & 0 \end{pmatrix}, \quad T_{12} = \frac{1}{2\sqrt{6}}\begin{pmatrix} 0 & 0 & 0 & 0 & 0 & -i & 0 \\ 0 & 0 & 0 & 0 & 0 & 0 & i\sqrt{2} \\ 0 & 0 & 0 & i & 0 & 0 & 0 \\ 0 & 0 & -i & 0 & 0 & 0 & 0 \\ 0 & 0 & 0 & 0 & 0 & 0 & -i\sqrt{2} \\ i & 0 & 0 & 0 & 0 & 0 & 0 \\ 0 & -i\sqrt{2} & 0 & 0 & i\sqrt{2} & 0 & 0 \end{pmatrix}$$

$$T_{13} = \frac{1}{2\sqrt{6}}\begin{pmatrix} 0 & 0 & 0 & 0 & -1 & 0 & 0 \\ 0 & 0 & 0 & 1 & 0 & 0 & 0 \\ 0 & 0 & 0 & 0 & 0 & 0 & \sqrt{2} \\ 0 & 1 & 0 & 0 & 0 & 0 & 0 \\ -1 & 0 & 0 & 0 & 0 & 0 & 0 \\ 0 & 0 & 0 & 0 & 0 & 0 & \sqrt{2} \\ 0 & 0 & \sqrt{2} & 0 & 0 & \sqrt{2} & 0 \end{pmatrix}, \quad T_{14} = \frac{1}{2\sqrt{6}}\begin{pmatrix} 0 & 0 & 0 & 0 & i & 0 & 0 \\ 0 & 0 & 0 & -i & 0 & 0 & 0 \\ 0 & 0 & 0 & 0 & 0 & 0 & i\sqrt{2} \\ 0 & i & 0 & 0 & 0 & 0 & 0 \\ -i & 0 & 0 & 0 & 0 & 0 & 0 \\ 0 & 0 & 0 & 0 & 0 & 0 & -i\sqrt{2} \\ 0 & 0 & -i\sqrt{2} & 0 & 0 & i\sqrt{2} & 0 \end{pmatrix}$$

And thus we obtain the corresponding multiplication table (see **Figure 5**).

T_a/T_b	T_1	T_2	T_3	T_4	T_5	T_6	T_7	T_8	T_9	T_{10}	T_{11}	T_{12}	T_{13}	T_{14}
T_1	0	T_3	T_2	T_7	T_6	T_5	T_4	0	T_{12}	T_{11}	T_{10}	T_9	0	0
T_2	T_3	0	T_1	T_6	T_7	T_4	T_5	0	T_{11}	T_{12}	T_9	T_{10}	0	0
T_3	T_2	T_1	0	T_5	T_4	T_7	T_6	0	T_{10}	T_9	T_{12}	T_{11}	0	0
T_4	T_7	T_6	T_5	0	T_3/T_8	T_2	T_1	T_5	T_{14}	T_{13}	0	0	T_{10}	T_9
T_5	T_6	T_7	T_4	T_3/T_8	0	T_1	T_2	T_4	T_{13}	T_{14}	0	0	T_9	T_{10}
T_6	T_5	T_4	T_7	T_2	T_1	0	T_3/T_8	T_7	0	0	T_{14}	T_{13}	T_{12}	T_{11}
T_7	T_4	T_5	T_6	T_1	T_2	T_3/T_8	0	T_6	0	0	T_{13}	T_{14}	T_{11}	T_{12}
T_8	0	0	0	T_5	T_4	T_7	T_6	0	T_{10}	T_9	T_{12}	T_{11}	T_{14}	T_{13}
T_9	T_{12}	T_{11}	T_{10}	T_{14}	T_{13}	0	0	T_{10}	0	T_3/T_8	T_2	T_1	T_5	T_4
T_{10}	T_{11}	T_{12}	T_9	T_{13}	T_{14}	0	0	T_9	T_3/T_8	0	T_1	T_2	T_4	T_5
T_{11}	T_{10}	T_9	T_{12}	0	0	T_{14}	T_{13}	T_{12}	T_2	T_1	0	T_3/T_8	T_7	T_6
T_{12}	T_9	T_{10}	T_{11}	0	0	T_{13}	T_{14}	T_{11}	T_1	T_2	T_3/T_8	0	T_6	T_7
T_{13}	0	0	0	T_{10}	T_9	T_{12}	T_{11}	T_{14}	T_5	T_4	T_7	T_6	0	T_8
T_{14}	0	0	0	T_9	T_{10}	T_{11}	T_{12}	T_{13}	T_4	T_5	T_6	T_7	T_8	0

Figure 5. Lie algebra and structure constants of G2.

where

$$f_{123}=\frac{1}{\sqrt{2}};\ f_{147}=f_{516}=f_{246}=f_{257}=f_{345}=f_{637}=\frac{1}{2\sqrt{2}};$$

$$f_{1093}=f_{11123}=f_{1291}=f_{9414}=f_{11011}=f_{21012}=f_{5913}=f_{41013}=f_{51014}=f_{61411}=f_{71214}=f_{71113}=f_{61213}=\frac{1}{2\sqrt{2}}; \quad (13)$$

$$f_{458}=f_{678}=\frac{\sqrt{3}}{2\sqrt{2}};\ f_{9810}=f_{81211}=\frac{1}{2\sqrt{6}};\ f_{81314}=\frac{1}{\sqrt{6}}$$

are non-vanishing, totally anti-symmetric structure constants.

Notice that SU(2) Pauli matrices as well as SU(3) Gell-Mann matrices do not allow some general form that can describe all the matrices. I guess that the G2 (T1 to T14) also do not allow to do so.

4. Equations of Motion of Non-Abelian Waves

Consider an elementary particle whose motion is parametrized by the external position $x_j; j=1,2,3;$ velocity $\dot{x}_j; j=1,2,3;$ and internal gauge charges $T_a; a=1,\cdots,n$, which are the non-Abelian analogs of electromagnetic charge; n is the dimension of the vector space formed by those charges. Then the defining commutation relations are

$$\begin{aligned}\left[x_j,x_k\right]&=0\\ \left[x_j,\dot{x}_k\right]&=i\delta_{jk}\\ \left[T_a,T_b\right]&=if_{abc}T_c\\ \left[x_j,T_a\right]&=0\end{aligned} \quad (14)$$

where $j,k=1,2,3$ and $a,b,c=1,\cdots,n$.

In general, the equations of particle motion are Newtonian equations

$$m\ddot{x}_j=F_j\left(x,\dot{x},t\right) \quad (15)$$

and generalized Wong's equations [2]

$$\dot{T}_a+gf_{abc}A_j^bT^c\dot{x}_j=0;\ j=1,2,3;\ a,b,c=1,\cdots,n \quad (16)$$

(in the time axial gauge $A_0=0$). A_j is the vector potentials of the external gauge fields

$$A_j=A_j^aT_a;\ \ j=1,2,3;\ a,b,c=1,\cdots,n \quad (17)$$

Particle motion affected by the generalized Lorentz force

$$F_j\left(x,\dot{x},t\right)=gE_j\left(x,t\right)+g\varepsilon_{jkl}\dot{x}_kB_l\left(x,t\right) \quad (18)$$

where

$$E_j\left(x,t\right)\equiv E_j^a\left(x,t\right)T_a \ \text{ and } \ B_j\left(x,t\right)\equiv B_j^a\left(x,t\right)T_a \quad (19)$$

are three-dimensional vectors in outer particle space and n- dimensional vectors in the inner particle space. They are the expected solutions of the generalized Yang-Mills [12]-Shaw [13]-Lee [3]-Wong [2] equations

$$\partial_jB_j^a+gf^{abc}A_j^bB_j^c=0 \quad (20)$$

$$\frac{\partial B_i^a}{\partial t}+\varepsilon_{ijk}\left(\partial_jE_k^a+gf^{abc}A_j^bE_k^c\right)=0 \quad (21)$$

$$\partial_iE_i^a+gf^{abc}A_i^bE_i^c=\rho^a \quad (22)$$

$$-\frac{\partial E_i^a}{\partial t}+\varepsilon_{ijk}\left(\partial_jB_k^a+gf^{abc}A_j^bB_k^c\right)=j_i^a \quad (23)$$

In particular, for $n=1$ we have Maxwell-Faraday electromagnetic theory; for $n=3$ we have the Weinberg-Salam-Glashow electroweak model; for $n=8$ we have SU(3) QCD and for $n=14$ we obtain G2 generalization of Yang-Mills theory that may also have some relevance to the unified theory of fundamental interactions.

However, neither SU(3) nor G2 are based on seven-dimensional space of internal parameters in obvious contradiction to the requirement that $n=7$ from [7] and [8].

5. Color

So far we have considered matrices with the real and complex matrix elements. There are numerous ways to obtain hypercomplex extensions of these matrices. The simplest is:

$$\begin{aligned} e_1 &= -i\cdot\begin{pmatrix} 0 & 1 \\ 1 & 0 \end{pmatrix} = -i\sigma_1; \quad \sigma_1 = ie_1 \\ e_2 &= -i\cdot\begin{pmatrix} 0 & -i \\ i & 0 \end{pmatrix} = -i\sigma_2; \quad \sigma_2 = ie_2 \\ e_3 &= -i\cdot\begin{pmatrix} 1 & 0 \\ 0 & -1 \end{pmatrix} = -i\sigma_3; \quad \sigma_3 = ie_3. \end{aligned} \tag{24}$$

These expressions may be treated as a substitution of 2×2 matrices containing complex matrix elements by 1×1 matrices containing quaternion matrix elements. This treatment is legitimate since quaternions do allow for matrix representation while octonions, as stated previously, cannot be represented by matrices. Nevertheless, (25) give us an idea of how to introduce a special definition of charges and currents that do satisfy the $n=7$ requirement. Namely,

$$T_j = ie_j; \quad j=1,\cdots,7 \tag{25}$$

Then the structure constants are: $f_{abc} = f_{123} = f_{246} = f_{435} = f_{651} = f_{572} = f_{714} = f_{367} = 1$

We assume that these are the color charges and currents in the unified theory of the fundamental interactions. Our confidence is based on the discovery made by I. Newton [14]:

Red	Orange	Yellow	Green	Blue	Indigo	Violet

6. Conclusion

It looks like a long way to go until the comparison with the experimental results could be obtained within this approach. However, definitely it provides an interesting extension of the current version of the quantum field theory.

References

[1] Dyson, F.J. (1990) *American Journal of Physics*, **58**, 209-211. http://dx.doi.org/10.1119/1.16188

[2] Wong, S.K. (1970) *Il Nuovo Cimento A*, **65**, 689-694. http://dx.doi.org/10.1007/BF02892134

[3] Lee, C.R. (1990) *Physics Letters A*, **148**, 146-148. http://dx.doi.org/10.1016/0375-9601(90)90769-K

[4] Sepunaru, D. (2015) *Journal of Modern Physics*, **6**, 698-709. http://dx.doi.org/10.4236/jmp.2015.65075

[5] Silagadze, Z.K. (2002) *Annales de Fondation Louis de Broglie*, **27**, 241-255. http://arxiv.org/abs/hep-ph/0106235

[6] Tanimura, S. (1992) *Annals of Physics*, **220**, 229-247. http://dx.doi.org/10.1016/0003-4916(92)90362-P

[7] Eckmann, B. (1943) *Commentarii Mathematici Helvetici*, **15**, 318-339. http://dx.doi.org/10.1007/BF02565648

[8] Rost, M. (1996) *Documenta Mathematica*, **1**, 209-214.

[9] Behrends, R.E., Dreitlein, J., Fronsdal, C. and Lee, W. (1962) *Reviews of Modern Physics*, **34**, 1. http://dx.doi.org/10.1103/RevModPhys.34.1

[10] Noether, E. (1918) Gottingen Math. Physic., Nachr. kgl. Ges.. Wiss. Kl., 235-257.

[11] Carone, C.D. and Rastogi, A. (2008) *Physical Review D*, **77**, 035011. http://dx.doi.org/10.1103/PhysRevD.77.035011

[12] Yang, C.N. and Mills, R.L. (1954) *Physical Review*, **96**, 191- 201. http://dx.doi.org/10.1103/PhysRev.96.191

[13] Shaw, R. (1955) Ph.D. Diss., Cambridge University, Cambridge, pt. II, ch. III.

[14] Newton, I. (1704) Opticks: Or, A Treatise of the Reflections, Refractions, Inflexions and Colours of Light. Also Two Treatises of the Species and Magnitude of Curvilinear Figures. London.

Journal of Modern Physics, 2016, 7, 1091-1097
Published Online June 2016 in SciRes. http://www.scirp.org/journal/jmp
http://dx.doi.org/10.4236/jmp.2016.710097

Scientific Research Publishing

What Is Wrong with Bohm's Mechanics? An Analysis of a Hong-Ou-Mandel Type Experiment

Sofia Wechsler

Kyriat Motzkin, Israel
Email: sofia10@012.net.il

Received 19 April 2016; accepted 15 June 2016; accepted 20 June 2016

Abstract

The predictions of the Bohmian mechanics are compared with the predictions of the standard quantum mechanics. The analysis is done on a recently performed experiment of Hong-Ou-Mandel type. To the difference from the experiment of Hong, Ou, and Mandel with photons, the new one used bosons possessing rest-mass, ^{4}He atoms. Another novelty is that vis-à-vis the old experiment with identical photons, the recent one proves that distinguishable states of identical bosons can be used on condition that those states can transform into one another. The analysis here is done separately in the standard quantum formalism, and on base of the Bohmian velocities. Calculating the Bohmian trajectories, a contradiction arises. A major advantage of the present work over previous works that found the Bohmian mechanics problematic—typically based on counterfactual reasoning—is that the analysis here uses no counterfactual reasoning. Also, there is an advantage vis-à-vis the Brida experiment based on a thought-experiment of P. Ghose that also showed a contradiction between the quantum and Bohm's mechanics. Brida's experiment is done with photons, for which Bohm's mechanics is not valid, while the experiment analyzed here is carried with particles possessing rest-mass.

Keywords

Gratings of Light, Bragg Scattering, Bohmian Velocity, Bohmian Trajectory

1. Introduction

The Standard Quantum Mechanics (SQM) is plagued by the collapse postulate which besides being alien to the SQM formalism, leads to various contradictions. A famous example is offered by the so-called Hardy's paradox

How to cite this paper: Wechsler, S. (2016) What Is Wrong with Bohm's Mechanics? An Analysis of a Hong-Ou-Mandel Type Experiment. *Journal of Modern Physics*, **7**, 1091-1097. http://dx.doi.org/10.4236/jmp.2016.710097

with a two-particle entanglement [1], in which the collapse postulate in conjunction with the special relativity produces a contradiction [2] [3].[1]

Vis-à-vis these problems, different "interpretations" of the quantum mechanics were proposed, suggesting different solutions. It is beyond the scope of this work to examine all these interpretations and their weak points. A review of the interpretations most often discussed in the literature can be found in [5]. We focus here on D. Bohm's interpretation [6] [7] in the spirit of the guide-wave idea of L. de Broglie [8], since it is the most thoroughly elaborated and investigated.

Bohm's Mechanics (BM) eliminates the collapse postulate by assuming the existence of a quasi-classical particle—called in the literature *Bohmian particle*—that has at once a well-defined position and velocity, and therefore follows a well-defined *trajectory*. Thus, BM depicts a clear picture on how the measurements' outcomes are produced: the detector through which passes the Bohmian particle, makes a recording, while the other detectors remain silent although different parts of the wave-function impinge on them too. Thus, the collapse postulate becomes futile.

Unfortunately, the BM encounters hard problems.

One problem is that the BM is unfit for photons, as the formula of the Bohmian velocity involves the mass of the particle. Trials to take, for instance, the quantity $\hbar\omega/c^2$ as mass of a photon, encounter difficulties [9].

Another problem is that reasoning from the point of view of observers in relative movement, as in Hardy's analysis [1]-[3], the Bohmian trajectories predicted by the different observers are different. The contradiction would be avoided only if the wave-function would be valid in one single frame—a *preferred frame*—and invalid in all the other frames [10]. But the theory of relativity doesn't allow preferred frames.

Though, searches for frames in which the wave-function was violated were done in different ways, with moving detectors [11] or beam-splitters [12], or supposing some ether moving together with the Earth [13]. The experimental results didn't reveal any such invalidating frames.

P. Ghose pointed to one more problem, appearing in two-particle interferometry [14]-[16], and *working with one single frame*, the lab frame. In experiments with more than one particle, the Bohmian trajectories make predictions compatible with SQM if the particles are *distinguishable*. However, if the particles are *indistinguishable* and their wave-functions overlap, one cannot follow the evolution of each particle individually simply because one cannot distinguish between them. P. Ghose proposed an experiment with indistinguishable bosons, each boson passing through a different slit, and showed that the BM predictions differ clearly from those of the SQM.

A simulation of this proposal was realized with down-conversion photons by G. Brida and his co-workers [17] [18]. It confirms the SQM predictions, but it is questionable if that can be taken as disproving the BM because *the BM is not applicable to photons*.

For this reason, another experiment is analyzed here, recently performed at the Charles Fabry labs [19]. The experiment is a realization of the Hong-Ou-Mandel (HOM) experiment, with bosons possessing rest-mass, ^{4}He atoms, instead of photons. This analysis shows a contradiction which appears between BM and SQM when the wave-function is a superposition of different states of two identical particles. This analysis is also done *only in the lab frame*, and the proof is much simpler than that of P. Ghose.

The next sections are organized as follows: Section 2 describes the experiment main line. Section 3 presents the QM analysis of the experiment. Section 4 calculates the Bohmian trajectories of the two involved particles. Section 5 comprises discussion.

2. A Hong-Ou-Mandel Type Experiment with Bosons

The first step in the HOM-type experiment is the generation of pairs of atoms, **Figure 1**. On a trapped Bose-Einstein condensate (BEC) is superimposed a moving optical lattice created by two counter-propagating laser beams between which there is a small difference in frequency, $\delta\nu$. Thus, the atoms in the BEC appear as having a relative movement with respect to the lattice, with a mean z-component of the linear momentum, p_0, dependent on $\delta\nu$.

Under such conditions, if a collision of two atoms occurred, and was also accompanied by interaction with the lattice, the z-linear momenta of the atoms is changed to new values, P and p, $P > p$, see figure 1, **a** in [20] or

[1]Hardy's analysis was focused on ruling out local hidden variables, but it was immediately realized that it implies that the collapse clashes with the relativity, even without involving hidden variables. Berndl and Goldstein suggested that the clash is due to drawing conclusions on non-performed measurements [4]. Their suggestion is in line with the claim that the wave-function has an epistemological character, but it brings no contribution to the effort of understanding the measurement process.

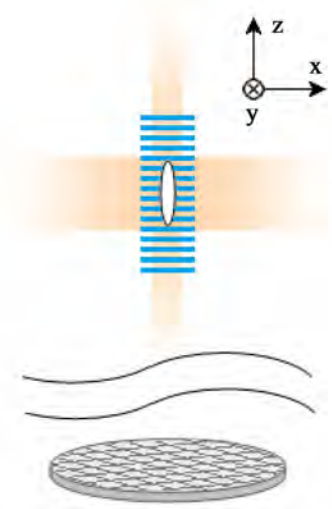

Figure 1. Generation and detection of the atom pairs. (not to scale) This figure is similar with the figure 1, **a** in [19] and represents schematically the elements used in producing and detecting atom pairs. On a BEC (white vertical oval) located in an optical trap (pink shaded) is superimposed a moving optical lattice (blue). When the lattice and the trap are switched off, the atoms fall toward a micro-channel plate detector located below the BEC.

[21] (these articles contain a detailed explanation of the pair generation process). The values P and p are quite well-defined due to the restrictions imposed by the conservation laws of linear momentum and energy, and by the lattice constant, see figure 1, **b** in [20]. Thus, a pair of atoms is created, one atom labeled below as **a**, with z-linear momentum P, the other, labeled **b**, with z-linear momentum p.

At a time t_1 the optical lattice is switched off, and 200 μs later the optical trap is switched off too. Since this moment on, the atoms fall freely under the action of the gravity and of their initial linear momenta. Due to the difference in linear momentum along the axis z, they separate spatially, see **Figure 2**.

At a time $t_2 = t_1 + 500\ \mu s$ the atoms meet a second optical lattice, non-running, with the fringes in the plane x-y. The lattice is sufficiently thick in the z-direction for being felt by both atoms although there is a distance between them. The lattice is kept active for 100 μs, and the effect is that the z-linear momenta of the atoms are swapped.

From now on, the distance along the axis z between the two atoms decreases steadily and they meet again at a time t_3 that satisfies $t_3 - t_2 = t_2 - t_1$, see **Figure 2**. At t_3 the second optical lattice is switched on again, but only for an interval of 50 μs. This shorter interval of atom-lattice interaction has the effect that the lattice acts similarly with a beam-splitter that transmits and reflects in equal proportion. In consequence, both atoms leave the lattice with the same z-linear momentum, either both with P (the output **c**), or both with p (the output **d**).[2]

3. Analysis of the Experiment According to the Quantum Mechanics

In this analysis only the evolution along the z-axis is relevant, because the velocity of the atoms in the plane x-y had quite a narrow peak around zero, as shows the figure 2(c) in [19]. The fringes of all the optical lattices were perpendicular to the z-axis and so the detector plate. Therefore, the calculi below are done in one dimension, on the axis z.

Between the times t_1 and t_2 the atoms are distinguishable by their linear momentum s.t. the wave-function of the boson pair is

$$\left|\mathbf{a},\mathbf{b}\right\rangle_1 = \hat{\mathbf{a}}_P^\dagger \hat{\mathbf{b}}_p^\dagger \left|0\right\rangle = \left|1_{\mathbf{a},P}\right\rangle \left|1_{\mathbf{b},p}\right\rangle, \tag{1}$$

As said in Section 2, at t_2 the second optical lattice is switched on.

[2]Since the time the trap is switched off, on the atoms acts the gravitational acceleration which alters the linear momenta P and p. However, inside the interferometer the alteration is small, moreover, inside the optical lattices activated at t_2 and t_3 compensation is done for this acceleration.

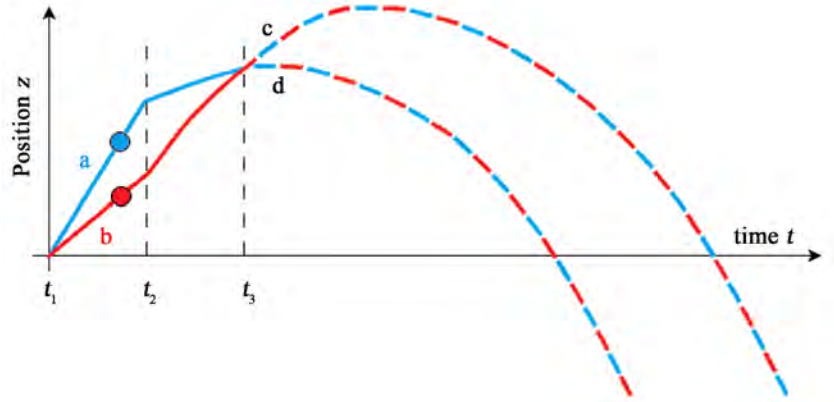

Figure 2. The time-evolution of the atom pairs. (Not to scale). This picture is similar with the figure 1**, b** in [19]. The origin of the vertical axis is at the point where the pair is supposed to have been generated. The horizontal axis represents time of flight. Each one of the curves after t_3 symbolize that both atoms got the same linear momentum.

According to [19] the behavior of the wave-packets in this lattice is well described by the Rabi formalism of a two-state system driven by an oscillatory field. The two states allowed by the interaction with the lattice under the energy and momentum conservation constraints, correspond to the linear momenta P and p. Thus, the evolution of an atom **q** in the field is described by a linear superposition

$$\hat{\mathbf{q}}_P^\dagger \to A(\tau)\hat{\mathbf{q}}_P^\dagger + B(\tau)\hat{\mathbf{q}}_p^\dagger,\ \ \hat{\mathbf{q}}_p^\dagger \to C(\tau)\hat{\mathbf{q}}_P^\dagger + D(\tau)\hat{\mathbf{q}}_p^\dagger, \tag{2}$$

where the symbol $\to$ means "transforms into", τ is the interval of exposure to the field, and

$$|A(\tau)|^2 + |B(\tau)|^2 = |C(\tau)|^2 + |D(\tau)|^2 = 1. \tag{3}$$

As reported in [19], after an interval of 100 μs the coefficients $A(\tau)$ and $D(\tau)$ became zero, therefore the linear momenta of the two atoms were swapped,

$$\hat{\mathbf{a}}_P^\dagger \to \imath e^{-\imath\varphi_2}\hat{\mathbf{a}}_p^\dagger,\ \text{ and }\ \hat{\mathbf{b}}_p^\dagger \to \imath e^{\imath\varphi_2}\hat{\mathbf{b}}_P^\dagger,$$

s.t. the following transformation occurred (leaving aside constant phase-factors)

$$|\mathbf{a},\mathbf{b}\rangle_2 = \hat{\mathbf{a}}_p^\dagger\,\hat{\mathbf{b}}_P^\dagger\,\hat{\mathbf{a}}_P\,\hat{\mathbf{b}}_p\,|1_{\mathbf{a},P}\rangle|1_{\mathbf{b},p}\rangle = |1_{\mathbf{a},p}\rangle|1_{\mathbf{b},P}\rangle, \tag{4}$$

At the time $t_3 = t_2 + 500\ \mu s$ the second optical lattice is switched on again. Since t_3 obeys $t_3 - t_2 = t_2 - t_1$ the wave-packets of **a** and **b** *overlap*, rendering the two atoms indistinguishable. With the lattice active for only 50 μs, it was found that the Equations (2) and (3) yielded,

$$\hat{\mathbf{a}}_p^\dagger \to \frac{1}{\sqrt{2}}\left(\hat{\mathbf{d}}_p^\dagger + \imath e^{\imath\varphi_3}\hat{\mathbf{c}}_P^\dagger\right),\qquad \hat{\mathbf{b}}_P^\dagger \to \frac{1}{\sqrt{2}}\left(\hat{\mathbf{c}}_P^\dagger + \imath e^{-\imath\varphi_3}\hat{\mathbf{d}}_p^\dagger\right). \tag{5}$$

Thus, the lattice acted similarly to a b eam-splitter equally transmitting and reflecting (see section "The HOM effect" in [19]).

In the rest of the text the subscripts p and P will be omitted for the outputs **c** and **d**, because the beam **c** is produced only with linear momentum P, and **d** only with the linear momentum p.

Therefore, after $t_3 + 50\ \mu s$ the pair passes into the state

$$|\mathbf{c},\mathbf{d}\rangle = \frac{1}{2}\left\{\imath\left(e^{\imath\varphi_3}\hat{\mathbf{c}}^{\dagger 2} + e^{-\imath\varphi_3}\hat{\mathbf{d}}^{\dagger 2}\right) + \left(-\hat{\mathbf{c}}^\dagger\hat{\mathbf{d}}^\dagger + \hat{\mathbf{d}}^\dagger\hat{\mathbf{c}}^\dagger\right)\right\}\hat{\mathbf{a}}_p\,\hat{\mathbf{b}}_P\,|1_{\mathbf{a},p}\rangle|1_{\mathbf{b},P}\rangle. \tag{6}$$

The content of the second pair of round parentheses on the RHS vanishes because of the indistinguishability of the particles. The resulting wave-function is,

$$|\mathbf{c},\mathbf{d}\rangle = \frac{\imath}{\sqrt{2}}\left(e^{\imath\varphi_3}\,|2_{\mathbf{c},P}\rangle + e^{-\imath\varphi_3}\,|2_{\mathbf{d},p}\rangle\right), \tag{7}$$

which means that both atoms exit the lattice with the same linear momentum.

For the benefit of the next section it is useful to write the wave-functions (4) and (7) in coordinate representation

$$\psi_2\left(z_{\mathbf{a}}, z_{\mathbf{b}}\right) = \left\langle z_{\mathbf{a}} \middle| 1_{\mathbf{a},p} \right\rangle \left\langle z_{\mathbf{b}} \middle| 1_{\mathbf{b},P} \right\rangle = \frac{1}{2\pi} \mathrm{e}^{\imath\left(pz_{\mathbf{a}} + Pz_{\mathbf{b}}\right)}, \tag{8}$$

$$\begin{aligned} \psi\left(z_{\mathbf{c}}, z_{\mathbf{d}}\right) &= \frac{\imath}{2\sqrt{2}\pi}\left\{ \mathrm{e}^{\imath\left(\varphi + 2Pz_{\mathbf{c}}\right)/\hbar} + \mathrm{e}^{\imath\left(-\varphi + 2pz_{\mathbf{d}}\right)/\hbar} \right\} \\ &= \frac{1}{\sqrt{2}\pi} \mathrm{e}^{\imath\left(Pz_{\mathbf{c}} + pz_{\mathbf{d}}\right)/\hbar} \cos\left(\frac{Pz_{\mathbf{c}} - pz_{\mathbf{d}}}{\hbar} + \varphi \right). \end{aligned} \tag{9}$$

In these wave-functions were omitted leading constant phase-factors.

4. Analysis of the Experiment According to the Bohmian Mechanics

Bohm's interpretation of the QM is based on the concept of particles that move along well-defined trajectories. The BM predicts that an atom should have at each time t a well-defined coordinate $\mathbf{r}$ and a well-defined velocity $\dot{\mathbf{r}}$. Given a system of two quantum objects, **a** and **b**, of space-coordinate u and v respectively, if the joint wave-function is expressed as

$$\Psi\left(u,v,t\right) = R\left(u,w,\mathfrak{e}\right) \ \mathrm{xp}\left[\imath S\left(u,v,t\right)/\hbar\right], \tag{10}$$

BM predicts for each object the velocity

$$\dot{u}_{\mathbf{a}}^{\mathrm{BM}}\left(u,v,t\right) = \frac{1}{\mu_{\mathbf{a}}} \frac{\partial}{\partial u} S\left(u,v,t\right), \qquad \dot{v}_{\mathbf{b}}^{\mathrm{BM}}\left(u,v,t\right) = \frac{1}{\mu_{\mathbf{b}}} \frac{\partial}{\partial v} S\left(u,v,t\right), \tag{11}$$

where $\mu_{\mathbf{a}}$ and $\mu_{\mathbf{b}}$ are the masses of the particles, in our case, both equal to the mass μ of ^{4}He.

For the present analysis we are interested in the velocities before t_3, and those after the transformation (5) takes place.

The wave-function (8) gives according to the formulas (10) and (11) that between $t_2 + 100\,\mu\mathrm{s}$ and t_3,

$$\dot{z}_{\mathbf{a}} = \frac{1}{\mu} \frac{\partial S\left(z_{\mathbf{a}}, z_{\mathbf{b}}\right)}{\partial z_{\mathbf{a}}} = \frac{p}{\mu}, \qquad \dot{z}_{\mathbf{b}} = \frac{1}{\mu} \frac{\partial S\left(z_{\mathbf{a}}, z_{\mathbf{b}}\right)}{\partial z_{\mathbf{b}}} = \frac{P}{\mu}. \tag{12}$$

The wave-function (9) gives according to (10) and (11) that after the transformations (5),

$$\frac{\partial S\left(z_{\mathbf{c}}, z_{\mathbf{d}}\right)}{\partial z_{\mathbf{c}}} = P, \qquad \frac{\partial S\left(z_{\mathbf{c}}, z_{\mathbf{d}}\right)}{\partial z_{\mathbf{d}}} = p\,, \tag{13}$$

$$\dot{z}_{\mathbf{c}} = \frac{1}{\mu} \frac{\partial S\left(z_{\mathbf{c}}, z_{\mathbf{d}}\right)}{\partial z_{\mathbf{c}}} = \frac{P}{\mu}, \qquad \dot{z}_{\mathbf{d}} = \frac{1}{\mu} \frac{\partial S\left(z_{\mathbf{c}}, z_{\mathbf{d}}\right)}{\partial z_{\mathbf{d}}} = \frac{p}{\mu}. \tag{14}$$

Comparing the velocities (14) with (12) one may assume that in each trial of the experiment a fast particle—**c**, and a slow particle—**d**, leave the beam-splitter. However, that is disconfirmed by the experiment.

In [19] it is reported that precise measurements of the atoms' velocities were done. It was found that what emerged in the single trials of the experiment were two atoms of the same speed, either both fast, or both slow, as predicts the wave-function (7) and its subsequent forms, and not one fast atom and one slow, see the dip in figure 3 in [19].

Therefore in the formulas (14) the velocity of one particle should be calculated by dividing by 2μ not by μ, since there are two atoms in the beam **c**, not one. Similarly for the beam **d**. By doing so one would obtain

$$\dot{z}_{\mathbf{c}} = \frac{P}{2\mu}, \qquad \dot{z}_{\mathbf{d}} = \frac{p}{2\mu}. \tag{15}$$

Let's now remind that the meaning of the action function S is the Lagrangian of the *total* system integrated over time. In an experiment in which two identical particles, each one traveling with linear momentum P, and

moving together, *i.e.* having the same space-coordinate $z_{\mathbf{c}}$, the classical Hamilton-Jacobi formalism predicts $\partial S\left(z_{\mathbf{c}}, z_{\mathbf{d}}\right)/\partial z_{\mathbf{c}} = 2P$, not only P as in (13). Similarly, for two identical particles, each one of linear momentum p, and moving together with the same space-coordinate $z_{\mathbf{d}}$, $\partial S\left(z_{\mathbf{c}}, z_{\mathbf{d}}\right)/\partial z_{\mathbf{d}} = 2p$, to the difference from (13).

In continuation, the velocity of one single particle should be obtained by division to 2μ, $\dot{z}_{\mathbf{c}} = P/\mu$ and $\dot{z}_{\mathbf{d}} = p/\mu$ to the difference from (15).

Thus, an incompatibility resulted between the experiment and the BM definitions.

5. Discussion

The Bohmian mechanics is a hidden-variable, non-local theory, in which the hidden variables are the initial position of the Bohmian particles, at some time t_0. For $t > t_0$, the definitions (11) together with the form (10) of the wave-function allow obtaining the position of each particle step by step,

$$z_{\mathbf{x}}\left(t+\Delta t\right) = z_{\mathbf{x}}\left(t\right) + \dot{z}_{\mathbf{x}}\left(z_{\mathbf{a}}\left(t\right), z_{\mathbf{b}}\left(t\right), t\right)\Delta t \text{, where } \mathbf{x} = \mathbf{a}, \mathbf{b}. \tag{16}$$

In this way one can obtain a unique trajectory for each particle.

However, as the Equation (16) shows, the Bohmian velocity of each particle at a given time t may depend on the position of both particles at t. In this case the BM becomes problematic vis-à-vis the theory of relativity. In the lab frame the two particles have at a given time t certain positions, e.g. $z_{\mathbf{a}}$ and $z_{\mathbf{b}}$. Though, according to the time-axis of another frame, in movement with respect to the lab, by the time the particle **a** has the position $z_{\mathbf{a}}$, the particle **b** has the position $z'_{\mathbf{b}}$. The Bohmian trajectories of such a system of particles are therefore frame-dependent.

For avoiding this ambiguity the BM has to postulate the existence of a preferred frame. The question whether the wave-function evolves according to a preferred frame is an issue of debate.

Here is the advantage of the present analysis, which, as Ghose's analysis, is done in the lab frame only. However, the present analysis is much simpler than that of P. Ghose, and is based on an experiment with particles possessing rest-mass, to which the BM can be applied.

Acknowledgements

This work was inspired by the thought-experiment proposed by Ghose in 2000, by the experiment performed by Brida in 2002, and by the HOM-type experiments recently performed at the Laboratoire Charles Fabry. It is a deep pleasure for me to thank to Prof. Christoph Westbrook for the detailed explanations about the HOM-type experiment reported in [19].

References

[1] Hardy, L. (1992) *Physical Review Letters*, **68**, 2981-2984. http://dx.doi.org/10.1103/PhysRevLett.68.2981

[2] Wechsler, S. (2003) Where Was the Particle? https://arxiv.org/ftp/quant-ph/papers/0301/0301098.pdf

[3] Wechsler, S. (2016) Contextual Experiments, Influence from Future, and the Wave-Function "Collapse". https://www.researchgate.net/publication/281210065_Contextual_Experiments_Influence_from_Future_and_the_Wave-Function_Collapse

[4] Berndl, K. and Goldstein, S. (1994) *Physical Review Letters*, **72**, 780. http://dx.doi.org/10.1103/PhysRevLett.72.780

[5] Bassi, A. and Ghirardi, G.-C. (2003) *Physics Reports*, **379**, 257-426. http://arxiv.org/abs/quant-ph/0302164

[6] Bohm, D. (1952) *Physical Review*, **85**, 166-179.

[7] Bohm, D. (1952) *Physical Review*, **85**, 180-193. http://dx.doi.org/10.1103/PhysRev.85.180

[8] de Broglie, L. (1926) Ondes et mouvements. Gauthier-Villars, Paris.

[9] Tumulka, R. (2012) Private Communications.

[10] Berndl, K., Dürr, D., Goldstein, S. and Zanghì, N. (1995) EPR-Bell Nonlocality, Lorentz Invariance, and Bohmian Quantum Theory. http://arxiv.org/abs/quant-ph/9510027

[11] Zbinden, H., Brendel, J., Tittel, W. and Gisin, N. (2001) *Journal of Physics A: Mathematical and General*, **34**, 7103-7110. http://dx.doi.org/10.1088/0305-4470/34/35/334

[12] Stefanov, A., Zbinden, H., Gisin, N. and Suarez, A. (2003) *Physical Review A*, **67**, 042115. http://dx.doi.org/10.1103/PhysRevA.67.042115

[13] Salart, D., Baas, A., Branciard, C., Gisin, N. and Zbinden, H. (2008) *Nature*, **454**, 861-864. http://dx.doi.org/10.1038/nature07121

[14] Ghose, P. (2003) Incompatibility of the de Broglie-Bohm Theory with Quantum Mechanics. https://arxiv.org/abs/quant-ph/0001024

[15] Ghose, P. (2003) An Experiment to Distinguish between de Broglie-Bohm and Standard Quantum Mechanics. http://arxiv.org/abs/quant-ph/0003037

[16] Ghose, P. (2003) On the Incompatibility of Standard Quantum Mechanics and the de Broglie-Bohm Theory. http://arxiv.org/abs/quant-ph/0103126v8

[17] Brida, G., Cagliero, E., Falzetta, G., Genovese, M., Gramegna, M. and Novero, C. (2002) *Journal of Physics B*: *Atomic, Molecular and Optical Physics*, **35**, 4751. http://dx.doi.org/10.1088/0953-4075/35/22/316

[18] Brida, G., Cagliero, E., Falzetta, G., Genovese, M., Gramegna, M. and Predazzi, E. (2002) *Physical Review A*, **68**, 033803. http://dx.doi.org/10.1103/PhysRevA.68.033803

[19] Lopes, R., Imanaliev, A., Aspect, A., Cheneau, M., Boiron, D. and Westbrook., C.I. (2015) An Atomic Hong-Ou-Mandel Experiment. https://arxiv.org/abs/1501.03065 http://dx.doi.org/10.1038/nature14331

[20] Bonneau, M., Ruaudel, J., Lopes, R., Jaskula, J.-C., Aspect, A., Boiron, D. and Westbrook, C.I. (2013) *Physical Review A*, **87**, 061603(*R*).

[21] Campbell, G.K., Mun, J., Boyd, M., Streed, E.W., Ketterle, W. and Pritchard, D.E. (2006) *Physical Review Letters*, **96**, 020406. http://dx.doi.org/10.1103/PhysRevLett.96.020406

Journal of Modern Physics, 2016, 7, 1098-1104
Published Online June 2016 in SciRes. http://www.scirp.org/journal/jmp
http://dx.doi.org/10.4236/jmp.2016.710098

Scientific Research Publishing

Did LIGO Really Detect Gravitational Waves?

—The Existence of Electromagnetic Interaction Made the Experiments of LIGO Invalid

Xiaochun Mei[1], Ping Yu[2]

[1]Institute of Innovative Physics, Fuzhou, China
[2]Cognitech Calculating Technology Institute, Los Angeles, CA, USA
Email: ycwlyjs@yeah.net, yupingpingyu@yahoo.com

Received 1 May 2016; accepted 15 June 2016; accepted 20 June 2016

Abstract

The paper proves that due to the existence of electromagnetic interaction, the experiments of LIGO cannot detect gravitational waves. This is also the reason why Weber's experiments of gravitational waves failed. In fact, the formulas of general relativity that gravitational waves affect distances are only suitable for particles in vacuum. LIGO experiments are carried out on the earth. The laser interferometers are fixed on the steel pipes on the earth's surface in the balanced state of electromagnetic force. Electromagnetic force is 10^{40} times greater than gravity. Gravitational waves are too weak to overcome electromagnetic force and change the length of steel pipes. Without considering this factor, the design principle of LIGO experiment has serious problem. The experiments to detect gravitational waves should move to space to avoid the influence of electromagnetic interaction. Besides, LIGO experiments have the following problems. 1) No explosion source of gravitational waves is really founded. 2) The argument that the Einstein's theory of gravity is verified is a vicious circle and invalid in logic. 3) The results of experiments cause sharp contradiction for the energy currents of gravitational waves. The difference reaches to 10^{24} times and is unacceptable. 4) The method of numerical relativity causes great errors due to the existence of singularities. The errors are enlarged by the effect of butterfly due to the non-linearity of Einstein's equation of gravity. 5) The so-called change of length 10^{-18} m between two glasses of interferometers detected in the experiment exceeds the ability of current technique. This kind of precise has entered micro-scalar. The uncertain principle of quantum mechanics makes it impossible. The signs appeared in LIGO experiments are not caused by distance change. 6) LIGO experiments have not detected gravitational waves. What detected may be the signs of disturbances coming from the middle region between two laser interferometers.

Keywords

LIGO Experiments, Gravitational Waves, General Relativity, Electromagnetic Interaction, Laser Interferometer, Weber Experiment, Singularity Black Holes

How to cite this paper: Mei, X.C. and Yu, P. (2016) Did LIGO Really Detect Gravitational Waves? *Journal of Modern Physics*, **7**, 1098-1104. http://dx.doi.org/10.4236/jmp.2016.710098

1. Introduction

February 11, 2016, LIGO announced that for the first time mankind detected gravitational waves and observed a binary black hole merger directly. This piece of news becomes headline of many global leading media. However, there are many problems in the experiments of LIGO. Physicists should cool down to think the following problems carefully.

2. Where Was the Source of Gravitational Waves?

According to normal pressures of experiments, we should determine or observe the event of binary black hole merger which really happened in space by some methods at first. For example, the experiment observed optical afterglow caused by the material around black holes in merger process. Suppose the speed of gravitational wave is the same as that of light. When the light reached the earth, gravitational waves also arrived and caused stripe changes in interferometers.

The problem was, did LIGO really observe binary black hole merger? The authors read the PRL paper of LIGO but find no word to say they had observed astronomical phenomena about binary black hole merger [1]. They used the method of backward to deduce the event. Based on the signs detected in laser interferometers and the Einstein's theory of gravity, by fitting them with computer, LIGO declared that the event happened in a distance galaxy 1.3 billion years ago.

Therefore, so-called binary black hole merger is only the result of computer simulation, rather than a really observed event in astronomy and physics. By using so-called matching filter method, LIGO declared to find gravitational waves and binary black hole merger from their waveform library which had been established in advance, rather than find them from sky.

As well-known, we need to input many free parameters in the processes of computer simulations. If the method is used to deal with the Einstein's equation of gravity, dozen free parameters are needed. Just like Feynman's joke, using four free parameters may fit out an elephant and using five free parameters may let the elephant swing its nose.

Let's estimate the influence of gravitational wave's explosion on the material around the source of wave declared by LIGO. The corresponding energy of 3 solar mass is 5.4×10^{47} J. When they were transformed into energy in one second, the energy current density on the surface of sphere with radius 10 light's yeas was 4×10^{12} J/m$^2\cdot$s. We compare it with Hiroshima atomic bomb of 20,000 ton TNT corresponding energy to be 8.4×10^{13} J. Suppose that the explosion lasted one second, the energy current density was also 4×10^{12} J/m$^2\cdot$s on the surface of sphere with radius 1.3 meter. So the gravitational wave's explosion declared by LIGO was able to raise the temperature of material around the source to thousand degrees even dozens thousand degrees and destroyed all object's construction within the distance of 10 light's years.

The star density for common galaxies is about 2.5×10^{-3} sun/light's yeas. The sphere with radius 10 light's years contains 10.5 suns. Suppose that the mass of non-luminous material is 5 times more than that of luminous material, the material in the sphere with radius of 10 light's years re is about 50 solar mass. If theses material was vibrated 100 times in one second and heated to thousand degrees even dozens thousand degrees, a great amount of radiations with various frequencies would be produced. According to some informed reports, Gamma rays were detected in two places of south sky at the same time of gravitational wave's explosion. According the estimation, if the explosion of gravitational waves were true, what we observed would be the radiations of various frequencies, rather than Gamma rays only. Meanwhile, the radiations would last more than 10 years, rather than disappearing immediately. They would be observable phenomena, but astronomers did not find them.

However, the paper of LIGO described that the experiment was the first observation of binary black hole merger. That is to say, they really observed binary black hole's collision and merger.

3. Did the Experiment Verify the Einstein's Theory of Gravity?

According to the interpretation of LIGO, the experiments verified the gravitational wave theory of Einstein. However, what they observed were only two signs in laser interferometers, without really observing binary black hole merger and 3 solar mass being transformed into gravitational waves, how could they say that the gravitational wave theory of Einstein was verified?

The real conclusion should be that if the Einstein's theory of gravity was true and what LIGO detected were

real signs of gravitational waves, an event of binary black hole merger happened in a distant galaxy 1.3 billion years ago, in which 3 solar mass was transformed into gravitational waves and emitted into the universal space. That's all! We cannot say any more.

On the other hand, the logic of LIGO has some problem. At first, based on the datum observed in laser interferometer and the gravitational theory of Einstein (reason), they deduced that there was an event of binary black hole merger happened in a distance galaxy 1.3 billion years ago (result). Then, based on the so-called consistence between the event and the datum observed (reason), the Einstein's theory of gravity is verified (result). Obviously, the argument of LIGO is a vicious circle and invalid logically.

Besides, the Einstein's theory of gravity is not the only one. Up to now, many gravity theories have been put forward, for example, the gravity theory in flat space-time. All of these theories predict the existence of gravitational waves. The difference is that the gravitational wave of general relativity involves quadrupole moment, but the gravitational wave of flat space-time involves dipole moment, besides quadrupole moment [2] [3]. The effect of dipole moment is greater than quadrupole moment.

If fitting gravity theory in flat space-time with the signs detected in interferometers, we can also deduce different processes of astronomy and astrophysics. For example, the binary black hole merger (there are also black holes in the Newtonian theory) happened in the Milky Way Galaxy, instead of distance Galaxy. In the process, much less mass is transformed into gravity waves, rather than 3 solar mass.

Further on, there are two arms in laser interferometer. There is a pair of reflect glass in each arm. According to general relativity, gravitational wave's radiation involves quadrupole moment. By the actions of gravitational actions, four glasses are affected simultaneously. While the distance between one pair glasses increases, the distance of another pair glasses decreases. If gravitational wave's radiation involves dipole moment, there are three main models for the same process at least. 1) One pair glass's distance changes, another does not change. 2) One pair glass's distance increase while another decreases. Two pair glass's distances increases or decreases simultaneously.

The experiments of LIGO had not considered these possibilities. No methods were used to distinguish quadrupole moment and dipole moment. There were no wave forms of dipole moment in their waveform library, for they had not thought this possibility. Therefore, even though what detected were the gravitational waves of dipole moment radiations, the computer of LIGO may misunderstand them as that of quadrupole moment. The experiments to verify the theory of gravity in flat space-time may be considered as that to verify the theory of gravity in curved space-time. So, the experiment of LIGO has not verified the Einstein's theory of gravity.

4. There Are Contradictions Caused by the Energy Current Density of Gravitational Waves

According to general relativity, gravity causes space-time curved which changes the distance between objects. The basic principle of LIGO experiment was that gravitational waves affected the lengths of interferometer's two arms. Because two arms were vertical each other, the effects on them were different which leaded to the change of interference stripe.

However, according to general relativity strictly, the formulas of gravitational wave's effect of distances were only suitable for two particles moving along geodesic lines in vacuum [4]. This is the precondition of calculation. Whether or not are they also suitable for the experiments carried out on the earth's surface?

We should understand what the length change of interferometer's arm means. The Interferometers of LIGO were fixed on the vacuum steel pipes and the poles are fixed on the earth's surface. Reflect glasses hanged in interferometers through special fibers. So there are two possibilities in the experiments. The first was that the positions of hang glasses were unchanged, but the lengths of steel pipes were changed. The second was that the lengths of steel pipes were unchanged, but the positions of hang glasses were changed by the vibrations. The first is the standard opinion of general relativity which emphasizes spatial curvature and is used to explain the experiments of LIGO. But the second is not the standard opinion of general relativity. It represents the action of force to cause the vibration of glasses. In general relativity, there is no the concept of force. We only have the concept of spatial curvature caused by material.

The interferometer system was acted by electromagnetic force and reached balance. In the first case, only when the balance was destroyed, the distance between two glasses could change. Because electromagnetic interaction is 10^{40} times greater than gravitational interaction, gravitational waves cannot break the balance of electromagnetic force. So the effect of gravitational waves cannot be observed.

In the second situation, reflect mirrors hanged on interferometers, not be free in vacuum. Because the connections of mirrors with fiber are also controlled by electromagnetic force, in LIGO experiments, electromagnetic interaction cannot be avoided. Many important factors are neglected in the analysis of experiments.

Because the Einstein theory of gravity is equivalent to that of Newtonian under the condition of weak fields, we can a simplified method to estimate the energy current density of gravitational waves on the earth's surface. At first, we assume that two reflect mirrors suspend in vacuum and discuss the actions of gravitational waves on the motions of mirrors. After that, we discuss the effect of electromagnetic interaction on LIGO experiments.

For the stability of experiments, the mass of suspend glass is 40 kg. Suppose that the vibration frequency of gravitational wave is 100 Hz. In order to estimate the energy of gravitational waves roughly. The force acted on grass caused by gravitational wave is F which causes an acceleration a. For simplification, we suppose a to be a constant. Under the action of F, each glass moves $\Delta L = 0.5\times10^{-18}$ m in time 10^{-2} s. According to the formula of the Newtonian, we have

$$F = ma, \quad \Delta L = \frac{1}{2}a(\Delta t)^2 \tag{1}$$

$$\text{so} \quad F = \frac{2m\Delta L}{(\Delta t)^2} = 4\times10^{-13}\ \text{N} \tag{2}$$

The moving distance of glass is $\Delta L = 0.5\times10^{-18}$ m in 10^{-2} s, in which the work that gravitational wave does is

$$P = F\Delta L = 2\times10^{-31}\ \text{J} \tag{3}$$

In the unite time (1 second), the work that gravitational wave does is

$$T = 10^2\times2\times10^{-31} = 2\times10^{-29}\ \text{J}/\text{m}^2\cdot\text{s} \tag{4}$$

Suppose the surface area of glass is 0.5 m^2, correspondently, the energy current density of gravitational waves is

$$W_1 = \frac{2\times10^{-29}}{0.5} = 4\times10^{-29}\ \text{J}/\text{m}^2\cdot\text{s} \tag{5}$$

This is a very small quantity.

On the other hand, according to the calculation of LIGO, 3 solar mass was transformed into the energy of gravitational waves in a second and was emitted into space. Let's estimate the energy current density accepted on the earth's surface. The solar mass is 2×10^{30} kg, the energy of 3 solar mass is

$$E = 3mc^2 = 6\times10^{30}c^2 = 5.4\times10^{47}\ \text{J} \tag{6}$$

The distance of 1.3 billion light years is $R = 13\times365\times24\times3600\times10^8 c = 4.1\times10^{16}c$. The energy current density on the surface of the earth is

$$W_2 = \frac{E}{4\pi R^2} = \frac{6\times10^{30}\text{c}^2}{4\times3.14\times4.1^2\times10^{32}c^2} = 2.9\times10^{-4}\ \text{J}/\text{m}^2\cdot\text{s} \tag{7}$$

The ratio of energy current densities for two calculation methods is

$$\frac{W_2}{W_1} = \frac{2.9\times10^{-4}}{4\times10^{-29}} = 7.25\times10^{24} \tag{8}$$

Even we consider that the energy of gravitational waves absorbed by glasses was ten thousandth, the energy current density in (5) was increased ten thousand times, the ratio was still 10^{20}. The difference is so great that it cannot be accepted in physics. Unfortunately, physicists of LIGO have not noticed this contradiction.

5. The Effects of Electromagnetic Interaction Can Not Be Neglected

As mentioned above, the interferometers of LIGO are fixed on the earth's surface which are controlled by electromagnetic force and reach the situation of balance. To change the lengths of steel pipes, an extract force with

the same magnitude as electromagnetic force is needed at least. However, electromagnetic force is 10^{40} times greater than gravity. So wear gravitational waves on the earth's surface can not violate the balance of electromagnetic force to change the lengths of steel pipes and produce signs in LIGO experiments.

In fact, if we consider the action of gravitational waves on the objects fixed on the earth's surface, electromagnetic interaction between charged particles will be invoiced. In this case, the Einstein equation of gravity cannot be solved. No any problem can be discussed.

Therefore, in general relativity, electromagnetic interaction is not considered in general. The formulas about the effect of gravitational wave on the distances are only suitable for two particles located in vacuum [4]. For the interferometers of LIGO, controlled by electromagnetic interaction, the formulas are invalid. This is most foundational reason that LIGO experiments fail.

According to the calculation of LIGO, the distance change of two glasses was 10^{-18} m, corresponding to 3 solar masses was transformed into gravitational waves in one second in a distance galaxy 1.3 billion light years far away. But this calculation had not considered the effect of electromagnetic interaction. If electromagnetic interaction was considered, suppose that the distance change between two glasses was still 10^{-18} m, the energy of gravitational waves should be greater 10^{40} times. The energy current density of gravitational waves would reach $10^{12}\ \mathrm{J/m^2 \cdot s}$.

What is that mean? On the earth's equator, the energy current density of solar light is $1.33\times10^{3}\ \mathrm{J/m^2 \cdot s}$. So $10^{12}\ \mathrm{J/m^2 \cdot s}$ corresponds to the radiation energy of 750 million suns on the surface of the earth, vibrating hundred times in one second. Under the action of this strong gravitational energy, let alone the laser interferometer of LIGO, even the earth itself would be destroyed.

In this way, we can explain why J. Weber's gravitational wave experiments failed. Weber put forward a method to detect gravitational waves. He used metal to made antenna and believed that gravitational waves would cause antenna resonance. He declared that he had accepted the signs of gravitational waves coming from the center of the Milky Way Galaxy. However, Weber's experiments cannot be repeated by other physicists. The signs Weber accepted was considered too great so that the Milky Way Galaxy would be exhausted in 1 billon years. Now, what Weber accepted is considered to be occasional interference signs, rather than gravitational waves.

The fail reason of Weber's experiments is the same as the experiments of LIGO. Gravitational waves are too weak to overcome electromagnetic force between irons in metal and cause antenna vibrating. In this meaning, all laser interferometers on the surface of the earth including LIGO, and Virgo in Italy and France, GEO600 in Germen, TAMA300 in Japan and so on cannot really observe gravitational wave's signs.

The experiment of gravitational waves should move to space, not only to avoid noises, mainly to avoid electromagnetic interaction. In fact, because there was no the effect of electromagnetic force, the J. H. Taylor and R. A. Hulse's observational of gravitational waves for double pulsar radio was credible [5].

6. Is the Method of Numerical Relativity Reliable?

The Einstein's equations of gravity are non-linear and difficult to be solved. Up to now, only a few strict solutions are obtained, most of them are static solutions. If the motions of source material are considered, motion speeds are contained in energy momentum tensor, so that the equations cannot be solved.

The process of binary black hole merger involved speeds, so the normal method of mathematical analysis losses efficacy. The method of numerical relativity is put forward to deal with this kind of problems [6]. However, black holes involved singularities and the law of physics invalid in singularities. The concrete realization of mathematical infinite is the crash of computer in the simulation process.

In order to make calculation possible, lots of revisions had to be introduced which cause great errors. The boundary and initial conditions have to be reset each time when computer is near to crash, so that the errors are introduced again and again. Because the Einstein's gravity field equations are non-linear, the Butterfly effect enlarged the errors.

The LIGO experiments used numerical relativity to calculate binary black hole merger. This was also another cause which leads to inconsistence. Because the Butterfly effect of non-linear process cannot be avoided, the effectiveness of numerical relativity is worth suspending.

Of course, most essential problem is, do singularity black holes with infinite great densities and infinite small volumes exist in nature [6]-[9]?

7. Can the Length's Change of 1000 Times Less than Nuclear Radius Be Measured?

According to the declaration of LIGO, the signs of gravitational waves correspond to the length change of 10^{-18} m for the interferometer's arms, 1000 times less than nuclear radius. What does this mean? As we know that the radius of atom is about 10^{-18} m. At this scalar, an object's boundary has become fuzzy. Looking it closely, the surface of an object is a pile of dazzle electron group, moving in very high speeds. How can the length change of 1000 times less than nuclear radius be distinguished and measured?

In fact, when laser shot at the mirrors of interferometers, the atomic displaces on mirror's surface were far more than 10^{-18} meters. It was meaningless to say that the length change of 10^{-18} m can be measured. This kind of precise has entered micro-scalar. Not only it is far beyond the limitation of mankind technology, it also violates the foundational principle of physics. According the uncertainty principle $\Delta x \cdot \Delta p \sim h$ in quantum mechanics, if atomic thermal motions are limited in the region of 10^{-18} meter, their momentum changes will reach the magnitude order of 10^{-16}. The speed changes of atoms will be very near light's speed and the mirrors cannot exist again.

Therefore, it is meaningless to say that gravitational waves caused the length change of 10^{-18} meter of interferometer's arms. The signs only come from mirror's vibrations caused by a certain unknown reason, or certain force. It had nothing to do with the length change of steel pipes. According to the formulas of general relativity, this kind of sign is not caused by gravitational waves. In the gravitational theory of curved space-time, there is no the concept of force. Gravitational waves only change the distances of space (the earth's surface).

8. What LIGO Accepted Was Really the Signs of Gravitational Waves?

In fact, this kind of vibrations happened frequently and were considered as noises and neglected by the computer of LIGO. Only when the source of vibrations just located at a place near middle position and accepted by two interferometers nearly simultaneously on September 14, 2015, it may be misunderstand as the signs of gravitational waves.

For example, LIGO declared that they had excluded the possibility of earthquake. But we still mention it. As we know, 5 million earthquakes happen on the earth each year which are perceptive by earthquake instruments. More small earthquakes cannot be detected by seismic detectors. The frequencies of perceptive earthquakes are below 20 Hz. The frequencies of slight earthquakes which cannot be detected by earthquake instruments are high than 20 Hz.

The frequencies detected by the interferometers of LIGO are 35 - 150 Hz, similar to that of slight earthquakes. Suppose that there was slight earthquake occurring at the point near the middle palace of two interferometers. The earthquake instruments did not detect it, but the interferometers of LIGO detected it. Though slight earthquakes are not the events of small possibility, it is not commonly possible to occur at the middle palace of two interferometers. The waves of earthquakes reached two interferometers with time difference of 7 milliseconds. Whether or not the computer of LIGO misunderstands it as the signs of gravitational waves? This possibility cannot be excluded.

Besides earthquake's waves, air vibration can also cause the disturbances of same frequencies (the frequencies of sound waves are 20 - 16,000 Hz). These disturbances may transit to the laser interferometers through earth's crust and cause the false judgment of computer. For example, a gust of wine occasionally blows at a rock which was just located at the middle place between two interferometers of LIGO and caused a vibration of shirt time. The computer of LIGO might consider it as an event of gravitational wave.

9. Conclusions

In general relativity, the formulas about the influences of gravitational waves on space distances are only suitable for particles in vacuum. If electromagnetic interactions exist, these formulas are invalid due to the fact that electromagnetic forces are 10^{40} times stronger than gravity. The interferometers of LIGO are fixed on steel pipes which are fixed on the earth's surface. The system is acted by electromagnetic force and reaches balance. The actions of gravitational waves are too weak to break the balance to cause the change of distance. So what LIGO interferometers detected were not the signs of gravitational waves. They may be caused by the vibrations happened on the surface of the earth, just located at the middle region of two interferometers. The signs were received almost simultaneously so that the computer of LIGO judged them as the signs of gravitational waves

wrongly.

In this meaning, all laser interferometers on the earth's surfaces including LIGO cannot really detect gravitational waves. The detections should move to space, not only to eliminate noises, but also to eliminate electromagnetic interaction more importantly. We should also consider the possibility of dipole radiations and the rationality of singularity black holes.

Besides, no explosion source of gravitational waves was found in LIGO experiments. The argument of LIGO about the verification of the Einstein theory of gravity was a vicious circle and invalid in logic. The results of experiments would cause serious contradiction for the energy current density of gravitational waves.

In sum, the LIGO experiments, the faster-than-light experiment of neutron in 2012, the gravitational wave experiment of early universe in 2014, as well as the GP-B experiment of Stanford University in 2011 provide us the lessons that the possibility of failure is great to establish huge scientific equipments to detect small effects. Especially, for gravitational experiments, the risk is very high.

Meanwhile, physicists should be cautious when they evaluate their academic achievement. It is improper to say too much to pursue sensational effect before the results are fully examined.

The authors are grateful to Professors Sheng Zhiyuan and Huang Zhixun's beneficial discussion.

References

[1] Abbott, B.P., *et al*. (2016) *Physical Review Letters*, **116**, 061102. http://dx.doi.org/10.1103/PhysRevLett.116.061102

[2] Wang, Y.J. and Tang, M.Z. (1990) The Theory and Effect of Gravity. Hunan Science and Technology Publishing Company, Changsha, p. 592.

[3] Mei, X.C. (2015) The Third Theory of Space-Time and Gravity as Well Cosmology in Flat Space-Time. Intellectual Property Publishing Company, Beijing, p. 249.

[4] Liu, L. and Zhao, Z. (2004) General Relativity. High Education Publishing Company, Beijing, p. 140.

[5] Weiberg, J.M. and Taylor, J.H. (1984) *Physical Review Letters*, **52**, 1348. http://dx.doi.org/10.1103/PhysRevLett.52.1348

[6] Yimingleon. Numerical Relativity. http://astroleaks.lamost.org/?p=5334

[7] Mei, X.C. (2011) *International Journal of Astronomy and Astrophysics*, **1**, 109-116. http://dx.doi.org/10.4236/ijaa.2011.13016

[8] Mei, X.C. (2013) *Journal of Modern Physics*, **4**, 974-982. http://dx.doi.org/10.4236/jmp.2013.47131

[9] Mei, X.C. (2014) *International Journal of Astronomy and Astrophysics*, **4**, 656-667. http://dx.doi.org/10.4236/ijaa.2014.44060

Journal of Modern Physics, 2016, 7, 1105-1111
Published Online June 2016 in SciRes. http://www.scirp.org/journal/jmp
http://dx.doi.org/10.4236/jmp.2016.710099

Memory Effect in Chemotaxis Equation

Bhupendra Singh[1], Loukrakpam Kennedy Meitei[2*], Ranjit Kumar[2], Varun Malik[2], Yogesh Kumar[2], Nihal Kumar[2]

[1]Department of Physics, Atmaram Sanatan Dharma College, University of Delhi, Delhi, India
[2]Department of Physics, Dyal Singh College, University of Delhi, Delhi, India
Email: *kennedy4mangang@gmail.com

Received 3 April 2016; accepted 15 June 2016; published 20 June 2016

Abstract

Diffusion-Reaction (DR) equation has been used to model a large number of phenomena in nature. It may be mentioned that a linear diffusion equation does not exhibit any traveling wave solution. But there are a vast number of phenomena in different branches not only of science but also of social sciences where diffusion plays an important role and the underlying dynamical system exhibits traveling wave features. In contrast to the simple diffusion when the reaction kinetics is combined with diffusion, traveling waves of chemical concentration are found to exist. This can affect a biochemical change, very much faster than straight diffusional processes. This kind of coupling results into a nonlinear (NL) DR equation. In recent years, memory effect in DR equation has been found to play an important role in many branches of science. The effect of memory enters into the dynamics of NL DR equation through its influence on the speed of the travelling wavefront. In the present work, chemotaxis equation with source term is studied in the presence of finite memory and its solution is compared with the corresponding chemotaxis equation without finite memory. Also, a comparison is made between Fisher-Burger equation and chemotaxis equation in the presence of finite memory. We have shown that nonlinear diffusion-reaction-convection equation is equivalent to chemotaxis equation.

Keywords

Chemotaxis, Nonlinear Diffusion-Reaction Equation, Finite Memory Effect, Solitary Wave Solutions

1. Introduction

Diffusion-Reaction (DR) equation has been used to explain many phenomena in nature [1]. On the other hand, DR equation with finite memory transport has played important role in recent years [2]-[6]. The diffusion

*Corresponding author.

How to cite this paper: Singh, B., Meitei, L.K., Kumar, R., Malik, V., Kumar, Y. and Kumar, N. (2016) Memory Effect in Chemotaxis Equation. *Journal of Modern Physics*, **7**, 1105-1111. http://dx.doi.org/10.4236/jmp.2016.710099

equation with finite memory have been used to explain the forest fire [7], population growth models [8], the effect of legalisation of abortion law on life of women in Italy [9], diffusion of drugs through skin membrane [10].

In addition to diffusion, there are many phenomena in nature in which convection velocity term also becomes important [11]-[13]. Convective velocity is a measure of the bias in the system (think of a dye injected into a running stream). The case when convective velocity became time-dependent was studied by Franosch and Nelson [11]. They studied numerically how this time-dependent convection or the so called "wind" affected the population near a hot spot of favorable growth rates (an oasis) surrounded by a less favorable "desert region". Nonlinear convective velocity term arises in many physical problems including one dimensional turbulence, sound waves in viscous medium, shock waves in viscous medium and so on [14].

Nonlinear convective flux term arises naturally in the study of chemotaxis equation [15]. While diffusion arises due to random motion of the organism, the movement of certain species can be influenced by the presence of chemoattractant (which can generate the directed movement in the population) [1]. For example, insects, single cell organism, bacteria and animals rely on an acute sense of smell for conveying information between members of the species and the chemicals which are involved in this process are called pheromones. Movement of organism in response to environmental agents (chemical stimulus) is called taxis and movement induced by chemical stimulus is referred to as chemotaxis [1] [15]-[19]. Thus chemically directed movement is called chemotaxis.

For example, the female silk moth *Bombyx mori* exudes a pheromone, called bombykol, as a sex attractant for the male, which has a remarkably efficient antenna filter to measure the bombykol concentration, and it moves in the direction of increasing concentration. The acute sense of smell of many deep sea fish is particularly important for communication and predation [1] [20]. It is not only in animal and insect ecology that the mechanism of chemotaxis is important. It can equally be crucial in biological processes. For example, when a bacterial infection invades the body it may be attacked by movement of cells towards the source as a result of chemotaxis.

It has been shown that certain species of bacteria and insects can move toward higher concentrations of nutrients [1]. Concentration $s(x,t)$ of the substrate or attractant is governed by the equation [17]

$$\frac{\partial s}{\partial t} = -G(s)u + D_0 \frac{\partial^2 s}{\partial x^2}, \tag{1}$$

where $G(s)$ is the concentration of the attractant per cell, $u(x,t)$ is the density of the bacteria and D_0 is the diffusion constant of the attractant. For most of the practical purpose, $G(s)$ is taken as constant and diffusion constant D_0 is also neglected [21]. Arguments to justify this approximation are given in Ref [21]. Under this assumption Equation (1) reduces to

$$\frac{\partial s}{\partial t} = -Gu. \tag{2}$$

On the other hand concentration of the bacteria is described by the equation [16]

$$\frac{\partial u}{\partial t} = \frac{\partial}{\partial x}\left[\mu(s)\frac{\partial u}{\partial x}\right] - \frac{\partial}{\partial x}\left[u\chi(s)\frac{\partial s}{\partial x}\right] + f(u), \tag{3}$$

where the first tern on the right side represent the motion of the bacteria in the absence of chemotaxis. In the absence of chemical gradient $\left(\frac{\partial s}{\partial x} = 0\right)$, Equation (3) becomes identical to the diffusion-reaction equation in the presence of source term $f(u)$. Here motility factor, μ, takes the place of the diffusion coefficient *D*. In Equation (3) μ is taken as function of substrate concentration *s*. In principle μ could also vary with bacterial concentration *u* and space variable *x*. But the effect of substrate concentration is not known at present [16]. For most of the practical purpose μ is taken as constant.

The second tern on the right side of Equation (3) describes the chemotactic response of the species. In Equation (3), $u\chi(s)\left[\frac{\partial s}{\partial x}\right]$ is flux of species due to chemotaxis where $\chi(s)$ is a measure of strength of chemotaxis, and is termed as chemotactic coefficient. The function χ is also called the chemotactic sensitivity

function. In the next section we will discuss memory effect in DR equation.

2. Memory Effect in DR Equation

Memory effect in DR equation arises when dispersal of the particle is not mutually independent [2]-[6]. In particular, note that the solution of the one dimensional diffusion equation (the boundary of the problem is at infinity, *i.e.*, $-\infty < x < \infty$)

$$\frac{\partial u}{\partial t} = D\frac{\partial^2 u}{\partial x^2}$$

is given by

$$u(t,x) = \frac{1}{\sqrt{4D\pi t}}\exp\left(-\frac{x^2}{4Dt}\right)$$

At $t = 0$, the solution of the equation is Dirac delta function, *i.e.*,

$$u(x, t = 0) = \delta(x)$$

Thus, at $t = 0$ all the particles are sitting at $x = 0$. For $t > 0$, the solution of the equation is non zero for all x. If we take a value of x such that $|x| > ct$, where c is the speed of light, we see that there is a finite probability, however small, for particles to diffuse at superluminal speeds. The error lies in the diffusion equation itself, which does not recognize any limiting propagation speed. Thus it becomes necessary to include memory effect, which takes care of the finite speed. When memory effect is taken into account then we have the following modification of Fick's law [2] in the presence of nonlinear convection term

$$J(x, t+\tau) = -D\frac{\partial u}{\partial x} + g(u)v, \tag{4}$$

$$\frac{\partial u}{\partial t} = -\frac{\partial J}{\partial x} + f(u), \tag{5}$$

where $u = u(x,t)$, is the concentration or the density variable depending on the phenomenon under study; v is the coefficient of nonlinear convective flux term $g(u)$ and D is the diffusion coefficient. Here $\frac{\partial u}{\partial t}$ is the time rate of change of concentration at time t and $J(x, t+\tau)$ is the flux at a later time $t+\tau$, while $f(u)$ is the source term. Here τ is delay time and its value depends on the system under study [9] [22] [23]. For experimental determination of τ, see ref. [22] [23]. After simplifying Equations (4) and (5) we get

$$u_{tt} - \beta D u_{xx} - f'(u)u_t + \beta\left(u_t - f(u)\right) + \beta v g'(u)u_x = 0. \tag{6}$$

Here $\beta \equiv \frac{1}{\tau}$, $f'(u) = \frac{\mathrm{d}f}{\mathrm{d}u}$ and $g'(u) = \frac{\mathrm{d}g}{\mathrm{d}u}$. In particular for $f(u) = \alpha u - \gamma u^2$ and $g(u) = u^2$, Equation (6) reduces to Fisher-Burger equation with finite memory [6]

$$u_{tt} - \beta D u_{xx} - f'(u)u_t + \beta\left(u_t - f(u)\right) + k\beta u u_x = 0$$

where $k \equiv 2v$. Note that Equation (6) describe a transport phenomenon in which both diffusion and convection processes are of equal importance. After using the transformation $\xi = x - wt$ in Equation (6), we get

$$\left(w^2 - \beta D\right)u'' + \left(f'(u) - \beta\right)wu' - \beta f(u) + \beta v g'(u)u' = 0. \tag{7}$$

By taking $\tau = 1/\beta = 0$ in Equations (6) and (7) one obtain the corresponding DR equation without finite memory transport

$$u_t + v g'(u)u_x = D u_{xx} + f(u), \tag{8}$$

and

$$Du'' + wu' - v g'(u)u' + f(u) = 0. \tag{9}$$

One can see from above that Equations (6) and (7) are hyperbolic nonlinear DR equation while Equations (8) and (9) are parabolic nonlinear DR equation.

3. Memory Effect in Chemotaxis Equation

In the presence of finite memory, Equation (5) remains unchanged while Equation (4) gets modified to

$$J(x,t+\tau)=-\left[\mu(s)\frac{\partial u}{\partial x}-u\chi(s)\frac{\partial s}{\partial x}\right]. \tag{10}$$

Simplifying Equations (5) and (10) one obtains

$$u_{tt}+\left(\beta-f'(u)\right)u_t-\beta f(u)-\beta\frac{\partial}{\partial x}\left[\mu(s)\frac{\partial u}{\partial x}\right]+\beta\frac{\partial}{\partial x}\left[u\chi(s)\frac{\partial s}{\partial x}\right]=0. \tag{11}$$

In Equation (11) we will take $\mu(s)=\mu_0$, $\chi(s)=\chi_0$. Afetr this substitution Equation (11) becomes

$$u_{tt}+\left(\beta-f'(u)\right)u_t-\beta f(u)-\beta\mu_0 u_{xx}+\beta\chi_0 s_x u_x+\beta\chi_0 u s_{xx}=0. \tag{12}$$

Now using the transformation $\xi=x-wt$ in Equations (2) and (12) we get

$$s'=\frac{G}{w}u, \tag{13}$$

$$\left(w^2-\beta\mu_0\right)u''+\left(f'(u)-\beta\right)wu'-\beta f(u)+\beta\chi_0 s'u'+\beta\chi_0 u s''=0. \tag{14}$$

For $\tau=1/\beta=0$, Equations (12) and (14) becomes

$$u_t-\mu_0 u_{xx}+\chi_0 s_x u_x+\chi_0 u s_{xx}=f(u), \tag{15}$$

$$\mu_0 u''+wu'-\chi_0 s'u'-\chi_0 u s''+f(u)=0. \tag{16}$$

From Equation (13) one can see that $s''=Gu'/w$. Substituting the value of s' and s'' from Equation (13) into Equation (14) one obtains

$$\left(w^2-\beta\mu_0\right)u''+\left(f'(u)-\beta\right)wu'-\beta f(u)+\frac{2\beta\chi_0 G}{w}uu'=0. \tag{17}$$

In Equation (7) if we take $g(u)=u^2$, then we obtain the following equation

$$\left(w^2-\beta D\right)u''+\left(f'(u)-\beta\right)wu'-\beta f(u)+2\beta vuu'=0. \tag{18}$$

Now comparing Equations (17) and (18) one can see that $D=\mu_0$ and $v=\chi_0 G/w$. Under this condition Equations (7) and (17) becomes identical. Note that here v is coefficient of nonlinear convection term and from Equation (17) one can see that this coefficient depends on χ_0, G and wave velocity w. Thus, we have mapped the chemotaxis equation to nonlinear diffusion-reaction-convection equation. In this mapping we have assumed that $v=\dfrac{\chi_0 G}{w}$ and hence by measuring χ_0, G and w, experimentally, we can find the velue of convective velocity term v. Similarly, by measuring μ_0 experimentally, we can determine the diffusion coefficient D.

4. Solutions

For Fisher type reaction term $f(u)=\alpha u-\gamma u^2$, Equation (17) or (18) takes the form

$$\left(w^2-\beta D\right)u''+w(\alpha-\beta)u'+(k\beta-2\gamma w)uu'-\beta\alpha u+\beta\gamma u^2=0, \tag{19}$$

where $k\equiv 2v=\dfrac{2\chi_0 G}{w}$. By taking $\tau=1/\beta=0$ in Equation (19) one obtain the corresponding nonlinear DR equation without finite memory transport

$$Du''+wu'-kuu'+\alpha u-\gamma u^2=0. \tag{20}$$

Solutions of Equations (19) and (20) is already obtained by us in ref. [6]. Here we will write the solution of Equation (19) as

$$u(\xi)=\frac{\alpha}{2\gamma}\left[1-\tanh\left(\frac{\gamma k\alpha(\alpha+\beta)}{\left(4D\beta\gamma^2-\alpha^2k^2\right)}\xi\right)\right], \tag{21}$$

and

$$u(\xi)=\frac{\alpha}{2\gamma}\left[1-\coth\left(\frac{\gamma k\alpha(\alpha+\beta)}{\left(4D\beta\gamma^2-\alpha^2k^2\right)}\xi\right)\right], \tag{22}$$

where wave velocity w is given by

$$w=\frac{\beta\left(\alpha k^2+4D\gamma^2\right)}{2\gamma k(\alpha+\beta)}. \tag{23}$$

Equation (21) is a solitary wave solution of Equation (19) whereas solution (22) diverges. Since $u(\xi)$ represent the concentration of certain species which cannot go to infinity hence solution (22) is physically not acceptable. On the other hand solutions of Equation (20) is given by

$$u(\xi)=\frac{\alpha}{2\gamma}\left[1-\tanh\left(\frac{\alpha k}{4\gamma D}\xi\right)\right], \tag{24}$$

and

$$u(\xi)=\frac{\alpha}{2\gamma}\left[1-\coth\left(\frac{\alpha k}{4\gamma D}\xi\right)\right], \tag{25}$$

and wave speed w as

$$w=\frac{\alpha k^2+4D\gamma^2}{2\gamma k}. \tag{26}$$

Equation (24) is again a solitary wave solution of Equation (20) while Equation (25) is physically not acceptable. Now using Equation (13), we have

$$s(\xi)=\int\frac{G}{w}u(\xi)\,\mathrm{d}\xi+C, \tag{27}$$

where C is constant of integration. Substituting the value of $u(\xi)$ from Equations (21) and (22) in Equation (27), we obtain the following value of $s(\xi)$ of Equation (13) as

$$s(\xi)=\frac{G\alpha}{2\gamma w}\left[\xi-\frac{\left(4D\beta\gamma^2-\alpha^2k^2\right)}{\gamma k\alpha(\alpha+\beta)}\ln\left[\cosh\left(\frac{\gamma k\alpha(\alpha+\beta)}{\left(4D\beta\gamma^2-\alpha^2k^2\right)}\xi\right)\right]\right]+C, \tag{28}$$

and

$$s(\xi)=\frac{G\alpha}{2\gamma w}\left[\xi-\frac{\left(4D\beta\gamma^2-\alpha^2k^2\right)}{\gamma k\alpha(\alpha+\beta)}\ln\left[\sinh\left(\frac{\gamma k\alpha(\alpha+\beta)}{\left(4D\beta\gamma^2-\alpha^2k^2\right)}\xi\right)\right]\right]+C, \tag{29}$$

where w is given by Equation (23). Similiarly, substituting the value of $u(\xi)$ from Equations (24) and (25) in Equation (27), we obtain the following value of $s(\xi)$ of Equation (13) as

$$s(\xi)=\frac{G\alpha}{2\gamma w}\left[\xi-\frac{4\gamma D}{\alpha k}\ln\left[\cosh\left(\frac{\alpha k}{4\gamma D}\xi\right)\right]\right]+C, \tag{30}$$

and

$$s(\xi)=\frac{G\alpha}{2\gamma w}\left[\xi-\frac{4\gamma D}{\alpha k}\ln\left[\sinh\left(\frac{\alpha k}{4\gamma D}\xi\right)\right]\right]+C, \tag{31}$$

where w is given by Equation (26). From Equations (28)-(31) one can see that concentration $s(x,t)$ of attractant increases with G and decreases as wave speed w increases. Also, it is directly proportional to coefficient of linear term α and inversely proportional to coefficient of nonlinear term γ.

5. Concluding Remarks

Certain aspects ignored earlier [10] in the studies of the chemotaxis equation involving quadratic nonlinearity are now investigated in this work. We have studied the chemotaxis equation with the source term and finite memory transport in particular. The existence of solitary wave solutions of Equations (19) and (20) is demonstrated explicitly. We have also obtained an exact solutions for concentration $s(x,t)$. Also, a correspondence between nonlinear Diffusion-Reaction-Convection and chemotaxis equation is established. It is shown that nonlinear DR equation with nonlinear convection term is equivalent to chemotaxis equation. Thus, nonlinear convection terms arise naturally in the study of chemotaxis [10]. Also, from Equation (17) one can see that coefficient of non-linear convective flux, $v=\frac{\chi_0 G}{w}$, decreases as wave speed w increases. Thus, using the nonlinear Diffusion-Reaction-Convection equation one can find the coefficient of nonlinear convective flux v, of chemotaxis equation.

Although result obtained in this paper is highly simplified, the solutions obtained here can explain such physical phenomena which is governed by chemotaxis equation. The case when μ and χ depend on bacteria concentration u and space variable x will be discussed in a separate paper. Such studies are in progress.

Acknowledgements

We would like to thank R. S. Kaushal, Awadhesh Prasad and Ram Ramaswamy for helpful discussion. We would also like to thank Dyal Singh College for providing us the computational facility during the course of this work.

References

[1] Murray, J.D. (1993) Mathematical Biology. Springer-Verlag, New York.

[2] Cattaneo, C. (1958) *Comptes Rendus de l'Académie des Sciences*, **247**, 431-433.

[3] Abramson, G., Bishop, A.R. and Kenkre, V.M. (2001) *Physical Review E*, **64**, 066615.

[4] Kar, S., Banik, S.K. and Ray, D.S. (2002) *Physical Review E*, **65**, 061909. http://dx.doi.org/10.1103/PhysRevE.65.061909

[5] Kar, S., Banik, S.K. and Ray, D.S. (2003) *Journal of Physics A*: *Mathematical and General*, **36**, 2771. http://dx.doi.org/10.1088/0305-4470/36/11/308

[6] Mishra, A. and Kumar, R. (2012) *Physical Review A*, **376**, 1833.

[7] Méndez, V. and Llebot, J.E. (1997) *Physical Review E*, **56**, 6557. http://dx.doi.org/10.1103/PhysRevE.56.6557

[8] Méndez, V. andCamacho, J. (1997) *Physical Review E*, **55**, 6476. http://dx.doi.org/10.1103/PhysRevE.55.6476

[9] Caputo, M. and Gloria-Bottini, F. (2011) *Natural Science*, **3**, 694-701. http://dx.doi.org/10.4236/ns.2011.38093

[10] Caputo, M. and Cametti, C. (2009) *Journal of Physics D*: *Applied Physics*, **42**, 125505. http://dx.doi.org/10.1088/0022-3727/42/12/125505

[11] Franosch, T. and Nelson, D.R. (2000) *Journal of Statistical Physics*, **99**, 1021-1030. http://dx.doi.org/10.1023/A:1018607932123

[12] Mishra, A. and Kumar, R. (2010) *Physics Letters A*, **374**, 2921-2924. http://dx.doi.org/10.1016/j.physleta.2010.03.039

[13] Gilding, B.H. and Kersner, R. (2004) Traveling Waves in Nonlinear Diffusion-Convection Reaction. Birkhäuser Verlag, Basel. http://dx.doi.org/10.1007/978-3-0348-7964-4

[14] Debnath, L. (1997) Nonlinear Partial Differential Equations for Scientists and Engineers. Birkhäuser, Boston. http://dx.doi.org/10.1007/978-1-4899-2846-7

[15] Benguria, R.D., Depassier, M.C. and Méndez, V. (2004) *Physical Review E*, **69**, 031106. http://dx.doi.org/10.1103/PhysRevE.69.031106

[16] Keller, E.F. and Segel, L.A. (1971) *Journal of Theoretical Biology*, **30**, 235-248. http://dx.doi.org/10.1016/0022-5193(71)90051-8

[17] Rosen, G. (1976) *Journal of Theoretical Biology*, **59**, 371-380. http://dx.doi.org/10.1016/0022-5193(76)90177-6

[18] Sherratt, J.A. (1994) *Bulletin of Mathematical Biology*, **56**, 129-146. http://dx.doi.org/10.1007/BF02458292

[19] Adler, J. and Dahl, M. (1967) *Microbiology*, **46**, 161-173. http://dx.doi.org/10.1099/00221287-46-2-161

[20] Di Francesco, M. Mathematical Models in Life Sciences. Lecture Notes.

[21] Segel, L.A. (1972) Lecture Notes on Mathematics in the Life Sciences, Vol. 4. American Mathematical Society, Providence, 1-47.

[22] Aoki, K. and Xiang, C.Y. (2007) *The Journal of Physical Chemistry C*, **111**, 15433-15439. http://dx.doi.org/10.1021/jp071757g

[23] Iaffaldano, G., Caputo, M. and Martino, S. (2006) *Hydrology and Earth System Sciences*, **10**, 93-100. http://dx.doi.org/10.5194/hess-10-93-2006

Journal of Modern Physics, 2016, 7, 1112-1119
Published Online June 2016 in SciRes. http://www.scirp.org/journal/jmp
http://dx.doi.org/10.4236/jmp.2016.710100

On the Cosmical Zero Point Energy Density

Bo Lehnert

Alfvén Laboratory, Royal Institute of Technology, Stockholm, Sweden
Email: bo.lehnert@ee.kth.se

Received 28 April 2016; accepted 16 June 2016; published 21 June 2016

Abstract

The frequency spectrum of the cosmical Zero Point Energy (ZPE) and its total density are so far unknown in their details. In the present complementary investigation, a revised theory forms the basis for studies of this concept in two respects. It first applies to the observable universe considered as an entity, as well as to included subregions such as the galaxies with supermassive black holes. Second, experiments are proposed on the maximum Casimir force arising between two metal plates of different materials and with a vanishing air gap in their spacing. This serves the purpose of making an indirect determination of the ZPE energy density in the laboratory, *i.e.* at the Earth's orbit. The ZPE energy density is interpreted as dark matter density and its pressure gradient as dark energy force density.

Keywords

Zero Point Energy, Casimir Force, Dark Matter, Dark Energy

1. Introduction

In his pioneering studies of the harmonic oscillator Planck [1] showed that there existed a lowest nonzero ground state energy level, now called Zero Point Energy (ZPE). An example of the related electromagnetic vacuum fluctuations was later given by Casimir [2] who predicted that two metal plates would attract each other when being sufficiently close together. This force was first confirmed experimentally by Lamoreaux [3]. It reveals the existence of a real *macroscopic* pressure and energy density, originating from photon-like fluctuations of the ZPE. Consequently the vacuum is not a state of empty space.

The low-frequency part of the ZPE fluctuations has to be accepted as an experimental fact, but a problem arises with its high-frequency part. The earlier performed conventional analysis leads namely to a spectrum having an infinite total energy density, as demonstrated by Terletskii [4], Milonni [5] and Loudon [6] among others. As pointed out by the author [7]-[11], this is unacceptable from the physical point of view, as well as due to the facts that such an analysis both becomes *underdetermined* and is based on states of the ensemble which all

How to cite this paper: Lehnert, B. (2016) On the Cosmical Zero Point Energy Density. *Journal of Modern Physics*, **7**, 1112-1119. http://dx.doi.org/10.4236/jmp.2016.710100

have the equal probabilities of *unity*. Also Riess and Turner [12] and Heitler [13] have thrown doubts upon this conventional theory on the ZPE spectrum.

To overcome this difficulty, the author [9]-[11] has proposed the ensemble of ZPE modes to be treated separately, on the condition of a *finite* integrated total energy, and being relevant also at the temperature $T = 0$. This has been done in the standard way of considering oscillations of frequency ν populating the available states of an ensemble in statistical equilibrium, *i.e.* with a probability equal to a Boltzmann factor $\exp(-\nu/\bar{\nu})$. Here $\frac{1}{2}h\bar{\nu}$ is the average and finite member energy of these states, having the corresponding average frequency $\bar{\nu}$. This leads to a physically acceptable, self-consistent and finite total pressure of the ZPE "photons".

The purpose of the complementary investigations presented in this paper is twofold. First, the theory of the ZPE spectrum will be used in models on dark matter and dark energy, applied both to the observable universe considered as an entity, and to galaxies including supermassive black holes at their centra. Second, an experimental determination is desirable which aims at the so far unknown value of the average frequency $\bar{\nu}$ of the ZPE spectrum, measured at the position of the Earth. As to be shown here, this can possibly be realized by means of measurements on the maximum available Casimir force acting on metals of different electromagnetic skin depths.

2. Theory on the Zero Point Energy

2.1. The ZPE Spectrum

In the present revised theory on the ZPE spectrum [8]-[10], the contribution to the local energy density u in the spectral range $(\nu, \nu + \mathrm{d}\nu)$ becomes

$$\mathrm{d}u = \left(4\pi h/c^3\right)\nu^3 \exp\left(-\nu/\bar{\nu}\right)\mathrm{d}\nu \tag{1}$$

This results in a finite integrated energy density

$$u = 24\pi h\bar{\nu}^4/c^3 \tag{2}$$

where the average frequency $\bar{\nu}$ is unknown so far.

2.2. An Interpretation of Dark Matter and Dark Energy

The self-consistent spectrum of Equations (1) and (2) has been proposed as the basis for a new interpretation of dark matter and dark energy [8] [9]. The corresponding analysis is here limited to an isotropic pressure $p = u/3$ in spherically symmetric geometry. With the radial coordinate r, a local *expansive* force density in the outward direction arises from the pressure gradient, as given by

$$f_p = -\frac{1}{3}\frac{\mathrm{d}u}{\mathrm{d}r} \tag{3}$$

This represents the local contribution to dark energy.

The integrated relativistic mass due to ZPE further becomes

$$M(r) = \left(4\pi/c^2\right)\int_0^r u r^2 \mathrm{d}r \tag{4}$$

as being contained within a sphere of radius r. Here cases will also be considered where there exists a supermassive black hole of mass M_b at the centre $r = 0$. The total local *contracting* gravitational force density in the negative radial direction then becomes

$$f_g = -\left(Gu/c^2r^2\right)\left[M(r) + M_b\right] \tag{5}$$

where $G = 6.67\times10^{-11}\ \mathrm{m^3\cdot kg^{-1}\cdot s^{-2}}$ is the constant of gravitation. This force density thus represents the total and local contribution to dark matter. Two cases will be considered here. The first concerns a local balance of the forces in absence of a black hole mass M_b. Then an exact solution can be found. The second case includes the mass M_b and where only a solution for an average balance so far becomes available.

2.2.1. Local Balance

A local balance between the expansive and contracting forces is given by $f_p + f_g = 0$, leading to

$$-\frac{\mathrm{d}u}{\mathrm{d}r} = \left(3Gu/c^2r^2\right)\left[M_b + \left(4\pi/c^2\right)\int_0^r ur^2\mathrm{d}r\right] \tag{6}$$

So far local forms of $u(r)$ have not been found which satisfy this equation when $M_b \neq 0$.

In the case $M_b = 0$, a local solution of the form $u = u_c\left(r_c/r\right)^2$ is on the other hand available [8]. It results in the relations

$$6\pi G u_c r_c^2/c^4 = 1 \tag{7}$$

and

$$M(r) = 2c^2 r/3G \tag{8}$$

2.2.2. Average Balance

The condition of an average balance can still be obtained by substituting $u(r)$ by a mean value $u = u_0 = \text{const}$. This value then prevails within a spherical volume of radius R, with $u = 0$ at points $r > R$. The local expansive force of Equation (3) is then replaced by an integrated total pressure force

$$F_p = \frac{4}{3}\pi R^2 u_0 \tag{9}$$

at the boundary $r = R$. Integrating the gravitational force (5) over the total volume further yields a total contracting force

$$F_g = -\left(4\pi G u_0 M_b R/c^2\right) - \left(4\pi^2 G u_0^2 R^4/3c^4\right) \tag{10}$$

The condition $F_p + F_g = 0$ of average balance then leads to

$$u_0 = \left(c_1/R^2\right)\left[1 - \left(c_2/R\right)\right] \tag{11}$$

having a maximum

$$u_{0\max} = \left(4c_1/27c_2^2\right) = 4c^8/243\pi G^3 M_b^2 \tag{12}$$

at $R = R_{\max} = 3c_2/2$ where $c_1 = c^4/\pi G$ and $c_2 = 3M_b G/c^2$. At this maximum the total ZPE mass becomes

$$M_{\max} = \frac{4}{3}\pi R_{\max}^3 u_{0\max}\Big/c^2 = 4\pi c_1 c_2/9c^2 = 4M_b/3 \tag{13}$$

The energy density (11) has the following properties as a function of R:

- A balance is only possible for $R > c_2$ because c_1 and c_2 are by definition positive, as well as the mean energy density u_0.
- The density u_0 increases from zero at $R = c_2$, to the maximum $u_{0\max}$ at $R = R_{\max}$. This relatively large value of $u_{0\max}$, and the related ZPE mass (13), can be considered as the result of a reinforcement of dark matter by the black hole mass, in the case of an existing equilibrium.
- For values $R > R_{\max}$, u_0 further decreases and approaches the form $u_0 = c_1/R^2$ at large R where u_0 becomes independent of the black hole mass M_b.

2.3. Cosmical Applications

The present theoretical concepts and interpretations can here be applied to two examples:

- The observable universe considered as an entity, with mean properties at its largest scale corresponding to an averaged ZPE energy density.
- Subregions of the universe, on a smaller scale such as that of the galaxies within which there can exist gravitationally contracted local parts of higher ZPE energy density.

2.3.1. The Observable Universe

The radius of the observable universe is estimated to about 10^{26} m by astronomers. In its present stage of expansion it contains about 4% of normal matter, about 23% of dark matter, and about 73% of dark energy as given by Linder and Permutter [14] and Perlmutter [15]. This state thus deviates to a certain extent from an equilibrium. The normal matter has thereby an average density of about 10^{-26} kg·m^{-3} according to Linde [16]. The estimated ZPE energy density then becomes about 5×10^{-9} J·m^{-3}.

Turning first to the imagined case of local balance between dark matter and dark energy in absence of normal matter, this leads to Equations (6)-(8) for $M_b = 0$. Equation (8) then results in an average energy density

$$u = c^4/2\pi GR^2 \tag{14}$$

in local equilibrium. With the radius R in the range from 5×10^{25} to 2×10^{26} m, this would result in an energy density ranging from 6×10^{-9} to 4×10^{-10} J·m^{-3}, respectively.

We next consider the present state of a certain deviation from equilibrium. As an approximation, the average density u_0 is then determined from expressions (9) and (10) with $M_b = 0$ and under the condition $|F_p/F_g| = k_{pg} = 73/23$. It results in

$$u_0 = c^4/k_{pg}\pi GR^2 \tag{15}$$

With R in the range from 5×10^{25} to 2×10^{26} m this corresponds to an average density in the range from 5×10^{-9} to 3×10^{-10} J·m^{-3}, respectively. The density obtained from Equation (15) is thus within the same range as the estimated one. This can be taken as a support of the present theory.

2.3.2. The Milky Way

As subregion we now take the Milky Way as an example, having a radius of about 5×10^{20} m and a thickness of about 1.5×10^{20} m. According to Ghez *et al.* [17] there is a supermassive black hole at its centre, with a mass of about 8×10^{36} kg, *i.e.* 4×10^{6} solar masses. Its volume is reduced to 10^{-7} of the solar volume, corresponding to a radius of about 3×10^{6} m.

Turning to the average balance of Equations (9)-(13), we notice the following results obtained with $c_1 = 3.86\times10^{43}$ J·m^{-1} and $c_2 = 1.77\times10^{10}$ m:

- In the balance between the expansive and contracting forces, relation (11) permits several possible values of u_0. This introduces some uncertainty in the interpretation. It may also not become necessary to satisfy the balance condition exactly, in analogy with the case of Equation (15) of the universe as an entity.
- There is a smallest possible radius equal to $c_2 = 1.77\times10^{10}$ m.
- The maximum of u_0 occurs at $R = 3c_2/2 = 2.66\times10^{10}$ m which is much larger than the radial extension of the supermassive black hole. It leads to $u_{0\max} = 1.8\times10^{22}$ J·m^{-3}. This is an extremely high value, corresponding to a total ZPE mass $4M_b/3$ of Equation (15). It might be realized only under special conditions.
- The branch of Equation (11) at large $R \gg c_2$ is almost independent of M_b, and it leads to the limit $u_0 \to c^4/\pi GR^2$. Choosing a radius of the order of the thickness of the Milky Way, and which roughly corresponds to the position of the Earth within it, this results in a local density of about $u_0 = 2\times10^3$ J·m^{-3}. This density value is substantially higher than the average ZPE energy density of the universe considered as an entity.

3. Experimental Determination of the Dark Energy Density

There is no exact theoretical indication so far about the magnitude of the dark ZPE energy density at the position of the Earth's orbit. Here a possible experimental procedure will be presented for determination of it.

3.1. The Casimir Force

The first investigations on the Casimir force were performed on a small but nonzero air gap between two metal plates. The largest available force of this kind would on the other hand arise in the case of a vanishing air gap [10]. Then the electromagnetic skin depths of the plates will play the rôle of an equivalent gap.

Starting from the spectrum of Equations (1) and (2), the Casimir force arises from the difference in pressure

on the in- and outsides of the metal plates. Whereas the full ZPE pressure acts on their outsides, there is a reduced pressure on their insides due to the boundary condition which sorts out all frequencies below a certain limit $\hat{\nu}$. The latter corresponds to wavelengths larger than $\hat{\lambda} = c/\hat{\nu}$. The net Casimir pressure thus becomes

$$\hat{p} = \left(4\pi h/3c^3\right)\int_0^{\hat{\nu}} \nu^3 \exp\left(-\nu/\overline{\nu}\right) \mathrm{d}\nu \tag{16}$$

Normalizing by the introduction of $x = \nu/\overline{\nu}$ and $\hat{x} = \hat{\nu}/\overline{\nu}$, we obtain

$$\hat{p} = p_0 \Pi\left(\hat{x}\right) \tag{17}$$

where

$$p_0 = 8\pi h \overline{\nu}^4/c^3 \tag{18}$$

and

$$\Pi = \int_0^{\hat{x}} x^3 \exp\left(-x\right) \mathrm{d}x = 1 - \left(1 + \hat{x} + \frac{1}{2}\hat{x}^2 + \frac{1}{6}\hat{x}^3\right)\exp\left(-\hat{x}\right) \tag{19}$$

3.1.1. Results from a Nonzero Air Gap

We first consider the case of a nonzero air gap of the width d, being much larger than the electromagnetic skin depth of the plates at relevant frequencies. Then frequencies lower than $\hat{\nu} = c/2d$ and wavelengths larger than $\hat{\lambda} = 2d$ will be excluded. In the limit $\hat{x} \ll 1$, the function Π approaches the value $\hat{x}^4/24$, corresponding to a net pressure

$$\hat{p} = \pi hc/48d^4, \qquad \hat{x} \ll 1 \tag{20}$$

as shown by Casimir [2] and being applicable to earlier experiments. The result (20) only involves the low-frequency part of the spectrum. It therefore indicates that the full Casimir force should become substantially larger at ever decreasing gap widths, up to a certain limit which includes the entire ZPE spectrum. Thus the pressure (20) is *independent* of the average frequency $\overline{\nu}$ of Equation (1), and it appears first in the total pressure (18).

3.1.2. Results from a Vanishing Air Gap

We next turn to the maximum Casimir force of a vanishing air gap. Then the width d is replaced by the sum of the skin depths δ_1 and δ_2 of two plates (1) and (2) consisting of different metals, the choice of which will be described later. This leads to a total skin depth

$$\delta_1 + \delta_2 = 2\left(1/\pi\mu_0\sigma_{12}\nu\right)^{1/2} \tag{21}$$

where the effective electrical conductivity becomes

$$\sigma_{12} = \frac{4\sigma_1\sigma_2}{\sigma_1 + \sigma_2 + 2\sqrt{\sigma_1\sigma_2}} \tag{22}$$

with σ_1 and σ_2 standing for the electrical conductivities of each metal. In the limit where half a wavelength $\lambda/2 = c/2\nu$ is equal to the total skin depth (21), the corresponding frequency limit becomes

$$\hat{\nu} = \pi c^2 \mu_0 \sigma_{12}/16 \tag{23}$$

Since λ varies as $1/\nu$ and $\delta_1 + \delta_2$ as $1/\sqrt{\nu}$, all frequencies ν less than $\hat{\nu}$ are excluded by the boundary condition. Therefore $\hat{\nu}$ represents the Casimir frequency limit, as in the analogous case of a nonzero air gap.

We now consider a *given* total energy density u and a total pressure $p = u/3$ expressed by Equation (18), with $\hat{p}$ and Π given by Equations (17) and (19), and $\hat{\nu}$ by Equation (23). The Casimir pressure $\hat{p}$ then becomes a function of the average frequency $\overline{\nu}$ for a given effective conductivity (22). This dependence is shown in **Figure 1** for the combinations Ag/Cu, Al/Cr, Ni/Cd, Ta/Pb and Sb/Bi of plate pairs:

- The left-hand part of the figure relates to large values of $\hat{x}$ for which $\hat{p}$ already includes the full pressure p_0, and for which there is a *vanishing* difference between the various plate combinations.

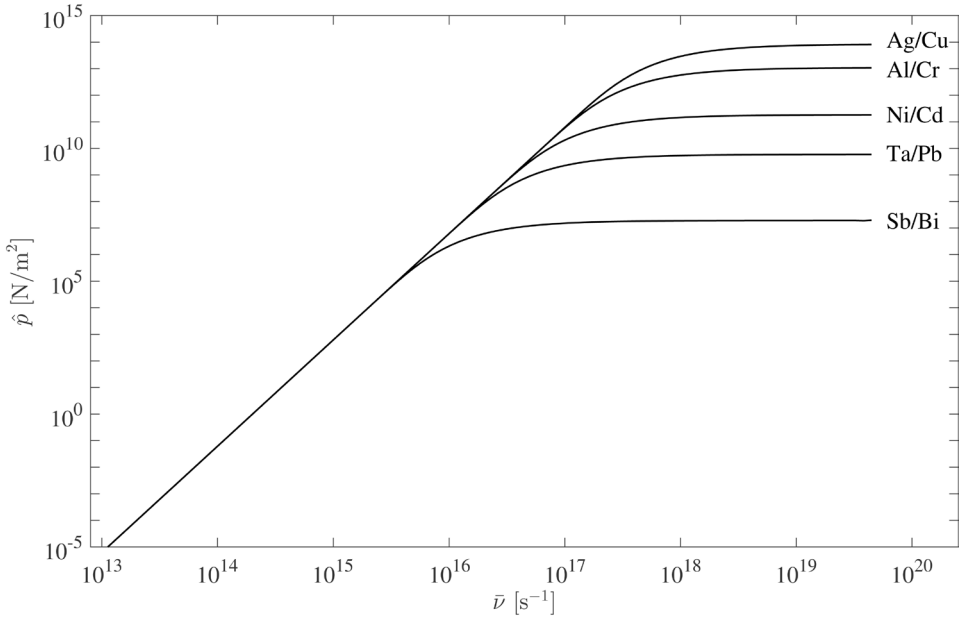

Figure 1. The Casimir pressure $\hat{p}$ as a function of various possible values of the so far unknown average frequency $\bar{\nu}$, for a number of metal plate pairs having different equivalent conductivities σ_{12}.

- The right-hand part of the same figure corresponds on the other hand to small $\hat{x}$ for which there is a difference due to the various effective resistivities. This part leads to a pressure $\hat{p}$ having the asymptotic limit

$$\hat{p}_\infty = \left(\pi h/3c^3\right)\hat{\nu}^4 \tag{24}$$

due to Equations (17)-(19), where the frequency limit $\hat{\nu}$ is given by Equation (23). Thus the limit $\hat{p}_\infty$, becomes *independent* of the average frequency $\bar{\nu}$, but depends strongly on the choice of plate material.

3.2. Proposed Experimental Investigations

A vanishing air gap has the advantage of a maximum Casimir force. The latter may even become recordable by means of a simple lever balance. This is gained at the expense of the following questions:

- To avoid effects from the air pressure, the measurements should take place in vacuo.
- To avoid microscopic matching between the metal structures, plate pairs of different metals should be chosen, as pointed out by Abramson [18] and Brodin [19]. Metals with any form of ferromagnetism should also be excluded.
- Even with a maximum Casimir force, other surface and sticking mechanisms may interfere with the measurements, such as the Van der Waals forces. To minimize this problem, many independent measurements with various plate combinations have to be made, to sort out the special behaviour on the skin depths represented by **Figure 1**.

3.2.1. Estimations from Existing Data

The possible relation between the Casimir force and the magnitude of the ZPE energy density at the orbit of the Earth, can be used in first estimations of this density:

- From the results of the previous Section 2.3.2, the density u_0 at the Earth's orbit has roughly been estimated to give rise to a total pressure $p_0 = u_0/3 = 10^3\ \mathrm{N\cdot m^{-2}}$. In **Figure 1** this would correspond to a parameter range around $\hat{p} = 10^3\ \mathrm{N\cdot m^{-2}}$ and $\bar{\nu} = 10^{15}\ \mathrm{s^{-1}}$.
- In earlier experiments with an air gap as small as $d = 6\times10^{-7}$ m, the net Casimir pressure (20) becomes $\hat{p} = 0.1\ \mathrm{N\cdot m^{-2}}$. With air gaps of this magnitude, the pressure $\hat{p}$ is then expected to be much smaller than

the pressure p_0 of the total spectrum. Due to **Figure 1** this then implies that $\bar{\nu}$ should in any case be larger than $10^{14}\ s^{-1}$.

3.2.2. Experiments on the Maximum Casimir Force

A detailed research on the total ZPE energy density in the laboratory is proposed here, and may be performed in a series of measurements of the Casimir pressure $\hat{p}$ with various plate combinations. With these values of $\hat{p}$ introduced into **Figure 1**, corresponding values of the average frequency would be found, as predicted by the theory. This leads to the following situation:

- If all obtained values of $\hat{p}$ point to the same value of $\bar{\nu}$ then the latter is with high probability to be identified as the average frequency of the ZPE spectrum of Equation (1).
- If the measured values of $\hat{p}$ would on the other hand point to different values of $\bar{\nu}$, the measured result is likely to be disturbed by other unknown effects.

4. Conclusions

The frequency spectrum of the zero Point Energy and its total density on cosmical scale are unknown in their details. The present complementary investigation includes a revised theory, forming the basis for determinations of this energy density. First, this concerns the values of the latter within the observable universe considered as an entity, as well as in subregions such as the galaxies including supermassive black holes. Second, experiments are proposed on the maximum Casimir force between metal plates with vanishing gap distance, with the purpose of determining the ZPE energy density in the laboratory, *i.e.* at the orbit of the Earth. These problems thus concern the ZPE on cosmical scale, with its interaction with gravity.

In the present approach the ZPE energy density is interpreted as a dark matter density, and its pressure gradient as a dark energy force density. The lack of emitted radiation is reconcilable with this picture. Thereby the crucial coincidence problem of equal orders of magnitude of dark matter and dark energy cannot be explained by the cosmological constant. This problem is instead resolved by the present variable concepts originating from the *same* ZPE photon gas balance.

An additional and different effect due to ZPE arises on the microscopical scale of elementary particles, as explained earlier by the author [20] [21]. This concerns the ZPE connection with the particle rest masses, as obtained from a nonzero divergence of the electric field strength in *vacuo*. It leads among other things to a composite boson, having the same basic properties and mass as the 125 GeV particle detected by CERN, but with *no* relation to the theory by Higgs.

References

[1] Planck, M. (1901) *Annalen der Physik*, **309**, 553-563. http://dx.doi.org/10.1002/andp.19013090310

[2] Casimir, H.B.G. (1948) *Proc. K. Ned. Akad. Wet.*, **51**, 793-795.

[3] Lamoreaux, S.K. (1997) *Physical Review Letters*, **78**, 5-8. http://dx.doi.org/10.1103/PhysRevLett.78.5

[4] Terletskii, Yu.D. (1971) Statistical Physics. North-Holland Publishing Comp., Amsterdam and London.

[5] Milonni, P.W. (1994) The Quantum Vacuum. American Press Inc., Harcourt Brace and Company, Boston, San Diego, New York, London, Sydney, Tokyo and Toronto.

[6] Loudon, R. (2000) The Quantum Theory of Light. 3rd Edition, Oxford University Press, Oxford.

[7] Lehnert, B. (2010) *International Review of Physics* (*IREPHY*), **4**, 237-241.

[8] Lehnert, B. (2013) *Journal of Plasma Physics*, **79**, 327-334. http://dx.doi.org/10.1017/S0022377812001055

[9] Lehnert, B. (2014) *Journal of Electromagnetic Analysis and Applications*, **6**, 319-327. http://dx.doi.org/10.4236/jemaa.2014.610032

[10] Lehnert, B. (2014) *Progress in Physics*, **10**, 76-78.

[11] Lehnert, B. (2015) *Journal of Modern Physics*, **6**, 448-452. http://dx.doi.org/10.4236/jmp.2015.64048

[12] Riess, A.G. and Turner, M.S. (2004) Scientific American, **290**, 50-55.

[13] Heitler, W. (1954) The Quantum Theory of Radiation. 3rd Edition, Clarendon Press, Oxford, 57, 409.

[14] Linder, E. and Perlmutter, S. (2007) *Physics World*, 24-30.

[15] Perlmutter, S. (2003) *Physics Today*, **56**, 53-60. http://dx.doi.org/10.1063/1.1580050

[16] Linde, A. (1994) *Scientific American*, 32-39.

[17] Ghez, A.M., Klein, B.L., Morris, M. and Becklin, E.E. (1998) *The Astrophysical Journal*, **509**, 678-686. http://dx.doi.org/10.1086/306528

[18] Abramson, N. (2012) Private Communication.

[19] Brodin, G. (2012) Private Communication.

[20] Lehnert, B. (2013) Revised Quantum Electrodynamics. Nova Science Publications, Inc., New York.

[21] Lehnert, B. (2015) *Journal of Modern Physics*, **6**, 2074-2079. http://dx.doi.org/10.4236/jmp.2015.614214

Journal of Modern Physics, 2016, 7, 1120-1131
Published Online June 2016 in SciRes. http://www.scirp.org/journal/jmp
http://dx.doi.org/10.4236/jmp.2016.710101

Stability Analysis of Electromagnetic Ordinary and Extraordinary Modes

N. Noreen[1], S. Zaheer[1], H. A. Shah[2]

[1]Forman Christian College, Chartered University, Lahore, Pakistan
[2]Government College University, Lahore, Pakistan
Email: nailanoreen@fccollege.edu.pk

Received 5 April 2016; accepted 16 June 2016; published 21 June 2016

Abstract

By using kinetic theory, we derived the general dispersion relations for ordinary mode (O-mode) and Extra-ordinary mode (X-mode) in anisotropic magnetized plasma. The effects of energy anisotropy, magnetic field to density ratio (Ω_0/ω_p) and the plasma beta $\beta_\parallel$ on the propagation characteristics, have been analyzed. The stability analysis and the growth rates have been presented. The marginal threshold condition for oscillatory and purely growing mode has been obtained for higher harmonics and we have also calculated their growth rates in terms of plasma beta $\beta_\parallel$ and energy anisotropy $T_\perp/T_\parallel$. The X-mode satisfies the instability condition according to difference of geometry with the O-Mode. These modes are important for spherical tokamaks, and their coupling leads to the generation of the Bernstein mode, which causes the heating effects.

Keywords

Instabilities, Growth Rate, Anisotropy

1. Introduction

The ordinary mode (O-mode) is a linearly polarized electromagnetic perpendicularly propagating wave, which propagates only when wave frequency is greater than the plasma frequency. The work is related to the electromagnetic cyclotron harmonic instability for its possible role in solar and interplanetary radio emission processes where the ratio ω_p/Ω_0 (where ω_p is the electron plasma frequency and Ω_0 is the electron cyclotron frequency) is relatively high *i.e.*, the ratio is of the order of 10 or can be as high as 50 or even 100 near 1 a.u. It may be useful for the heating and current drive mechanism in the spherical tori like the NSTX [1] and MAST [2] where the $\omega_p > \Omega_0$.

It is found that extraordinary mode (X-mode) power is not absorbed at the cyclotron resonance but uniquely at the upper hybrid resonance, displaced to the low field side of the cyclotron resonance. O-mode power, however,

How to cite this paper: Noreen, N., Zaheer, S. and Shah, H.A. (2016) Stability Analysis of Electromagnetic Ordinary and Extraordinary Modes. *Journal of Modern Physics*, **7**, 1120-1131. http://dx.doi.org/10.4236/jmp.2016.710101

is absorbed at the cyclotron resonance as well. The displacement of the upper hybrid resonance to the low field side with O-mode launch is significantly smaller than that with X-mode launch because of the lower densities produced by O-mode launch at the same microwave power level [3]. Hamasaki [4] [5] investigated the electromagnetic o-mode instability with perpendicularly propagating waves for a two temperature Maxwellian distribution function. Lee [6] studied the same mode in counterstreaming plasmas and showed that the ordinary mode became unstable as the magnetic field changed. Later Bornatici and Lee [7] worked on O-mode and determined that for counterstreaming plasmas an instability occurred if the streaming velocity exceeded a certain threshold value which can be below the required velocity to excite the electrostatic two-stream instability. They also concluded that whereas the perpendicular temperature stabilized the effect the parallel temperature enhanced the instability. Shivamoggi [8] also discussed the destabilization of the O-mode due to magnetic field and thermal effects. Ibscher *et al.* [9] investigated the nonresonant Wieble mechanism which can drive the O-mode unstable. They studied the instability on the basis of a threshold which gave the instability conditions and upper limits of the growth rate. Their problem was restricted for fundamental harmonic only. Iqbal *et al.* [10] studied the O-mode in degenerate anisotropic plasmas and proposed the excitation of a new banded type of instability which grew at some particular values of temperature anisotropy. Hadi *et al.* [11] also revised the analysis of the O-mode instability with Maxwellian parallel distribution coupled with thermal ring perpendicular distribution. They demonstrated that O-mode for thermal ring distribution may be excited for cyclotron harmonics as well as for the purely growing branch, depending on the value of the normalized ring speed. Lazar *et al.* [12] concluded that O-mode instability was driven by an excess of parallel temperature where $A = \frac{T_\perp}{T_\parallel} < 1$ for $\beta_\parallel > 1$. Vafin *et al.* [13] derived the analytical marginal instability condition for magnetized plasmas when charged particles were distributed in counter-streams with equal temperatures. They confirmed the O-mode instability at small plasma beta values, when the parallel counter-stream free energy exceeded the perpendicular bi-Maxwellian free energy. Farrell [14] presented a theory in which he described the direct generation of electromagnetic O-mode emission via mildly energetic electron beams in a highly dense and warm plasma.

In this manuscript, the energy anisotropic Heaviside distribution function is used for understanding the behavior of O-mode and X-mode. Such distribution function provides the detailed information about banded emission of O-mode instability. Such type of emission has been observed in space plasmas, where $\omega_p / \Omega_0 > 10$ e.g. solar wind. Satellite wave instruments commonly detect banded magnetospheric emissions between harmonics of the electron gyrofrequency in the outer magnetosphere [15]. This type of banded emission has been observed in the terristial magnetosphere. Frequency-banded electromagnetic waves up to 2000 Hz are observed concurrently with warm energy-banded ions in the low latitude auroral and sub-auroral zones during every large geomagnetic storm, observed by the FAST and DEMETER satellites. The appearance of the banded wave activity suggests that there may be distinct changes in the geospace system that characterize large magnetic storms [16].

Coupling of the O-mode and X-mode is a necessary tool for generation of the bernstein mode which is a powerful source of heating in spherical tokamaks. Literature shows the different methods of their coupling. But their unstable regions are a major problem in the coupling. Padoba *et al.* [17] first time demonstrated the conversion from an O-mode to an X-mode by probe measurements of amplitude and phase of the wave field in the conversion region. Cairns *et al.* [18] used sheared magnetic field to calculate the linear conversion of the O-mode to the X-mode. Because electron Bernstein waves are analyzed as possible candidates for heating spherical tokamaks. Ram *et al.* [19] developed a kinetic model for studying the energy flow transfer between the X-mode, the O-mode and the EBW in the mode conversion region in the vicinity of the cold plasma upper hybrid resonance. Sodha *et al.* [20] derived the dispersion relation for modulational instabilities of a Gaussian electromagnetic beam propagating in the two modes: O-mode and X-mode, along the externally applied d.c. magnetic field, in a homogeneous magnetoplasma.

The layout of this paper is as follow. Section 2 gives information about the mathematical model of O-mode and X-mode. This section presents the stability analysis and calculates the maximum growth rate. A brief summary of results and discussions is given in Section 3. Section 4 will conclude the results.

2. Mathematical Model

2.1. The Ordinary Mode (O-Mode)

By using kinetic model, the general dispersion relation for perpendicularly propagating O-mode with $k_\parallel = 0$ in

collionless plasma is as follow [21]

$$\frac{c^2k_\perp^2}{\omega^2}=1+\frac{2\pi}{\omega}\omega_p^2\int_{-\infty}^{\infty}p_\parallel^2\mathrm{d}p_\parallel\int_0^\infty\mathrm{d}p_\perp\chi_1\sum_{n=-\infty}^{\infty}\frac{\left[J_n(z)\right]^2}{(\omega-n\Omega_0)}$$
$$-\frac{2\pi}{\omega^2}m\omega_p^2\int_{-\infty}^{\infty}\mathrm{d}p_\parallel\int_0^\infty p_\perp\mathrm{d}p_\perp\left[\frac{p_\parallel}{p_\perp}\left(\frac{p_\parallel}{m}\frac{\partial f_0}{\partial p_\perp}-\frac{p_\perp}{m}\frac{\partial f_0}{\partial p_\parallel}\right)\right] \tag{1}$$

Here $\chi_1=\dfrac{\partial f_0}{\partial p_\perp}$ and f_0 is distribution function.

The energy anisotropic Heaviside distribution function is [22] [23]

$$f_0=\frac{1}{2\pi\hat{p}_\perp}\delta(p_\perp-\hat{p}_\perp)\frac{1}{2\hat{p}_\parallel}H(\hat{p}_\parallel^2-p_\parallel^2) \tag{2}$$

$$p_{\perp,\parallel}^2=mT_{\perp,\parallel}$$

where $T_\perp$ and $T_\parallel$ are the effective temperatures in the perpendicular and parallel directions defined as follows

$$T_\perp=d^3p\frac{p_\perp^2}{2m}F(p_\perp^2,p_\parallel)$$

$$T_\parallel=2d^3p\frac{p_\parallel^2}{2m}F(p_\perp^2,p_\parallel)$$

and their corresponding integrations yields the results

$$T_\perp=\frac{p_\perp^2}{2m},\ T_\parallel=\frac{p_\parallel^2}{3m}$$

Using Equations (1) and (2), we obtain

$$\frac{c^2k_\perp^2}{\omega^2}=1-\frac{\omega_p^2}{\omega^2}\left[1+\sum_{n=1}^{\infty}\frac{\eta_o}{A}\left(\frac{2n^2\Omega_0^2}{\omega^2-n^2\Omega_0^2}\right)\right] \tag{3}$$

where

$$\eta_o=2\sum_{n=1}^{\infty}\hat{z}J_n(\hat{z})J_n'(\hat{z})$$

$$\hat{z}=\frac{k_\perp\hat{v}_\perp}{\Omega_0}$$

$$A=\frac{T_\perp}{T_\parallel}=\frac{\hat{v}_\perp^2}{\hat{v}_\parallel^2}$$

For principle harmonic *i.e.*, $n=1$, we get the following linear dispersion relation

$$\omega^4-\left(\Omega_0^2+c^2k_\perp^2+\omega_p^2\right)\omega^2+\omega_p^2\Omega_0^2\left(\frac{\hat{z}^2}{A\beta_\parallel}+1-\frac{\eta_o}{A}\right)=0 \tag{4}$$

where $\beta_\parallel=\dfrac{\omega_p^2v_\parallel^2}{c^2\Omega_0^2}$.

We note that $\left(\dfrac{\hat{z}^2}{A\beta_\parallel}+1-\dfrac{\eta_1}{A}\right)<0$ is the condition for instability.

However, for higher harmonics, the linear dispersion relation takes the form

$$\frac{\omega^2}{\omega_p^2}-\frac{\hat{z}^2}{A\beta_{\|}}=1+\sum_{n=1}^{\infty}\frac{\eta_o}{A}\left(\frac{2n^2\Omega_0^2}{\omega^2-n^2\Omega_0^2}\right) \tag{5}$$

2.2. The Extra-Ordinary Mode (X-Mode)

The general dispersion relation of the X-mode is as

$$\frac{c^2k_{\perp}^2}{\omega^2}=1+\frac{2\pi}{\omega}\omega_p^2\int_{-\infty}^{\infty}p_{\|}^2\mathrm{d}p_{\|}\int_0^{\infty}\mathrm{d}p_{\perp}\chi_1\sum_{n=-\infty}^{\infty}\frac{p_{\perp}J_n'^2(z)}{m(\omega-n\Omega_0)} \tag{6}$$

By using the simple mathematical analysis, the dispersion relation of the X-mode is

$$\frac{c^2k_{\perp}^2}{\omega^2}=1-\frac{\omega_p^2}{\omega^2}\sum_{n=1}^{\infty}\eta_x\left(\frac{2\omega^2}{\omega^2-n^2\Omega_0^2}\right) \tag{7}$$

In terms of A and $\beta_{\|}$, the relation can be expressed as

$$\frac{\omega^2}{\omega_p^2}-\frac{\hat{z}^2}{A\beta_{\|}}=\sum_{n=1}^{\infty}\eta_x\left(\frac{2\omega^2}{\omega^2-n^2\Omega_0^2}\right) \tag{8}$$

where

$$\eta_x=\left[2\hat{z}J_n'(z)J_n''(z)+2\left[J_n'(z)\right]^2\right]$$

3. Results and Discussion

In this section we will discuss the stability condition and calculate the growth rate for different combinations of A and $\beta_{\|}$.

We first numerically discussed the results obtained for the O-mode from Equation (3). Lee [12] has calculated O-mode for three harmonics with the Maxwellian distribution function and concluded that the mode is stable for the Maxwellian distribution. Ichimaru [24] has discussed the O-mode for higher harmonics with nonlocal effects and confirmed the existence of Azbel-Karner resonance when the wave frequency is multiple of electron cyclotron frequency.

The banded emission is observed in plots of A vs $\hat{z}$ in the case of energy anisotropic Heaviside distribution **Figure 1**. This banded emission strongly agrees with the results of Iqbal *et al*. [10] where the anisotropic Fermi Dirac distribution function was used. The wave provides a wide range of stable and unstable regions.

In **Figure 1**, the relation of $\beta_{\|}$ and anisotropy A is plotted, it provides a marginal threshold value. The dotted curve shows that $\frac{\hat{z}^2}{A\beta_{\|}}+1=\frac{\eta_O}{A}$, this curve plays the role of threshold value between stable and unstable O-mode. Below the dotted curve the condition $\frac{\hat{z}^2}{A\beta_{\|}}+1<\frac{\eta_O}{A}$ satisfies and mode is unstable which is presented by dashed curve. Above that dotted curve the condition is $\frac{\hat{z}^2}{A\beta_{\|}}+1>\frac{\eta_O}{A}$, it means that there is a stable region *i.e*., the solid curve. The comparison of plots defines that for small $\hat{z}^2$ the $\beta_{\|}$ contains large value, this is the region where $\beta_{\|}$ is large enough to provide a growth rate much larger than the oscillatory frequency $\omega_r \ll \omega_i$ so these results strongly agree with the environment *i.e*., solar wind. For large anisotropy, $T_{\|}/T_{\perp}>10$, or for large $\beta_{\|}>10$, the O-mode instability is faster than the firehose instability. Larger values of $\beta_{\|}$ means low magnetic fields or more dense and hotter plasma, these conditions can come across at different altitudes in the solar wind regime.

In series of **Figures 2-5**, growth rates of higher harmonics have been plotted. For analytical threshold we consider complex form $\omega^2=(\omega_r+i\omega_i)^2$, in plots the solid lines represent the ω_r and dashed shows the ω_i, where $\beta_{\|}=4.0$ for **Figures 2-5**.

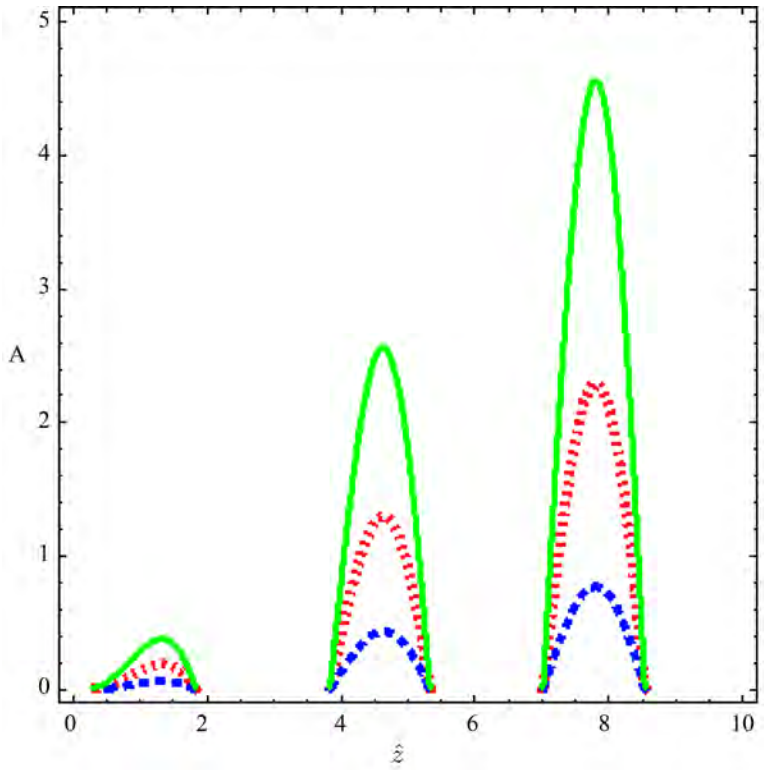

Figure 1. Marginal stability condition.

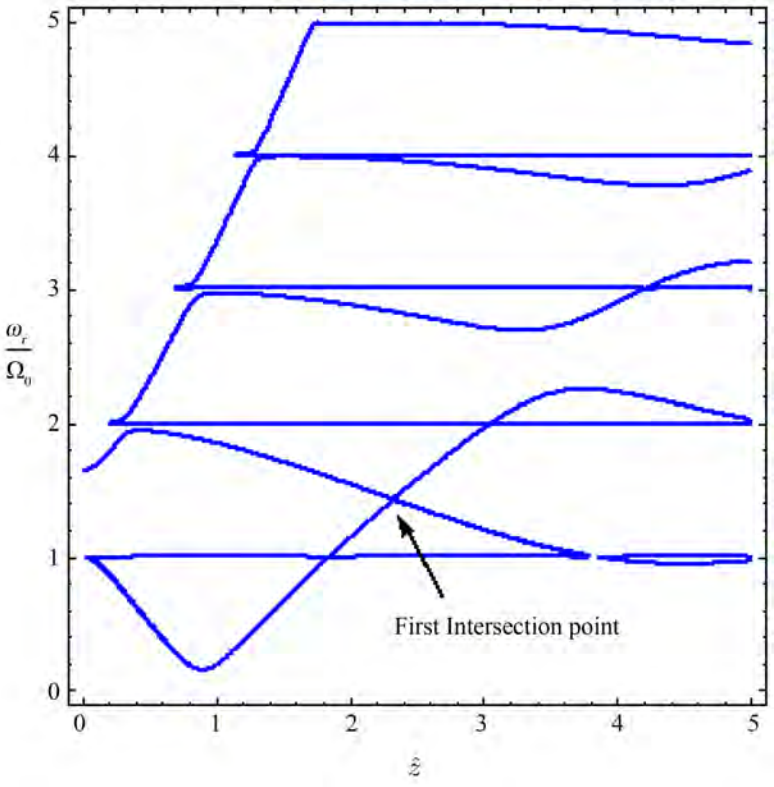

Figure 2. $A = 0.1,\ \ \Omega_0^2/\omega_p^2 = 0.37$.

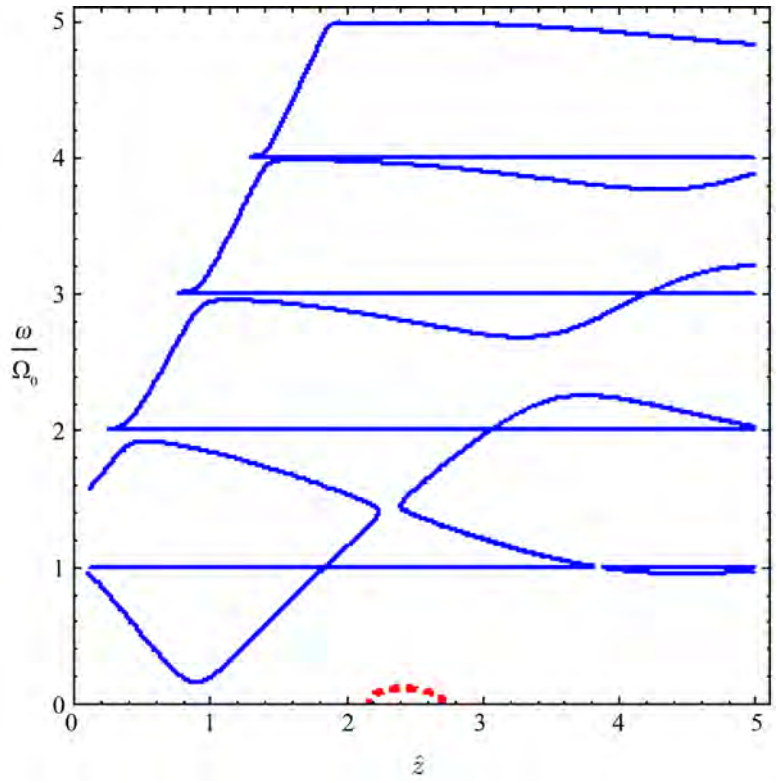

Figure 3. $A = 0.1 \quad \Omega_0^2/\omega_p^2 = 0.43$.

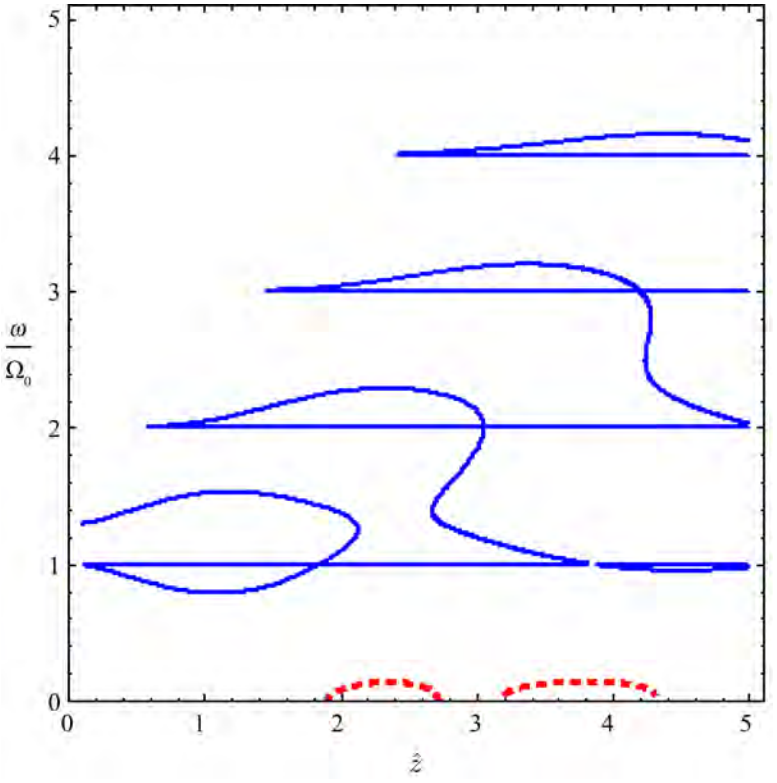

Figure 4. $A = 0.6 \quad \Omega_0^2/\omega_p^2 = 0.9$.

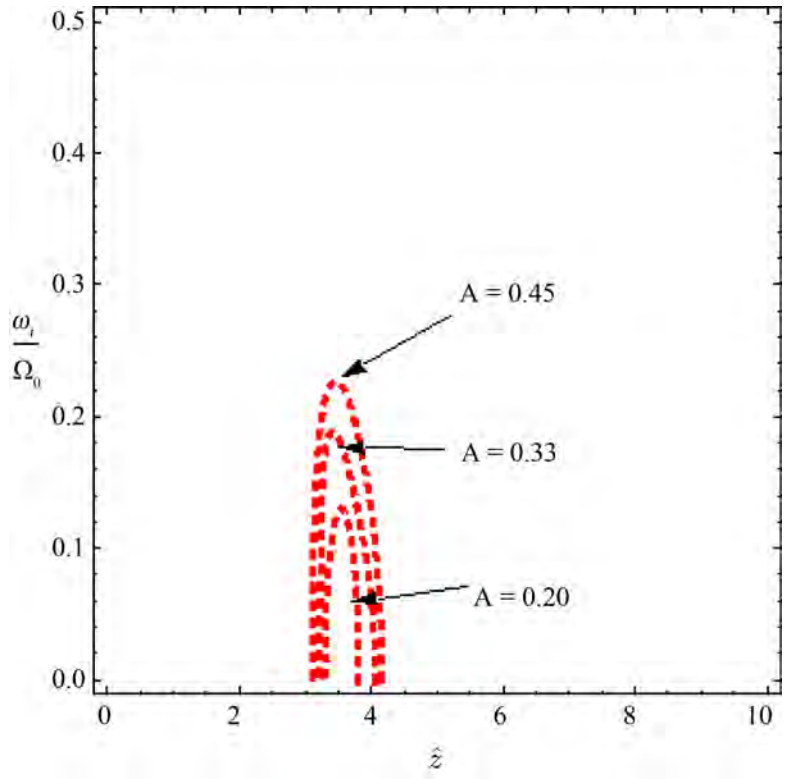

Figure 5. Growth rate for different A.

In **Figure 2**, there is a s table form of O-mode but at $A = 0.1$ and $\Omega_0^2/\omega_p^2 = 0.37$ the harmonics start to intersect with each other.

Figures 3-5 show the real part of dispersion relation and dependence of O-mode on magnetic field. As we increase values of magnetic field, $\Omega_0^2/\omega_p^2 = 0.43$ it becomes unstable and the first unphysical state generates as in **Figure 3**. These results also satisfy the marginal instability condition as discussed earlier numerically. In above plots, noticeable thing is the value of $A = 0.1$. The parallel streaming is dominating in O-mode and playing a role to destabilize the wave. The plasma beta is greater than one so these effects satisfy the high plasma beta regimes.

On further increasing the magnetic field, unstable regions are obtained and at $\Omega_0^2/\omega_p^2 = 0.6$ and A = 0.9, the wave becomes totally unstable as in **Figure 4**.

The growth rate shows that parallel streaming responsible to grow the wave. The complex part of the dispersion relation tells that the wave is growing in the gaps. **Figure 5** shows the growing parts of the first two gaps.

The O-mode instability divides in two branches for complex ω. First branch is oscillatory when $\omega_i = 0$ and second branch is aperiodic or purely growing when $\omega_r = 0$ as in **Figure 6**. Further increasing the value of parallel streaming, the aperiodic branch is obtained. For oscillatory branch the magnetic field plays a role to destabilize the wave and increase the growth of the wave.

For second branch, which is aperiodic or purely growing, the trend totally reverses . The growth rate increases with the decreasing value of A. The result proves that the anisotropy stabilizes the purely growing part. **Figure 7** shows the increasing growth rate of aperiodic mode with decreasing value of A. The noticeable thing is that this part also satisfies the condition of the firehose instability *i.e.*, $T_{\parallel} > T_{\perp}$ and $\beta_{\parallel} > 1$. The purely growing wave is also called non-propagating firehose instability [25] The study of variation of anisotropy tells us that with the increasing value of A, the growth rate is also increases that means by increasing value of A destabilizes the wave. When $T_{\parallel} > T_{\perp}$ and $\beta_{\parallel} > 1$, then wave becomes more unstable this result proves that O-mode instability satisfies the condition of the firehose instability.

For number of harmonics, the X-mode is also unstable but for this mode perpendicular temperature is

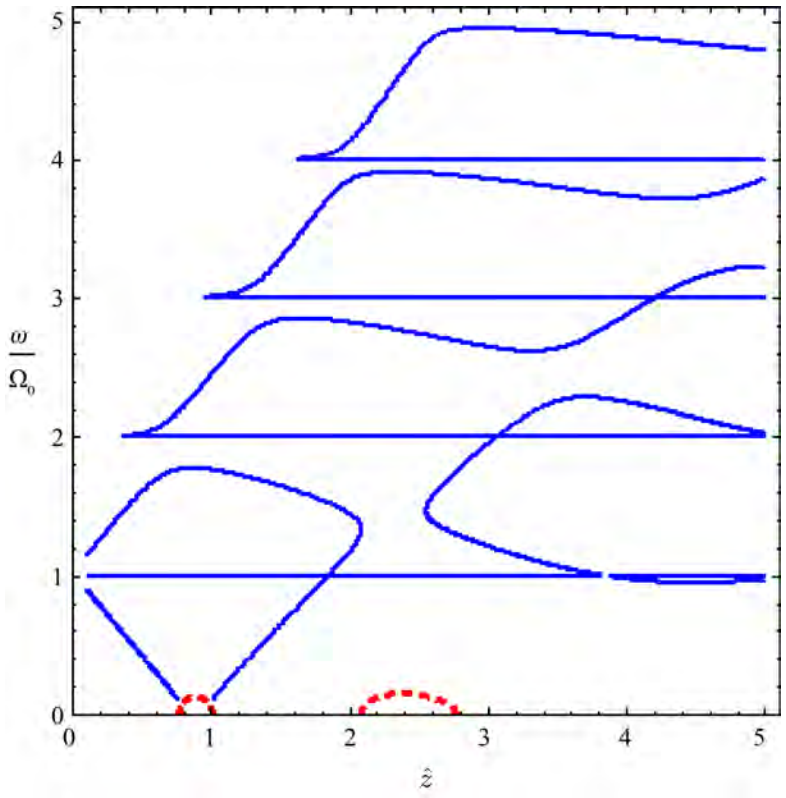

Figure 6. $A = 0.09 \quad \Omega_0^2/\omega_p^2 = 0.9$.

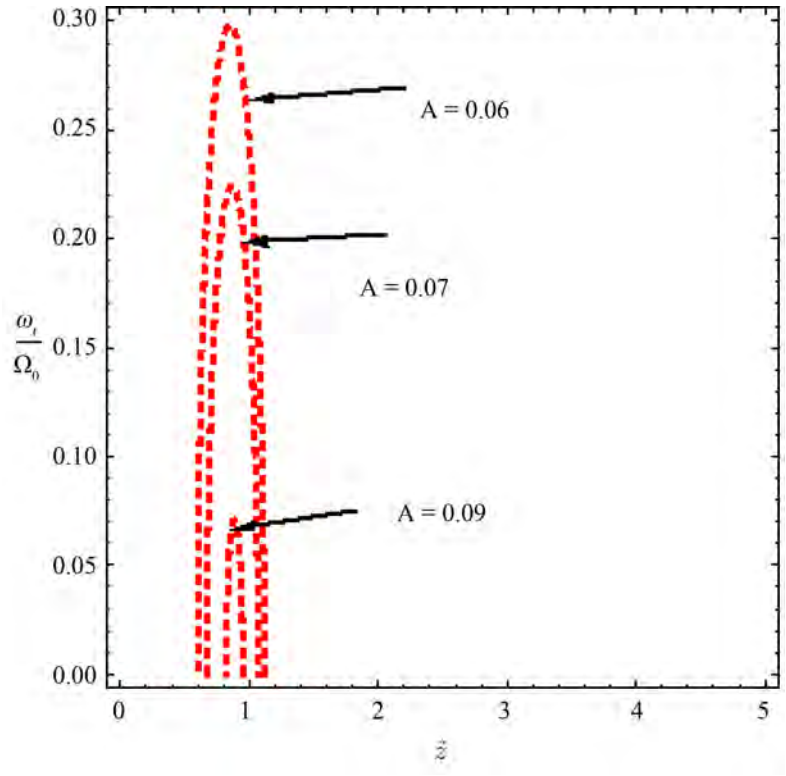

Figure 7. Growth rate for aperiodic branch.

dominating. The wave becomes unstable for larger value of A. In **Figure 8** when $A = 6.5$, the wave is stable. But after that when $A = 6.96$, the harmonics overlap each other and wave starts to be unstable as in **Figure 9**.

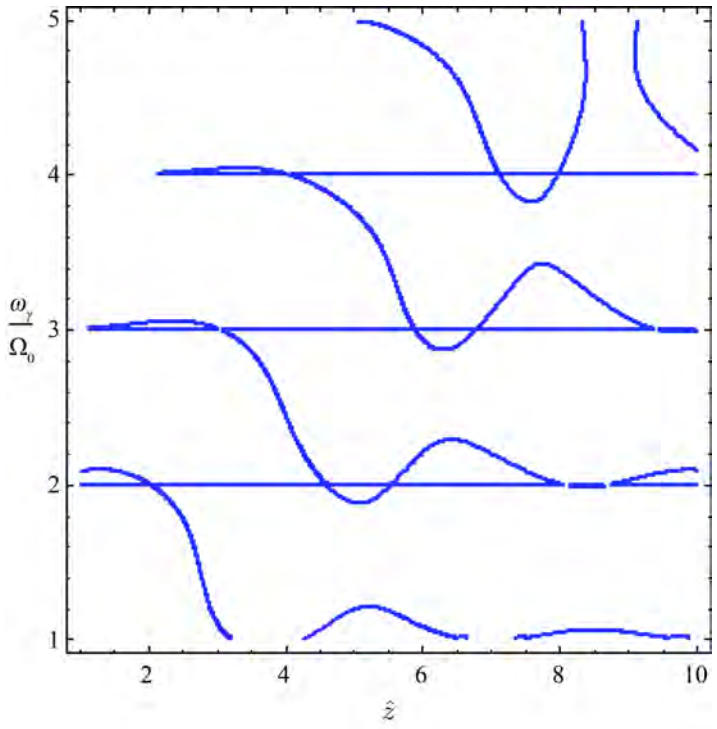

Figure 8. $A = 6.5 \quad \Omega_0^2/\omega_p^2 = 0.09 \quad \beta = 4.0$.

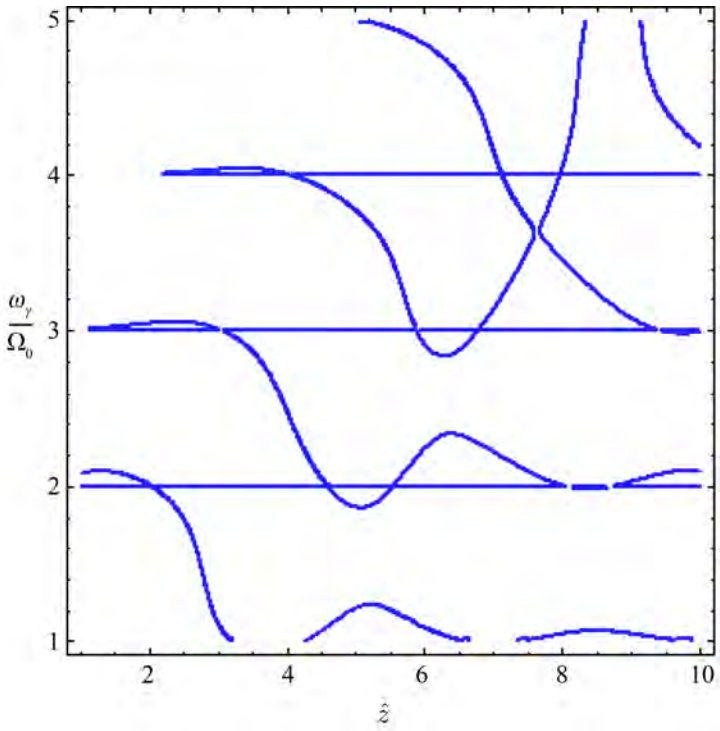

Figure 9. $A = 6.69 \quad \Omega_0^2/\omega_p^2 \quad \beta = 4.0$.

On further increasing the value of A the mode becomes more unstable as in **Figure 10** the value of A is 8 and $\Omega_0^2/\omega_p^2 = 0.09$. The solid curves show the real part of the wave and dashed curves show the growth of the said wave. The increasing value of A shows that in X-mode instability perpendicular streaming is dominating. At A = 11, it becomes totally unstable **Figure 11**.

Figure 12 discusses that the growth rate increases with the increasing value of anisotropy. Anisotropy destabilizes the X-mode, the X-mode follows the same trend as that of the O-mode.

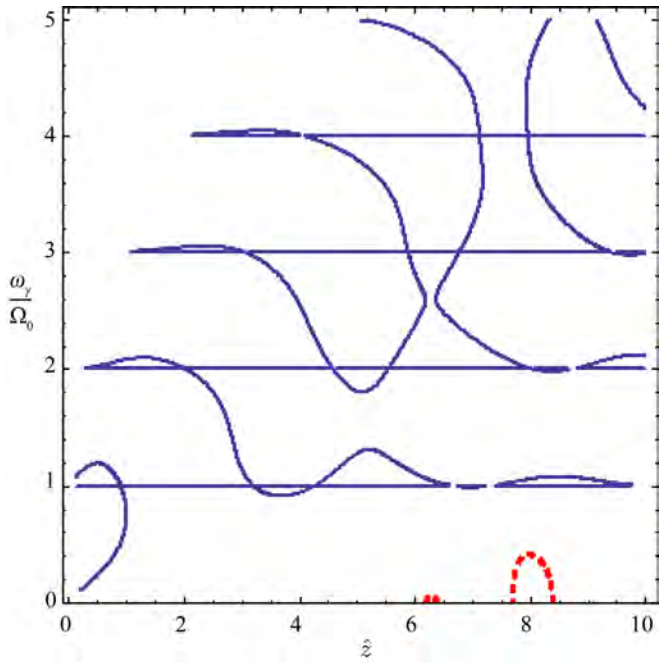

Figure 10. $A = 8.0 \quad \Omega_0^2/\omega_p^2 = 0.09 \quad \beta = 4.0$.

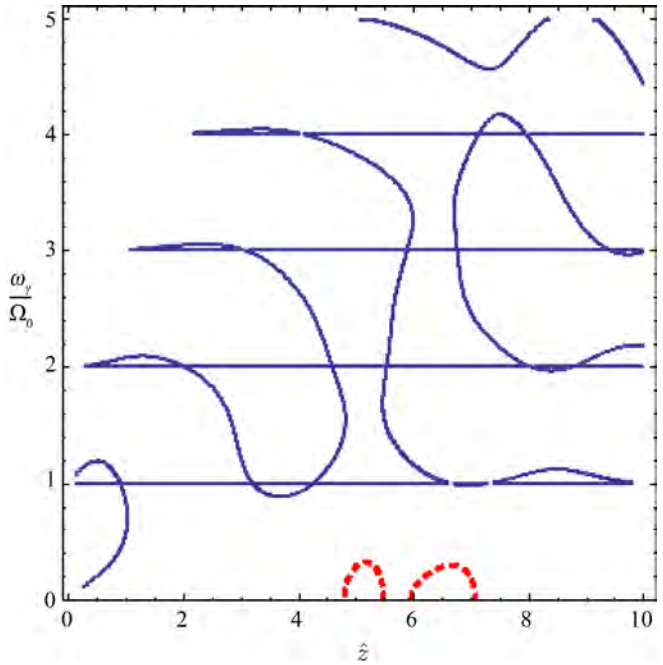

Figure 11. $A = 11 \quad \Omega_0^2/\omega_p^2 = 0.09 \quad \beta = 4.0$.

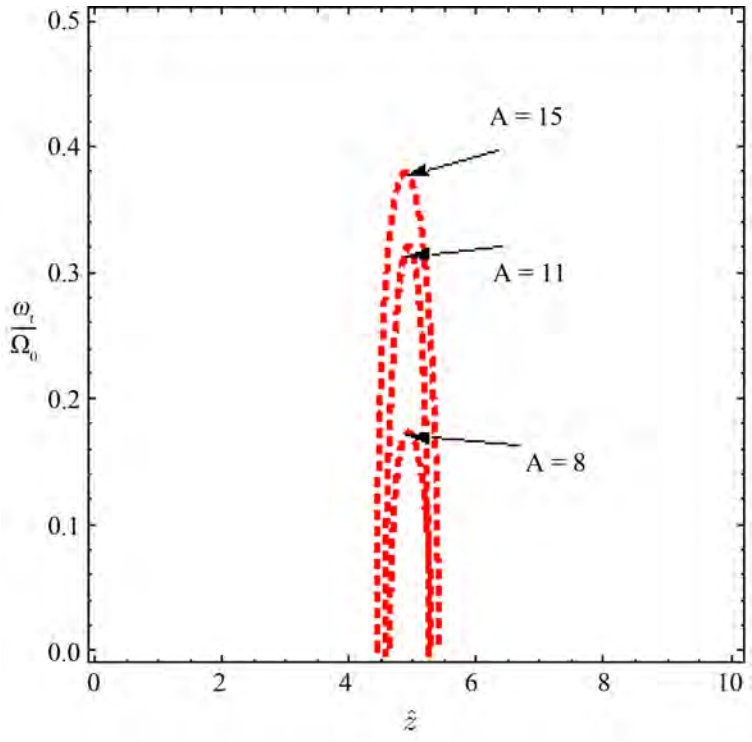

Figure 12. Growth rate of X-mode for different values of A.

4. Conclusion

O-mode instability, for principle harmonic, depends upon the magnetic field even it is weaker. The instability generates due to temperature anisotropy and free energy of anisotropy converted in the magnetic induction which is the reason of growing wave. The growth rate varies directly with the value of ratio of anisotropy. Here we have calculated the marginal threshold condition in form of plasma parameters A and $\beta_{\|}$ for principle harmonic. For higher harmonics, oscillatory branch satisfies the statement and purely growing part inverts the condition. It varies inversely with the anisotropy. The oscillatory and purely growing mode both satisfies the conditions of firehose instability *i.e.*, $T_{\|} > T_{\perp}$ and $\beta_{\|} > 1$ as $B_0 \| E$ in O-mode. The stability analysis of the X-mode tells that perpendicular temperature is dominating. The mode is unstable for $T_{\perp} > T_{\|}$, according to geometry of the X-mode that is $B_0 \perp E$. Coupling of these two modes converts them into the Bernstein mode which is responsible of heating effects in tokamak. The O-X conversion is the method of achieving the Bernstein mode.

Acknowledgements

Authors are thankful to the Department of Physics, FC College (A Chartered University) for financial assistance.

References

[1] Ono, M., *et al*., (2004) *Nuclear Fusion*, **44**, 452. http://dx.doi.org/10.1088/0029-5515/44/3/011

[2] Akers, R.-J., *et al*., (2002) *Physics of Plasmas*, **9**, 3919. http://dx.doi.org/10.1063/1.1490928

[3] Whaley, D.R., *et al*. (1992) *Nuclear Fusion*, **32**, 757. http://dx.doi.org/10.1088/0029-5515/32/5/I04

[4] Hamasaki, S. (1968) *Physics of Fluids*, **11**, 12.

[5] Hamasaki, S. (1968) *Physics of Fluids*, **6**, 11.

[6] Lee, K.F. (1969) *Physics Review*, **1**, 181.

[7] Bornatici, M. and Lee, K.F. (1971) *Physics Fluids*, **13**, 42.

[8] Shivamoggi, B.K. (1982) *Astrophysics and Space Science*, **82**, 481-483. http://dx.doi.org/10.1007/BF00651455

[9] Ibschar, D., Lazar, M. and Schlickeiser, R. (2012) *Physics of Plasmas*, **19**, 072116. http://dx.doi.org/10.1063/1.4736992

[10] Iqbal, Z., Hussain, A., Murtaza, G. and Tsintsadze, N.L. (2014) *Physics of Plasmas*, **21**, 032128. http://dx.doi.org/10.1063/1.4870007

[11] Hadi, F., Yoon, P.H. and Qamar, A. (2015) *Physics of Plasmas*, **22**, 022112. http://dx.doi.org/10.1063/1.4907657

[12] Lazar, M., Schlickeiser, R., Poedts, S., Stockem, A. and Van, S. (2014) http://arxiv.org/abs/1411.1508

[13] Vafin, S., Schlickeiser, R. and Yoon, P.H. (2014) *Physics of Plasmas*, **21**, 104504. http://dx.doi.org/10.1063/1.4897373

[14] Farrell, W.M. (2001) *Journal of Geophysical Research*: *Space Physics*, **106**, 15701-15709. http://dx.doi.org/10.1029/2000JA000156

[15] Colpitts, C.A., Cattell, C.A., Kozyra, J.U. and Parrot, M. (2012) *Journal of Geophysical Research*: *Space Physics*, **117**. http://dx.doi.org/10.1029/2011JA017329

[16] LaBelle, J., Ruppert, D.R. and Treumann, R.A. (1999) *Journal of Geophysical Research*, **104**, 293-303. http://dx.doi.org/10.1029/1998JA900050

[17] Podoba, Y.Y., Laqua, H.P., Warr, G.B., Schubert, M., Otte, M., Marsen, S. and Wagner, F. (2007) *Physical Review Letters*, **98**, 255003. http://dx.doi.org/10.1103/PhysRevLett.98.255003

[18] Cairns, R.A. and Lashmore-Daviesa, C.N. (2000) *Physics of Plasmas*, **7**, 4126-4134.

[19] Ram, A.K., Bers, A. and Lashmore-Davies, C.N. (2002) *Physics of Plasmas*, **9**, 409-418. http://dx.doi.org/10.1063/1.1429634

[20] Sodha, M.S., Sharma, R.P., Maheshwari, K.P. and Kaushik, S.C. (1977) *Plasma Physics*, **20**, 585. http://dx.doi.org/10.1088/0032-1028/20/6/009

[21] Bashir, M.F. and Murtaza, G. (2012) *Brazilian Journal of Physics*, **42**, 487-504.

[22] Yoon, P.H. and Davidson, R.C. (1987) *Physical Review A*, **35**, 2718-2721.

[23] Bashir, M.F., Noreen, N., Murtaza, G. and Yoon, P.H. (2014) *Plasma Physics and Controlled Fusion*, **56**, Article ID: 055009.

[24] Ichimaru, S. (1973) Basic Principles of Plasma Physics: A Statistical Approach. Addison-Wesley Publishing Company, New York, 104.

[25] Lazar, M., Poedts, S., Schlickeiser, R. and Ibscher, D. (2014) *Solar Physics*, **289**, 369-378. http://arxiv.org/abs/1307.0768

Journal of Modern Physics, 2016, 7, 1132-1137
Published Online June 2016 in SciRes. http://www.scirp.org/journal/jmp
http://dx.doi.org/10.4236/jmp.2016.710102

The Nature, Origin and Propagation of the Electric Field: A New Insight to Fundamental Physics

Narahari V. Joshi

Department of Physics, University of Los Andes, Merida, Venezuela
Email: joshi@ula.ve

Received 25 April 2016; accepted 16 June 2016; published 21 June 2016

Abstract

The nature, origin and propagation of the electric field are discussed for the first time on the basis of the presence of vibrating strings in the space and their self-excitation process. It is considered that the electron is formed from strings and it has specific vibrational frequency. This excites the strings which are close by with the self-excitation process. This procedure which is continuous in the space according to the symmetry and vibrational energy in the form of waves spreads near the electron (or the charge particle), which behaves and carries energy known as electric field. In fact, the electron does not continuously emit energy in any form but induces (or excites) and organizes energy in a self-sustain vibrational form and extends in three dimensional space. Only on the basis of the presence of strings (vibrational energy), several electromagnetic phenomena have been explained in a consistent way. The vibrational nature of the electric field is also examined with the help of Stark effect and X-ray diffraction approach to support the present view.

Keywords

Electric Field, Strings as Compact Liquid, Self Excitation

1. Introduction

In spite of several years of research work, important aspects of electric field are not well understood, particularly its nature and how it propagates in vacuum. According to the accepted theory [1] a charge particle like the electron emits energy continuously in some form. Following laws of symmetry, it is propagated in a spherical shape. At a time t the sphere of radius ct is filled with electric energy where c is the velocity of light. After time dt the sphere of radius c(t + dt) is filled with energy. The most important aspect is that the intensity of the field within

How to cite this paper: Joshi, N.V. (2016) The Nature, Origin and Propagation of the Electric Field: A New Insight to Fundamental Physics. *Journal of Modern Physics*, **7**, 1132-1137. http://dx.doi.org/10.4236/jmp.2016.710102

the radius ct is not altered and extra energy or field is observed in the outer shell of thickness cdt. It is worth mentioning that during this process the mass of the electron is the same. This means that energy is not conserved and the electron or the charge particle cannot emit energy (or field) continuously.

This observation has no explanation on the basis of classical electrodynamics. However, in the frame work of Quantum Field Theory (QFT) some explanation is provided. According to it (QFT), there exist intermediate energy states. The sum of these states forms an integral which includes all energy states and momentum. Integrals related with momentum become divergent. The renormalization route converts them into virtual (off shell) particles. This results in absorption and emission of virtual particles by the electron (ultraviolet divergence). This hypothesis based on QFT theory helps to explain the conservation of the charge of the electron [2].

A virtual particle is an explanatory conceptual entity that is originated in mathematical calculations in quantum field theory and it is a confusing subject. This is a highly speculative assumption and the absorption of the virtual particle is neither conformed theoretically nor experimentally. Sometimes, it is considered as disturbances in the field. Meanwhile, the absorption of the field in vacuum by vibrating strings and its feedback process given by Van der Pol nonlinear differential equation do explain satisfactorily the conservation of charge and mass [3].

The other very significant and fundamental aspect is that the charge particle (positive or negative) forms equivi-potential circles (or points) and a field of lines (or sometimes field of force) are directed from the positive charge outwards in the space meanwhile for the negative charge the field of lines are attracted towards it [1]. This explains the charge distribution in three dimensional space and the force can be calculated at any point. However, it is never discussed why the field is directed towards the negative charge and it originates from the positive charge. Meanwhile, the equi-potential surfaces have exactly the same properties. This contradiction, which forms the base for electromagnetism, is completely overlooked. Recently, this paradox has been discussed due to the motion of organized vibrating strings which not only explains the detail mechanism of formation of equi-potential circles but also elucidates why they have clock wise and anti-clock wise properties [3] [4]. Moreover, it provides information about how and why the forces of attraction and repulsion are originated in between two charge particles *i.e.* force at a distance [4].

Recently, some work has been carried out in this direction and Gauss law has been re-examined and it is established that the energy does absorb in vacuum and space is filled with an excitable medium [5]. This is also confirmed by Casimir effect [6] which is associated with zero point energy of quantized field. The direct experimental confirmation for the presence of energy in vacuum has been investigated and several experimental data and patents have been reported [7]-[9]. Important aspect is that vacuum energy can be converted into electromagnetic energy and not any other form. According to the quantum field theory also, the field can be visualized assuming that the space is filled with interconnecting vibrating units similar to strings.

A re-examination of Gauss law [5] also shows that the absorption of energy is roughly proportional to the inverse of the square of the distance from the electron, indicating that a considerable energy is absorbed very close to the electron. This has a vibrational nature and it partly provides a feed back to the vibrational energy of the electron [3] [5] and in some way gives pressure on the electron which can be associated with the Poincare stress. In fact, the details and the origin for the stress has not received due attention [1]. However, the absorption of energy by strings very close to the electron does provide a possible explanation.

Moreover, the above point of view, namely the considerable absorption of vibrational energy associated with strings very close to the electron does explain the cloudy nature around the electron. The density of the cloud varies from point to point very close to the electron and this cloud moves with the electron. A careful measurement shows that the intensity of the electric field is slightly altered because of the shielding effect of clouds. In fact, the distribution of charge of the electron can be written as

$$\alpha_{\text{observed}} = \alpha_{\text{naked}} + \alpha_{\text{cloud}} \tag{1}$$

where α_{observed} is the charge of the electron that is observed (1.6×10^{-19} Coulombs); α_{naked} is the true charge which is not measured and α_{cloud} is the charge distribution around the central part. According to the quantum mechanical model, at the central part of the electron the cloud density is maximum, while it reduces considerably outside.

This origin for the presence of clouds near the electron has never been examined critically. However, in the frame work of quantum field theory, it is explained on the basis of ultra-violet divergence of fields by using renormalization process. According to it, the contribution in the divergent integrals associated with the correction

term to the mass or charge of the particle. However, the most important aspect namely the origin for α_{cloud}, the correction term to the cloud of electron, is not addressed in QFT [2]. It is worth mentioning that the point of view expressed above indicates that the origin for clouds lies in the vibrational energy very close to the electron absorbed by the mechanism mentioned earlier [5].

Recently, several fundamental aspects of electromagnetic fields such as Maxwell's equations [10], Lorentz force [11] electrostatic attraction or repulsion [4] etc. have been re-examined on the basis of strings as a compact incompressible liquid. According to the string theory the space is filled with small vibrating units of the order of Planck's length (10^{-33} cm). Several interesting aspects of the electric and magnetic fields are explained with branes, which are a physical entity that generalizes a point particle to higher dimensions. D_1 brane is like a string, it vibrates and it also has quantum fluctuations. Several properties related with elementary particles have been explained with the extra dimensions of branes. According to the string theory, the D-brane plays a crucial role. It is assumed that it carries the electric or magnetic field and open strings couple to the electromagnetic field at their end points. Maxwell fields are associated with the attachment of the open string and D-brane (in an extra dimension). Even though a considerable work has been reported in this direction, a totally different approach is taken in the present work. It is worth mentioning that in this discussion only the presence of strings in the vacuum is taken into account as vibrating units and no other aspects of the string theory such as the presence of branes of any dimension (D_0 (point), D_1 (line), D_2 (surface) and so on) are considered. Quantum harmonic oscillators (or vibrating units) in space permit us to consider conversion of energy into kinetic, potential and also in storage form. The direct consequence of it is that the space becomes an excitable medium through which the energy in some form can be transported (not by flow, motion or stream of any kind) by a non-conventional mechanism like propagation of induced "self-excited vibrations" in strings.

The other significant aspect of string theory is that particles are not point like. Instead they are vibrational modes. This means that elementary particles are formed from a specific arrangement of vibrating strings and therefore all particles have vibrating nature with specific frequency. In addition to this, the electron has a rotational motion (or spin). By considering the vibrational and rotational motions of electron, several properties of electromagnetism have been coherently explained earlier just by taking into account strings in a compact form of dry liquid [3]-[5] [10] [11]. However, it differs from the conventional liquid as every element of it (vibrating string) has significant amount of energy in a storage form which is convertible into kinetic and potential energy. As mentioned earlier because of the feedback mechanism based on Van der Pol equation, the energy is conserved due to self-sustained vibrations. This includes the conservation of the charge and mass (both structural and electromagnetic) of the electron and details have been discussed extensively earlier by Joshi [3].

2. Self-Excited Vibrations and Propagation

In fact, as mentioned earlier, the electron does not emit energy or field. The vibrations associated with electrons induce excitations in vibrating strings with which the space is filled. A self-excitation process [12]-[14] of vibrational energy advances in 3-D space and gives the impression that the electron or charge particle is emitting continuously energy or electric field in the space.

Self- excited systems begin to vibrate with their own accord under special conditions [12]. The energy required for these vibrations is obtained from a uniform source associated with the system itself (in the present case, vibrational energy of strings) and there is some inherent mechanism which supplies energy to start and maintain harmonic oscillations with certain frequency. If the system is disturbed for any reason the forces are created and they may lead the system away from the equilibrium position and then it will start oscillations provided that the conditions are suitable. When the cause for self-oscillations stops, the forces related with it disappear.

It is known from string theory that strings behave like quantum harmonic oscillators with quantum fluctuations (zero point energy) [15] and form a self-excitable system. The self-excitation process can be originated from several mechanisms but the most obvious in the present system is due to "Stick slip" process according to which one surface slides on another with dry friction [13]. This process is also known as friction induced self-excited vibration. Earlier investigation reveals that this is more probable when vibrating elements are very small as it is the present case. Favorable conditions for this type of excitation are that the surface should be in close contact for some time and then move with a low velocity. These conditions are completely fulfilled in strings as a compact form of liquid. Self-excitation can also take place due to flow induce vibrations in a com-

pact liquid of strings [12] [13]. Both processes are obvious and effective which help the vibrations of electrons to excite and organize scheme of strings.

Now, let us imagine a vibrating electron (or charge particle) in three dimensional space which will induce self-activated vibrational energy in the nearest region. According to the symmetry, the nearest region will activate vibrations in strings which lie in the next circle and so on. After time t, the strings in radius ct will have vibration energy due to the self-activation process. However, it is worth to mention that the amplitude of vibrations (or the intensity) will go on reducing from one stage to another as the number of participating layers of strings increases [3]. Thus, the electron or the charge particle does not emit energy in any form but the vibrations associated to it induce self-activated vibrations in the surrounding system which in turn propagates in three dimensional space. This means that the field energy is directly associated with the vibrational energy.

3. Interaction of the Electric Field with Vibrating Systems

To appreciate the nature of the electric field and its association with vibrations, it is necessary to examine the interaction of the electric field with vibrating systems as it is difficult to estimate or evaluate the properties directly because of unknown parameters of strings related with vibrations and quantum harmonic oscillators.

According to the string theory also, some of the properties of strings are associated with quantum harmonic oscillators [15]. Because of their compact nature, it can be assumed that they form a system of strongly coupled harmonic oscillators.

Morse potential is an interatomic interaction model between two atoms or molecules. It is better approximated to the potential associated with the vibrational nature of the system [13] [14]. Obviously, it in teracts strongly with other vibrating systems like the electric field. An important characteristic feature of strong coupling interaction is the splitting of the energy levels and it is frequently associated with the perturbation in Morse potential, as in strong coupling the potential energy interacts with each other. The effects of the external electric field on Morse potential have been investigated earlier [13] [14] and an analytical formulation had been developed which explains successfully the frequency and the bond length dependence for diatomic molecules.

Delly [14] added an extra term in Morse potential

$$V(r) = De(1-\eta)^2 + f(E)\cdot r \tag{2}$$

$$\eta = \mathrm{e}^{-a(r-r_o)}$$

where $f(E)$ is the perturbation induced by the applied electric field. Here r is the distance between two nucleus of interest and r_o is the equilibrium distance. Obviously "a" has dimensions of $(\text{length})^{-1}$. De is the energy associated with the dissociation of the bond length. Taking into account the additional term, the frequency and the bond length have been examined for some molecules like Nacl, H_2O and experimental data are in agreement with the calculated values. The addition of the term $f(E)\cdot r$ in the potential of the harmonic oscillator also implies that the energy associated with the electric field is related with the vibrational energy. This approach has been further extended by Hashjin and Mott [13].

The detailed calculations of energy splitting have been carried out earlier by Novotny [16] by considering the equation of motion for a coupled system in which the constant of coupling can be varied and its effect on energy splitting is clearly determined experimentally. In the adiabatic limit, it is possible to transfer energy from one oscillator to the other through resonance [14] [16]. Therefore, it is necessary to examine the effect of the electric field on oscillating systems such as coupled quantum dots or a system of atoms and molecules in the external electric field. This means Stark effect.

4. Vibrational Stark Effect (VSE)

It is known that an electric field, internal or externally applied, perturbs molecular vibrations considerably. The changes induced by the applied electric field are measured by VSE, thus it provides a direct mapping between vibrational modes and electric field.

One of the few experimental evidences where the electric field is directly related with the vibrational energy of the system at atomic or molecular level is Stark effect; which shows the shifting and splitting of energy states due to the presence of the external electric field. VSE provides a direct relation between the observed variation in the vibrational modes and the applied electric field. Recently, it has been suggested that the external electric

field alters the potential energy of the surface perturbing the Morse potential of the molecule. This causes the change in the bond length and hence changes in the frequency. The field induced changes in the frequency and the force constant are given by [13].

$$d\nu = \nu_E - \nu_0 \tag{3}$$

$$dk = k_E - k_0 \tag{4}$$

where the subscript E shows the value perturbed by steady state electric field and subscript o denotes a free field value.

A detailed calculation has been carried out for the applied electric field and the field induced frequency is given [13]

$$V_E = K\nu_0 \tag{5}$$

where K is a constant and whose value depends upon the magnitude and direction of the applied electric field. The obtained results are compared with the calculated values for several molecules like H_2, N_2, O_2 and F_2 (homo-nuclear) and HF, HCl, CO (hetero-nuclear) and they are in agreement .The details are given by Hashjin and Matt [13]. It is worth to point out that the theory is tested for strongly covalent bonds which are described by harmonic oscillators and whose energy states lie at the bottom of the Morse potential well.

The additional effect is also observed by X-ray diffraction technique where the electric field induces the changes in the bond length or inter- atomic distances [17]. The above studies reveal that electric field, which is associated with vibrational motion, interacts with the oscillating system of the atoms and molecules. The above mentioned experimental techniques strongly support the vibrational nature of the electric field. This might help to understand the conversion of field into particles (photons) or vice versa as the energy of both depends upon the frequency. This is mathematically explained with the help of the creation and annihilation operatorsin QFT.

The electron and its associated field have vibrational nature. Therefore, it is interesting to examine other elementary particles and the nature of the corresponding fields. In a compact liquid, as considered in the present case, the mechanism associated with Van der Pol equation is not valid. However, a liquid in a confined region like the nucleus has several particles and their interacting fields which give rise to the damping coefficient and increase the magnitude of the constant of string μ. Van der Pol equation, therefore, might play a crucial role in the system which is given by [3]

$$\frac{\mathrm{d}^2x}{\mathrm{d}t^2} + \zeta\left(1-x^2\right)\frac{\mathrm{d}x}{\mathrm{d}t} + \mu x = 0 \tag{6}$$

Here ζ is a damping coefficient. Recently this equation has been solved by the algebraic method and it is found that constants ζ and μ play a very crucial role. The solution of the above equation is given [18]

$$x = \mathrm{e}^{-\zeta t}\left[b\sin\left(\omega t + \phi\right)\right] \tag{7}$$

where b and ϕ are constants which depend upon the initial conditions. A detailed analysis reveals that the frequency mainly depends upon the value of μ meanwhile ζ determines the exponential fall. The value of μ is related with the potential energy of the oscillator which becomes considerably high in the presence of particles and their interactions. Naturally fields have high frequency. Obviously, for higher values of ζ (damping coefficient), the forces have very short range. A further systematic investigation with this approach might provide information about the range of the force and their interactions. If so, the presence of vibrating strings in the form of a compact liquid might be a step ahead in the unification process.

5. Conclusion

The nature, origin and details of the propagation of the electric field on the basis of self-excitation process are discussed. Contrary to the accepted theories, it is found that the electron induced vibrational energy by self-excitation mechanism. The excitation process continues in space and the vibrational energy in the form of electric field spreads. Unexplained properties like electron cloud and Poincare stress become the natural consequences of the proposed theory. The electric field is examined with the help of VSE and X ray diffraction approaches. It is worth mentioning that several electromagnetic properties have been explained in a consistent manner by assuming only the presence of vibrating strings in the space.

References

[1] Feynman, R.P., Leighton, R.B.M. and Sands, M. (1969) The Feynman Lectures on Physics, Vol. 2, Chapter 4. Addison-Wesley, Boston.

[2] Bogolyubov, N.N. and Shirkov, D.V. (1982) Introduction to the Theory of Quantized Fields, Chapter 3. Benjamin, Reading.

[3] Joshi, N.V. (2013) *Physics Essays*, **26**, 61-67.

[4] Joshi, N.V. (2013) *World Journal of Mechanics*, **3**, 307-309. http://dx.doi.org/10.4236/wjm.2013.37032

[5] Joshi, N.V. (2015) *Journal of Modern Physics*, **6**, 2035-2039.

[6] Milonni, P. (1994) The Quantum Vacuum. An Introduction to Quantum Electro-Dynamics, Chapter 1. Academic Press, San Diego.

[7] Bearden, T.E. (2004) Energy from the Vacuum, Chapter 7. Cheniere Press, Santa Barbara.

[8] Haisch, B. and Moddel, G. (2008) Quantun Vacuum Energy Extraction. US. Patent No. 7379286.

[9] Maclay, G., Hammer, J.R., Clark, G.M., Kim, Y. and Kir, A. (2004) Study of Vacuum Energy for Breakthrough Propulsion. NASA Report OR-213311.

[10] Joshi, N.V. (2015) *Journal of Modern Physics*, **6**, 921-926. http://dx.doi.org/10.4236/jmp.2015.67096

[11] Joshi, N.V. (2014) *World Journal of Mechanics*, **4**, 247-250.

[12] D'Souza, A.F. and Dweib, A.H. (1990) *Journal of Sound and Vibration*, **137**, 177-190. http://dx.doi.org/10.1016/0022-460X(90)90787-Z

[13] Hashjin, S.S. and Matt, C.F. (2013) *Journal of Chemical Physics*, **139**, 144101-144112. http://dx.doi.org/10.1063/1.4820487

[14] Delley, B. (1998) *Journal of Molecular Structure*: *Theochem*, **434**, 229-237.

[15] Zwiebach, B.A. (2009) First Course in String-Theory, Chapter 12. Cambridge University Press, Cambridge. http://dx.doi.org/10.1017/CBO9780511841620

[16] Novotny, L. (2010) *American Journal of Physics*, **78**, 1199-1202. http://dx.doi.org/10.1119/1.3471177

[17] Semen, V.G., Vladimir, G.T. and Ullrich, P. (2005) *Acta Crystallographica Section A*, **61**, 387-396.

[18] Akbari, M.R., Ganji, D.D., Mujidian, A. and Ahmadi, A.R. (2014) *Frontiers of Mechanical Engineering*, **9**, 177-190. http://dx.doi.org/10.1007/s11465-014-0288-8

Journal of Modern Physics, 2016, 7, 1138-1149
Published Online June 2016 in SciRes. http://www.scirp.org/journal/jmp
http://dx.doi.org/10.4236/jmp.2016.710103

Monochrome HUD's Imaging Projector Based on Laser-DMD System

Sayed Sajjad Mousavi Fard*, Masood Kavosh Tehrani, Mehrdad Mehrani

College of Opto-Electronics Engineering, Malek Ashtar University of Technology (MUT), Shahin Shahr, Iran
Email: *s.moosavifard@gmail.com

Received 9 May 2016; accepted 16 June 2016; published 21 June 2016

Abstract

Design and tolerance of a new head up display's projector system is reported. It is based on laser-micro display modules. We designed optical diffraction limited modules and some of our novelties were compactness, using common material and spherical lenses in optical design, easy and economical manufacturing process, uniform intensity and minimum aberrations of final image, economical and repairable designed system. Projector magnification is 10.0X and diagonal of image plane is 76.2 mm. ZEMAX software is employed for optical design and tolerance.

Keywords

Head-Up Display (HUD), Head Mounted Display (HMD), Deformable Micro Mirror Displays (DMD), Polarizer Beam Splitter (PBS)

1. Introduction

One of the most important requirements for the pilot's cockpit is the type of display through which the most important flight information with the outdoor image is simultaneously provided for the pilot. Two types of display instruments were used: Head-Up Displays or HUDs and Helmet Mounted Displays or HMDs. HUD is a type of display instrument mounted in the cockpit and the most important flight information, the image of outside area, comes in its combiner-collimator beam splitter display surface and thus, a composite image of the outside world with the flight information is available to the pilot. HMD has the same structure, but its main specification is the compactness structure of the projection mounted on the pilot's helmet building the output image in its exit pupil [1] [2]. In this article, the HUD type has been designed. Creating high quality image is a common concern for optoelectronic designers. The image quality for this system is a function of: light source, image source and image projector's optical design. Therefore, there are three fundamental challenges that must respond

*Corresponding author.

How to cite this paper: Fard, S.S.M., Tehrani, M.K. and Mehrani, M. (2016) Monochrome HUD's Imaging Projector Based on Laser-DMD System. *Journal of Modern Physics*, **7**, 1138-1149. http://dx.doi.org/10.4236/jmp.2016.710103

in a favorable method [3] [4]. Historically, four types of light sources have been introduced for these displays; they are: Arc lamps, Halide-metal lamps, LED and Lasers. The laser light source has been used according to its unique features that lead to the quality of the output image. Image source has been a constant concern; indeed, different generations of HUDs are identified by this module. The first-generation of displays is Cathode Ray Tube or CRT that is still used in common HUDs. They had weaknesses that led to the appearance of other generation. The main problems of these types are: low intensity, brightness and contrast, cost limitation, high power consumption, saturated image with time, low operating endurance, cooling problems, phosphor's erosion and limitation of gray scale. These problems led to its sharp decline in popularity. The second generation of the image source is liquid crystal display or LCD; in an overall classification, this type is divided into two types: transmission and reflection. Reflective type is Liquid Crystal On Silicon platform or LCOS, its benefits are: small dimension, high resolution, more rigid and reliable structure, but its limitations such as polarized light source requirement, less efficiency in comparison to DMD type, temperature control requirement, high intensity light source requirement made it less popular [5] [6]. The third generation is holographic displays that made desired images by reconstruction of the Fourier transforms. Reflective structure made its output more brightness. Its potential limitations should also be noted: first, this type is limited to monochromatic light source, second, its complex structure increases the charges, and third, speckle phenomena decrease the final image quality [7]-[9]. Deformable Micro Mirror Displays or DMD is the fourth generation of the image sources that appeared in 1997 with Texas instrument and was vastly considered by optical systems designers. Its disadvantages are: more complex to drive, higher price compared to other micro displays, limitations in reducing the pixel dimensions, but it offers wide advantages such as high contrast and reflective efficiency, reliable and rigid structure, high operating temperature range, independence on polarized light and lower intensity light source requirement [10] [11]. Its optimum benefits compelled us to apply them in our system. In the final step, there was the most important challenge: "optical design", it was a challenge because of the following requirements: high compacted projector element, eliminating the aberrations in diffraction limit and making a uniform bright image [12]. In this article, comprehensive reviews of essential elements have been explained and the elements optical design is carried out with "ZEMAX" program based on constraints; and finally, tolerance analysis is made for the feasibility of fabrication [13]. Our designed system's specifications are: compacted structure, diffractive limited optical design, economic considerations, simplification and high image quality.

2. Principal Modules

The layout of this designed system has been illustrated in **Figure 1**. As can be seen in this figure, projection system is composed of three main parts: first the light source (marked with 1 #), second the image source (marked with 5#), and third adapting and the projection optics (marked with 2-4# and 6# respectively). The light emitted from the laser diode source enters the first beam expander with 1.0mm diameter and exits from it with a diameter of 5.0 mm, then this beam with Gaussian profile is transmitted from diffractive optic element, becomes top hat shaped, then this 5.0 mm top hat profile beam enters the second beam expander and exits from it with a diameter of 7.8 mm and enters a beam splitter cube and is reflected on DMD surface perfectly illuminating it, then the modulated light is reflected again from DMD surface and entersa projector. This module creates a 10X magnified image on its gain type diffuser screen. First and second beam expanders with diffractive elements make an adapting module that converts the 1.0 mm diameter Gaussian beam into 7.8 mm top hat ones. This module makes a fit and uniform beam profile to illuminate the DMD micro display, and this is an important requirement for making a high quality image.

2.1. The Light Source

Light source is a primary component of this system, and the correct choice will facilitate the process of setting up the system. This part is made of a green diode laser with a wavelength of 532 nm, and its output power is 1 watt, which is being control by using a mechanical shutter. The output light intensity is controlled to create different levels of brightness. Dimensions of used laser are 40(W) × 36(H) × 90(L) and its specifications are according to **Table 1**. Inherent parallel beams of laser light placed in the light cone are faced to the image source thus creating minimal waste and desired thumbnail display clarity.

This light source is reliable, highly durable, with a very limited and narrow wavelength range, and has desired brightness for avionic applications. Its radiation safety measurement at field of view is critical; this will be

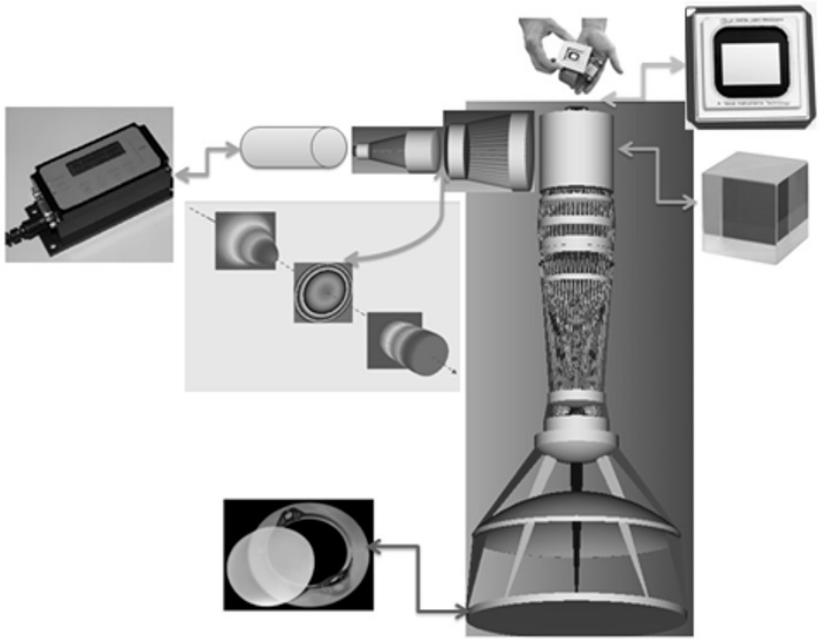

Figure 1. Block diagram of DMD based projectors for HUD.

Table 1. Dimensions and performance specifications of used diode laser [14].

Specifications	Quantity
Wavelength	532 ± 1 nm
Exit power	1.5 mw
Power stabilization	99%
Noise variability in range of 20 MHz	≤1%
Mode of operation	Continuous
Cross section diameter	1.0 ± 0.1 mm
Laser beam divergence	0.5 mrad
The opticalelement	Aspherical AR-coated
Operating voltage	3 - 5 Vdc (9 - 12 Vdc)
Operating current	≤500 mA
Operating temperature imension (mm)	−10 to +50˚C
Holding chamber	40 (W) × 36 (H) × 90 (L)
	hard anodized aluminum

calculated in terms of these parameters: the output light intensity, wavelength range and photo of perception [15]. The bandwidth of this laser and losses caused by intermediate elements (optical or electro optical elements) will cause the final light intensity to become safe. In addition, the light intensity can be adjusted for various applications such as day and night and high or low light outdoor intensity. Laserability to couple with DMD micro display in higher efficiency than other light sources made it an ideal choice to use in our system.

2.2. The Image Source

As mentioned in section one, the selected image source type is DMD, the DMD is fabricated in c-si using similar processing technologies as those applied to integrated circuit fabrication. It consists of an array of mirrors, one per pixel, suspended over CMOS circuitry. **Figure 2** shows photographs of the device. In **Figure 2(a)**, the micro mirrors are shown. In **Figure 2(b)**, one of the micro mirrors has been removed to show the underlying structure. **Figure 2(c)** shows a magnified view of this underlying structure.

The mirror assembly consists of a square mirror on top of a post attached to a torsion-hinge-suspended yoke. The yoke can rotate about ±12˚ (±10˚ in older DMDs) before it contacts the mechanical stop. For this deflection, the torsion effects in the hinges are fully elastic. On the silicon substrate, push-pull address electrodes are connected to the CMOS circuitry. The CMOS electronics in the underlying silicon substrate consists of a six transistor SRAM cell per pixel plus other circuits. With the appropriate bias, the mirrors move in response to the voltages on the address electrodes. In the +12˚ position, light incident onto the mirror will be reflected on to the projection lens, and in the −12˚ position, the light is directed away from the lens input and is internally absorbed. Thus, the light from any position on the mirror array is either present or not present, *i.e.* the projected intensity is binary. The mirrors can switch positions in about 15 μs, which allows achieving gray scales by time-multiplexing the mirror position. Luminance between the full-on and full-off values is obtained by selecting the appropriate on- and off-times. Furthermore, DMD micro display has other benefits: first a reflection structure of micro display caused the surface to become warm later, which can also cause high thermal power.

2.3. The Adapting Optics and Projection

The final part of HUD system design requirement is the optical design. Optical design is divided in to two parts: first; adapting light module, and second: projector module. The first module is used to make a proper illuminating light profile and the second part is used to make a perfect magnified final image.

3. Optical Modules Design

3.1. The Adapting Optics Design

Although the use of laser light is very useful, its output light profile is Gaussian. Since making a uniform image in the whole field of view is a very important consideration**,** this problem should be eliminated as much as possible**.**It is possible to design an adapting light module; which is composed of two elements: diffractive optic and beam expander element. Diffractive optic element shown in **Figure 3**, changes the Gaussian profile of laser light to top hat ones that have a high uniform distribution [17]. This uniform light is necessary to make a fit image in the final surface. Its specifications are according to **Table 2**.

The second necessary element is beam expander; which consists of two 1:5 and 5:7.8 mm element shown with 2# and 4# markers in **Figure 1**. The first, 1:5 mm element makes entrance light beam for diffractive element and the second 5:7.8 mm makes entrance light beam for beam splitter type prism. These designs are diffractive limited, and no more aberrations are added to its output according to **Figure 4** and **Figure 5**, respectively.

3.2. The Projector Design

This module is the main optical element in this electro-optical system. As shown in **Figure 6**. Number 1 element

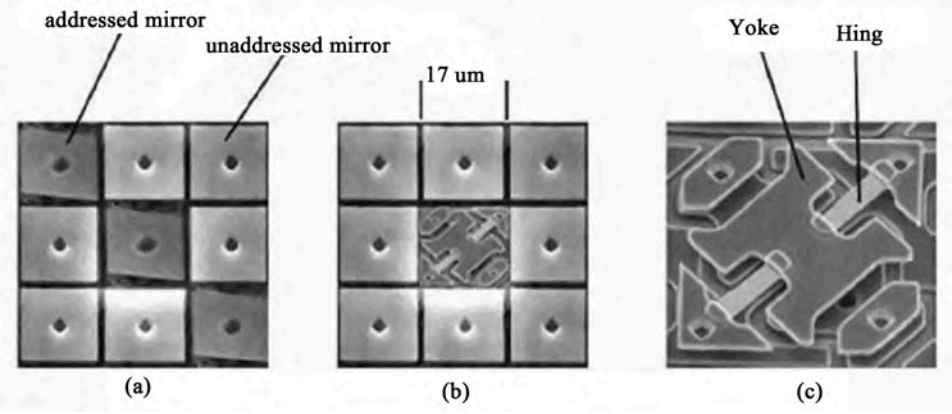

Figure 2. Photomicrographs of the DMD: (a) 16 μm mirrors on 17 μm centers, with mirrors shown in both the on and off positions; (b) one mirror removed to show underlying structure; and (c) magnified view [16].

Table 2. Specifications of diffractive beam shaper [17].

Factor	Quantify
Function	Top Hat
Dimension	circular with 5.0 mm
Operating wave length	532 ± 1 nm
Entrance pupil diameter	1.0 mm
Operating range	infinity
Exit pupil diameter	5.0 mm
Uneven spots Output	less than 0.5%

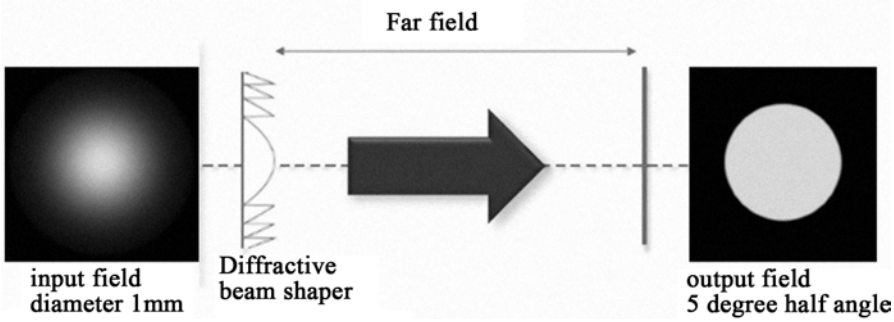

Figure 3. Overall schematic of diffractive beam shaper operation [17].

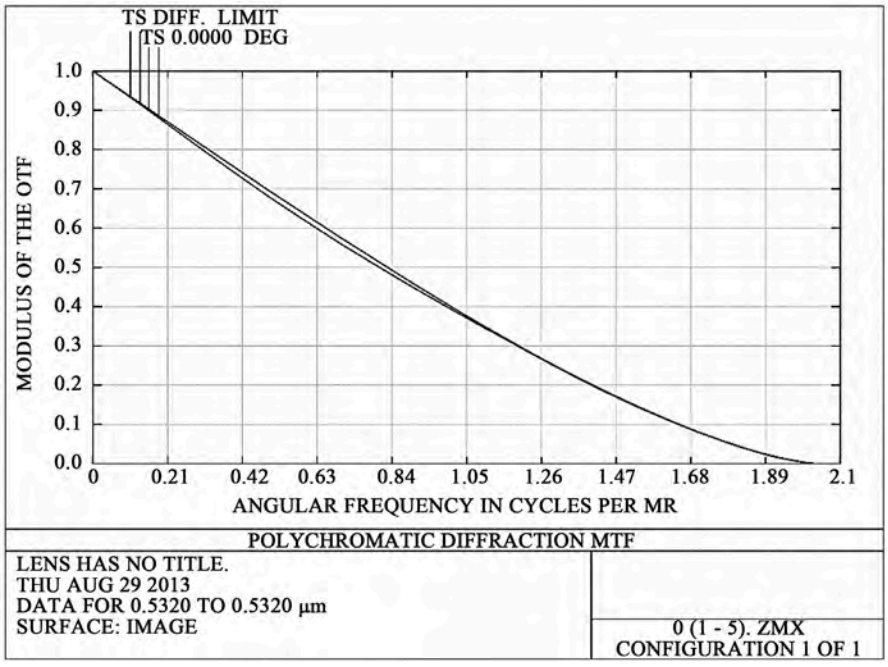

Figure 4. MTF diagram of designed beam expander 1:5 mm.

represents the effective area of the used DMD micro display. This element is considered a circle form with a diameter of 7.62 mm to cover up the maximum area of this micro display. Number 2 element represents the beam splitter prism. This prism is made of SF2 material and is considered as a cubic glass with 25.4 mm dimensions. This prism is considered as a transparent cube in optical design. Numbers 3 - 5 and 7 - 11 elements represent spherical lenses.

Number 6 element represents the system's stop. Nominal stop is the metal diaphragm with 26.0 mm inside

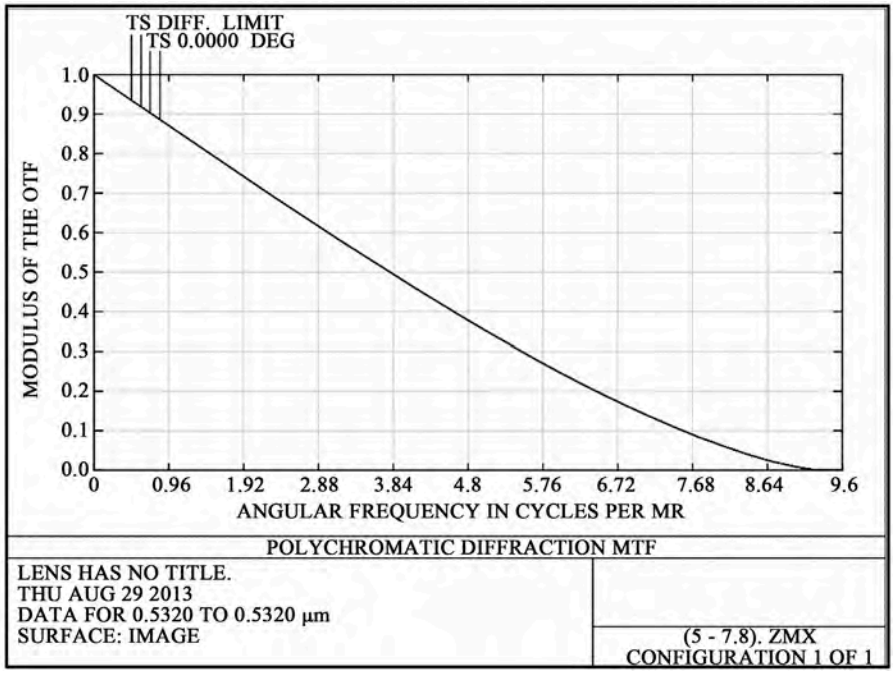

Figure 5. MTF diagram of designed beam expander 5:7.8 mm.

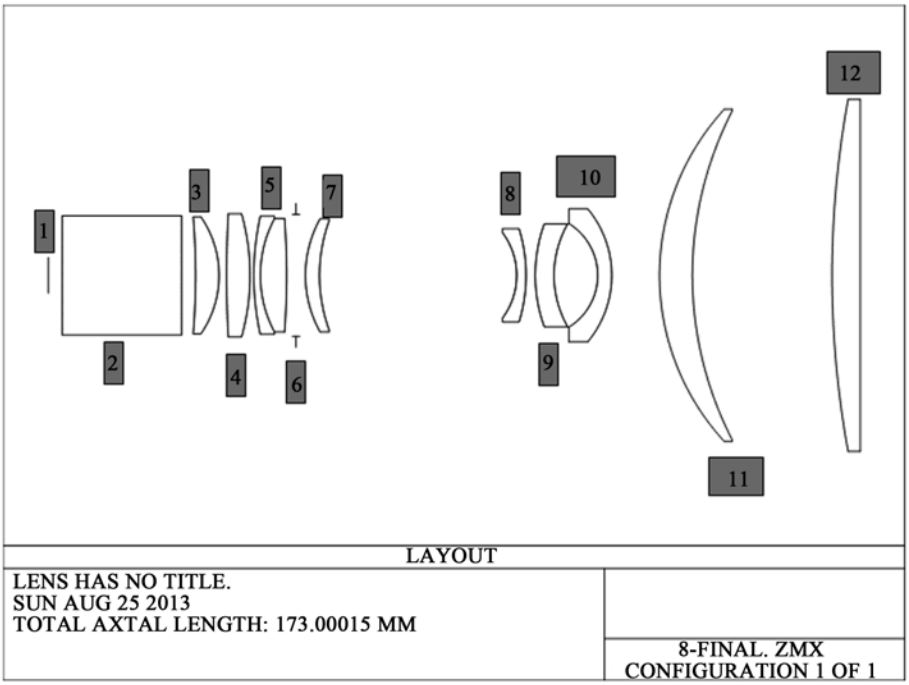

Figure 6. Schematic of 12 elements of designed projector.

diameter that can be changed up to 3.0 mm tolerances to illumination settings. Number 12 optical element is added to correct aberrations for convergence of projection module's output radiation. The tube length is equivalent to 173 mm that is equal to the distance from the DMD micro display to diffuser display screen, which represents a compact projector system. High compact optical element creates problems in its design. The most important problems are; excessive aberrations, extreme changes in image brightness level and excessive f/#, reduction aberrations techniques, and optimization of these three factors will be presented. The overall features of

the designed system are: the length of the projector is equal to 173 mm that is highly desirable and represents a compact system, this module's optical zoom is 10X, which leads to a 76.2 mm diameter image, it includes 9 spherical lenses. The great benefit of this design compared to other types is its simplicity in manufacturing, assembly, test process and its being more economical. Using a DMD micro display reduces light losses in secondary reflections from its surface, and the image spot diameter created by the projector must be less than 120 μm according to CRT spot diameter. This amount is equal to 15 μm and is approximately 8 times as good as defined value. Important results of our designed module listed in **Table 3**.

Analysis related to image quality are as follows: the maximum spot diameter of the created image is equal to 15.4 μm according to **Figure 7**, the distortion aberration amount in the full range of image display is less than five percent and field curvature aberration in the full range of image display is less than 5 mm. According to **Figure 8**, point spread function for this design is shown in **Figure 9**. As shown in this figure, an optimized design is carried out.

Figure 10 shows diagrams of relative brightness depending on the height of the beam. As seen the maximum variation in the whole field of view is 5%, which is very desirable. Here is a reminder point: as mentioned later, the gain type diffusers were used to create more uniform illumination in the field of view. Performance of this diffuser image surface is so that the light intensity in the corner is less than other points, and this phenomenon is corrected by an optical design trick. The polymeric elements present interesting abilities as a fit and designed diffuser display surface in a particular field of view is grossly different from the other parts; and therefore, without the excessive brightness from the lighting source, you can easily build a clearer picture in your desired viewing angle.

4. Tolerance Setting on the Designed Projector Module

Since the projector module is the most critical optical module of this imaging system, it is important to put a tolerance on its criteria. We use Monte Carlo analysis, and in this method produce a series of random lenses that fit desired tolerances, and then the index is calculated [18]. Shaded model of this module, after setting tolerances, is shown in **Figure 11**. The Monte Carlo analysis estimates the real-world performance of a system, which meets the specified tolerances. When performing the Monte Carlo analysis, all tolerances are considered simultaneously. For each Monte Carlo cycle, all of the parameters, which have specified tolerances, are randomly set using the defined range of the parameter and a statistical model of the distribution of that parameter over the specifiedrange. By default, all parameters are assumed to follow the same normal distribution with a total width of fourstandard deviations between the extreme minimum and maximum allowed values. For example, a radius of 100.00 mm with a tolerance of +4.0/−0.0 mm will be assigned a random radius between 100.00 mm and 104.00 mm, with a normal distribution centered on 102.00 mm and a standard deviation of 1.0 mm.

Spot diagram information is according to **Figure 12**. As seen from this figure, spot diameter variation is negligible, this verified the image quality. Also, distortion and field of curvature aberrations are according to **Figure 13**, and their changes are negligible too.

Table 3. Important factors in the design of the projector module.

Factor	Amounts
The number of surfaces	22 surfaces
Stop diameter	26.0 mm
The catalogue of used glass	SCHOTT MISC OHARA CDGM
Effective focal length	9.9 mm
Back focal length	97.25 mm
Image space f/#	0.23
Entrance pupil diameter	42.7 mm
Exit pupil diameter	10.07 mm

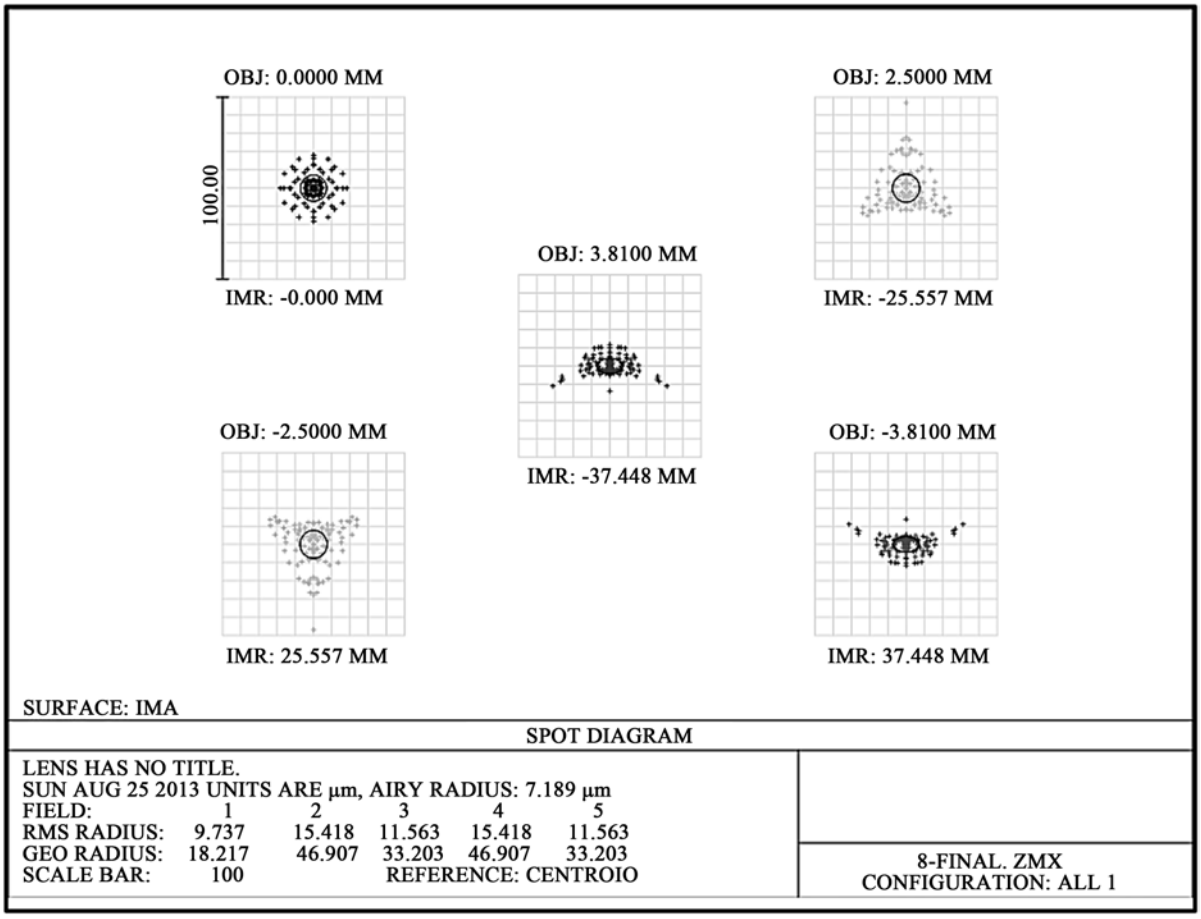

Figure 7. Schematic of spot diameter of image created by this system.

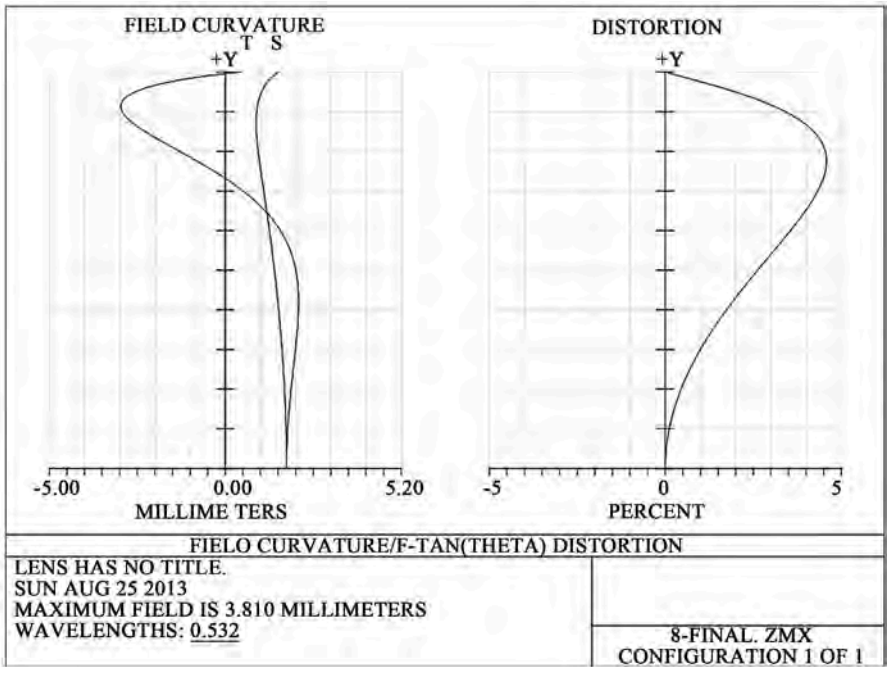

Figure 8. Diagram of distortion aberration and field curvature.

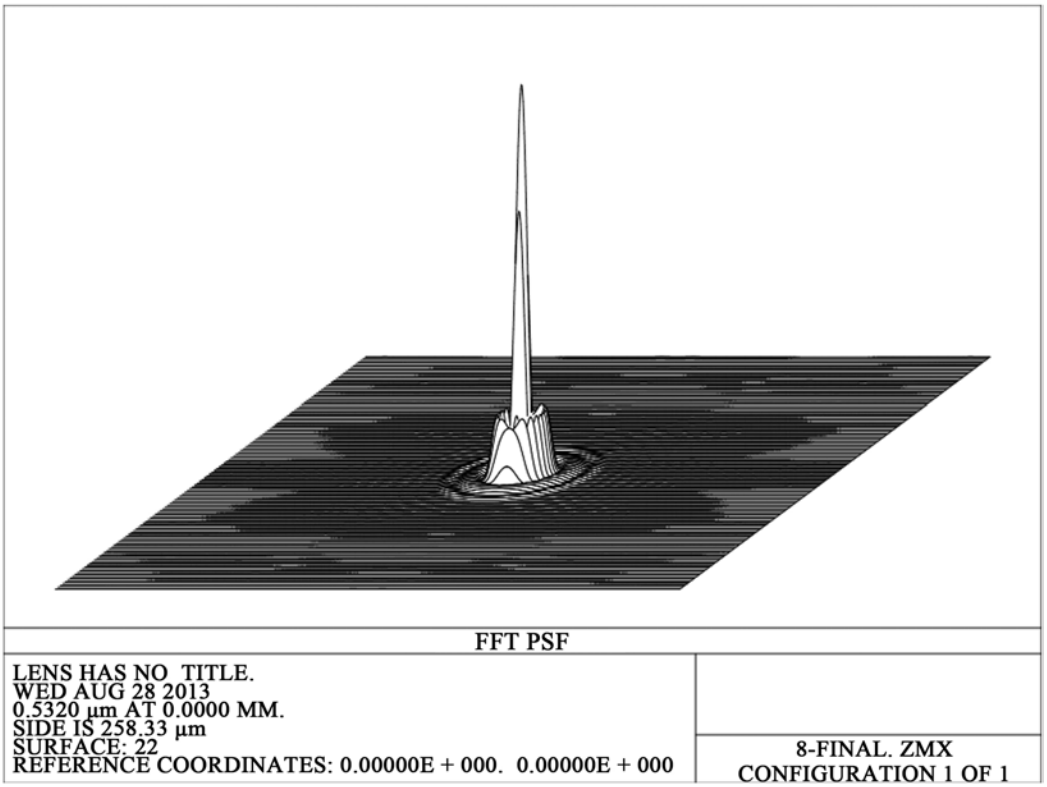

Figure 9. Point spread function of this system.

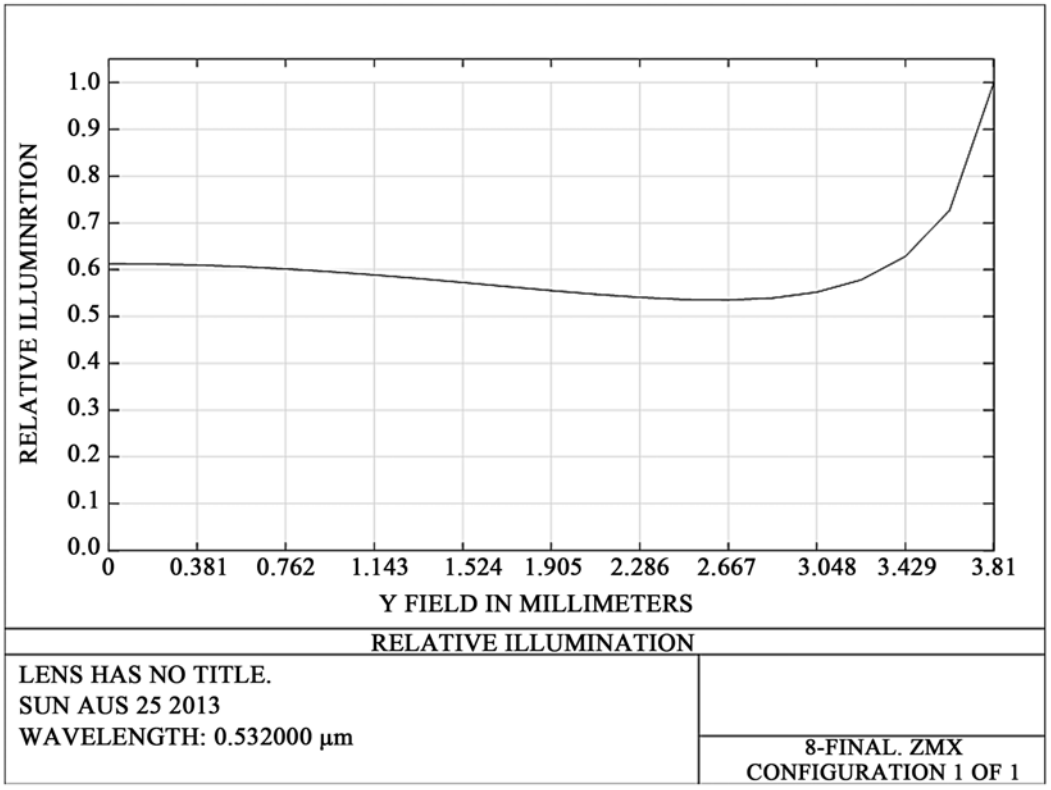

Figure 10. Schematic of relative illumination in image plan according to the beam height.

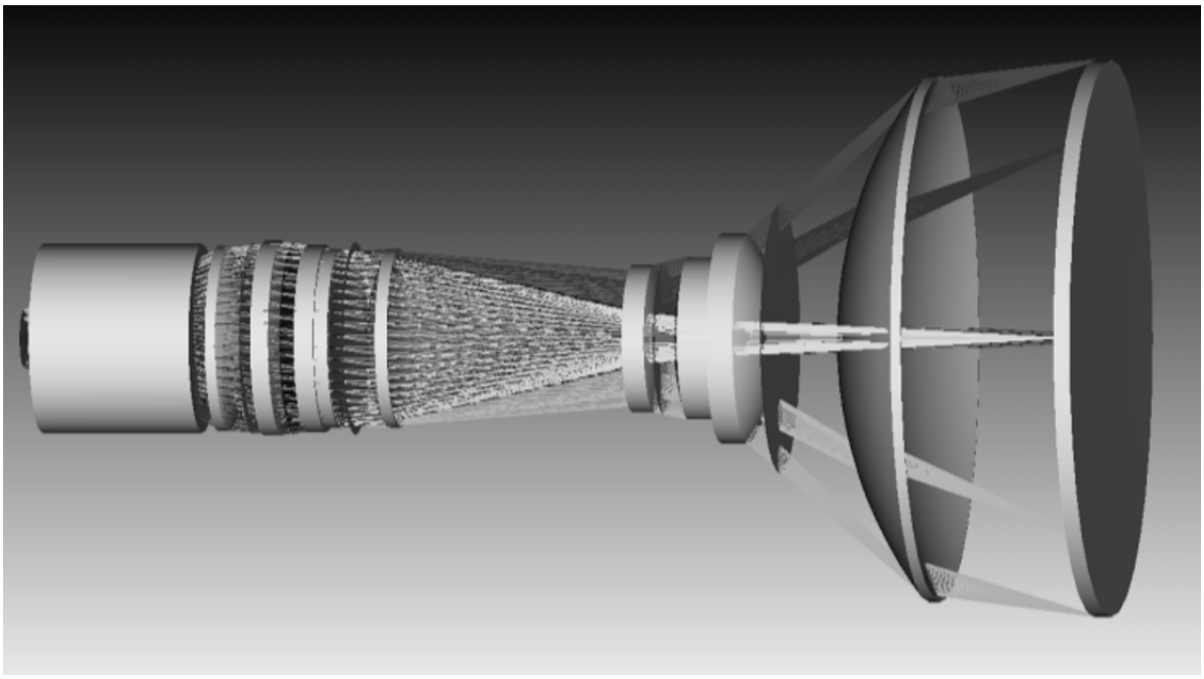

Figure 11. Three dimensional image of projector module after making tolerances.

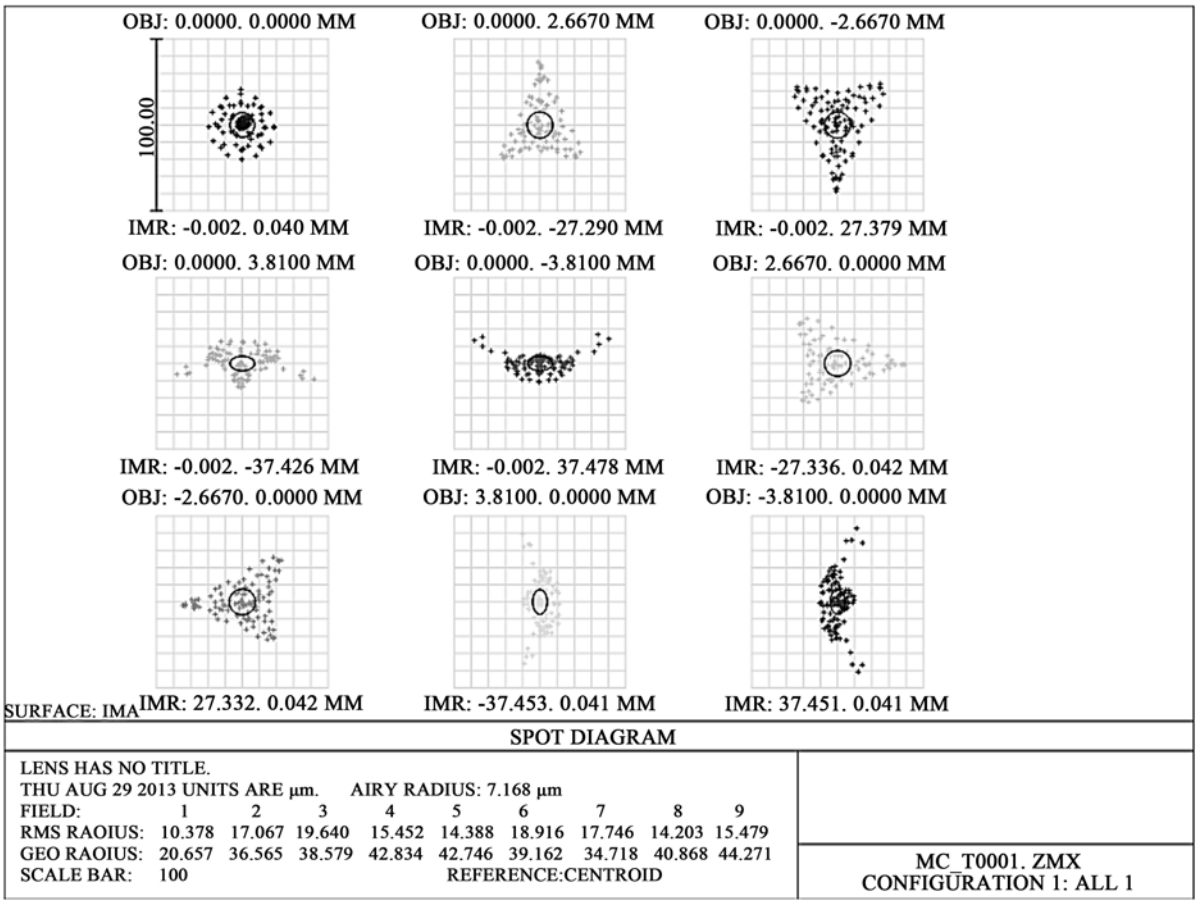

Figure 12. Spot diagram after tolerance.

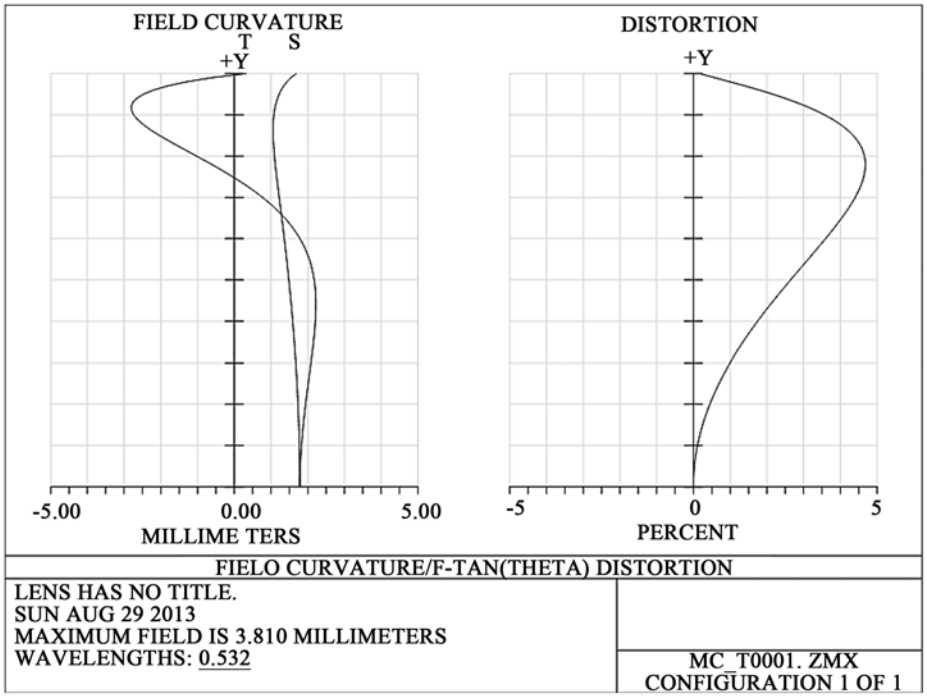

Figure 13. Field curvature and distortion figures after tolerance.

5. Conclusion

All used optical lenses are spherical, and common materials are utilized in optical design process; therefore, the manufacturing process becomes easy and economical. Making compactness system problems is responded perfectly and the whole of this system will be put in the box with 200 × 200 × 200 mm^3 dimensions. As previously mentioned the following factors are important in image quality evaluation [19]: First: created spot diameter, second: uniform intensity on the screen and third: lack of excessive distortion aberration (less than 5% of the total range of the image). Designed system has a high lifetime because of its durable elements and materials, all system components are interchangeable and cost effective.

References

[1] Paul, L. (2008) A Digital Head-Up Display System as Part of an Integrated Autonomous Landing System Concept. SPIE 6957, 695700-10.

[2] Zhaoa, Q.-L., Wangb, Z.-Q. and Liua, T.-G. (2007) *Optik*, **118**, 29-33.

[3] Wisely, P. (2008) Enhancing the Performance of a Pilot's Head-Up Display. SPIE.

[4] Billings, M., Fernandez, J., Cashen, R., Large, R., Wang, S. and Tisdale, G. (2003) Development of Digital Light Engine Based Head-Up Displays. SPIE 5080, 308-319.

[5] Brown, R.-D., Modro, D.-H., Quast, G., Wallace, D.-L., Vancleef, M.-G. and Wood, R.-B. (2004) Performance Assessment of a LCOS-Based Head-Up Display. SPIE 5443, 146-155.

[6] Zhao, Q.-L., Wang, Z.-Q., Guo, H.-Q., Sun, Q., Lu, Z.-W. (2004) *Optik*, **115**, 11-14. http://dx.doi.org/10.1078/0030-4026-00324

[7] Buckley, E. (2008) Holographic Laser Projection Technology, Information Display.

[8] Zheng, H., Yu, Y. and Dai, C. (2009) *Optik*, **120**, 431-436.

[9] Elmorshidy, A. (2010) *Journal of Telecommunications*, **2**, 104-112.

[10] Shia, Z. and Gao, Y. (2012) *Optik*, **123**, 1640-1645.

[11] Bechtela, C., Knobbeb, J., Grügerb, H. and Laknerb, H. (2014) *Optik*, **125**, 876-882. http://dx.doi.org/10.1016/j.ijleo.2013.07.091

[12] Hua, H., Ha, Y. and Rolland, J.-P. (2003) *Applied Optics*, **42**, 97-107. http://dx.doi.org/10.1364/AO.42.000097

[13] Focus Software ZEMAX Development Corporation (2008) ZEMAX Optical Design Program User's Guide, Version 10.

[14] (2013) TOPAG, 532 nm Diode Lasers, Last Modified. http://www.TOPAG.com

[15] Boyd, R.-W. (1983) Radiometry and the Detection of Optical Radiation. John Wiley and Sons.

[16] Stupp, E. and Brennesholtz, M. (1999) Projection Displays. Wiley.

[17] Billings, M. (2003) Development of Digital Light Engine Based Head-Up Displays. SPIE 5080, 308-319.

[18] Tompkins, K.R. (2000) Projection Displays Technology for Avionics Applications. SPIE 4022, 63-72.

[19] Christopher, T.-B. (2000) The Flat Panel Head up Display. SPIE 4022, 399-410.

Journal of Modern Physics, 2016, 7, 1150-1159
Published Online June 2016 in SciRes. http://www.scirp.org/journal/jmp
http://dx.doi.org/10.4236/jmp.2016.710104

Scientific Research Publishing

The Integer-Fraction Principle of the Digital Electric Charge for Quarks and Quasiparticles

Ding-Yu Chung

Utica, MI, USA
Email: dy_chung@yahoo.com

Received 8 April 2016; accepted 17 June 2016; published 21 June 2016

Abstract

In the integer-fraction principle of the digital electric charge, individual integral charge and individual fractional charge are the digital representations of the allowance and the disallowance of irreversible kinetic energy, respectively. The disallowance of irreversible kinetic energy for individual fractional charge brings about the confinement of individual fractional charges to restrict irreversible movement resulted from irreversible kinetic energy. Collective fractional charges are confined by the short-distance confinement force field where the sum of the collective fractional charges is integer. As a result, fractional charges are confined and collective. The confinement force field includes gluons in QCD (quantum chromodynamics) for collective fractional charge quarks in hadrons and the magnetic flux quanta for collective fractional charge quasiparticles in the fractional quantum Hall effect (FQHE). The collectivity of fractional charges requires the attachment of energy as flux quanta to bind collective fractional charges. The integer-fraction transformation from integral charges to fractional charges consists of the three steps: 1) the attachment of an even number of flux quanta to individual integral charge fermions to form individual integral charge composite fermions, 2) the attachment of an odd number of flux quanta to individual integral charge composite fermions to form transitional collective integral charge composite bosons, and 3) the conversion of flux quanta into the confinement force field to confine collective fractional charge composite fermions converted from composite bosons. The charges of quarks are fractional, because QCD (the strong force) emerges in the universe that has no irreversible kinetic energy. Kinetic energy emerged in the universe after the emergence of the strong force. The charges of the quasiparticles in the FQHE are fractional because of the confinement by a two-dimensional system, the Landau levels, and an extremely low temperature and the collectivity by high energy magnetic flux quanta. From the integer-fraction transformation from integral charge electrons to fractional charge quarks, the calculated masses of pion, muon and constituent quarks are in excellent agreement with the observed values.

How to cite this paper: Chung, D.-Y. (2016) The Integer-Fraction Principle of the Digital Electric Charge for Quarks and Quasiparticles. *Journal of Modern Physics*, **7**, 1150-1159. http://dx.doi.org/10.4236/jmp.2016.710104

Keywords

Electric Charge, Integral Charge, Fractional Charge, Quarks, Kinetic Energy, Confinement, The Fractional Quantum Hall Effect, The Theory of Everything, The Masses of Quarks, The Mass of Muon, The Mass of Pion, Cosmology

1. Introduction

The elementary charge denoted as e or q is a fundamental physical constant for electric charge. One elementary charge has a measured value of approximately 1.602×10^{-19} coulombs. The electric charge of any isolated object is an integer multiple of e. Quarks and quasiparticles have fractional charges. Quarks have fractional electric charge values 1/3 or 2/3 times the elementary charge. There have been a large number of experiments searching for fractional charge, isolatable, elementary particles using a variety of methods, but no evidence has been found to confirm existence of free fractional charge particles, which leads to the quark confinement concept that the quarks in collective groupings are permanently confined within the hadrons whose charges are integer multiples of e [1]-[4]. Fractional charge quasiparticles in the fractional quantum Hall effect (FQHE) also exist in collective groupings in the confinement of a two-dimensional system, the Landau levels, and an extremely low temperature [5]-[7]. Confinement and collectivity are the common features in fractional charge quarks and quasiparticles. This paper posits that the origin of integral electric charge and fractional electric charge is the integer-fraction principle of digital electric charge. The principle relates to the confinement and collectivity of fractional charges.

Section 2 describes the integer-fraction principle. Section 3 explains the origin of the strong force as the confinement force field for fractional charge quark and the calculations of pion, muon and quark masses. Section 4 describes the fractional quantum Hall effect for fractional charge quasiparticles.

2. The Integer-Fraction Principle

There are integral electric charge and fractional electric charge. The two types of fractional charge particles are fractional charge quarks in hadron and fractional charge quasiparticles in the FQHE. The origin of integral electric charges and fractional electric charges is unknown. This paper posits that the origin of integral electric charge and fractional electric charge is the integer-fraction principle of digital electric charge. In the integer-fraction principle of the digital electric charge, individual integral charge with irreversible kinetic energy to cause irreversible movement is allowed, while individual fractional charge with irreversible kinetic energy is disallowed. Individual integral charge and individual fractional charge are the digital representations of the allowance and the disallowance of irreversible kinetic energy, respectively. The disallowance of irreversible kinetic energy for individual fractional charge brings about the confinement of individual fractional charges to restrict the irreversible movement resulted from kinetic energy. Collective fractional charges are confined by the short-distance confinement force field where the sum of the collective fractional charges is integer. As a result, fractional charges are confined and collective. The confinement force field includes gluons in QCD (quantum chromodynamics) for collective fractional charge quarks in hadrons and the magnetic flux quanta for collective fractional charge quasiparticles in the fractional quantum Hall effect (FQHE).

The collectivity of fractional charges requires the attachment of energy as flux quanta to bind fractional charges. As a result, the integer-fraction transformation from integral charges to fractional charges involves the integer-fraction transformation to incorporate flux quanta similar to the composite fermion theory for the FQHE [8] [9]. There are two steps in the composite fermion theory for the FQHE. The first step is the formation of composite fermion by the attachment of an even number of magnetic flux quanta to electron. Composite fermions in the Landau levels are the "true particles" to produce the FQHE, while electrons in the Landau level are the true particles to produce the integral quantum Hall effect (IQHE). The IQHE is a manifestation of the Landau level quantization of the electron kinetic energy. The second step is the conversion of integral charges to fractional charges in the collective mode of composite fermions. The IQHE in the collective mode of composite fermions is the FQHE as expressed by the filling factors υ's related to electric charges.

$$\begin{aligned}
&\text{the composite fermion theory}\\
&\text{the first step :}\\
&\text{electrons} \xrightarrow{\text{even numbers of magnetic flux quanta}} \text{composite fermions}\\
&\text{the second step for the collective mode of composite fermions :}\\
&\nu^* = m \ \text{ for the IQHE}\\
&\nu = \frac{\nu^*}{2n\nu^* \pm 1} = \frac{m}{2mn \pm 1} \ \text{ for the FQHE}\\
&\text{for } \nu^* = 1,\ \nu = \frac{1}{2n+1} \ \text{ for the Laughlin wavefunction of the FQHE}
\end{aligned} \tag{1}$$

where m and n are integers, and υ and υ^* are the filling factors for electrons and composite fermions, respectively in the Landau levels. The composite fermion theory is used to compute precisely a number of measurable quantities, such as the excitation gaps and exciton dispersions, the phase diagram of composite fermions with spin, the composite fermion mass, etc.

The first step of the integer-fraction transformation from integral charge to fractional charge is same as the first step in the composite fermion theory. The first step is the attachment of an even number of flux quanta to individual integral charge fermions to form individual integral charge composite fermions [6]. Flux quanta are the elementary units which interact with a system of integral charge fermions. The attachment of flux quanta to the fermions transforms them to composite particles. The attached flux quanta change the character of the composite particles from fermions to bosons and back to fermions. Composite particles can be either fermions or bosons, depending on the number of attached flux quanta. A fermion with an even number of flux quanta becomes a composite fermion, while a fermion with an odd number of flux quanta becomes a composite boson. Fermions, such as electrons and protons, follow the Pauli exclusion principle which excludes fermions of the same quantum-mechanical state from being in the same position. Bosons, such as photons or helium atoms, follow the Bose-Einstein statistics which allows bosons of the same quantum-mechanical state being in the same position. As a result, fermions are individualistic, while bosons are collectivistic. Composite fermions are individualistic, while composite bosons are collectivistic. In the first step, the attachment of an even number of flux quanta to each integral charge fermion provides these fermions individual integral charge composite fermions which follow the Pauli exclusion principle.

The second step involves the traditional composite bosons. The second step explains the origin of $1/(2n + 1)$ in Equation (1) in the second step of the composite fermion theory which does not explain the origin of $1/(2n + 1)$. The second step is the attachment of an odd number of flux quanta to individual integral charge composite fermions to form transitional collective integral charge composite bosons [6]. Individual integral charge composite fermions with an odd number $(2n + 1)$ of flux quanta provide collective integral charge composite bosons which allow bosons of the same quantum-mechanical state being in the same position. The collective integral charge composite bosons allow the connection of collective flux quanta from collective integral charge composite bosons. Each flux quantum represents an energy level. In individual integral charge composited fermions, the degenerate energy levels are separated. In collective integral charge composite bosons, the $2n$ +1 degenerate energy levels are connected into $2n + 1$ sites in the same energy level.

The third step is the conversion of collective flux quanta into the confinement force field to confine collective fractional charge composite fermions converted from the collective integral charge composite bosons. In collective fractional charge fermions, each site in the same energy level has $\pm 1/(2n + 1)$ fractional charge.

$$\text{fractional charge per site in the same energy level} = \frac{\pm 1}{2n+1} \tag{2}$$

Fractional charges are the integer multiples of $\pm 1/(2n + 1)$ fractional charge to explain the origin of $1/(2n + 1)$ in Equation (1) for the composite fermion theory. The products in the third step also include individual integral charge fermions to conserve electric charge. The sum of all collective fractional charges and individual integral charges is integer. The integer-fraction transformation from individual integral charge fermions to collective fractional charge fermions is as follows.

$$\text{individual IC fermions} \xrightarrow{\text{even number of flux quanta}} \text{individual IC composite fermions} \xrightarrow{\text{odd number of flux quanta}} \text{tramsitional collective IC composite bosons} \xrightarrow{\text{confinement force field}} \text{collective FC composite fermions} + \text{individual IC fermions} \quad (3)$$

where IC is integral charge and FC is fractional charge.

3. The Origin of the Strong Force and the Calculations of Pion, Muon and Quark Masses

The charges of quarks are fractional, because QCD (the strong force) emerged in the universe that had no irreversible kinetic energy. Kinetic energy emerged in the universe after the emergence of the strong force as described in the cyclic dual universe model previously [10] [11]. As described previously [10] [11], there are three postulates in the dynamic and reversible theory of everything. The first postulate of the dynamic and reversible theory of everything is the oscillating M-theory as the oscillating membrane-string-particle whose space-time dimension number oscillates between 11D and 10D and between 10D and 4D dimension by dimension reversibly. There is no compactization. Matters in oscillating M-theory include 11D membrane (2_{11}) as membrane (denoted as 2 for 2 space dimensions) in 11D, 10D string (1_{10}) as string (denoted as 1 for 1 space dimension) in 10D, and variable D particle ($0_{4 \text{ to } 11}$) as particle (denoted as 0 for 0 space dimension) in 4D to 11D. Space-time dimension number between 10 and 4 decreases with decreasing speed of light, decreasing vacuum energy, and increasing rest mass. The second postulate is the digital transitional Higgs-reversed Higgs fields postulate as the digital attachment-detachment spaces postulate. Attachment space (denoted as 1) attaches matter, and relates to rest mass and reversible movement. Detachment space (denoted as 0) detaches matter, and relates to irreversible kinetic energy. The combination of n units of attachment space as 1 and n units of detachment space as 0 brings about three different digital space structures: binary partition space, miscible space, or binary lattice space as below.

$$\underset{\text{attachment space}}{(1)_n} + \underset{\text{detachment space}}{(0)_n} \xrightarrow{\text{combination}} \underset{\text{binary partition space}}{(1)_n(0)_n}, \underset{\text{miscible space}}{(1+0)_n}, \text{ or } \underset{\text{binary lattice space}}{(1\ 0)_n} \quad (4)$$

Binary partition space, $(1)_n(0)_n$, consists of two separated continuous phases of multiple quantized units of attachment space and detachment space. In miscible space, $(1 + 0)_n$, attachment space is miscible to detachment space, and there is no separation of attachment space and detachment space. Binary lattice space, $(1\ 0)_n$, consists of repetitive units of alternative attachment space and detachment space. Binary partition space $(1)_n(0)_n$, miscible space $(1 + 0)_n$, and binary lattice space $(1\ 0)_n$ account for quantum mechanics, special relativity, and the force fields, respectively. In this paper, the integer-fraction principle is an extension of the digital space structure consisting of attachment space for rest mass and reversible movement and detachment space for irreversible kinetic energy.

Our universe is in the reversible multiverse. In the third postulate for reversible multiverse, all physical laws and phenomena are permanently reversible, and temporary irreversibility of entropy increase is allowed through reversibility breaking, symmetry violation, and low entropy beginning. One irreversible phenomenon which is not allowed is the collision of expanding universes. The collision of expanding universes which have the inexhaustible resource of space-time to expand is permanently irreversible due to the impossibility to reverse the collision of expanding universes. To prevent the collision of expanding universes, every universe is surrounded by the interuniversal void that is functioned as the permanent gap among universes. The space in the interuniversal void is detachment space [10] which detaches matter and relates to kinetic energy. The interuniversal void has zero-energy, zero space-time, and zero vacuum energy, and detachment space only, while universe has non-zero-energy, the inexhaustible resource of space-time to expand, zero or/and non-zero vacuum energy, and attachment space with or without detachment space. Attachment space attaches matter and relates to rest mass. The detachment space of the interuniversal void has no space-time, so it cannot couple to particles with space-time in universes, but it prevents the advance of expanding universes to the interuniversal void to avoid the collision of expanding universes.

A zero-sum energy dual universe of positive-energy universe and negative-energy universe can be created in the zero-energy interuniversal void, and the new dual universe is again surrounded by the interuniversal void to avoid the collision of universes. Under symmetry, the new positive-energy universe and the new negative-energy universe undergo mutual annihilation to reverse to the interuniversal void immediately. Our universe is

the dual asymmetrical positive-energy-negative-energy universe where the positive-energy universe on attachment space absorbed the interuniversal void on detachment space to result in the combination of attachment space and detachment space, and the negative-energy universe did not absorb the interuniversal void. Within the positive-energy universe, the absorbed detachment space with space-time can couple to particles in the positive-energy universe to result in massless particles with irreversible kinetic energy. The formation of our universe involves symmetry violation between the positive-energy universe and the negative energy universe. Irreversible kinetic energy from detachment space is the source of irreversible entropy increase, so the positive-energy universe is locally irreversible, while the negative-energy universe without irreversible kinetic energy from detachment space is locally reversible. The locally reversible negative-energy universe guides the reversible process of the dual universe. As a result, our whole dual universe is globally reversible. Our dual universe is the globally reversible cyclic dual universe as shown in **Figure 1** for the evolution of our universe as described previously [10] [11].

The four reversible steps in the globally reversible cyclic dual universe are 1) the formation of the 11D membrane dual universe, 2) the formation of the 10D string dual universe, 3) the formation of the 10D particle dual universe, and 4) the formation of the asymmetrical dual universe.

1) The formation of the 11D membrane dual universe

As described previously [10] [11], the reversible cyclic universe starts in the zero-energy interuniversal void, which produces the dual universe of the positive-energy 11D membrane universe and the negative-energy 11D membrane universe as in **Figure 1**. In some dual 11D membrane universes, the 11D positive-energy membrane universe and the negative-energy 11D membrane universe coalesce to undergo annihilation and to return to the interuniversal void as in **Figure 1**.

2) The formation of the 10D string dual universe

Under the reversible oscillation between 11D and 10D, the positive-energy 11D membrane universe and the negative-energy 11D membrane universe are transformed to the positive-energy 10D string universe and the negative-energy 10D string universe, respectively, as in **Figure 1**. The positive-energy 11D membrane universe is transformed to the positive-energy 10D string universe as in Equations (5a) and (5b).

The RS1 Membrane Transformation

$$\text{step 1}: 2_{11} \xrightarrow{\text{from 11D membrane to 10D string}} 1_{10} \text{ in the 11D AdS space} \tag{5a}$$

$$\text{step 2}: 2(1_{10}) \xrightarrow{\text{the close string vibration}} 1_{10}\, 0_{10} = 1_{10}\, g_e \text{ in the 11D AdS space}$$

$$2(2_{11}) \xleftarrow{\text{the close string and the open string vibrations}} (s1_{10})\, g_e \tag{5b}$$

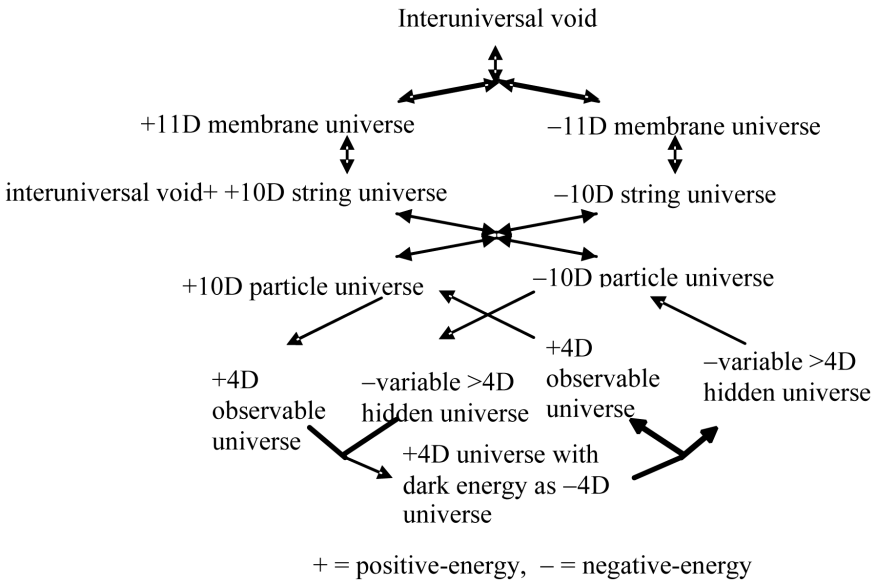

Figure 1. The globally reversible cyclic dual universe.

where 2_{11} is membrane (denoted as 2) in 11D, s is the pre-strong force, 1_{10} is string (denoted as 1) in 10D, 0_{10} is particle (denoted as 0) in 10D, AdS is anti-de Sitter, and g_e is the external graviton.

According Randall and Sundrum, the RS1 (Randall-Sundrum model 1) in an anti-de Sitter (AdS) space consists of one brane with extremely low graviton's probability function and another brane with extreme high graviton's probability function [12] [13]. The formation of the 10D string dual universe involves the RS1. As shown in Equation (5a), one of the possible membrane transformations from the 11D membrane to the 10D string is the RS1 membrane transformation which involves two steps. In the Step 1, the extra spatial dimension of the 11D membrane in the transformation from the 11D membrane to the 10D string becomes the spatial dimension transverse to the string brane in the bulk 11D anti-de Sitter space [12]. This transformation is derived from the transformation from membrane to string. In the transformation from the two-dimensional membrane to the one-dimensional string, the extra spatial dimension of the two-dimensional membrane on the x-y plane becomes the x-axis transverse to the one-dimensional string on the y-axis in the two-dimensional x-y space. In the Step 2, for the RS1 membrane transformation, two string branes are combined to the combined string brane. The external 10D particles generated by the close string vibration of the combined string brane are the 10D external gravitons which form the external graviton brane as the Gravitybrane (Planck Plane) in the RS1 of the Randall-Sundrum model [12] [13]. As in the RS1 of the Randall-Sundrum model, the two branes with equal mass-energy in the 11D anti-de Sitter space are the string brane with weak gravity and the external graviton brane with strong gravity. The weak gravity in the string brane is the predecessor of the observed weak gravity generated during the Big Bang [14] [15]. The external graviton in the external graviton brane is the predecessor of a part of the observed dark energy [16]. The 10D string brane and the 10D external graviton brane correspond to the predecessors of the observed universe (without dark energy) and a part of observed dark energy, respectively [14] [15]. The reverse transformation from 10D to 11D is the RS1 string transformation.

In Equation (5b), the particles generated from the 10D open string vibration are the 10D particles for the pre-strong force (denoted as s) in addition to the external graviton from the close string vibration in the 11D AdS. The pre-strong force is the same for all strings without positive or negative sign. This pre-strong force is the prototype of the observed strong force for fractional charge quarks generated during the Big Bang [14] [15].

In the negative universe through symmetry, the 11D anti-membrane (2_{-11}) is transformed to 10D antistring (1_{-10}) with external anti-graviton $\overline{g_e}$ and the pre-strong force s as follows.

$$2\left(2_{-11}\right) \longleftrightarrow \left(s1_{-10}\right)\overline{g_e} \tag{6}$$

The dual universe of the positive-energy 10D string universe with n units of $(1_{10})_n$ and the negative-energy 10D string universe with n units of $(1_{-10})_n$ is as follows.

$$\left(\left(s1_{10}\right)g_e\right)_n\left(\overline{g_e}\left(s1_{-10}\right)\right)_n \tag{7}$$

There are four equal regions: the positive-energy 10D string universe, the external graviton, the external anti-graviton, and the negative-energy 10D string universe [16].

Some dual 10D string universes return to the dual 11D membrane universes under the reversible oscillation between 11D and 10D. Alternatively, under symmetry violation as in the case of our universe, the positive-energy 10D string universe absorbs the interuniversal void, while the negative-energy 10D string universe does not absorb the interuniversal void. The interuniversal void has zero vacuum energy. In our universe, the absorption of the interuniversal void by the positive-energy 10D string universe forced the positive-energy 10D universe with high vacuum energy to be transformed to the universe with zero vacuum energy that was the vacuum energy of the 4D universe. However, the transformation from 10D to 4D was not immediate, because the strings had to be 10D, and it could not be transformed to 4D, therefore, strings had to be transformed to particles that allowed the change of its dimension number freely to accommodate the transformation from the 10D universe to the 4D universe driven by the absorption of the inter universal void.

1) The formation of the 10D particle dual universe

As described previously [15], the transformation from strings to particles came from the emergence of positive charge and negative charge that allowed the mutual annihilation of positively charge 10D strings and negatively charge 10D antistrings in the 10D string universes to produce positively charge 10D particles and negatively pre-charge 10D antiparticles in the 10D particle universes as follows.

$$\left(\left(s\,0_{10}\,e^{+}e^{-}\,0_{-10}\;s\right)g_{e}\right)_{n}\left(\overline{g_{e}}\left(s\,0_{10}\,e^{+}e^{-}\;0_{-10}\,s\right)\right)_{n}, \tag{8}$$

where s and e are the pre-strong force and the pre-charge force in the flat space, g_e is the external graviton, $\overline{g_e}$ is the external graviton, and $0_{10}0_{-10}$ is the particle-antiparticle. There are four equal regions: the 10D positive-energy particle universe, the external graviton, the 10D negative-energy particle universe, and the external anti-graviton. The emergence of positive charge and negative charge provides the prototype of the observed electromagnetic force with charge generated during the Big Bang [14] [15].

2) The formation of the asymmetrical dual universe

The formation of our current universe follows immediately after the formation of the 10D particle dual universe through the asymmetrical dimensional oscillations, leading to the asymmetrical dual universe. The 10D positive-energy universe was transformed immediately to the 4D positive-energy particle universe with zero vacuum energy. The 10D negative-energy particle universe undergoes the stepwise dimension number oscillation between 10D and 4D. Without absorbing the inter universal void, the external graviton and the anti-graviton also undergo the stepwise dimension number oscillation between 10D and 4D. The result is the asymmetrical dual universe consisting of the four equal regions of the 4D positive-energy particle universe, the variable D external graviton, the variable D negative-energy particle universe, and the variable D external anti-graviton. The asymmetrical dual universe is manifested as the asymmetry in the weak interaction in our observable universe as follows.

$$\begin{aligned}&\text{the 4D positive-energy particle universe and the external graviton}\\&\left(\left(s\,0_{4}\,e^{+}w^{+}\,e^{-}w^{-}\,0_{-4}\,s\right)g_{e}\right)_{n}\\&\text{the variable D negative-energy particle universe and the external anti-graviton}\\&\left(\overline{g_{e}}\left(s\,0_{4\text{ to }10}\,e^{+}w^{+}\,e^{-}w^{-}\,0_{-4\text{ to }-10}\,s\right)\right)_{n}\end{aligned} \tag{9}$$

where s, g_e, $\overline{g_e}$ e, and w are the strong force, external graviton, external anti-graviton, electromagnetism, and weak interaction, respectively for the observable universe, and where 0_40_{-4} and $0_{4\text{ to }10}\;0_{-4\text{ to }-10}$ are 4D particle-antiparticle for the 4D positive-energy particle universe and variable D particle-antiparticle for the variable D negative-energy particle universe, respectively. For our asymmetrical dual universe, the step 3 for the transformation from 10D string to 10D particle had to be followed by the step 4, so the electromagnetic interaction from the step 3 was unified with the weak interaction from the step 4 to become the electroweak interaction, which was generated during the Big Bang [14] [15].

In the reversible cyclic dual universe, the strong force emerged before the emergence of kinetic energy, while electromagnetism and the weak force after the emergence of kinetic energy. As a result, quarks associated with the strong force have fractional charges, while the fermions associated with electromagnetism and the weak force are integral charge electron and neutral charge neutrino, respectively. The strong force binding the quarks increases with distance, unlike the electromagnetic force whose strength decreases with distance. When one attempts to separate quarks, bond energy increases up to a point where it becomes more favorable to decay to other particles. As a result, fractional charge quarks are confined by the strong force, while integral charge electron is not confined by electromagnetism to follow the integer-fraction principle of the digital electric charge. The strong force is the confinement force field to confine fractional charge quarks. No isolated fractional charge quark has been observed directly, and collective fractional charge quarks can be observed within hadron. Fractional charges can be observed only in the confinement of collective fractional charges.

According the integer-fraction transformation from integral charge to fractional charge, the formation of quarks from electrons is as follows.

$$\begin{aligned}&\text{individual } e\,\overline{e}\xrightarrow{\text{2 electric flux quanta}}\text{individual } F_c\;\overline{F_c}\\&\xrightarrow{\text{3 electric flux quanta}}\text{transitional collective } B_c\;\overline{B_c}\xrightarrow{\text{QCD}}\\&\text{collective 2 } Q_c\;\overline{Q_c}\text{ of }\pm\frac{1}{3}\text{ and }\pm\frac{2}{3}\text{ charge with 3 gluons + individual } e\,\overline{e}\end{aligned} \tag{10}$$

where F_c, B_c, and Q_c are the composite fermion the composite boson, and the composite quark, respectively. The first step of the integer-fraction transformation from electron to quark is the attachment of 2 flux quanta to indi-

vidual integral charge electrons to form individual composite fermions (F_c's). The flux quanta (70.0252 MeV) are the electric flux quanta as proposed by Peter Cameron to calculate accurately the masses of pion, muon, and proton [17]. The quantum of 70.0252 MeV is also the bosonic mass quantum proposed by Malcolm H. MacGregor for a basic building block to calculate accurately the masses of hadrons [18]. According the oscillating M-theory postulate, the electric flux quantum is B_6 the boson which one mass dimension higher than F_5 that is electron as fermion as follows [10] [11].

$$M_{B6} = M_{F5}/\alpha = M_e/\alpha = 70.0252 \text{ MeV} \tag{11}$$

where α is the fine structure constant for electromagnetism. The F_c (the composite fermion) consists of two B_6 as electric flux quanta.

$$M_{Fc} = 2M_{B6} = 140.0505 \text{ MeV} \tag{12}$$

The mass of pion (boson) is the mass of the composite fermion (F_c) minus the mass of electron (fermion) [17].

$$M_\pi = M_{Fc} - M_e = 139.5395 \text{ MeV} \tag{13}$$

which is in excellent agreement with the observed 139.5702 MeV.

The second step is the attachment of 3 flux quanta (B_6's) to the individual integral charge composite fermions (F_c's) to form the transitional collective integral charge composite bosons (B_c's). The transitional composite bosons are derived from the combination of the three composite fermions (3 F_c's) with the three flux quanta (3 B_6's) which are connected and located at the same position in the same 3-F_c energy level. One 3-F_c energy level consists of the three connected F_c sites with the connected three flux quanta (3 B_6's). The mass of the transitional composite bosons B_c is as follows.

$$M_{Bc} = 3M_{Fc} + 3M_{B6} = 630.227 \text{ MeV} \tag{14}$$

In the third step, 3 electric flux quanta (B_6's) are converted to 3-color gluons (red, green, and blue) in QCD to confine the collective fractional charge composite quarks (Q_c's) conversed from the transitional composite bosons (B_c's). The integer-fraction transformation explains the origin of the three colors in gluons. Each of the three F_c sites in the energy level has ±1/3 charge. The fractional charges of quarks are the integer multiples of ±1/3e. One composite boson (B_c) is converted into two composite quarks (fermions) in the same way as the conversion of one photon (boson) into two fermions (electron-positron). As a result, the composite quark (Q_c) has 1/2 mass of the composite boson (B_c) in addition to the mass of 0, 1, 2, or 3 electrons for the three F_c sites for different electric charges.

$$\begin{aligned} M_{Qc} &= M_{Bc}/2 + 0,1,2,\text{or}\,3M_e \\ &= 315.1136.\ 315.6246,\ 316.1356, \text{ or } 316.6646 \text{ MeV} \end{aligned} \tag{15}$$

The fully occupied integral charge composite quark (316.6646 MeV) decays into three muons (one muon and one muon-anti-muon pair). The mass of muon is as follows.

$$M_\mu = M_{Qc}/3 = M_e + \frac{3M_{Fc}}{2} = M_e + \frac{3M_e}{2\alpha} = 105.5489 \text{ MeV} \tag{16}$$

which is in excellent agreement with the observed 105.6584 MeV. The muon mass formula in Equation (16) is identical to the Barut lepton mass formula for the masses in the periodic table of elementary particles [14] [19]. Equation (16) explains the origin of 3/2 which cannot be explained easily by Cameron, MacGregor, and Barut [17]. In Equation (15), the composite quark at 315.1136 MeV without the addition of electron is not really a true fermion, so the 1/3 of the composite quark without the addition of electron is used as the fermionic mass quantum at 105.0379 MeV for a mass building block to calculate accurately the masses of hadrons by MacGregor [18].

The composite quark is the starting quark for all quarks [14]. The composite quark at the high energy condition is a low-mass current quark surrounded by three-color gluons to confine quarks. The composite quark at the low energy condition is a high-mass constituent quark with a small amount of binding energy. The calculated mass of neutron is equal to 939.54 MeV as the combined constituent quarks minus a small amount of binding energy [20] [21] in excellent agreement with observed mass of 939.57 MeV.

4. The Fractional Quantum Hall Effect

The charges of the quasiparticles in the FQHE are fractional, because of the confinement by a two-dimensional system, the Landau levels, and an extremely low temperature and the collectivity by high energy magnetic flux quanta. The Hall effect allows the observation of fractional charges [6].

When an electric current flows through a conductor in a magnetic field, the magnetic field exerts a transverse force on the moving charge carriers which tends to push them to one side of the conductor. A buildup of charge at the sides of the conductors produces a measurable voltage (the hall voltage for the Hall effect) between the two sides of the conductor. The Hall effect has become a standard tool for the determination of the density of free electrons in electrical conductors, particularly, the electron density of semiconductors. In semiconductors, electrons can be confined in a two-dimensional system, such as in the interface between silicon and silicon oxide. Electrons can be confined further by the Landau levels derived from the vortices generated by the high energy magnetic field. Some of the electrons get trapped (localized) and isolated in the Landau levels. At an extremely low temperature, electrons can be confined even further by suppressing the disturbing scattering process originating from electron-phonon interactions. Electrons are confined by a two-dimensional system, the Landau levels, and an extremely low temperature.

The collectivity of fractional charge quasiparticles is provided by the strong magnetic flux quanta from the strong magnetic field in the Hall effect. As in Equation (3), the integer-fraction transformation from individual integral charge electron to collective fractional charge quasiparticles consists of 1) the attachment of an even number of magnetic flux quanta to individual integral charge electrons to form individual integral charge composite fermions, 2) the attachment of an odd number of magnetic flux quanta to individual integral charge composite fermions to form transitional collective integral charge composite bosons, and 3) the conversion of magnetic flux quanta to the confinement force field to confine collective fractional charge quasiparticles. The integer-fraction transformation for the FQHE is similar to the composite fermion theory for the FQHE [8] [9]. The integer-fraction transformation explains the origin of $1/(2n + 1)$ in the composite fermion theory through the transitional composite boson as described in Section 2. The transformation is possible under the strict confinement condition and the strong magnetic field to generate magnetic flux quanta to attach to electrons and composite fermions. Without the strict confinement condition and the strong magnetic field, only the ordinary Hall effect without quantum Hall effect is possible.

5. Summary

In the integer-fraction principle of the digital electric charge, individual integral charge and individual fractional charge are the digital representations of the allowance and the disallowance of irreversible kinetic energy, respectively. The disallowance of irreversible kinetic energy for individual fractional charge brings about the confinement of individual fractional charges to restrict irreversible movement resulted from irreversible kinetic energy. Collective fractional charges are confined by the short-distance confinement force field where the sum of the collective fractional charges is integer. As a result, fractional charges are confined and collective. The confinement force field includes gluons in QCD (quantum chromodynamics) for collective fractional charge quarks in hadrons and the magnetic flux quanta for collective fractional charge quasiparticles in the fractional quantum Hall effect (FQHE). The collectivity of fractional charges requires the attachment of energy as flux quanta to bind collective fractional charges. The integer-fraction transformation from integral charges to fractional charges consists of the three steps: 1) the attachment of an even number of flux quanta to individual integral charge fermions to form individual integral charge composite fermions, 2) the attachment of an odd number of flux quanta to individual integral charge composite fermions to form transitional collective integral charge composite bosons, and 3) the conversion of flux quanta into the confinement force field to confine collective fractional charge composite fermions converted from composite bosons. The charges of quarks are fractional, because QCD (the strong force) emerged in the universe that had no irreversible kinetic energy. Kinetic energy emerged in the universe after the emergence of the strong force. The charges of the quasiparticles in the FQHE are fractional because of the confinement by a two-dimensional system, the Landau levels, and an extremely low temperature and the collectivity by high energy magnetic flux quanta. From the integer-fraction transformation from integral charge electrons to fractional charge quarks, the calculated masses of pion, muon and constituent quarks are in excellent agreement with the observed values.

References

[1] Abbiendi, G., *et al.* (2003) *Physics Letters*, **B572**, 8-20. http://dx.doi.org/10.1016/S0370-2693(03)00639-7

[2] The MACRO Collaboration (2000) *Physics Review*, **D62**, 052003. http://dx.doi.org/10.1103/PhysRevD.62.052003

[3] Halyo, V., *et al.* (2000) *Physics Review Letters*, **84** 2576-2579. http://dx.doi.org/10.1103/PhysRevLett.84.2576

[4] Bian, J. and Wang, J. (2012) *Journal of Instrumentation*, **7**, 7020. http://dx.doi.org/10.1088/1748-0221/7/07/P07020

[5] Tsui, D., Stormer, H. and Gossard. A. (1982) *Physical Review Letters*, **48**, 1559. http://dx.doi.org/10.1103/PhysRevLett.48.1559

[6] Stormer, H. (1999) *Reviews of Modern Physics*, **71**, 875. http://dx.doi.org/10.1103/RevModPhys.71.875

[7] Laughlin, R. (1983) *Physical Review Letters* **50**, 1395. http://dx.doi.org/10.1103/PhysRevLett.50.1395

[8] Kamilla, R., Wu. X. and Jain, J. (1996) *Physics Review. Letters*. **76**, 1332. http://dx.doi.org/10.1103/PhysRevLett.76.1332

[9] Jain, J. (2007) Composite Fermions. Cambridge University Press, New York. http://dx.doi.org/10.1017/CBO9780511607561

[10] Chung, D. (2015) *Journal of Modern Physics*, **6**, 1820-1832. http://dx.doi.org/10.4236/jmp.2015.613186

[11] Chung, D. (to Be Published in April, 2016) *Journal of Modern Physics*, **7**, 642-655. http://dx.doi.org/10.4236/jmp.2016.77064

[12] Randall, L. (2005) Warped Passages: Unraveling the Mysteries of the Universe's Hidden Dimensions. Harper Collins, New York.

[13] Randall, L. and Sundrum, R. (1999) *Physics Review Letter*, **83**, 3370-3373. http://dx.doi.org/10.1103/PhysRevLett.83.3370

[14] Chung, D. (2014) *Journal of Modern Physics*, **5**, 1234-1243. http://dx.doi.org/10.4236/jmp.2014.514123

[15] Chung, D. (2015) *Journal of Modern Physics*, **6**, 1249-1260. http://dx.doi.org/10.4236/jmp.2015.69130

[16] Chung, D. and Krasnoholovets, V. (2013) *Journal of Modern Physics*, **4**, 77-84. http://dx.doi.org/10.4236/jmp.2013.47A1009

[17] Cameron, P. (2011) *Apeiron*, **18**, 29-42.

[18] MacGregor, M. (2007) The Power of Alpha: The Electron Elementary Particle Generation with Alpha-Quantized Life-times And Masses. World Scientific Publishing, Singapore.

[19] Barut, A. (1979) *Physical Review Letter*, **42**, 1251. http://dx.doi.org/10.1103/PhysRevLett.42.1251

[20] Chung, D. (1999) *Speculations in Science and Technology*, **21**, 277-289. http://dx.doi.org/10.1023/A:1005513404873

[21] Chung, D. (2001) The Periodic Table of Elementary Particles and the Composition of Hadrons. arXiv:hep-th/0111147v5

Journal of Modern Physics, 2016, 7, 1160-1165
Published Online June 2016 in SciRes. http://www.scirp.org/journal/jmp
http://dx.doi.org/10.4236/jmp.2016.710105

Scientific Research Publishing

Considerations on the Unification of Quantum Physics with the General Theory of Relativity

Guido Zbiral

Klosterneuburg, Austria
Email: guido@zbiral.at

Received 25 April 2016; accepted 17 June 2016; published 21 June 2016

Abstract

From a holistic perspective of a physical space of any given size[1], it is invariably necessary to consider its energy content, since no physical means exists of making a physical space completely devoid of energy. Such a space would therefore only be a fictive "geometric space"—that can be intellectually conceived and treated according to the rules of the appropriate geometry—although not existing in reality in the cosmos. Cosmic space always contains energy in one form or another, limited by the space under consideration. Therefore, each space possesses an energy density—no matter how low, which never becomes zero. Because of the mass-energy equivalence relationship $E \equiv m.c^2$, cosmic space also possesses a mass equivalent and is therefore "materialistic" in nature. If this is considered in association with Einstein's space-time, what is obtained instead is an "energy-time", *i.e.* an energy effect, which is based on Planck's action quantum h. Under this condition, a close relationship would appear to exist between the General Theory of Relativity and Quantum Physics. Furthermore, it will be shown that the physical conditions of space are such that a natural quantisation of space and time exists, thus obviating the need for any artificial or arbitrary quantisation.

Keywords

Spacetime, Energy Effect, Planck's Action Quantum h, Adapted Spacetime, Quantisation of Space and Time

1. Introduction

The Energy ↔ Space-Dualism

Due to the equivalence of mass and energy, energy can only ever appear physically—*i.e.* in a three-dimensional

[1]Each part of cosmic space is itself a real physical space.

How to cite this paper: Zbiral, G. (2016) Considerations on the Unification of Quantum Physics with the General Theory of Relativity. *Journal of Modern Physics*, **7**, 1160-1165. http://dx.doi.org/10.4236/jmp.2016.710105

form. The existence (or presence) of any given state and any given "quantum" of energy thus indispensably requires the existence of a three-dimensional space in order to be able to create an "energy effect".

Axiom: everything that exists in the cosmos is energy in one or other of its diverse manifestations and nothing exists that does not contain energy.

Cosmic space can only exist in association with energy, since cosmic space itself has been created in the course of world history by the process of dispersion of energy. For example, the energy density of the almost perfectly isotropic[2] cosmic background radiation (photon radiation) in space—a relic of the Big Bang, now having a temperature of approx. 2.7 K—is currently ca. 6×10^{-20} J/cm^3 or 0.38 eV/cm^3.

It is the nature of cosmic space to invariably be completely filled or pervaded (penetrated) with energy. As energy only manifests itself in a quantised (discrete) form, it follows that cosmic space—as the "carrier" of energy quanta—must also be structured in a quantum manner.

The properties (or parameters) of a given space under consideration are complexly related (in accordance with physical laws) to the energy situation of this space. For this reason, energy can only ever be simultaneously considered with the physical space claimed by it. This physical space is a part of the entire cosmic space invariably. Energy without space and space without energy do not exist anywhere in the entire cosmos! From this, it follows that:

1) Energy requires space in order to yield an energy effect after a specific time (as a consequence of its inertia).

2) Space requires energy in order to be a physical space (a completely empty space void of energy would "invalidate" the concept of space)[3].

3) Energy and space are mutually dependent and are mutually inseparably associated from a physical perspective; they should therefore always be considered "holistically". This applies equally both to the cosmos as a whole and to each single photon as a fundamental component of the entire cosmos. The frequency ν of the photon determines its energy E, while its wavelength λ determines the space claimed by the photon. As far as the physical size is concerned [energy density × volume], energy and cosmic (physical) space are coessential or identical!

4) $E = h \times \nu$ (Planck's Equation), h (Planck's action quantum) = 6.626×10^{-34} J·s, $\nu = c/\lambda$ [1].

Due to the fundamental importance of the theses 1) to 3) for the following considerations, I shall attempt—even at the risk of repeating myself—to formulate even more precisely as well as justify this:

Space, considered holistically, contains energy—always and without exception.

Energy, considered holistically, claims a specific and hence limited space—always and without exception.

Note: *At the very beginning*, *only energy existed in the highest concentrated form*! *As a result of the ensuing* "*energy dispersion*", *the constantly expanding cosmic space came into being and started to expand* (*associated by the simultaneous decrease in the energy density*). *Cosmic space is completely flooded by energy—always and everywhere—and is thus identical to energy. Cosmic space can therefore be considered as* "*inflated energy*".

Cosmic space consists solely of energy in all possible existing states and energy densities. Therefore, space and energy, considered holistically from a physical perspective, are one and the same!

However, we have become accustomed in our daily life to consider the two identical physical quantities as separate entities (essences), because in one case the subject of our interest is only the volume of the space (or its geometrical form)—while in the other case it is only the amount (or density) of the energy within the space!

"Pure" space, *i.e.* an absolute vacuum, devoid of any energy content, is not a physical space, and thus has no physical dimension—it is only a "geometrical space" (*i.e.*, a graphic space that can be imagined intellectually and analysed from a geometrical and mathematical perspective). Albeit possessing the geometrical spatial dimensions [R^3], say, [cm^3], it is not real in the sense of existing in the cosmos.

The complete energy vacuum of a space cannot be represented by any physical state; neither has such a space ever existed anywhere in the cosmos nor is it possible to create one—even with the most extreme technical efforts imaginable. According to quantum theory, it is not even possible to produce an ideal vacuum in the cosmos, since a field energy will never become precisely zero, its field quanta only fluctuate in an indeterminate manner around the zero value. It is these quantum fluctuations that therefore always result in a certain residual energy. This means that a supposedly "completely empty space—devoid of energy" can never exist in the cosmos, but

[2]No preference exists with respect to position and direction of radiation, *i.e.*, it is uniform in all places and directions.

[3]According to Leibnitz: "Space is the relationship of objects to each other; space is nothing without objects present in the space." Each form of energy (≡mass) shall be physically assigned the term "object". Therefore cosmic space is "material".

must contain a certain residual field energy, no matter how small. For this reason, no heat accumulator can exist, from which it is possible to completely extract its heat content. It will always retain a residual quantity of heat—no matter how small.

"Real = physical space", *i.e.* the entire universe as well as any arbitrarily small part of it, always possesses an energy density $\varepsilon = [E/R^3]$, its "physical dimension" therefore being $[R^3 \cdot \varepsilon]$ = energy = $[E]$, e.g. W·s or J or N·m. Thus, for example, the energy density of the universe due to the cosmic background radiation is given by $\varepsilon = 6 \times 10^{-20}$ J/cm^3 or 0.38 eV/cm^3.

From this, it follows that:

Cosmic space is energy and for this reason must be classified as "material" in nature, since the entire cosmos has emerged exclusively from energy (three-dimensional) in the course of world time t, and it is at all times another energy effect, *i.e.* the product of energy multiplied by time.

Even by applying the greatest possible technical effort, it is physically impossible to completely separate the "energy of space" from its particular space under consideration[4]. Every arbitrarily small or large space remains therefore inseparably associated with its intrinsic residual energy. Exactly as is the case with energy, no part of real (physical) space—no matter how small, created by the dissipation of energy, can be annihilated; it remains in existence forever (in the expansion phase of the cosmos).

Therefore in all physical considerations, the particular space under consideration must be regarded together with its energy content, which is present at all times without exception. Considering only the geometrical dimensions of space $[R^3]$, may result in a physically false picture, because:

It is energy that makes space into a real physical space and provides space with both its internal structure and external form by means of the gravitation inseparably associated with energy!

In other words: each arbitrary quantum of energy is inextricably associated with space and gravitation, or alternatively, each physical space contains energy and gravitation.

2. Association between Spacetime and Energy Effect

1) In Einstein's spacetime, space contains no energy (and therefore no gravitational force)—it is a continuum.

Spacetime thus possesses only the geometrical dimension R^3 multiplied by time t and—in the sense of the axiom set forth in Chapter 1—cannot be ascribed any real existence. It is merely a mathematical-geometrical construct, in which gravitation is interpreted not as a force but as the geometry of space.

Notwithstanding being an extremely successful theory of gravitation, all attempts to combine the General Theory of Relativity with Quantum Physics into one single united theory of quantum gravitation have hitherto failed. The unification of the two great theories of the 20th century is regarded as one of the great challenges of physics, and yet it is not certain whether this will be successful based on the premises currently existing. The requirements for the unification of the two theories would, of necessity, include the quantisation of time and space.

As a continuum, the completely empty geometrical space is only divisible to an arbitrary fine extent from a geometrical perspective—but not, however, from a physical perspective. A space completely devoid of energy, e.g. spacetime, is thus not physically quantisable, but only geometrically quantisable—by being assigned arbitrary (fictitious) space quanta, e.g. in units of the Planck length (L_P) or a multiple thereof. In this manner, however, it is not possible to bring about a unification of these two great theories. For this purpose, it will be necessary to seek a different path.

2) If the insights obtained from Chapter 1 are included in the following physical considerations—*i.e.* that a "cosmic space ≡ energy" equivalence exists-then it becomes possible to interpret the expression for cosmic space

"spacetime = space × time" as "space × energy density × time = energy × time",

possessing the physical dimension $[R^3 \cdot \varepsilon t] = [E \cdot t]$, *i.e.* an "energy effect". Under this condition, Planck's energy effect (quantum theory) and Einstein's adapted spacetime (adapted General Relativity Theory) can be unified. As it is an incontestable fact that the entire cosmic space with its energy content represents an energy effect in the course of the world time to date, then the above interpretation must be permissible. The spacetime thereby "adapted" is therefore an "energy effect" and not a continuum. From a holistic perspective, cosmic space re-

[4]It corresponds to the 3rd Law of Thermodynamics: no heat accumulator exists, from which it is possible to completely extract its heat content. There will always remain a residual amount of heat-no matter how small.

mains today what it has always been since its creation, namely energy. Expressing this more precisely:

As cosmic space (from a holistic perspective) and cosmic energy are coessential or identical, then adapted spacetime = energy × time = energy effect are similarly identical, as already determined in Chapter 1, item c) above! By incorporating the always present space-energy into "spacetime", the latter is transformed into an "energy effect", based on the Planck's action quantum $h = 6.626 \times 10^{-34}$ J·s. In this manner, a close relationship between the two great theories of the 20th century is discerned, which leads me to believe that a unification of these two theories ought to be possible in principle, because—adapted spacetime is quantisable!

3. Considerations on a Quantisation of Real Physical Space

As far as the quantisation of cosmic space is concerned, no confirmed research results from the community of physicists as yet exist [2]-[4].

As already indicated, the entire cosmic space can be interpreted as an "energy effect". For this reason, no element of space can exist—no matter how small—that is completely devoid of energy.

It would therefore be possible to interpret Planck's action quantum has the smallest elementary unit of energy-effect, from which the entire cosmic space is composed.

Under this condition, the internal structure of cosmic space is essentially determined by the action quantum h. In consequence, this would mean that cosmic space cannot be physically divided up into arbitrarily small amounts, but rather it is possible to imagine a smallest physical element of space, say, a "space quantum", which contains an energy quantum, such as a cosmic photon, whereby the dimensions of this space quantum are dependent on the energy situation present[5].

Each energy quantum of cosmic space possesses its own (energy-specific) space quantum, and they are both identical—in precisely the same manner that energy and cosmic space are identical.

As the photons in cosmic space are "free (non-bounded) particles", the energy of the photons can, in principle, assume any arbitrary positive value. As the energy of photons in cosmic space is therefore continually changeable, so the energy density and the dimensions of each cosmic element of space are also continually changeable. We owe this situation to the continual growth (or constant expansion) of cosmic space (by contrast, we owe the stability of matter to the quantisation of energy of the system of particles that are in a bound state due to their interaction with each other).

The energetic state of each cosmic element of space is determined by the frequency of the photon acting in this element of space in accordance with Planck's Equation $E = h \times \nu$, $\nu = c/\lambda$.

As the photons on their path through cosmic space constantly generate entropy (being unable to escape the 2nd Law of Thermodynamics), they gradually lose their energy. In the case of the cosmic background radiation, the decrease of energy entails a decrease in the frequency ν (or an increase in the wavelength λ) of the cosmic photons[6]. A low-energy photon therefore requires a greater spatial component, in order to be able to oscillate with the lower frequency (or greater wavelength). The photon effectively expands the space it claims against the effect of gravitation, thus creating more space for its movement.

Note: *The wavelength λ of blackbody radiation photons is inversely proportional to its absolute temperature T and, at T = 1 K, is approx.* 2.9 mm. *The typical wavelength λ of cosmic photons associated with the current cosmic background radiation for T = 2.7 K is approx.* 1 mm, *corresponding to a frequency ν of approx.* 0.3×10^{12} Hz.

In contrast to the space quanta created by the photons associated with the cosmic background radiation, the highest-energy photons in the history of the cosmos—and thus smallest possible space quanta—occurred immediately following the Big Bang, once the physically unimaginable, immeasurably high "initial temperature" of the cosmos at time t = 0 had fallen to approx. 10^{32} K. *This temperature is known as Planck's temperature T_P.*

With the wavelength λ of photons at T = 1 K being approx. 2.9×10^{-3} m, *the wavelength λ_P at $T_P = 10^{32}$ K can be approximately calculated as* $10^{-3}/10^{32} = 10^{-35}$ m, *this being known as the Planck length λ_P and—as the physically smallest possible length—also defines the dimensions of the smallest (and highest-energy) space quanta (in physics books, the Planck length is typically denoted by L_P).*

[5]The smallest space quanta are therefore those currently occupied by the highest-energy photons. No space quanta smaller in scale may exist. Notwithstanding this, if the intellectual attempt is made to divide such a space quantum, then 2 space quanta would be obtained—each with a photon of half the wavelength, *i.e.* with twice the energy. This however is physically impossible. Therefore the smallest space quanta do indeed exist and cannot be further divided from a physical perspective.

[6]The typical wavelength of cavity photon radiation λ also corresponds to the mean distance between the photons.

Given the speed of light $c = 3 \times 10^8$ m·s^{-1}, *the frequency* $\nu_P = c/\lambda_P$ *can be approximately calculated at* 10^8 m·s^{-1}/10^{-35} m = 10^{43} s^{-1} (*or* Hz,) *and is known as the Planck frequency* ν_P.

To travel the length of λ_P, *a ray of light requires the time* $t_P = \lambda_P/c = 10^{-35}$ m/3 × 10^8 m·s^{-1} = 10^{-43} s, *this time being known as the Planck time* t_P (*the shortest interval of time physically possible*).

The Planck values calculated here on a scale of orders of magnitude only represent the first-possible physical parameters in the history of the cosmos immediately following the Big Bang at $T_P = 10^{32}$ K, derived from the first (and thus most energy-rich) photons of cosmic radiation energy, which should therefore be referred to as Planck photons. These physical parameters change in the course of world time, *i.e.*, the temperature, frequency, energy of cosmic photons is steadily decreasing, while the wavelength is steadily increasing. For this reason, the "physical quantisation of cosmic space" cannot be based on the constant Planck length $\lambda_P^3 = (10^{-35}$ m$)^3$—instead it is necessary to refer to the current energy situation of the cosmic photons.

Since the temperature and thus the energy of cosmic photons decrease everywhere uniformly with the falling thermal state of equilibrium of the cosmic background radiation—this corresponding to a universal uniform increase in entropy taking place, more space is required uniformly everywhere for this entropy to be deposited. This space is thereby created by the universal uniform increase in the wavelength λ of all cosmic photons. This means that the growth rate of cosmic space is everywhere the same—the universe is expanding uniformly and isotropically. An unequivocal correlation thus emerges between Planck's formula for the energy of the cosmic background radiation and the universal uniform growth (expansion) of cosmic space. This energy-space behaviour exhibited by all cosmic photons (or space quanta) precisely corresponds to Hubble's Law[7], which thus finds a physical explanation that is not derivable from the Big Bang Theory [5].

Furthermore, each quantum of space evidently possesses a three-dimensional structure and is spatially limited by the wavelength λ^3 of its photon. For this reason, the entire energy-filled cosmic space (as the sum total of all space quanta) must possess the same properties as its smallest energy-filled components. Everything we know about the cosmic photons and the Planck action quantum h must also apply to the cosmos as a whole. The world of the infinitesimal thus has a direct effect on the cosmos in its entirety!

Summary of the key statements contained in Chapter 3:

No space quantum exists in the cosmos without an energy quantum—were this not the case, this space quantum would be devoid of energy, and this is not possible in a physical situation. The entire cosmic space is therefore composed of energy quanta (e.g. cosmic photons), where each energy quantum in cosmic space possesses its own (energy-specific) space quantum. In the course of world time, each cosmic photon (like everything else) constantly generates entropy, the deposition of which constantly requires more cosmic space. This increase in entropy causes the photon to constantly lose energy, this being expressed in a constant increase in its wavelength λ. The increase in λ is tantamount to a uniform expansion in the space required by each cosmic photon in all directions in order to be able to oscillate with the ever greater wavelength λ. As a result of this quantum phenomenon, all cosmic photons taken together are the cause of the constant and isotropic expansion of the entire cosmic space, precisely corresponding to Hubble's Law.

4. Considerations on a Quantisation of Time

The quantisation of time is an area of research still in its infancy, concerning which there are at the present time no as yet generally recognised or confirmed results from the community of physicists available [6]. Since in General Relativity, space and time are interlocked in the spacetime continuum, if one of them is quantised, then so must the other.

To use the shortest possible constant Planck time ($t_P = 10^{-43}$ secs) for the quantisation of time would not be physically justifiable, but merely an arbitrary imposition. The time quanta of cosmic space will not have remained constant in the course of world time to date, but rather—in analogy to the dimensions of space quanta depending on the variable energy of the cosmic photon radiation—are dependent on the variable energetic ambient conditions of the space in question. I therefore propose to draw on the frequency $\nu = 1/t$ of cosmic photons for the physical quantisation of time, since Planck's Equation $E = h \times \nu$ also provides a correlation between space quanta and time quanta.

At the present time, the typical wavelength λ of the cosmic photons of the cosmic background radiation is

[7]The same situation arises everywhere—irrespective of the point of view of the observer, *i.e.* an increase in the speed of expansion in proportion to the distance from the respective observer.

approx. 1 mm at a cosmic temperature $T = 2.7$ K, this corresponding to a frequency ν of 0.3×10^{12} Hz and t (at $T = 2.7$ K) = ca. 3×10^{-12} s.

For λ (at $T = 273$ K = 0˚C) = 10^{-2} mm, $\nu = 0.3 \times 10^{14}$ Hz, t (at 273 K) = 3×10^{-14} s

For λ (at $T = 3000$ K) = 0.9×10^{-3} mm, $\nu = 0.3 \times 10^{15}$ Hz, t (at 3000 K) = 3×10^{-15} s …and so on.

For λ_P (at $T = 10^{32}$ K) = 10^{-35} m, $\nu_P = 10^{43}$ Hz, t_P (at 10^{32} K) = 10^{-43} s.

Under these considerations, the time quanta t of cosmic space is variable within the above threshold values of frequency and temperature of cosmic photons (cosmic background radiation).

Remark on spacetime: space and time, as understood by Einstein, are not independent entities but interwoven in spacetime, *i.e.*, a physical dependence exists between them. From this it thus follows: if cosmic space is quantifiable as a perpetual carrier of energy, then cosmic time must also be quantifiable, as is seen above. Furthermore, a correlation must exist between space quanta and time quanta. Both apply in Chapter 3 and 4. However, no evidence of spacetime quantisation currently exists, and in General Relativity, space and time are continuous and not quantisable.

5. Conclusions

This paper depicts how it is possible to undertake a quantisation of space based on physical arguments, whereby each space quantum is fully occupied by an energy quantum (e.g. cosmic background radiation photon). Space quanta and energy quanta are identical in the same manner that cosmic space and energy are.

The quantisation of time is derived from the frequency of the energy quanta and is thus physically associated with the space quanta. The quantisation of space and time is an absolute prerequisite to achieve a unification of Quantum Physics with the General Theory of Relativity.

Acknowledgements

My warmest thanks go to my translator C. A. Szwaja (M.A. Physics, Oxon), both for translating my manuscript from German into English and his numerous valuable suggestions on the text itself.

References

[1] Barrow, J.D. (2002) The Constants of Nature; From Alpha to Omega Wikipedia—Planck's Constant: https://en.wikipedia.org/wiki/Planck_constant

[2] Odenwald, S. (2011) The Astronomy Cafe—Ask the Astronomers: Is Space Really Quantized? www.astronomycafe.net/qadir/BackTo286.html

[3] (2013) Physics Forums: Is Space Itself Quantized? https://www.physicsforums.com/threads/is-space-itself-quantized.707694/

[4] (2011) Physics Forums: Are Space and Time Really Quantized? https://www.physicsforums.com/threads/are-space-and-time-really-quantized.509659/

[5] Zbiral, G. (2013) *International Journal of Theoretical and Applied Physics*, **3**, 25-35.

[6] Ben Crowell, June 13, 2013 in Physics Stack Exchange: Is Time Quantized? Is There a Fundamental Time Unit That Cannot Be Divided? http://physics.stackexchange.com/questions/67899/is-time-quantized-is-there-a-fundamental-time-unit-that-cannot-be-divided

Journal of Modern Physics, 2016, 7, 1166-1180
Published Online June 2016 in SciRes. http://www.scirp.org/journal/jmp
http://dx.doi.org/10.4236/jmp.2016.710106

Dynamics of Nerve Pulse Propagation in a Weakly Dissipative Myelinated Axon

Nkeh Oma Nfor[1], Mebu Tatason Mokoli[2]

[1]Complex Systems and Theoretical Biology Group, Laboratory of Research on Advanced Materials and Nonlinear Science(LaRAMaNS), Department of Physics, Faculty of Science, University of Buea, Buea, Cameroon
[2]Laboratory of Research on Advanced Materials and Nonlinear Science (LaRAMaNS), Department of Physics, Faculty of Science, University of Buea, Buea, Cameroon
Email: omnkeh@gmail.com

Received 3 May 2016; accepted 17 June 2016; published 21 June 2016

Abstract

We analytically derived the complex Ginzburg-Landau equation from the Liénard form of the discrete FitzHugh Nagumo model by employing the multiple scale expansions in the semidiscrete approximation. The complex Ginzburg-Landau equation now governs the dynamics of a pulse propagation along a myelinated nerve fiber where the wave dispersion relation is used to explain the famous phenomena of propagation failure and saltatory conduction. Stability analysis of the pulse soliton solution that mimics the action potential fulfills the Benjamin-Feir criteria for plane wave solutions. Finally, results from our numerical simulations show that as the dissipation along the myelinated axon increases, the nerve impulse broadens and finally degenerates to front solutions.

Keywords

Ginzburg-Landau Equation, Liénard Form, Fitz Hugh Nagumo Model, Semidiscrete Approximation, Saltatory Conduction, Benjamin-Feir Criteria, Dissipation

1. Introduction

Wave p ropagation a nd p attern f ormation i n a v ariety o f ex citable media ca n b e e ffectively d escribed b y reaction-diffusion e quations. The F itzHugh N agumo (FHN) model [1] [2] is o ne o f t he simple e xamples o f a two-dimensional e xcitable d ynamics t hat governs such systems. T his model ha ve b een us ed a s a s implified version of t he Hodgkin-Huxley m odel [3] of ne uron firing. The F HN m odel w hich i s characterized b y a recovery m echanism furnishes us with a b etter und erstanding o f the essential d ynamics o f t he i nteraction of

How to cite this paper: Nfor, N.O. and Mokoli, M.T. (2016) Dynamics of Nerve Pulse Propagation in a Weakly Dissipative Myelinated Axon. *Journal of Modern Physics*, **7**, 1166-1180. http://dx.doi.org/10.4236/jmp.2016.710106

membrane potential and qualitatively captures the general properties of an excitable membrane. Even though its simplicity allows very valuable insight to be gained, the accuracy of reproducing real experimental results is limited.

Myelinated axons modelled by discrete FHN equations incorporate a richer dynamics than its continuous counterparts. Also, the mathematical study of spatially discrete models is challenging because of special and poorly understood phenomena occurring in them that are absent if the continuum limit of these models is taken. For example, in the discrete FHN model, there exists a coupling threshold for its propagation while the continuous system sustains propagation of all coupling strengths [4]-[7]. Enormous efforts to understand propagation failure in FHN system were made by Booth *et al*. [6], in which they considered slow recovery and very special limiting values of the parameters characterizing the bistable source and the spatial diffusivity in the FHN system. By imposing some special boundary conditions, they studied the evolution of localized front from one cell to another until it failed to propagate. Also, by using the Morris-Lecar model for myelinated nerve fiber, Hastings *et al*. [8] demonstrated that travelling waves could be observed even though they had difficulties to extend their results to the FHN system. Our main focus is to capture the various profiles of nerve impulses along a myelinated axon when the dissipative effects is reduced to its minimum value. This will be experimentally very difficult to be realized, but we hope to theoretically investigate this effect by using perturbation techniques.

The effects of dissipation is prominent in most physical and biological systems [9]-[11], such as the myelinated FHN fiber which is a discrete system made of periodic structures called Ranvier nodes [12]. Dissipative systems are spatiotemporally organized patterns that are far from a steady state configuration because of the dynamic imbalance between spatial interactions and temporal instabilities. This dissipative effect spread thoughout a neural network because of the spatially localized connectivity between adjacent group of neurons, leading to the diffusive transmissions to neighboring cells. In fact, from experimental and theoretical standpoint, waves travelling over dissipative neural network mostly vanish due to collision [13]-[15] and lack of an external energy source to take care of attenuation [16]. However, we still observe localized short excitations of nerve impulses [17], ultrashort pulses from passively mode-locked lasers, travelling waves in cortical networks, Bose-Einstein condensates in cold atoms [18], in various autonomous dissipative media, suggesting that more stable solitonic profiles can be observed provided measures are taken to minimize dissipation.

The control of pulse propagation in dissipative media can also be achieved by subjecting the system to high frequency periodic perturbations. For a discrete system like myelinated axons, this method has the advantage that the external frequency can either suppress or enhance the pulse propagation [19]. The purpose of this study is to examine the evolution of a nerve impulse, responsible for carrying electrical signals along a weakly dissipative myelinated axon. This issue is brought into sharp focus because neurons effectively participate in a collective spatiotemporal sharing of vital information. For some conservative media like in optical fibers, such crucial signals are conveyed by trains of solitons [20]-[22] which are robust to external perturbations. We derived the Complex Ginzburg-Landau (CGL) equation from a weakly dissipative FHN model, where the pulse solution clearly depicts the action potential typical in neural networks. The linear stability analysis of the action potential generally shows that the nerve impulse is relatively unstable to small pertubations.

The rest of the work is organized as follows; in Section 2, after a brief introduction of the FHN model, we derived the model CGL equation in a weak dissipative medium using the multiple scale expansion in the semi-discrete approach. The analytic solution of the CGL equation is obtained in Section 3 following the method highlighted in [23], to obtain the Pereira and Stenflo [24] pulse soliton solution. A linear stability analysis is carried out in Section 4 to check the robustness of the nerve impulse when subjected to a minimal perturbation. Consequently, the Benjamin-Feir criteria is satisfied from the qualitative analysis of the modulational instability. Numerical simulations of the CGL equation depict the evolution of the pulse soliton whose width increases as the dissipation increases. In the absence of dissipation, we observe a stable profile of the nerve impulse. Finally Section 5 gives a summary of the entire work.

2. Model Equations

We consider a one-dimensional chain of FitzHugh-Nagumo equations [1] [2]:

$$\dot{u}_n = u_n - \frac{u_n^3}{3} - v_n + K\left(u_{n+1} - 2u_n + u_{n-1}\right) \tag{1a}$$

$$\dot{v}_n = a + bu_n - cv_n. \tag{1b}$$

Here u_n and v_n are the membrane potential and the recovery variable respectively at the n^{th} excitable membrane site known as Ranvier node. The recovery variable v_n depicts the slow dynamics because the parameters $a,b,c \ll 1$. For Equation (1a), the first term, u_n, accounts for the positive feedback, where depolarization enhances more depolarization through the voltage-gated sodium channel. The second term, $-u_n^3/3$, is a rapid negative feedback loop, corresponding to the auto-inactivation of the sodium channel. The third term $-v_n$ represents a recovery process which may be physically responsible for regulating the outward potassium currents that oppose depolarization. The last term is the discrete diffusive term with coupling strength K, that is proportional to the difference in internodal currents through a given Ranvier node. The first term of (1b) *i.e.* a mainly measures the potassium leakage current while bu_n captures the activation of the voltage-gated potassium channel by the membrane potential u_n, which increases the magnitude of v_n. Lastly, $-cv_n$ controls the pumping of potassium ions out of the neuron.

Differentiating Equation (1a) with respect to time and substituting the value of $\dot{v}_n$ from (1b) yields

$$\ddot{u}_n + \Omega_0^2 u_n + \left(u_n^2 - \gamma_2\right)\dot{u}_n - \gamma_1 u_n^3 + \gamma_0 = D_0\left(u_{n+1} - 2u_n + u_{n-1}\right) + D_1\left(\dot{u}_{n+1} - 2\dot{u}_n + \dot{u}_{n-1}\right), \tag{2}$$

where $\Omega_0, \gamma_0, \gamma_1, \gamma_2, D_0$ and D_1 are all constants.

System (2) is the Liénard form of the FHN model of a myelinated nerve fiber which may be considered as the modified form of the van der Pol equation. For $D_0 = D_1 = 0$, Equation (2) becomes the cubic Liénard equation with linear damping and it is sometimes regarded as a generalization of damped oscillations. Furthermore, within the linear regime and when the dissipation is neglected, we obtain the well known linear harmonic oscillator that finds numerous applications in both classical and quantum physics. The Liénard type of equations have been intensively investigated from both mathematical and physical perspectives, and their study remains an active field of research in mathematical physics [25]-[28].

Equation (2) also mimics a one dimensional chain of atoms with unit mass, harmonically coupled to their nearest neighbors, characterized by dissipation and subjected to nonlinear on-site potential. A lot of difficulties is encountered to analytically solve this equation, however we will use a perturbation technique to minimize the effects of dissipation and also attempts to find appropriate solutions. In this light, all the dissipative coefficients γ_2, D_1 are perturbed to the order ε^2, where $\varepsilon \ll 1$ is a slow variable parameter. Also, we greatly minimize the rate at which the leakage potassium ions are discharged from the neuron by perturbing γ_0 to order ε^3. Consequently keeping just terms up to order ε^2, Equation (2) is rewritten as

$$\ddot{u}_n + \Omega_0^2 u_n - D_0\left(u_{n+1} - 2u_n + u_{n-1}\right) + u_n^2\dot{u}_n - \gamma_1 u_n^3 = \varepsilon^2 D_1\left(\dot{u}_{n+1} - 2\dot{u}_n + \dot{u}_{n-1}\right) + \varepsilon^2\gamma_2\dot{u}_n. \tag{3}$$

There are always frequency limits within which normal propagation of nerve impulse signals are observed across the FHN myelinated axon. In order to define the appropriate frequency range, we employ a perturbative technique where a suitable solution of the FHN model containing ε parameter is used. Upon substitution of this solution into the diffusive FHN model (3), the dispersion relation is obtained with terms at order of $\varepsilon^0 e^{i\theta_n}$. Hence, we consider a simplified solution of our FHN model (3) of the form;

$$u_n(t) = \varepsilon\psi(n,t)e^{i\theta_n} + \varepsilon\psi^*(n,t)e^{-i\theta_n} + O\left(\varepsilon^3\right), \tag{4}$$

with $\theta_n = qn - \omega t$ where q is the normal mode wave number and ω is the angular frequency.

In the semidiscrete approximation, $\psi(n,t)$ is supposedly independent of the "fast" variables t and n. Instead, it depend on the "slow" variables defined by $X_i = \varepsilon^i x$ and $T_i = \varepsilon^i t$, for $i \geq 1$. A continuum limit approximation is then made with the wave amplitudes while the discrete nature of the phase in maintained, details of this method is given in [25] [29].

Collecting terms at order $\varepsilon^0 e^{i\theta_n}$ gives the dispersion relation

$$\omega^2 = \Omega_0^2 + 4D_0\sin^2\left(\frac{q}{2}\right), \tag{5}$$

which is plotted in **Figure 1**. From Equation (5), the linear spectrum has a gap $\omega_{\min} = \Omega_0$ and it is limited by the cut-off frequency $\omega_{\max} = \left(\Omega_0^2 + 4D_0\right)^{1/2}$ due to discreteness.

The variation of the diffuseness of the plasma membrane through the dispersion coefficient D_0, physically

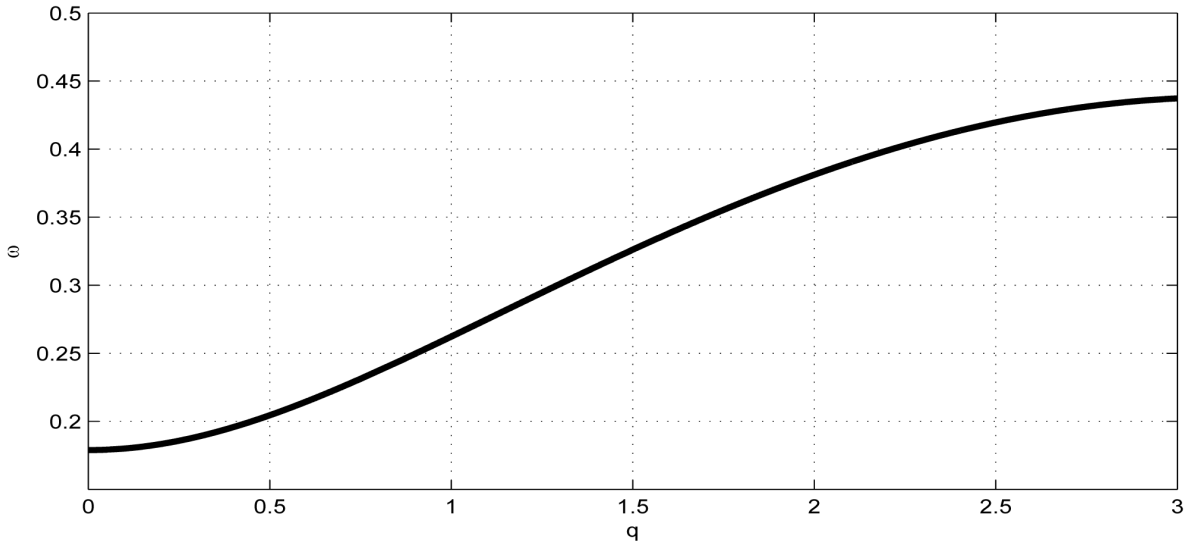

Figure 1. Linear dispersion curve of the nerve impulse for $D_0 = 0.04$ and $\Omega_0^2 = 0.032$. There is a lower cutoff mode $q = 0$ with frequency $\omega_0 = \Omega_0$ and upper cutoff mode $q = \pi$ with frequency $\omega_{\max} = \left(\Omega_0^2 + 4D_0\right)^{1/2}$.

accounts for the alteration of ions movement across pumps and ion channels at the Ranvier nodes. Clearly for normal propagation of action potential across the myelinated axon, there exists a frequency range $f_0 \le f \le f_{\max}$, where $f_0 = \Omega_0/2\pi$ (lower cutoff mode $q = 0$) and $f_{\max} = \left(\Omega_0^2 + 4D_0\right)^{1/2}/2\pi$ (upper cutoff mode $q = \pi$). In this frequency range, the voltage-gated sodium ions channels are highly concentrated in the Ranvier nodes which are myelin free. When an action potential is generated at the axon hillock, the influx of sodium ions causes the adjacent Ranvier nodes to depolarize, resulting in an action potential at the node. This also triggers depolarization of the next Ranvier node and the eventual initiation of an action potential. Action potentials are successively generated at neighboring Ranvier nodes; therefore, the action potential in a myelinated axon appears to jump from one node to the next, a process called saltatory conduction. For $f < f_0$, the action potential initially generated from one Ranvier node jumps to the next in a discontinuous manner. This process allows the speed of conduction to be greatly increased and completely distorts switching between adjacent Ranvier nodes. Consequently, this leads to propagation failure because of the inability of the nerve impulse to move across the axon. Lastly, for $f > f_{\max}$, the nerve impulse cannot propagate because its amplitude exponentially decays to zero. However considering the nonlinearity of the medium, it may be possible to observe normal propagation along the axon provided the amplitude exceeds a certain threshold value. This mode of propagation called supratransmission has been realized in many physical systems [30]-[33].

Terms of order $\varepsilon^1 e^{i\theta_n}$ gives

$$\frac{\partial \psi}{\partial T_1} + v_g \frac{\partial \psi}{\partial X_1} = 0, \tag{6}$$

where $v_g = \dfrac{D_0 \sin q}{\omega}$ is the group velocity as depicted in **Figure 2**.

Finally, we collect terms proportional to $\varepsilon^2 e^{i\theta_n}$ to have

$$\begin{aligned} \frac{\partial^2 \psi}{\partial T_1^2} - 2i\omega \frac{\partial \psi}{\partial T_2} &= D_0 \cos(q) \frac{\partial^2 \psi}{\partial X_1^2} + 2iD_0 \sin(q) \frac{\partial \psi}{\partial X_2} \\ &\quad + \left[3\gamma_1 + i\omega\right] |\psi|^2 \psi + i\omega \left[4D_1 \sin^2\left(\frac{q}{2}\right) - \gamma_2 \right] \psi. \end{aligned} \tag{7}$$

By considering the reference mobile frame $\xi_i = X_i - v_g T_i$ and $\tau_i = T_i$ with v_g being the group velocity of

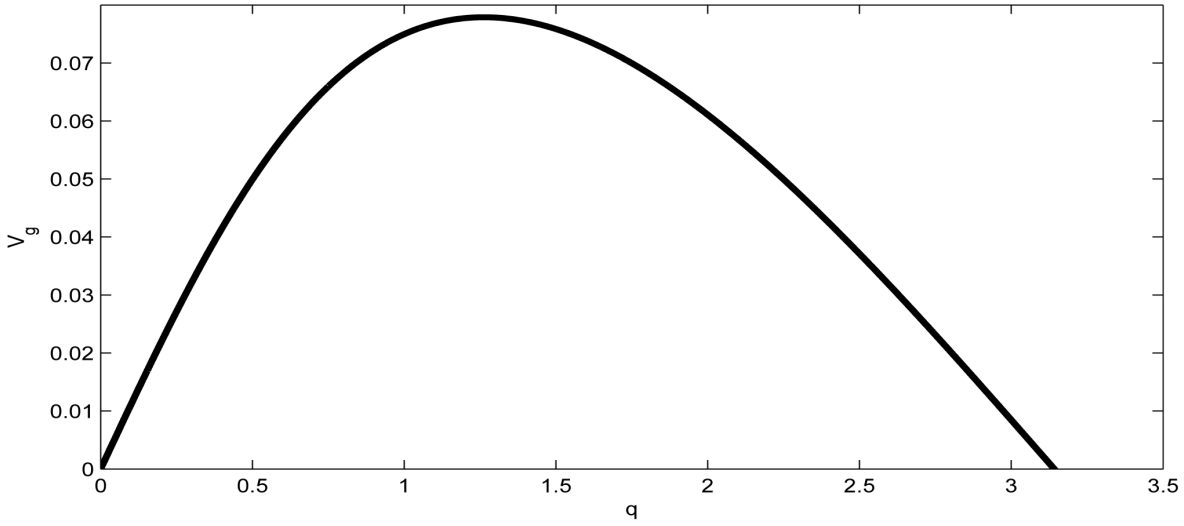

Figure 2. Group velocity of the nerve impulse for $D_0 = 0.02$ and $\Omega_0^2 = 0.032$.

the wave, we obtain

$$i\frac{\partial \psi}{\partial \tau_2} + \frac{P}{2}\frac{\partial^2 \psi}{\partial \xi_1^2} + \left(Q_r + iQ_i\right)\left|\psi\right|^2 \psi + i\frac{R}{2}\psi = 0, \tag{8}$$

where P, is the real dispersion coefficient, Q_r and Q_i are respectively the real and imaginary parts of the nonlinear coefficient, while $R < 0$ is the dissipative coefficient that causes the attenuation of action potential because of lost of energy during propagation. These parameters are given by;

$$P = \frac{D_0 \cos(q) - v_g^2}{\omega}, \tag{9}$$

$$Q_r = \frac{3\gamma_1}{2\omega}, \tag{10}$$

$$Q_i = \frac{1}{2}, \tag{11}$$

$$R = -\gamma_2 + 4D_1 \sin^2\left(\frac{q}{2}\right). \tag{12}$$

Equation (8) is the CGL equation and generally speaking, it represents one of the most-studied nonlinear equations in the physics world today. This is because it gives a qualitative and quantitative description of a myriad of physical activities [11] [25] [34]. In neural networks, the propagation of modulated nerve impulses observed is governed by CGL equation, which clearly demonstrates how neurons participate in processing and sharing of information [25]. In this study which we focus on the propagation of action potential along a myelinated axon, it is incumbent on us to obtain appropriate solutions that depicts the asymmetric structural features of action potential. Physically in most conservative media [35], solitary waves are understood as carriers of energy, however in this our context where dissipation is still prominent we need to balance the energy outflow in order to observe stable nerve impulses.

3. Solution of the Equation of Motion

Since we are dealing with a CGL equation, it is incumbent on us to look for a propagating wave solution of the form:

$$\psi\left(\xi_1, \tau_2\right) = a\left(\xi_1\right) e^{i\phi(\xi_1) - i\omega'\tau_2}, \tag{13}$$

which upon substitution into Equation (8) to obtain

$$\left(\omega' - \frac{P}{2}\phi_{\xi_1}^2\right)a + \frac{P}{2}a_{\xi_1\xi_1} + Q_r a^3 = 0, \tag{14a}$$

$$\left(\frac{R}{2} + \frac{P}{2}\phi_{\xi_1\xi_1}^2\right)a + P\phi_{\xi_1}a_{\xi_1} + Q_i a^3 = 0. \tag{14b}$$

Let us assume that

$$\phi(\xi_1) = \phi_0 + d\ln\left[a(\xi_1)\right], \tag{15}$$

where d is the chirp parameter and ϕ_0 is an arbitrary phase which we set to zero (*i.e.* $\phi_0 = 0$) without loss of generality. Equation (15) is obviously a constraint imposed on $\phi(\xi_1)$ because the chirp could have a more general functional dependence on ξ_1. However this restriction allows us to find all possible analytic pulse-like solutions of the modified CGL Equation (8). Consequently, Equation (14) becomes

$$\omega' a + \frac{P}{2}a_{\xi_1\xi_1} - \frac{P}{2}\frac{d^2 a_{\xi_1}^2}{a} + Q_r a^3 = 0, \tag{16a}$$

$$\frac{R}{2}a + \frac{P}{2}d\,a_{\xi_1\xi_1} + \frac{P}{2}\frac{d\,a_{\xi_1}^2}{a} + Q_i a^3 = 0. \tag{16b}$$

We now have two second order ordinary differential equations (ODE) relative to the same dependent variable, $a(\xi_1)$. To have a common solution, the two equations must be compatible which generally in most systems is not the case. However, for this particular system, they can be made compatible by a proper choice of the parameters.

The following procedure is employed in order to find the compatibility conditions of the two equations; initially we eliminate the first derivatives from Equation (16) to have

$$\left(\frac{Pd}{2} + \frac{P}{2d}\right)a_{\xi_1\xi_1} + \left(\frac{R}{2} + \frac{\omega'}{d}\right)a + \left(\frac{Q_r}{d} + Q_i\right)a^3 = 0, \tag{17}$$

which upon integration and setting the integration constant to zero yields

$$\frac{Pd}{2}\left(1 + \frac{1}{d^2}\right)a_{\xi_1}^2 + \left(\frac{R}{2} + \frac{\omega'}{d}\right)a^2 + \frac{1}{2}\left(\frac{Q_r}{d} + Q_i\right)a^4 = 0. \tag{18}$$

On the other hand, we eliminate the second derivative from Equation (16), obtaining

$$\frac{Pd}{2}\left(1 + d^2\right)a_{\xi_1}^2 + \left(\frac{R}{2} - \omega' d\right)a^2 + \left(Q_i - Q_r d\right)a^4 = 0. \tag{19}$$

Equations (18) and (19) must coincide, consequently leading to the following conditions:

$$d = -3Q_r \pm \sqrt{9Q_r^2 + 2} \quad \omega' = \frac{R\left(1 - d^2\right)}{4d}. \tag{20}$$

In order for us to obtain pulse solutions with real amplitudes, we assume that $R < 0, Q_r < 0.50, P > 0,$ and without loss of generality, we set $d = 1$, leading to $\omega' = 0$. The solution of CGL Equation (8) obtained by by Pereira and Stenflo [24] now reads

$$\psi(\xi_1, \tau_2) = \left[\sqrt{\frac{-R}{2(0.5 - Q_r)}}\operatorname{sech}\left(\sqrt{\frac{-R}{2P}}\xi_1\right)\right]^{1+i} \mathrm{e}^{-i\omega'\tau_2}, \tag{21}$$

with the amplitude of the solution plotted in **Figure 3**.

We now obtain the exact analytic solution of the nerve impulse propagating along the myelinated axon by substituting (21) into the FHN model solution (4) to have;

$$u_n(t) = 2\varepsilon\left[A\operatorname{sech}\left(B\xi_1\right)\cos\left[\ln\left(A\operatorname{sech}B\xi_1\right)\right]\right]\cos\theta_n - 2\varepsilon\left[A\operatorname{sech}\left(B\xi_1\right)\sin\left[\ln\left(A\operatorname{sech}B\xi_1\right)\right]\right]\sin\theta_n, \tag{22}$$

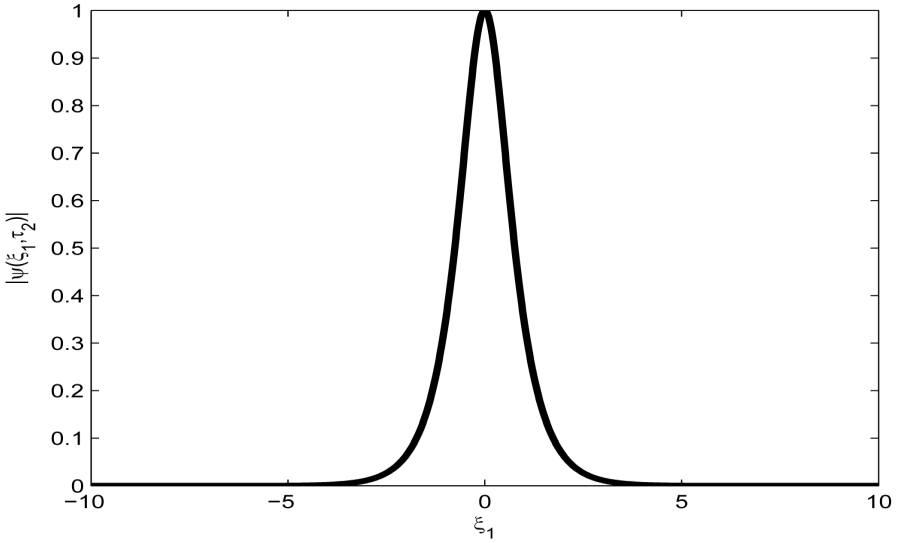

Figure 3. Spatial solution (21) of the CGL Equation (9), for $\Omega_0^2 = 0.032$, $D_0 = 0.020$, $\gamma_1 = 0.020, \gamma_2 = 0.667, D_1 = 0.001, q = 0.00$ and $d = 1.0$.

where

$$A = \sqrt{\frac{-R}{2(0.5 - Q_r)}},\ B = \sqrt{\frac{-R}{2P}}.$$

Figure 4 depicts the spatial profile of this nerve impulse which may be considered as an electrical signal that propagates over a long distance without a change in amplitude.

Also, when the parameter ε is varied, the form of the wave is greatly distorted as in **Figure 5**. Finally, **Figure 6** depicts the spatiotemporal

4. Linear Stability and Numerical Analysis

Stability is a very important property of a wave profile in a neural network, since it determines whether such patterns can be observed experimentally, or utilized for diagnostic purposes. Recall that the phenomenon of modulational in stability results when a steady-state solution is subjected to a weak perturbation, which eventually leads to the exponential growth of its amplitude along the line of propagation due to the interplay between the nonlinearity and dispersive effects of the medium. Initially, we consider the stability of the trivial homogeneous solution $\psi(\xi_1, \tau_2) = 0$ by substituting the perturbations of the form $e^{iq\xi_1 + \lambda\tau_2}$ in the linearized part of Equation (8). This leads to the characteristic equation

$$\Gamma(\lambda) = 2\lambda + R + iPq^2 = 0, \tag{23}$$

where q is a spatial wavenumber of the perturbation and λ determines the growth rate. The corresponding dispersion relation reads

$$2\lambda(q) = -R - iPq^2, \tag{24}$$

and when all the eigenvalues $\lambda(q)$ have negative real parts, the homogeneous solution is asymptotically stable. Clearly the stability depends on the dissipative coefficient R and we conclude that the trivial solution is unstable since $R < 0$.

We now study the existence and stability of plane wave solutions $\psi = \psi_0 e^{i(q\xi_1 + \omega\tau_2)}$ of Equation (8). We obtain the relation between the unknown amplitude ψ_0, wavenumber q and frequency ω of the plane wave solution as follows;

$$\omega = -\frac{1}{2}Pq^2 + \frac{1}{2}iR + (Q_r + iQ_i)\psi_0^2. \tag{25}$$

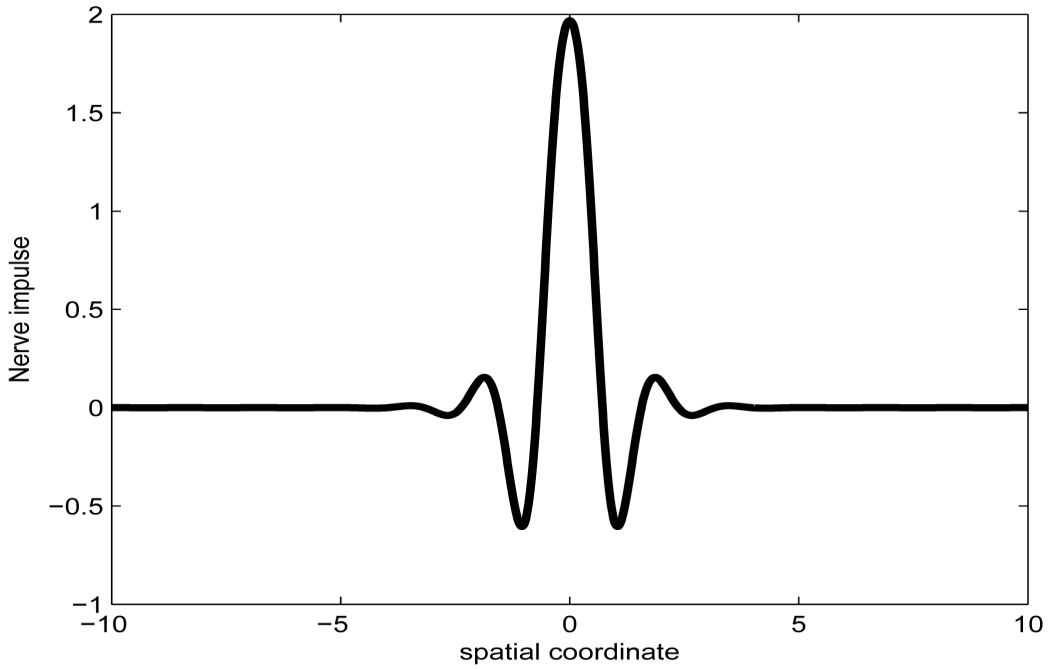

Figure 4. Spatial solution (22) of the FHN model (3), for $\Omega_0^2 = 0.032$, $D_0 = 0.020$, $\gamma_1 = 0.020$, $\gamma_2 = 0.667$, $D_1 = 0.001$, $q = 0.00$, $t = 1.0$, $d = 1.0$ and $\varepsilon = 1.0$.

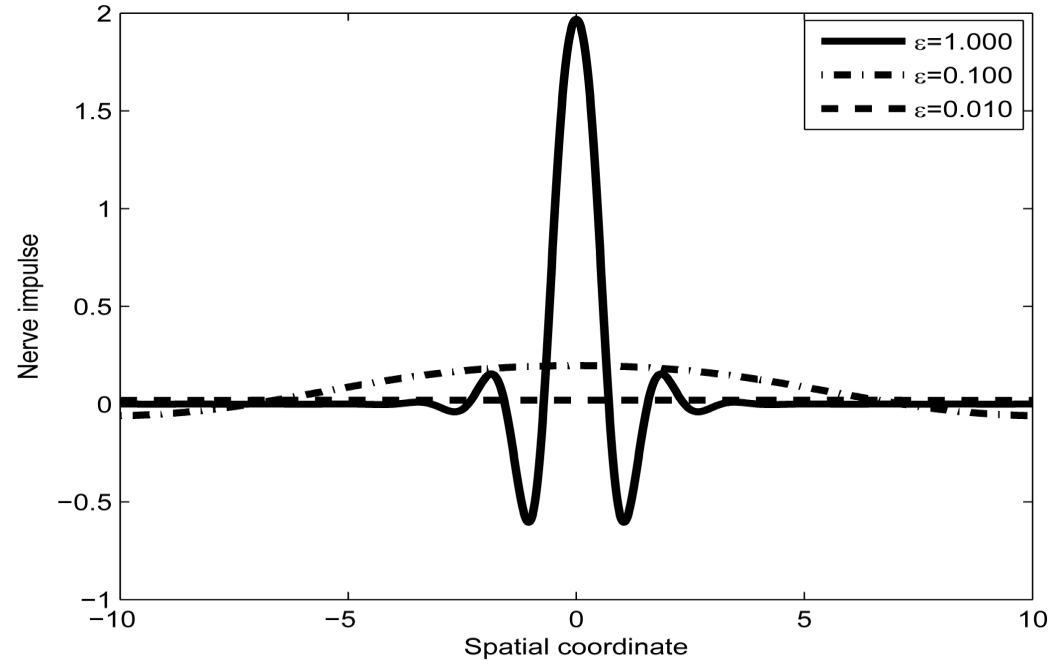

Figure 5. Spatial variation of solution (22) of the FHN model (3) as parameter ε is varied. This is for $\Omega_0^2 = 0.032$, $D_0 = 0.020$, $\gamma_1 = 0.020$, $\gamma_2 = 0.667$, $D_1 = 0.001$, $q = 0.00$, $t = 1.0$, and $d = 1.0$.

Due to the symmetry property of the CGL Equation (8) *i.e.* $\psi \to -\psi$, this equation is symmetric under the reflection $\psi_0 \to -\psi_0$, and we restrict our analysis to the case $\psi_0 \geq 0$. The real and imaginary parts of Equation (25) give the expressions for the amplitude ψ_0^2 and the frequency $\omega(q)$ at a given wavenumber q:

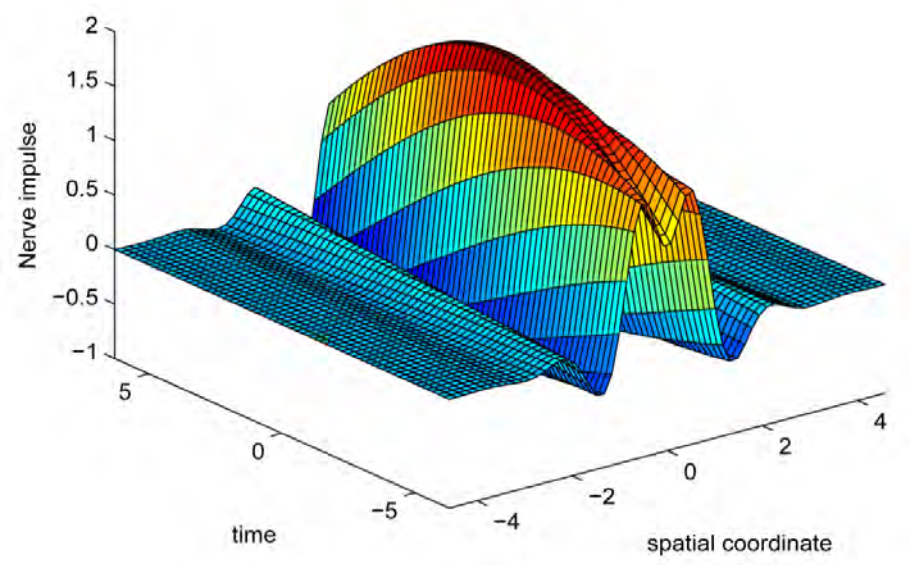

(a)

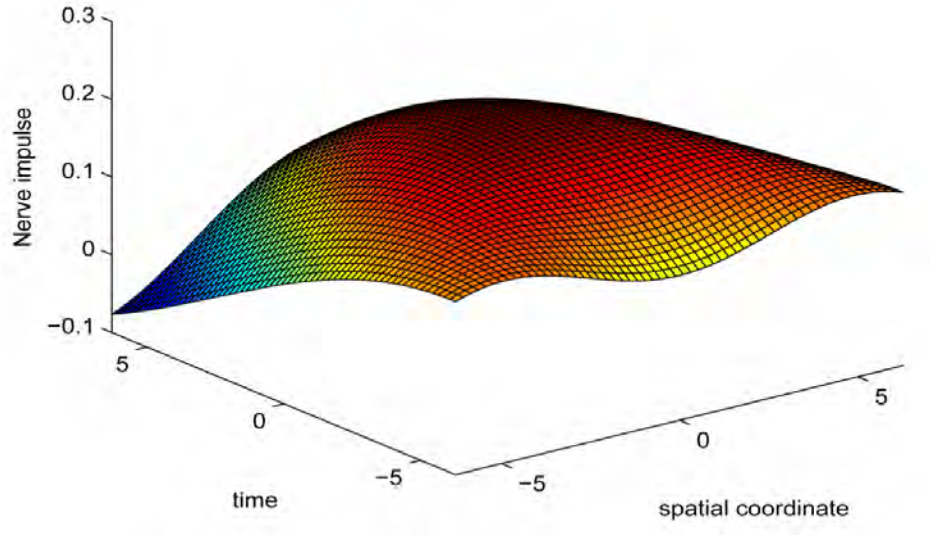

(b)

Figure 6. Spatiotemporal evolution of nerve impulse solution (22) for $\Omega_0^2 = 0.032$, $D_0 = 0.020$, $\gamma_1 = 0.020$, $\gamma_2 = 0.667$, $D_1 = 0.001$, $q = 0.00$, $d = 1.0$. (a) $\varepsilon = 1.000$ (b) $\varepsilon = 0.100$.

$$\omega(q) = -\frac{1}{2}Pq^2 + Q_r\psi_0^2,\ Q_i\psi_0^2 + \frac{R}{2} = 0. \tag{26}$$

Figure 7 shows the amplitude of the plane wave solution ψ_0 as a function of the dissipative parameter $-R$ (since $R < 0$) for $Q_i = 0.50$.

We now perturb the plane wave solutions in order to have

$$\psi(\xi_1, \tau_2) = \left(\psi_0 + \psi_p\right)e^{i(q\xi_1 + \omega\tau_2)}, \tag{27}$$

where

$$\psi_p = \psi_+ e^{ik\xi_1 + \lambda\tau_2} + \psi_- e^{-ik\xi_1 + \bar{\lambda}\tau_2}, \tag{28}$$

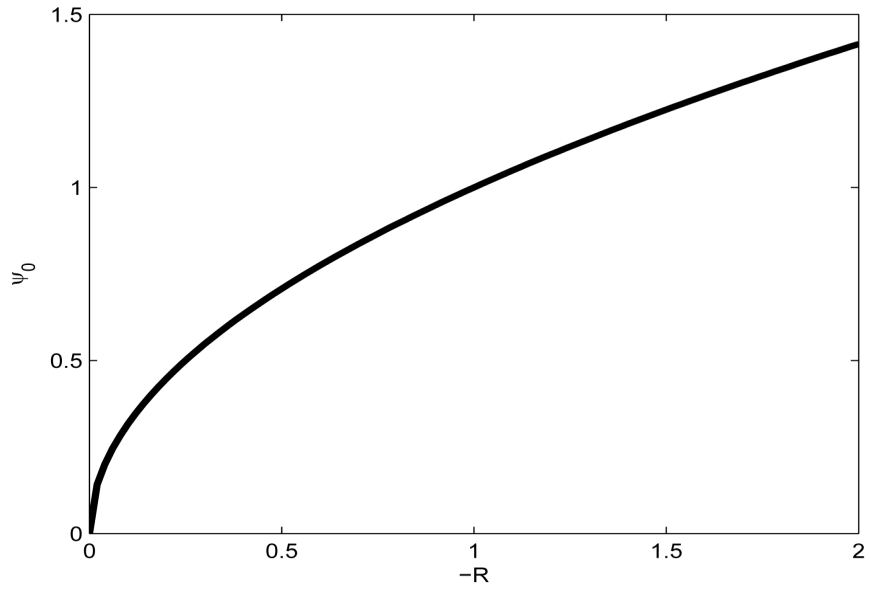

Figure 7. Amplitude of plane wave solution ψ_0 versus parameter $-R$ for $Q_i = 0.50$ according to Equation. (26).

is a small perturbation term with a growth rate λ. Here $\bar{\lambda}$ and ψ_- denote complex conjugation, and k stands for different perturbation modes. Substitution of (27) into CGL Equation (8) and linearization in ψ_p yields

$$\begin{aligned} &i\frac{\partial \psi_p}{\partial \tau_2} - \omega\left(\psi_0 + \psi_p\right) + \frac{P}{2}\left(\frac{\partial^2 \psi}{\partial \xi_1^2} + 2iq\frac{\partial \psi_p}{\partial x} - q^2\left(\psi_0 + \psi_p\right)\right) \\ &+\left(Q_r + iQ_i\right)\left(\psi_0^3 + 2\psi_0^2\psi_p + \psi_0^2\psi_p^*\right) + \frac{1}{2}iR\left(\psi_0 + \psi_p\right) = 0. \end{aligned} \tag{29}$$

After s ubstituting (28) in to (29) a nd us ing Equation (25), we obt ain a n e quation i nvolving t wo l inearly independent functions $e^{ik\xi_1 + \lambda\tau_2}$ and $e^{-ik\xi_1 + \bar{\lambda}\tau_2}$. Requiring that the coefficients of these functions are zero, we arrive at a system of linear equations for the unknowns ψ_+ and ψ_-:

$$\begin{pmatrix} m_{11} & m_{12} \\ m_{21} & m_{22} \end{pmatrix}\begin{pmatrix} \psi_+ \\ \psi_- \end{pmatrix} = \begin{pmatrix} 0 \\ 0 \end{pmatrix}, \tag{30}$$

with

$$m_{11} = i\lambda - \frac{1}{2}Pk^2 - Pkq + \left(Q_r + iQ_i\right)\psi_0^2,$$

$$m_{12} = \left(Q_r + iQ_i\right)\psi_0^2,$$

$$m_{21} = \left(Q_r - iQ_i\right)\psi_0^2,$$

$$m_{22} = -i\lambda - \frac{1}{2}Pk^2 + Pkq + \left(Q_r - iQ_i\right)\psi_0^2.$$

Since we ar e l ooking for n on-trivial s olutions $\left(\psi_+, \psi_-\right)$, th e c haracteristic e quation for t he p erturbation growth rate $\lambda(k)$ is obtained when the determinant of the coefficient matrix vanishes:

$$\lambda^2 + 2\left(Q_i\psi_0^2 + iPqk\right)\lambda + 2Pk\left(iqQ_i - kQ_r\right)\psi_0^2 + P^2k^2\left(k^4/4 - q^2\right) = 0. \tag{31}$$

Solutions $\lambda(k)$ can now be found explicitly and the maximum of their real parts determines the stability of plane waves. Consequently we solve Equation (31) to obtain

$$\lambda(k) = -\left(Q_i\psi_0^2 + iPqk\right) \pm \sqrt{\Delta}, \tag{32}$$

where $\Delta = Q_i^2\psi_0^4 - P^2k^2\left(\frac{k^2}{4} - 2\frac{Q_r}{P}\psi_0^2\right)$, is the discriminant of the quadratic Equation (31). It is a very useful component because it determines the nature of roots of the growth rate $\lambda(k)$ which is purely complex. Since this discriminant depends on different perturbation modes k, it is therefore clear that Δ is bound to have multiple values as will be demonstrated below.

For $\Delta = 0$, plane waves are modulationally stable since $Q_i > 0$.

For $\Delta < 0$, implying that $\frac{k^2}{4} - 2\frac{Q_r}{P}\psi_0^2 > 0$ we have that $\frac{Q_r}{P} < 0 (i.e\ PQ_r < 0)$ and the plane waves are always stable since $Q_i > 0$.

Lastly, for $\Delta > 0$, implying that $\frac{k^2}{4} - 2\frac{Q_r}{P}\psi_0^2 < 0$ we have that $\frac{Q_r}{P} > 0 (i.e\ PQ_r > 0)$. The perturbation grows exponentially with time resulting to the instability of the plane waves which tend to self-modulate with a wave vector k. The plane wave solutions of the CGL Equation (8) clearly manifest the the classical Benjamin-Feir scenario where plane waves are unstable for positive PQ_r, while they are stable for negative values. Consequently, one expects to find spatially localized nerve impulses along the myelinated axon, for any wave carrier whose wave vector is in the positive range of PQ_r.

The condition $PQ_r > 0$, is also the condition for the existence of solitons, the study of the long-term evolution of a plane wave injected as initial condition in the neural network shows that, after a period during which the waves start to self-modulate as predicted by the linear stability analysis we just performed, this change persists until the amplitude of the plane waves vanishes in some regions. Sometimes, this modulational instability leads to a train of pulses [36], but for our case, this effect generates a single nerve impulse produced by the superposition of continuous waves oscillating at a constant frequency shift.

We now perform the numerical simulations of the CGL Equation (8) by using a Runge-Kutta scheme with fixed step size and initial conditions obtained from the analytic solution (21) of the CGL equation to check the long term effects of modulational instability. **Figure 8** depicts the spatiotemporal evolution of the nerve impulse along the myelinated axon as the dissipative parameter is varied.

In the first case, *i.e.* **Figure 8(a)** where the dissipation is zero, we observe that the pulse conserves its shape, indicating that energy is not lost during propagation. This creates an ideal platform where vital information is transmitted along the myelinated axon with little or no distortion. As the dissipation increases as in **Figure 8(b)** & **Figure 8(c)**, the nerve impulse becomes wider and flatter and may be termed a flat-top soliton. As time tends to infinity, the flat top solitons becomes unstable and decomposes into two fronts.

The corresponding contour plot of the spatiotemporal evolution of the nerve impulse in **Figure 8** is given by **Figure 9**. This numerical results clearly confirms the prediction of our linear stability analysis by demonstrating that solutions for $PQ_r > 0$ are unstable, and furnishes us with the details beyond the linear limits. This shows that the nerve impulse degenerates to fronts which are also solutions of the CGL equation [37].

5. Conclusions

In this study, we addressed the issue of nerve pulse propagation along a weakly dissipative myelinated axon modelled by the discrete FHN model. The effect of dissipation is always a big nuisance during the transmission of electrical signals across a neural network, consequently crucial information is always lost. We transformed the FHN model to its Liénard form and minimized the effects of dissipation by perturbing the appropriate parameters to higher order. The proposed solution for the Liénard equation carried the ε parameter, where the dispersion relation that governed the propagation of nerve impulse was obtained at the first order of terms in ε. The second and third order terms in ε gave the group velocity and the CGL equation respectively. The pulse soliton solution of the CGL equation was derived analytically, and clearly mimiced the action potential typical in neural networks. We carried out linear stability analysis in Section 4, with results showing that the pulse soliton was generated as a result of modulational instability of the plane wave solution. By numerically integrating the CGL equation and varying the dissipation, we demonstrated that nerve impulses conserved its shape in a dissipative free medium. As the myelinated axon becomes more and more dissipative, the nerve impulse

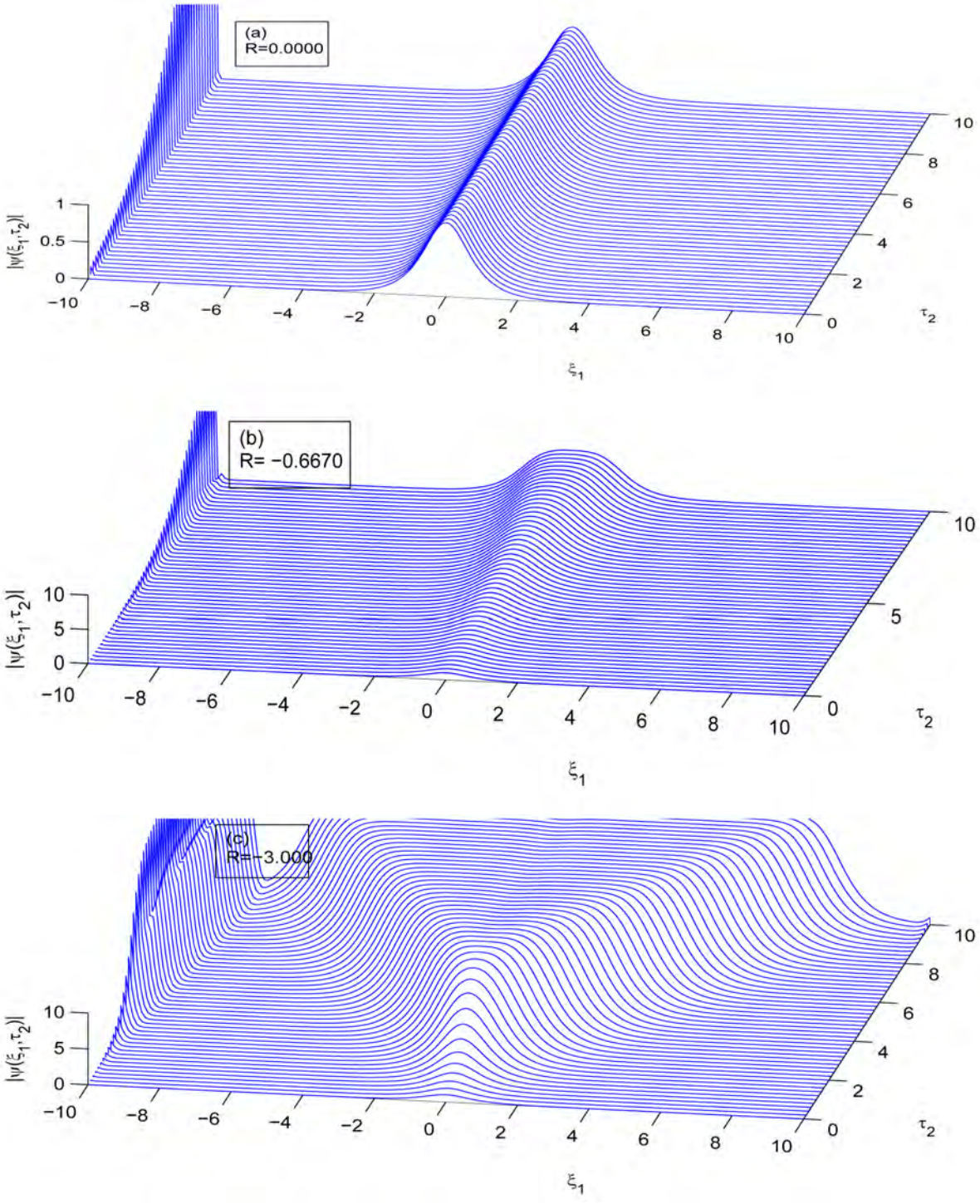

Figure 8. Spatiotemporal evolution of nerve impulse when the dissipation is varied for $P = 0.00064, Q_r = 0.600, Q_i = 0.50$. (a) $R = 0.000$, (b) $R = -0.6670$, (c) $R = -3.0000$.

becomes more unstable and degenerates to fronts.

From this theoretical study carried on a dissipative myelinated axon, we believe it will furnish us with the appropriate knowledge of predicting the physiological state of real neurons. For instance, a sick neuron which is usually considered as dissipative can be clearly distinguished from a healthy neuron and consequently lead to

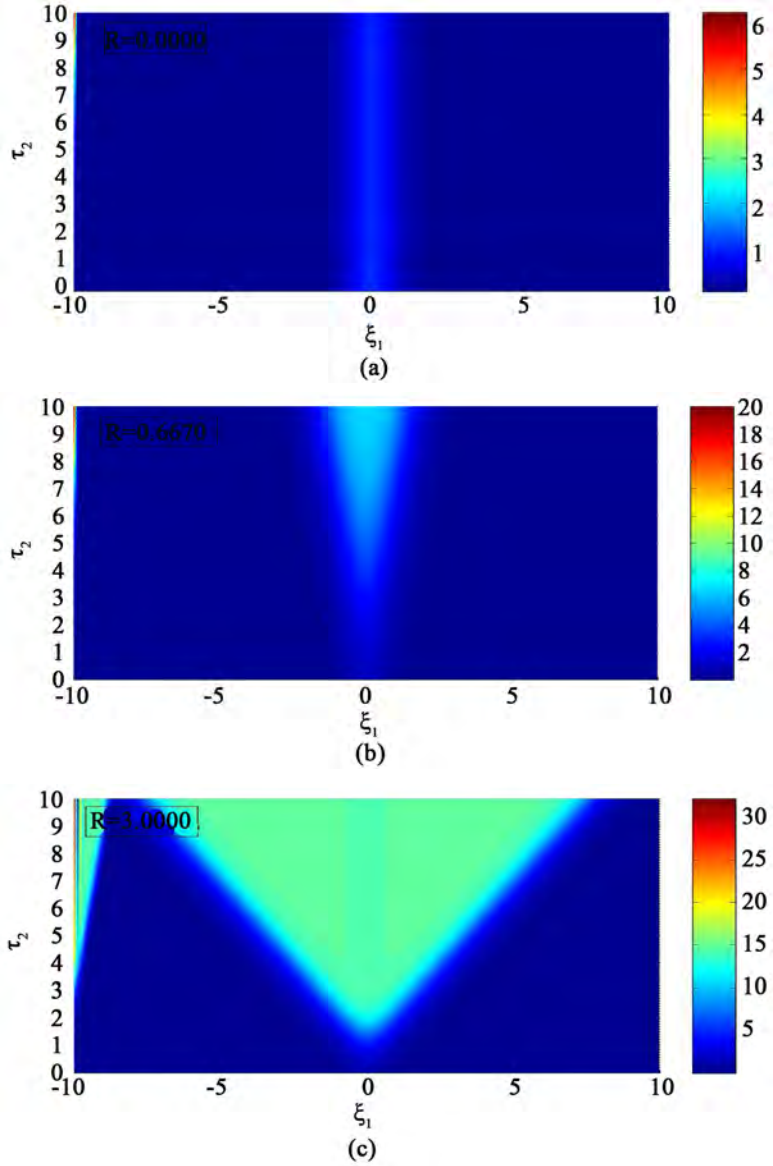

Figure 9. Corresponding contour plot of the evolution of bright nerve impulse in **Figure 8** when the dissipation is varied for $P = 0.00064$, $Q_r = 0.600$, $Q_i = 0.50$. (a) $R = 0.000$, (b) $R = -0.6670$, (c) $R = -3.0000$.

the appropriate therapeutic action.

Acknowledgements

N. Oma Nfor appreciates the enriching discussion with F. M. Moukam Kakmeni of the LaRAMaNS research group. The authors are very grateful to the referee for useful comments and the Journal of Modern Physics for subsidizing the publication fee.

References

[1] FitzHugh, R.A. (1961) *Biophysics Journal*, **1**, 445-446. http://dx.doi.org/10.1016/S0006-3495(61)86902-6

[2] Nagumo, J., Arimoto, S. andYoshitzawa, S. (1962) *Proceedings of the IRE*, **50**, 2061-2070. http://dx.doi.org/10.1109/JRPROC.1962.288235

[3] Hodgkin, A.L. and Huxley, A.F. (1952) *The Journal of Physiology*, **117**, 500-544. http://dx.doi.org/10.1113/jphysiol.1952.sp004764

[4] Keener, J.P. (1987) *SIAM Journal on Applied Mathematics*, **47**, 556-572. http://dx.doi.org/10.1137/0147038

[5] Erneux, T. and Nicolis, G. (1993) *Physica D*: *Nonlinear Phenomena*, **67**, 237-244. http://dx.doi.org/10.1016/0167-2789(93)90208-I

[6] Booth, V. and Erneux, T. (1995) *SIAM Journal on Applied Mathematics*, **55**, 1372-1389. http://dx.doi.org/10.1137/S0036139994264944

[7] Carpio, A. and Bonilla, L.L. (2001) *Physical Review Letters*, **86**, 6034. http://dx.doi.org/10.1103/PhysRevLett.86.6034

[8] Hastings, S.P. and Chen, X. (1999) *Journal of Mathematical Biology*, **38**, 1-20. http://dx.doi.org/10.1007/s002859970001

[9] Nicolis, G. andPrigogine, I. (1977) Self-Organization in Nonequilibrium Systems: From Dissipative Structures to Order through Fluctuations. Wiley, New York.

[10] Haken, H. (1983) Synergetics: An Introduction. 3rd Edition, Springer, Berlin. http://dx.doi.org/10.1007/978-3-642-88338-5

[11] Kuramoto, Y. (1984) Chemical Oscillations, Waves, and Turbulence. Springer, Berlin. http://dx.doi.org/10.1007/978-3-642-69689-3

[12] Keener, J. and Sneyd, J. (2001) Mathematical Physiology. Springer, Berlin.

[13] Wu, J.Y., Guan, L. and Tsau, Y. (1999) *The Journal of Neuroscience*, **19**, 5005-5015.

[14] Murray, J.D. (2002) Mathematical Biology II: Spatial Models and Biomedical Applications. 3rd Edition, Springer-Verlag, New York.

[15] Lu, Y., Sato, Y. and Amari, S. (2011) *Neural Computation*, **23**, 1248-1260. http://dx.doi.org/10.1162/NECO_a_00111

[16] Chang, W., Ankiewicz, A., Soto-Crespo, J.M. and Akhmediev, N. (2008) *Physical Review A*, **78**, 023830. http://dx.doi.org/10.1103/PhysRevA.78.023830

[17] Dikande, A.M. and Bartholomew, G.A. (2009) *Physical Review E*, **80**, 041904. http://dx.doi.org/10.1103/PhysRevE.80.041904

[18] Akhmediev, N. and Ankiewicz, A. (2008) Dissipative Solitons: From Optics to Biology and Medicine. Springer, Berlin.

[19] Ratas, I. and Pyragas, K. (2012) *Physical Review E*, **86**, 046211.

[20] Fandio, D.J. J., Dikande, A.M. and Sunda-Meya, A. (2015) *Physical Review A*, **92**, 053850. http://dx.doi.org/10.1103/PhysRevA.92.053850

[21] Amrani, F., Niang, A., Salhi, M., Komarov, A., Leblond, H. and Sanchez, F. (2011) *Optics Letters*, **36**, 4239-4241. http://dx.doi.org/10.1364/OL.36.004239

[22] Haboucha, A., Leblond, H., Salhi, M., Komarov, A. and Sanchez, F. (2008) *Physical Review A*, **78**, 043806.

[23] Akhmediev, N.N. and Afanasjev, V.V. (1996) *Physical Review E*, **53**, 1190-1201.

[24] Pereira, N.R. and Stenflo, L. (1977) *Physics of Fluids*, **20**, 1733-1734. http://dx.doi.org/10.1063/1.861773

[25] Kakmeni, F.M.M., Inack, E.M. and Yamakou, E.M. (2014) *Physical Review E*, **89**, 052919. http://dx.doi.org/10.1103/PhysRevE.89.052919

[26] Pandey, S.N., Bindu, P.S., Senthilvelan, M. and Lakshmanan, M. (2009) *Journal of Mathematical Physics*, **50**, 102701. http://dx.doi.org/10.1063/1.3204075

[27] Banerjee, D. and Bhattacharjee, J.K. (2010) *Journal of Physics A*: *Mathematical and Theoretical*, **43**, 062001. http://dx.doi.org/10.1088/1751-8113/43/6/062001

[28] Messias, M. and Gouveia, M.R.A. (2011) *Physica D*: *Nonlinear Phenomena*, **240**, 1402-1409. http://dx.doi.org/10.1016/j.physd.2011.06.006

[29] Dauxois, T. and Peyrard, M. (2006) Physics of Solitons. Cambridge University Press, Cambridge.

[30] Khomeriki, R. (2004) *Physical Review Letters*, **92**, 063905. http://dx.doi.org/10.1103/PhysRevLett.92.063905

[31] Susanto, H. (2008) *SIAM Journal on Applied Mathematics*, **69**, 111-125. http://dx.doi.org/10.1137/070698828

[32] Susanto, H. and Karjanto, N. (2008) *Journal of Nonlinear Optical Physics & Materials*, **17**, 159-165. http://dx.doi.org/10.1142/S0218863508004147

[33] Motcheyo, T.A.B., Tchawoua, C., Siewe, M.S. and Tchameu, J.D.T. (2013) *Communications in Nonlinear Science and Numerical Simulation*, **18**, 946-952. http://dx.doi.org/10.1016/j.cnsns.2012.09.005

[34] Pismen, L.M. (1999) Vortices in Nonlinear Fields. Oxford University/Clarendon Press, Oxford/New York.

[35] Newell, A.C. (1985) Solitons in Mathematics and Physics. SIAM, Philadelphia. http://dx.doi.org/10.1137/1.9781611970227

[36] Akhmedieva, N.N., Eleonski, V.M. and Kulagin, N.E. (1985) *Soviet Physics—JETP*, **62**, 894-899.

[37] Marcq, P., Chaté, H. and Conte, R. (1994) *Physica D*: *Nonlinear Phenomena*, **73**, 305-317. http://dx.doi.org/10.1016/0167-2789(94)90102-3

Journal of Modern Physics, 2016, 7, 1181-1191
Published Online June 2016 in SciRes. http://www.scirp.org/journal/jmp
http://dx.doi.org/10.4236/jmp.2016.710107

A Basis for Causal Scattering Waves, Relativistic Diffraction in Time Functions

Salvador Godoy, Karen Villa

Depto de Física, Facultad de Ciencias, Universidad Nacional Autónoma de México, Mexico City, Mexico
Email: sgs@ciencias.unam.mx, ksva@ciencias.unam.mx

Received 3 March 2016; accepted 18 June 2016; published 22 June 2016

Abstract

Relativistic diffraction in time wave functions can be used as a basis for causal scattering waves. We derive such exact wave function for a beam of Dirac and Klein-Gordon particles. The transient Dirac spinors are expressed in terms of integral defined functions which are the relativistic equivalent of the Fresnel integrals. When plotted versus time the exact relativistic densities show transient oscillations which resemble a diffraction pattern. The Dirac and Klein-Gordon time oscillations look different, hence relativistic diffraction in time depends strongly on the particle spin.

Keywords

Diffraction in Time, Relativistic Diffraction in Time, Causal Scattering Basis, Transient Quantum Processes

1. Introduction

Similarities between optics and quantum mechanics have long been recognized. One example of this symmetry was obtained by Moshinsky [1] who addressed the following non-relativistic, quantum, 1D shutter problem. Consider a monoenergetic beam of free particles moving parallel to the x-axis. For negative times, the beam is interrupted at $x=0$ by a perfectly absorbing shutter perpendicular to the beam. Suddenly, at time $t=0$, the shutter is opened, allowing for $t>0$ the free time-evolution of the beam of particles. What is the transient density observed at a distance x from the shutter? The shutter problem implies solving, as an initial value problem, the time-dependent Schrödinger equation with an initial condition given by

$$\psi(x,0)=\mathrm{e}^{ikx}\theta(-x), \tag{1}$$

where $\theta(x)$ denotes the step function defined as: $\theta(x)=(1 \text{ if } x>0) \text{ or } (0 \text{ if } x<0)$. For $x\geq 0$, Moshinsky proves that the free propagation of the beam has the exact solution given by:

How to cite this paper: Godoy, S. and Villa, K. (2016) A Basis for Causal Scattering Waves, Relativistic Diffraction in Time Functions. *Journal of Modern Physics*, **7**, 1181-1191. http://dx.doi.org/10.4236/jmp.2016.710107

$$M(x,t;k)=\frac{1}{\sqrt{2i}}e^{i(kx-\omega t)}\left\{\frac{1+i}{2}+\int_0^{\xi(x,t)}e^{i\pi u^2/2}\,du\right\}\theta(t), \tag{2}$$

where the integral is the complex Fresnel function: $\int_0^{\xi}\exp\left(i\pi u^2/2\right)du\equiv C(\xi)+iS(\xi)$ and ξ is given by $\xi(x,t)\equiv\sqrt{m/\pi\hbar t}\,(\hbar kt/m-x)$. For $x\geq 0$ the probability density ρ is then

$$\rho(x,t)=\frac{1}{2}\left[C(\xi)+\frac{1}{2}\right]^2+\frac{1}{2}\left[S(\xi)+\frac{1}{2}\right]^2\theta(t). \tag{3}$$

The right-hand side in Equation (3) is similar to the mathematical expression for the light intensity in the optical Fresnel diffraction by a straight edge [2]. For a fixed position $x=1$, the plot of the probability density $\rho(1,t)$ as a function of time is shown in **Figure 1**.

These temporal oscillations are a pure quantum phenomenon, and similar oscillations arise at the moment of closing and opening gates in nanoscopic circuits [3]. With adequate potentials added to the model, it has been used to study transient dynamics of tunneling matter waves [4]-[7], and the transient responses to abrupt changes of the interaction potential in semiconductor structures and quantum dots [8] [9]. For a review on the subject see [10] [11]. There is, in summary, a strong motivation for a thorough understanding of transient time oscillation in beams of matter.

One of the main problems in physics is to find, for the S matrix of an interaction, restrictions which proceed from general principles such as causality [12]. Notice that there is a close relation between diffraction in times wave functions and those wave functions which are needed for a causal description. From Equation (2) we see that for $x\geq 0$ the wave function $M(x,t;k)$ is *causal* and the shutter solution can then be used as a basis function for causal scattering. Indeed, for an arbitrary function, $f(x)\equiv\int_{-\infty}^{\infty}F(k)e^{ikx}dk$, and assuming an initial condition given by:

$$\Psi(x,0)=f(x)\theta(-x), \tag{4}$$

then the free time evolution of the initial condition becomes

$$\Psi(x,t)=\theta(t)\int_{-\infty}^{\infty}M(x,t;k)F(k)dk. \tag{5}$$

It is evident that if we want a relativistic solution for $\Psi(x,t)$, we need, instead of $M(x,t;k)$, the corresponding relativistic solution to the shutter problem.

As far as we know nobody has ever reported the exact relativistic solution to the shutter problem. Moshinsky worked this problem and gave an approximated answer. In a couple of articles [13] [14], he discussed the shutter problem using the Klein-Gordon and the Dirac equations. Using approximated solutions Moshinsky arrives to the conclusion that only for the Schrödinger equation the wave function ψ does resemble the expression that appear in the optical theory of diffraction. In his conclusions [13], Moshinsky emphatically denies the existence

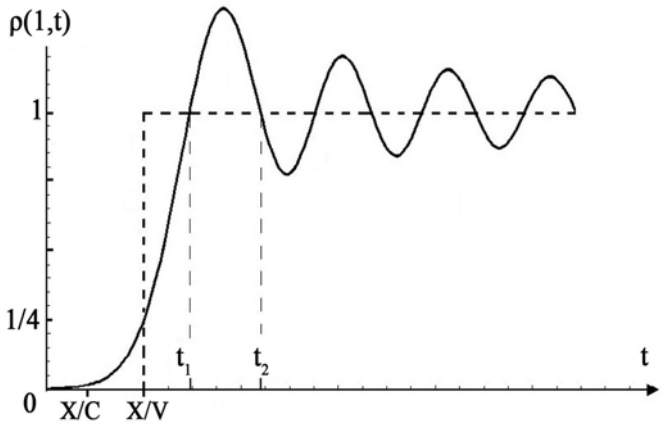

Figure 1. Probability density for non-relativistic diffraction in time.

of diffraction in time in the relativistic case. In the case of photons this is obviously true, the d'Alembert's solution does not allow such time oscillations. However, for particles with mass different from zero, in full disagreement with Moshinsky's conclusions, we report here that relativistic diffraction in time oscillations is indeed present.

The purpose of the present paper is to derive the exact solutions for the Dirac and Klein-Gordon shutter problems. The exact transient Dirac spinors are expressed in terms of integral-defined-functions which are the relativistic equivalent of the Fresnel integrals. In partial agreement with Moshinsky's conclusions we find that indeed the relativistic densities do not resemble the mathematical expression for intensity of light that appears in the theory of diffraction in Optics. In spite of this, when our exact relativistic densities are plotted versus time, the plots show transient oscillations which resemble a diffraction pattern. For this reason in this article we claim that impressive diffractions in time oscillations do exist in the relativistic realm. Furthermore, the Dirac and Klein-Gordon densities look quite different, which implies that relativistic diffraction in time distinguishes between spin 0 and 1/2.

2. The Dirac Shutter Problem

Consider, for relativistic particles of spin 1/2, the shutter problem. We want to find out the spinor wave function $\psi(z,t)=(\psi_1,\psi_2,\psi_3,\psi_4)^{\mathrm{T}}$ which is the solution of the one-dimensional Dirac equation:

$$\left\{\begin{pmatrix} I & 0 \\ 0 & I \end{pmatrix}\frac{1}{i}\frac{\partial}{\partial(ct)}+\begin{pmatrix} 0 & \sigma_z \\ \sigma_z & 0 \end{pmatrix}\frac{1}{i}\frac{\partial}{\partial z}+\mu\begin{pmatrix} I & 0 \\ 0 & -I \end{pmatrix}\right\}\psi=0, \tag{6}$$

where σ_z is the 2×2 Pauli matrix and $\mu^{-1}\equiv\hbar/mc\equiv\lambda_C$ the Compton length. The initial condition corresponds, for $t\le 0$, to a plane wave to the left of the shutter and zero to the right. Three quantum numbers are needed to classify the Dirac free particle solutions, namely, the momentum $\boldsymbol{p}\equiv\hbar\boldsymbol{k}$, the positive or negative energies $\epsilon=\pm\hbar\omega$, where $\omega=c\left(k^2+\mu^2\right)^{1/2}$, and helicity $\Lambda_S=\boldsymbol{S}\cdot\boldsymbol{p}/p$. We select the initial condition assuming a positive energy $\epsilon=+\hbar\omega$ and a plane wave propagating along the z direction $\boldsymbol{k}=(0,0,k)$. As for the initial helicity,

$$\Lambda_S=S_z=\frac{\hbar}{2}\begin{pmatrix} \sigma_z & 0 \\ 0 & \sigma_z \end{pmatrix}, \tag{7}$$

we choose the initial state with a well defined direction of spin, for instance parallel to the direction of motion, $S_z=+1/2$. Then in the shutter problem we have an incident plane wave given by

$$\psi(z,t)=N\left(1,0,\frac{k}{\mu+\omega/c},0\right)^{\mathrm{T}}\mathrm{e}^{i(kz-\omega t)}\theta(-z)\quad(t\le 0). \tag{8}$$

For free particles, the helicity Λ_S is a constant of motion. The initial direction of spin, $S_z=1/2$, will be conserved at all positive times. As a consequence the two components of the wave function (ψ_2 and ψ_4) which are zero at the initial time will remain zero at all positive times:

$$\psi_2(z,t)=\psi_4(z,t)=0.\quad(t\ge 0). \tag{9}$$

In terms of the remaining two components (ψ_1,ψ_3) the Dirac shutter problem is the solution of the equation,

$$\left\{\begin{pmatrix} 1 & 0 \\ 0 & 1 \end{pmatrix}\frac{1}{i}\frac{\partial}{\partial(ct)}+\begin{pmatrix} 0 & 1 \\ 1 & 0 \end{pmatrix}\frac{1}{i}\frac{\partial}{\partial z}+\mu\begin{pmatrix} 1 & 0 \\ 0 & -1 \end{pmatrix}\right\}\begin{pmatrix}\psi_1\\ \psi_3\end{pmatrix}=0, \tag{10}$$

with the initial condition:

$$\begin{pmatrix}\psi_1(z,0)\\ \psi_3(z,0)\end{pmatrix}=\begin{pmatrix}N\\ \gamma\end{pmatrix}\mathrm{e}^{ikz}\theta(-z), \tag{11}$$

where $\gamma\equiv Nk/(\mu+\omega/c)$. The normalization factor N is chosen as $N\equiv\sqrt{1+\omega/c\mu}$; in this way the probability density ρ and the density current $\boldsymbol{j}/c$ transform initially, as a four-vector $(\rho,\boldsymbol{j}/c)=(2/\mu)(\omega/c,\boldsymbol{k})$.

We use the Compton length $\lambda_C \equiv \hbar/mc$ to define dimensionless variables: $\chi \equiv z/\lambda_C$, $\tau \equiv ct/\lambda_C$, $\kappa \equiv k\lambda_C$, and $\Omega \equiv \omega\lambda_C/c = \sqrt{1+\kappa^2}$. Using these variables we derive in **Appendix A** the exact solution of the Dirac shutter problem. To simplify the notation, for n integer, we denote by G_n the integral-defined complex functions

$$G_n(\chi,\tau) \equiv \int_\chi^\tau du\, e^{i\Omega(\tau-u)} \frac{J_n\left(\sqrt{u^2-\chi^2}\right)}{\left(u^2-\chi^2\right)^{n/2}} \equiv C_n + iS_n \qquad (\tau \geq \chi) \tag{12}$$

where $J_n(z)$ is the Bessel function of the first kind of order n. Notice that $z=0$ is a removable singularity for $J_n(z)/z^n$, hence the functions G_n are analytic. In fact the integrand can be explicitly written analytic by eliminating the denominator. Indeed, using repeatedly the recurrence relation for the Bessel functions, $2nJ_n(z)/z = J_{n-1}(z) + J_{n+1}(z)$, we we can write

$$\begin{aligned}
\frac{J_1(z)}{z} &= \frac{1}{2}\left[J_0(z)+J_2(z)\right] \\
\frac{J_2(z)}{z^2} &= \frac{1}{24}\left[3J_0(z)+4J_2(z)+J_4(z)\right] \\
\frac{J_3(z)}{z^3} &= \frac{1}{480}\left[10J_0(z)+15J_2(z)+6J_4(z)+J_6(z)\right]
\end{aligned} \tag{13}$$

Clearly the real and imaginary parts of $G_n \equiv C_n + iS_n$ are analytic oscillating functions.

From **Appendix A**, for the right side of the shutter $\chi > 0$, we have the exact Dirac shutter solution:

$$\begin{aligned}
-2\begin{pmatrix}\psi_1(\chi,\tau)\\ \psi_3(\chi,\tau)\end{pmatrix}\Big/\theta(\tau-\chi) = \begin{pmatrix}\gamma\\ N\end{pmatrix}\Bigg\{ & i\kappa\left(\frac{\sin\left[\Omega(\tau-\chi)\right]}{\Omega} - \frac{\chi}{\Omega}S_1\right) \\
& -\left(\cos\left[\Omega(\tau-\chi)\right] - \frac{\chi}{2}\frac{\sin\left[\Omega(\tau-\chi)\right]}{\Omega} + \frac{1}{\Omega}S_1 + \frac{\chi^2}{\Omega}S_2\right)\Bigg\} \\
& -\begin{pmatrix}N\\ \gamma\end{pmatrix}\Bigg\{\cos\left[\Omega(\tau-\chi)\right] \pm i\frac{\sin\left[\Omega(\tau-\chi)\right]}{\Omega} \mp \chi\left(C_1 \pm \frac{i}{\Omega}S_1\right) \\
& -\frac{i}{\kappa}\Bigg(-\left(\frac{\chi}{2}\pm i\right)e^{\mp i(\tau-\chi)} + \begin{pmatrix}G_1^*\\ G_1\end{pmatrix}_{\kappa=0} + \chi^2\begin{pmatrix}G_2^*\\ G_2\end{pmatrix}_{\kappa=0} \\
& +\Omega\sin\left[\Omega(\tau-u)\right] + \frac{\chi}{2}\cos\left[\Omega(\tau-\chi)\right] - C_1 - \chi^2 C_2 \\
& \pm i\left[\cos\left[\Omega(\tau-\chi)\right] - \frac{\chi}{2}\frac{\sin\left[\Omega(\tau-\chi)\right]}{\Omega} + \frac{1}{\Omega}S_1 + \frac{\chi^2}{\Omega}S_2\right]\Bigg)\Bigg\}
\end{aligned} \tag{14}$$

Notice the function $\theta(\tau-\chi)$ which shows the relativistic condition that no wave function exists until $ct \geq z$. This property is missing in the Schrödinger solution.

3. Dirac Diffraction in Time

Given the Dirac wave function $\psi(z,t)$ in Equation (14), we can calculate the probability density ρ given by

$$\rho(\chi,\tau;\kappa) = |\psi|^2 = |\psi_1|^2 + |\psi_3|^2 \equiv \rho_1 + \rho_3 \tag{15}$$

In **Figure 2**, for fixed values of $\kappa = 1$ ($v/c = 0.7$) and $\chi = 5$, we show a typical plot of the Dirac density $\rho(\tau)$. Surprisingly we find damped oscillations which resemble the Schrödinger diffraction in time oscillations. For this reason we call this plot a relativistic diffraction in time process. However, the Dirac oscillations are clearly different from the Schrödinger ones (see **Figure 1**). For ρ_1 notice the impressive double oscillations which are unique to the Dirac theory.

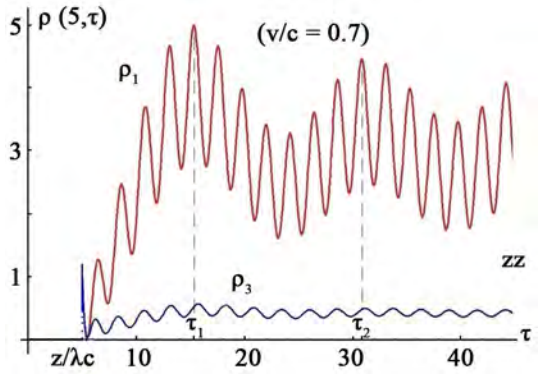

Figure 2. Dirac diffraction in time probability densities ρ_1 and ρ_3.

As expected, for a relativistic solution, the Dirac density vanishes for times $0 \le t \le z/c$. The down oscillation, immediately following, $t = z/c$, is also a relativistic property.

4. The Klein-Gordon Shutter Problem

For relativistic particles with spin 0, the Klein-Gordon shutter problem is, by definition, the solution $\psi(z,t)$ of the equation:

$$\frac{\partial^2\psi}{\partial z^2} - \frac{\partial^2\psi}{\partial(ct)^2} = \mu^2\psi, \tag{16}$$

where $\mu \equiv 1/\lambda_C \equiv mc/\hbar$. The initial conditions correspond to a plane wave to the left of the shutter and zero to the right.

$$\psi(z,t) = \mathrm{e}^{i(kz-\omega t)}\theta(-z), \qquad (t \le 0) \tag{17}$$

where $\omega = c\left(k^2+\mu^2\right)^{1/2}$. Therefore at $t = 0$, when the shutter is suddenly opened, we have the initial conditions:

$$\psi(z,0) = \mathrm{e}^{ikz}\theta(-z), \qquad \frac{\partial\psi(z,0)}{\partial t} = -i\omega\mathrm{e}^{ikz}\theta(-z). \tag{18}$$

Similar to the Dirac problem, in terms of the dimensionless variables: $\chi \equiv z/\lambda_C$, $\tau \equiv ct/\lambda_C$, $\kappa \equiv k\lambda_C$, and $\Omega \equiv \omega\lambda_C/c = \sqrt{1+\kappa^2}$, we find the exact solution of this Klein-Gordon problem in **Appendix B**. At a fixed distance $\chi > 0$, on the right side of the shutter, we have the exact Klein-Gordon shutter solution:

$$\psi(\chi,\tau;\kappa) = \frac{1}{2}\theta(\tau-\chi)\left\{\mathrm{e}^{i\Omega(\chi-\tau)} - \int_\chi^\tau \mathrm{d}u\ \mathrm{e}^{i\Omega(u-\tau)}\left[\chi\frac{J_1\left(\sqrt{u^2-\chi^2}\right)}{\sqrt{u^2-\chi^2}} + i\kappa J_0\left(\sqrt{u^2-\chi^2}\right)\right]\right\} \tag{19}$$

or in simplified notation

$$\psi(\chi,\tau) = \frac{1}{2}\theta(\tau-\chi)\left\{\mathrm{e}^{i\Omega(\chi-\tau)} - \chi G_1^* - i\kappa G_0^*\right\}. \tag{20}$$

The presence of $\theta(\tau-\chi)$ means, as expected, that the wave function vanishes for $t < z/c$, where z is the distance from shutter to the particle detector.

Given the Klein-Gordon wave function $\psi(\chi,\tau)$, we have a charge density given by (charge $q = 1$),

$$\rho(\chi,\tau) = -Im\left[\psi^*(\chi,\tau)\frac{\partial\psi(\chi,\tau)}{\partial\tau}\right] \tag{21}$$

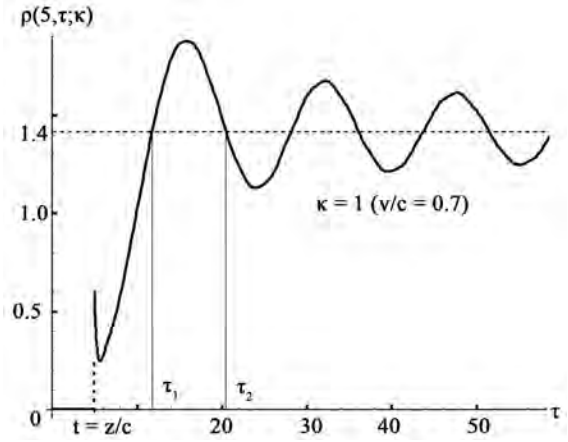

Figure 3. Typical Klein-Gordon diffraction in time for the charge density, $\chi = 5$.

In **Figure 3**, for fixed values of $\kappa = 1$ and $\chi = 5$, we show a typical plot of the charge density versus time for the Klein-Gordon solution. The impressive damped oscillations, shown in **Figure 3**, clearly resemble the optical Fresnel diffraction pattern by an straight edge. The double oscillation which is present in the Dirac solution is missing now.

Notice that the asymptotic behavior of ρ is not 1, as it occurs in the Schrödinger solution. In the particular case of $\chi = 5$ and $\kappa = 1$ ($v/c = 0.7$) shown in **Figure 3**, the stationary density is $\rho = 1.4$, which is the correct prediction for the shutter's initial conditions (18). In fact

$$\rho(\chi,0) = -Im\left[\psi^*(\chi,0)\frac{\partial\psi(\chi,0)}{\partial\tau}\right] = \sqrt{1+\kappa^2} \tag{22}$$

Therefore, for $\kappa = 1$ the predicted stationary density is 1.4.

5. Conclusions

We derived the exact solutions for the Klein-Gordon and the Dirac shutter problems. In agreement with Moshinsky we find that the relativistic solutions do not resemble the analytic expression that appears in the theory of diffraction in Optics. In spite of this, we prove that when the exact Dirac and Klein-Gordon densities are plotted versus time, the following happens: 1) both densities show transient oscillations which in some way resemble the optical diffraction pattern; 2) the Dirac density looks quite different from the Klein-Gordon one, which implies that transient time oscillations depend strongly on the particle spin.

For these reasons and in total disagreement with Moshinsky's conclusions [13], we claim that impressive diffractions in time oscillations do exist in the relativistic realm. For spin 0 and 1/2 particles, we prove that diffraction in time oscillations exists only for particles of rest mass different from zero; photons do not show such time oscillations.

References

[1] Moshinsky, M. (1951) *Physical Review*, **84**, 525. http://dx.doi.org/10.1103/PhysRev.84.525

[2] Born, M. and Wolf, E. (1965) Principles of Optics. Pergamon Press, Oxford, 192-195.

[3] Schneble, D., Hasuo, M., Anker, T., Pfau, T. and Mlynek, J. (2003) *Journal of the Optical Society of America B*, **20**, 648-651. http://dx.doi.org/10.1364/JOSAB.20.000648

[4] Brouard, M. and Muga, J.G. (1996) *Physical Review A*, **54**, 3055.

[5] García-Calderón, G. and Rubio, G. (1997) *Physical Review A*, **55**, 3361.

[6] García-Calderón, G., Villavicencio, J., Delgado, F. and Muga, J.G. (2002) *Physical Review A*, **66**, 042119.

[7] Stevens, K.W.H. (1980) *European Journal of Physics*, **1**, 98.

[8] Delgado, F., Cruz, H. and Muga, J.G. (2002) *Journal of Physics A*: *Mathematical and General*, **35**, 10377.

[9] Delgado, F., Muga, J.G. and Garca-Calderón, G. (2005) *Journal of Applied Physics*, **97**, 013705. http://dx.doi.org/10.1063/1.1826215

[10] García-Calderón, G., Rubio, G. and Villavicencio, J. (1999) *Physical Review A*, **59**, 1758.

[11] Delgado, F., Muga, J.G., Ruschhaput, A., Garca-Calderón, G. and Villavicencio, J. (2003) *Physical Review A*, **68**, 032101.

[12] Hilgevoord, J. (1960) Dispersion Relations and Causal Descriptions. North Holland Publishing, Amsterdam, 13-33.

[13] Moshinsky, M. (1952) *Physical Review*, **88**, 625. http://dx.doi.org/10.1103/PhysRev.88.625

[14] Moshinsky, M. (1952) *Revista Mexicana de Fsica*, **I**, 3.

[15] Abramowitz, M. and Stegun, I.A. (1965) Handbook of Mathematical Functions. Dover Publications, New York, 1019-1030.

[16] Duffy, D.G. (2001) Green Functions with Applications. Chapman and Hall/CRC, London, 82-84. http://dx.doi.org/10.1201/9781420034790

Appendix A

With the help of the dimensionless variables given by: $\chi \equiv z/\lambda_C$, $\tau \equiv ct/\lambda_C$, $\kappa \equiv k\lambda_C$, and $\Omega \equiv \omega\lambda_C/c = \sqrt{1+\kappa^2}$, the Dirac Equation (10) may be rewritten as

$$\left\{\begin{pmatrix}1 & 0\\ 0 & 1\end{pmatrix}\frac{\partial}{\partial\tau}+\begin{pmatrix}0 & 1\\ 1 & 0\end{pmatrix}\frac{\partial}{\partial\chi}+i\begin{pmatrix}1 & 0\\ 0 & -1\end{pmatrix}\right\}\begin{pmatrix}\psi_1\\ \psi_3\end{pmatrix}=0, \tag{23}$$

and the initial condition becomes:

$$\psi(\chi,0)\equiv\begin{pmatrix}\psi_1(\chi,0)\\ \psi_3(\chi,0)\end{pmatrix}=\begin{pmatrix}N\\ \gamma\end{pmatrix}e^{i\kappa\chi}\theta(-\chi). \tag{24}$$

Taking the Laplace transform ($\tau\to s$) in Equation (23), and denoting $\mathcal{L}\left[\psi(\chi,\tau)\right]\equiv\phi(\chi,s)=\left(\phi_1(\chi,s),\phi_3(\chi,s)\right)^{\mathrm{T}}$, Equation (23) becomes a matrix differential equation

$$\frac{\mathrm{d}\phi}{\mathrm{d}\chi}+\left(\sigma_x s+\sigma_y\right)\phi=\begin{pmatrix}\gamma\\ N\end{pmatrix}e^{i\kappa\chi}\theta(-\chi) \tag{25}$$

which holds in the range $-\infty<\chi<\infty$. Due to the presence of the step function $\theta(-\chi)$, the origin $\chi=0$ is a singular point where we demand that the function $\phi(\chi,s)$ must be continuous. We break the infinite range into the ranges ($\chi\le 0$) and ($\chi\ge 0$). For the left side of the shutter, $\phi_<(\chi,s)$ denotes the solution of the differential equation:

$$\frac{\mathrm{d}\phi_<}{\mathrm{d}\chi}+\left(\sigma_x s+\sigma_y\right)\phi_<=\begin{pmatrix}\gamma\\ N\end{pmatrix}e^{i\kappa\chi},\qquad(\chi\le 0) \tag{26}$$

and for the right side, $\phi_>(\chi,s)$ denotes the solution of

$$\frac{\mathrm{d}\phi_>}{\mathrm{d}\chi}+\left(\sigma_x s+\sigma_y\right)\phi_>=0,\qquad(\chi\ge 0). \tag{27}$$

Both functions $\phi_<$ and $\phi_>$ must be bounded ($\phi_<$ at $-\infty$) and ($\phi_>$ at $+\infty$), and must be continuous at the interface $\chi=0$.

Because the matrix

$$\sigma_x s+\sigma_y=\begin{pmatrix}0 & s-i\\ s+i & 0\end{pmatrix} \tag{28}$$

has eigenvalues given by: $\lambda_1=\sqrt{s^2+1}=-\lambda_2$, with corresponding orthogonal eigenvectors given by:

$$u_1=\begin{pmatrix}\sqrt{s-i}\\ \sqrt{s+i}\end{pmatrix},\qquad u_2=\begin{pmatrix}-\sqrt{s-i}\\ \sqrt{s+i}\end{pmatrix}, \tag{29}$$

then, taking into account the boundary conditions at $\pm\infty$, we have the general solutions for the matrix differential equations:

$$\phi_>(\chi,s)=A\begin{pmatrix}\sqrt{s-i}\\ \sqrt{s+i}\end{pmatrix}e^{-\chi\sqrt{s^2+1}}\quad(\chi\ge 0) \tag{30}$$

$$\phi_<(\chi,s)=B\begin{pmatrix}-\sqrt{s-i}\\ \sqrt{s+i}\end{pmatrix}e^{+\chi\sqrt{s^2+1}}-\frac{1}{s^2+\Omega^2}\begin{pmatrix}i\kappa\gamma-(s-i)N\\ i\kappa N-(s+i)\gamma\end{pmatrix}e^{i\kappa\chi}\quad(\chi\le 0) \tag{31}$$

where $\Omega^2=1+\kappa^2$. The constants A and B are fixed from the condition at the interface: $\left(\phi_{1<}(0,s),\phi_{3<}(0,s)\right)^{\mathrm{T}}=\left(\phi_{1>}(0,s),\phi_{3>}(0,s)\right)^{\mathrm{T}}$. We have then a set of two algebraic equations with solutions:

$$A=\frac{-1}{2}\frac{1}{s^2+\Omega^2}\left[\frac{1}{\sqrt{s-i}}\left(i\kappa\gamma-(s-i)N\right)+\frac{1}{\sqrt{s+i}}\left(i\kappa N-(s+i)\gamma\right)\right] \tag{32}$$

$$B=\frac{-1}{2}\frac{1}{s^2+\Omega^2}\left[\frac{1}{\sqrt{s+i}}\left(i\kappa N-(s+i)\gamma\right)-\frac{1}{\sqrt{s-i}}\left(i\kappa\gamma-(s-i)N\right)\right] \tag{33}$$

Substituting Equation (32) into Equation (30) and Equation (33) into Equation (31), we get the solution for Dirac shutter problem in the (χ,s) space. For $\chi\geq 0$, where the particle detector is located, we have the solution:

$$-2\begin{pmatrix}\phi_1(\chi,s)_>\\ \phi_3(\chi,s)_>\end{pmatrix}=\frac{\mathrm{e}^{-\chi\sqrt{s^2+1}}}{s^2+\Omega^2}\left\{\begin{pmatrix}i\kappa\gamma\\ i\kappa N\end{pmatrix}-(s\mp i)\begin{pmatrix}N\\ \gamma\end{pmatrix}-\sqrt{s^2+1}\begin{pmatrix}\gamma\\ N\end{pmatrix}+\frac{\sqrt{s\mp i}}{\sqrt{s\pm i}}\begin{pmatrix}i\kappa N\\ i\kappa\gamma\end{pmatrix}\right\} \tag{34}$$

Notice the singular points at $s=\pm i\Omega$ (simple poles) and $s=\pm i$ (branch points), all of them locate in the imaginary axis. Therefore, by the Nyquist stability criterion, the time dependent solution $\psi(\chi,\tau)$ is an oscillatory bounded solution.

To simplify the final notation, we express the inverse Laplace transforms ($s\to\tau$) with the help of the integral-defined complex functions ($\tau\geq\chi$):

$$G_n(\chi,\tau;\kappa)\equiv\int_\chi^\tau \mathrm{d}u\,\mathrm{e}^{i\Omega(\tau-u)}\frac{J_n\left(\sqrt{u^2-\chi^2}\right)}{\left(u^2-\chi^2\right)^{n/2}}\equiv C_n+iS_n \qquad n=0,1,2,\cdots \tag{35}$$

Using Laplace Transforms Tables [15] and the convolution theorem we find the following results, valid for $\chi\geq 0$,

$$\mathcal{L}^{-1}\left[\frac{\mathrm{e}^{-\chi\sqrt{s^2+1}}}{s^2+\Omega^2}\right]=\theta(\tau-\chi)\left\{\frac{\sin\left[\Omega(\tau-\chi)\right]}{\Omega}-\frac{\chi}{\Omega}S_1\right\} \tag{36}$$

$$\mathcal{L}^{-1}\left[\frac{e^{-\chi\sqrt{s^2+1}}}{s^2+\Omega^2}(s+i)\right]=\theta(\tau-\chi)\left\{\cos\left[\Omega(\tau-\chi)\right]+i\frac{\sin\left[\Omega(\tau-\chi)\right]}{\Omega}-\chi\left(C_1+\frac{i}{\Omega}S_1\right)\right\}. \tag{37}$$

Next, we use the relation

$$-\frac{\mathrm{d}}{\mathrm{d}\chi}\frac{\mathrm{e}^{-\chi\sqrt{s^2+1}}}{s^2+\Omega^2}=\frac{\mathrm{e}^{-\chi\sqrt{s^2+1}}}{s^2+\Omega^2}\sqrt{s^2+1} \tag{38}$$

to obtain

$$\mathcal{L}^{-1}\left[\frac{\mathrm{e}^{-\chi\sqrt{s^2+1}}}{s^2+\Omega^2}\sqrt{s^2+1}\right]=\theta(\tau-\chi)\left\{\cos\left[\Omega(\tau-\chi)\right]-\frac{\chi}{2}\frac{\sin\left[\Omega(\tau-\chi)\right]}{\Omega}+\frac{1}{\Omega}S_1+\frac{\chi^2}{\Omega}S_2\right\} \tag{39}$$

Finally, using the identities

$$\frac{\mathrm{e}^{-\chi\sqrt{s^2+1}}}{s^2+\Omega^2}\frac{\sqrt{s-i}}{\sqrt{s+i}}=\frac{\mathrm{e}^{-\chi\sqrt{s^2+1}}}{s^2+\Omega^2}\frac{\sqrt{s^2+1}}{s+i} \tag{40}$$

and

$$\frac{1}{\left(s^2+\Omega^2\right)(s+i)}=\frac{1}{\Omega^2-1}\left(\frac{-s+i}{s^2+\Omega^2}+\frac{1}{s+i}\right) \tag{41}$$

we obtain

$$\begin{aligned}\mathcal{L}^{-1}\left[\frac{\mathrm{e}^{-\chi\sqrt{s^2+1}}}{s^2+\Omega^2}\frac{\sqrt{s-i}}{\sqrt{s+i}}\right]=\frac{\theta(\tau-\chi)}{\Omega^2-1}\Bigg\{&-\left(\frac{\chi}{2}+i\right)\mathrm{e}^{-i(\tau-\chi)}+G_1^*(\kappa=0)+\chi^2G_2^*(\kappa=0)\\&+\Omega\sin\left[\Omega(\tau-u)\right]+\frac{\chi}{2}\cos\left[\Omega(\tau-\chi)\right]-C_1-\chi^2C_2\\&+i\left[\cos\left[\Omega(\tau-\chi)\right]-\frac{\chi}{2}\frac{\sin\left[\Omega(\tau-\chi)\right]}{\Omega}+\frac{1}{\Omega}S_1+\frac{\chi^2}{\Omega}S_2\right]\Bigg\}\end{aligned} \tag{42}$$

Therefore, for $\chi \geq 0$, the Dirac final solution is given by:

$$\begin{aligned}-2\begin{pmatrix}\psi_1(\chi,\tau)_> \\ \psi_3(\chi,\tau)_>\end{pmatrix} &= \mathcal{L}^{-1}\left[\frac{\mathrm{e}^{-\chi\sqrt{s^2+1}}}{s^2+\Omega^2}\right]\begin{pmatrix}i\kappa\gamma \\ i\kappa N\end{pmatrix} - \mathcal{L}^{-1}\left[\frac{\mathrm{e}^{-\chi\sqrt{s^2+1}}}{s^2+\Omega^2}(s\mp i)\right]\begin{pmatrix}N \\ \gamma\end{pmatrix} \\ &\quad - \mathcal{L}^{-1}\left[\frac{\mathrm{e}^{-\chi\sqrt{s^2+1}}}{s^2+\Omega^2}\sqrt{s^2+1}\right]\begin{pmatrix}\gamma \\ N\end{pmatrix} + \mathcal{L}^{-1}\left[\frac{\mathrm{e}^{-\chi\sqrt{s^2+1}}}{s^2+\Omega^2}\frac{\sqrt{s\mp i}}{\sqrt{s\pm i}}\right]\begin{pmatrix}i\kappa N \\ i\kappa\gamma\end{pmatrix}\end{aligned} \tag{43}$$

where each inverse Laplace transform has been previously calculated. We claim that Equation (43) is the exact Dirac wave function for the shutter problem, valid for $\chi \geq 0$ and $\Omega \neq 1$ ($k \neq 0$).

Appendix B

In a similar way to the Dirac solution, the Klein-Gordon shutter problem can be written in terms of dimensionless variables:

$$\frac{\partial^2\psi}{\partial\chi^2} - \frac{\partial^2\psi}{\partial\tau^2} = \psi \tag{44}$$

with initial conditions given by:

$$\psi(\chi,0) = \mathrm{e}^{i\kappa\chi}\theta(-\chi), \qquad \frac{\partial\psi(\chi,0)}{\partial\tau} = -i\Omega\mathrm{e}^{i\kappa\chi}\theta(-\chi). \tag{45}$$

Taking the Laplace transform ($\tau \to s$) of Equation (44) we find the differential equations:

$$\frac{\mathrm{d}^2\phi_<}{\mathrm{d}\chi^2} - (s^2+1)\phi_< = -(s-i\Omega)\mathrm{e}^{i\kappa\chi}, \quad (\chi \leq 0) \tag{46}$$

and

$$\frac{\mathrm{d}^2\phi_>}{\mathrm{d}\chi^2} - (s^2+1)\phi_> = 0. \quad (\chi \geq 0) \tag{47}$$

Here both functions $\phi_<$ and $\phi_>$ must be bounded: ($\phi_<$ at $-\infty$) and ($\phi_>$ at $+\infty$). The two functions and their first derivatives must be continuous at the interface $\chi = 0$.

Taking into account the boundary conditions at $\pm\infty$, the solutions of Equations (46) and (47) are:

$$\phi_<(\chi,s) = A\mathrm{e}^{\chi\sqrt{s^2+1}} + \frac{1}{s+i\Omega}\exp(i\kappa\chi) \qquad (\chi \leq 0) \tag{48}$$

$$\phi_>(\chi,s) = B\mathrm{e}^{-\chi\sqrt{s^2+1}} \qquad (\chi \geq 0) \tag{49}$$

where $\Omega = \sqrt{1+\kappa^2}$. The constants A and B are fixed from the conditions at the interface: $\phi_<$ and $\phi_>$, and their first derivatives, $\mathrm{d}\phi_</\mathrm{d}\chi$ and $\mathrm{d}\phi_>/\mathrm{d}\chi$, must be continuous at $\chi = 0$. We have then a set of two coupled algebraic equations with solutions given by:

$$A = \frac{-1}{2}\frac{1}{s+i\Omega}\left(1+\frac{iK}{\sqrt{s^2+1}}\right) \tag{50}$$

$$B = \frac{1}{2}\frac{1}{s+i\Omega}\left(1-\frac{iK}{\sqrt{s^2+1}}\right) \tag{51}$$

Substituting Equation (50) into Equation (48) and Equation (51) into Equation (49) we have the solutions:

$$\phi_<(\chi,s) = \frac{-1}{2}\frac{1}{s+i\Omega}\left(1+\frac{iK}{\sqrt{s^2+1}}\right)\exp\left(+\chi\sqrt{s^2+1}\right) + \frac{1}{s+i\Omega}\exp(i\kappa\chi), \tag{52}$$

$$\phi_>(\chi,s) = \frac{1}{2}\frac{1}{s+i\Omega}\left(1-\frac{iK}{\sqrt{s^2+1}}\right)\exp\left(-\chi\sqrt{s^2+1}\right). \tag{53}$$

Finally, we need to invert the Laplace transforms ($s \to \tau$). We find in Laplace Transforms Tables [15] the following results valid for $\chi \geq 0$:

$$\mathcal{L}^{-1}\left[\frac{\mathrm{e}^{-\chi\sqrt{s^2+1}}}{(s+i\Omega)\sqrt{s^2+1}}\right] = \theta(\tau-\chi)\int_{|\chi|}^{\tau} \mathrm{d}u\ \mathrm{e}^{-i\Omega(\tau-u)} J_0\left(\sqrt{u^2-\chi^2}\right) \tag{54}$$

$$\mathcal{L}^{-1}\left[\frac{\mathrm{e}^{-\chi\sqrt{s^2+1}}}{s+i\Omega}\right] = \theta(\tau-\chi)\left[\mathrm{e}^{-i\Omega(\tau-|\chi|)} - \chi\int_{\chi}^{\tau} \mathrm{d}u\ \mathrm{e}^{-i\Omega(\tau-u)} \frac{J_1\left(\sqrt{u^2-\chi^2}\right)}{\sqrt{u^2-\chi^2}}\right] \tag{55}$$

We have then the final solutions, for $\chi \geq 0$:

$$\psi_{>}(\chi,\tau) = \frac{1}{2}\theta(\tau-\chi)\left\{\mathrm{e}^{-i\Omega(\tau-\chi)} - \int_{\chi}^{\tau} \mathrm{d}u\ \mathrm{e}^{-i\Omega(\tau-u)}\left[\chi\frac{J_1\left(\sqrt{u^2-\chi^2}\right)}{\sqrt{u^2-\chi^2}} + i\kappa J_0\left(\sqrt{u^2-\chi^2}\right)\right]\right\} \tag{56}$$

and for $\chi \leq 0$ we get the incident and reflected wave:

$$\psi_{<}(\chi,\tau) = \mathrm{e}^{i(\kappa\chi-\Omega\tau)} - \frac{1}{2}\theta(\tau+\chi)\left\{\mathrm{e}^{-i\Omega(\chi+\tau)} + \int_{-\chi}^{\tau} \mathrm{d}u\ \mathrm{e}^{-i\Omega(\tau-u)}\left[\chi\frac{J_1\left(\sqrt{u^2-\chi^2}\right)}{\sqrt{u^2-\chi^2}} + i\kappa J_0\left(\sqrt{u^2-\chi^2}\right)\right]\right\} \tag{57}$$

We claim that Equations (56) and (57) are the exact Klein-Gordon wave functions for the shutter problem. It's no s urprising t o f ind t he B essel functions $J_0\left(\sqrt{u^2-\chi^2}\right)$ and $J_1\left(\sqrt{u^2-\chi^2}\right)\Big/\sqrt{u^2-\chi^2}$, t hey a re j ust t he Green's function and its derivative respectively for the Klein-Gordon equation [16].

Journal of Modern Physics, 2016, 7, 1192-1199
Published Online June 2016 in SciRes. http://www.scirp.org/journal/jmp
http://dx.doi.org/10.4236/jmp.2016.710108

Time, Length, and Mass Are Derived Quantities

Tower Chen[1], Zeon Chen[2]

Unit of Mathematical Sciences, College of Natural and Applied Sciences, University of Guam, UOG Station, Mangilao, Guam
Email: tower_c@yahoo.com, zeon_chen@yahoo.com

Received 20 April 2016; accepted 21 June 2016; published 24 June 2016

Abstract

Fundamental units of measurements are kilograms, meters, and seconds—in regards to mass length, and time. All other measurements in mechanical quantities including kinetic quantities and dynamic quantities are called derived units. These derived units can be expressed in terms of fundamental units, such as acceleration, area, energy, force, power, velocity and volume. Derived quantities will be referred to as time, length, and mass. In order to explain that fundamental units are not equivalent with fundamental quantities, we need to understand the contraction of time and length in Special Relativity. If we choose the velocity of light as fundamental quantity and length and time as derived quantities, then we are able to construct three-dimensional space-time frames. Three-dimensional space-time frames representing time with polar coordination, time contraction and length contraction can be shown graphically.

Keywords

Fundamental Units, Fundamental Quantities, Derived Units, Derived Quantities, Special Relativity, Constant Velocity of Light, Three-Dimensional Space-Time Frame

1. Introduction

The following statements were written in the paper "Time Dilation and Length Contraction Shown in Three-Dimensional Space-Time Frames" published in Concepts of Physics, Vol. VI, No. 2, 2009. "*Since the concept of the movement phenomenon of an object is more fundamental than the concepts of space and time, its unit of velocity is more fundamental than the units of space* (*length*) *and time, which are derivations. Furthermore, without gravitational force, we would be unable to measure the gravitational mass of an object; without spring force, we would be unable to measure the inertial mass of an object. Since the concept of the force phenomenon ap-*

How to cite this paper: Chen, T. and Chen, Z. (2016) Time, Length, and Mass Are Derived Quantities. *Journal of Modern Physics*, **7**, 1192-1199. http://dx.doi.org/10.4236/jmp.2016.710108

plied to an object is more fundamental than the concept of mass, the unit of force is more fundamental that the unit of mass, which is also a derivation."

In this paper, we like to have a further discussion about this issue. In order to measure something, we need to define a *unit of measurement*. In this way, all measurements are multiples or fractions of that unit. The units of measurement are defined as standard. The International System of Units (SI) defined seven fundamental units of measure based on conventional and historical reasons from which all other SI units are derived [1]. For this paper, the topic is limited to mechanics. These SI fundamental units are commonly called metric units. The definitions of fundamental units are based on physical objects such as standard second clocks, standard meter sticks and standard kilogram bars. A day is divided in 24 hours, each hour divided in 60 minutes, each minute divided in 60 seconds. A second clock is equal to 1/(24 × 60 × 60) of the day. A meter stick is equal to 1/10,000,000 of the distance from the Earth's equator to the North Pole measured on the circumference through Paris. A kilogram bar is equal to the mass of one liter of water. A liter is one thousandth of a cubic meter. In classical physics, time and length are absolute and independent, so fundamental units match with fundamental quantities. In modern physics, time and length are relative and dependent; thus fundamental units are not equivalent to fundamental quantities.

2. Special Relativity

Einstein placed two guns at the middle of the train with moving velocity u, he fired a pair of photons from these two gun at the same time on **Figure 1**. The length of a car of the train is $2d$.

Light has a duality including wave and photon. The velocity of light is the limit velocity of particles in the universe. The velocity of light, $c = 3\times10^8$ m/sec which is the fixed value measured by any observers, no matter which direction of photons are fired.

1) For observers on the train:

The velocities of both photons are same. The time of a photon hitting the front wall is $t = \frac{d}{v}$. The time of photon hitting the back wall is $t = \frac{d}{v}$. Therefore, observers on the train will see the two photons hits both the front wall and back wall simultaneously.

2) For the observers on the platform:

The time for the photon hitting the front wall is $(d + u\times t)/c$ which is longer. The time for the photon hitting the back wall is $(d - u\times t)/c$ which is shorter. This shows that one photon will hit the back wall earlier than the front wall. Thus, these two events are not happening simultaneously.

Classical physics shows that two events happen simultaneously are absolute, so space and time are independent. Einstein's thought experiment shows that two events happening simultaneously are relative, so space and time are dependent.

Now, let's modify Einstein's thought experiment by firing a photon from the floor to the ceiling on **Figure 2**.

The platform with S frame, the train with S' frame, and the train travels to the right with velocity u. Observers on the train see a photon moving from the floor to the ceiling vertically and the track of motion is h. Observers on the platform see a photon moving from the floor to the ceiling slantingly and the track of motion is r. The distance of train traveled from the time a photon leaving the floor to the time reaching the ceiling is x. Three lengths r, x, h form the right triangle, and we can derive the formula

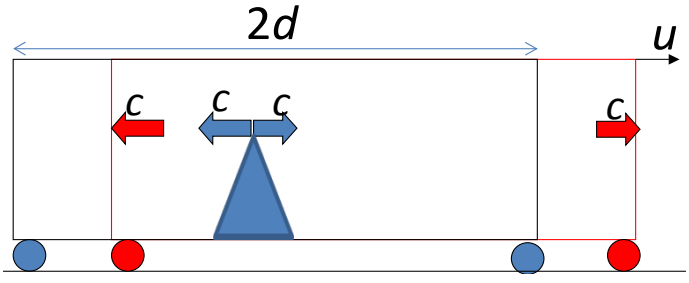

Figure 1. Einstein's famous thought experiment: A pair of photons are fired at middle of the train.

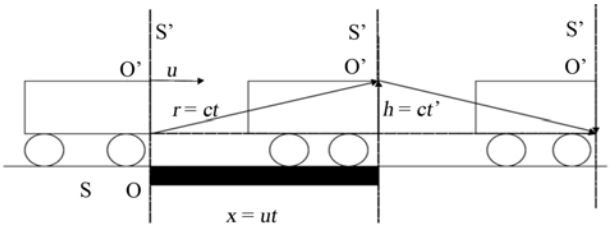

Figure 2. Modified Einstein's thought experiment by firing a photon from the floor to the ceiling. The sides r, x, h of a triangle form the right triangle.

$$h^2 = r^2 - x^2$$

from the Pythagorean theorem. Replacing h by ct', r by ct, and x by ut and by simplifying the equation, we derive the time contraction formula [2]

$$t' = \left(\sqrt{1-\left(\frac{u}{c}\right)^2}\right)t\ .$$

For example, the velocity of the train measured by observers on the platform is $u = 0.6c$, and the train traveled 25 sec. When we input these data into the time contraction formula measured on the train, we get

$$t' = \left(\sqrt{1-\left(\frac{u}{c}\right)^2}\right)t = \left(\sqrt{1-\left(\frac{0.6c}{c}\right)^2}\right)25 = 20 \text{ sec}$$

measured on the train which is shorter then $t = 25$ sec. Special Relativity shows that the time that light moves from the floor to the ceiling are not absolute. Because there are two different possible values of 25 sec or 20 sec for the same event, time cannot be treated as a fundamental quantity.

From the time contraction formula of

$$t' = \left(\sqrt{1-\left(\frac{u}{c}\right)^2}\right)t$$

multiplying u on the equation of both sides, we get the formula of

$$ut' = \left(\sqrt{1-\left(\frac{u}{c}\right)^2}\right)ut$$

ut' is the distance traveled by the train measured from observers on the train denoted by x', ut is the distance traveled by the train measured from observers on the platform denoted by x on **Figure 3**. The length contraction formula can be expressed as

$$x' = \left(\sqrt{1-\left(\frac{u}{c}\right)^2}\right)x\ .$$

Using the formulas, the velocity of the train is $u = 0.6c$ and travels 25 sec measured by the observers on the platform. The distance traveled by the train is $x = ut = 0.6c \times 25 \text{ sec} = 15 \text{ lsec}$. Input these data into the formula of length contraction, then we can calculate the distance traveled by the train measured from the train is

$$x' = \left(\sqrt{1-\left(\frac{u}{c}\right)^2}\right)x = \left(\sqrt{1-\left(\frac{0.6c}{c}\right)^2}\right)\times 15 \text{ lsec} = 12 \text{ lsec}$$

This result is the same as the result from another formula

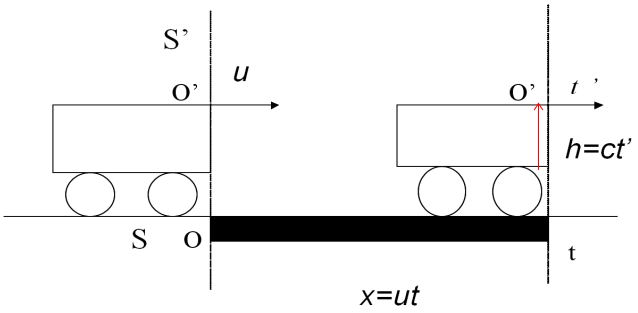

Figure 3. Modified Einstein's thought experiment by shooting a photon from the floor to the ceiling. The distance, x, traveled by the train is measured from the platform.

$$x' = ut' = 0.6c \times 20 \text{ sec} = 12 \text{ lsec}$$

It is shorter than x = 15 lsec. Special Relativity shows that the length (distance) of the train travels from the photon leaving the floor to reach the ceiling is not absolute. Because there are two different possible values of 15 lsec or 12 lsec for the same travel event, so length cannot be treated as a fundamental quantity.

3. Construct a New Space-Time Frame

In *The Trouble with Physics*, the author mentions that: "Descartes and Galileo made a most wonderful discovery. In this way, time is represented as if it were another dimension of space. This 'spatialization' of time is useful but may be challenged as representing a static and unchanging world" [3].

We construct a new space-time frame by presenting time using polar coordinates.

If the unit of time is sec, then the unit of radius for polar circle is chosen to be light second (lsec), then the unit of x-axis should be chosen as light second (lsec) on **Figure 4**. We construct this new space-time frame to make space and time dependent by using the unit of lsec.

If the unit of time is year, then the unit of radius for polar circle is chosen to be light year (lyr), then the unit of x-axis should be chosen to be light year (lyr) on **Figure 5**. We construct this new space-time frame to make space and time dependent by using the unit of lyr.

The advantage of this coordinate frame is that line OA not only represents the motion of the train observed from the platform, but also represents the tract of the photon traveling observed from the platform on **Figure 6**. From the figure on the new space-time frame, it shows that $(\mathrm{OA})^2 = (\mathrm{OO}')^2 + (\mathrm{O}'\mathrm{A})^2$ because OO′A is right triangle. We are able to derive time contraction formula

$$t' = \left(\sqrt{1-\left(\frac{u}{c}\right)^2}\right) t$$

and length contraction formula

$$x' = \left(\sqrt{1-\left(\frac{u}{c}\right)^2}\right) x$$

replacing OA by ct, OO′ by ut, and O′A by ct' which were discussed on the previous section [4].

The advantage is that the O′B can represent the motion of the platform, and O′A can represent the motion of the train from observer's perspective on **Figure 7**. The point B and the point A are on the same circle with the radius of ct'. In order to find the direction of the line O′B, we should find the value of O′Q which is equal to x'. From these polar coordinate frames, the triangle O′BQ is proved to be similar to the triangle OAO′ because the value of the fraction of $\frac{u}{c}$ multiplied by t on the numerator and denominator is the same value as $\frac{u}{c}$ multiplied by t'. Therefore $\frac{ut}{ct} = \frac{ut'}{ct'} \rightarrow \frac{x}{r} = \frac{x'}{r'}$. As long as x, r, r' are given, x' can be calculated.

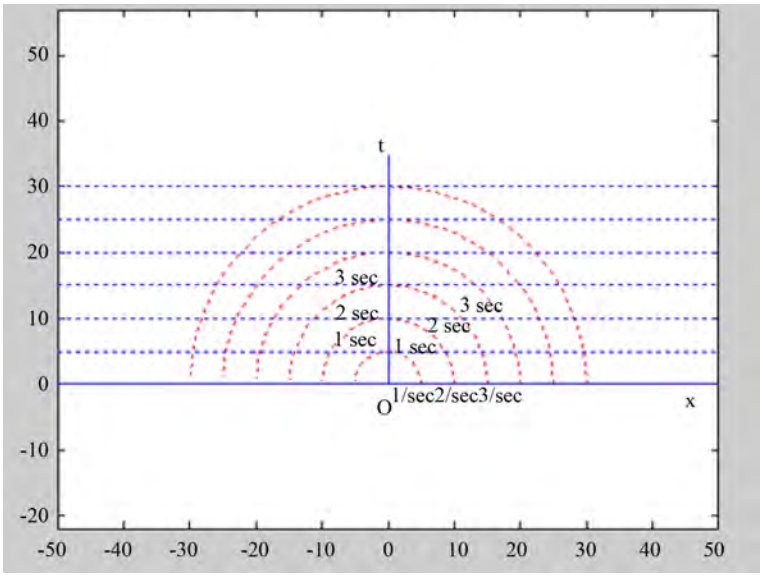

Figure 4. Construct a new space-time frame by presenting time with unit of 1 sec using polar coordinates.

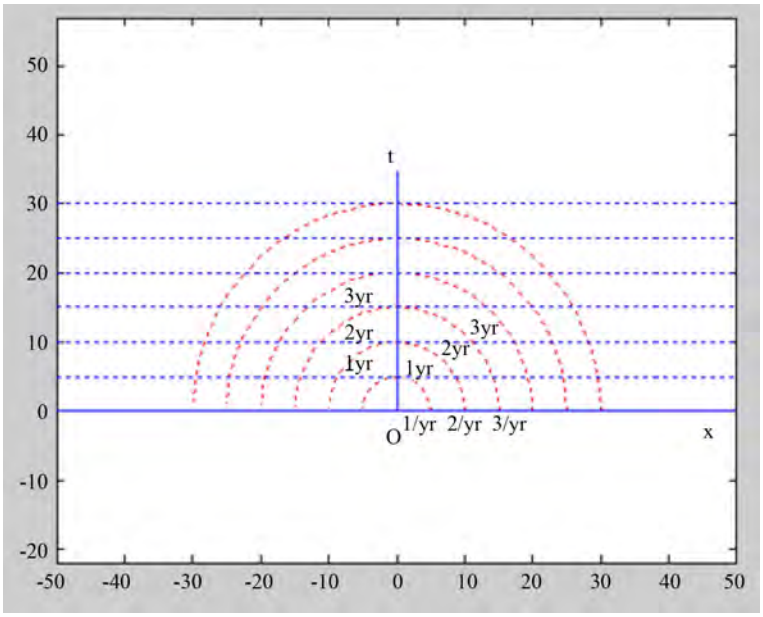

Figure 5. Construct a new space-time frame by presenting time with unit of lyr using polar coordinates.

The ratios of distance to time are proved to be same for both frames. From the previous result $\frac{x}{r}=\frac{x'}{r'}$ $\rightarrow$ $\frac{x}{ct}=\frac{x'}{ct'}$ $\rightarrow$ $\frac{x}{t}=\frac{x'}{t'}$ $\rightarrow$ $u=u'$. The velocity of train traveling measured from observers on the platform is same as the velocity of platform measured from observers on the train. It shows that the traveling train and the platform are a pair of inertial frames [5].

In order to describe the motion of an object in 3-dimensional space along the locations of x-axis, y-axis, and z-axis, we can construct a new space-time frame. Spheres with different radius representing different outgoing time, polar coordinates will be formed from circles of intersections between spheres and x-y plane, y-z plane,

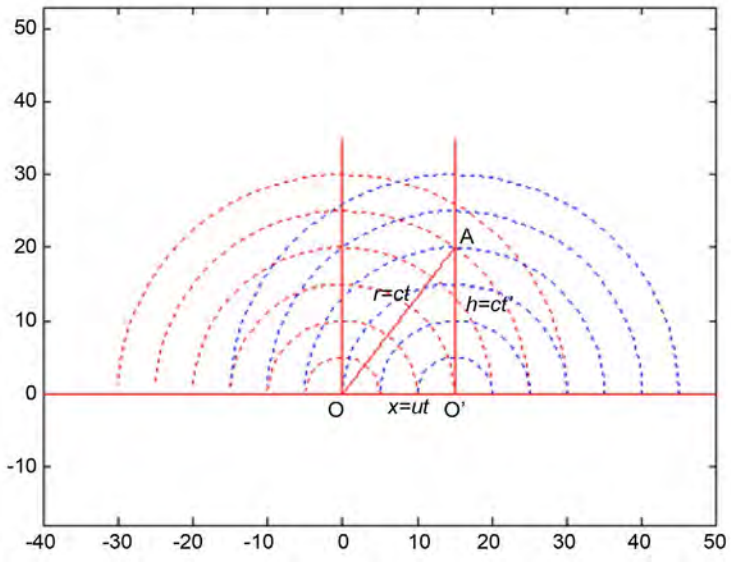

Figure 6. Red circles represent the polar coordinates on the platform. We are able to construct a new space-time frame by presenting time with polar coordinates on the platform to describe the motion of the train using the line OA.

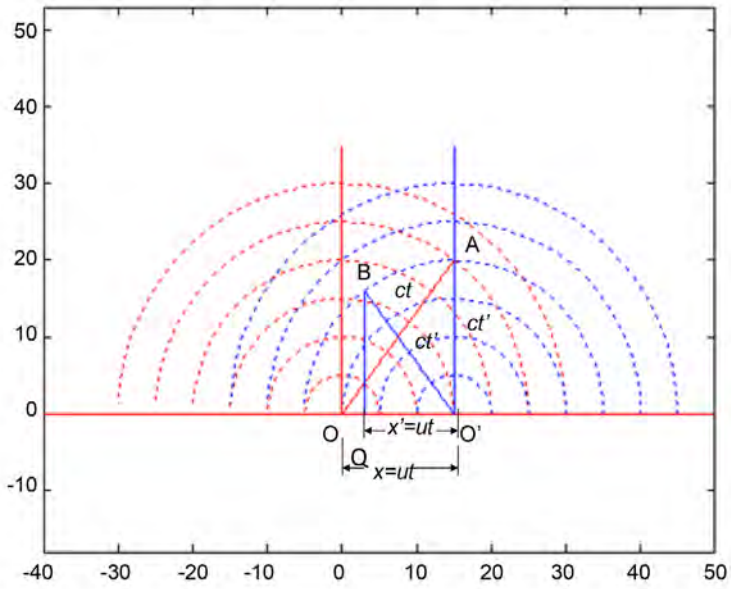

Figure 7. Blue circles represent the polar coordinate on the train. We are able to construct a new space-time frame by presenting time with polar coordinate on the train to describe the motion of the platform using the line O′B.

and z-x plane on **Figure 8**. We are able to use the red polar coordinates of x-y plane, the blue polar coordinates of y-z plane, and the gray polar coordinates of z-x plane to describe the locations of a moving object moving along x-axis, y-axis, and z-axis [6]. This kind of new coordinate frame embedding time axis into space axes is called three-dimensional space-time frame which saves one dimension. We won't be puzzled by being not able to visualize four-dimensional space-time frame.

4. Fundamental Units International System (SI) of Units

The General Conference on Weights and Measures has replaced all but one of the definitions of its fundamental

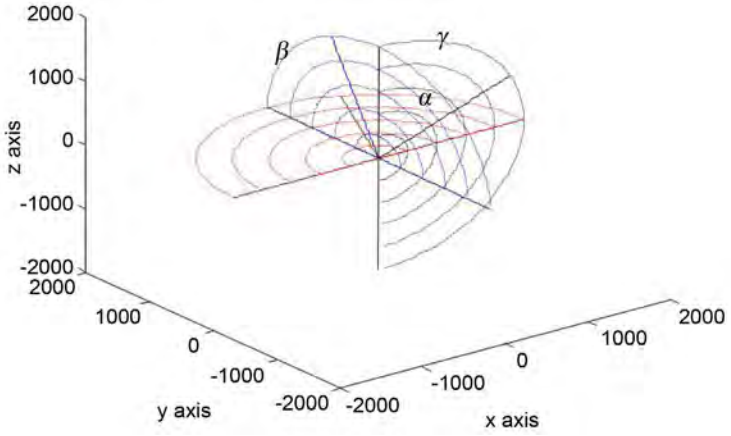

Figure 8. Three-dimensional space-time frame formed by three polar planes on three different planes.

units based on physical objects (such as standard time clocks, standard meter sticks, or standard kilogram bars) with physical descriptions of the units based on stable properties of the Universe. SI fundamental units are current (2005) formal definition [1].

The meter is the length of the path traveled by light in vacuum during a time interval of 1/299,792,458 of a second. From $d = ct$ and c = 299,792,485 m/sec in order to travel 1 meter distance, then the time taken by light is $t = d/c = 1\,\text{m}/(299792458\,\text{m/sec}) = (1/299792458)\,\text{sec}$. We use the velocity of light to define the unit of length 1 meter (1 m).

The second is the duration of 9,192,631,770 cycles of the radiation corresponding to the transition between the two hyperfine levels of the ground state of the caesium-133 atom. From the wave property of light, $c = \frac{\lambda}{T} = \lambda \times f$, then $f = \frac{1}{T}$ or $T = \frac{1}{f}$ The light is emitted by a caesium atom, its frequency is 9,192,631,770 cycles/sec. $T = \frac{1}{f} = \frac{1}{\frac{9192631770\ \text{cycles}}{\text{sec}}} = \frac{1\,\text{sec}}{9192631770\ \text{cycles}}$ then $T \times 9192631770\ \text{cycles} = 1\,\text{sec}$.

We use velocity of light $c = \frac{\lambda}{T} = \lambda \times f$ to define the unit of time, 1 second.

These physical definitions allow scientists to reconstruct meter standards or standard clocks anywhere in the world, or even on other planets, without referring to a physical object kept in a vault somewhere.

In fact, the kilogram is the only fundamental unit still defined by a physical object. The International Bureau of Weights and Measures (BIPM) keeps the world's standard kilogram in Paris, and all other weight standards, such as those of Britain and the United States, are weighed against this standard kilogram.

My opinion, about that the definition of kilogram defined by BIPM, is that they still use gravitational constant, G, as a hidden value, through the action of weighting $W = G\frac{Mm}{R^2} = gm$, where $g = G\frac{M}{R^2}$ (M is the mass of the earth, R is the distance from the scale to the center of the earth) is exactly same value for both mass on the scale at the same location. Under the balance of the scale, the weight of the standard mass on left side is equal to the weight of the prototype mass on the right side of scale. We can conclude that the standard mass is equal to the prototype mass. Without gravitational force, we are not able to check the balance of the standard mass with the prototype mass.

5. Conclusions

If we want to understand time and space, we cannot study them separately. It is our misconception to believe that time and space own innate properties. Actually without movement, we are not able to measure the elapsed time or the distance of traveled. The movement of an object helps us better understand the concept of time and

space.

Since the concept of movement is more fundamental than the concept of space and time, then choosing the velocity of light as a fundamental quantity is reasonable. Since we are able to measure the mass of an object through gravitational force, then choosing force as a fundamental quantity is reasonable.

Because of the constant velocity of light, we should treat velocity of light as fundamental quantity and time and length become derived quantities. In the International System of Units, the velocity of light is already used to define 1 sec and 1 meter, and gravitational force is also used to define 1 kg of mass by balancing with the prototype on scale. In modern physics, we should treat physical events as fundamental elements of thoughts instead of individual objects.

Here we have summarize the discussion in the conclusion of Contextual Principle: We are able to cognize the being of an individual through the existence of phenomena and are able to describe the properties of that individual through the individual's possession of contextual attributes. We are not able to cognize the being of an individual through the existence of individual itself and are not able to describe the properties of that individual through the individual's possession of innate attributes. Physical events are much fundamental than individual objects.

References

[1] International System of Units. http://physics.nist.gov/cuu/Units/current.html

[2] Chen, T. and Chen, Z. (2011) Advantages of Three-Dimensional Space-Time Frames. *Journal of Frontiers in Science*, Sciences Academic Publisher. http://www.sapub.org/journal/archive.aspx?journalid=1015&issueid=337

[3] Smolin, L. (2006) The Trouble with Physics. Houghton Mifflin Company, New York, 256-258.

[4] Chen, T. and Chen, Z. (2009) *Concepts of Physics*, **VI**, 221-235. http://merlin.phys.uni.lodz.pl/concepts/www/VI_2/221.pdf

[5] Chen, T. and Chen, Z. (2008) *Concepts of Physics*, **V**, 523-534. http://merlin.fic.uni.lodz.pl/concepts/www/V_3/523.pdf

[6] Chen, T. and Chen, Z. (2005) Motions of Particles Described in a Three-Dimensional Space-Time Frame. *Proceedings of* 10*th Asian Technology Conference in Mathematics*, Korea National University of Education. http://epatcm.any2any.us/EP/EP2005/2005P163/fullpaper.pdf

Journal of Modern Physics, 2016, 7, 1200-1209
Published Online June 2016 in SciRes. http://www.scirp.org/journal/jmp
http://dx.doi.org/10.4236/jmp.2016.710109

Scientific Research Publishing

The Real Reason Why the Electron's Bare *g*-Factor Is 2 Times Classical

Donald Bowen

Independent Researcher, Concord, MA, USA
Email: quark377@aol.com

Received 24 May 2016; accepted 21 June 2016; published 24 June 2016

Abstract

When analyzing an Electron's orbit's and movements, a "classical" bare *g*-factor of "1" must be used, but when analyzing just the Electron itself, a bare *g*-factor and gyromagnetic ratio of twice the "classical" value is needed to fit reality. Nobody has fully explained this yet. By examining the electromagnetic wave nature of the electron, it is possible to show a simple reason why its bare *g*-factor must be 2, without resorting to superluminal velocities or dismissing it as mystically intrinsic. A simple charged electromagnetic wave loop (CEWL) model of the electron that maintains the same electromagnetic wave nature as the high-energy photons from which electron-positron pairs form, will have exactly half of its energy in the form of magnetic energy who's field lines are perpendicular to the direction of the charge rotation, which leads to the conclusion that only half of the electron's electromagnetic mass is rotational mass, from which it is easy to calculate a bare *g*-factor of 2 using Feynman's equation for the electron's *g*-factor.

Keywords

Electron *g*-Factor, Magnetic Moment, Spin, Angular Momentum, Magnetic Energy, Charged Electromagnetic Wave Loop, CEWL, Pair Production, General Relativity Mass, de Broglie Wave

1. Introduction

The *g*-factor for an electron [1] is actually composed of two elements. The first element is the "bare" *g*-factor of exactly 2 and then the second element is a small correction to this, the anomalous magnetic moment. Total electron *g*-factor = 2 × (1.00116) = 2.00232. The anomalous magnetic moment correction of 1.00116 [2] is best explained by the virtual photons of QED theory [3] (see section 5 of the discussion section). In this paper, only the roots of the "bare" *g*-factor are investigated since the anomalous corrections due to QED's virtual photons represent a different entity, the value of which varies from particle to particle. The reason that the electron has a bare

How to cite this paper: Bowen, D. (2016) The Real Reason Why the Electron's Bare *g*-Factor Is 2 Times Classical. *Journal of Modern Physics*, **7**, 1200-1209. http://dx.doi.org/10.4236/jmp.2016.710109

g-factor of exactly 2 rather than 1 has been a source of mystery ever since spin was discovered. This paper should help solve this mystery.

What is the electron's g-factor? The g-factor is a part of the calculation for the gyromagnetic ratio [4], which is the ratio of the magnetic moment of a particle to the angular momentum of the same particle. G-factors are used for example in equations to calculate the various Larmor frequencies for MRI imaging purposes. Feynman shows, with a very simple equation, that if the mass and charge of an electron are distributed equally about a given radius, then the "classical" g-factor for the electron must be exactly "1" [5], and in fact for calculations where the electron is orbiting a nucleus, the orbital g factor is indeed exactly one.

$$\mu = IA = \frac{qv}{2\pi r} \times \pi r^2 = \frac{q}{2m_e} \times m_e vr = \frac{q}{2m_e} \times L \quad \text{(Feynman) [5]} \tag{1}$$

μ = Magnetic moment (I = current, A = area enclosed by I, q = electron charge, m_e = electron mass)
L = angular momentum.

$$\text{Therefore, the Gyromagnetic ratio} = \frac{\mu}{L} = g_e\left(\frac{q}{2m_e}\right) \text{ where the } g\text{-factor } g_e = 1 \tag{2}$$

1.1. History of the g-Factor

A problem arose in the early days of trying to make quantum mechanical equations fit reality. It became apparent from experiments that the electron's internal g-factor (as opposed to it's orbital g-factor) needed to be 2 instead of 1.

i.e. the electron's Gyromagnetic ratio = $\frac{\mu}{L} = g_e\left(\frac{q}{2m_e}\right)$, Where g_e takes the value of 2 rather than 1.

When Uhlenbeck and Goudsmit first discovered electron "spin", they proposed that an electron has a magnetic moment due to a physically spinning sphere [6] but this led to two problems; First; a quick calculation based on the existing classical spherical model of the electron [7] showed that even if the charge were only on the surface of that sphere, it would need to exceed the speed of light in order to produce the correct magnetic moment [8]. The second problem was that the Fine-Structure and Zeeman spectral lines could not be accounted for correctly with a g-factor of one. *i.e.* only with a bare g-factor of "2", (combined with a separate relativistic Thomas correction) could quantum mechanical equations reproduce the correct spectral lines [9].

Note: See section 3 of the Discussions at end of paper for Dirac's later insight into the mathematical necessity for the g-factor of 2 as well as the Thomas correction.

When Uhlenbeck and Goudsmit realized that the surface of their sphere would need to exceed the speed of light in order to produce the correct magnetic moment they had no explanation for how this could work, so they just submitted a note in their spin paper [6] explaining that there was a superluminal velocity issue. Note: The superluminal velocity problem goes away if one uses the Charged Electromagnetic Wave Loop (CEWL) model for the electron [10], but first it is interesting to explore why Uhlenbeck and Goudsmit relied on a spherical model for the electron. They probably did so for the simple reason that a spherical model was already in use by other physicists, *i.e.* the classical radius model of 2.818×10^{-15} m [7] that had been developed by Lorentz before spin was discovered. Another reason they used a spherical model was that they (incorrectly) thought that the necessary g-factor of 2 could be arrived at by using a surface charged spherical model. At the suggestion of their mentor Ehrenfest, they had used an existing g-factor calculation, previously done by another famous physicist [6], which suggested that the necessary g factor of 2 could be accounted for by assuming that the charge of an electron resides only on the surface of a solid sphere. This previous calculation, which they included in their famous spin paper, produced the correct g-factor of two, which seemed to support the spherical model. However, a correct calculation, as shown below, will show that their spherical model would actually produce a g-factor of 5/3 (too small).

For a sphere of; M = mass, p_m = density, w = angular frequency, the angular momentum "J" is:

$$J = wp_m \int\int\int_{0,0,0}^{R,\pi,2\pi} (r\sin\theta)^2 r^2 \sin\theta \mathrm{d}r\mathrm{d}\theta\mathrm{d}\varphi = w2MR^2/5 \tag{3}$$

For the same sphere, if charge Q resides only on the surface, the magnetic moment "u" is:

$$u = \frac{w}{2}\frac{Q}{\left(4\pi R^2\right)} R^4 \int\int_{0,0}^{\pi,2\pi} \sin\theta^2 \sin\theta \mathrm{d}\theta \mathrm{d}\varphi = wQR^3/3 \tag{4}$$

Therefore $\gamma = \frac{u}{J} = \left(wQR^3/3\right)/\left(w2MR^2/5\right) = (5/3)(Q/2M)$ (5)

If the surface-charged-spherical model produces a g-factor of 5/3 instead of the necessary 2, then it can't be correct. But in those early years of quantum mechanics this mistake was not known, and since it looked right, people moved on with the right answer of 2 for the wrong reason. The superluminal conflict was dismissed at the time by just saying the electron has an "intrinsic" spin that can't be understood classically.

Both the erroneous g-factor explanation and the superluminal velocity issues go away if the Charged-Electromagnetic-Wave-Loop (CEWL) Model is used, *i.e.* the charge can now rotate within Einstein's laws of relativity, and the g-factor of 2 can easily be derived from the model. It can also be demonstrated that no other shape or diameter besides the CEWL model can get rid of the superluminal violations of relativity. The CEWL model, as described in the paper "An Electron Model Consistent with Electron-Positron Pair Production from High Energy Photons" [10] will also exactly generate the correct de Broglie matter-wave base frequency to over 6 decimal places while matching the known magnetic moment of the electron to over 6 decimal places simultaneously (Getting the de Broglie frequency to match was another problem with the original spherical superluminal model). Below is a quick summary of the CEWL model followed by some diagrams to help explain how it generates the correct g-factor of 2.

1.2. The CEWL Model

The CEWL model starts with the premise that since electron-positron pairs form from purely electromagnetic photons (of energy > 1.022 Mev [11]), and since the resulting pairs of electrons and positrons (of energy 0.511 Mev each) have the same electromagnetic nature (as witnessed by their de Broglie wavelengths), then they must have the same electromagnetic wave nature as the photons from which they originated, except for one detail; The magnetic field lines of electrons and positrons can close back on themselves allowing matter to exist at rest, whereas the magnetic field lines of photons do not (and hence the magnetic and electric fields of photons chase each other forward at the speed of light).

Note: Maxwell was the first to be able to calculate the speed of light "c" with his equation $c^2 = \frac{1}{\epsilon\mu}$, where ϵ and μ are the electric and magnetic permittivity constants of free space. Where does the mass come from? One can combine Maxwell's equation above with Einstein's $E = mc^2$ to get $m = E\epsilon\mu$ where mass can be equated to the purely electromagnetic terms on the right. The electromagnetic energy tensor equations of general relativity theory are also shown to contribute to space time distortion exactly the same as mass does (see below).

2. From Photon to Fermion

2.1. From Photon

Modern modelling of photons generally focuses on the "potential" E and B fields (Electric and Magnetic fields), but as Maxwell first envisioned a photon, it is actually composed of a charge separation spiralling through space at the speed of light [12] (the electric permittivity constant of free space ϵ describes the capacitance like ability to induce a charge separation in free space). **Figure 2** "before" shows how Maxwell envisioned the charge separations of a photon (the spiral can be either right hand or left polarity). Note: The cross section perpendicular to the direction of travel is of the general form of an ellipse [13], with "circularly" polarized light having a circular elliptical cross section, and regular "polarized" photons having a more elongated elliptical cross section (circularly polarized photons can be changed into "regular" elliptically polarized photons and "regular" photons can be changed to circularly polarized by sending the photon through non-linear optics such as "quarter wave plates" [14]) The right hand or left hand spiral "spin" rotation direction however stays constant unless the photon is reflected by a mirror etc.)

2.2. To Fermion

When high energy gamma ray photons (of at least 1.011 Mev energy) collide with matter, they produce elec-

tron-positron pairs [11] (see **Figure 1**).

The CEWL model for electron positron pair production is shown below by the transition from a high energy photon in **Figure 2** "before" to two charged loops in **Figure 2** "after". The positively charged loop is a Positron and the negatively charged loop is an Electron. Due to the original spin rotation of each at formation, the magnetic fields are opposed at the moment of formation, allowing the electron and positron to separate despite their enormous electrostatic attraction at that scale. The original paper [10] contains the math to show that the opposing magnetic field at initial formation of an electron-positron pair would exceed the electrostatic attraction between them.

The simplest definition of the *g*-factor of an electron is that it represents the ratio between the radius of the rotating charge, and the radius of the rotating mass. For example if we look at an electron orbiting in a circle, we know that it will generate a bare *g*-factor of one because the mass and the charge are both orbiting at the same radius around the atom. The CEWL electron model may look similar, with a rotating charged component, but unlike the case where an electron orbits a nuclei (where all the mass of the electron contributes to rotational mass), in the CEWL model only half the electron's mass contributes to rotational mass. The electric energy, *i.e.* the rotating charge component, contributes to the rotational mass, but the magnetic energy, because the direction of its components only act in a plane perpendicular to the direction of the charge, as shown in **Figure 3**, the magnetic energy will not add "rotational" mass. (See the difference between electric energy mass and magnetic energy mass below).

2.3. Electromagnetic Energy and Mass

MIT Physics professors' emeriti Slater & Frank have solved Maxwell's Electromagnetic equations for the general case of plane wave propagation of photons to show that the total Electro-Magnetic Energy Density in free space, *i.e.* with no resistive component is:

$$\text{Total Electro-Magnetic Energy Density} = U = \frac{1}{2}\left(\epsilon_0 E^2 + \frac{1}{\mu_0} B^2\right) \text{ [16]} \tag{6}$$

As further explained by Slater & Frank, the average magnetic component (the B half of this equation) is only greater than the average Electric component when a resistive component is present [16]. In any given rest frame, photons and electrons do not lose energy, *i.e.* internally they have no resistive component, so therefore if the electrons and positrons maintain the same electromagnetic wave nature as the photon from which they originated, then the average electric energy must exactly equal the average magnetic energy in both cases.

Using $E = mc^2$, one can divide the above Energy density Equation (6) by c^2 to get Mass density:

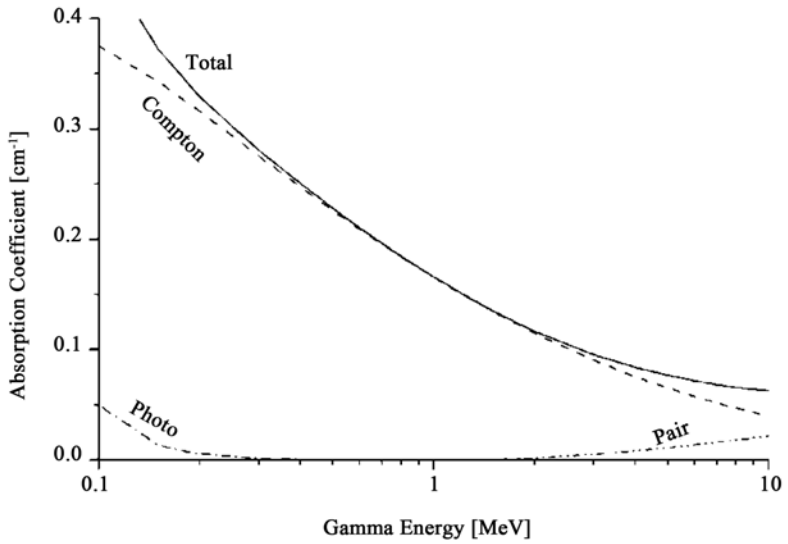

Figure 1. Electron-positron pair production in aluminum [15].

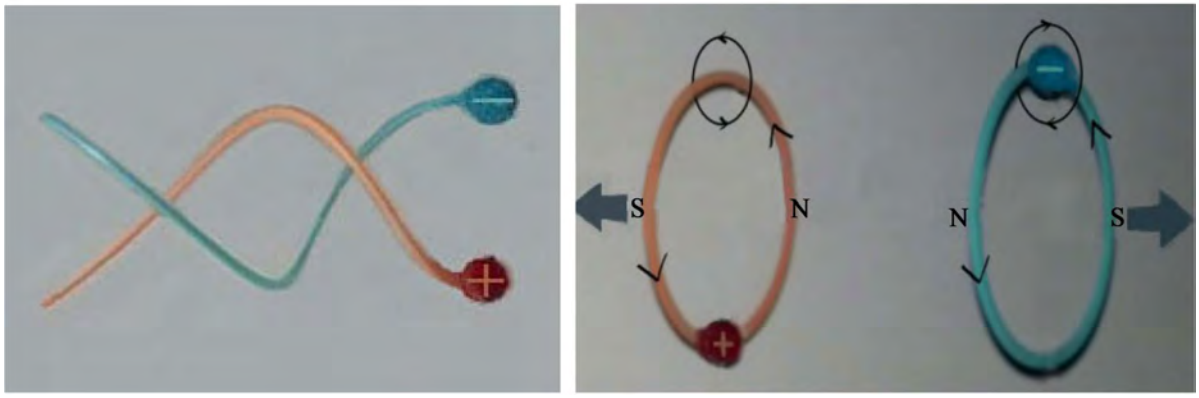

Figure 2 "Before" and **Figure 2** "After" show the transition from a 1.022 Mev photon to positive and negative loops that are closed and repelling away from each other magnetically. The positive loop is a positron and the negative loop is an electron. Note: The wavelength in **Figure 2**."Before" and the loop diameters in **Figure 2**. "After" are roughly in scale relative to each other, but the other dimensions such as the size, shape and distribution of the charged regions would differ from what is shown. Due to the compressive forces of the magnetic field lines inside and outside the loop, the thickness of this charged layer would most likely be a very thin in the same way that a barrel hoop is, with the charge most likely sinusoidally distributed as it rotates around the loop.

Figure 2. "Before" Photon $\lambda = 12.13 \times 10^{-13}$ m. "After" Loop Diam = 7.723×10^{-13} m.

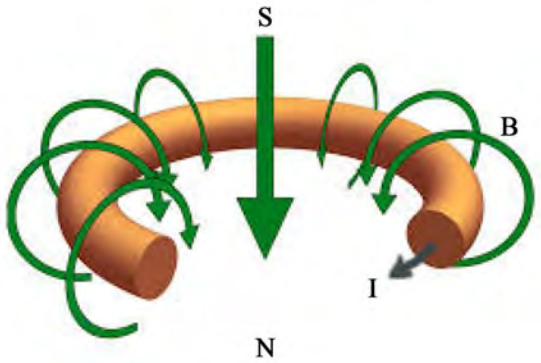

Figure 3. The Magnetic "B" field lines which are due to the rotation of the charge inside an electron/positron have no component in the direction of the "I" current/charge rotation and hence can add no rotational energy/mass. Note: the positive charge in a positron would rotate as shown, but the negative charge of an electron would rotate in a direction opposite to that of the "I" arrow in order to conform to the North and South polarity shown. Due to its electromagnetic wave nature, the charge amount would most likely vary sinusoidally as it progresses around the loop at the speed of light (inside a loop of much smaller volume relative to radius than shown in this figure).

$$\text{Mass density} = \frac{U}{c^2} = \frac{1}{2c^2}\left(\epsilon_0 E^2 + \frac{1}{\mu_0} B^2\right) \tag{7}$$

Note: Using Maxwell's $c^2 = \dfrac{1}{\epsilon\mu}$ to get rid of μ, it is easy to show that this is exactly the same equation as the Electromagnetic Stress-Energy tensor form for mass used in Einstein's General Relativity [17]

Electromagnetic Tensor equation for Mass: $T = \dfrac{\epsilon_0}{2}\left(\dfrac{E^2}{c^2} + B^2\right)$ [17] (8)

Since only half the electromagnetic mass contributes to angular momentum, then we can simply substitute $L/2$ for L into Feynman's electron gyromagnetic equation, Equation (2) above, and we get:

$$\text{Gyromagnetic ratio} = \frac{\mu}{L/2} = 2 \times \left(\frac{q}{2m_e}\right) \tag{9}$$

The electron *g*-factor g_e is now twice classical, *i.e.* $g_e = 2$ instead of 1.

Note: See the Conclusions section for a more detailed explanation.

This is similar to the Faraday Paradox in which a magnet rotating inside a conductive loop can impart no rotational energy out to the loop. [18].

3. No Other Model Can Match Reality without Violating either Einstein's General Relativity or Maxwell's Equations

The fact that the Tensor equations of general relativity show that the space time distortions due to electromagnetic energy density are no different from the space time distortions of "mass" suggests that they are one and the same. Furthermore, if we invoke some mystical "other" form of mass such as a sphere or disk on which the charge rotates, we run into a problem; If there is another form of "mass" (besides the electromagnetic energy components), then by Einstein's $E = mc^2$, that mass would come at the expense of the electromagnetic energy. We know that the base de Broglie frequency of an electron is exactly the same as the frequency of a purely electromagnetic photon of equal energy [10], so this by itself should rule out any subtraction from the original electromagnetic energy (with which to make this different form of matter). Additionally, the charge cannot rotate at any diameter except the CEWL diameter (see below), and since the magnetic energy of any loop of moving charge would, of necessity, be both inside and outside the loop (see **Figure 3**), then the total mass cannot be completely inside the loop diameter. This rules out a charge on the edge of a disk of some hypothetical different form of mass for example. This also rules out any other exotic shape where all the mass is completely inside the CEWL diameter.

No other diameter except a circular loop of exactly the CEWL diameter can fit reality. This is because unless the charge is rotating in a circular loop of diameter 7.723×10^{-13} Meter, at the speed of light, the correct magnetic moment and the correct de Broglie frequency will not be generated simultaneously. Only at precisely the correct CEWL diameter, will both match reality to over 6 decimal places [10]. Any smaller diameter requires superluminal velocities to generate the correct magnetic moment, and any larger diameter requires superluminal velocities to generate the correct de Broglie frequency. For the same reason, any loop besides a circle doesn't work either; If for example we investigate an oval loop (instead of a circular loop), who's transit frequency at the speed of light matches the de Broglie frequency, then the magnetic moment will be too small due to the fact that the magnetic moment depends on multiplying the amperage times the area enclosed inside the loop. It is only at precisely the CEWL diameter that all elements of reality can be met exactly and simultaneously [10].

4. Discussions

1) When the Grand Master of Physics Lorentz first heard of Uhlenbeck's and Goudsmit's ground-breaking spin paper, he pointed out a possible problem; *i.e.* since the magnetic energy is roughly the magnetic moment squared divided by the radius cubed, *i.e.* $\frac{U^2}{r^3}$ [6], then the radius would have to be roughly 10^{-14} meter *i.e.* too big. This had also reinforced the concept that the spin must be "intrinsic" and physics moved on. But apparently Lorentz's only objection to that size was that it conflicted with the then current estimates of atomic nuclei cross sections, and since he was aware that electron's can be emitted from nuclei (beta decay), hence the size didn't make sense to him. But the original CEWL model paper shows that the Muon and Tau higher energy states of the electron have a much smaller size [10], and since the electron would most likely be in the form of a Muon while it still resides inside a neutron, Lorentz's size estimate would not actually be the conflict he thought it to be. Lorentz's rough estimate of size was not far from the Electron's CEWL loop radius of 3.86×10^{-13} Meter. The CEWL model predicts that the Muon form of the electron would be about 207 times smaller than the electron [10], *i.e.* roughly 1.86×10^{-15} Meter (much closer to what Lorentz was expecting).

2) Two other distinguished physicists have suggested the same diameter as that of the CEWL model: Just before publishing the original paper, a book by Mac Gregor [19] was discovered, in which he had proposed a spherical model of exactly the same diameter as the CEWL model. Mac Gregor, (who studied under Uhlenbeck), suggests that a charge spins around the equator of this spherical model in order to produce the correct magnetic moment for an electron. The CEWL model differs in that it doesn't use a spherical "scaffolding" to support the charge as it rotates since it has not been demonstrated what the spherical scaffolding would be made of or how it would form.

Another paper [20], written in 1952 by the distinguished MIT professor emeritus Kerson Huang, has just come

to light as well. In his 1952 paper Professor Huang explores the same diameter within the context of quantum mechanical equations. Professor Huang uses the same diameter for the same reason, *i.e.* because it generates the correct magnetic moment for the electron, but his interpretation of the electron is different from the CEWL model in that by using the quantum mechanical approach, he does not address the internal structure of the electron itself, or what it might be made of, and suggests that the mysterious matter of the electron can be either physically localized or physically spread out over large regions of space depending on the measurement. The CEWL model by contrast addresses the internal structure of the electron itself and says that it is a charged electromagnetic wave internally. (See next section for a comparison to the quantum mechanical approach).

3) A few years after Uhlenbeck's and Goudsmit's ground breaking spin paper, the famous physicist Dirac was able to derive an amazing 4 × 4 matrix version of quantum mechanics which included relativity corrections, and was able to show that both the *g*-factor of 2 as well as the Thomas correction of 2 could both be inferred as necessary from his more advanced mathematical descriptions of the electron [21]. This is similar to the way that the speed of light "*c*" can be inferred from either Maxwell's equations or Einstein's $E = mc^2$ equation). Dirac however was working from a quantum-mechanical approach, which did not require presenting a physical model for the electron in the same way that Maxwell had put forth a rotating charge model of the photon in order to explain how Maxwell's equations would generate the speed of light for a photon. The end result was that even decades after Uhlenbeck's and Guoudsmit's discovery of spin, the *g*-factor of 2 was still viewed as a mysterious mathematical necessity. As Einstein famously said towards the end of his life, "You know, it would be sufficient to really understand the electron." [19].

The CEWL model matches all known values for the electron, so it is compatible with the amazing equations of quantum mechanics, but it goes a step further by proposing an internal structure for the electron itself. Quantum mechanical equations were developed to fit the known spectral line data generated by quantum energy jumps of electrons as they transition between orbital levels within the ecosystems of atoms (electrons have characteristic wavelengths as they move through space, and because of this, only atomic orbits whose circumferences are integer values of these wavelengths are stable). The quantum energy jump equations address the energy level jumps within the ecosystem of an atom, but do not address the internal structure of the electron itself. Richard Feynman, one of the founders of QED theory, (one of the most advanced forms of quantum mechanics), lamented at the end of his 1985 book on QED that there is no theory that explains the masses of particles [3]. Other versions of quantum mechanics are also silent on what the internal structure of the electron might be. The CEWL model by contrast addresses the internal structure of the electron itself, showing it to be an electromagnetic wave internally, just like the photon from which it originated (with the only difference between a fermion and a photon being that the magnetic field lines of a fermion can close back on themselves allowing a fermion to exist a rest). The electromagnetic wave nature of the CEWL model, in addition to showing why the *g*-factor must be 2, also shows how the rotating charge would add both a positive and negative speed of light component to the average velocity of a moving electron as predicted by Dirac [21], and also explains how the de Broglie wave nature of the electron can arise from the model [10]. (The de Broglie wave nature of the electron explains why quantum energy jumps are required within the ecosystem of atoms).

4) The CEWL model addresses the previously mysterious *g*-factor of 2 needed to make quantum mechanical equations fit reality, but how does this fit with the mysterious Pauli's exclusion principle of quantum mechanics? And is it compatible with the mysterious "superposition of spin" demonstrated by the Stern Gerlach experiment [22]? Here's a quick and easy trick to show how everything fits together: Take two magnetic compasses as shown in **Figure 4** "before" and then put one on top of the other as shown in **Figure 4** "after". Voila! One has spin up and the other has spin down! This is the nature of Pauli's exclusion principle. Within the "ecosystem" of an atom, pairs of electrons within the same orbit interact with each other such that their magnetic field lines are minimized in the same way that the two compasses have done. This is a lower energy state than having both electrons "spin" in the same direction.

The heavier neutrons and protons of the nuclei have magnetic moments too, they are just much heavier than an electron. Imagine strapping a pound of lead to the needle of one of the compasses (assuming the heavy compass could still rotate freely); the two compasses would still align themselves as before, except that the lighter "electron" would respond to a magnetic field quicker than the heavy "nuclei". In any atom, the first electron in any orbital pair would align itself with the nuclei, and the second would align itself with the first, and each successive electron pair in an atomic "ecosystem" would do likewise. The Stern-Gerlach experiment consisted of shooting randomly oriented silver atoms (which have one unpaired electron in the outer shell) through a strong magnet [22]. The

Figure 4. "Before" two isolated electrons. "After" electrons form pairs of one "Up" and one "Down".

result was that the stream of silver atoms split into two streams and this result was used to demonstrate that electrons exist in a "superposition". "Superposition" implies something mystical about an electron, but it's not really that mysterious; what was really happening was that the heavy nuclei didn't have time to react while going through the magnet, but the unpaired electron did. If the heavier nuclei were already somewhat aligned with the magnet, the electron flipped out of its normal state opposing the nuclei spin, and into a spin state closer to that of the nuclei (adding to the total magnetic moment). If on the other hand the nuclei happened to already be aligned somewhat opposite to the magnet, then the final orientation of the electron subtracted from the nuclei magnetic moment. The net effect is two magnetic states (of the atomic ecosystem) depending on whether the electron now adds to, or subtracts from, the original nuclei magnetic moment after going through the magnet (an electron by itself would not show a two state "superposition" since it would simply rotate into full alignment with the magnet).

5) The circular loop of the CEWL electron model is similar to the nature of an inductive loop antenna [23] in that the circumference around a loop antenna must match the wavelength of the received/transmitted electromagnetic radio wave photons. Likewise, the circumference of the CEWL model exactly matches the Compton wavelength of a photon of energy equal to that of an electron. (in the CEWL model, the electron has exactly the same nature as the electromagnetic photon that generated it, with the only difference being that the magnetic field lines have closed back on themselves allowing it to exist "at rest" rather than travel at the speed of light). Antenna theory subdivides electromagnetic interactions into 3 regions [24]; 1) The "Near Field" where electromagnetic oscillations are induced near the antenna, but leads to no net loss of energy from the antenna (all "virtual photon" energy is reabsorbed by the antenna), 2) The "Fresnel" intermediate region, and 3) The "Far Field" where photons fully form and can propagate away (leading to net energy loss from the antenna). The "virtual photons" (and virtual particles) that start to form near the electron but then get immediately reabsorbed is the basis for how Feynman and Shwinger calculated the anomalous magnetic moment correction of 1.00116 for the electron's *g*-factor [3]. The ability of electrons, positrons and other forms of matter to induce oscillations in the vacuum of free space is what distinguishes modern quantum type physics from the previous more "classical" interpretations of physics, *i.e.* interactions of particles with a pure vacuum cannot be calculated as simply "one-way" interactions, but rather the energy fluctuations of all the virtual photons (and virtual particles) induced near matter must also be calculated, both for their effect back on the original particle as well as for their effect on nearby photons and matter [3].

By investigating the antenna nature of the CEWL model it may be possible to investigate, among other things, the directionality and polarity of the "virtual" photons of QED theory that are emitted (and immediately reabsorbed) in the vicinity of electrons. As semiconductors shrink down to sizes where ever smaller numbers of electrons are channelled through ever smaller channels, CEWL modelling of the antenna and spin characteristics at scales close to the CEWL size of the electron may provide insight into how to further reduce resistance losses in semiconductors.

6) The electron's *g*-factor of 2 represents the highest gyromagnetic moment of any form of matter and this is most likely connected to the fact that the electron is an indivisible unit of matter and a building block for other forms of matter [10]. When for example the neutron's *g*-factor is represented as −3.826, this does not mean that the gyromagnetic moment of a neutron is 3.826 times higher than an electron, *i.e.* it just represents an offset to an arbitrary gyromagnetic ratio equation. The *g*-factor equation for the heavier neutron looks similar to the electron's equation, except that instead of using the charge and mass of the electron (which would require a *g*-factor correction 3 orders of magnitude smaller than the electrons *g*-factor), it instead arbitrarily uses the mass of one proton, m_p (while still using the charge of one electron).

This same arbitrary equation: $\mu = g\left(\frac{e}{2m_p}\right)I$ [4] (10)

Is used for neutrons and protons and all nuclei "For simplicity and consistency" [4]. In the same way that the electron's *g*-factor gives a clue to its internal structure, the various *g*-factors of other nuclear components can most likely be investigated for information on how their internal building blocks are arranged.

5. Conclusions

By looking at how Feynman derived the electron's gyromagnetic ratio in equation #2 from his equation #1, it is easy to see that when investigating an electron's orbit around an atom, where both all the mass and all the charge of the electron orbit at the same radius around the atom, the bare *g*-factor must be exactly 1, so it has been a mystery why a bare *g*-factor of 2 is needed to make quantum mechanical equations fit reality. This paper shows that if a simple Charged-Electromagnetic-Wave-Loop (CEWL) model is used for the electron itself, whereby the electron maintains the same electromagnetic characteristics as the photon from which it originated, then it follows that only half of the electron's mass contributes to the angular momentum inside the electron. This is due to the fact that the magnetic field lines inside the electron are perpendicular to the direction of the charge rotation internally (see **Figure 3**), and hence the magnetic energy half of the mass cannot add to the angular momentum inside the electron, which leads to the conclusion that the angular momentum inside the electron is exactly half of what it would be if the entire electromagnetic energy contributed to angular momentum (see Equations (6)-(8) and reference [16]). This shows that inside the electron itself, the angular momentum as used by Feynman in Equation (2) would now need to take the value of L/2 instead of L, leading to a necessary correction to the other side of Feynman's equation by increasing the *g*-factor to $g_e = 2$ instead of 1 in order to keep the two halves of the equation equal. This explains the mystery of why quantum mechanical equations require an electron to have a bare *g*-factor of 2 rather than 1 in order to fit reality.

The CEWL model, in addition to explaining why a bare *g*-factor of 2 is needed for calculations involving the electron's internal spin, also explains all other known values for the electron as well as showing how electron-positron pairs can form from high energy photons.

Acknowledgements

Many thanks to Robert V. Mulkern PhD for reviewing this paper as well as for the calculations to demonstrate that a surface charged spherical model can't work, and for helpful discussions.

References

[1] Wikipedia (2015) *g*-Factor_(Physics). https://en.wikipedia.org/wiki/*G*-factor_(physics)

[2] Wikipedia (2015) Anomalous Magnetic Dipole Moment. https://en.wikipedia.org/wiki/Anomalous_magnetic_dipole_moment

[3] Feynman, R.P. (1985) QED, The Strange Theory of Light and Matter. Princeton University Press, Princeton, 115-118, 152.

[4] Wikipedia (2015) Gyromagnetic Ratio. https://en.wikipedia.org/wiki/Gyromagnetic_ratio

[5] Feynman, Leighton, Sands, The Feynman Lectures on Physics. Vol. III, Basic Books, New York, 34-3.

[6] Pais, Abraham, Inward Bound. Oxford University Press, Oxford, 276-279.

[7] Wikipedia (2015) Classical Electron Radius. https://en.wikipedia.org/wiki/Classical_electron_radius

[8] Wikipedia(2015) Electron Magnetic Moment . https://en.wikipedia.org/wiki/Electron_magnetic_moment

[9] Jackson, J.D. (1998) Classical Electrodynamics. 3rd Editon, John Wiley & Sons, Hoboken, 548.

[10] Bowen, D. and Mulkern R.V. (2015) An Electron Model Consistent with Electron-Positron Pair Production from High Energy Photons. Scientific Research Publishing. http://www.scirp.org/Journal/PaperInformation.aspx?PaperID=59188

[11] Wikipedia (2016) Pair_Production. https://en.wikipedia.org/wiki/Pair_production

[12] Maxwell, J.C. (1873) A Treatise On Electricity & Magnetism. Vol. II, Clarendon Press, London, 403.

[13] Wikipedia (2015) Elliptical Polarization. http://en.wikipedia.org/wiki/Elliptical_polarization

[14] Wikipedia (2015) Waveplate. https://en.wikipedia.org/wiki/Waveplate

[15] Paul, H. (2014) Gamma Abs Al.png. Wikipedia. http://commons.wikimedia.org/wiki/File:Gamma_Abs_Al.png

[16] Slater, J.C. and Frank, N.H. (2015) Electromagnetism. Dover Publications, New York, 94-103.

[17] Wikipedia (2015) Stress-Energy_Tensor. https://en.wikipedia.org/wiki/Stress–energy_tensor

[18] Wikipedia (2015) Faraday_Paradox. https://en.wikipedia.org/wiki/Faraday_paradox

[19] Mac Gregor, M.H. The Enigmatic Electron, Chapters 7, 17. 2nd Edition El Mac Books, Santa Cruz, 2013 Reprint of 1992 Original.

[20] Huang, K. (1952) On the Zitterbewegung of the Dirac Electron. Department of Physics, MIT, Cambridge.

[21] Dirac P.A.M. (2011) The Principles of Quantum Mechanics. 4th Edition, Oxford University Press, Oxford, Reprinted 2011, 165 & 261-267.

[22] Wikipedia (2015) Stern-Gerlach Experiment. https://en.wikipedia.org/wiki/Stern–Gerlach_experiment

[23] Wikipedia (2015) Loop Antennae. https://en.wikipedia.org/wiki/Loop_antenna

[24] Wikipedia (2015) Near and Far Field. https://en.wikipedia.org/wiki/Near_and_far_field

Journal of Modern Physics, 2016, 7, 1210-1227
Published Online June 2016 in SciRes. http://www.scirp.org/journal/jmp
http://dx.doi.org/10.4236/jmp.2016.710110

Scientific Research Publishing

We Are Living in a Computer Simulation

Ding-Yu Chung

Utica, MI, USA
Email: dy_chung@yahoo.com

Received 10 May 2016; accepted 24 June 2016; published 28 June 2016

Abstract

This paper posits that we are living in a computer simulation to simulate physical reality which has the same computer simulation process as virtual reality (computer-simulated reality). The computer simulation process involves the digital representation of data, the mathematical computation of the digitized data in geometric formation and transformation in space-time, and the selective retention of events in a narrative. Conventional physics cannot explain physical reality clearly, while computer-simulated physics can explain physical reality clearly by using the computer simulation process consisting of the digital representation component, the mathematical computation component, and the selective retention component. For the digital representation component, the three intrinsic data (properties) are rest mass-kinetic energy, electric charge, and spin which are represented by the digital space structure, the digital spin, and the digital electric charge, respectively. The digital representations of rest mass and kinetic energy are 1 as attachment space for the space of matter and 0 as detachment space for the zero-space of matter, respectively, to explain the Higgs field, the reverse Higgs field, quantum mechanics, special relativity, force fields, dark matter, and baryonic matter. The digital representations of the exclusive and the inclusive occupations of positions are 1/2 spin fermion and integer spin boson, respectively, to explain spatial translation by supersymmetry transformation and dark energy. The digital representations of the allowance and the disallowance of irreversible kinetic energy are integral electric charges and fractional electric charges, respectively, to explain the confinements of quarks and quasiparticles. For the mathematical computation component, the mathematical computation involves the reversible multiverse and oscillating M-theory as oscillating membrane-string-particle whose space-time dimension (D) number oscillates between 11D and 10D and between 10D and 4D to explain cosmology. For the selective retention component, gravity, the strong force, electromagnetism, and the weak force are the retained events during the reversible four-stage evolution of our universe, and are unified by the common narrative of the evolution.

Keywords

Computer Simulation, Physical Reality, Virtual Reality, Digital Computer, Computer-Simulated Physics, Digital Representation, Selective Retention, M-Theory, Space Structure, Higgs Field,

How to cite this paper: Chung, D.-Y. (2016) We Are Living in a Computer Simulation. *Journal of Modern Physics*, **7**, 1210-1227. http://dx.doi.org/10.4236/jmp.2016.710110

Reverse Higgs Field, Fractional Electric Charge, Spin, Multiverse, Cosmology, Force Fields, Cyclic Universe

1. Introduction

In the simulation hypothesis by Nick Bostrom [1], physical reality is actually a computer simulation. We are living in a computer simulation which is derived from the mathematical computation based on the fundamental laws of physics. In the future, the computer will be powerful enough to compute all details in physical reality, and will create a computer-simulated world. Currently, it is possible to simulate virtual reality by digital computer. Virtual reality is digital computer-simulated reality. Virtual reality is used in flight simulation to train people to be pilots. The model of the typical digital computer is often called the von Neumann computer as **Figure 1**.

In a digital computer, input data from the input unit are converted into digitized data. For the computer simulation process for virtual reality, the computation section of the Central Process Unit (CPU) computes digitized data in geometric formation and transformation in space-time, while the control section of the CPU handles the logistics of digitized data. Selective digitized data are retained in memory. The computed digitized data are converted into data which appear as output data in the output unit. As a result, the computer simulation process for virtual reality involves the three components consisting of the digital representation component, the mathematical computation component, and the selective retention component. In the digital representation component, data are represented by digital representations. Both data and digital representations of data exist. The mathematical computation component computes digitized data in geometric formation and transformation in space-time. The selective retention component retains selectively events in a narrative. There is no logical relation among all retained events. The retained events are unified by the common narrative.

This paper posits that we are living in a computer simulation to simulate physical reality which has the same computer simulation process as virtual reality (computer-simulated reality). Both computer simulation processes for physical reality and virtual reality involve the digital representation of data, the mathematical computation of the digitized data in geometric formation and transformation in space-time, and the selective retention of events in a narrative. For the digital representation component of physical reality, the three intrinsic data (properties) are rest mass-kinetic energy, electric charge, and spin which are represented by the digital space structure [2]-[4], the digital spin, and the digital electric charge [5], respectively. As described previously for the digital space structure [2]-[4], the digital representations of rest mass and kinetic energy are 1 as attachment space for the space of matter and 0 as detachment space for the zero-space of matter, respectively. In the digital space structure, attachment space attaches to matter permanently or reversibly. Detachment space detaches from the object at the speed of light. Attachment space relates to rest mass and reversible movement, while detachment space relates to irreversible kinetic energy. Attachment space and detachment space are the origins of the Higgs field and the reverse Higgs field, respectively. The combination of n units of attachment space as 1 and n units of detachment space as 0 brings about the three digital structures: binary partition space $(1)_n(0)_n$, miscible space $(1 + 0)_n$, and binary lattice space $(1\ 0)_n$ to account for quantum mechanics, special relativity, and the force fields, respectively. The digital representations of the exclusive and the inclusive occupations of positions are 1/2 spin fermion and integer spin boson, respectively. Fermions, such as electrons and protons, follow the Pauli exclusion principle which excludes fermions of the same quantum-mechanical state from being in the same position. Bosons, such as photons or helium atoms, follow the Bose-Einstein statistics which allows bosons of the same quantum-mechanical state being in the same position. The exclusion-inclusion brings about spatial translation by the supersymmetry transformations between fermion and boson. As described previously for the digital electric

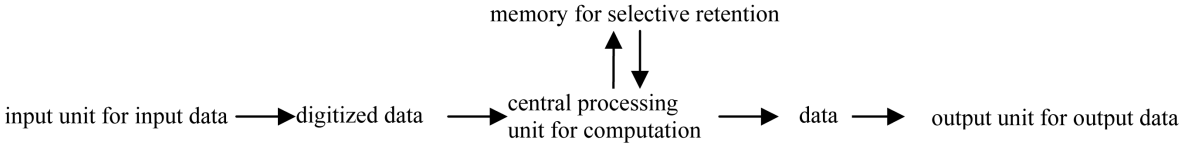

Figure 1. The model of the typical digital computer.

charge [5], the digital repre-sentations of the allowance and the disallowance of irreversible kinetic energy are integral electric charges and fractional electric charges, respectively. Quarks in hadrons and quasiparticles in the Fractional Quantum Hall Effect (FQHE) have fractional electric charges whose irreversible movement caused by irreversible kinetic energy is restricted within hadrons and within the confinement of two-dimensional systems, respectively.

For the mathematical computation of physical reality, the mathematical computation involves geometric formation and transformation in space-time, and as described before [3] [4], physical reality involves oscillating M-theory instead of conventional fixed M-theory. In oscillating M-theory as oscillating membrane-string-particle, space-time dimension (D) number oscillates between 11D and 10D and between 10D and 4D. Space-time dimension number between 10 and 4 decreases with decreasing speed of light, decreasing vacuum energy, and increasing rest mass.

The selective retention component for physical reality is narrative. For physical reality, the unification of the four force fields (gravity, the strong force, electromagnetism, and the weak force) based on a symmetry group has not been successful. There is no logical relation among the four force fields. In the computer simulation process for virtual reality, it is possible to retain events at different times in a narrative in such way that different events are unified by the common narrative. As described before [6]-[9], the four force fields in our universe are the retained events during the four-stage evolution of our universe, and are unified by the common narrative of the evolution.

Conventional physics cannot explain the reality of quantum mechanics easily. Conventional physics cannot explain the origins of the confinement of quarks and the fractional charges of quasiparticles. The geometry in conventional physics is fixed M-theory which has no experimental proof. Conventional physics cannot unify the four force fields. Conventional physics cannot explain physical reality clearly, while computer-simulated physics can explain physical reality clearly [4] [5] by using the computer simulation process consisting of the digital representation component, the mathematical computation component, and the selective retention component. We are living in a computer simulation.

Section 2 describes the mathematic computation component for oscillating M-theory. Section 3 explains the digital representation component consisting of the digital space structure, the digital spin, and the digital electric charge. Section 4 describes the narrative of the evolution of our universe to unify the four force fields.

2. The Mathematical Computation Component

The geometry in the mathematic computation component for the computer simulation process is oscillating M-theory. M-theory with eleven-dimensional membrane is an extension of string theory with ten-dimensional string, in contrast to the observed 4D. In conventional M-theory, space-time dimensional number (D) is fixed. As a result, the observed 4D results from the the compactization of the extra space dimensions in 11D M-theory, However, there is no experimental proof for compactized extra space dimensions, and there are numerous ways for the compactization of the extra space dimensions [10]. As described before [3] [4], the geometry for the mathematical computation is oscillating M-theory derived from oscillating membrane-string-particle whose space-time dimension number oscillates between 11D and 10D and between 10D and 4D dimension by dimension reversibly. There is no compactization. Matters in oscillating M-theory include 11D membrane (2_{11}) as membrane (denoted as 2 for 2 space dimensions) in 11D, 10D string (1_{10}) as string (denoted as 1 for 1 space dimension) in 10D, and variable D particle ($0_{4\text{ to }11}$) as particle (denoted as 0 for 0 space dimension) in 4D to 11D.

As described previously [3] [4], the QVSL (quantum varying speed of light) transformation transforms both space-time dimension number (D) and mass dimension number (d). In the QVSL transformation, the decrease in the speed of light leads to the decrease in space-time dimension number and the increase of mass in terms of increasing mass dimension number from 4 to 10,

$$c_{\mathrm{D}} = c/\alpha^{\mathrm{D}-4}, \tag{1a}$$

$$E = M_0 \cdot \left(c^2/\alpha^{2(\mathrm{D}-4)}\right) \tag{1b}$$

$$= \left(M_0/\alpha^{2(\mathrm{d}-4)}\right)\cdot c^2. \tag{1c}$$

$$c_{\mathrm{D}} = c_{\mathrm{D}-n}/\alpha^{2n}, \tag{1d}$$

$$M_{0,\mathrm{D,d}} = M_{0,\mathrm{D}-n,\mathrm{d}+n}\alpha^{2n}, \tag{1e}$$

$$\mathrm{D},\ \mathrm{d} \xrightarrow{\mathrm{QVSL}} (\mathrm{D} \mp n),\ (\mathrm{d} \pm n) \tag{1f}$$

$$E_{\mathrm{vacuum,D}} = E - M_{0,\mathrm{D}}c^2, \tag{1g}$$

where c_{D} is the quantized varying speed of light in space-time dimension number, D, from 4 to 10, c is the observed speed of light in the 4D space-time, α is the fine structure constant for electromagnetism, E is energy, M_0 is rest mass, D is the space-time dimension number from 4 to 10, d is the mass dimension number from 4 to 10, n is an integer, and E_{vacuum} = vacuum energy. For example, in the QVSL transformation, a particle with 10D4d is transformed to a particle with 4D10d from Equation (1f). Calculated from Equation (1e), the rest mass of 4D10d is $1/\alpha^{12} \approx 137^{12}$ times of the mass of 10D4d. In terms of rest mass, 10D space-time has 4d with the lowest rest mass, and 4D space-time has 10d with the highest rest mass. Rest mass decreases with increasing space-time dimension number. The decrease in rest mass means the increase in vacuum energy ($E_{\mathrm{vacuum,D}}$), so vacuum energy increases with increasing space-time dimension number. The vacuum energy of 4D particle is zero from Equation (1g). The mass dimension number is limited from 4 to 10, because 4D is the minimum space-time, and 11D membrane and 10D string are equal in the speed of light, rest mass, and vacuum energy. Since the speed of light for > 4D particle is greater than the speed of light for 4D particle, the observation of > 4D superluminal particles by 4D particles violates casualty. Thus, > 4D particles are hidden particles with respect to 4D particles. Particles with different space-time dimensions are transparent and oblivious to one another, and separate from one another if possible.

As described previously [3] [4], another part of the mathematical computation component is the reversible multiverse. In the reversible multiverse, all physical laws and phenomena are permanently reversible, and temporary irreversibility of entropy increase is allowed through reversibility breaking, symmetry violation, and low entropy beginning. We live in the universe with such temporary irreversible entropy increase. The reversible universe is shown in cosmology which is in Section 4.

3. The Digital Representation Component

In the digital representation component for the computer simulation process, data in physical reality are represented by digital representations. Both data and digital representations exist. In physical reality, the three intrinsic data (properties) are rest mass-kinetic energy, spin, and electric charge which have the three digital representations consisting of the digital space structure, the digital spin, and the digital electric charge for the intrinsic data (properties) of rest mass-kinetic energy, spin, and electric charge, respectively.

3.1. Digital Space Structure

The digital representations of rest mass and kinetic energy are 1 as attachment space for the space of matter and 0 as detachment space for the zero-space of matter, respectively. In the digital space structure, attachment space attaches to matter permanently or reversibly. Detachment space detaches from the object at the speed of light. Attachment space relates to rest mass and reversible movement, while detachment space relates to irreversible kinetic energy.

In conventional physics, space does not couple with particles. In the Higgs field, space is the passive zero-energy ground state space. Under spontaneous symmetry breaking, the passive zero-energy ground state is converted into the active, permanent, and ubiquitous nonzero-energy Higgs field, which couples with massless particle to produce the transitional Higgs field-particle composite. Under spontaneous symmetry restoring, the transitional Higgs field-particle composite is converted into the massive particle with the longitudinal component on zero-energy ground state without the Higgs field as follows.

$$\begin{aligned}&\text{zerro-energy groud state space} \xrightarrow{\text{spontaneous symmetry breaking}} \text{nonzero-energy scalar Higgs field}\\ &\xrightarrow{\text{massless particle}} [\text{the transitional nonzero-energy Higgs field-particle composite}]\\ &\xrightarrow{\text{spontaneous symmetry restoring}} \text{massive particle with the longitudinal component}\\ &\text{on zero-energy ground state space without the Higgs field}\end{aligned} \tag{2}$$

In conventional physics, the nonzero-energy scalar Higgs Field exists permanently in the universe. The problem

with such nonzero-energy field is the cosmological constant problem from the huge gravitational effect by the nonzero-energy Higgs field in contrast to the observation [11].

As described before [4], in the digital space structure, space as the zero-energy ground state space couples with particles, unlike passive space in conventional physics. Attachment space is the origin of the Higgs field. Under spontaneous symmetry breaking, attachment space as the active zero-energy ground state space couples with massless particle to form momentarily the transitional non-zero energy Higgs field-particle composite. The Higgs field is momentary and transitional, avoiding the cosmological constant problem. Under spontaneous symmetry restoring, the transitional nonzero-energy Higgs field-particle composite is converted into massive particle with the longitudinal component on zero-energy attachment space without the Higgs field as follows.

$$\begin{aligned}&\text{massless particle} + \text{zero-energy attachment space} \xrightarrow{\text{spontaneous symmetry breaking}}\\&\left[\text{the transitional non-zero energy Higgs field-particle composite}\right]\\&\xrightarrow{\text{spontaneous symmetry restoring}} \text{massive particle with the longitudinal}\\&\text{component on zero-energy attachment space without the Higgs field}\end{aligned} \tag{3}$$

Detachment space is the origin of the reverse Higgs field. Unlike the conventional model, detachment space actively couples to massive particle. Under spontaneous symmetry breaking, the coupling of massive particle to zero-energy detachment space produces the transitional nonzero-energy reverse Higgs field-particle composite which under spontaneous symmetry restoring produces massless particle on zero-energy detachment space without the longitudinal component without the reverse Higgs field as follows.

$$\begin{aligned}&\text{massive particle} + \text{zero-energy detachment space} \xrightarrow{\text{spontaneous symmetry breaking}}\\&\left[\text{the transitional nonzero-energy reverse Higgs field-particle composite}\right]\\&\xrightarrow{\text{spontaneous symmetry restoring}} \text{massless particle without the longitudinal}\\&\text{component on zero-energy detachment space without the reverse Higgs field}\end{aligned} \tag{4}$$

For the electroweak interaction in the Standard model where the electromagnetic interaction and the weak interaction are combined into one symmetry group, under spontaneous symmetry breaking, the coupling of the massless weak W, weak Z, and electromagnetic A (photon) bosons to zero-energy attachment space produces the transitional nonzero-energy Higgs fields-bosons composites which under partial spontaneous symmetry restoring produce massive W and Z bosons on zero-energy attachment space with the longitudinal component without the Higgs field, massless A (photon), and massive Higgs boson as follows.

$$\begin{aligned}&\text{massless WZ} + \text{zero-energy WZ attachment space} + \text{massless A} + \text{zero-energy A attachment space A}\\&\xrightarrow{\text{spontaneous symmetry breaking}} \left[\text{the transitional nonzero-energy WZ Higgs field -WZ composite}\right]\\&+\left[\text{nonzero-energy A Higgs field -A composite}\right] \xrightarrow{\text{partial spontaneous symmetry restoring}}\\&\text{massive WZ with the longitudinal component on attachment space without the Higgs field}\\&+ \text{massless A} + \text{the nonzero energy massive Higgs boson}\end{aligned} \tag{5}$$

From the periodic table of elementary particles, the theoretical calculated mass of the Higgs boson is 128.8 GeV in good agreements with the observed 125 or 126 GeV [12]. In terms of mathematical expression, the conventional permanent Higgs field model and the posited transitional Higgs field model are identical. The interpretations of the mathematical expression are different for the permanent Higgs field model and the transitional Higgs field model. The transitional Higgs field model avoids the cosmological problem in the permanent Higgs field model.

As shown in Section 4, our universe is the dual asymmetrical positive-energy-negative-energy universe where the positive-energy universe on attachment space absorbed the interuniversal void on detachment space to result in the combination of attachment space and detachment space, and the negative-energy universe did not absorb the interuniversal void. The combination of n units of attachment space as 1 and n units of detachment space as 0 brings about three different digital space structures: binary partition space, miscible space, or binary lattice space as below.

$$\begin{aligned}&(1)_n + (0)_n \xrightarrow{\text{combination}} (1)_n(0)_n, \quad (1+0)_n, \text{ or } (1\,0)_n\\&\text{attachment space, detachment space, binary partition space, miscible space, binary lattice space}\end{aligned} \tag{6}$$

Binary partition space, $(1)_n(0)_n$, consists of two separated continuous phases of multiple quantized units of attachment space and detachment space. In miscible space, $(1+0)_n$, attachment space is miscible to detachment space, and there is no separation of attachment space and detachment space. Binary lattice space, $(1\,0)_n$, consists of repetitive units of alternative attachment space and detachment space. In conventional physics, space does not couple with particles, and does not contain detailed structure. In the digital space structure, space couples with particles, and contains the three different digital structures.

Binary partition space $(1)_n(0)_n$ can be described by the uncertainty principle. The uncertainty principle for quantum mechanics is expressed as follows.

$$\sigma_x \sigma_p \geq \frac{\hbar}{2} \tag{7}$$

The position, x, and momentum, p, of a particle cannot be simultaneously measured with arbitrarily high precision. The uncertainty principle requires every physical system to have a zero-point energy (non-zero minimum momentum) and to have a non-zero minimum wavelength as the Planck length. In terms of the space structure, detachment space relating to kinetic energy as momentum is σ_p, and attachment space relating to space (wavelength) for a particle is σ_x. In binary partition space, neither detachment space nor attachment space is zero in the uncertainty principle, and detachment space is inversely proportional to attachment space. Quantum mechanics for a particle follows the uncertainty principle defined by binary partition space. Binary partition space $(1)_n(0)_n$ can also be described by the Schrodinger in quantum mechanics where total energy equals to kinetic energy related to $(0)_n$ plus potential energy related to $(1)_n$. In binary partition space, an entity is both in constant motion as standing wave for detachment space and in stationary state as a particle for attachment space, resulting in the wave-particle duality.

Detachment space contains no matter that transmits information. Without transmitting information, detachment space is outside of the realm of causality. Without causality, distance (space) and time do not matter to detachment space, resulting in non-localizable and non-countable space-time. The requirement for the system (binary lattice space) containing non-localizable and non-countable detachment space is the absence of net information by any change in the space-time of detachment space. All changes have to be coordinated to result in zero net information. This coordinated non-localized binary lattice space corresponds to nilpotent space. All changes in energy, momentum, mass, time, space have to result in zero [13]. The non-local property of binary lattice space for wave function provides the violation of Bell inequalities [14] in quantum mechanics in terms of faster-than-light influence and indefinite property before measurement. The non-locality in Bell inequalities does not result in net new information. Binary partition space explains the nonlocal pilot-wave theory (Bohmian mechanics) where the trajectories of particles are nonlocal and fully determined by the pilot wave [15].

In binary partition space, for every detachment space, there is its corresponding adjacent attachment space. Thus, no part of the mass-energy can be irreversibly separated from binary partition space, and no part of a different mass-energy can be incorporated in binary partition space. Binary partition space represents coherence as wavefunction. Binary partition space is for coherent system. Any destruction of the coherence by the addition of a different mass-energy to the mass-energy causes the collapse of binary partition space into miscible space. The collapse is a phase transition from binary partition space to miscible space.

$$\underset{\text{binary partition space}}{(0)_n\,(1)_n} \xrightarrow{\text{collapse}} \underset{\text{miscible space}}{(0+1)_n} \tag{8}$$

Another way to convert binary partition space into miscible space is gravity. Penrose [16] pointed out that the gravity of a small object is not strong enough to pull different states into one location. On the other hand, the gravity of large object pulls different quantum states into one location to become miscible space. Therefore, a small object without outside interference is always in binary partition space, while a large object is never in binary partition space.

The information in miscible space is contributed by the miscible combination of both attachment space and detachment space, so information can no longer be non-localized. Any value in miscible space is definite. All observations in terms of measurements bring about the collapse of wavefunction, resulting in miscible space that leads to eigenvalue as definite quantized value. Such collapse corresponds to the appearance of eigenvalue, E, by a measurement operator, H, on a wavefunction, Ψ.

$$H\Psi = E\Psi \tag{9}$$

In miscible space, attachment space is miscible to detachment space, and there is no separation of attachment space and detachment space. In miscible space, attachment space contributes zero speed, while detachment space contributes the speed of light. For a moving massive particle consisting of a rest massive part and a massless part, the massive part with rest mass, m_0, is in attachment space, and the massless part with kinetic energy, K, is adjacent to detachment space. The combination of the massive part in attachment space and massless part in detachment leads to the propagation speed in between zero and the speed of light. To maintain the speed of light constant for a moving particle, the time (t) in moving particle has to be dilated, and the length (L) has to be contracted relative to the rest frame.

$$\begin{aligned} t &= t_0 \Big/ \sqrt{1-\upsilon^2/c^2} = t_0\gamma, \\ L &= L_0 \big/ \gamma, \\ E &= K + m_0c^2 = \gamma m_0c^2 \end{aligned} \tag{10}$$

where $\gamma = 1\Big/\left(1-v^2/c^2\right)^{1/2}$ is the Lorentz factor for time dilation, and length contraction, E is the total energy, and K is the kinetic energy.

Bounias and Krasnoholovets [17] propose that the reduction of dimension can be done by slicing dimension, such as slicing 3 space dimension object (block) into infinite units of 2 space dimension objects (sheets). As shown in Section 4, the positive-energy 10D4d particle universe as our observable universe with high vacuum energy was transformed into the 4D10d universe with zero vacuum energy at once, resulting in the inflation. During the Big Bang following the inflation, the 10d (mass dimension) particle in attachment space denoted as 1 was sliced by detachment space denoted as 0. For example, the slicing of 10d particle into 4d particle is as follows.

$$\begin{gathered} 1_{10} \xrightarrow{\text{slicing}} 1_4 \qquad \sum_{\mathrm{d}=5}^{10}\left(0_4\ 1_4\right)_{n,\mathrm{d}} \\ \text{10d particle} \quad \text{4d core particle} \quad \text{binary lattice space} \end{gathered} \tag{11}$$

where 1_{10} is 10d particle, 1_4 is 4d particle, d is the mass dimension number of the dimension to be sliced, n as the number of slices for each dimension, and $(0_4\ 1_4)_n$ is binary lattice space with repetitive units of alternative 4d attachment space and 4d detachment space. For 4d particle starting from 10d particle, the mass dimension number of the dimension to be sliced is from d = 5 to d = 10. Each mass dimension is sliced into infinite quantized units (n = ∞) of binary lattice space, $(0_4\ 1_4)_\infty$. For 4d particle, the 4d core particle is surrounded by 6 types (from d = 5 to d = 10) of infinite quantized units of binary lattice space. Such infinite quantized units of binary lattice space represent the infinite units (n = ∞) of separate virtual orbitals in a gauge force field, while the dimension to be sliced is "dimensional orbital" (DO), representing a type of gauge force field. The mass-energy in each dimensional orbital increases with the number of dimension number, and the lowest dimension orbital with d = 5 has the lowest mass-energy [9] [18]. 10d particle was sliced into six different particles: 9d, 8d, 7d, 6d, 5d, and 4d equally by mass. Baryonic matter is 4d, while dark matter consists of the other five types of particles (9d, 8d, 7d, 6d, and 5d).

$$\begin{gathered} \text{10D4d} \xrightarrow{\text{the inflation}} \text{4D10d} \xrightarrow{\text{the Big Bang}} \\ \text{baryonic matter}\left(\left(\text{4D4d}\right) + \text{dark matter}\ \left(\text{4D5d, 4D6d, 4D7d, 4D8d, 4D9d}\right) + \text{kinetic energy}\right. \end{gathered} \tag{12}$$

The mass ratio of dark matter to baryonic matter is 5 to 1. At 72.8% dark energy, the calculated values for baryonic matter and dark matter (with the 1:5 ratio) are 4.53% (= (100 − 72.8)/6) and 22.7% (= 4.53 × 5), respectively, in excellent agreement with observed 4.56% and 22.7%, respectively [9] [19] [20]. The dimensional orbitals of baryonic matter provide the base for the periodic table of elementary particles to calculate accurately the masses of all elementary particles, including quarks, leptons, gauge bosons, the Higgs boson, and the knees-ankles-toe in cosmic rays [12] [18] [21]. The calculated masses of all elementary particles are in good agreement with the observed values. For examples, the calculated mass of top quark and the Higgs boson are 176.5 GeV and 128.8 GeV in good agreement with the observed 173.34 GeV and 125 or 126 GeV, respectively.

As shown in the periodic table of elementary particles described previously [18], the lowest dimensional orbital is for electromagnetism. Baryonic matter with maximum number of gauge force fields (dimensional orbit-

als) is the only one with the lowest dimensional orbital for electromagnetism. With higher dimensional orbitals, dark matter does not have this lowest dimensional orbital [6] [18]. Without electromagnetism, dark matter cannot emit light, and is incompatible to baryonic matter with electromagnetism, like the incompatibility between oil and water. Derived from the incompatibility between dark matter and baryonic matter, the modified interfacial gravity (MIG) between homogeneous baryonic matter region and homogeneous dark matter region to separate baryonic matter region and dark matter region explains galaxy evolution and unifies the CDM (Cold Dark Matter) model, MOG (Modified Gravity), and MOND (Modified Newtonian Dynamics) [22] [23]. The digital space structure based on the combination of binary partition space and binary lattice space explains superconductivity [24] and superstar without singularity to replace black hole with singularity [25] [26]. Singularity is permanently irreversible by losing information permanently, forbidden in the reversible multiverse.

3.2. The Digital Spin

The digital representations of the exclusive and the inclusive occupations of positions are 1/2 spin fermion and integer spin boson, respectively. Fermions, such as electrons and protons, follow the Pauli exclusion principle which excludes fermions of the same quantum-mechanical state from being in the same position. Bosons, such as photons or helium atoms, follow the Bose-Einstein statistics which allows bosons of the same quantum-mechanical state being in the same position. As a result, the digital representations of the exclusive and the inclusive occupations of positions are 1/2 spin fermion and integer spin boson, respectively. The symmetry between fermion and boson is supersymmetry. Two supersymmetry transformations from boson to fermion and from fermion to boson yield a spatial translation. In physical reality, supersymmetry is varying supersymmetry [3] [4]. In varying supersymmetry, the repetitive transformation between fermion and boson brings about a spatial translation and the transformation into the adjacent mass dimension number. Varying supersymmetry transformation is one of the two steps in transformation involving the oscillation between 10D particle and 4D particle. The transformation during the oscillation between 10D particle and 4D particle involves the stepwise two-step transformation consisting of the QVSL transformation and the varying supersymmetry transformation. As described in Section 2, the QVSL transformation involves the transformation of space-time dimension, D whose mass increases with decreasing D for the decrease in vacuum energy. The varying supersymmetry transformation involves the transformation of the mass dimension number, d whose mass decreases with decreasing d for the fractionalization of particle, as follows.

stepwise two-step varying transformation

$$\text{(1)}\quad \mathrm{D},\ \mathrm{d} \xleftrightarrow{\text{QVSL}} (\mathrm{D}\mp 1),(\mathrm{d}\pm 1) \tag{13}$$

$$\text{(2)}\quad \mathrm{D},\ \mathrm{d} \xleftrightarrow{\text{varying supersymmetry}} \mathrm{D},(\mathrm{d}\pm 1)$$

The repetitive stepwise two-step transformation between 10D4d and 4D4d as follows.

$$10\mathrm{D}4\mathrm{d} \leftrightarrow 9\mathrm{D}5\mathrm{d} \leftrightarrow 9\mathrm{D}4\mathrm{d} \leftrightarrow 8\mathrm{D}5\mathrm{d} \leftrightarrow \cdots \leftrightarrow 4\mathrm{D}5\mathrm{d} \leftrightarrow 4\mathrm{D}4\mathrm{d} \tag{14}$$

In this two-step transformation, the transformation from 10D4d to 9D5d involves the QVSL transformation as in Equation (1d). Calculated from Equation (1e), the mass of 9D5d is $1/\alpha^2 \approx 137^2$ times of the mass of 10D4d. The transformation of 9D5d to 9D4d involves the varying supersymmetry transformation. In the normal supersymmetry transformation, the repeated application of the fermion-boson supersymmetry transformation carries over a boson (or fermion) from one point to the same boson (or fermion) at another point at the same mass. In the varying supersymmetry transformation, the repeated application of the fermion-boson supersymmetry transformation carries over a boson from one point to the boson at another point at different mass dimension number in the same space-time number. The repeated varying supersymmetry transformation carries over a boson $\mathrm{B_d}$ into a fermion $\mathrm{F_d}$ and a fermion $\mathrm{F_d}$ to a boson $\mathrm{B_{d-1}}$, which can be expressed as follows

$$M_{\mathrm{d,F}} = M_{\mathrm{d,B}}\alpha_{\mathrm{d,B}}, \tag{15a}$$

$$M_{\mathrm{d-1,B}} = M_{\mathrm{d,F}}\alpha_{\mathrm{d,F}}, \tag{15b}$$

where $M_{\mathrm{d,B}}$ and $M_{\mathrm{d,F}}$ are the masses for a boson and a fermion, respectively, d is the mass dimension number, and $\alpha_{\mathrm{d,B}}$ or $\alpha_{\mathrm{d,F}}$ is the fine structure constant that is the ratio between the masses of a boson and its fermionic partner. Assuming α's are the same, it can be expressed as

$$M_{\mathrm{d,B}} = M_{\mathrm{d+1,B}}\alpha_{\mathrm{d+1}}^2 . \tag{15c}$$

The mass of 9D4d is $\alpha^2 \approx (1/137)^2$ times of the mass of 9D5d through the varying supersymmetry transformation. The transformation from a higher mass dimensional particle to the adjacent lower mass dimensional particle is the fractionalization of the higher dimensional particle to the many lower dimensional particles in such way that the number of lower dimensional particles becomes

$$N_{\mathrm{d-1}} = N_{\mathrm{d}}/\alpha^2 \approx N_d\,(137)^2 \tag{15d}$$

The fractionalization also applies to D for 10D4d to 9D4d, so

$$N_{\mathrm{D-1}} = N_{\mathrm{D}}/\alpha^2 \tag{15e}$$

Since the supersymmetry transformation involves translation, this stepwise varying supersymmetry transformation leads to a translational fractionalization, resulting in the cosmic expansion. Afterward, the QVSL transformation transforms 9D4d into 8D5d with a higher mass. The two-step transformation repeats until 4D4d, and then reverses stepwise back to 10D4d for the cosmic contraction. The oscillation between 10D and 4D results in the reversible cyclic fractionalization-contraction for the reversible cyclic expansion-contraction of the universe which does not involve irreversible kinetic energy.

3.3. The Digital Electric Charge

As described before [5], the digital representations of the allowance and the disallowance of irreversible kinetic energy are integral electric charges and fractional electric charges, respectively. Individual integral charge with irreversible kinetic energy to cause irreversible movement is allowed, while individual fractional charge with irreversible kinetic energy is disallowed. The disallowance of irreversible kinetic energy for individual fractional charge brings about the confinement of individual fractional charges to restrict the irreversible movement resulted from kinetic energy. Collective fractional charges are confined by the short-distance confinement force field where the sum of the collective fractional charges is integer. As a result, fractional charges are confined and collective. The confinement force field includes gluons in QCD (quantum chromodynamics) for collective fractional charge quarks in hadrons and the magnetic flux quanta for collective fractional charge quasiparticles in the fractional quantum Hall effect (FQHE) [27]-[29].

The collectivity of fractional charges requires the attachment of energy as flux quanta to bind fractional charges. As a result, the integer-fraction transformation from integral charges to fractional charges involves the integer-fraction transformation to incorporate flux quanta similar to the composite fermion theory for the FQHE [30] [31]. There are two steps in the composite fermion theory for the FQHE. The first step is the formation of composite fermion by the attachment of an even number of magnetic flux quanta to electron. Composite fermions in the Landau levels are the "true particles" to produce the FQHE, while electrons in the Landau level are the true particles to produce the integral quantum Hall effect (IQHE). The IQHE is a manifestation of the Landau level quantization of the electron kinetic energy. The second step is the conversion of integral charges to fractional charges in the collective mode of composite fermions. The IQHE in the collective mode of composite fermions is the FQHE as expressed by the filling factors υ's related to electric charges.

$$\begin{aligned}
&\text{the composite fermion theory}\\
&\text{the first step :}\\
&\text{electrons} \xrightarrow{\text{even numbers of magnetic flux quanta}} \text{composite fermions}\\
&\text{the second step for the collective mode of composite fermions :}\\
&\nu^* = m \quad \text{for the IQHE}\\
&\nu = \frac{\nu^*}{2n\nu^* \pm 1} = \frac{m}{2mn \pm 1} \quad \text{for the FQHE}\\
&\text{for } \nu^* = 1,\ \nu = \frac{1}{2n+1} \quad \text{for the Laughlin wavefunction of the FQHE}
\end{aligned} \tag{16}$$

where m and n are integers, and υ and υ^* are the filling factors for electrons and composite fermions, respective-

ly in the Landau levels. The composite fermion theory is used to compute precisely a number of measurable quantities, such as the excitation gaps and exciton dispersions, the phase diagram of composite fermions with spin, the composite fermion mass, etc.

The integer-fraction transformation from integral charges to fractional charges consists of the three steps: 1) the attachment of an even number of flux quanta to individual integral charge fermions to form individual integral charge composite fermions, 2) the attachment of an odd number of flux quanta to individual integral charge composite fermions to form transitional collective integral charge composite bosons, and 3) the conversion of flux quanta into the confinement force field to confine collective fractional charge composite fermions converted from composite bosons. The first step of the integer-fraction transformation from integral charge to fractional charge is same as the first step in the composite fermion theory. The first step is the attachment of an even number of flux quanta to individual integral charge fermions to form individual integral charge composite fermions [28]. Flux quanta are the elementary units which interact with a system of integral charge fermions. The attachment of flux quanta to the fermions transforms them to composite particles. The attached flux quanta change the character of the composite particles from fermions to bosons and back to fermions. Composite particles can be either fermions or bosons, depending on the number of attached flux quanta. A fermion with an even number of flux quanta becomes a composite fermion, while a fermion with an odd number of flux quanta becomes a composite boson. Fermions, such as electrons and protons, follow the Pauli exclusion principle which excludes fermions of the same quantum-mechanical state from being in the same position. Bosons, such as photons or helium atoms, follow the Bose-Einstein statistics which allows bosons of the same quantum-mechanical state being in the same position. As a result, fermions are individualistic, while bosons are collectivistic. Composite fermions are individualistic, while composite bosons are collectivistic. In the first step, the attachment of an even number of flux quanta to each integral charge fermion provides these fermions individual integral charge composite fermions which follow the Pauli exclusion principle.

The second step involves the traditional composite bosons. The second step explains the origin of $1/(2n + 1)$ in Equation (16) in the second step of the composite fermion theory which does not explain the origin of $1/(2n + 1)$. The second step is the attachment of an odd number of flux quanta to individual integral charge composite fermions to form transitional collective integral charge composite bosons [28]. Individual integral charge composite fermions with an odd number $(2n + 1)$ of flux quanta provide collective integral charge composite bosons which allow bosons of the same quantum-mechanical state being in the same position. The collective integral charge composite bosons allow the connection of collective flux quanta from collective integral charge composite bosons. Each flux quantum represents an energy level. In individual integral charge composited fermions, the degenerate energy levels are separated. In collective integral charge composite bosons, the $2n + 1$ degenerate energy levels are connected into $2n + 1$ sites in the same energy level.

The third step is the conversion of collective flux quanta into the confinement force field to confine collective fractional charge composite fermions converted from the collective integral charge composite bosons. In collective fractional charge fermions, each site in the same energy level has $\pm 1/(2n + 1)$ fractional charge.

$$\text{fractional charge per site in the same energy level} = \frac{\pm 1}{2n+1} \tag{17}$$

Fractional charges are the integer multiples of $\pm 1/(2n + 1)$ fractional charge to explain the origin of $1/(2n + 1)$ in Equation (16) for the composite fermion theory. The products in the third step also include individual integral charge fermions to conserve electric charge. The sum of all collective fractional charges and individual integral charges is integer. The integer-fraction transformation from individual integral charge fermions to collective fractional charge fermions is as follows.

$$\begin{aligned} &\text{individual IC fermions} \xrightarrow{\text{even number of flux quanta}} \text{individual IC composite fermions} \\ &\xrightarrow{\text{odd number of flux quanta}} \text{tramsitional collective IC composite bosons} \\ &\xrightarrow{\text{confinement force field}} \text{collective FC composite fermions} + \text{individual IC fermions} \end{aligned} \tag{18}$$

where IC is integral charge and FC is fractional charge. From the integer-fraction transformation from integral charge electrons to fractional charge quarks, the calculated masses of pion, muon and constituent quarks are in excellent agreement with the observed values [5].

4. The Selective Retention Component

The selective retention component retains selectively events in a narrative. The retained events are unified by the common narrative. The narrative of physical reality is the four-stage evolution of our cyclic dual universe. The four force fields are unified by the four-stage evolution. For the narrative of our universe, our universe is in the reversible multiverse where all physical laws and phenomena are permanently reversible, and temporary irreversibility of entropy increase is allowed through reversibility breaking, symmetry violation, and low entropy beginning. The multiverse has been studied extensively. For example, Brian Greene [32] described the nine types of the multiverse which produce complicated collections of universes. The reversible multiverse model is a simple and neat version of the multiverse to exclude all permanently irreversible phenomena and physical laws. One irreversible phenomenon which is not allowed is the collision of expanding universes. The collision of expanding universes which have the inexhaustible resource of space-time to expand is permanently irreversible due to the impossibility to reverse the collision of expanding universes. To prevent the collision of expanding universes, every universe is surrounded by the interuniversal void that is functioned as the permanent gap among universes. The space in the interuniversal void is detachment space [6] which detaches matter and relates to kinetic energy. The interuniversal void has zero-energy, zero space-time, and zero vacuum energy, and detachment space only, while universe has nonzero-energy, the inexhaustible resource of space-time to expand, zero or/and non-zero vacuum energy, and attachment space with or without detachment space. Attachment space attaches matter and relates to rest mass. The detachment space of the interuniversal void has no space-time, so it cannot couple to particles with space-time in universes, but it prevents the advance of expanding universes to the interuniversal void to avoid the collision of expanding universes.

A zero-sum energy dual universe of positive-energy universe and negative-energy universe can be created in the zero-energy interuniversal void, and the new dual universe is again surrounded by the interuniversal void to avoid the collision of universes. Under symmetry, the new positive-energy universe and the new negative-energy universe undergo mutual annihilation to reverse to the interuniversal void immediately. Our universe is the dual asymmetrical positive-energy-negative-energy universe where the positive-energy universe on attachment space absorbed the interuniversal void on detachment space to result in the combination of attachment space and detachment space, and the negative-energy universe did not absorb the interuniversal void. Within the positive-energy universe, the absorbed detachment space with space-time can couple to particles in the positive-energy universe to result in massless particles with irreversible kinetic energy. The formation of our universe involves symmetry violation between the positive-energy universe and the negative energy universe. Irreversible kinetic energy from detachment space is the source of irreversible entropy increase, so the positive-energy universe is locally irreversible, while the negative-energy universe without irreversible kinetic energy from detachment space is locally reversible. The locally reversible negative-energy universe guides the reversible process of the dual universe. As a result, our whole dual universe is globally reversible. Our dual universe is the globally reversible cyclic dual universe as shown in **Figure 2** for the evolution of our universe as described previously [6]-[9].

The four reversible stages in the globally reversible cyclic dual universe are 1) the formation of the 11D membrane dual universe, 2) the formation of the 10D string dual universe, 3) the formation of the 10D particle dual universe, and 4) the formation of the asymmetrical dual universe.

1) The formation of the 11D membrane dual universe

As described previously [6]-[9], the reversible cyclic universe starts in the zero-energy interuniversal void, which produces the dual universe of the positive-energy 11D membrane universe and the negative-energy 11D membrane universe as in **Figure 2**. In some dual 11D membrane universes, the 11D positive-energy membrane universe and the negative-energy 11D membrane universe coalesce to undergo annihilation and to return to the interuniversal void as in **Figure 2**.

2) The formation of the 10D string dual universe

Under the reversible oscillation between 11D and 10D, the positive-energy11D membrane universe and the negative-energy 11D membrane universe are transformed into the positive-energy 10D string universe and the negative-energy 10D string universe, respectively, as in **Figure 2**. The positive-energy 11D membrane universe is transformed into the positive-energy 10D string universe as in Equations (19a) and (19b).

$$\begin{aligned}&\text{The RS1 Membrane Transformation}\\&\text{step}1: 2_{11} \xrightarrow{\text{from 11D membrane to 10D string}} 1_{10} \text{ in the 11D AdS space}\\&\text{step}2: 2(1_{10}) \xrightarrow{\text{the close string vibration}} 1_{10}\, 0_{10} = 1_{10}\ g_e \text{ in the 11D AdS space}\end{aligned} \tag{19a}$$

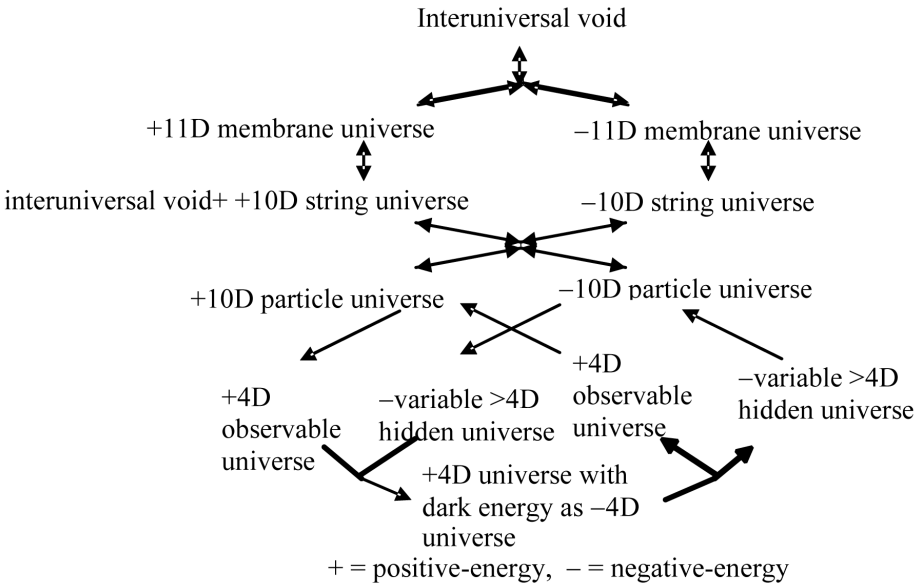

Figure 2. The globally reversible cyclic dual universe.

$$2\left(2_{11}\right) \xleftarrow{\text{the close string and the open string vibrations}} \left(s1_{10}\right) g_e \tag{19b}$$

where 2_{11} is membrane (denoted as 2) in 11D, s is the pre-strong force, 1_{10} is string (denoted as 1) in 10D, $0_{10}$is particle (denoted as 0) in 10D, AdS is anti-de Sitter, and g_e is the external graviton.

According Randall and Sundrum, the RS1 (Randall-Sundrum model 1) in an anti-de Sitter (AdS) space consists of one brane with extremely low graviton's probability function and another brane with extreme high graviton's probability function [33] [34]. The formation of the 10D string dual universe involves the RS1. As shown in Equation (19a), one of the possible membrane transformations from the 11D membrane to the 10D string is the RS1 membrane transformation which involves two steps. In the Step 1, the extra spatial dimension of the 11D membrane in the transformation from the 11D membrane to the 10D string becomes the spatial dimension transverse to the string brane in the bulk 11D anti-de Sitter space [33]. This transformation is derived from the transformation from membrane to string. In the transformation from the two-dimensional membrane to the one-dimensional string, the extra spatial dimension of the two-dimensional membrane on the x-y plane becomes the x-axis transverse to the one-dimensional string on the y-axis in the two-dimensional x-y space. In the Step 2, for the RS1 membrane transformation, two string branes are combined into the combined string brane. The external 10D particles generated by the close string vibration of the combined string brane are the 10D external gravitons which form the external graviton brane as the Gravitybrane (Planck Plane) in the RS1 of the Randall-Sundrum model [33] [34]. As in the RS1 of the Randall-Sundrum model, the two branes with equal mass- energy in the 11D anti-de Sitter space are the string brane with weak gravity and the external graviton brane with strong gravity. The weak gravity in the string brane is the predecessor of the observed weak gravity generated during the Big Bang [6] [17]. The external graviton in the external graviton brane is the predecessor of a part of the observed dark energy [3] [4]. The 10D string brane and the 10D external graviton brane correspond to the predecessors of the observed universe (without dark energy) and a part of observed dark energy, respectively [6] [17]. The reverse transformation from 10D to 11D is the RS1 string transformation.

In Equation (19b), the particles generated from the 10D open string vibration are the 10D particles for the pre-strong force (denoted as *s*) in addition to the external graviton from the close string vibration in the 11D AdS. According to Maldacena, the AdS/CFT correspondence is a correspondence between quantum gravity in AdS space and quantum field theory of conformal field theory (CFT) in one dimension lower [35]. The AdS/CFT correspondence describes Equation (19b) as the correspondence between the external graviton in the 11D AdS and the pre-strong force of 10D CFT in one dimension lower. The pre-strong force is the same for all strings without positive or negative sign. This pre-strong force is the prototype of the observed strong force generated during the Big Bang [6] [17]. Kinetic energy emerged in the universe after the emergence of the pre-strong force,

so the strong force becomes the confinement force for fractionally charge quarks which do not allow irreversible kinetic energy [5].

In the negative universe through symmetry, the 11D anti-membrane (2_{-11}) is transformed into 10D antistring (1_{-10}) with external anti-graviton $\overline{g_e}$ and the pre-strong force s as follows.

$$2\left(2_{-11}\right)\longleftrightarrow\left(s1_{-10}\right)\overline{g_e} \tag{20}$$

The dual universe of the positive-energy 10D string universe with n units of $(1_{10})_n$ and the negative-energy 10D string universe with n units of $(1_{-10})_n$ is as follows.

$$\left(\left(s1_{10}\right)g_e\right)_n\left(\overline{g_e}\left(s1_{-10}\right)\right)_n \tag{21}$$

There are four equal regions: the positive-energy 10D string universe, the external graviton, the external anti-graviton, and the negative-energy 10D string universe.

Some dual 10D string universes return to the dual 11D membrane universes under the reversible oscillation between 11D and 10D. Alternatively, under symmetry violation as in the case of our universe, the positive-energy 10D string universe absorbs the interuniversal void, while the negative-energy 10D string universe does not absorb the interuniversal void. The interuniversal void has zero vacuum energy. In our universe, the absorption of the interuniversal void by the positive-energy 10D string universe forced the positive-energy 10D universe with high vacuum energy to be transformed into the universe with zero vacuum energy that was the vacuum energy of the 4D universe. However, the transformation from 10D to 4D was not immediate, because the strings had to be 10D, and it could not be transformed into 4D, therefore, strings had to be transformed into particles that allowed the change of its dimension number freely to accommodate the transformation from the 10D universe to the 4D universe driven by the absorption of the interuniversal void.

3) The formation of the 10D particle dual universe

As described previously [9] [17], the transformation of strings into particles came from the emergence of positive charge and negative charge that allowed the mutual annihilation of positively charged 10D strings and negatively charged 10D antistrings in the 10D string universes to produce positively charged 10D particles and negatively pre-charged 10D antiparticles in the 10D particle universes as follows.

$$\left(\left(s0_{10}e^+e^-0_{-10}s\right)g_e\right)_n\left(\overline{g_e}\left(s0_{10}e^+e^-0_{-10}s\right)\right)_n, \tag{22}$$

where s and e are the pre-strong force and the pre-charged force in the flat space, g_e is the external graviton, $\overline{g_e}$ is the external graviton, and $0_{10}0_{-10}$ is the particle-antiparticle. There are four equal regions: the 10D positive-energy particle universe, the external graviton, the 10D negative-energy particle universe, and the external anti-graviton. The emergence of positive charge and negative charge provides the prototype of the observed electromagnetic force with charge generated during the Big Bang [6] [17].

4) The formation of the asymmetrical dual universe

The formation of our current universe follows immediately after the formation of the 10D particle dual universe through the asymmetrical dimensional oscillations, leading to the asymmetrical dual universe. The 10D positive-energy universe was transformed immediately into the 4D positive-energy particle universe with zero vacuum energy. The 10D negative-energy particle universe undergoes the stepwise dimension number oscillation between 10D and 4D. Without absorbing the interuniversal void, the external graviton and the anti-graviton also undergo the stepwise dimension number oscillation between 10D and 4D. The result is the asymmetrical dual universe consisting of the four equal regions of the 4D positive-energy particle universe, the variable D external graviton, the variable D negative-energy particle universe, and the variable D external anti-graviton. The asymmetrical dual universe is manifested as the asymmetry in the weak interaction in our observable universe as follows.

$$\begin{gathered}\text{the 4D positive-energy particle universe and the external graviton}\\ \left(\left(s0_4e^+w^+e^-w^-0_{-4}s\right)g_e\right)_n\\ \text{the variable D negative-energy particle universe and the external anti-graviton}\\ \left(\overline{g_e}\left(s0_{4\text{ to }10}e^+w^+e^-w^-0_{-4\text{ to }-10}s\right)\right)_n\end{gathered} \tag{23}$$

where s, g_e, $\overline{g_e}$ e, and w are the strong force, external graviton, external anti-graviton, electromagnetism, and weak interaction, respectively for the observable universe, and where $0_4 0_{-4}$ and $0_{4\text{ to }10}\,0_{-4\text{ to }-10}$ are 4D particle-antiparticle for the 4D positive-energy particle universe and variable D particle-antiparticle for the variable D negative-energy particle universe, respectively. For our asymmetrical dual universe, the stage 3 for the transformation of 10D string into 10D particle had to be followed by the stage 4, so the electromagnetic interaction from the stage 3 was unified with the weak interaction from the stage 4 to become the electroweak interaction, which was generated during the Big Bang [6] [17].

4a) the formation of the 4D positive-energy particle universe

The formation of 4D positive-energy particle universe involved the two-step transformation: 1) the inflation and 2) the Big Bang. In the first step, the inflation is the transformation from 10D4d to 4D10d immediately. Calculated from Equation (1e), the rest mass of 4D10d is $M_{0,10} = M_{0,4} \big/ \alpha^{2(10-4)} \approx 137^{12}$ times of the rest mass of 10D4d, resulting in the first step of the inflation as the rapid expansion of space from the high vacuum energy 10D4d to the zero vacuum energy 4D10d as follows [8].

$$\begin{aligned} &1.\ \underline{\text{the inflation}} \\ &10\text{D4d} \xrightarrow{\text{quick QVSL transformation}} 4\text{D10d} \end{aligned} \tag{24}$$

In the second step of the transformation, the Big Bang is a two-step process. The first step is the coupling of detachment space and the the massive particles on attachment space in the positive-energy universe that absorbed the interuniversal void on detachment space. The result is the total conversion to generate massless particles on detachment space in the positive-energy universe and the external attachment space surrounded the positive-energy universe as described in Equation (4). In the second step, the coupling of attachment space and the massless particles in the positive-energy universe that absorbed the external attachment space surrounded the positive-energy universe. The partial conversion resulted in massive particles such as weak bosons, leptons, the Higgs boson, and massless particles such as photon. The second step is described in Equation (5) through the Higgs mechanism. The irreversible kinetic energy resulted from detachment space started the positive-energy universal expansion. The positive-energy universe has the combination of attachment space and detachment as follows.

$$\begin{aligned} &2.\ \underline{\text{The Big Bang}} \\ &1.\ \text{massive particles on attachment space} + \text{detachment space} \xrightarrow{\text{total conversion}} \\ &\quad \text{massless particles on detachment space} + \text{the external attachment space} \\ &2.\ \text{massless particles on detachment space} + \text{the external attachment space} \\ &\quad \xrightarrow{\text{partial conversion}} \text{massless particles} + \text{massive particles} \\ &\quad + \text{detachment space} + \text{attachment space} + \text{the Higgs boson} \end{aligned} \tag{25}$$

In the second law of thermodynamics, the entropy (a measure of the disorder of a system) of an isolated system can increase, but not decrease. In other words, the entropy of a closed system will never decrease into the future. There are two mysteries about this irreversible entropy increase as described in "From Eternity to Here: The Quest for the Ultimate Theory of Time" by Sean Carroll [36]. Firstly, this irreversible entropy increase of a macroscopic collection of particles is different from all microscopic reversible processes where for every allowed process there exists a time-reversed process that is also allowed. Secondly, the universe started with the very low entropy state as the inflation-Big Bang in a very small space, not with the high entropy state near equilibrium state in a large space. Such low entropy beginning is a mystery. In this paper, the mysteries of the irreversible entropy increase are explained by the presence of irreversible kinetic energy which induces irreversible entropy increase. In the Boltzmann formula of thermodynamic, the absolute entropy S of an ideal gas to the quantity W, which is the number of the arrangements of particles corresponding to a given macroscopic collection of particles:

$$S = k_B \ln W \tag{26}$$

where k_B is the Boltzmann's constant. The Boltzmann formula shows the relationship between entropy and the number of ways the atoms or molecules of a thermodynamic system can be arranged. The various atoms or molecules have different positions and momenta for irreversible entropy increase, because the increase in the num-

ber of different arrangements of particles in a macroscopic collection of particles requires the movements of individual particles in a macroscopic collection of particles. (There is no entropy increase in a single microscopic particle.) Individual momenta from kinetic energy are required for irreversible entropy increase in a macroscopic collection of particles. In other words, kinetic energy transforms a macroscopic collection of particles from one way of the arrangement of particles (order) into many ways of the arrangements of particles (disorder), and the process from order to disorder is irreversible in an isolated macroscopic collection of moving particles.

In our universe, the interuniversal void on detachment space was by the 10D positive-energy string universe which was very small. (The rest mass of 4D10d is $1/\alpha^{12} \approx 137^{12}$ times of the mass of 10D4d.) To have exactly reversible absorption-desorption of the interuniversal void for the reversible dual universe, the absorption and desorption have to be uniform. The space of the universe where the absorption-desorption occurs has to be small enough for the uniform absorption-desorption. The 10D string was small mass to allow the uniform absorption-desorption for reversible absorption-desorption of the interuniversal void, resulting in low entropy beginning. (The subsequent irreversible absorption of the interuniversal void is forbidden.) In the reversible multiverse postulate, all physical laws and phenomena are permanently reversible, and temporary irreversibility of entropy increase is allowed through reversibility breaking, symmetry violation, and low entropy beginning. Our 4D positive-energy particle universe is an example of irreversibility of entropy increase through reversibility breaking, symmetry violation, and low entropy beginning.

4b) the formation of the variable D negative-energy particle universe

The the formation of the variable D negative-energy particle universe involves the stepwise two-step transformation: the QVSL transformation and the varying supersymmetry transformation from 10D4d to 4D4d. (The particles in the 10D dual particle universe are 10D4d.) The QVSL transformation involves the transformation of space-time dimension, D. The repetitive stepwise two-step transformation from 10D4d to 4D10d as follows.

$$\begin{aligned} &10\text{D4d} \to 9\text{D5d} \to 9\text{D4d} \to 8\text{D5d} \to \cdots \to 4\text{D5d} \to 4\text{D4d} \\ &\mapsto \text{hidden} \quad \text{dark} \qquad \text{universe} \quad \leftarrow\mapsto \text{dark} \quad \text{energy} \quad \leftarrow \end{aligned} \tag{27}$$

The variable D negative-energy particle universe consists of two periods: the hidden variable D negative-energy particle universe and the dark energy universe. The hidden variable D negative-energy particle universe composes of the > 4D particles. As mentioned before, particles with different space-time dimensions are transparent and oblivious to one another, and separate from one another if possible. Thus, > 4D particles are hidden and separated particles with respect to 4D particles in the 4D positive-energy particle universe (our observable universe). The hidden variable D negative-energy particle universe with D > 4 and the observable universe with D = 4 are the "parallel universes". The 4D particles transformed from hidden > 4D particles in the variable D negative-energy particle universe are observable dark energy for the 4D positive-energy particle universe, resulting in the accelerated expanding universe. Since the variable D negative-energy particle universe does not have detachment space, the presence of dark energy is not different from the presence of the cosmological constant. According to the theoretical calculation based on the asymmetrical dual universe, dark energy started in 4.47 billion years ago in agreement with the observed 4.71 ± 0.98 billion years ago [9]. Our asymmetrical dual universe consists of the four equal regions of the 4D positive-energy particle universe, the variable D external graviton, the variable D negative-energy particle universe, and the variable D external anti-graviton, so the percentage the variable D area is 75%, three out of four regions, as the maximum percentage of dark energy. In terms of quintessence, such dark energy can be considered the tracking quintessence [37] from the variable D area with the space-time dimension number as the tracker.

After the maximally connected universe, 4D dark energy transforms back to > 4D particles that are not observable. The removal of dark energy in the observable universe results in the stop of accelerated expansion and the start of contraction of the observable universe. The end of dark energy starts another "parallel universe period". Both hidden universe and observable universe contract synchronically and equally. Eventually, the Big Crush and the two-step deflation occur in the 4D positive-energy particle universe. In the first step of the deflation, the 4D positive-energy particle universe loses all detachment space, kinetic energy, light, cosmic radiation, and force fields as dimensional orbitals, resulting in returning to 4D10d. In the second step of the deflation, without irreversible kinetic energy, the reversible direct dimension number oscillation resumes to transform the low vacuum energy 4D10d into the high vacuum energy 10D4d for the rapid contraction of space. Meanwhile, hidden > 4D particles-antiparticles in the hidden universe transform into 10D4d particles-antiparticles. The dual universe can undergo another cycle of the cyclic dual universe. On the other hand, both universes can undergo the reverse

Table 1. The computer simulation process of physical reality.

Components	Parts	Descriptions	Account for
Digital representation	Digital space structure	The digital representations of rest mass and kinetic energy are 1 as attachment space for the space of matter and 0 as detachment space for the zero-space of matter, respectively	Higgs field, reverse Higgs field, quantum mechanics, special relativity, force fields, dark matter, baryonic matter
	Digital spin	The digital representations of the exclusive and the inclusive occupations of positions are 1/2 spin fermion and integer spin boson, respectively	The expanding universe by spatial translation from supersymmetry transformation, dark energy
	Digital electric charge	The digital representations of the allowance and the disallowance of irreversible kinetic energy are integral electric charges and fractional electric charges, respectively	The confinements of fractional charge quarks and quasiparticles
Mathematical computation	Oscillating M-theory	Oscillations between 11D and 10D and between 10D and 4D	Cosmology
	Reversible multiverse	All physical laws and phenomena are permanently reversible, and temporary irreversibility of entropy increase is allowed	Cosmology
Selective retention	Selective retention of events	Selective retention of events in the narrative of the reversible four-stage evolution	Gravity, the strong force, electromagnetism, and the weak force as the retained events in the common narrative

charge transformation to become the 10D dual string universe, which in turn can return to the 11D dual membrane universe that in turn can return to the zero-energy universe as **Figure 2**.

5. Summary

This paper posits that we are living in a computer simulation to simulate physical reality which has the same computer simulation process as virtual reality (computer-simulated reality). Both computer simulation processes for physical reality and virtual reality involve the digital representation of data, the mathematical computation of the digitized data in geometric formation and transformation in space-time, and the selective retention of events in a narrative. We are living in a computer simulation consisting of the digital representation component, the mathematical computation component, and the selective retention component.

For the digital representation component of physical reality, the three intrinsic data (properties) are rest mass-kinetic energy, electric charge, and spin which are represented by the digital space structure, the digital electric charge, and the digital spin, respectively. For the digital space structure, the digital representations of rest mass and kinetic energy are 1 as attachment space for the space of matter and 0 as detachment space for the zero-space of matter, respectively. Attachment space and detachment space are the origins of the Higgs field and the reverse Higgs field, respectively. The combination of n units of attachment space as 1 and n units of detachment space as 0 brings about the three digital structures: binary partition space $(1)_n(0)_n$, miscible space $(1+0)_n$, and binary lattice space $(1\ 0)_n$ to account for quantum mechanics, special relativity, and the force fields, respectively.

For the digital spin, the digital representations of the exclusive and the inclusive occupations of positions are 1/2 spin fermion and integer spin boson, respectively. The exclusion-inclusion brings about spatial translation by the supersymmetry transformations between fermion and boson. For the digital electric charge, the digital representations of the allowance and the disallowance of irreversible kinetic energy are integral electric charges and fractional electric charges, respectively. The disallowance of irreversible kinetic energy of fractional electric charges brings about the confinement of fractional electric charges for quarks and quasiparticles in hadrons and two dimensional systems, respectively.

Without the digital space structure, physical reality would have been like classical (Newtonian) mechanics without the Higgs field, quantum mechanics, special relativity, force fields, and dark matter. Without the digital spin, dark energy would have not existed through the expansion of the negative-energy universe by supersym-

metry transformation. Without the digital electric charge, fractional charge quarks would have not existed to constitute nucleus in atom.

The mathematical computation involves the reversible multiverse and oscillating M-theory as oscillating membrane-string-particle whose space-time dimension (D) number oscillates between 11D and 10D and between 10D and 4D. Space-time dimension number between 10 and 4 decreases with decreasing speed of light, decreasing vacuum energy, and increasing rest mass. The mathematical computation component explains cosmology. Gravity, the strong force, electromagnetism, and the weak force in our universe are the retained events during the four-stage evolution of our universe, and are unified by the common narrative of the evolution in the selective retention component.

Conventional physics cannot explain the reality of quantum mechanics easily. Conventional physics cannot explain the origins of the confinement of quarks and the fractional charges of quasiparticles. The geometry in conventional physics is fixed M-theory which has no experimental proof. Conventional physics cannot unify the four force fields. Conventional physics cannot explain physical reality clearly, while computer-simulated physics can explain physical reality clearly by using the computer simulation process consisting of the digital representation component, the mathematical computation component, and the selective retention component. We are living in a computer simulation. **Table 1** is the summary of the computer simulation process of physical reality

References

[1] Bostrom, N. (2003) *Philosophical Quarterly*, **53**, 243-255. http://dx.doi.org/10.1111/1467-9213.00309

[2] Chung, D. and Krasnoholovets, V. (2013) *Journal of Modern Physics*, **4**, 27-31. http://dx.doi.org/10.4236/jmp.2013.44A005

[3] Chung, D. (2015) *Journal of Modern Physics*, **6**, 1820-1832. http://dx.doi.org/10.4236/jmp.2015.613186

[4] Chung, D. (2016) *Journal of Modern Physics*, **7**, 642-655. http://dx.doi.org/10.4236/jmp.2016.77064

[5] Chung, D. (2016) *Journal of Modern Physics*, **7**, 1150-1159.

[6] Chung, D. (2015) *Journal of Modern Physics*, **6**, 1249-1260. http://dx.doi.org/10.4236/jmp.2015.69130

[7] Chung, D. and Krasnoholovets, V. (2007) *Scientific Inquiry*, **8**, 165-182.

[8] Chung, D. (2015) *Journal of Modern Physics*, **6**, 1189-1194. http://dx.doi.org/10.4236/jmp.2015.69123

[9] Chung, D. and Krasnoholovets, V. (2013) *Journal of Modern Physics*, **4**, 77-84. http://dx.doi.org/10.4236/jmp.2013.47A1009

[10] Woit, P. (2006) Not Even Wrong: The Failure of String Theory and the Search for Unity in Physical Law. Basic Books, New York.

[11] Weinberg, S. (1989) *Review Modern Physics*, **61**, 1-23. http://dx.doi.org/10.1103/RevModPhys.61.1

[12] Chung, D. and Hefferlinm, R. (2013) *Journal of Modern Physics*, **4**, 21-26. http://dx.doi.org/10.4236/jmp.2013.44A004

[13] Diaz, B. and Rowlands, P. (2003) *American Institute of Physics Proceedings of the International Conference of Computing Anticipatory Systems*, Liege, 11-16 August 2003, 203-218.

[14] Bell, J. (1964) *Physics*, **1**, 195-199.

[15] Mahler, D., *et al*. (2016) *Science Advances*, **2**, e1501466.

[16] Penrose, R. (2000) Wavefunction Collapse as a Real Gravitational Effect. In: Fokas, A., Grigoryan, A., Kibble, T. and Zegarlinski, B., Eds., *Mathematical Physics* 2000, Imperial College, London, 266-282. http://dx.doi.org/10.1142/9781848160224_0013

[17] Bounias, M. and Krasnoholovets, V. (2003) *The International Journal of Systems and Cybernetics*, **32**, 1005-1020.

[18] Chung, D. (2014) *Journal of Modern Physics*, **5**, 1234-1243. http://dx.doi.org/10.4236/jmp.2014.514123

[19] Chung, D. (2014) *Journal of Modern Physics*, **5**, 464-472. http://dx.doi.org/10.4236/jmp.2014.56056

[20] Jarosik, N., Bennett, C.L., Dunkley, J., Gold, B., Greason, M.R., Halpern, M., *et al*. (2011) *The Astrophysical Journal Supplement Series*, **192**, 14. http://dx.doi.org/10.1088/0067-0049/192/2/14

[21] Chung, D. (2014) *Journal of Modern Physics*, **5**, 1467-1472. http://dx.doi.org/10.4236/jmp.2014.515148

[22] Chung, D. (2014) *International Journal of Astronomy and Astrophysics*, **4**, 374-383. http://dx.doi.org/10.4236/ijaa.2014.42032

[23] Chung, D. (2015) *Global Journal of Science Frontier Research A*, **15**, 119-125.

[24] Chung, D. (2015) *Journal of Modern Physics*, **6**, 26-36. http://dx.doi.org/10.4236/jmp.2015.61005

[25] Chung, D. and Krasnoholovets, V. (2013) *Journal of Modern Physics*, **4**, 1-6. http://dx.doi.org/10.4236/jmp.2013.47A1001

[26] Chung, D. (2014) *Global Journal of Science Frontier Research A*, **14**, 1-8.

[27] Tsui, D., Stormer, H. and Gossard, A. (1982) *Physical Review Letters*, **48**, 1559-1562. http://dx.doi.org/10.1103/PhysRevLett.48.1559

[28] Stormer, H. (1999) *Reviews of Modern Physics*, **71**, 875-889. http://dx.doi.org/10.1103/RevModPhys.71.875

[29] Laughlin, R. (1983) *Physical Review Letters*, **50**, 1395-1398. http://dx.doi.org/10.1103/PhysRevLett.50.1395

[30] Kamilla, R., Wu, X. and Jain, J. (1996) *Physics Review Letters*, **76**, 1332-1335. http://dx.doi.org/10.1103/physrevlett.76.1332

[31] Jain, J. (2007) Composite Fermions. Cambridge University Press, New York. http://dx.doi.org/10.1017/CBO9780511607561

[32] Greene, B. (2011) The Hidden Reality: Parallel Universes and the Deep Laws of the Cosmos. Alfred A. Knopf, New York.

[33] Randall, L. (2005) Warped Passages: Unraveling the Mysteries of the Universe's Hidden Dimensions. Harper Collins, New York.

[34] Randall, L. and Sundrum, R. (1999) *Physics Review Letter*, **83**, 3370-3373. http://dx.doi.org/10.1103/PhysRevLett.83.3370

[35] Maldacena, J. (1998) *Advances in Theoretical and Mathematical Physics*, **2**, 231-252. http://dx.doi.org/10.4310/ATMP.1998.v2.n2.a1

[36] Carroll, S. (2010) From Eternity to Here: The Quest for the Ultimate Theory of Time. Dutton, New York.

[37] Padmanabhan, T. (2003) *Physics Reports*, **380**, 235-320. http://dx.doi.org/10.1016/S0370-1573(03)00120-0

Journal of Modern Physics, 2016, 7, 1228-1246
Published Online June 2016 in SciRes. http://www.scirp.org/journal/jmp
http://dx.doi.org/10.4236/jmp.2016.710111

Hypothesis of the Hidden Multiverse Explains Dark Matter and Dark Energy

Alexander Alexandrovich Antonov

Research Center of Information Technologies "TELAN Electronics", Kiev, Ukraine
Email: telan@bk.ru

Received 12 May 2016; accepted 24 June 2016; published 28 June 2016

Abstract

Analysis of WMAP and Planck spacecraft data has proved that we live in an invisible Multiverse, referred to as hidden, that has a quaternion structure. It explains the reason for the mutual invisibility of parallel universes contained in the hidden Multiverse. It is shown that the hidden Multiverse includes most likely twenty parallel universes from different dimensions, six of which are adjacent to our universe. Besides, edges of the hidden Multiverse are connected to other (from one to four) Multiverses, which are observable neither by electromagnetic nor by gravitational manifestations. The Multiverse described contains four matter-antimatter pairs, annihilation of which is prevented by relative spatial position of the universes. The experimental proof of existence of the hidden Multiverse is explained to be the phenomenon of dark matter and dark energy that correspond to other invisible parallel universes, except ours, included in the hidden Multiverse. General scientific principle of physical reality of imaginary numbers, refuting some of the statements of the existing version of the special theory of relativity, is a physical and mathematical foundation of the outlined conception of the hidden Multiverse. The article presents relativistic formulas of the theory of special relativity adjusted in accordance with the principle. It also offers appropriate interpretation of multidimensional space of the hidden Multiverse.

Keywords

Multiverse, Imaginary Numbers, Dark Matter, Dark Energy, Special Theory of Relativity

1. Introduction

In what kind of world do we live in: In Monoverse or Multiverse? And what are dark matter and dark energy like in this world? These are main questions of astrophysics, which are attempted to be answered in this article.

In modern physics there are two main theories: the theory of relativity and the quantum mechanics, which are

How to cite this paper: Antonov, A.A. (2016) Hypothesis of the Hidden Multiverse Explains Dark Matter and Dark Energy. *Journal of Modern Physics*, **7**, 1228-1246. http://dx.doi.org/10.4236/jmp.2016.710111

absolutely contradictive, since they use different mathematics, different axioms and different physical pictures of the world. There is also a string theory, which attempts to unite quantum mechanics and theory of relativity, but so far without success.

To date, numerous hypotheses of Multiverse [1]-[11] have been proposed according to these theories. However, according to many scientists, they are not scientific [12] [13], because they do not comply[1] with the falsification criterion proposed by Popper [14]. In other words, these hypotheses are such that they can neither be confirmed nor denied. Given this circumstance, the majority of scientists believe that we live in a single universe, *i.e.*, in a Monoverse.

But still there is no answer[2] for the second question. Therefore, the phenomenon of dark matter and dark energy [15] [16] remains unexplained.

These theories either give no answers for many other fundamental questions of astrophysics:

- Why is there no antimatter in our universe [17]?
- Where do tachyons locate [18] [19]?
- Are imaginary numbers physically real [20] [21]?, etc.

So, starting with answering the latter question (whether imaginary numbers[3] are physically real), which seems to have nothing to do with direct content of the article, we proceed to description of a new proposed conception of the Multiverse, which gives answers to the remaining questions mentioned above.

2. Physical Reality of Imaginary Numbers

Imaginary numbers in mathematics were discovered about five hundred years ago by Scipionedel Ferro, Niccolò Fontana Tartaglia, Gerolamo Cardano, Lodovico Ferrari and Rafael Bombelli [22]. However, unlike other numbers, such as integer, fractional, positive and negative, etc., the meaning of which becomes immediately clear as they are appearing, physical sense of imaginary numbers has remained unclear following their discovery. And it is still unclear, despite the fact that:

- To date, the theory of functions of complex variables [22] was developed by Abraham de Moivre, Leonhard Euler, Jean Le Rond D'Alembert, Caspar Wessel, Pierre-Simon de Laplace, Jean-Robert Argand, Johann Carl Friedrich Gauss, Augustin Louis Cauchy, Karl Theodor Wilhelm Weierstrass, William Rowan Hamilton, Pierre Alphonse Laurent, Georg Friedrich Bernhard Riemann, Oliver Heaviside, Jan Mikusiński and many others;
- Currently, complex numbers are widely used in all the exact sciences.

It is still unclear also despite the fact that at the beginning of the 20th century Joseph Larmor, Nobel Prize winner Hendrik Antoon Lorentz, Jules Henri Poincaré, Nobel Prize winner Albert Einstein and others developed the special theory of relativity (STR) [23] [24], which actually postulated the absence of any physical sense in imaginary numbers.

However, this STR statement seems unconvincing [25], as, firstly, it was proposed on the basis of the obvious fact that imaginary mass, imaginary time and other imaginary physical quantities, which were beyond explanation, appeared in relativistic formulas at superluminal speeds. Without explanation of their physical sense, STR turned out to be incomplete. Therefore, in order to avoid the necessity to explain them, the original formulation of the second postulate proposed by Albert Einstein [26], which is now referred to as the principle of light speed constancy, has been, de facto, extended[4] by two more formulations which are actually non-identical to the original one:

- The principle of light speed non-exceedance;
- The statement on lack of physical sense in imaginary numbers.

And secondly, explanation of inability to overcome the light speed barrier was so unconvincing that it could be refuted even at the mundane level. For example, inability to get from one into another room of an apartment through a wall separating them does not mean the inability:

- to get into adjacent room through a door;
- absence of the adjacent room.

[1]Unlike the conception of the hidden Multiverse considered in the article (see below).
[2]Except that proposed in the article (see below)
[3]We'll actually hereinafter discuss concrete numbers, *i.e.* numbers provided with references to corresponding physical units.
[4]However, it is not customary in science to provide several different formulations for axioms, postulates, theorems and laws, especially if they are non-identical

Therefore, extended interpretation of the second STR postulate did not seem convincing to all physicists. And in the 21st century MINOS [27] and OPERA [28] experiments were conducted at the American Tevatron Collider and the European Large Hadron Collider, respectively. They aimed to refute extended interpretation of the second postulate in the current version of the STR by detecting superluminal neutrinos and thus prove physical reality of imaginary numbers. However, physical community considered the experiments to be not enough reliable and refuted them by ICARUS [29] experiment.

Results of other experiments, which did prove physical reality of imaginary numbers, were published [20] [21] [30] [31] almost at the same time. And since these experiments were conducted using oscillation processes in the linear electric circuits, they could be verified in any electronic laboratory, and therefore be considered as absolutely reliable. These alternative experiments cannot be ever refuted. And they actually have not been refuted by physical community.

We give a brief description of theoretical and experimental studies. They are very important, because they allow using experimentally based approach to invention of theories, which is more consistent with the subject of the study, instead of the axiomatic approach[5] so popular in modern physics. Therefore, the principle of physical reality of imaginary numbers, which is basic due to the conception of the Multiverse described below, has been rather experimentally proved, than postulated. Moreover, it has been proved many times in different ways, so as not to leave the slightest doubt about its reality.

2.1. The First Proof of the Principle of Physical Reality of Imaginary Numbers

The first proof [30] [31] uses Ohm's law[6] [32] known to all educated people in the interpretation proposed by Charles Proteus Steinmetz [33] for electric AC circuits. According to this interpretation, electrical reactance of capacitors and inductors are measured by heteropolar imaginary numbers, unlike the electric resistance of resistors measured by real numbers. Therefore, total reactance of any electric LCR-circuit is measured by complex numbers. In accordance with this interpretation of Ohm's law, when electric LCR-circuit is affected by sinusoidal voltage, sinusoidal electric current with amplitude equal to the ratio of applied voltage amplitude and complex impedance modulus flows through it.

This is open information contained in any textbook on the theory of electric circuits. However, none of textbooks admits that this information is the evidence of physical reality of imaginary numbers, as well as there is no any reference that the principle of physical reality of imaginary numbers is a scientific discovery.

Instead, the authors of textbooks, when wondering how they could answer these inevitable questions asked by students, chose not to develop this topic. Especially, they could refer to the STR, which asserts that there is no physical sense in imaginary numbers. Therefore, students are still told that capacitive and inductive imaginary resistances measured by imaginary numbers are imaginary, *i.e.*, nonexistent.

Nevertheless, this is a misconception. Should capacitive and inductive imaginary resistances be physically nonexistent, amplitude of current flowing through LCR-circuits should not have been changed at change in applied voltage frequency. However, electrical and radio frequency engineers have long known that it does change. Therefore, despite its name "imaginary", capacitive and inductive imaginary resistances are quite real. They are just as real as the resistance of resistors.

Moreover, should inductive and capacitive imaginary resistances be physically nonexistent, there would be no resonance in electric LCR-circuits discovered by Galileo di Vincento Bonaiutide' Galilei in 1602 [34]. And even such science as radiotechnics also wouldn't have existed.

However, they do exist. Their existence proves physical reality of complex (including imaginary) numbers, and thus refutes extended interpretation of the second STR postulate [25].

2.2. The Second Proof of the Principle of Physical Reality of Imaginary Numbers

For decades students have been explained that imaginary resistances of capacitors and inductors are imaginary and, therefore, physically nonexistent, readers have some doubts about correctness of the given evidence.

Therefore, we provide the second proof [20], which is also very simple. It is so simple, that it should eliminate any suspicion of errors in it.

[5]Still being more appropriate in mathematics. However, due to Oliver Heaviside even mathematics is an experimental science.
[6]Discovered by Ohm in 1826 for electric DC-circuits.

This proof is based on the undeniable fact of existence of shock oscillations in nature, including tsunami, sound of church bells and even a kid's swing being pushed by parents to get a swinging motion. Existence of shock oscillations turns out to be possible only if imaginary numbers are physically real[7]. Let us prove this.

Any processes in linear electric circuits, including shock oscillations, are described by differential equation (usually second-order)

$$a_n \frac{\mathrm{d}^n y}{\mathrm{d}t^n} + a_{n-1} \frac{\mathrm{d}^{n-1} y}{\mathrm{d}t^{n-1}} + \cdots + a_o y = b_m \frac{\mathrm{d}^m x}{\mathrm{d}t^m} + b_{m-1} \frac{\mathrm{d}^{m-1} x}{\mathrm{d}t^{m-1}} + \cdots + b_0 x \tag{1}$$

where $x(t)$ is the input action (or the input signal);

$y(t)$ is the response to the action (or the output signal);

$a_n, a_{n-1}, \cdots, a_0, b_m, b_{m-1}, \cdots, b_0$ are constant coefficients;

$n, n-1, \cdots, 0, m, m-1, \cdots, 0$ are the order of derivatives;

Solution of the differential Equation (1) contains two terms

$$y(t) = y_{free}(t) + y_{forc}(t) \tag{2}$$

where $y_{free}(t)$ is the free (or transient) component of response;

$y_{forc}(t)$ is the forced component of response.

Moreover, relative duration of these processes is different in different cases. In case of shock oscillations[8] duration of the component $y_{forc}(t)$ is always much less than duration of the component $y_{free}(t)$. Therefore, it does not prevent observation of transients in experiments. The particular type of the transient $y_{free}(t)$ in the form of a certain function of time is found in the result of solving the so-called algebraic characteristic equation (usually second-order) correspondent to the original differential Equation (1)

$$a_n p^n + a_{n-1} p^{n-1} + \cdots + a_0 = 0 \tag{3}$$

where $a_n, a_{n-1}, \cdots, a_o$ are the same constant coefficients as in Equation (1);

$n, n-1, \cdots, 0$ are exponents with value equal to the order of the corresponding derivatives in the differential Equation (1);

p is the variable that, in case it takes on values in the form of complex numbers $-\sigma \pm i\omega$ is often referred to as complex frequency;

Certain type of transient processes that always exists (aperiodic, critical or oscillatory) is determined on the basis of the result of Equation (3). And for oscillatory transient solution of the algebraic Equation (3) is a pair of complex conjugate numbers. Besides, the solution of algebraic Equation (3) for oscillatory transient process would be a pair of complex conjugate numbers. Therefore, in the case of solution of the characteristic Equation (3) on the set of real numbers, the result $-\sigma \pm i\omega$ could not be obtained. In this case it would have to be concluded that shock oscillations should be nonexistent[9].

However, they do exist. Their existence proves physical reality of complex (including imaginary) numbers, and thus refutes extended interpretation of the second STR postulate [25].

2.3. The Third Proof of the Principle of Physical Reality of Imaginary Numbers

Finally, to definitively dispel any doubts as to the validity of the principle of physical reality of imaginary numbers, which is the base for the new conception of the Multiverse, we provide another proof [21]. This time, we analyze resonance process which (in contrast to the shock oscillations) is characterized by the fact that a forced component $y_{forc}(t)$ of the oscillation process far exceeds the transient process $y_{free}(t)$ in duration. Therefore, the component $y_{free}(t)$ does not interfere with the observations of the forced component $y_{forc}(t)$ in the relevant experiments.

Textbooks on the theory of linear electric circuits state that resonance is characterized by the following features:

- at resonant frequency the forced component of response $y_{forc}(t)$ takes on extreme absolute value;
- at resonant frequency phase shift between force and forced component of response $y_{forc}(t)$ becomes zero;

[7]Consequently, if the current version of STR was true, there would be no tsunami and kid's swing would not be swinging after been pushed by parents.

[8]Occurring under impulse action.

[9]Therefore, characteristic algebraic equations are solved only on the set of complex numbers.

- resonant frequencies corresponding to the previous two features are equal to each other and to the frequency of free oscillations.

Indeed, such features are peculiar to resonance only in LC-circuits. In LCR-circuits such result is only due to their approximate analysis. Accurate analysis of resonance in LCR-circuits reveals numerous unexplained oddities[10] contradicting the common sense.

For example, accurate formulas for electric LCR-circuit depicted in **Figure 1** corresponding to the first feature of resonance would be as follows

$$\begin{cases} \omega'_{res1} = 0 \\ \omega''_{res1} = \sqrt{\omega_0^2 - 4\sigma_0^2} = \omega_0 \dfrac{\sqrt{Q^2 - 1}}{Q} \end{cases} \tag{4}$$

Accurate formulas corresponding to the second feature of resonance would have the following form

$$\begin{cases} \omega'_{res2} = 0 \\ \omega''_{res2} = \sqrt{\omega_0 \sqrt{\omega_0^2 + 8\sigma_0^2} - 4\sigma_0^2} = \omega_0 \dfrac{\sqrt{Q\sqrt{Q^2 + 2} - 1}}{Q} \end{cases} \tag{5}$$

And accurate formula corresponding to the third feature of resonance would be as follows

$$\omega_{free} = \sqrt{\omega_0^2 - \sigma_0^2} = \omega_0 \frac{\sqrt{4Q^2 - 1}}{2Q} \tag{6}$$

where $\omega = 2\pi f$; $2\sigma_0 = \dfrac{R}{L}$; $\omega_0 = \dfrac{1}{\sqrt{LC}}$; $Q = \dfrac{\omega_0}{2\sigma_0} = \dfrac{1}{R}\sqrt{\dfrac{L}{C}}$.

As can be seen, there are, for some reason, many resonant frequencies, though according to the definition resonant frequency should be single. And different features of resonance correspond to different formulas. Some of resonant frequencies even equal zero. Formulas for determining resonant frequencies when applying to different electric LCR-circuits are also different[11]. Frequency of free oscillations is never equal to any of the resoant frequencies[12]. Such a list of unexplained oddities of the existing resonance interpretation is, perhaps, enough to prove its imperfection.

The difference between the accurate formulas for ω''_{res1}, ω''_{res2} and approximate formula given in all textbooks $\omega_{res} \approx 1/\sqrt{LC}$ is very small and does not exceed the experimental error.

On the one hand, practical use of a simpler, but approximate, formula $\omega_{res} \approx 1/\sqrt{LC}$ *is* justified. On the other hand, since there is still a difference between the accurate and approximate formulas, it requires explanation.

It sometimes happens in physics that a slight discrepancy between obtained and expected results can lead to discoveries. For example, Cherenkov radiation was found in this way. In 1958 Pavel Alekseyevich Cherenkov,

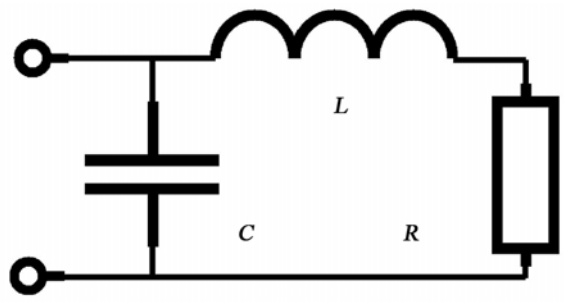

Figure 1. Electric LCR-circuit concerned.

[10]Which are not admitted in textbooks. Therefore, resonance in LCR-circuits is explained in textbooks only on the basis of approximate formulas, masking the real situation.

[11]It can be easily showed.

[12]However, the attempt [36] to explain this circumstance was unsuccessful.

Igor Evgenyevich Tamm and Ilya Mikhaylovich Frank received the Nobel Prize [35] for its discovery and explanation.

The situation concerned is also the case of discovery, as it has been proved that resonance actually exists at complex frequencies, rather than at real ones, as is commonly believed. As for the real frequencies, only some near-resonance oscillation processes are observed. Moreover, as it turned out, real resonance can occur even when affected by exponential radio and video pulses.

Physical reality of resonance at complex frequencies is confirmed by numerous experiments. Let us describe one of them, which can be repeated by any interested reader. It is all the more convincing because it is inexplicable within the existing theory of electric circuits.

Figure 2 shows two similar, but slightly different, electric diagrams the inputs of which are supplied by the same signals. These signals U_{inp} can be represented as a sum of rectangular U_1 and exponential U_2 radio

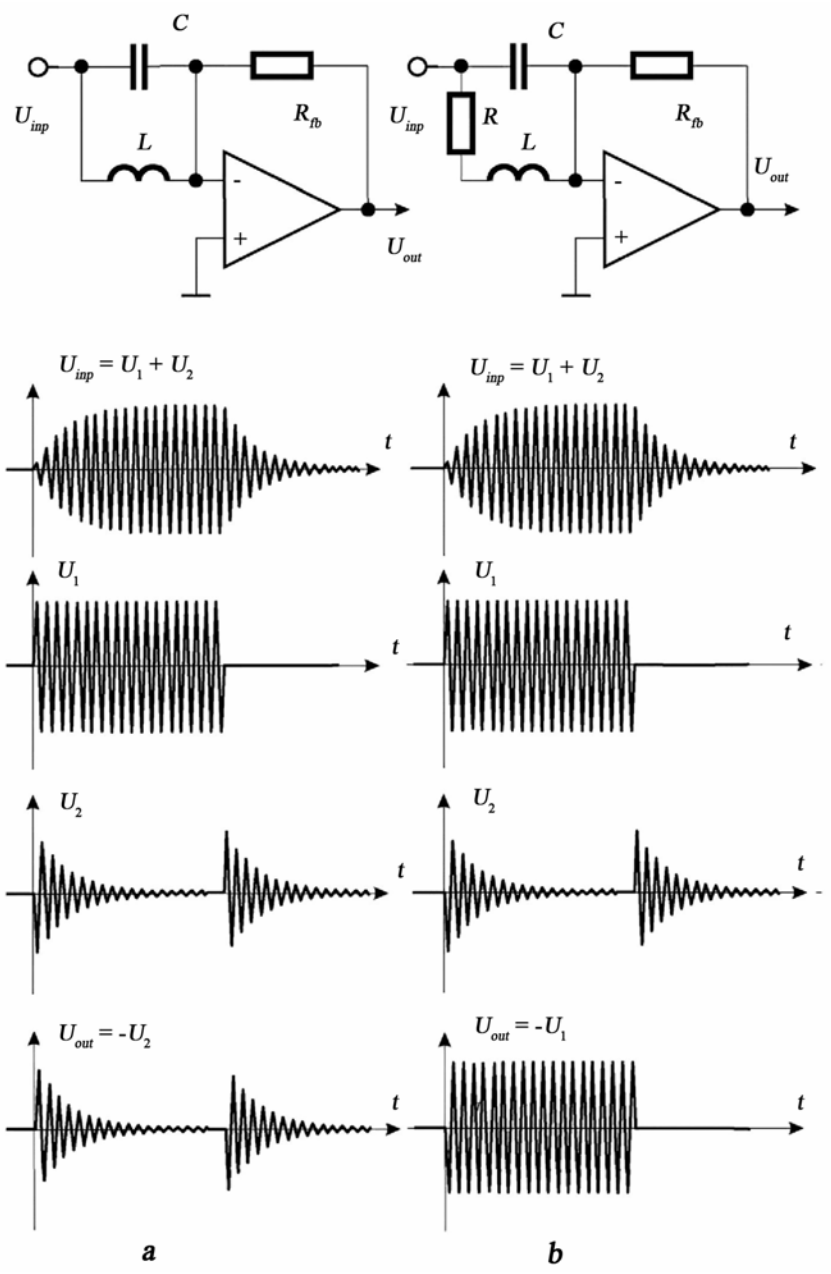

Figure 2. The proof of resonance at complex frequencies.

pulses that cannot be separated by existing filters because their spectra substantially interfere with each other. However, since their complex frequencies $p = \pm i\omega$ and $p = -\sigma \pm i\omega$ are different, they are easily separated by filters of complex frequencies, which are actually electric diagrams depicted. The diagram in **Figure 2(a)** depicts electric LC-circuit in the input, complex resonant frequencies of which $\pm i\omega$ coincide with complex frequencies of rectangular radio pulses U_1. Therefore, rectangular radio pulses are not supplied[13] to the output of such a diagram, whereas exponential radio pulses $U_{out} = -U_2$ are. The diagram in **Figure 2(b)** presents electric LCR-circuit in the input, complex resonant frequencies of which $-\sigma \pm i\omega$ coincide with complex frequencies of exponential radio pulses U_2. Therefore, exponential radio pulses are not supplied to the output of such a diagram, whereas rectangular radio pulses $U_{out} = -U_1$ are.

Similarly, rectangular and exponential video pulses corresponding to different complex frequencies $p = 0$ and $p = -\sigma$ can be separated.

Similar resonant processes take place in different electric circuits at complex frequencies. The existence of such a resonance proves, in turn, physical reality of complex frequencies, and, thus, physical reality of any other[14] complex (and therefore imaginary) numbers. And, therefore, denies the extended interpretation of the second postulate of STR [25].

Resonance at complex frequencies is even patented [37].

3. Physical Nature of Imaginary Numbers

If the proofs of reality of imaginary numbers mentioned above were known to a physical community, there would be no need in such extremely difficult experiments as MINOS, OPERA and ICARUS, as the alternative radio-electronic experiments which are much simpler would comprehensively solve the problem.

To understand the problem more deeply it would be also appropriate to explain what physical entities imaginary numbers correspond to in nature. As people do not have senses allowing them to register imaginary[15] physical entities, to believe that imaginary numbers are physically real they should somehow ascertain their existence experimentally. This requires at least a small number of situations to be provided as examples where imaginary numbers are proved to be physically real.

Processes in electric LCR-circuits, analyzed given the actual physical existence of the so-called 'imaginary' capacitive and inductive imaginary resistances, are one of the examples of such situations, as shown above. These imaginary resistances are measured by instruments available in any electronic laboratory, just as the resistance of resistors, physical reality of which has never been in doubt. Consequently, capacitive and inductive imaginary resistances[16] in the theory of electric circuits are an example of actually existing imaginary physical entities, known to everyone.

Another popular example, confirming physical reality of imaginary numbers is shock oscillations in the form of tsunami, sound of church bells, kid's swing being pushed by parents to get a swinging motion, etc., existing in nature only because their complex frequencies are physically real.

One more example that confirms physical reality of imaginary numbers is a well-known phenomenon of resonance, which turns out to exist at physically real complex frequencies.

Since the Nature is unified and consistent, the Science, striving to cognize It, should also be consistent, even being divided into many different scientific disciplines because of limited intellectual capacity of people. Consequently, the principle of physical reality of imaginary numbers proved in the theory of electric circuits is generally scientific. All exact sciences, such as theory of relativity, quantum mechanics optics, radioelectronics and others, should be adjusted in accordance with this principle.

Let us provide an example of how it can be done in the STR. Adjusted version of the STR will serve as one more proof of actual existence of imaginary physical entities.

4. Adjustment of the STR

Imaginary mass, imaginary time and other imaginary physical quantities appearing at superluminal speeds in re-

[13]As the filter is band-stop.
[14]Let us remember that resonance can be also in oscillation systems of other physical nature.
[15]And not only imaginary. People cannot hear infra and ultrasounds, see dark matter and dark energy, feel magnetic field and X-ray radiation and touch elementary particles, stars and many other physical entities, the parameters of which are measured by real numbers.
[16]As well as values derived from them: electric currents, voltages, capacities and energies.

lativistic formulas of the STR [38] adjusted due to the principle of physical reality of imaginary numbers should be recognized as actually existing. They also should be considered as imaginary quantities that have a certain physical sense, which is now to be explained. For example, with respect to the Lorentz-Einstein formula

$$m = \frac{m_0}{\sqrt{1-(v/c)^2}} \tag{7}$$

where m_0 is the rest mass of a moving entity;
m is the relativistic mass of a moving entity;
v is the velocity of a physical entity;
c is the speed of light.

The explanation is as follows. As can be seen from the formula (7), relativistic mass of moving entities, e.g. tachyons [18] [19], becomes imaginary at $v > c$. Since, according to the principle of physical reality of imaginary numbers, the moving entities really exist, they are in some another place. Owing to the condition $v > c$ this another place is beyond the event horizon and is therefore invisible to us. For clarity we should call it a tachyon universe. Subsequently, our universe should be called "tardyon" by the name of elementary particles, moving with sub-light speed.

It should be logically concluded that we live in a Multiverse [39], which includes at least tardyon and tachyon universes. And since the Multiverse is invisible, it should be referred to as hidden [40].

In this regard it is appropriate to note that the MINOS and OPERA experiments could be successful only if mass of neutrinos was zero, since at $v > c$ it would remain to be a real number. Otherwise, neutrinos with non-zero mass at $v > c$ would have imaginary mass and be invisible to us just as other tachyons. Therefore, a negative result of the OPERA and MINOS experiments, as mentioned in [41] [42], can be considered as evidence of non-zero neutrino mass.

The Nobel Prize in Physics 2015 was awarded jointly to Takaaki Kajita and Arthur B. McDonald "for the discovery of neutrino oscillations, which shows that neutrinos have mass", which has been proved as a result of similar arguments, but with the use of the results of previously conducted experiment [43].

However, let's return to the hidden Multiverse. According to the first postulate of the STR tachyon universe is an inertial reference system, *i.e.*, it has the same physical and other laws of nature that operate in our universe. Consequently, inhabitants of tachyon universe perceive their universe just as people of the Earth perceive their tardyon universe.

However, the formula (7) does not correspond to this condition and should, therefore, be adjusted as follows:

$$m = \frac{m_0 \exp(iq\pi/2)}{\sqrt{1-(v/c-q)^2}} = \frac{m_0 \exp(iq\pi/2)}{\sqrt{1-(w/c)^2}} \tag{8}$$

where $q = \lfloor v/c \rfloor$ is the discreet 'floor' function of argument v/c;
$w = v - qc$ is the local velocity for each universe, which can take values only in the range $0 \le w \le c$;
v is the velocity measured from our tardyon universe, which, therefore, can be called a tardyon velocity.
Other relativistic formulas of the STR can be adjusted in a similar manner.

5. The Hidden Multiverse

As follows from the formula (8), tardyon universe corresponds to the parameter $q = 0$, and tachyon universe[17] corresponds to the parameter $q = 1$. However, the hidden Multiverse can contain more than two universes. Tardyon antiverse[18] corresponds to $q = 2$, tachyon antiverse[19] corresponds to $q = 3$, another tardyon universe corresponds to $q = 4$ and another tachyon universe corresponds to $q = 5$ and so on[20]. There can be muchof the universes. They can be called parallel, because universes never intersect despite their infinity. Annihilation of universes and antiverses, both tardyon and tachyon, is certainly excluded, as they alternate in a strictly defined order in the Multiverse. Besides, the order is that the structure of the hidden Multiverse can be called heli-

[17]In which time flows in perpendicular direction in relation to the time in our tardyon universe, *i.e.* for us it "stands still".
[18]In which time flows in opposite direction in relation to the time in our tardyon universe.
[19]In which time also flows in perpendicular direction in relation to the time in our tardyon universe, but in opposite direction in relation to time in tachyon universe, *i.e.* for us it "stands still".
[20]Here we got an answer for the question about the location of antimatter and tachyons.

cal (see **Figure 3**, **Figure 4** and **Figure 7**).

The structure may be either closed or open. If the structure is closed, as shown in **Figure 3**, our Multiverse would be the only one. If the structure is open, as shown in **Figure 4** and **Figure 7**, the Multiverse would probably be connected by its edges to other Multiverses[21], together forming Supermultiverse. Other Multiverses of the Supermultiverse are unavailable to us not only by electromagnetic, but also by gravitational manifestations.

If the parameter q in the formula (8) is assumed to be independent variable[22], universes of the hidden Multiverse could be assumed to exist in different dimensions. These dimensions are, in a way, always beside us, wherever we are. Therefore, appropriate technologies, which are still unavailable to us, will allow transiting from one dimension to another[23].

Relative spatial position of parallel universes in such multidimensional space is stabilized by some automatic regulation process still unknown to us, without which the hidden Multiverse would have ceased to exist long ago.

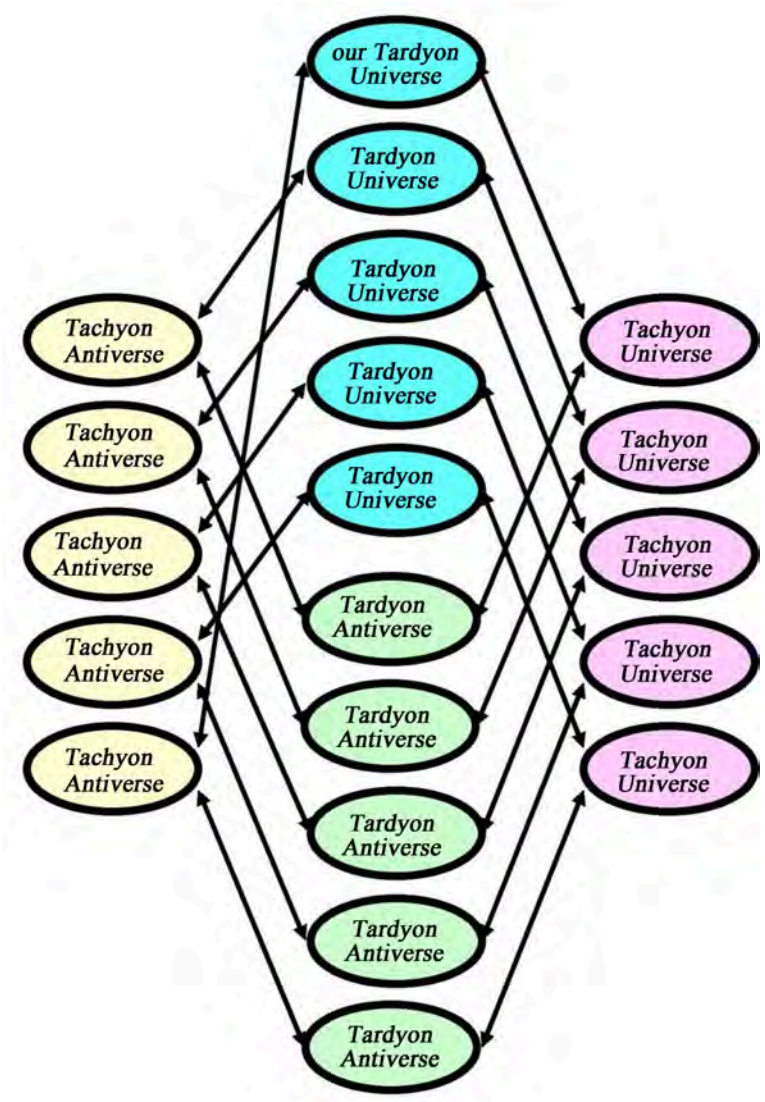

Figure 3. Possible structure of the hidden Multiverse corresponding to the principle of physical reality of complex numbers.

[21]If existence of other Multiverses is not recognized, it would be very difficult to explain what is behind open edges of our Multiverse.

[22]As the value q under the influence of unknown factors changes in accordance with the function $\exp(iq\pi/2)$ in portals (see below), through which transition from one parallel universe to another is available.

[23]Or, equivalently, from one parallel universe to another.

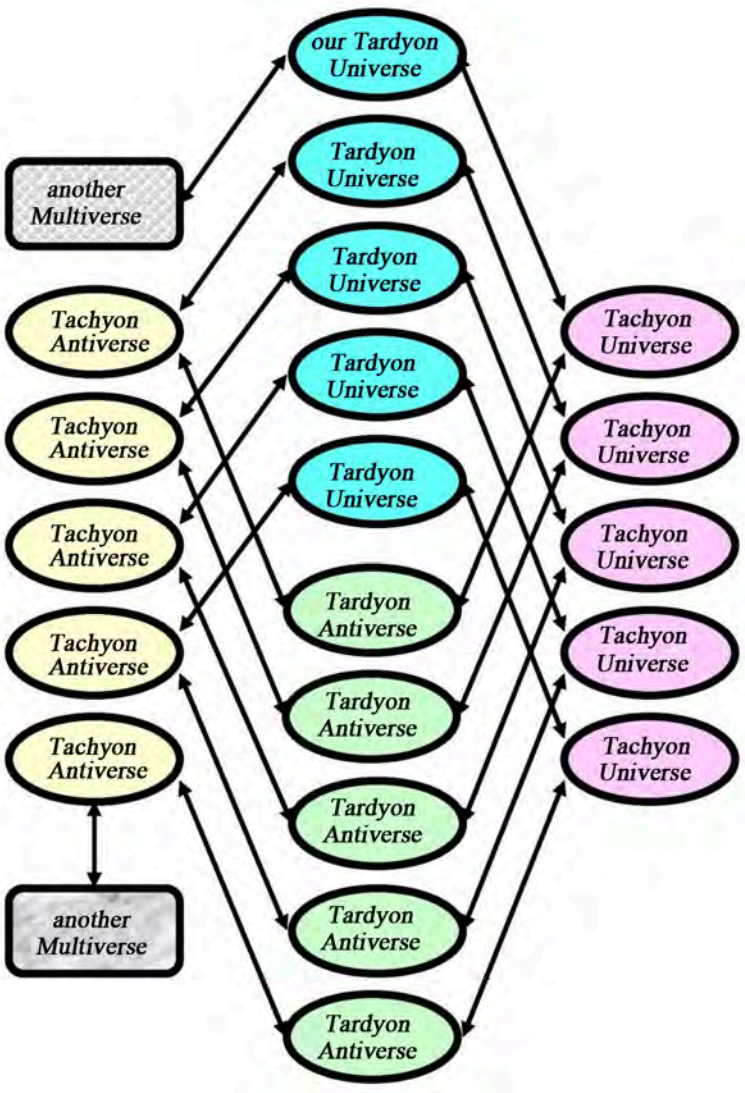

Figure 4. Another possible structure of the hidden Multiverse corresponding to the principle of physical reality of complex numbers.

In the course of such process, as well as other processes of automatic regulation, the regulated objects, *i.e.* parallel universes, slightly move relative to each other and sometimes even partially penetrate into each other in some spots. Such penetration generates certain transition zones, which are also referred to as portals or star gates[24] [44]. Relatively small physical bodies, such as elementary particles and inhabitants of universes, can pass from one universe to another through the portals. Exception is stars, planets and galaxies, as otherwise universes could be destabilized.

On the other hand, transition of material objects from one universe to another allows averaging mass-energy of different universes to some extent. Transitions through portals are likely to be relatively safe[25], since according to the law of communicating vessels characteristics of pre-portal and after-portal areas of space should be almost identical[26]. In the examples of possible structures of the hidden Multiverse given in **Figures 3-7** portals between adjacent universes are denoted by single bidirectional arrows. Indeed, there are a lot of such portals.

[24]Which have nothing to do with molehills and wormholes.
[25]As, for instance, mains are relatively safe, if no one touches them.
[26]Therefore, should at least one portal between the Earth and space be opened, the Earth would have remained without its atmosphere and hydrosphere. This might supposedly have once happened on Mars.

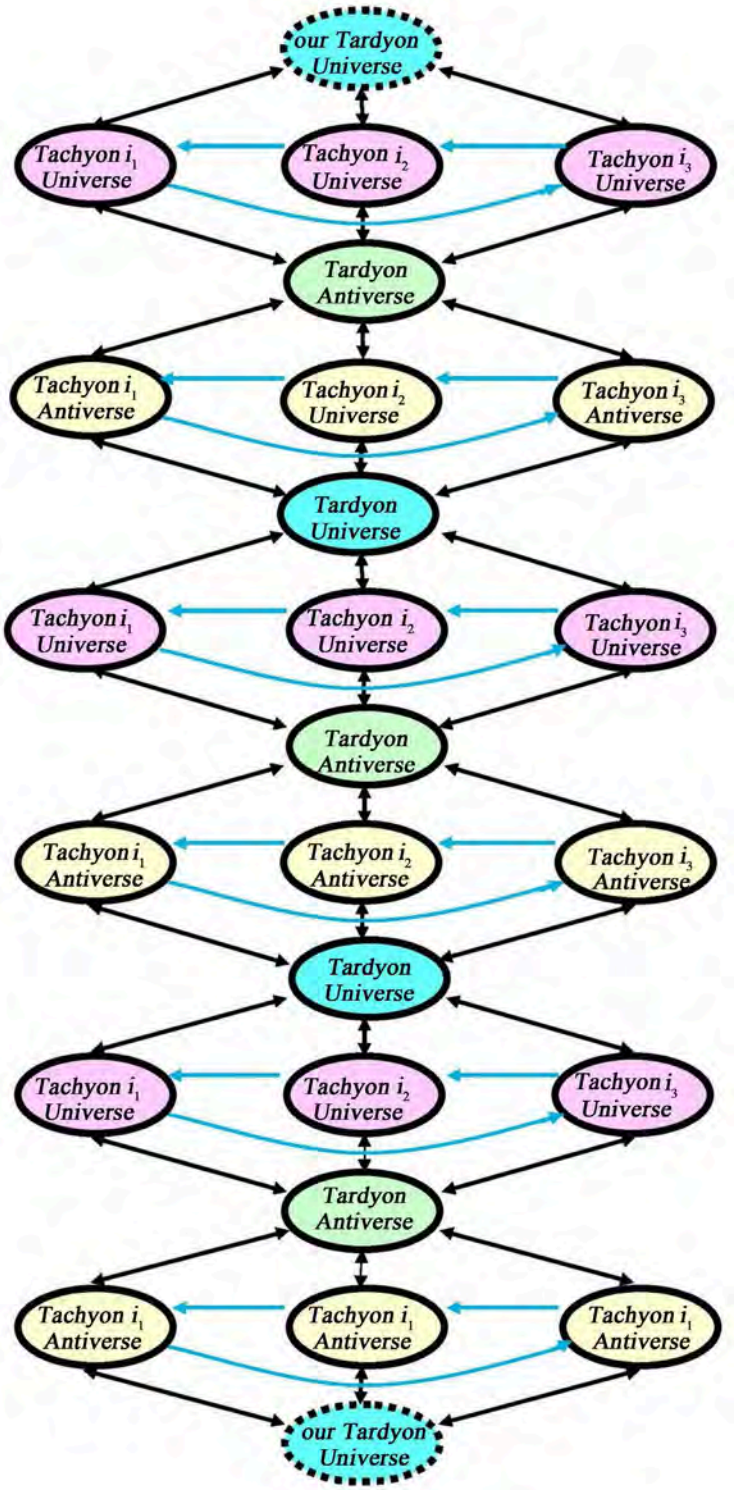

Figure 5. Possible structure of the hidden Multiverse, corresponding to the principle of physical reality of hypercomplex numbers.

6. Explanation of Dark Matter and Dark Energy

Description of the structure of the actually existing hidden Multiverse will be incomplete without explanation of

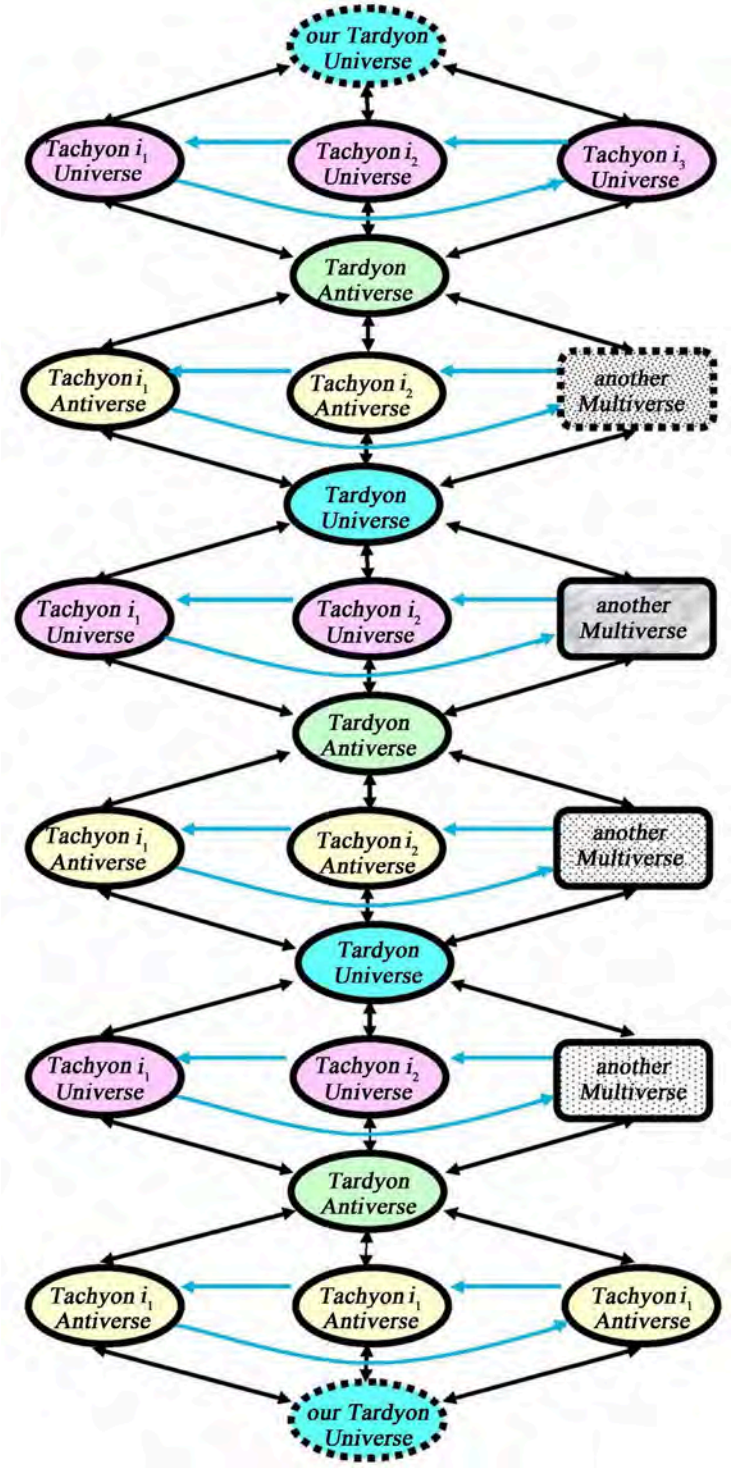

Figure 6. The most probable structure of the hidden Multiverse, corresponding to the principle of physical reality of hypercomplex numbers.

the phenomenon of dark matter and dark energy [15] [16]. Dark matter has become known as a result of research carried out by Jan Hendrik Oort and Fritz Zwikky in 1932-33, and dark energy has been discovered by Nobel Prize winners Saul Perlmutter, Brian P. Schmidt and Adam G. Riess in 1998-99. However, this astrophysical phenomenon is still incomprehensible. It is absolutely invisible. Therefore, it could be detected only

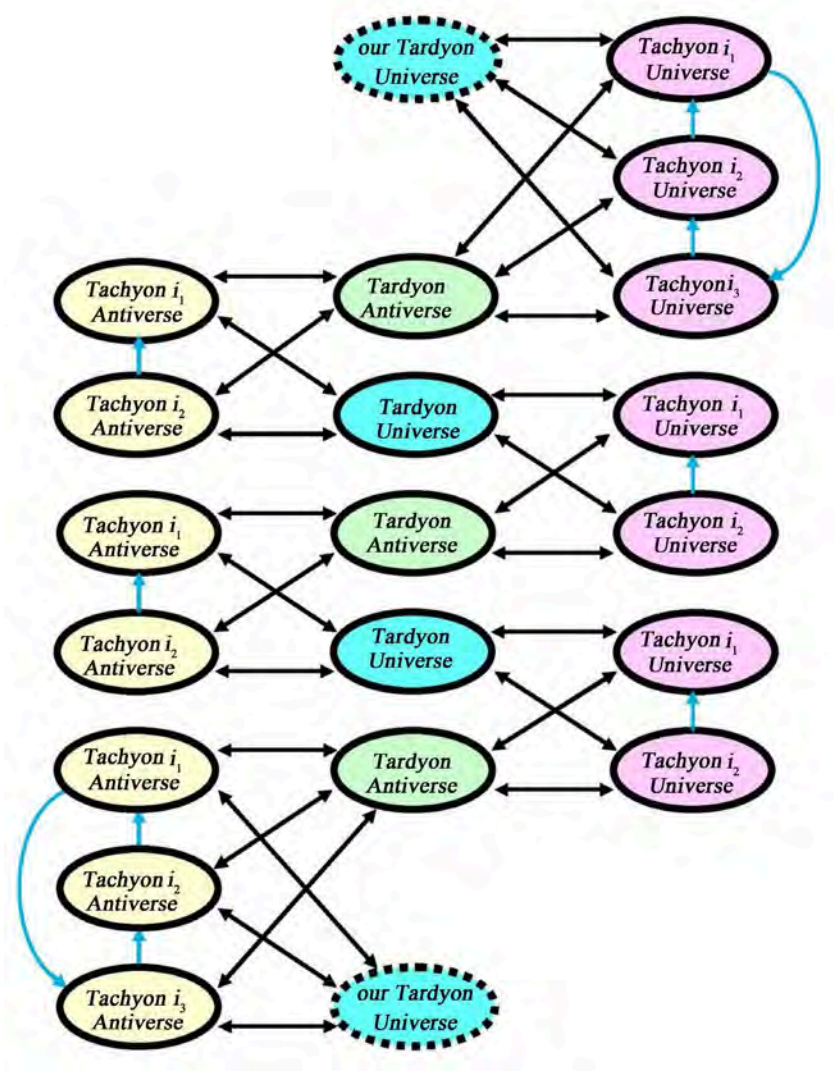

Figure 7. Structure of the hidden Multiverse, corresponding to WMAP and Planck spacecraft data.

indirectly by the effect of gravitational lensing. Dark matter and dark energy contain no chemical elements known to us. It would seem to even destroy the modern understanding of the term "matter". Although a very large number of research results have been published over the past few years, scientists have failed to get closer to understanding its nature.

Given the situation it can be assumed that the current formulation of the problem concerning explanation of the phenomenon of dark matter and dark energy within the conception of Monoverse, corresponding to the existing version of the STR, is wrong, as wrong is this version of STR itself.

Alternative explanation of dark matter and dark energy is as follows. They are the other parallel universes of the hidden Multiverse [45]-[47] unobservable from our universe. That is why dark matter and dark energy are invisible. As they are in other parallel universe, rather than in ours, their chemical composition cannot be determined. Whereas, the Earth, having available all tools for chemical analysis, contains no chemical elements of other universes.

7. Analysis of WMAP and Planck Spacecraft Data

Explanation of dark matter and dark energy given above based on WMAP [48] and Planck [49] spacecraft observations allows us to determine basic parameters of the hidden Multiverse, and thus clarify its structure.

Since according to Planck data total mass-energy of the whole Multiverse consists of 4.9% ordinary (baryonic) matter (earlier WMAP estimate-4.6%), 26.8% dark matter (according to WMAP-22.4%) and 68.3% dark energy (according to WMAP-73%),

- the hi dden M ultiverse c onsists o f $100\%/4.9\% = 20.4$ parallel u niverses a ccording t o P lanck an d o f $100\%/4.6\% = 21.7$ parallel universes according to WMAP;
- dark matter consists of $26.8\%/4.9\% = 5.5$ parallel universes according to Planck and of
- $22.4\%/4.6\% = 4.9$ parallel universes according to WMAP;
- dark energy consists of $68.3\%/4.9\% = 13.9$ parallel universes according to Planck and of $73.9\%/4.6\% = 15.9$ parallel universes according to WMAP.

Therefore, taking into account possible measurement errors and some inequality of mass-energy of different parallel universes, it is permissible to assume that the hidden Multiverse contains twenty parallel universes, six of which are adjacent to our universe.

However, the structure of the hidden Multiverse shown in **Figure 3** and **Figure 4** does not correspond to the results of calculations. Besides that it is unclear why the hidden Multiverse contains twenty parallel universes, it is even more unclear why six parallel universes turned out to be adjacent to ours, rather than two.

Thus, the principle of physical reality of imaginary numbers within the STR wouldn't seem to justify our expectations, because the experimental data obtained from WMAP and Planck spacecrafts, do not correspond to the possible structure of the hidden Multiverse given in **Figure 3** and **Figure 4**.

8. Quaternion Structure of the Hidden Multiverse

Let us try, however, to find solution to the situation. Why there are six adjacent universes? This means that three parallel tachyon universes and three parallel tachyon antiverses are adjacent. However, several parallel universes presented in **Figure 3** and **Figure 4** cannot be parallel in one and the same dimension, because the structure of such parallel dimensions is determined by complex numbers, including a single imaginary unit.

In other words, WMAP and Planck data actually refute compliance of the structure of the hidden Multiverse with the principle of physical reality of complex numbers, rather than the principle of physical reality of imaginary numbers.

However, imaginary units are part of not only complex, but also hypercomplex numbers [50]. Besides, quaternions $a + bi_1 + ci_2 + di_3$ include exactly three imaginary units i_1, i_2, i_3 connected by the following relations

$$i_1^2 = i_2^2 = i_3^2 = -1 \tag{9a}$$

$$i_1 i_2 i_3 = i_2 i_3 i_1 = i_3 i_1 i_2 = -1 \tag{9b}$$

$$i_1 i_3 i_2 = i_2 i_1 i_3 = i_3 i_2 i_1 = 1 \tag{9c}$$

As can be seen, the relation (9a) is the same as for the imaginary units in complex numbers. Relations (9b) and (9c) are possible only with respect to quaternions. Consequently, they allow tachyon universes and antiverses operate in parallel. In other words, WMAP and Planck data actually correspond to the assertion, that the structure of the hidden Multiverse is based on the principle of physical reality of quaternions.

The structure of such hidden Multiverse is determined by the formula of Lorentz-Einstein, adjusted once more

$$\begin{aligned} m &= \frac{m_0 \exp\left(i_1 q\,\pi/2\right)\exp\left(i_2 r\,\pi/2\right)\exp\left(i_3 s\,\pi/2\right)}{\sqrt{1-\left[v/c-\left(q+r+s\right)\right]^2}} \\ &= \frac{m_0 \exp\left(i_1 q\,\pi/2\right)\exp\left(i_2 r\,\pi/2\right)\exp\left(i_3 s\,\pi/2\right)}{\sqrt{1-\left(w/c\right)^2}} \end{aligned} \tag{10}$$

where q is the total number of parallel universes, penetration into which was made through bidirectional portals, corresponding to the imaginary unit i_1, with increasing distance from our tardyon universe;

r is the total number of parallel universes, penetration into which was made through bidirectional portals, corresponding to the imaginary unit i_2, with increasing distance from our tardyon universe;

s is the total number of parallel universes, penetration into which was made through bidirectional portals, corresponding to the imaginary unit i_3, with increasing distance from our tardyon universe;

v is the velocity measured from our tardyon universe, which, therefore, can be called tardyon velocity;

c is the speed of light;

$w = v - (q + r + s)c$ is the local velocity for corresponding universe, which can take values only in the range $0 \le w < c$.

Other relativistic formulas of the STR can be adjusted in a similar manner.

Consequently, the structure of multidimensional space containing parallel universes of the hidden Multiverse is determined by three independent variables q, r and s. Therefore, the total number of parallel universes given the helical structure of the Multiverse should be a multiple of eight. According to the WMAP and Planck date it is likely equaled to twenty-four for a closed helical structure, as shown in **Figure 5**. In this figure, as in **Figure 3**, our tardyon universe is denoted by a dashed line in the form of a screw collar. In the structure of the Multiverse it serves as the beginning and the end, so it is depicted twice.

The structure of the hidden Multiverse in **Figure 6** and **Figure 4** is depicted as partially closed. Therefore, it can be connected by its unclosed edges with other Multiverses, collectively forming Supermultiverse. However, while, as noted above, other Multiverses, external to our Multiverse, are unobservable not only by electromagnetic, but also gravitational manifestations, WMAP and Plank data enables determination of their number. As shown in **Figure 6** it equals the difference between the theoretically expected twenty-four and the experimentally observed twenty universes, *i.e.*, four Multiverses. Therefore, information obtained by WMAP and Plank devices corresponds to the block diagram[27] depicted in **Figure 7**.

Thus, WMAP and Plank data conclusively demonstrates not only that our hidden Multiverse contains exactly twenty parallel universes, six of which are adjacent to our universe, but also the fact that one to four[28] other Multiverses are also adjacent to our hidden Multiverse. Besides, these data prove quaternion structure of the hidden Multiverse and, thus, physical reality of quaternions.

A peculiarity of quaternion structure of the hidden Multiverse is that in addition to bidirectional portals based on the relation (9a), which are denoted by bidirectional black arrows, it contains unidirectional portals[29] based on the relations (9b) and (9c), which are denoted by unidirectional blue arrows. Location of these portals in **Figure 6** and **Figure 7** are consistent with the principles of their operation discussed below in relation to one of the links of the hidden Multiverse (see **Figure 8**), including tardyon and tachyon universes and tardyon antiverses.

To explain these principles of operation, corresponding to the relation (9b), we should rewrite it as a set of non-commutative products

$$\begin{aligned} i_1 i_2 &= i_3 \\ i_2 i_3 &= i_1 \\ i_3 i_1 &= i_2 \end{aligned} \tag{11}$$

The first product $i_1 i_2 = i_3$ means that penetration from the tachyon universe i_1 into the tachyon universe i_3 is possible through the unidirectional portal i_2. The second product $i_2 i_3 = i_1$ means that penetration from the tachyon universe i_2 into the tachyon universe i_1 is possible through the unidirectional portal i_3. The third product $i_3 i_1 = i_2$ means that that penetration from the tachyon universe i_3 into the tachyon universe i_2 is possible through the unidirectional portal i_1.

The algorithm of operation of unidirectional portals is shown in **Figure 8(b)**. Besides, penetration from tardyon universeinto tachyon universes i_1, i_2, i_3, and from tachyon universes i_1, i_2, i_3 into tardyon antiverse is possible through the respective bidirectional portals i_1, i_2, i_3. The algorithm of operation of bidirectional portals i_1, i_2, i_3 is shown separately in **Figure 8(a)** and jointly with the algorithm of operation of unidirectional portals i_1, i_2, i_3 in **Figure 8(b)** and **Figure 8(c)**.

Relation (9c) can also be rewritten in the form of a set of non-commutative products

$$\begin{aligned} i_1 (-i_3) &= i_2 \\ i_2 (-i_1) &= i_3 \\ i_3 (-i_2) &= i_1 \end{aligned} \tag{12}$$

[27]Which does not depict other Multiverses, as they have not been detected by WMAP and Plank devices.

[28]Since our hidden Multiverse can touch the same Multiverses by its edges several times.

[29]From and through which one cannot return to its universe.

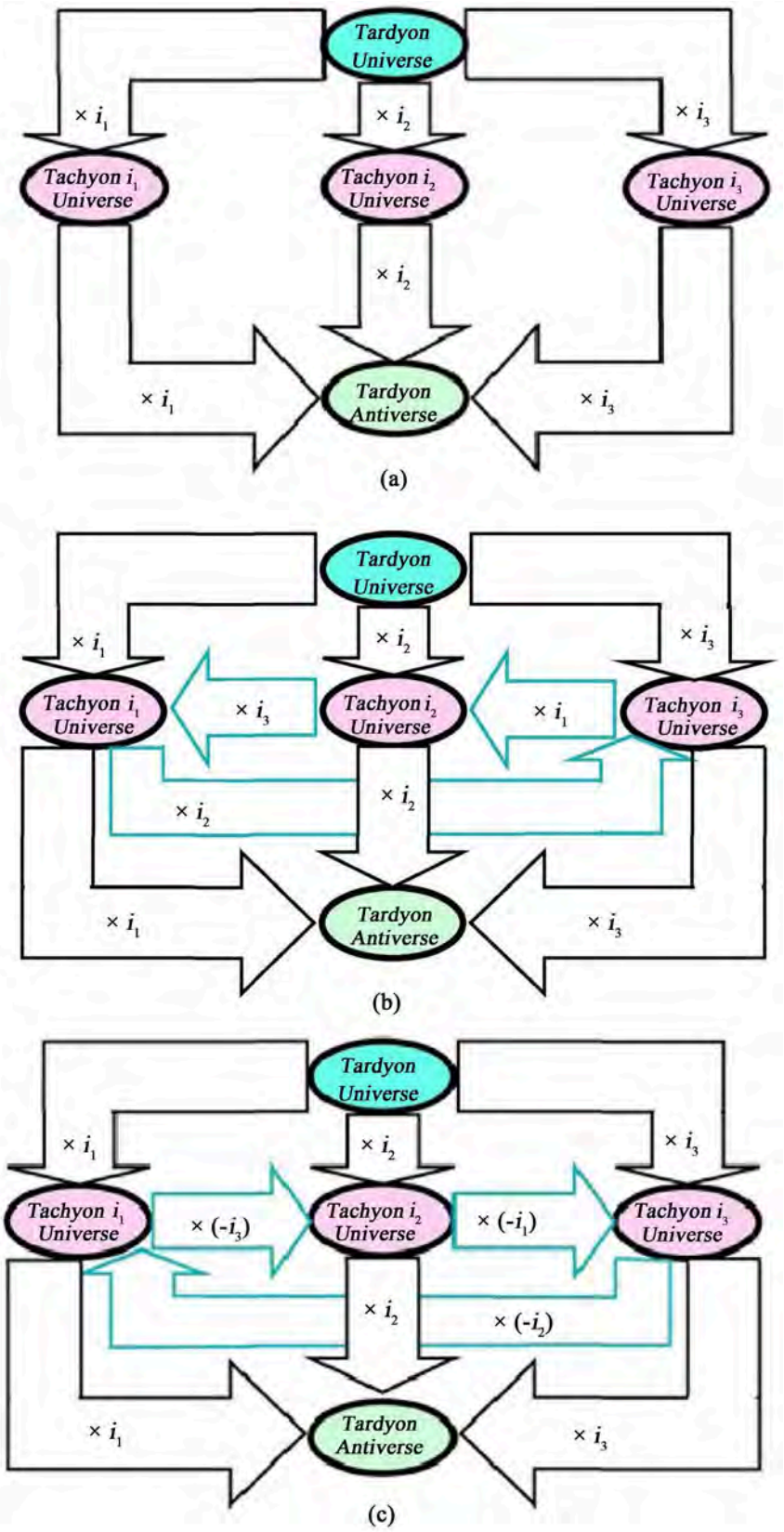

Figure 8. The algorithm of operation of hidden Multiverse's portals.

It would seem that products of imaginary units included in the set (12) differ from the products of imaginary units included in the previous set. However, they actually don't (see **Figure 8(c)**). Indeed, according to the reasoning given above the product $i_1 i_3 = i_2$ can mean that penetration from the tachyon universe i_1 into the tachyon universe i_2 is possible through the unidirectional portal i_3. But then the first product $i_1(-i_3) = i_2$ in the set (12) means that movement is also possible in the opposite direction, *i.e.* penetration from the tachyon universe i_2 into the tachyon universe i_1 may be done through the unidirectional portal i_3. Such transition corresponds to the non-commutative product $i_2 i_3 = i_1$. And this is the second product in the set (11). Similarly, the product $i_2 i_1 = i_3$ can mean that penetration from the tachyon universe i_2 into the tachyon universe i_3 is possible through the unidirectional portal i_1. But then the second product $i_2(-i_1) = i_3$ in the set (12) means that movement is possible in the opposite direction, *i.e.* penetration from the tachyon universe i_3 into the tachyon universe i_2 may be done through the unidirectional portal i_1. Such transition corresponds to the product $i_3 i_1 = i_2$. And this is the third product in the set (11). Finally, the product $i_3 i_2 = i_1$ can mean that penetration from the tachyon universe i_3 into the tachyon universe i_1 is possible through the unidirectional portal i_2. But then the third product $i_3(-i_2) = i_1$ in the set (12) means that movement is possible in the opposite direction, *i.e.* penetration from the tachyon universe i_1 into the tachyon universe i_3 may be done through the unidirectional portal i_2. Such transition corresponds to the product $i_1 i_2 = i_3$. And this is the first product in the set (11). Consequently, the algorithm corresponding to the set of non-commutative products of imaginary units (12) shown in **Figure 8(c)** is actually equivalent to the previous algorithm corresponding to the set of non-commutative products of imaginary units (11) shown in **Figure 8(b)**.

The remaining links of the hidden Multiverse operate in a similar manner, as is easy to show.

Thus, the foregoing allows us to give the following answer for a question about existence of antimatter and tachyons, put in the beginning of the article: Quaternion Multiverse contains four pairs of different types of matters and antimatters, as well as tachyons in six different types of tachyon universes and antiverses.

9. Review of the Conception of the Hidden Multiverse for Compliance with Popper's Falsification Criterion

So, presentation of the conception of hidden Multiverse is completed.

There is the last question, whether this conception complies with Popper's falsification criterion, or, in other words, whether this conception can be confirmed or refuted experimentally.

It turns out that it can, for example, as follows.

Existence of the hidden Multiverse has been allegedly confirmed by those experiments at the Large Hadron Collider, which showed that there was a mass defect near the point of singularity when $v \to c$. *i.e.*, there were situations, when total mass of elementary particles at the beginning of the experiment turned out to be greater than total mass of elementary particles at the end of the experiment[30]. In such situations mass defect can be explained by formation of tachyons that, having overcome the light speed barrier, disappeared in tachyon universes and/or tachyon antiverses, e.g., as a result of formation of short-term micro and mini portals, similar to formation of macro portal in the episode with the Eldridge destroyer. Therefore, such situations can be interpreted as experimental confirmation of tachyon existence, and, thus, the existence of the hidden Multiverse containing tachyon universes and antiverses.

10. Conclusions

So, the article provides answers to all the questions raised therein:

- physical reality of imaginary, complex and hypercomplex numbers has been proved theoretically and experimentally;
- resonance has been proved to exist at complex frequencies, rather than real ones;
- extended interpretation of the second postulate of the current version of the STR has been thereby refuted;
- it has been shown that failure of attempts to explain the phenomenon of dark matter and dark energy is caused by incorrect formulation of task aimed at searching for explanation within the conception of Monoverse, corresponding to the current incorrect version of the STR;
- the adjusted formulation of the task aimed at searching for explanation of the phenomenon of dark matter

[30]For example, with frequent disappearance of elementary particles before their collision.

and dark energy within the conception of Multiverse has been suggested;
- relativistic formulas of the STR have been suggested given the principle of physical reality of imaginary numbers;
- conception of quaternion structure of the hidden Multiverse, which, according to the WMAP and Planck data, contains twenty mutually invisible universes existing in different dimensions, has been suggested on the basis of the adjusted relativistic formulas of the STR;
- according to the WMAP and Planck data six parallel universes among those twenty mutually invisible universes existing in different dimensions are adjacent to our universe;
- it has been shown that dark matter and dark energy correspond both to other invisible parallel universes of the hidden Multiverse, except ours;
- it has been shown that dark matter corresponds to the adjacent invisible parallel universes and dark energy corresponds to the rest of the parallel universes, shielded from us by parallel universes of dark matter;
- it has been explained how portals sometimes appear between adjacent parallel universes of the hidden Multiverse, enabling inhabitants of one universe to penetrate into another;
- since time in different parallel universes of the hidden Multiverse flows in different directions, movement through portals make it possible to travel not only through space, but also through time;
- it has been shown that quaternion structure of the hidden Multiverse contains four pairs of different matters-antimatters, and that their annihilation is prevented;
- it has been shown that tachyons locate in tachyon universes and antiverses of six different types;
- and, finally, it has been shown how the outlined hypothesis of the hidden Multiverse can be subjected to review for compliance with Popper's falsification criterion.

Acknowledgements

The author is grateful for participation in the discussion of the paper to my wife Dr. Olga Ilyinichna Antonova, whose criticism and valuable comments contributed to improvement of the article.

References

[1] Deutch, D. (1998) The Fabric of Reality: The Science of Parallel Universes and Its Implications. Penguin Books, London.

[2] Greene, B. (2000) The Elegant Universe: Superstrings, Hidden Dimensions, and the Quest for the Ultimate Theory. Random House Inc., New York.

[3] Kaku, M. (2006) Parallel Worlds. A Journey through Creation, Higher Dimensions, and the Future of the Cosmos. Doubleday, New York.

[4] Steinhardt, P.J. and Turok, N. (2007) Endless Universe: Beyond the Big Bang. Doubleday, New York.

[5] Vilenkin, A. (2007) Many Worlds in One: The Search for Other Universes. Macmillan, London.

[6] Weinberg, S. (2008) Cosmology. Oxford University Press, New York.

[7] Carr, B., Ed. (2009) Universe or Multiverse? Cambridge University Press, Cambridge.

[8] Lucash, V.N. and Mikheyeva, E.V. (2010) Physical cosmology. Physmathlit, Moscow.

[9] Greene, B. (2011) The Hidden Reality: Parallel Universes and the Deep Laws of the Cosmos. Random House Inc., New York.

[10] Deutsch, D. (2012) The Beginning of Infinity: Explanations That Transform the World. Reprint Edition. Penguin Books, London.

[11] Tegmark, M. (2015) Our Mathematical Universe: My Quest for the Ultimate Nature of Reality. Vintage, New York.

[12] Kragh, H. (2011) Higher Speculations: Grand Theories and Failed Revolutions in Physics and Cosmology. Oxford University Press, New York.

[13] Ellis, G. and Silk, J. (2014) *Nature*, **516**, 321-323. http://dx.doi.org/10.1038/516321a

[14] Popper, K.R. (1972) Conjectures and Refutations. The Growth of Scientific Knowledge. Routledge and Kegan Paul, London and New York.

[15] Freeman, K. and McNamara, G. (2006) In Search of Dark Matter. Springer, New York.

[16] Nicolson, I. (2007) Dark Side of the Universe: Dark Matter, Dark Energy, and the Fate of the Cosmos. Johns Hopkins University Press, Baltimore.

[17] Dirac, P.A.M. (1931) *Proceedings of the Royal Society A*, **133**, 60-72. http://dx.doi.org/10.1098/rspa.1931.0130

[18] Tanaka, S. (1960) *Progress of Theoretical Physics*, **24**, 171-200. http://dx.doi.org/10.1143/PTP.24.171

[19] Feinberg, G. (1967) *Physical Review*, **155**, 1089-1105. http://dx.doi.org/10.1103/PhysRev.159.1089

[20] Antonov, A.A. (2010) *General Mathematics Notes*, **1**, 11-16. http://dx.doi.org/10.17686/sced_rusnauka_2010-887

[21] Antonov, A.A. (2015) *General Mathematics Notes*, **31**, 34-53.

[22] Weisstein, E.W., Ed. (2005) The CRC Concise Encyclopedia of Mathematics. 3rd Edition, CRC Press, Boca Raton.

[23] Einstein, A. (1920) Relativity: The Special and General Theory. H. Holt and Company, New York.

[24] Hawking, SW. and Penrose, R. (2010) The Nature of Space and Time. Princeton University Press, Princeton. http://dx.doi.org/10.1515/9781400834747

[25] Antonov, A.A. (2014) *Global Journal of Science Frontier Research A*: *Physics and Space Science*, **14**, 51-59.

[26] Einstein, A. (1905) *Annalen der Physik*, **322**, 891-921. http://dx.doi.org/10.1002/andp.19053221004

[27] Adamson, P., Ashby, N. and Bumgarner, R. (2014) Measurement of the Velocity of the Neutrino with MINOS. arXiv:1408.6267v1

[28] Adam, T., *et al.* (2011) Measurement of the Neutrino Velocity with the OPERA Detector in the CNGS Beam. arXiv:1109.4897v4

[29] Antonello, M., Baibussinov, B., Boffelli, F., *et al.* (2012) Precision Measurement of the Neutrino Velocity with the ICARUS Detector in the CNGS Beam. arXiv:1208.2629

[30] Antonov, A.A. (2015) *American Journal of Electrical and Electronic Engineering*, **3**, 124-129.

[31] Antonov, A.A. (2015) *Global Journal of Physics*, **2**, 145-149.

[32] Ohm, G.S. (2015) Gesammelte Abhandlungen. Severus Verlag, Hamburg.

[33] Steinmetz, C.P. (2010) Theory and Calculation of Electric Circuits. Nabu Press, Charleston.

[34] Frova, A. and Marenzana, M. (2006) Thus Spoke Galileo: The Great Scientist's Ideas and Their Relevance to the Present Day. Oxford University Press, Oxford.

[35] Tamm, I.E. (1959) *Uspehi Fizicheskih Nauk*, **68**, 387-396.

[36] Mandelshtam, L.I. (1955) Lectures on Oscillation. Vol. 4, Academy of Sciences of USSR, Moscow.

[37] Antonov, A.A. and Bazhev, V.M. (1970) Means of Rising Deflecting Currents for Spiral Beam Sweep on the CRT Screen. Patent of USSR # 433650.

[38] Antonov, A.A. (2014) *American Journal of Scientific and Industrial Research*, **5**, 40-52.

[39] Antonov, A.A. (2011) *British Journal of Science*, **2**, 51-60. http://dx.doi.org/10.17686/sced_rusnauka_2011-892

[40] Antonov, A.A. (2015) *International Journal of Advanced Research in Physical Science*, **2**, 25-32. http://dx.doi.org/10.17686/sced_rusnauka_2015-903

[41] Antonov, A.A. (2011) *American Journal of Scientific and Industrial Research*, **2**, 890-891. http://dx.doi.org/10.5251/ajsir.2011.2.6.890.891

[42] Antonov, A.A. (2011) *European Journal of Scientific Research*, **65**, 321-328.

[43] 2015 Nobel Prize in Physics. Scientific American, 6 October 2015.

[44] Antonov, A.A. (2016) *Philosophy & Cosmology*, **6**, 11-27.

[45] Antonov, A.A. (2015) *American Journal of Modern Physics*, **4**, 180-188.

[46] Antonov, A.A. (2015) *Global Journal of Science Frontier Research* (*A*): *Physics and Space Science*, **15**, 33-38.

[47] Antonov, A.A. (2015) *Cosmology*, **19**, 40-61.

[48] Hinshaw, G., Larson, D., Komatsu, E., *et al.* (2012) Nine Year Wilkinson Anisotropy Probe (WMAP) Observations: Cosmological Parameter Results. http://arxiv.org/abs/1212.5226

[49] Adam, R., Ade, P.A.R., Aghanim, N., *et al.* (2015) Plank 2015 Results. 1. Overview of Products and Scientific Results. https://arxiv.org/abs/1502.01582

[50] Kantor, I.L. and Solodovnikov, A.S. (1989) Hypercomplex Numbers. Springer Verlag, Berlin.

Journal of Modern Physics, 2016, 7, 1247-1276
Published Online June 2016 in SciRes. http://www.scirp.org/journal/jmp
http://dx.doi.org/10.4236/jmp.2016.710112

A Model of the Universe that Can Explain Dark Matter, Dark Energy, and the Fourth Space Dimension

Donald J. Koterwas[1,2,3]

[1]Retired, Monument, CO, USA
[2]Department of Earth, Space, and Graphic Sciences, United States Military Academy, West Point, NY, USA
[3]Department of Civil Engineering and Engineering Mechanics, and Department of Optics, University of Arizona, Tucson, AZ, USA
Email: sdkoterwas@gmail.com

Received 29 April 2016; accepted 24 June 2016; published 28 June 2016

Abstract

This paper explains how a model of the universe can be constructed by incorporating time and space into geometry in a unique way to produce a 4-space dimension/1-time dimension model. The model can then show how dark matter can be the gravity that is produced by real matter that exists throughout our entire universe. The model can also show how dark energy is not an increase in energy that is causing the accelerated expansion of the universe, but is an accelerating decrease in matter throughout the universe as the stars and galaxies in the universe continue to convert matter into energy during their life cycles. And then the model can show how a fourth space dimension must exist in our universe to locate a point in space.

Keywords

Universe, Dark Matter, Dark Energy, Gravity, Fourth Space Dimension

1. Introduction

Dark matter and dark energy continue to be the subjects of many articles written in scientific papers and journals. Dark matter was proposed in the 1970's to account for the gravity that had to exist in a halo effect around galaxies to account for the faster than expected motion of stars in the outer orbits of the galaxies. It was called dark matter because it was not visible. It did not absorb, reflect, or emit light. It was estimated that the amount of dark matter had to be over 6 times the amount of visible matter that existed in the galaxies. Dark energy was pro-

posed by astronomers in 1998 to account for the accelerating expansion of the universe that had become evident from their observations of the motions of supernovae and galaxies.

Most of the research that is done to try to explain dark matter involves the search for some kind of exotic particle that is not visible, but does produce a gravitational effect. There is an alternative way to try to explain dark matter. Dark matter does not have to be matter; it can just be gravity.

Dark energy is still a mystery. It is thought to be some kind of energy that is spread throughout the universe and is increasing at an accelerating rate. There is an alternative way to explain dark energy. The accelerating expansion of the universe does not have to be caused by an increase in energy that we call dark energy; it can be caused by a decrease in gravity due to a decrease in the amount of matter in the universe.

Both of these explanations involve gravity, and it is not surprising that gravity is still a little bit of a mystery. Is it a force that acts between objects as described by Sir Isaac Newton, or is it a warping of space-time as described by Albert Einstein? Regardless of its true nature, the effects of gravity in our universe are well known, and they can be shown most effectively by the use of equations, graphs, and geometric models. We can construct a model of the universe that will show the relationships between gravity, dark matter, and dark energy. The model will also show that a fourth space dimension must exist in our universe to locate a point in space.

2. The Model

A model of the universe can be constructed that can explain the true nature of dark matter and dark energy. Current models of the universe do not incorporate time into space in a way that shows the whole universe as it really exists on a grand scale. Some of the models show how the universe developed over time since the beginning of time at the big bang. Some show time as a timeline and show the development of the parts of the universe, such as protons, molecules, forces, stars, and galaxies, along this timeline. Some present a model in two or three dimensions upon which accurate measurements involving space and time can be made, such as the Lambda CDM cosmological model. But they do not present a 5-dimensional model of our entire universe upon which accurate measurements involving space and time can be made.

In our real world, we know that when we look out into space, we are also simultaneously looking back in time. And no matter in which direction we look, we are looking back in time about 13.8 billion years to the beginning of the universe at the big bang. We know that the Hubble telescope will give us a similar picture of the beginnings of our universe no matter in which direction it is pointed. It does not give us a picture of our nearest galaxies as they exist now. It gives us a picture of them as they existed millions and billions of years ago, since it has taken millions and billions of years for their emitted light to reach the telescope.

Time and space can be incorporated into geometry to construct a model that reflects the reality that the Hubble space telescope reveals. When mathematicians and scientists need to include time in their calculations about the physical world, they generally represent it as another dimension along a straight line equivalent to the x, y, or z-axis in the Cartesian coordinate system. Most of the current models of the universe also treat time as a straight line in one direction; *i.e.*, as the arrow of time. However, if we consider the nature of time, we realize that it began at the creation of the universe, and it did not travel in a straight line in one direction in space. It progressed outward from the big bang in all directions. So, we can make a unique shift in incorporating time and space into geometry by treating time as a radius of a sphere in a coordinate system where time is the radius, and the three space coordinates, x, y, and z are on the surface of the sphere. As time proceeds forward and outward on the radii of the sphere, all matter in the universe moves outward and expands on the surface of the sphere. Measurements are made on this model by, first of all, placing the observer at a point in time on the radius, and then secondly, establishing his space coordinate system on the surface of the sphere which represents the universe, to make physical measurements in the usual manner. When time is involved in the measurement, the observer moves to the next point in time on the radius, and then on the surface of the sphere, which will now be a larger or smaller sphere (the universe), the space coordinate system is established to make the physical measurements.

We can visualize this model of the universe and how it works if we place some measurements and objects on it. Along the radii, time would be measured in years. Along the surface of the sphere, which represents all of space, distances are measured in light years. In this way, the model is scaled so that a unit of distance along the time line, say one inch representing one billion years, is equivalent to the same unit of distance along the surface of the sphere, which would be one inch representing one billion light years. This model is based on this equiva-

lency, which recognizes the fact that the speed of light is one of the fundamental building blocks of our universe. When Albert Einstein developed his theory of relativity and produced his famous equation, $E = mc^2$, he showed how fundamentally important the speed of light is in our universe. It is not light itself, or electromagnetic waves in general, but it is the speed at which they travel through space that is so important. The speed of light is a limit to which nothing can travel faster. It actually presents a boundary to our universe. Speed is measured in units of distance divided by time, such as kilometers per second, or miles per hour. Thus the speed of light gives us a way of making measurements of distance, equivalent to measurements of time; *i.e*. one year of time is equivalent to one light year of distance in our universe. In our model, a length along the radius of the sphere, which represents time, is the same length along the radius that represents a measurement of one light year, and is also the same length along the surface of the sphere, which represents a distance in space. Because our model of the universe is based on this real equivalence, it will give us accurate measurements of space and time in our universe.

In our model, the beginning of time at t = 0 at the center of the sphere, occurs at the time of the big bang after an assumed period of super inflation (proposed by Alan Guth in the early 1980's) where the universe suddenly jumped in size by an enormous factor such as 10^{25} times, implying, according to Paul Davies in his book, *The Goldilocks Enigma*, that "the entire observable universe leapt from about the size of a proton to the size of a grapefruit virtually instantaneously. The actual magnification factor was unimportant so long as it was very big" [1]. He goes on to say, that after this initial instant of time and inflation of size, "inflation shuddered to a halt and normal expansion resumed" [1]. Our beginning model assumes that this normal expansion of the universe (outward along the radii of the sphere) takes place at the speed of light beginning when the universe was about the size of a grapefruit. Thus, a unit of measurement of time, say 1 billion years, is equal to a unit of distance, say 1 billion light years, along both the time axes and the space/distance axes along the surface of the sphere.

In our model, the radius of the sphere is increasing at the speed of light. This is because light travels outward from the beginning of time at the speed of light, so if the age of the universe is about 13.8 billion years old, the radius is at least 13.8 billion light years. We will show later how and why it is much greater than that. It is important to note that the surface of the sphere, which represents the universe, is not expanding at the speed of light. Actually, it is expanding currently by about 7 percent every billion years as indicated by recent observations. We will make calculations on our model later that will produce this same rate of expansion. It is also important to note that the entire universe is on the surface of the sphere in this model. All three space dimensions exist on the surface of the sphere. The x and y dimensions extend laterally, and the z dimension extends perpendicularly to these through the thickness of the sphere, and this will be discussed in more detail later. However, it should be emphasized at this point, that in this model, only time exists inside and outside of the sphere. Past time is inside the sphere, and future time is outside the sphere.

It is important to realize that the orientation of the 3 space directions on the surface of the sphere will depend on the orientation of the observer and local conditions, such as whether the observer, for example, is standing on the earth or floating in space. Thus, all 3 space directions are treated equally, although the thickness direction appears to be much smaller than the other 2 directions. It also appears in the model that we are overlapping the time and space dimensions in the thickness region on the surface of the sphere. This is true, but what does it really mean? Here is where the value of the model becomes evident. Everything inside the sphere is time, past time or history, to be exact. Everything outside of the sphere is also time, which is the future. When someone asks, "What is outside of our universe; *i.e*., what is outside of the sphere?", the model shows that the simple correct answer is, "It is our future, just as everything inside the sphere is our past." In other words, nothing real exists outside of the sphere, since the outside of the sphere is where the universe (the surface of the sphere) will be in the future. The inside of the universe, so to speak, is where the universe was in the past. The inside is nothing but the past. Everything on the surface of the sphere, including the thickness, is the present time. What this basically says is that space exists in time, and time exists in space. If one asks, "How thick is the thickness of the sphere?", one is also asking, "How long does present time last?" This is a question for the philosophers, but in our everyday lives, the present time does seem to last for some, although small, period of time before it becomes the past. We will return to this subject later, including a discussion of how thick the thickness is when measurements of height, width or depth are to be made.

We can now place some objects on the model. To keep the size of the model on a single sheet of paper, we can place galaxies spaced one billion light years apart on the surface of the sphere. We can construct the model to show our universe at the present time, which is now widely accepted as approximately 13.8 billion years. For simplicity, we will use 14 billion years as the age of the universe and show the spherical model in cross-section. When time, t, is equal to 14 billion years, the circumference of the sphere can be calculated to be approximately

88 billion light years, ($C = 2\pi r$, or $C = 2\pi(14)$, or $C = 87.96$). Thus there will be 88 galaxies spaced 1 billion light years apart along the circumference of the sphere, which represents the universe. This is not the actual size of our universe at the present time, as we will explain later. We do know that the universe is at least this size, though, since light has been traveling in all directions since shortly after the big bang, at the speed of light, for 13.8 billion years over a distance of at least 13.8 billion light years. The size of the model is now based on the universe expanding at a constant rate (which we will adjust later to show the actual expansion rates), but we will continue to use this simplified version to show how the model works.

The model, as developed so far, is represented in **Figure 1**. The entire universe is shown on the surface of the sphere. There are 88 galaxies spaced 1 billion light years apart along the surface of the sphere. We will locate our galaxy at the north pole of the sphere. As time proceeds forward, the radius of the sphere increases.

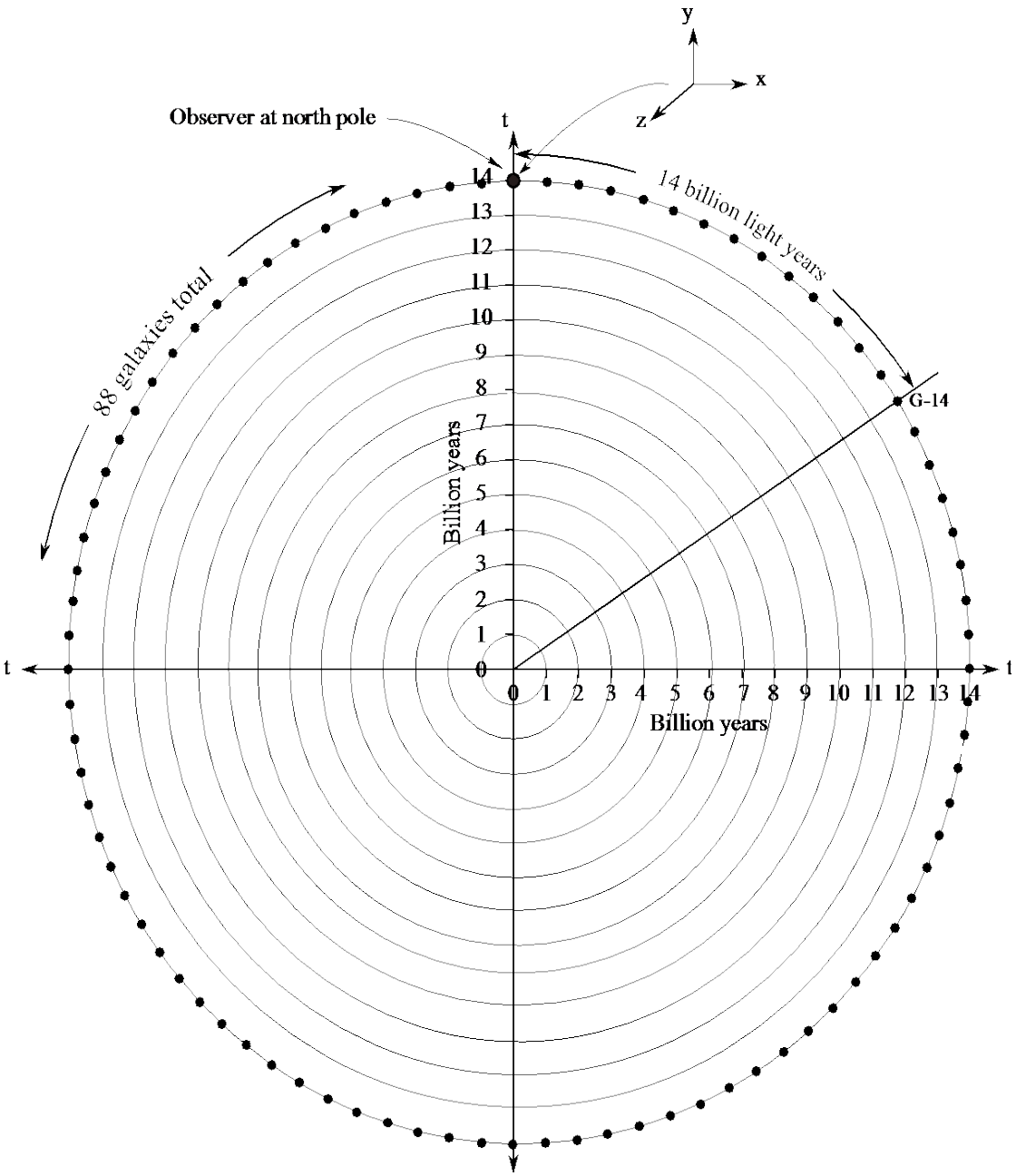

Figure 1. The model.

3. The Expanding Universe

Now that we have established the size of the model representing the universe, we can answer the question of how the model shows how the universe is expanding. The model shows the expansion every billion years by the ever increasing circles in the model that represent the universe as it expands every billion years. For example, if we use the circumference (in cross-section) of our model universe at a time of 14 billion years and compare it to the expanded circumference at a time of say, 15 billion years, the circumference of the sphere (our universe) will have expanded by approximately 7.1 percent. This number is obtained as follows: at t = 14 billion years, $C = 2\pi r$, or $C = 2\pi(14)$, or $C = 87.9$; at t = 15 billion years, $C = 2\pi(15)$ or $C = 94.2$; therefore, the percent of expansion of the universe along the surface of the sphere is (94.2 - 87.9) divided by 87.9, which is equal to 0.071 or 7.1 percent. It is interesting to note that Stephen Hawking in his book, *A Brief History of Time*, states that the universe is expanding by 5 to 10 percent every 1 billion years, based on measurements of the velocities at which other galaxies are moving away from us, using the Doppler effect [2]. What is even more interesting is that the Hubble constant, which is the current value used to determine the universes' expansion, agrees almost exactly with the above number. In a paper titled "Is the universe expanding faster than the speed of light?", Dave Rothstein from the Astronomy Department at Cornell University states that the Hubble constant "is approximately equal to 71, measured in the technically useful but conceptually confusing units of 'kilometers per second per megaparsec'. In more sensible units, the Hubble constant is approximately equal to 0.007% per million years-what it means is that every million years, all the distances in the universe stretch by 0.007%" [3]. This value is the same as 7% every billion years. His paper was written in September 2003. The present value for the Hubble constant, as determined by the Planck space mission and reported in March 2013, is now just under 68.

It should be noted that if, for example, our universe were twice as big and its circumference were 176 billion light years instead of 88 billion light years, the circumference would have to expand by approximately 12.3 billion light years over 1 billion years (instead of 6.3 billion light years) to equal 0.070 or 7 percent. This shows that the model can be easily adjusted to reflect actual experimental data.

Our model clearly shows how the size of the universe is expanding outwardly at the speed of light into the future (*i.e.*, 14 billion years of time is equivalent to 14 billion light years of distance), while the galaxies along the surface of the sphere (circumference in cross-section) are moving away from each other by approximately 7 percent over 1 billion years as we observe today. The model reflects reality in that, as we look out into space, we are looking back in time 14 billion years to the time of the big bang. As we do this, we are also looking out into space a distance of 14 billion light years. It is logical then, that the size of the universe (determined by the radius) can be expanding at approximately the speed of light while the galaxies are moving apart from each other by only 7 percent over 1 billion years as we observe today. Since this value corresponds with the actual value of approximately 7 per cent over 1 billion years, the model appears to be an accurate model.

The model shows, that if we choose a galaxy, galaxy G-7, that is now 7 billion light years away from our galaxy, located in our model on the surface of the sphere at a time of 14 billion years, it would have been 3.5 billion light years away from our galaxy 7 billion years ago at time t equals 7 billion years. The light emitted from that galaxy 7 billion years ago will travel toward our galaxy at the speed of light through an expanding universe presented by the expanding spheres in the model. We can calculate the distance light will have traveled every 1 billion years on the expanding spheres and show it on the model.

We first have to show how much the universe has expanded every billion years in the model. At time, t = 7 billion years, the circumference of the universe would be $2\pi r$, or $2\pi(7)$, which equals 43.96 billion light years. At time, t = 8 billion years, the circumference would be $2\pi(8)$ which equals 50.24 billion light years. The expansion is thus, 50.24 minus 43.96, or 6.28 billion light years. The distance increase in expansion per billion light years at time, t = 8 billion years, is 6.28 billion light years divided by 43.96 billion light years, or 0.1429 billion light years. We can make similar calculations for each year as the universe expands from 8 billion years old to 14 billion years old. While we are doing this, we can also make the similar calculations during the first 7 billion years of the universe's expansion. We are assuming that the expansion occurs at a constant rate during this time period; *i.e.*, the size of the universe, as determined by the radius, increases by 1 billion light years every 1 billion years. We will show later how the model can depict the expansion at the rates determined by current experimental data.

Now that we have calculated how much the universe has expanded from a time of 7 billion years to 8 billion years, we can determine how far the emitted light has traveled during this 1 billion year time period.

4. Light Traveling through Expanding Space

To do this, we need to know how light travels through expanding space. For example, if 2 galaxies are 1 billion light years apart, and after 1 billion years, they are now 1.1 billion years apart due to the expansion of space, how far did light travel when it was emitted from one of the galaxies 1 billion years ago? We can show by analogy presented in Appendix A, that light would have traveled the 1 billion light years (the speed of light is 1 billion light years per billion years) plus 1/2 the expanded distance. It thus would have traveled 1.05 billion light years and still be 0.05 billion light years away from the other galaxy.

We can now return to our previous example and determine how far the emitted light has traveled during this 1 billion year time period from time, t = 7 to time, t = 8. It is simply 1 billion light years plus 1/2 the expanded distance, or 1 billion light years plus 1/2 of 0.1429 light years or 1.0714 billion light years. We can again make similar calculations for the remainder of the time from 8 billion years to 14 billion years, and also, all the way back to the beginning of the universe. We will begin the calculations at a time of 380 thousand years after the big bang, which is now considered to be the time at which light was first emitted from the early universe. To be consistent, we started our calculations for the expansion of the universe at the same time, 0.00038 billion years, which is practically zero on the scale of our model. If the universe expanded at a constant rate of 1 billion light years per 1 billion years during its first billion years, the expansion per billion years is approximately 1 billion light years. The distance light traveled during this time period is the distance it traveled at the speed of light from the time light was first emitted to 1 billion years, or approximately 1 billion light years, plus 1/2 the expanded distance (1/2 of 1 billion light years), or a total of 1.5 billion light years. These calculations are shown in **Table 1**.

Using **Table 1**, we can now show how the light emitted from galaxy, G-7, at a time of 7 billion years travels toward our galaxy. We have plotted the light beginning at time, t = 7, and calculated what the remaining distance

Table 1. Expansion at a constant rate.

Time, t (BY)	Radius, r (BLY)	Circumference, C (BLY) & diff.		Expansion per BLY, (BLY)*	Distance light traveled (BLY)	% Expansion**
14	14	87.90	6.28	0.0769	1.0385	7.7
13	13	81.64	6.28	0.0833	1.0417	8.3
12	12	75.36	6.28	0.0909	1.0455	9.1
11	11	69.08	6.28	0.1000	1.0500	10.0
10	10	62.80	6.28	0.1111	1.0555	11.1
9	9	56.52	6.28	0.1250	1.0625	12.5
8	8	50.24	6.28	0.1429	1.0714	14.3
7	7	43.96	6.28	0.1667	1.0833	16.7
6	6	37.68	6.28	0.2000	1.1000	20.0
5	5	31.40	6.28	0.2500	1.1250	25.0
4	4	25.12	6.28	0.3333	1.1667	33.3
3	3	18.84	6.28	0.5000	1.2500	50.0
2	2	12.56	6.28	1.0000	1.5000	100
1	1	6.28	6.28	1.0000	1.5000	100
0+	0.00038	0.002	N/A	N/A	N/A	N/A
					16.0901 total	

BY = billion years. BLY = billion light years. *Increase in circumference divided by the previous circumference. **Increase in circumference divided by the previous circumference in percent.

is to our galaxy as it travels through expanding space. For example, as the emitted light travels from time, t = 7 to t = 8, we calculate the total distance the universe expanded between our galaxy and the place at which the light was emitted during this time, which is 3.5 billion light years, plus (0.1429 times 3.5 billion light years), and then subtract the distance light traveled, 1.0714 billion light years, during this time period. The result is 2.9288 billion light years remaining to our galaxy. Similar calculations can be performed as the light continues to travel toward our galaxy each billion years. These calculations are shown in **Table 2**. The table shows that the emitted light will have reached our galaxy after traveling through expanding space for 4.52 billion years, at a time of 11.52 billion years. This is also shown in **Figure 2**.

5. Our Visible Universe

Now that we know how the stage 1 model represents the universe and know how calculations are made with it, we can show how the model describes our visible universe. Remember, our entire universe, as it exists now, is shown on the surface (circumference in cross-section) of the sphere at a time of t = 14 billion years. Our visible universe will be shown on the model as a shape determined by the light beams now reaching our galaxy from all the galaxies in the universe from the time they first emitted light. Just as in the previous example where we plotted the light emitted 7 billion years ago from galaxy, G-7, to where it reached our galaxy a little over 2 billion years ago, we can begin plotting the light which we are now receiving at our galaxy at a time of 14 billion years, and trace it backwards in space and time on the model. We can use the calculations presented in **Table 1** to plot the light back to a time of 380 thousand years after the big bang. This is shown in **Figure 3**. The shape of the visible universe appears as a tear drop shaped figure in cross section, with a slightly indented bottom, in 3 dimensions (2 space and 1 time).

When we look far out into space with our telescopes, we are seeing galaxies as they existed billions of years ago. We can, for example, select galaxy G-28, which is now 28 billion light years away from our galaxy, and determine by our model that it is now in our visible universe, and we are just now seeing it as it existed when our universe was about 2 billion years old. We can also determine that our galaxy and galaxy G-28 were about 4 billion light years apart when the light which we are seeing was emitted from galaxy G-28. (This is the distance between the 2 galaxies measured along the circumference at a radius of 2 billion light years). The visible universe in the model is a tear drop shaped globe that extends from our galaxy out in all directions along the surface of the globe for a distance of 16.09 billion light years.

Now that we have created our basic stage 1 model, we can make some adjustments to it. We mentioned earlier that we developed the model based on our universe expanding at a constant rate. Data obtained recently by telescope shows that the expansion of the universe was actually decelerating for its first 8 billion years, and then the expansion began to accelerate. Zosia Rostomian, Lawrence Berkeley National Laboratory, and Nick Ross, BOSS Lyman-alpha team, Berkeley Lab, have developed a graph based on data from a spectroscopic survey

Table 2. Light emitted from G-7 at time, t = 7 billion years.

Time, t (BY)	Radius, r (BLY)	Circumference, C &diff. (BLY)		Expansion per BLY, (BLY)*	Distance light traveled (BLY)	Distance remaining (BLY)
14	14	87.90	6.28	0.0769	1.0385	
13	13	81.64	6.28	0.0833	1.0417	
12	12	75.36	6.28	0.0909	1.0455	−0.4811
11	11	69.08	6.28	0.1000	1.0500	0.5174
10	10	62.80	6.28	0.1111	1.0555	1.4249
9	9	56.52	6.28	0.1250	1.0625	2.2324
8	8	50.24	6.28	0.1429	1.0714	2.9288
7	7	43.96	6.28	0.1667	start	3.5

BY = billion years. BLY = billion light years. *Increase in circumference divided by the previous circumference.

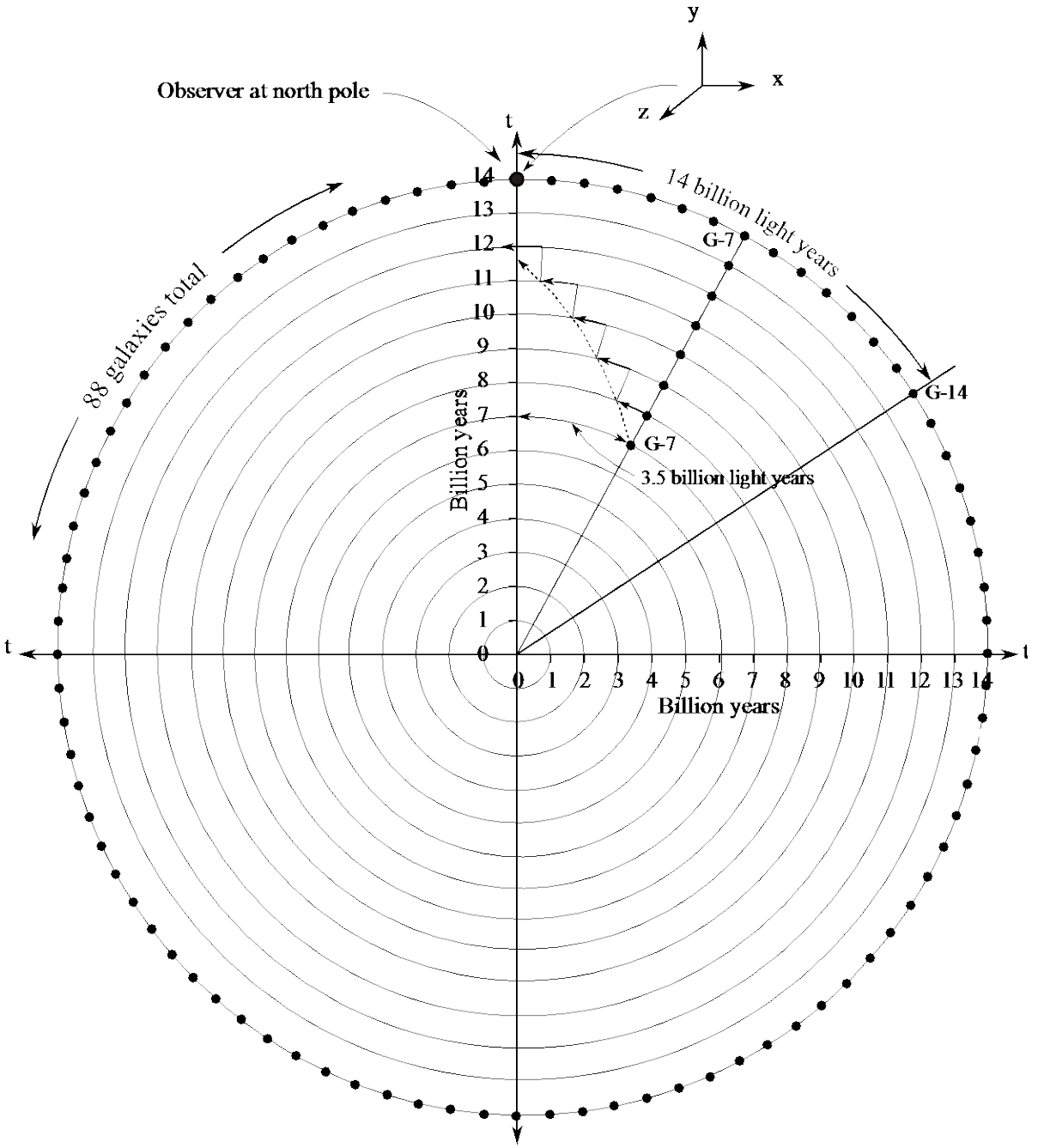

Figure 2. Light emitted from galaxy G-7.

(Boss Sloan Digital Sky Survey-III, November, 2012) that depicts this changing expansion [4]. This graph is shown in **Figure 4**.

We can change our model to mirror the data in this graph by increasing or decreasing the size of our model (circumference in cross-section) each billion years to match the deceleration and acceleration shown in the graph. For example, to show the rapid decrease in expansion during the first billion years, the size of the universe, as determined by the radius of the model, had to be expanding by billions of light years during the first billion years. Then, as the deceleration slowed down and leveled out at about a time of 8 billion years, the radius was expanding at a rate considerably slower than its current rate of about 6.9% every billion years. The expansion then began to slowly accelerate. The radius of the expanded model has to be large enough to mirror this expansion.

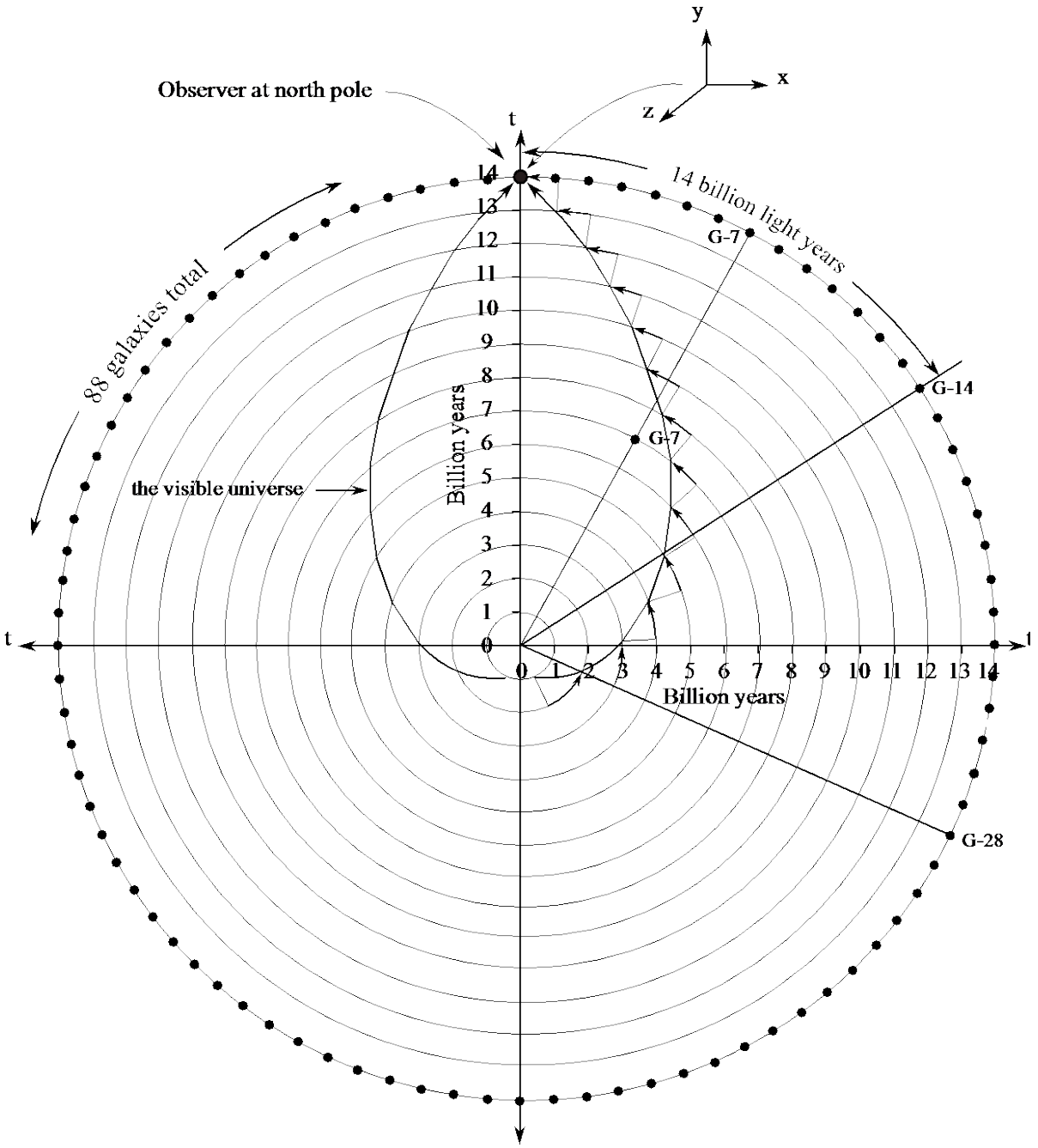

Figure 3. The visible universe.

It also has to reflect current consensus about the size of our visible universe. The most important for our model is the general agreement in the literature that the galaxies that we can observe when the universe was less than a billion years old, and their light has taken over 17 billion years to reach us, are now about 46 billion light years away from us. This is shown as galaxy, G-46 on the model. To reflect this result, the radius of the model has to be about 40 billion light years. This is all shown in **Table 3**, in column 2 (change in radius), and in column 6 (% Expansion). It is also shown in **Figure 5**. It should be noted that at a time of 14 billion years (now), the model shows that the universe is expanding at a rate of 6.9%, which relates very closely to the current value of the Hubble constant.

The model in **Figure 5** shows both the new time and corresponding radius measurement on the vertical axes.

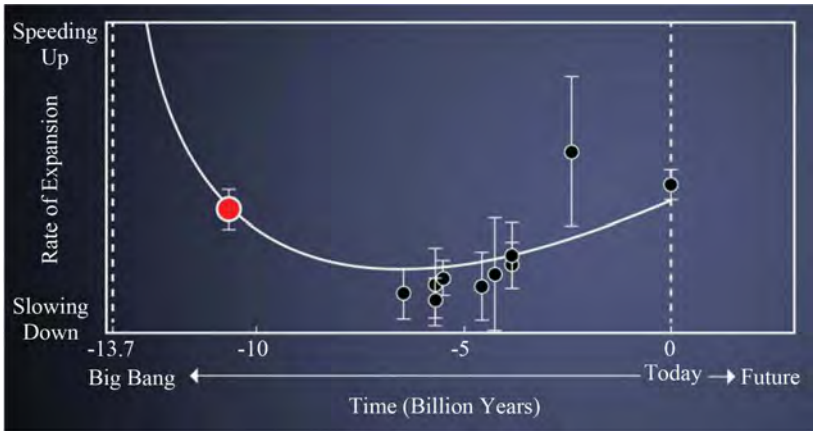

Figure 4. Expansion of the universe (Credit: Zosia Rostomian, LBNL; Nic ross, Boss lyman-alpha team, LBNL).

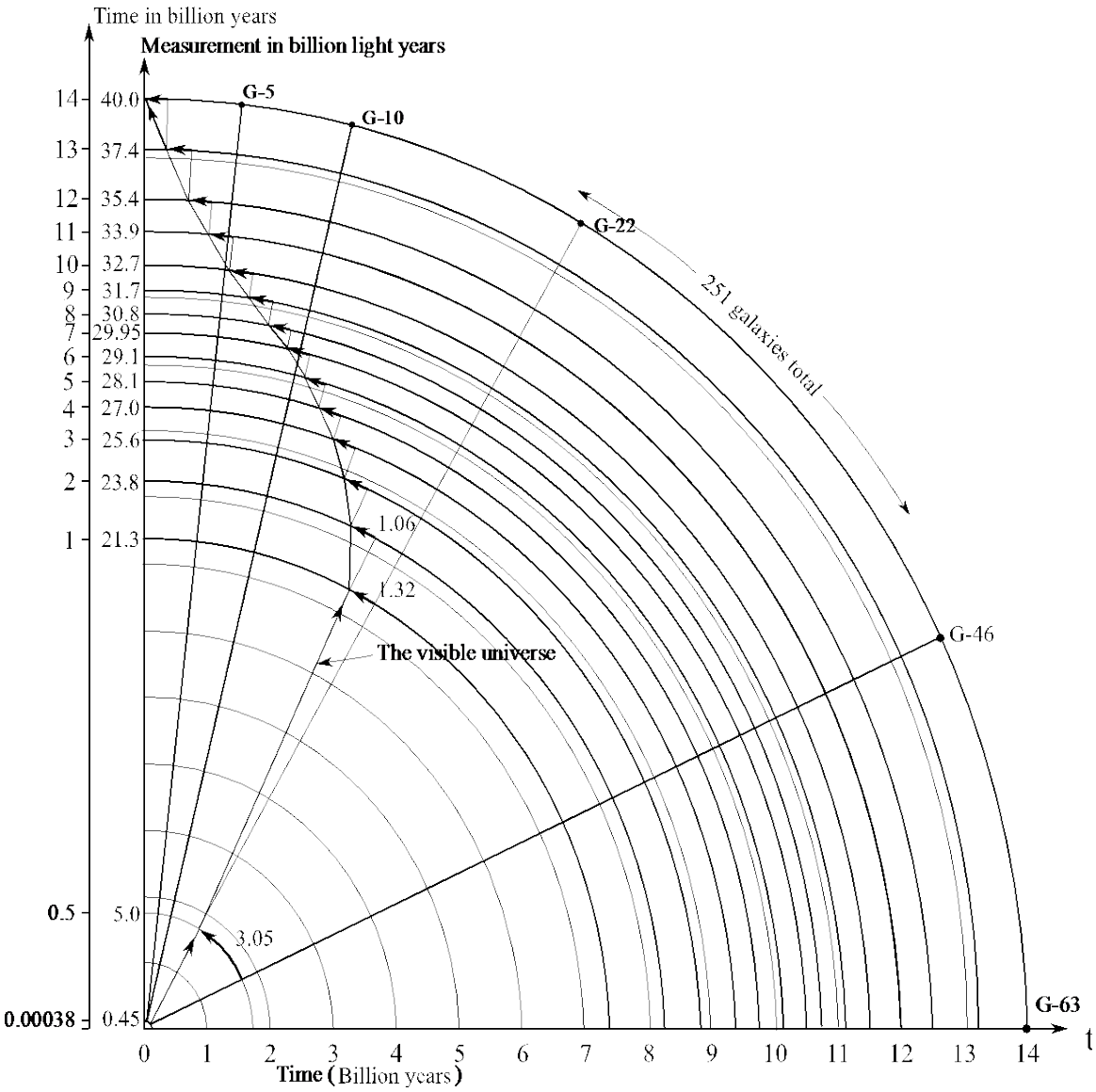

Figure 5. Expansion of the universe at observed rate.

Table 3. Expansion at observed rate.

Time, t (BY)	Radius, r (BLY)	Circumference, C (BLY) & diff.		Expansion per BLY, (BLY)*	Distance light traveled (BLY)	% Expansion**
14	40.0	251.2	16.3	0.0694	1.0347	6.9
13	37.4	234.9	12.6	0.0567	1.0284	5.7
12	35.4	222.3	9.4	0.0442	1.0221	4.4
11	33.9	212.9	7.5	0.0365	1.0183	3.7
10	32.7	205.4	6.3	0.0316	1.0158	3.2
9	31.7	199.1	5.7	0.0295	1.0148	3.0
8	30.8	193.4	5.3	0.0282	1.0141	2.8
7	29.95	188.1	5.4	0.0296	1.0148	3.0
6	29.1	182.7	6.2	0.0351	1.0176	3.6
5	28.1	176.5	6.9	0.0407	1.0204	4.1
4	27.0	169.6	8.8	0.0547	1.0274	5.5
3	25.6	160.8	11.3	0.0756	1.0378	7.6
2	23.8	149.5	15.7	0.1173	1.0587	11.7
1	21.3	133.8	102.4	3.2611	1.3153	326
0.5	5.0	31.4	28.6	10.20	3.0500	1020
0.00038	0.45	2.8	2.8	N/A	N/A	N/A
0	0	0	0	N/A	N/A	N/A
					17.6902	

BY = billion years. BLY = billion light year. *Increase in circumference divided by previous circumference. **Increase in circumference divided by the previous circumference in percent per BLY.

Note that at a time of 380,000 years when light was first emitted throughout our universe, its radius was 450 million light years. The galaxies that were just being formed at that time are now about 46 billion light years away from our galaxy. They are represented by galaxy G-46 on the model. Galaxies that are more distant than that, such as galaxy G-63, are not in our visible universe. We have also shown galaxy G-5 that was in our visible universe at a time of 10 billion years, galaxy G-10 at a time of 6.5 billion years, and galaxy G-22 at a time of 0.5 billion years. These will be used later when timelines are needed.

6. The Fourth Space Dimension

The next adjustment we can make on the model presents us with a paradigm shift in how we view our universe. Earlier, when we first developed our model, we described how all 3 space dimensions exist on the surface of the sphere and how the height dimension (thickness of the sphere) also represents the present time. To develop the true height dimension at any point on the sphere, we can rotate the sphere at that point.

If we look at **Figure 1**, which we will now call stage 1 of the model, and locate ourselves at the north pole of the sphere at t = 14 billion years, we can visualize the universe as the surface of the sphere in 2 lateral dimensions. To obtain the third dimension; *i.e.*, the height dimension, we can rotate the sphere 90 degrees about the north pole, and now the 2 lateral dimensions include the height dimension. As we rotate the sphere, it is important that we maintain our true distances along the surface of the sphere, which means, for example, that the distance of 17.69 billion light years from our galaxy to the most distant galaxy in our visible universe (and actually, back to the time light was first emitted in our universe about 380,000 years after the big bang) will become the new radius of our rotated sphere. We are changing the orientation of the sphere so that the original "up" direction is now pointing in the left horizontal direction in **Figure 6**. The important point is that this 4-space dimension universe is now experiencing the two different orientations at the same time. As 3 dimensional beings, we cannot do the same. We should also note that as the orientation of "up" changed, the center of the universe at t =

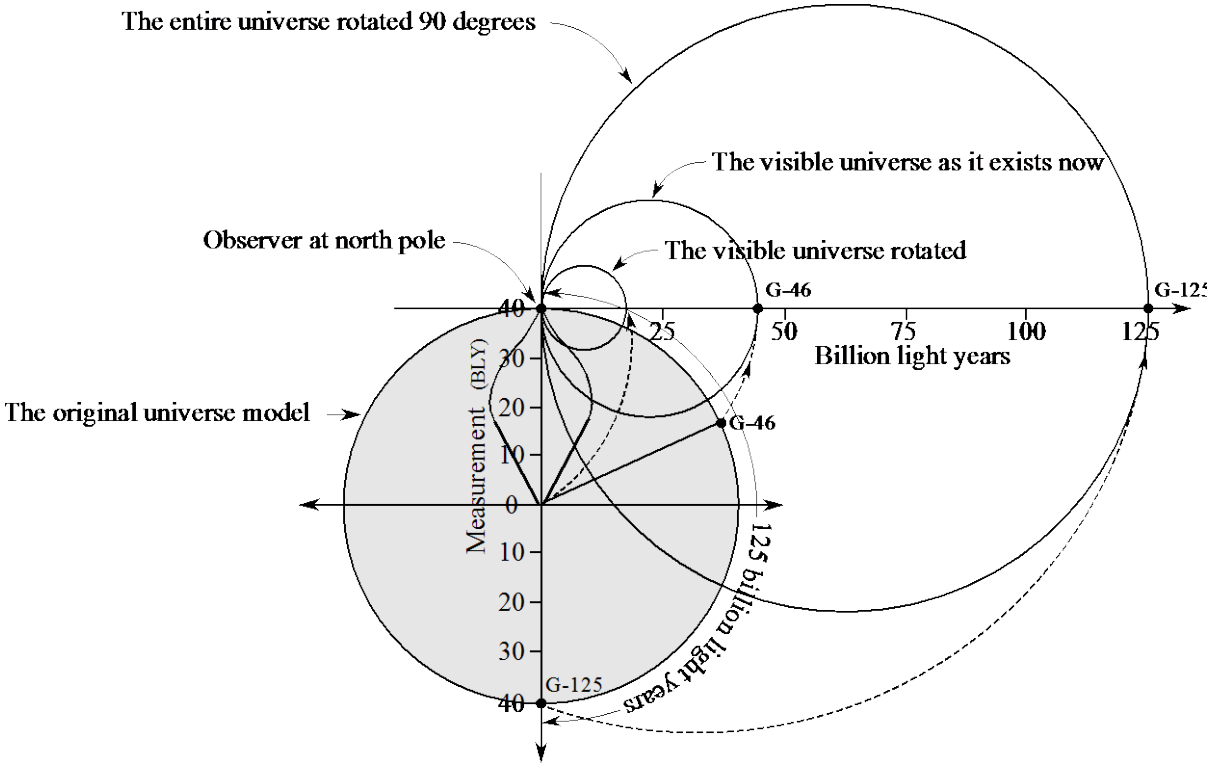

Figure 6. The universe rotated 90 degrees.

0; *i.e.*, the big bang, changed so that it is now also located in a horizontal direction to the right from the north pole as in **Figure 6**.

In **Figure 6**, we are not rotating the entire original universe model. We are rotating the spheres, which represent distances and space, into the radii which represent time, at the location of the observer at a single time of 13.8 billion years. We are rotating the surface of the sphere representing the entire universe which will have a radius of 125 billion light years, and the surface of the visible universe as it exists now, which will have a radius of 46 billion light years. Each will have the same timeline, as shown on the vertical axis in **Figure 5**, on its radius which we will show after its complete rotation in **Figure 7**. The rotation of the original visible universe is more complicated because it includes both distance and time, not just distance. The original visible universe represents the distances light traveled during 14 time periods from the observer back to 380,000 years. It is a representation of the distances light traveled over time which is speed, or velocity. The actual distances light traveled are the arrows on the 14 different circumferences in **Figure 5** that add up to a total distance of 17.69 billion light years. This is what is being rotated and shown in **Figure 6**. It will have its own timeline which stretches back to 380,000 years.

If we now change the "up" direction to all possible directions by rotating the spheres about the north pole in all possible directions, and the universe experiences all these different orientations at the same time, the model will now represent the entire universe with its center at the north pole. In addition, the surface of the initial universe will now have completely populated the volume of the large sphere, shown as the entire universe, as shown in cross-section in **Figure 7**. By changing the orientation of the surface of the sphere to all possible orientations, we have picked up all the galaxies that exist throughout the universe. By rotating the surface of the sphere (space) in all possible directions (time), we have merged space with time and developed 4-dimensional space-time which we experience in our real world today.

By using orientation as a 4th space dimension, our model, which we can now call stage 2, now reflects our 3-space dimension world as we know it. We are 3-dimensional beings who can experience only one orientation (or "up" direction) at a time. We cannot experience all possible orientations at the same moment in time; whereas the universe does "experience" all possible orientations at the same time as shown in **Figure 7**. We are 3-space dimensional beings living in a 4-space dimensional universe. This is analogous to the 2-dimensional

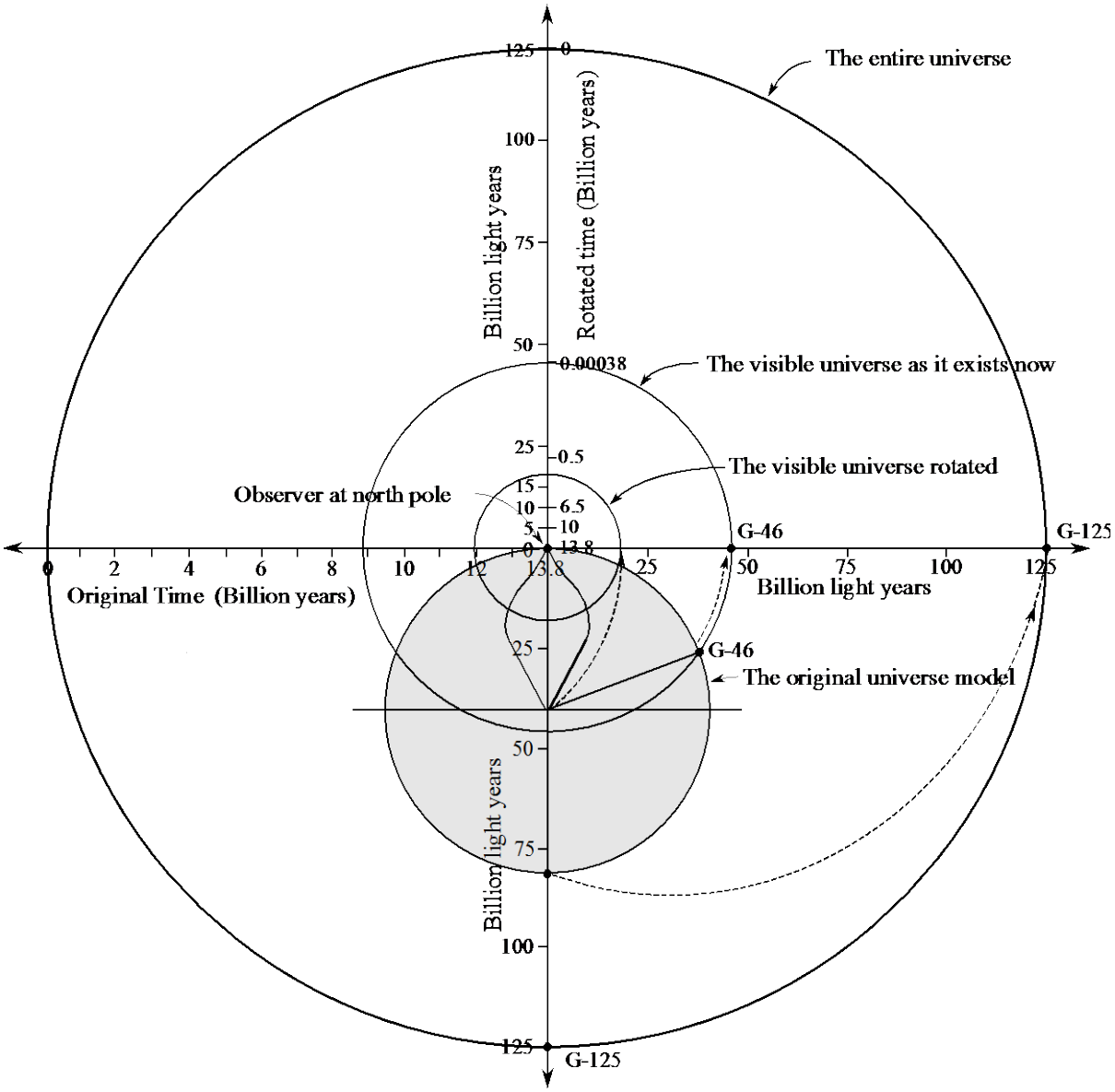

Figure 7. The stage 2 model with 4 space dimensions.

being living on a horizontal plane at one arbitrary height level who cannot experience the third dimension of height since there is no "up" direction in his flat 2-dimensional world. There are only 2 horizontal directions. In other words, in a 2-dimensional world, an intelligent square cannot become, or even conceptualize becoming a cube since the flat square can experience only one height level at a time. Being 2-dimensional, the square cannot experience many height levels at the same time, even though they may exist all around the square, or else the square could then become a 3-dimensional cube and no longer be 2-dimensional.

The model shown in **Figure 7** includes 4 space dimensions (width, height, depth, and orientation) and the time dimension. The timeline for the rotated distances of the entire universe, and the rotated distances of the visible universe as it exists now, are shown on the right side of the top of the vertical axis. They are based on the distances to galaxies G-5, G-10, G-22, and G-46 at the times at which they appeared in our visible universe as presented in **Figure 5**. For example, in **Figure 5**, the distance to galaxy G-10 along the circumference of the sphere at a time of 14 billion years (now) is 10 billion light years. When we track it back in time to where it intersects the line representing our visible universe, it appears in our visible universe at a time of 6.5 billion years (on the far left vertical axis). Thus, in **Figure 7**, a time of 6.5 billion years corresponds to a distance from the

observer (our galaxy) of 10 billion light years. Likewise, the distance of 46 billion light years to galaxy G-46 corresponds to a time of 380,000 years after the big bang, and the farthest distance to galaxy G-125 corresponds to a time of zero at the big bang. These last two distances and times are the numbers that will be used in the calculations to explain dark matter and dark energy. Another version of the model is shown in **Figure 8**, again in cross-section.

In **Figure 8**, the volume of the outer sphere represents our entire universe. It has a radius of 125 billion light years. The surface of the outer sphere represents the time of the creation of the universe, the big bang, at a time of 13.8 billion years ago. The volume of the middle sphere (The visible universe as it exists now, in **Figure 8**) represents all the galaxies in our visible universe as they exist now. It has a radius of 46 billion light years. This shows that the galaxies which were being formed, and we now observe just after the time of recombination at a time of 380,000 years, (and it has taken 17.7 billion years for their light to reach us), are now about 46 billion light years a way from us. The volume of the smallest sphere (The visible universe rotated, in **Figure 8**) represents our visible universe which we can observe in our telescopes. It has a radius of 17.7 billion light years. The surface of this sphere also represents the time of recombination when light was first emitted in the universe,

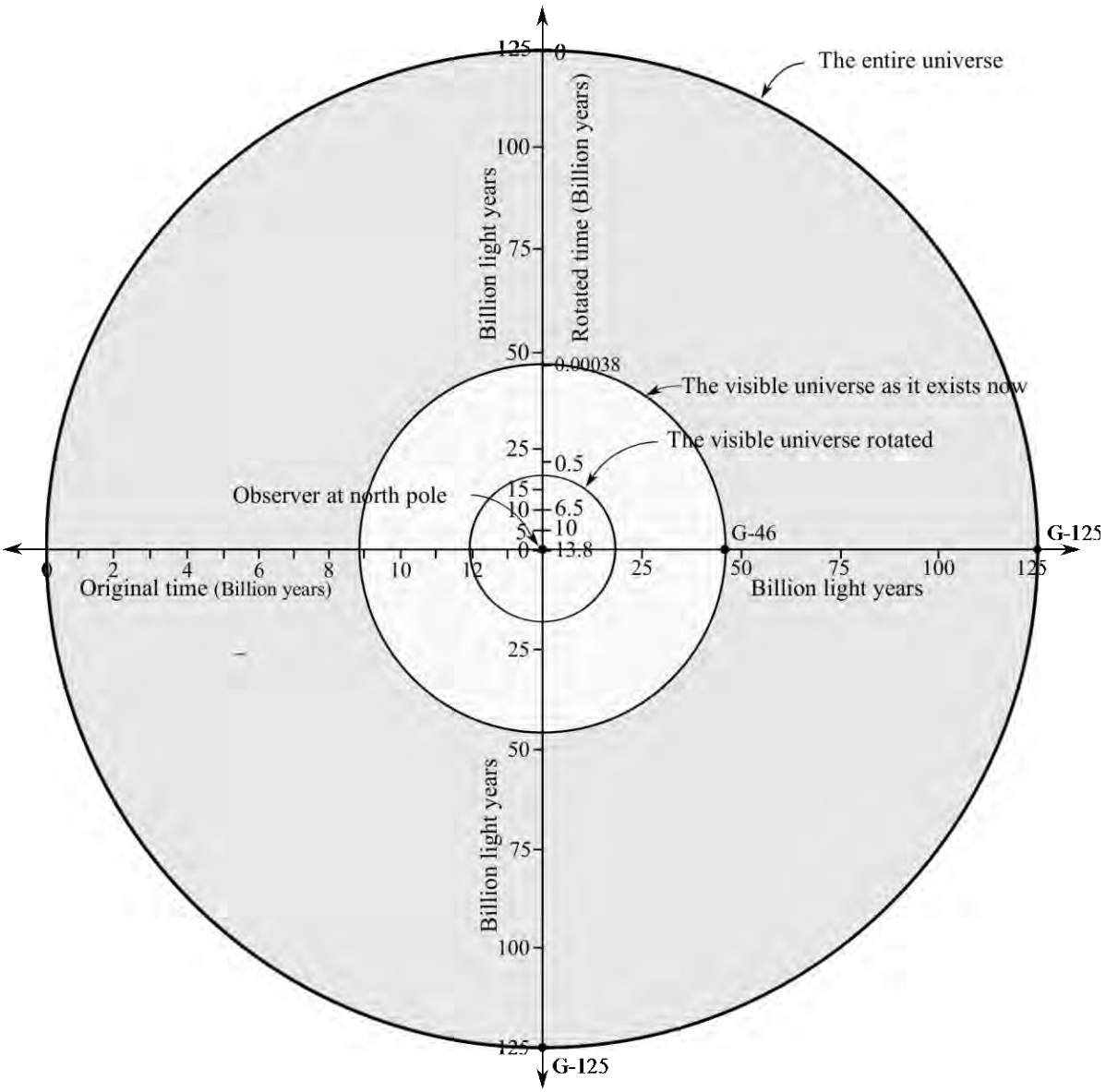

Figure 8. The simplified version of the stage 2 model.

at a time of 380,000 years after the big bang.

We can now make some calculations. We can compare the volume of the visible universe as it exists now (not as it existed in the past represented by the smaller visible universe), to the volume of the entire universe as it exists now. This will then give us the percentage of visible matter (baryonic) that we can now detect in our visible universe, compared to the amount of baryonic matter in the entire universe. Using the formula, $V = \frac{4}{3}\pi r^3$, the volume of the visible universe as it exists now, with a radius of r = 46 billion light years, is 407,513 cubic billion light years. The volume of the entire universe, with a radius of r = 125 billion light years, is 8,177,083 cubic billion light years. The ratio is thus, 20.7. This is almost exactly the same as the ratio of visible matter in the visible universe determined by the Planck space mission, compared to the total of all matter, including dark matter and dark energy, in the universe. Recent NASA Planck space mission data reported in March 2013 show that the early universe was 4.9 percent real (visible) matter in the form of atoms, 26.8 percent unseen dark matter and 68.3 percent unseen dark energy. Thus, the ratio of visible matter to all matter in the universe including dark matter and dark energy is 100 divided by 4.9, or 20.4. The model explains what the dark matter and dark energy is. It is the rest of the normal matter in the entire universe that is not visible to us because it is not in our visible universe.

We can now discuss dark matter and dark energy, but before we do, we should look again at the model in **Figure 8**. The dark area between the visible universe as it exists now, and the entire universe, contains the real matter (baryonic) that exists in the dark area that produces the gravity in our visible universe that we refer to as dark matter and dark energy. Dark matter and dark energy are in our visible universe simply as gravity, not as matter. This will be discussed in detail later. We know they are there because of their gravitational effects upon the stars in our galaxies and the accelerated expansion of the universe. They make up 20.7 times the amount of visible matter in our visible universe. The model also shows how time (on the top half of the vertical axis) extends from zero at the time of the big bang at a distance of 125 billion light years away from our galaxy, to a time of 0.00038 billion years at the beginning of our visible universe as it exists now at a distance of 46 billion light years away from our galaxy, to a time of 13.8 billion years after the big bang at our galaxy.

This stage 2 model reflects the reality of our world in several striking ways. Have you wondered why, for example, when the Hubble space telescope sends us a picture of galaxies in the universe many billions of light years distant from us and many billions of years back in time as they existed maybe only a billion years after the big bang, that the telescope can send us a similar picture when it is pointed in the opposite direction? In fact, it would send us a similar picture no matter in what direction it is pointed. In our real world, the big bang appears to be located out in space in all directions. The center of the universe where it all began appears to be located all around us in a sphere far, far away. This model explains why. Actually, our 3 space dimension model, stage 1, in **Figure 1** shows that the center of the universe began at a single point which is at time t = 0, just as our logic would tell us. If we are at the north pole in **Figure 1** and look out into space at a galaxy, say, 7 billion light years away, we are not looking out along the surface of the sphere that represents the universe as it exists now. As mentioned earlier, we are actually looking back in time 7 billion years, due to the fact that it took light from the galaxy 7 billion years to reach us, and see the galaxy as it existed in a smaller universe; *i.e.*, a smaller sphere with a radius equal to t = 7 billion years where all the galaxies are much closer together. If we look out farther and farther into space, we are looking back into time billions of years more to a much smaller sphere where all the galaxies are much closer together until eventually, at 14 billion years, and over 16 billion light years away (based on expansion at a constant rate), the sphere becomes a point no matter in what direction we look from the north pole.

There is another way to visualize this. We mentioned earlier when we were explaining how the model can represent the changing rates of expansion of the universe, that light was first emitted in the early universe about 380 thousand years after the big bang. This time is commonly referred to as the time of recombination. We are now receiving this light as radiation, detecting it in telescopes, and calling it the Cosmic Microwave Background (CMB) radiation. It is coming from hot clumps of gas and atoms, which would become stars and galaxies, which are spread throughout a sea of hot plasma. We are receiving it from all directions from outer space. When we look at a map of the CMB, we are looking at a flat projection of the radiation coming from the inside surface of a giant sphere, where we are at the center and located many billions of light years away from the surface. The CMB was first detected over 50 years ago. What we need to realize is that the CMB we are receiving now is not

the same CMB we received 50 years ago. The CMB we are receiving now is from matter in the early universe that was about 50 light years closer to the point at which the universe began, and 50 light years farther away from us than the CMB from 50 years ago.

We on earth, in the Milky Way galaxy, had our beginning in one of these hot clumps of gas and atoms located somewhere within this giant blob of extremely hot plasma. At the time of recombination, the universe had already expanded at such a rate that the clumps were moving apart from each other so fast that it is just now after more than 13 billion years, that light from some of these clumps is reaching us. We can visualize ourselves in this expanding blob where everything is moving away from us in all directions. The galaxies that are now closer to us were the clumps that were closer to us, and we received their first light, their CMB, billions of years ago. The CMB we are now receiving is from clumps so far away, or moving away so fast, that it has taken over 13 billion years for us to receive it. As the years go by, we will be receiving the CMB from the clumps that were even farther away from us at the time of recombination. As we go back deeper in space and farther in time, we encounter the rest of the universe that is not yet visible to us, back to the time of the big bang. Depending upon how fast the universe is expanding, we may never receive the CMB from the most distant clumps that are now galaxies 125 billion light years away from us in our model. This visualization shows how the model represents our perception of the universe as we look out into space. It shows how the big bang and the CMB can actually appear to exist in a sphere all around us, and come from all directions in space.

This 5-dimensional model (4 space dimensions and the time dimension) can be used to show another very interesting result. In **Figure 8**, if we look at the surface of the sphere at time, $t = 0$, the big bang, the model shows us that time is proceeding inward in the universe. In the model, this means that the sphere at time, $t = 0$, becomes larger as time progresses inward, and the time radius ends at the observer. In real life, this reflects the fact that time progresses from the past to the present where the observer exists. As the observer looks out into space in any direction, the observer is looking back in time and sees things as they were in the past. As the future develops into the present from the point of the observer, the timeline of the past increases, as shown in the model as the $t = 0$ sphere becomes larger. As the size of the entire universe increases, all the visible matter expands outward from the observer, just as current experimental data confirms. To be more exact, this shows that the observer is moving away at an increasing rate from all the matter observed all the way back to the big bang. For example, when current data using the Doppler effect shows that a galaxy 10 billion light years away from our galaxy is moving away at a faster rate than one that is 5 billion light years away, it shows that the distance between our galaxy and a galaxy that we now observe where it was 10 billion years ago, is increasing faster than the distance between our galaxy and a galaxy we now observe where it was 5 billion years ago. If these other two galaxies still exist now, it means that the galaxies are mutually moving away from each other in a universe that is expanding at an accelerating rate. This is what our model shows.

Another comment should be made regarding the model. Can "orientation" really be a 4^{th} space dimension? Included in the Appendices to this paper are two examples of how and why orientation needs to be considered as a 4^{th} space dimension. The examples are presented as stories, similar to thought experiments that a teacher in a space dimension class delivers to his students. The first one is titled, "The Space Dimension Class", and the second one is titled, "Lost in Space".

Also, in his book, *The Elegant Universe*, Brian Greene tells the story of how, in 1919, a mathematician named Theodore Kaluza suggested that there may be more than 3 space dimensions. His theory involved using equations analogous to those Albert Einstein used in his general theory of relativity, but included a 4^{th} space dimension and the time dimension instead of Einstein's 3 space dimensions and the time dimension. As a result, he found extra equations. He realized that the extra equations "were none other than Maxwell had written down in the 1880's for describing the electromagnetic force! By adding another space dimension, Kaluza had united Einstein's theory of gravity with Maxwell's theory of light" [5].

Brian Greene continues to relate how further detailed study of Kaluza's proposal showed that it conflicted with experimental data. "The simplest attempts to incorporate the electron into the theory predicted relations between its mass and its charge that were vastly different from their measured values" [6]. As a result, many physicists lost interest in Kaluza's idea. In the 1970's and 1980's, interest began again to focus on extra space dimensions as string theory evolved. String theory attempts to unify the fundamental forces of nature and requires up to 10 space dimensions and one time dimension. All the extra space dimensions are considered to be "curled-up" dimensions at every point in our familiar 3-dimensional space. They are required to be so microscopic that we cannot observe them. These are completely different than the proposed extra space dimension

called orientation. As discussed thus far, orientation is a large space dimension that is equivalent to height, width, and depth, and is a dimension we observe in our daily lives. We just cannot experience more than one particular orientation at a time, whereas the 4-dimensional universe does. It would be interesting if the physicists and mathematicians could formulate equations to represent orientation as the 4^{th} space dimension, and see if this would correct the experimental data problems experienced by Kaluza when he had united Einstein's theory of relativity with Maxwell's theory of light. It should be noted that orientation cannot be represented mathematically nor graphically as some combination of the 3 familiar space dimensions. There has to be an additional framework upon which the 3 space dimensions of height, width, and depth are oriented to show which way is "up". It is a completely different space dimension that is required to represent or describe an object in space.

Before we discuss dark matter, it is important to emphasize that this stage 2 model was developed from the perspective of the observer, which is how we view and study our universe. We are not at the center of our universe. All the galaxies 125 billion light years away from us at the surface of the larger sphere in the model are not at the edge of the universe any more than our galaxy is at the edge of the universe from the perspective of an observer in one of those galaxies who has developed a similar model. Again, everything on the outside of the model, which represents our universe, is the future.

7. Dark Matter

What is dark matter? Dark matter is commonly defined as a hypothetical form of matter that is believed to make up over 90 percent of the matter in the universe but is invisible in that it does not absorb or emit light, and does not collide with atomic particles but exerts gravitational force. Originally it was the so-called "missing matter" in the universe that was needed to account for the motions of the stars in numerous galaxies observed by astronomers. Once it was discovered that all observed galaxies had up to ten times more invisible or dark matter than visible matter, it was no longer called "missing" because it had then been discovered.

There is another form of dark matter that must exist if the big bang inflation theory is correct. This theory, among other things, is used to explain how matter in galaxies now very distant from each other could have communicated with other matter before, during, or immediately after the big bang. This has reintroduced a "missing matter" form of dark matter in addition to that in and around the galaxies. The inflation theory implies that there must be up to another ten times more dark matter than visible matter in the universe, which means that very little of the universe is composed of visible matter. Much of this "missing matter" may also be in the form of dark energy, which was postulated in the late 1990's to necessarily exist to cause the acceleration of the expansion of the universe and is detectable only through its gravitational effects. As mentioned earlier, NASA Planck space mission data show that the early universe was 4.9 percent real visible matter, 26.8 percent unseen dark matter and 68.3 percent unseen dark energy.

When we compared the volume of the entire universe to the volume of the visible universe in our model, the ratio came out to be 20.7 to 1. This means that if our visible universe contains only 4.9 percent real visible matter, then our entire universe must contain 20.7 times that, or a total of 101 percent matter that is real matter, but is not observable in our visible universe at the present time. This is an amazing result which can explain from where the dark matter and dark energy in our visible universe is coming. Since the entire universe contains 20.7 times as much real matter as there is in our visible universe, and we are calling it dark matter and dark energy, the value of 101 per cent is essentially the same as the 100 per cent total of visible matter, dark matter, and dark energy (4.9%, 26.8%, 68.3%) reported by the NASA Planck space mission. The dark matter and dark energy in our visible universe is not matter, it is gravity from all the real matter in our entire universe. Remember, dark matter was originally introduced to account for the gravity that has to exist in galaxies to cause the rotation of the stars in the galaxies. It does not have to be matter. It can simply be gravity.

An important point to realize is that this does not contradict current theories and explanations that dark matter and dark energy cannot be real matter made of atoms (baryonic) due to other reasons, such as nucleosynthesis, and calculations showing that our universe is flat and at its critical density. The result above still agrees with the results of other calculations that real matter can only be about 4.9% of all the matter (gravity) in the universe. The 4.9% real matter still remains in our model. The model shows that there is just 20.7 times more of it in our entire universe, which is producing 20.7 times more gravity in our entire universe (including our visible universe) than can be produced by the real visible matter in our much smaller visible universe. The percent of real matter in the entire universe is still 4.9%. We can now show how the gravity that exists in our visible, observable un-

iverse, which we now call dark matter and dark energy, is the gravity produced by all the real matter in the rest of the universe.

We first of all have to show how gravity can appear to act instantaneously throughout the universe, because an immediate argument is that we must disregard all matter outside of our visible universe because its effects or influence cannot travel faster than the speed of light. The counter argument is that all the dark matter and dark energy outside of our visible universe affects the expansion of our visible universe because it is part of the entire universe, not because its effects have to travel to the visible universe. We can show this by using one of Sir Isaac Newton's gravitational laws, and also using a modification of Alan Guth's inflation theory which will include gravity.

8. Gravity as Dark Matter and Dark Energy

One of Sir Isaac Newton's gravitational laws explains how the effects of gravity from all the stars and matter in a galaxy can be analyzed. For example, how do all the stars and matter in the Milky Way galaxy affect the sun in its orbit around the center of the galaxy? Donald Goldsmith, in his book, *The Astronomers*, presents a very good explanation of this law and how it predicts the motion of stars in galaxies [7]. The first part of Newton's law states that all the stars and matter outside the sun's orbit can be ignored, because their gravitational effect on the sun and its orbit cancels itself out. The second part states that the gravitational effect of all the stars and matter inside of the sun's orbit can be concentrated at the center. This by the way, was the law that was used to discover the dark matter that exists in a halo effect around galaxies to account for the faster than expected motion of stars in the outer orbits of the galaxies.

If we apply the second part of this law to our model in **Figure 8**, we can simply state that the gravitational effect from all the galaxies and matter inside the outer sphere (representing the entire universe) at a distance of 125 billion light years from the center, can be concentrated at the center. The center is where we exist as the observer in our galaxy. Any other observer in any other galaxy in the universe will likewise be at their center. This means that the gravitational effects of all the matter in the universe are spread out fairly uniformally throughout the universe. Each observer in each galaxy is feeling the concentrated effect of gravity from all the galaxies in the universe. This is how all the real matter in the entire universe, which is 20.7 times the visible matter in our visible universe, can produce the gravity in our visible universe which we are calling dark matter and dark energy.

A modification of Alan Guth's inflation theory can explain how the gravitational effects from all the galaxies in the universe can be spread throughout the universe, even though the galaxies are separated by distances much greater than light could have traveled between them. The first part of this modification relies on the fact that, in the evolution of the universe, gravity separated itself from the other forces of nature before the inflationary period of the universe began. Brian Cox, in his book, *Wonders of the Universe*, presents a graphic which shows the timeline of the universe from the beginning of time at the big bang, to the present [8]. It shows that the Planck Era, which is the time when gravity separated from the other forces of gravity, began at a time of 10^{-43} seconds. It shows that the Grand Unification Era, which is the time when the strong nuclear force splits from the other forces, began at a time of 10^{-36} seconds. The Inflation Era began at the end of the Grand Unification Era. It is generally agreed that the period of inflation occurred from 10^{-36} to 10^{-32} seconds. The point is, that gravity existed throughout the universe before inflation began.

The second part of the modification of Alan Guth's inflation theory introduces gravity into his original theory. Years ago, cosmologists, astronomers and astrophysicists wondered how objects (matter) in far distant reaches of the universe more than 13.8 billion light years apart (the age of the universe), could be so homogeneous and so much alike in many properties, such as composition and temperature, when there was no way that light or any type of information would have had the time to travel from one to the other. The solution was the inflation theory proposed by Alan Guth in the early 1980's, as mentioned earlier. The theory basically proposes that all of the matter in the universe, in some form, was initially close enough together to share its properties. As the big bang began and the matter expanded and clumps moved away from each other, an inflationary period took place in the expansion where the clumps, eventually to become stars and galaxies, moved away from each other much faster than the speed of light. After this rapid expansion much of the matter was separated by distances greater than the distance light could have ever traveled since the beginning of the universe. The distant regions of the universe could never again transfer information or have any influence upon each other (unless a deflationary pe-

riod should occur).

If the inflation theory, which after some modification is now widely accepted, can explain why the properties of similar objects in distant regions of the universe can be so uniform because they moved away from each other much faster than the speed of light, should not it also be able to explain why gravity could be "left behind", so to speak, around objects that rapidly moved apart from each other faster than the speed of light? If the effects of gravity cannot travel through space faster than the speed of light, as is generally believed based on Albert Einstein's General Theory of Relativity, and the matter separated faster than the speed of light, some of the gravity had to be "left behind". And as we discussed earlier, the total amount of this gravity is 20.7 times the amount produced by the real matter in our visible universe. This can be the gravity that exists in galaxies as dark matter, and the gravity that exists throughout the universe as dark energy.

The following example may make it easier to understand how gravity can be "left behind". Let us suppose that the early universe was similar to a very massive soccer ball with all the mass concentrated in the outer shell of the soccer ball, similar to our stage 1 model. There are indentations or seams in the soccer ball similar to a regular soccer ball, which usually has 20 hexagonal and 12 pentagonal sections. The shell of the soccer ball is a curved surface and all the regular hexagonal and pentagonal sections inside the seams of the soccer ball are likewise curved surfaces. See **Figure 9**.

The size of the soccer ball determines the amount of curvature of the soccer ball as a whole, and also the curvature of each individual section of the soccer ball. For simplicity, let us now look at a cross-section of the soccer ball. See **Figure 10**.

Figure 9. Soccer ball.

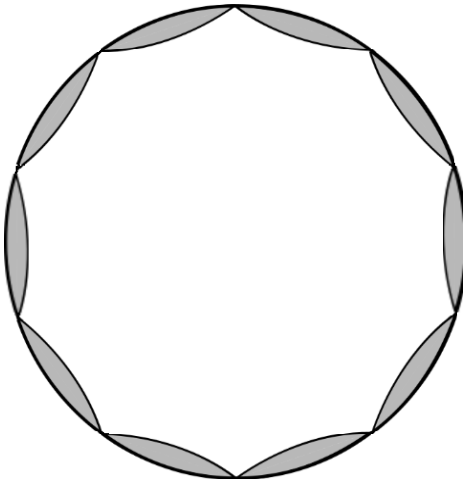

Figure 10. Soccer ball cross-section.

Suppose the soccer ball undergoes a large expansion, and the seams or indentations are very thin and much weaker, but much more elastic than the material inside the seams. The material inside the seams is very strong and thick and not very flexible. As the soccer ball expands, the space between the hexagonal and pentagonal sections stretches so that the sections are now spaced 5 times further apart than they were before the expansion. Because of their thickness and strength, they are still approximately the same size and *have about the same curvature* as before the expansion. The radius of the soccer ball will now be 5 times as large, and the curvature of the cross-section of the soccer ball as a whole, which is a circle, will now be 5 times less than before the expansion (since it is inversely proportional to the radius), but the curvature of each hexagonal and pentagonal section will be approximately the same as before the expansion. See **Figure 11**.

Let us now make the analogy between the soccer ball and our universe, but assume the universe has many, many more sections than the soccer ball since it is much, much larger. It follows that if the expansion of space occurs in the seams between the sections (space between the galaxies), the curvature (warped space-time) within the galaxies will remain about the same while the curvature (warped space-time) of the universe as a whole will be 5 times smaller (because the radius of the cross-section of the universe is now 5 times larger). Gravity, which is the force of attraction between the galaxies, and is also the warped space-time in and immediately around the galaxies, has been "left behind" in and around the galaxies as space has expanded *between* the galaxies. When we now look at the expanded universe where the galaxies are now 5 times farther apart then before, and calculate the amount of mass we can observe in the galaxies, it will be much less than is needed to account for the gravity (warped space-time) in and around the galaxies. Thus, the dark matter that is needed to exist in a spherical halo around the galaxies to account for the motions of the stars observed by our astronomers within the galaxies can be the gravity produced by all the galaxies when they were much closer together, that was "left behind" when the inflation occurred.

9. Dark Energy

Dark energy is commonly defined as an unknown form of energy which permeates all of space, and tends to accelerate the expansion of the universe. The NASA Planck space mission shows that it makes up 68.3% of the universe. It is important to note that, although the Planck space mission collected its data from a detailed study of the Cosmic Microwave Background (CMB) radiation, the values of 4.9%, 26.8%, and 68.3% are the *present day values* extrapolated from the CMB data. They are not the percentages that existed when the CMB radiation was emitted from a 380,000 thousand year old universe. Current thought is that dark energy is a negative pressure spread throughout space as a part of space itself, which acts as an anti-gravity force. As space expands, the dark energy is not diluted. Instead, more dark energy is created as space is created. However, this is not how energy, in general, behaves.

Our stage 2 model offers an alternative explanation. We can show with the model, that instead of dark energy

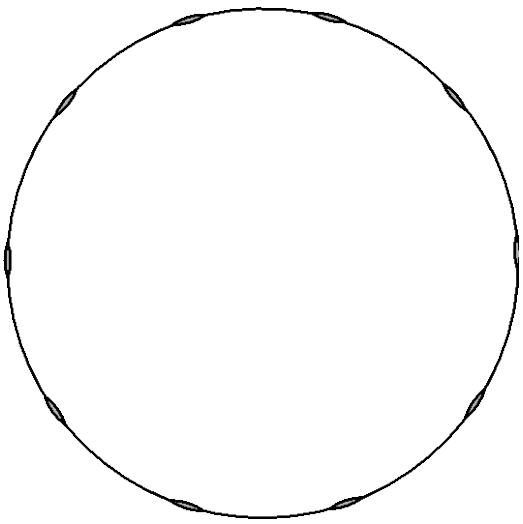

Figure 11. Soccer ball expanded.

increasing to cause the accelerated expansion of the universe, the total amount of matter in the universe is decreasing to cause the amount of gravity holding the universe together to decrease and allow the increased expansion.

Here is the theory. We know from physics that the amount of energy in a certain volume is diluted as the volume increases. The volume of a given amount of space increases by the cube of the radius as it increases, $\left(V = \frac{4}{3}\pi r^3\right)$. We also know from physics that the amount of gravity holding a given amount of space together decreases as the radius increases by square of the radius, $\left(G = \frac{1}{r^2}\right)$. Thus, if we look at our stage 2 model, the energy spread throughout the volume is decreasing faster (by the cube of the radius) than the gravity holding it together is decreasing (by the square of the radius). This means that the expansion should be slowing down. However, if the amount of gravity is reduced by conversion of matter into energy by the equation, $E = mc^2$, greater than the volume increases, the space will expand. We can use the model to calculate the numbers that will show this.

How is the amount of matter (gravity) being decreased? There are many books and articles written about the evolution of the universe, and how stars are formed, live, and die. We now have stars that are several generations old. The heavier elements in our universe are created in the life cycles of the stars. In the life cycle of a star, matter is continually being transformed into energy through the fusion process. When the life cycle of most stars ends in a supernova explosion, tremendous amounts of energy are released as heavier elements are created, and the amount of matter, although heavier, is much less. Since stars started forming in the universe about 13.3 billion years ago, the total amount of matter in the universe has been decreasing. We can calculate how much matter has been transformed into energy every billion years to cause the expansion of the universe to accelerate about 6 billion years ago.

We first of all, have to have an estimate of the number and type of stars that exist in the universe, and we also have to have an estimate of how long the life cycle of the average star lasts. The astronomers, astrophysicists, and cosmologists who have studied the stars have come up with some detailed results. They have learned that the greater a star's mass is when it formed, the faster it burns its fuel, and the shorter is its life cycle, which may be numbered in only millions of years. Many more stars, like the sun, will continue burning their fuel, and decreasing their mass, for about 10 billion years. The much smaller stars will burn their fuel much slower and may continue to do so for over 100 billion years.

The Milky Way galaxy is estimated to contain between 200 - 400 billion stars, and there are estimated to be over 100 billion galaxies in the universe. Each of these stars is converting tremendous amounts of matter into energy every second of every day. It is also estimated that the life cycle of the average star in the Milky Way galaxy is about 50 billion years. Astronomers can determine the age of stars in the universe very accurately. They have estimated that some of the stars in the Milky Way galaxy have been in existence for over 13 billion years, thus, the Milky Way galaxy must have been one of the earliest galaxies to form within the first billion years after the beginning of the universe.

We can now calculate how much matter has been transformed into energy every billion years to cause the expansion to accelerate about 6 billion years ago when the universe was almost 8 billion years old. When the expansion of the universe began to accelerate at about 8 billion years after its beginning, most of the stars in the Milky Way galaxy had already converted about 8 billion years worth of their 50 billion years of fuel, or about 16% of their matter, into energy. If the Milky Way galaxy is an average size galaxy in the universe (estimates are that it is somewhat smaller than average), then the amount of matter in the universe has decreased by at least 16% when the expansion of the universe began to accelerate.

In making the calculation, we need to realize that when the expansion of the universe began to accelerate, whatever was causing it was also accelerating. If it is in fact caused by the decreasing amount of matter in the universe, then the matter has to be decreasing at an accelerating rate. This is exactly what has been happening in our universe, when the initial dust and gas and clumps of matter in the early universe began to collapse and form the early stars and galaxies. As the stars and galaxies increased in numbers into the billions, they increasingly converted matter into energy, and the amount of matter in the universe decreased at an accelerating rate.

If the amount of decrease in matter during the first billion years was only 1/2 of 1%, and it increased by only 1/2 of 1% every billion years, it would be sufficient to account for the accelerating expansion of the universe

when it was almost 8 billion years old. This is when the rate of increase in volume of the universe (and corresponding decrease in energy) was less than the decrease of gravity holding it together. The ratio of the change in volume to the change in gravity, which had been much greater than one, was gradually decreasing as the matter in the universe decreased causing the decrease in gravity. Between 7 and 8 billion years, the ratio became less than one, and the expansion began to accelerate because gravity decreased at a greater rate than the amount of energy in the universe decreased. The following tables show how the changes (increase) in volume of the expanding universe (decrease in energy) compare to the changes in gravity (decrease) as the universe expanded over its almost 14 billion years of existence.

Table 4 shows how the rate of change in volume of the universe changed as the rate of change in the radius of the universe stopped slowing down and began to accelerate. After decreasing for about 8 billion years, it began to increase at an accelerating rate.

Table 5 shows how the amount of gravity in the universe decreased not only as the radius increased, but also as the amount of matter in the universe decreased. After about 8 billion years, the rate of decrease began to accelerate. This is caused by the increased acceleration in the loss of matter in the universe during the past 6 billion years (an additional increase of 1/2% every billion years) as shown in the Mass decrease column in the table.

Table 6 shows how the change (increase) in volume became less than the change (decrease) in gravity after 7 to 8 billion years; *i.e.*, ratio less than one, thus causing the expansion of the universe to accelerate rather than slow down as it had been doing.

These are the numbers that show how dark energy, which is causing the expansion of the universe, does not have to be some kind of increasing energy spread throughout the universe, but rather, can be a decreasing amount of gravity which can no longer prevent the expansion from accelerating. Whatever energy that existed at the big bang to cause the initial expansion can be the energy that is causing its acceleration due to the decrease of matter and gravity. These numbers have been developed from the recent data obtained by telescope and space missions that have been analyzing and studying the stars and galaxies in the universe. The astronomers, astrophysicists, and cosmologists, should be able to show how realistic the numbers are in determining the amount of

Table 4. Change in volume.

Time, t	Radius, r	Volume, $V=\frac{4}{3}\pi r^3$	Difference in volume	Change in volume	% Change
14	40.0	267,947	48,927	0.2234	22.3
13	37.4	219,020	33,292	0.1793	17.9
12	35.4	185,728	22,623	0.1387	13.9
11	33.9	163,105	16,715	0.1142	11.4
10	32.7	146,390	13,024	0.0977	9.8
9	31.7	133,366	11,040	0.0903	9.0
8	30.8	122,326	9850	0.0876	8.8
7	29.95	112,476	9307	0.0902	9.0
6	29.1	103,169	10,275	0.1106	11.1
5	28.1	92,894	10,488	0.1273	12.7
4	27.0	82,406	12,165	0.1732	17.3
3	256	70,241	13,799	0.2445	24.5
2	70,241	13,799	0.2445	0.3951	39.5
1	23.8	56,442	15,984	76	7600
0.5	21.3	40,458	39,935	523	52,300
0.00038	5.0	523	523	N/A	N/A
0	0				

Table 5. Change in gravity.

Time, t	Radius, r	Gravity, $\frac{1}{r^2}$	Difference in gravity	Gravity decrease	Mass decrease	Total decrease	% Change
14	40.0	0.000625	0.000090	0.12587	0.175	0.30087	30.1
13	37.4	0.000715	0.000083	0.10401	0.140	0.24401	24.4
12	35.4	0.000798	0.000072	0.08276	0.110	0.19276	19.3
11	33.9	0.000870	0.000065	0.06952	0.085	0.15452	15.5
10	32.7	0.000935	0.000060	0.06030	0.065	0.12530	12.5
9	31.7	0.000995	0.000066	0.06221	0.050	0.11221	11.2
8	30.7	0.001061	0.000054	0.04843	0.040	0.08843	8.8
7	29.95	0.001115	0.000066	0.05588	0.035	0.09088	9.1
6	29.1	0.001181	0.000085	0.06714	0.030	0.09714	9.7
5	28.1	0.001266	0.000106	0.07726	0.025	0.10226	10.2
4	27.0	0.001372	0.000154	0.10092	0.020	0.12092	12.1
3	25.6	0.001526	0.000239	0.13541	0.015	0.15041	15.0
2	23.8	0.001765	0.000439	0.19918	0.010	0.20918	20.9
1	21.3	0.002204	0.037796	0.94490	0.005	0.94990	95.0
0.5	5.0	0.040000	4.898272	0.99190	0.0025	0.99440	99.4
0.00038	0.45	4.938272	N/A	N/A	0.000	N/A	N/A
0	0						

Table 6. Ratio of change in volume to change in gravity.

Time, t	Radius, r	Change in volume	Change in gravity	Ratio
14	40.0	0.2234	0.30087	0.74
13	37.4	0.1793	0.24401	0.73
12	35.4	0.1387	0.19276	0.72
11	33.9	0.1142	0.15452	0.74
10	32.7	0.0977	0.12530	0.78
9	31.7	0.0903	0.11221	0.80
8	30.7	0.0876	0.08843	0.99
7	29.95	0.0902	0.09088	0.99
6	29.1	0.1106	0.09714	1.14
5	28.1	0.1273	0.10226	1.24
4	27.0	0.1732	0.12092	1.43
3	25.6	0.2445	0.15041	1.63
2	23.8	0.3951	0.20918	1.89
1	21.3	76	0.94990	80
0.5	5.0	523	0.99440	526
0.00038	0.45	N/A	N/A	N/A
0	0	N/A	N/A	N/A

matter that stars, and galaxies, are converting into energy during their life cycles. It is not so much a matter of the stars creating a tremendous amount of energy during the fusion process, which may or may not be significant, but more a matter of the loss of matter. The amounts shown in the above tables appear to be in agreement with what can be extrapolated from the current literature. The tables were also developed from our model of the universe. They show how our model of the universe can explain dark energy.

10. Conclusions

We have developed a model of the universe that can explain dark matter, dark energy, and the fourth space dimension. The model was developed by incorporating time into geometry by using time as a radius of an expanding sphere whose surface represented our entire universe. In the stage 1 model, all of space exists on the surface of the sphere, past history exists inside the sphere, and the future exists outside the sphere. The model shows that when we look out into space in any direction, we are looking back in time to the same point in space at the origin of our universe almost 14 billion years ago. It shows how light has been traveling through the expanding space of our universe for over 13.4 billion years. It shows how we can depict both our visible universe and our entire universe as they exist at the present time.

The stage 2 model was developed by rotating the surfaces of the stage 1 model in all directions about the observer. This was done because only 2 lateral space dimensions can be shown on a surface. For an observer to experience the third space dimension, the surface had to be rotated through a volume about the observer. By doing this, we developed a fourth space dimension which we called orientation, which also incorporated time into space. It is shown that to locate and describe a point in space, 4 space dimensions are required. Height, width, depth, and orientation are required. However, we are 3-dimensional beings living in a 4-dimensional world. We can experience only one orientation at a time, just as a flat 2-dimensional being can experience only one particular height dimension at a time.

The stage 2 model presents us a geometrical framework upon which we can calculate the volume (energy) and the amount of gravity that existed in our universe throughout its history. It thus presents us with a way to explain dark matter as the gravity produced by the real (baryonic) matter that exists throughout our entire universe. And it presents us with a way to explain dark energy as the energy that caused the original expansion of the universe at the big bang that is now accelerating due to the loss of matter and gravity in the universe.

This model of our universe represents a dramatic shift in how we view our universe. It shows how you can not only visualize a 3-dimensional space and one time dimension universe in a model on a flat piece of paper, but can also visualize a 4-dimensional space and one time dimension universe in a model on a piece of paper. The model gives us new insights into the nature of our universe, and presents a framework upon which theories can be developed to explain dark matter, dark energy, and the fourth space dimension. As we continue to explore our universe, and study and analyze the stars and galaxies, we can produce the experimental data that can show that this model can indeed explain dark matter, dark energy, and the fourth space dimension.

References

[1] Davies, P. (2006) The Goldilocks Enigma. Houghton Mifflin, New York, 56.

[2] Hawking, S. (1988) A Brief History of Time. Bantam, New York, 45. http://dx.doi.org/10.1063/1.2811637

[3] Rothstein, D. (2003) Is the Universe Expanding Faster than the Speed of Light? http://curious.astro.cornell.edu/the-universe/cosmology-and-the-big-bang/104-the-universe//expansion-of-the-universe/616-is-the-universe-expanding-faster-than-the-speed-of-light?

[4] Rostomian, Z. (2013) The Great Space Coaster. http://www.sdss3.org/press/lyabao.php

[5] Greene, B. (1999) The Elegant Universe. Norton, New York, 196.

[6] Greene, B. (1999) The Elegant Universe. Norton, New York, 197.

[7] Donald Goldsmith, D. (1991) The Astronomers. St. Martin's Press, New York, 37

[8] Cox, B. and Cohen, A. (2011) Wonders of the Universe. Harper Collins, New York, 110-111.

Appendix A: Light Traveling through Expanding Space

How is light affected by expanding space as light travels through it? We know that the speed of light is a constant. It will travel, say, a distance of one billion light years in a time of one billion years. If, for example, there were 2 galaxies that were 1 billion light years apart, and over a time of 1 billion years, space has expanded by 10 percent so that they are now 1.1 billion light years apart, how far will light have traveled from one galaxy to the other during the 1 billion years?

We first of all, have to make the distinction that the two galaxies have not moved apart relative to each other due to their motion; they have moved apart due to space expanding between them. And secondly, space, or spacetime to be more accurate, is something upon which measurements can be made as it expands. Using the above example, this means that after 1/2 billion years, we can locate a point in space between the two galaxies that will be midway between them, or 0.525 billion light years away from both of them. We can then realize that light, traveling for 1/2 billion years, will not have reached the half-way point of expanded space, or 0.525 billion light years. This is because the distance it had to travel was continually increasing as light traveled through it, and the last half of its journey, 0.525 billion light years, is still ahead of it, and will be continually expanding as light travels through it.

We can use the following analogy to make this clearer. Suppose we have an automobile traveling at 100 miles per hour on a roadway that is expanding by 10 percent, or a distance of 10 miles, every hour. There are mile markers every mile on the side of the road which is not expanding, (the base grid), and there are mile markers every mile on the expanding roadway. We can show how the automobile travels along the roadway in a time of 1 hour by the following graph. For simplification, the grid line markers on the base grid are shown every 5 miles, and the markers on the expanding roadway are shown every 25 miles. See **Figure A1**.

The graph shows that when the automobile travels on the roadway for the first 15 minutes, the length of the roadway is increasing ahead of it (the first 25 mile section will increase by 1/4 of the distance the 100 mile roadway increases in 15 minutes, or 1/4(2.5) = 0.625 miles) so that it will not reach the 25 mile marker on the roadway. When it has traveled, say, 1/2 the 25 miles (in 7.5 minutes), the remaining half of the 25 mile roadway will have increased by 1/2 of 0.3125 miles, so the automobile will be at least that much short of the 25 mile marker. As it travels the remaining half of the 25 mile roadway, the roadway continues to expand by the same amount, so the automobile will end up about 0.3125 miles short of the 25 mile marker. As the automobile continues to travel on each additional 25 mile expanding section, it will continue to fall short of each section mile marker by an increasing amount. But, note that the sections it has already traveled over also continue to expand, by 0.625 miles per 25 mile section, which will increase the distance the automobile has traveled in reference to the base grid. This is also shown in **Table A1**.

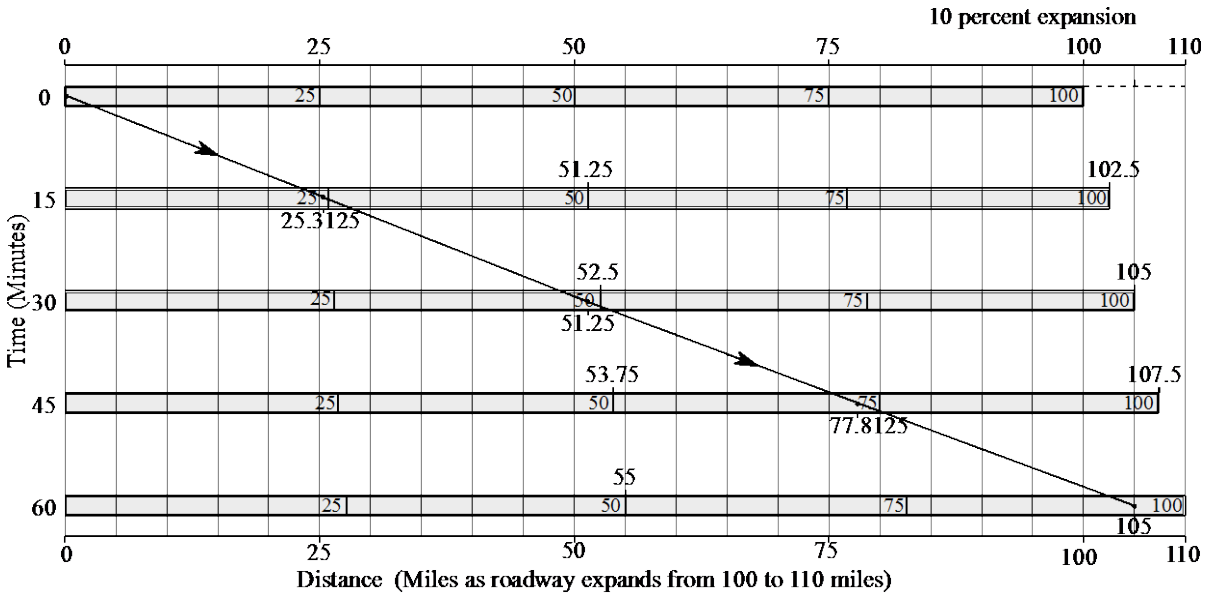

Figure A1. Analogy of an automobile traveling at 100 mph on an expanding roadway.

Table A1. Distance automobile travels in reference to base grid.

Time (minutes)	Distance traveled on original roadway as it expands (miles)				
	0 - 25	25 - 50	50 - 75	75 - 100	Total
0	0				0
15	25.3125				25.3125
30	25.3125 + 0.625	25.3125			51.25
45	25.3125 + 2 (.625)	25.3125 + 0.625	25.3125		77.8125
60	25.3125 + 3 (.625)	25.3125 + 2 (0.625)	25.3125 + 0.625	25.3125	105

The end result is that the automobile will have traveled a total of 105 miles on the roadway as it expanded from 100 to 110 miles in length. It has traveled 1/2 the expanded distance.

By analogy then, we can say that when light travels through expanding space, it will travel about 1/2 the distance by which space has expanded during the same time frame. This assumes, as mentioned earlier, that space, or spacetime, is actually something which can expand, and does expand. Albert Einstein assumed that spacetime was something that could be warped when he theorized about gravity. Astronomers have proven him to be correct when they have seen in pictures produced by the Hubble space telescope, that light is indeed bent by warped spacetime as it travels around massive galaxies in a lensing effect. The big bang theory assumes that space expanded enormously at the beginning of the universe, slowed down, and is now expanding at an accelerating rate. Thus, I believe we can state that when light travels through expanding space, it will travel 1/2 the expanded distance.

Appendix B: The Space Dimension Class

Suppose you were educated in a school system where it was required that you pass a space dimension class before you could graduate from high school. A prerequisite for the class was that you complete basic mathematics classes to include fractions, and complete basic geometry classes to include formulas for determining the area and volume of simple shapes and solid objects such as cubes and spheres. The space dimension class was a 2-hour class and consisted of a 1-hour lecture by the space dimension teacher followed by a 1-hour exam. If you failed the course, you would have to re-take it until you passed it, but if you had to re-take it, it would be a slightly different, more complicated course.

You are now one of 24 students in your first space dimension class. The space dimension teacher is standing behind his desk at the front of the classroom with a large chalkboard on the wall behind him. He begins his lecture and talks about the space dimension called height, which he explains is a length in the up and down direction. He then explains how the space dimension called width is a length in the left and right direction, and the space dimension called depth is a length in the forward and backward, or front and back direction. He also explains how these particular dimensions are based on a Cartesian coordinate system, which is also called a rectangular coordinate system, but there are also other possible coordinate systems, such as a cylindrical coordinate system that uses 2 lengths and 1 angle to locate a point in space or describe an object, or a spherical coordinate system that uses a length and 2 angles to locate a point in space or describe an object. He also mentions that there is a polar space coordinate system that uses a combination of the rectangular coordinate system and 1 length and 3 angles to locate a point in space. "However," he explains, "regardless of the coordinate system used, it is generally recognized that there are only 3 distinct space dimensions, which should be fairly obvious, because any object you can see and touch and feel appears to have height, width and depth".

He then reaches into a large, 5-gallon bucket sitting on his desk and pulls out a white Styrofoam cube about the size of his fist. He then explains how you could remove the top half of the cube by passing a horizontal plane through the middle of the cube. He also explains how you could remove the left half of the cube by passing a vertical plane through the original cube to separate the left half from the right half, and also how you could remove the front half of the cube by passing another vertical plane through the original cube to separate the front half from the back half. He then goes on to explain how you could remove only the top half *of* the left half of the

original cube by cutting along a portion of the horizontal and vertical planes so that the top left quarter (1/4) of the cube was removed (which is 1/2 times 1/2 equals 1/4 of the cube). To visually emphasize this, he picks up a razor blade from his desk and proceeds to make two cuts into the cube and removes the top left quarter of the cube, which is the top half of the left half of the cube. See **Figure B1**.

He places this cube on his desk and reaches into the large bucket and pulls out a second Styrofoam cube the same size as the first. He now explains how to remove the left third (1/3) *of* the top half *of* the front half of the cube. The part that would be removed would be 1/3 times 1/2 times 1/2 equals 1/12 of the cube. Again, he takes a razor blade and proceeds to make three cuts into the cube and removes the corner of the cube corresponding to the left third of the top half of the front half of the cube. See **Figure B2**.

The space dimension teacher places this cube on his desk and then tells all the students that the lecture is now over, and that it is time for them to take the final exam. He tells them that in order to pass the space dimension class, they will have to complete one problem. He then turns around, writes the problem on the chalkboard, and then walks out of the classroom. Here is what he writes on the chalkboard:

"Final Exam Problem:

Come up to my desk, reach into the bucket and remove one cube. Take the cube and one of the razor blades on my desk to your desk and remove the front half of the right half of the top half of the cube. You have one hour. Then take the remaining part of the cube to my office, place it on my desk, and compare it to my solution,

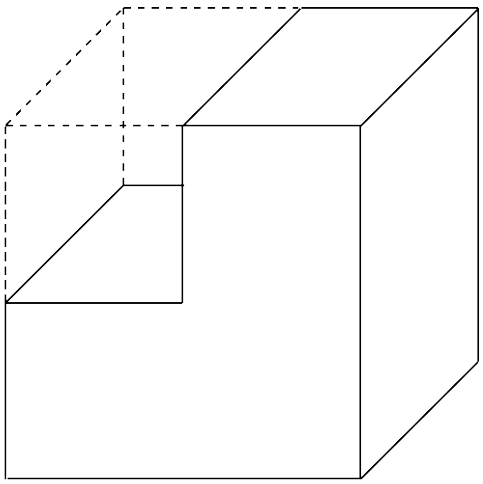

Figure B1. The top half of the left half removed.

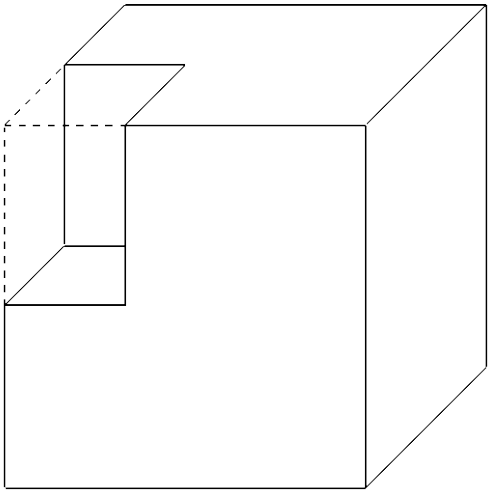

Figure B2. The left third of the top half of the front half removed.

which will be sitting in the middle of my desk. My original cube is identical to your original cube. If your cube looks the same as mine after you remove the specified section, you pass the course."

At this point, you think, "Hey, this is fairly easy!" since the lecture was not that difficult. You are very impressed by the space dimension teacher. He has very thick white hair, so he has probably been doing this for a long time. He appears to be very intelligent, and explains things in a very detailed, methodical manner. Anyway, you go up to the space dimension teacher's desk, reach into the bucket, and pick up a cube. When you look at the cube, you see that each of the 6 sides of the cube is a different color! One side is red, one side is black, another side is green, the fourth is blue, the fifth is yellow, and the sixth is white. All of the other students pick out an identically colored cube. Your heart starts to sink because you now realize that you have to decide which side of the cube is "up". The space dimension teacher will have obviously picked one of the colored sides of the cube to be in the "up" position when he made his 3 cuts into the cube to remove the top, right, front section of the cube. The orientation of your cube when you make the razor blade cuts, must be the same as his if your solution is to be the same as his. Unfortunately, you did not have the chance to ask the space dimension teacher which side of the cube was "up" since you assumed all sides of the white Styrofoam cube could be treated equally. Even if you had thought of the question, you did not have the opportunity to ask it.

You return to your desk, and after considerable thought, which leads you nowhere, arbitrarily pick the red side to be in the "up" position, and the blue side to be the "front" position, and make the 3 cuts to remove the top, right, front 1/8 section of the cube. At the end of the hour you take your cube to your space dimension teacher's office and place it on his desk next to his cube. You feel elated as you see that you chose the correct "up" side! Both your cube and the teacher's cube have the red side placed in the "up" direction! Furthermore, the top, right, front section that was removed on your cube corresponds to the same top, right, front section on the teacher's cube! But your heart sinks as you notice that the blue front side of your cube is not the same as the green front side of your space dimension teacher's cube. You flunked the class! See **Figure B3**.

Your fellow classmates go through the same experience that you just went through, and then you all return to the classroom with the space dimension teacher. He tells the class that only 1 student passed the course, which is exactly what he had expected, because each of the 24 students had only a 1 in 6 chance of arbitrarily picking the red side of the 6-sided cube to be the "up" side. In addition, of the 4 students that correctly picked the "up" side, each had only a 1 in 4 chance of picking the correct "front" side out of the 4 remaining vertical sides of the cube. He tells the students that according to custom, he will place the name of the student on the cube that was the same as his, and place it in the trophy case in his office to save for years to come. All other cubes will be discarded. He then tells the class that he hopes that all the students now realize the importance of this 4th space dimension called "orientation". To emphasize his point, he asks all the students to place themselves in the following situation:

"Suppose", he says, "you were a very tiny, though very intelligent microbe living inside one of the Styrofoam cubes and were able to move freely, although slowly about the cube. You could actually move to the surface of the cube, poke your head out, and see what color the surface happened to be. You had been living in your cube universe that was inside the 5-gallon bucket all your life. You had actually traveled up to the top of your universe to see which side was 'up'. You knew which side was 'up' because you felt the pull of gravity and could

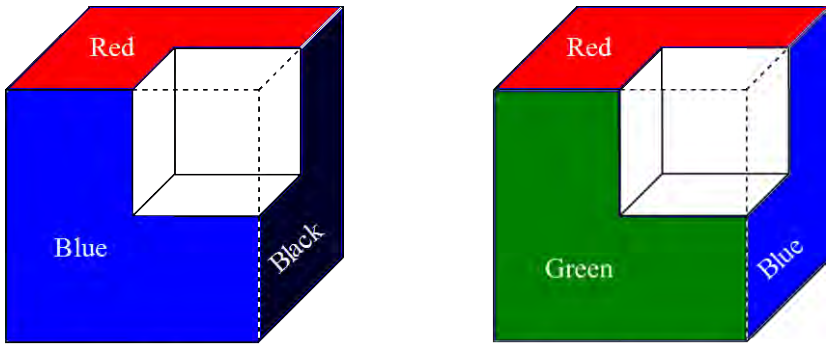

Figure B3. The student's and teacher's cube.

orient yourself so that 'up' was in the direction of the top of your head. You discovered that no side was truly 'up'. Because of the way your cube was positioned in the bucket, 'up' turned out to be a corner of the cube with a yellow side, a white side, and a green side each sloping downward at slightly different angles from the corner. That was fine with you because your entire universe was made of Styrofoam, and the color and shape of the outside had no influence upon your life. You were very comfortable living near the center of the cube, and you thus proceeded to go about your life as usual."

"You now suddenly feel your universe being moved about, turned upside down, and turned around, and then finally come to rest as a student places your universe on his desk. You hear someone muttering something about removing the top, right, front section of the cube within an hour and discarding it. You have a 1 in 8 chance of being removed from your universe and discarded, depending upon where you are located inside the cube. You know which side is now 'up', even though it is now much different than it was several minutes ago, because you can feel the pull of gravity pulling at your left ear. You quickly re-orient yourself inside your universe so that the pull of gravity is now at your feet and 'up' is now at the top of your head. You still have a major problem in that you have no idea which direction you should face so that your 'front' side corresponds to the student's 'front' side. However, since you are a very intelligent microbe, you quickly figure out that all you have to do is move down into the bottom half of the cube and you will have a 100% chance of surviving inside of your universe, provided your student understood the lecture about the 3 space dimensions. You don't know where the right side of the cube is, part of which will be removed; and you don't know where the front side of the cube is, part of which will also be removed; but you do know where the bottom half of the cube is, none of which will be removed. You start moving downward in your Styrofoam universe as quickly as possible, which unfortunately is slower than a snail's pace. Fortunately though, you make it into the bottom half just in time as the top, right, front of your universe disappears. You breathe a huge sigh of relief and thank your lucky stars that you knew all about the 3 space dimensions involving up and down, left and right, and front and back, and the other space dimension called orientation. You are also very thankful for the something in your life called gravity, which enabled you to determine which orientation was 'up'."

"You now feel yourself being picked up, carried around, and placed down on a surface again, and the pull of gravity is still at your feet. Your universe has just been placed on the space dimension teacher's desk, and unfortunately for you, the student that had your cube picked the white side of the cube to be the 'up' side instead of the red side, which was the teacher's determination of the correct 'up' side. Your whole universe will now be discarded because neither you nor the student knew what the correct orientation of the cube should be to agree with that of the authoritative space dimension teacher."

The space dimension teacher pauses for a bit and then tells the students how fortunate they all are that they are not tiny microbes living in a Styrofoam universe. He tells them that he hopes they have learned something worthwhile in his class, and is looking forward to seeing them again when they re-take the class. He tells them they will learn more about the dimension called orientation in the next class. He also invites the one student who passed the course to also re-take the class since it was only by chance that the student passed, not because of the student's superior understanding of the space dimensions. He then dismisses the class, wishing them well in their future endeavors.

This little story will hopefully cause you to think about the possibility of a fourth space dimension actually existing in our universe, and how it possibly could be something called orientation, but a kind of orientation that will be considered in a slightly different context than that which we now experience.

Appendix C: Lost in Space

Can "orientation" really be a 4^{th} space dimension? We should take time to visit another of the space dimension teacher's classes. One of his advanced classes is called "Orientation: The 4^{th} Dimension". In this class, he always begins with a little story. "Suppose," he says, "you were in a very large spaceship far out in space conducting a mission of exploring the universe, and had just recently entered a very unique-looking interstellar gas and dust cloud. The dust was not all that visible, but it quickly became thick enough so that your visibility was limited to several hundred miles in any direction, and neither stars nor any other objects were visible. Suppose the commander of the spaceship brought his spaceship to a stationary position and then asked you to board one of the spaceship's small personal reconnaissance vehicles and make an exploratory trip to see how distant the gas and dust cloud extended. To maintain direction and know where you were at all times, you were to keep de-

tailed notes as you left the exit port at the rear of the spaceship. You were to keep track of exactly how many miles you traveled in each of the 3 space dimensions; *i.e.*, forward/backward, left/right, and up/down, so that you would be able to retrace your travel and return easily."

"Suppose", he continues, "that during your trip, a burst of interstellar radiation suddenly occurred, and as it passed through your location, it caused your reconnaissance vehicle to spin and tumble about and disabled your gyroscope and propulsion and navigation systems. However, you had kept careful notes, and you knew that at this point, you had traveled a net of 650 miles in the forward direction, a net of 210 miles in the left direction, and a net of 360 miles in the upward direction since you had left the spaceship. Fortunately, although you had lost sight of the large spaceship several hundred miles ago, you still had a communication capability and immediately relayed the detailed directions to your location to the large spaceship, and asked the commander to come and rescue you. The commander of the spaceship responded that, unfortunately, they too had been hit by the burst of radiation that had also spun and tumbled their spaceship about and disabled their gyroscope and navigation system, but their propulsion system was still intact. You thought to yourself that you were extremely lucky that you had kept such good notes of the directions you traveled so that all the commander of the spaceship would have to do is send a rescue reconnaissance vehicle out of the same exit port of the spaceship and have it travel the same distances in the exact same directions you had traveled, and they would locate your position in space exactly. But then you realized at about the same time as did the commander of the spaceship that he needed to know in what direction the exit port of his spaceship was facing when you left the spaceship, now that the orientation of his spaceship had changed many times during the burst of interstellar radiation. He realized that he needed more than 3 dimensions to locate a point in space. He needed to know which direction on his spaceship was 'up'; *i.e.*, orientation, when your personal reconnaissance vehicle left the spaceship. He then had to place his spaceship in the exact same orientation to be able to rescue you. His spaceship had been spun and tumbled about in many different directions and combinations of up/down, left/right, and forward/backward. Since no objects were visible and there was no gravity, and his gyroscope and navigation system were disabled, there was no frame of reference in which he could determine which way was 'up', let alone position his spaceship in the same forward direction as it had been when your reconnaissance vehicle exited the spaceship."

"There was no way," said the space dimension teacher, "that the spaceship commander could locate your position in space since he needed a 4^{th} space dimension to provide a frame of reference, and we call that 4^{th} space dimension, orientation. We take this 4^{th} space dimension for granted in our everyday lives because we live on an earth with gravity that provides us an automatic frame of reference and an automatic orientation in the 'up' direction. However," he says, "the story ends happily in that the commander of the spaceship was able to repair his damaged systems, and by reviewing the computer tapes of all his damaged systems, he was able to re-establish his orientation as it was when you exited his spaceship, retrace your travel and rescue you." This little story should emphasize the point that you need 4 dimensions to locate a point in space, and orientation is that 4^{th} dimension.

Journal of Modern Physics, 2016, 7, 1277-1295
Published Online June 2016 in SciRes. http://www.scirp.org/journal/jmp
http://dx.doi.org/10.4236/jmp.2016.710113

Entropy at the Level of Individual Particles: Analysis of Maxwell's Agent with a Hidden-Variable Theory

Dirk J. Pons[1*], Arion D. Pons[2], Aiden J. Pons[3]

[1]Department of Mechanical Engineering, University of Canterbury, Christchurch, New Zealand
[2]University of Cambridge, Cambridge, UK
[3]Rangiora New Life School, Rangiora, New Zealand
Email: *dirk.pons@canterbury.ac.nz

Received 23 April 2016; accepted 26 June 2016; published 29 June 2016

Abstract

Problem: Maxwell's Agent (MA) is a thought experiment about whether the second Law is violated at smaller scales. This is a complex problem because the scale dependencies are unclear for perfect gas assumptions, quantum coherence, thermalisation, and contextual measurement. Purpose: The MA is explored from a non-local hidden-variable (NLHV) perspective. Approach: The Cordus theory, a specific NLHV solution, was applied at macroscopic to fundamental scales. Physical realism requires the Agent be included in the analysis. Findings: The primary function is sorting, *i.e.* a one-time separation of species by some attribute. The thermodynamic MA situation is merely a special case for reducing disorder (entropy). A one-time extraction of energy is possible. This requires input energy, hence the device only has thermodynamic leverage and is not a perpetual motion device. Inefficiencies arise from thermalisation causing short mean free path of Brownian motion, perfect gases having minimal interaction with the gate, ambiguity about spatial location arising from quantum superposition, contextual measurement interfering with the particle velocity, and bremsstrahlung hysteresis losses occurring when the Agent operates. Implications: Entropy is a group property at the bulk level, not a characteristic of the individual particle, and can be reversed at an energy cost at the particle level. Originality: The explanation spans multiple levels from macroscopic down to fundamental, which is unusual. Achieving an explanation from the NLHV sector is novel. The theory accommodates superposition, irreversibility, entropy, contextual measurement, coherence-discord transition, and Brownian motion.

Keywords

Entropy, Irreversibility, Ratchet, Demon, Thermodynamics, Contextual Measurement

*Corresponding author.

How to cite this paper: Pons, D.J., Pons, A.D. and Pons, A.J. (2016) Entropy at the Level of Individual Particles: Analysis of Maxwell's Agent with a Hidden-Variable Theory. *Journal of Modern Physics*, **7**, 1277-1295.
http://dx.doi.org/10.4236/jmp.2016.710113

1. Introduction

Maxwell's Agent (MA) is a thought experiment about whether it is possible to violate the second Law of thermodynamics at the microscopic scale. Maxwell's original idea [1] was that the motions of gas molecules in a vessel were variable, as evident in Brownian motion, so that a microscopic being with sufficiently sharp senses might detect the faster gas molecules in a container, and momentarily open a door to selectively let them into a second chamber. This would cause the temperature to drop in the first vessel, and rise in the second.[1] This is represented in **Figure 1**.

If this worked, it would appear to violate the second law because the temperature difference could subsequently be used to generate work, hence the paradoxical outcome of a perpetual motion machine. The essence of this is a process of measure -> decide -> act that sorts out the favourable outcomes. Other conceptual embodiments are the Brownian ratchet, and feedback engines.

The context was that Maxwell noted the second law applied statistically to bodies en-masse, and he questioned whether the law applied at the microscopic scale where the individual molecules became apparent. By implication he expected that the law could break down, that the being "would be able to do what is at present impossible to us". Technology is now approximately at the point where individual molecules can be sensed and controlled, so after many years of quiescence the MA is again a topic of interest [2]. However, there has arguably

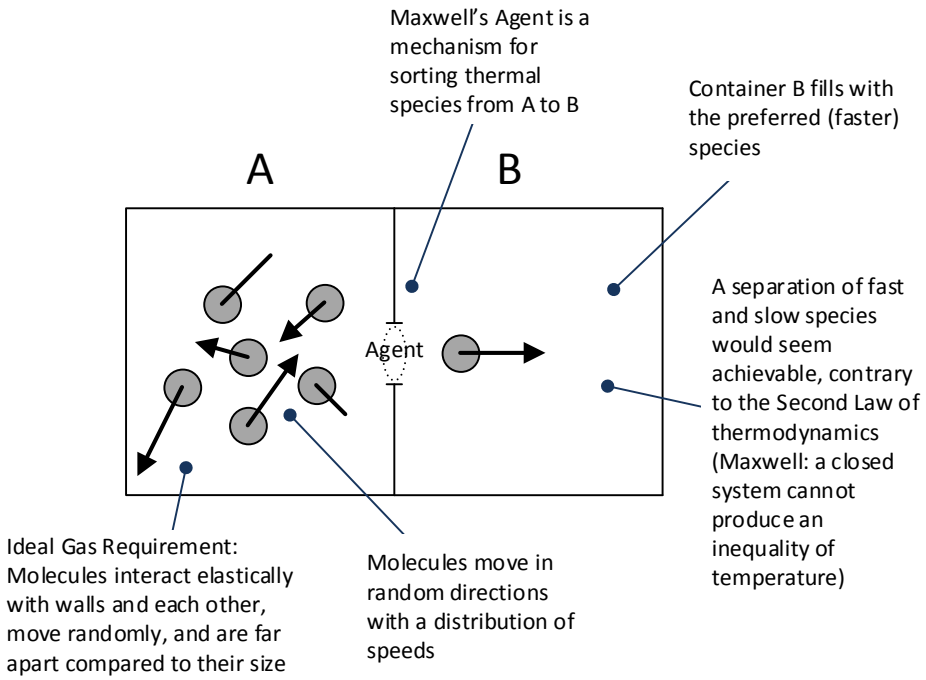

Figure 1. Maxwell's Agent is a thought experiment whereby the more energetic particles in vessel A are selectively admitted, by an active agent, into vessel B. The central question is whether this would allow work to be extracted from the random motions of the particles in A. If so, that would imply a violation of the second law. However there is also the possibility, identified by Maxwell which the second law only applies to the fluid as a whole, not to the individual particles.

[1]Maxwell (1891) (p. 338-339): "One of the best established facts in Thermodynamics is that it is impossible in a system enclosed in an envelope which permits neither change of volume nor passage of heat, and in which both the temperature and the pressure are everywhere the same, to produce any inequality of temperature or of pressure without the expenditure of work. This is the second law of thermodynamics, and it is undoubtedly true as long as we can deal with bodies only in mass, and have no power of perceiving or handling the separate molecules of which they are made up. But if we conceive of a being whose faculties are so sharpened that he can follow every molecule in its course, such a being, whose attributes are as essentially finite as our own, would be able to do what is impossible to us. For we have seen that molecules in a vessel full of air at uniform temperature are moving with velocities by no means uniform, though the mean velocity of any great number of them, arbitrarily selected, is almost exactly uniform. Now let us suppose that such a vessel is divided into two portions, A and B, by a division in which there is a small hole, and that a being, who can see the individual molecules, opens and closes this hole, so as to allow only the swifter molecules to pass from A to B, and only the slower molecules to pass from B to A. He will thus, without expenditure of work, raise the temperature of B and lower that of A, in contradiction to the second law of thermodynamics."

been no violation of the second law observed at these scales.

There are a number of questions: whether or not thermodynamics applies at the foundational level, whether or not a MA device could be built, and what the limitations of a real MA device might be. Maxwell's Agent does for the ontology of entropy what Schrodinger's Cat does for temporal superposition. The MA device is a thought experiment that provides a useful philosophical foil with which to probe the assumptions of thermodynamics at the fundamental level. Neither classical nor quantum perspectives of entropy definitively answer the question, so it is relevant to consider what the other sectors of physics make of the matter. These other sectors are primarily string theory—which has nothing specific to say on this topic and the non-local hidden-variable (NLHV) solutions—which do.

In keeping with the conjectural nature of Maxwell's question, the present paper treats the topic conceptually, using a thought experiment based on the NLHV solution provided by the prospective physics of Cordus theory. The NLHV theories all presume an internal structure at the sub-particle level, although such theories are exotic and not substantiated to the same degree as classical and quantum mechanics, neither are they frivolous. At times they have provided new insight into difficult problems (examples given below). Consequently it is worth evaluating Maxwell's question using new physics, for the ontological potential: doing this may suggest new ways of understanding the *possible* deeper causal mechanics of the second law of thermodynamics.

In keeping with the assumption of *physical realism* (*that physical observable phenomena have deeper causal mechanics involving parameters that exist objectively and correspond to some physical features of the particle*) that underpins NLHV theories, we use the term "Agent" to denote a physical mechanism, not necessarily either living or spiritual, with the ability to sense, make a decision, and perform a physical action, but not necessarily sentient. In comparison, Maxwell used the term "being", whereas others later substituted "demon".

2. Existing Theoretical Explanations and Empirical Applications

2.1. Empirical Applications

Macroscopic MA devices have occasionally been invented, but these are not perpetual motion machines, due to the effect of external fields or heat source and sinks, e.g. [3]. Practical applications of the MA exist, primarily as cooling [4] [5] or flow control [6] at the atomic level. However these devices require special setup including one-way barriers such as optical traps [7] [8], and external energy sources, thus do not raise thermodynamic paradoxes. The MA has been proposed as a mechanism in the vortex tube [9], though this too is not a perpetual motion effect, and there are other ways to explain that specific phenomenon. Other interesting applications of MA principles are in phase separation of grains in microgravity or vibrational suspension [10], and it has been proposed that the inelasticity of collisions causes clustering [11]. Molecular Brownian ratchets have also been proposed [12].

2.2. Theoretical Explanations

There are a number of theoretical explanations for why Maxwell's agent should not work. Szilárd's explanation, which was a prominent early contribution, was that the agent has to do work to assess the velocity of the molecules. Thus including the agent as part of the system means that the agent provides the work, see [13]. Another explanation was that there is an information cost to *measuring* [14] [15], *storing*, or *erasing* information about the state of a molecule, and this information requires work [16]. This is a popular theoretical approach, and the many different theories all suggest that the energy needed to operate the MA will be at least as great as the work done [17]. Similarly, the work required to erase the information has been predicted to be as much gained by the thermal difference in the engine [18]. A more controversial explanation is that there are no faster and slower particles, they are all stationary [19] [20]. However, this is problematic as it is difficult to reconcile with observed Brownian motion.

Statistical simulation has been applied to better understand the MA behaviour in classical fluids (billiard-type systems). Examples include velocity changes between collisions [21], and contacts between billiard spaces with different types of voids which change the geometric location of the balls [22]. This type of work has also shown that the MA creates a density gradient rather than temperature per se [23].

Numerous theoretical attempts have been made to explain the effect using quantum theory, e.g. [24] [25]. The process, as applied to a Szilard engine, is then considered to involve 1) insertion of a barrier wall, 2) measure-

ment, 3) expansion of the engine, and 4) removal of the barrier. Theoretical work suggests that the MA needs to know the number of entities involved in these condensates [26] [27], and that bosonic (as opposed to fermionic) condensates may give more work since the particles are identical [28]. Inverting the MA operation, it has been suggested that since measurement changes the energy of a quantum state, a MA could be used to power a heat engine via selective measurement [29]. However this idea does depend critically on the feasibility of making a reversible "pre-measurement". It has been suggested that a superconductor tunnel junction acts as a MA, hence providing cooling ("Brownian refrigerator") [30]. A limitation of the quantum approaches is the assumption that the working fluid is a coherent substance. This is evident in the many theories that depend on condensed substances and entangled states [31] [32]. This is a severe assumption since quantum coherence is not generally observed at the microscopic or macroscopic scales which Maxwell implicitly had in mind. Macroscopic states are characterised by discord (decoherence), which refers to non-superposition and non-entangled relationships between particles. This explicitly means that discord reduces the effectiveness of quantum-based MA mechanisms [33].

2.3. Difficulties

There are several obstacles to providing a complete scale-invariant explanation of the MA. One is the question of whether the perfect gas assumption is valid in the situation. Obviously real gases are imperfect, but how does this affect the MA outcome? Also, the question changes at a deeper level, since quantum mechanics assumes that particles are points. Another difficulty is how the Agent interacts with fields emitted by the particle. It is commonly stated that the Agent detects the energetic particles, but the methods of detection are seldom considered explicitly. The Agent cannot be permitted to generate photons and bounce them off the molecules, because that would involve adding energy to the system. So how does the detection occur, is it even possible to be non-intrusive from an energy perspective (c.f. Zeno effect), could it be lossless, and is it possible to use the fields emitted by the particle itself? Third, how to deal with the close-range thermalisation interactions that molecules make with each other in the moment between detection and admission? A simplistic assumption is that the whole operation of the Agent (detect-decide-open then close) operates instantly. However this is not physically possible since mass has to be moved and this takes time. Consequently the question is whether thermalisation invalidates the MA, and if so at what scales. Is there sufficient time between detection and action for the device to work? This is especially problematic if the particles have high velocity. How is quantum superposition to be included in the situation? Related to that is the difficulty of the transition from quantum to classical MA behaviour. Simple answers to these questions may be found by assuming that the Agent is outside the system, because then the Agent can be assigned powers that are not constrained by physical considerations. However such solutions are simplistic because they merely transfer part of the problem into the metaphysics domain.

Maxwell's question related to whether the thermodynamics at the foundational level are any different to those at the macroscopic, and that question is still incompletely answered. This is a complex problem because the scale dependencies are unclear for perfect gas assumptions, quantum coherence, thermalisation, and contextual measurement.

There is a need for analyses of the MA that 1) are based in physical realism (avoid resorting to metaphysical causation), and 2) span the scale from the macroscopic to the continuum represented by conventional thermodynamics, through to the level where particles display quantum properties, and potentially beyond to deeper physics at the sub-particle level. This is a challenging problem.

3. Purpose and Method

3.1. Purpose

The purpose of this paper is to explore the fundamental thermodynamic principles underpinning Maxwell's Agent. Specifically, we are interested in seeking insights from the hidden-variable sector. This sector has made little to no contribution to thermodynamics.

3.2. Methodology

Hidden-variable designs propose that matter particles have internal structures, the "hidden" variables. This is an intuitively attractive idea [34], but the difficulty has been finding suitable internal designs. Note that while the

Bell-type inequalities [35] [36] preclude *local* hidden-variable solutions, they do not eliminate *non-local* designs. Historically the only hidden variable theory of substance has been the de Broglie-Bohm pilot wave theory [37] [38], but that has not developed into a wider theory of physics. The recent development of the Cordus theory [39] offers another candidate solution, and this is applied here. The present paper uses Maxwell's Agent to explore how thermodynamics scale from the macroscopic to fundamental levels under the assumptions of this NLHV theory. The area under examination is Maxwell's simple gated two-chamber arrangement.

The conjectured Cordus theory is a conceptual physics. It started as a designed solution to wave-particle duality in the double-slit device [39]. By design is meant that the internal structures of the particle (*internal form*) were determined by what was necessary and sufficient to describe the empirically observed behaviour (*external functionality*) of the photon in the double-slit device. The theory was built on the assumption of physical realism, and that physically observable attributes, such as spin, correspond to some physical feature of the particle. In contrast quantum mechanics assumes that particles are structure-less zero-dimensional (0-D) points and their properties, such as spin, are mathematical properties or intrinsic variables. The theory has subsequently been expanded to include other areas including photon emission [40], matter-antimatter annihilation [41], neutrino attributes and beta decay processes [42], structure of the atomic nucleus [43], pair production [44], and asymmetrical baryogenesis [45].

3.3. Approach

Consistent with the position of physical realism, Maxwell's "being" is required to be a physical Agent: whether alive or inanimate it must be made of matter and operate according to physics, and may not have paranormal or metaphysical capabilities. The purpose of this paper concerns the intersection of thermodynamics with fundamental physics and consequently there is no value in permitting the MA mechanism to operate beyond time, matter, fields, and space. This is relevant to note since the MA problem is often framed by assuming *a priori* that the agent *must have* the ability to sort particles, without actually considering *how* it does that, and then looking at the logical consequences of having such an ability. Our position is that the Agent is an integral part of the system, and its capabilities must be included in the analysis from the outset.

The approach was to apply the *gedanken experiment* method. This method takes a given set of principles of physics, which are the starting lemmas. The starting point could be any theory of physics: continuum mechanics, quantum mechanics, string theory, NLHV theory, etc. In this case it was the Cordus theory. The method then applied logical inference on those lemmas, thereby predicting the physical causality for other parts of the problem not originally explicitly covered by the lemmas. Thus the process extended the theory beyond its original lemmas. The implications of this theoretical extension were then reconciled against known phenomena, and novel insights formulated into new explanations.

The operation of the Agent was considered at multiple scales. The first was the macroscopic level, where we imagine the interaction of perfectly elastic balls. The next was the level of molecules, at which the perfect-gas behaviour is examined. The third scale was that of the particle level of quantum mechanics. The fourth was at the Cordus level, to assess the foundational thermodynamic implications for this theory.

4. Results

4.1. Macroscopic Level: Thermodynamic Leverage and Sorting

First, consider the capabilities of the Agent at the macroscopic level, with *large vessels and perfectly elastic tennis balls*. This is not usually the level at which thermodynamics is applied, but it is fruitful to start at this level as there are scale issues that become apparent later. Assume that the velocities of the balls are subject to Newtonian mechanics, specifically that balls do not change their velocities for no reason.

The Agent has to determine the velocity of each ball in vessel A before deciding whether to admit it to vessel B. Assume, in the macroscopic case of the balls, that the Agent is permitted to use photons for measuring the velocity of each ball, e.g. radar, because the energy of the photons is negligible compared to that of the targets. Based on the information received the Agent may then open the gate selectively, and thus capture the faster balls. Generating and using photons adds energy to the system. Even so, this small work associated with measurement would seem, at least in some macroscopic cases, to be much less than the kinetic energy gained by admitting to the vessel B the ball with its large kinetic energy.

4.1.1. Thermodynamic Leverage

A once-off extraction of energy ex vessel B is then conceptually feasible. For example, the energetic balls in B could be made to strike a moveable plate, thereby performing work, see **Figure 2**. However, once this has been done, the energy states of vessels A and B would be the same, and there is no further energy that can be extracted. An alternative explanation is that once all the energetic balls have been sorted into vessel B, leaving the slower ones in A, there is nothing more for the Agent to do. Both approaches show that an infinite extraction of energy is not possible.

There are some candidate exemptions. If vessel A were infinitely large then the process could be sustained. However that requires two infinite volumes: one infinite volume A from which to extract fast species, another working space B in which to place them, and a third infinite volume C in which to dump the spent material after its energy is extracted. So this is not realistic. Another exemption would be to have finite volumes, and extract work as before, but heat the waste material from B before reintroducing it to A. However that makes the MA nothing more than a refrigeration circuit, and there is no net work extracted.

Even if the energetic balls in B are returned to A after harvesting their energy, as shown in **Figure 3**, this will not bring about a perpetual energy device. Once their energy is extracted the balls become slow, and adding them back to A causes them to be of no further thermodynamic usefulness.

A practical implementation of a macroscopic MA device seems feasible, using large balls, sparsely distributed, moving no faster than the Agent can respond. However one would need to overlook the energy cost of running the Agent: the measurement, decision-making, and gate-opening. At the macroscopic level that cost can be comparatively small relative to the large energy of the balls. Even so, this analysis suggests that even a perfect MA mechanism with perfectly elastic collisions between macroscopic balls would be unable to function as a perpetual energy device. Instead a perfect Agent operating at macroscopic level merely provides good thermodynamic leverage: the exertion of a small amount of energy in measurement and computing allows a large decrease in entropy and the extraction, though only once, of work. In summary:

A practical implementation of a macroscopic MA device seems feasible, using large objects that are sparsely distributed. A macroscopic MA device permits, at best, a one-time extraction of energy. This is at the cost of input energy or parasitic losses, hence thermodynamic leverage. This would not be a perpetual energy device.

4.1.2. Primary Macroscopic Outcome Is Sorting

The MA is often portrayed as a mechanism for perpetual motion. However, the present analysis shows that energy cannot be endlessly harvested, but rather that mixtures can be separated albeit with some energy operating cost. The Agent achieves sorting, *i.e.* a one-time separation of species by some attribute. That attribute is

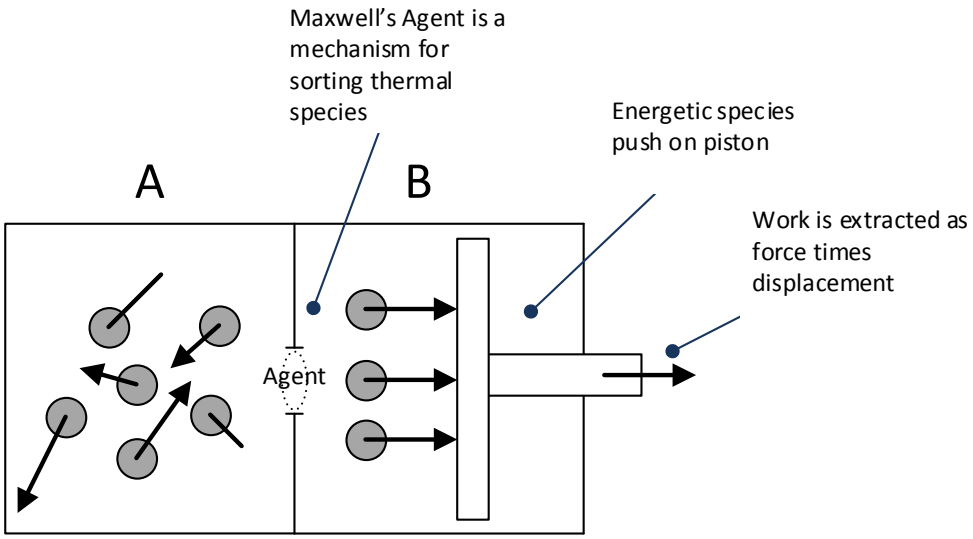

Figure 2. A once-off extraction of energy is feasible, if the Agent can sort out the more energetic species. The more captured energetic objects could, for example, be used to push a piston against an external resistance, thereby doing work.

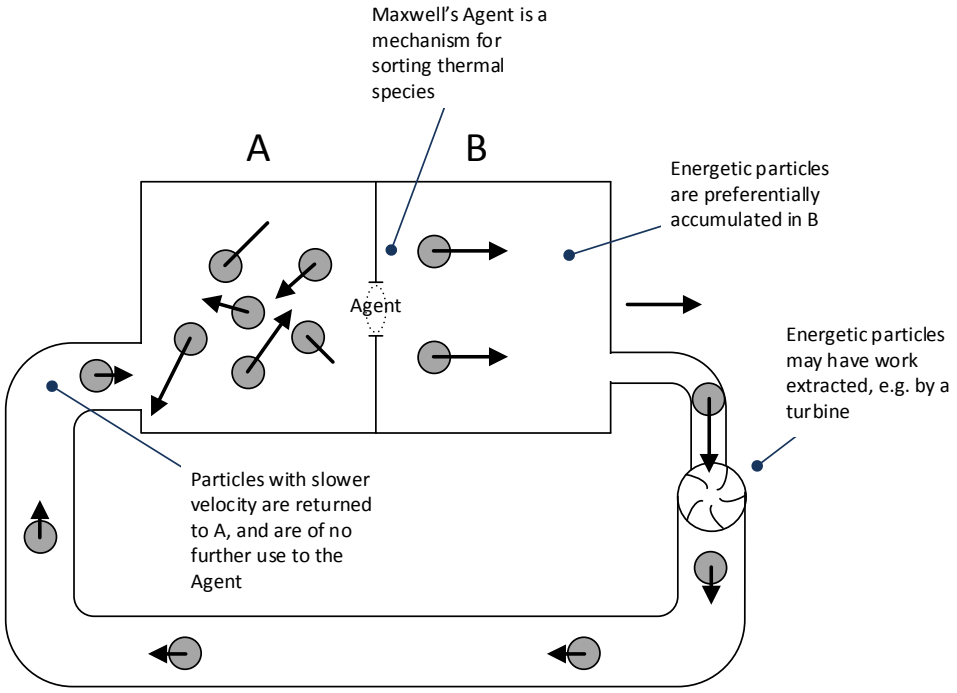

Figure 3. Extraction of energy is a one-time event. Return of the particles back to A causes the temperature to reduce in A, thereby limiting further energy extraction, even for a perfect Agent. So this is not a perpetual motion machine, though it may permit a one-time extraction of energy.

conventionally taken to be velocity, hence temperature in the vessels, and thus the problem is portrayed as a thermodynamic one. However the sorting could be by some other attribute, and at the macroscopic level this might be size, colour, charge etc. In such cases the problem is no longer primarily a thermodynamic one, but a reduction of disorder. In this context disorder refers to the degree of spread in the stochastic mixture of attributes: the MA reduces this spread by selective removal of objects with attributes within a certain range. In summary:

The primary function of a MA device is sorting and reducing disorder, i.e. a one-time separation of species by some attribute. The thermodynamic MA situation is merely a special case for sorting and reducing disorder, hence reduction of entropy.

Additional obstacles emerge that prevent an Agent from being perfect, and these become apparent at deeper levels of analysis.

4.2. Microscopic Level: Gas Interactions at the Molecular Level

Moving to the microscopic level, consider a fluid of perfect gas molecules. If we temporarily assume a perfect Agent—later we elaborate on the many imperfections and losses that a real Agent must have—then it is apparent that the same considerations apply as for the macroscopic balls: the Agent would function as a sorter of species and a reducer of disorder. If that sorting was by molecular velocity, then the outcomes would be thermodynamic, in the form of a once-off extraction of energy. The recycling of spent molecules back to vessel A would lower the temperature therein. Consequently, any energy that could be extracted would be limited by the temperatures of the vessels, hence the Carnot principle applies, and there is predicted to be no perpetual energy MA device at the molecular level (perfect gas) for vessels of finite volume. That is the optimistic loss-less situation and in reality there are more serious difficulties that the Agent must overcome, as follow.

4.2.1. Need for External Power to Operate the Agent

While the macroscopic balls may be detected with photons, we cannot permit this to be applied to the molecular scale because: 1) the momentum of the molecule may be appreciably affected, and 2) a larger number of photons are required to cope with the higher density of molecules, hence more work input. In this situation the energy

cost of measurement could be great compared to the work gained, *i.e.* poor thermodynamic leverage. Sensing the molecules will have to be done by detecting their fields, and additional problems arise (see below).

4.2.2. Momentum Transfer Eliminates the Difference in Velocity

The next difficulty for the Agent is that momentum transfer between molecules erases their velocity difference before the Agent can act to separate them. This also applies in the macroscopic case of elastic balls, but is less severe. At the microscopic level of gas molecules the process is termed thermalisation, whereby the interaction between particles causes equal distribution of energy, hence thermal equilibrium of the gas. A gas can still have Brownian motion even after thermalisation has occurred, as Maxwell pointed out. Increasing the density of the macroscopic balls or microscopic molecules (objects) makes things worse, because although the Agent has more candidate objects within a given time, the objects also have more opportunity to collide with each other and thereby make the distribution of kinetic energy more homogenous. Decreasing the density of the objects might help the situation. For example, if there is only one fast and one slow object in vessel A, then the Agent could hope to capture the fast one eventually, regardless of which was carrying the momentum. (Two objects of equal mass will swap momentum at impact). So in the simplest situation the principle works.

However as more interacting objects are added the momentum transfers become more complex. It is one of the assumptions of an ideal gas that collisions *between the gas particles* occur much more often than collisions with the *wall*. Thus the assumption of an ideal gas maximally works against the Agent: the gas molecules have maximal interaction to equalise their momenta, and they contact the wall relatively infrequently. So the Agent, which of necessity is positioned at the wall, will see relatively few molecules, and these will tend to be homogeneous in velocity.

A contrary argument is that thermalisation is a bulk process and merely results in homogeneous average momentum, whereas there is a degree of random variability for each individual molecule, hence Brownian motion, that the Agent might still harvest. However this will not do either, for reasons of time, as we come to next.

4.2.3. Time Is a Constraint on Efficiency

The difficulty for an Agent that seeks to sort based on random or Brownian motion is that the trajectory of any one molecule cannot be predicted until it is right at the wall, by which time it may be too late to capture it for vessel B. The Agent is static and must wait at its gate for an opportune moment when a high-velocity object happens to be naturally headed towards the gate. Thus the Agent needs time, in the form of waiting for a chance event, plus the time for measurement and capture. The same time provides a gap between the moment of detection and the moment of capture, and this time also allows the molecules to transfer momentum between each other at collisions, and thereby change or erase the initially measured velocity. The greater the particle density (number of participating molecules or objects per unit volume), the greater the momentum transfer opportunities, and the worse the problem for the Agent.

4.2.4. Mean Free Path and Operational Depth

For an Agent attempting to harness random or Brownian motion, it is preferable that the mean free path of the molecules is large. However circumstances do not favour this. The path length, *i.e.* distance between collisions, is inversely proportional to the product of the density (or pressure) and square of the particle diameter. This is problematic because the MA device prefers a denser gas (or higher pressure) with its greater energy density. The mean free path is of the order 0.1 um at 100 kPa, 373 K, for molecules of 3E−10 m diameter.[2]

We therefore introduce the concept that an Agent has an *operational depth*, this being the distance from the point where objects are detected, to vessel B. In the case of gas molecules this depth must be shorter than the mean free path of the molecules, so that the Agent may successfully complete all its detection and capture processes before the molecule changes velocity or direction. However the operational depth cannot be made arbitrarily short, because it depends on the time required to detect velocity (speed and direction), time for computation & decision-making, time to open and close the gate. Each of these requires other matter particles to be moved and then reset, hence the expenditure of energy and the consumption of time. While the operation of the Agent might be accelerated (e.g. faster electronics) to reduce the operational depth, the speed of light imposes a fundamental limit. Thus the further obstacle to constructing a working MA device is the necessity for fast operation, which is a challenge for implementation.

[2]http://hyperphysics.phy-astr.gsu.edu/hbase/kinetic/menfre.html#c3.

A further problem is that a short mean free path results in information about a molecule quickly becoming obsolete, and hence requires the Agent to undertake frequent re-measurement activities. These have an energy cost, which will need to be supplied externally or met by the harvested molecule.

The lower the particle density, in the extreme case only two objects in the vessel, the less the momentum transfer, but the longer the Agent must wait for a fortuitous alignment with the gate. If the Agent is expending energy in maintaining vigilant detection, then the temporal summation thereof must be offset against the once-off energy extraction possible from the system. This does not make for an easy energy breakeven point: the objects need have a certain minimum momentum to make the wait worthwhile. Also, it is preferable that the objects have high mass rather than high velocity. This is because higher velocity requires more frequent monitoring by the Agent and therefore more energy usage. In summary:

Practical difficulties exist for the Agent when operating on a molecular fluid, in that thermalisation erases the velocity difference between objects, such that the residual Brownian motion has a short mean free path. The Agent needs time to wait for a fortuitous incoming energetic object. However that same time also permits more thermalisation between the objects. This requires the Agent to undertake frequent re-measurement activities, with associated energy cost. The perfect gas assumption is incompatible with the Agent as it reduces the interaction of the objects with the wall. The larger the objects, and the fewer, the less the thermalisation and the greater the thermodynamic leverage, but the longer the Agent must wait for a fortuitous alignment with the gate. As the objects become smaller in momenta and more numerous, so the thermodynamic leverage decreases, and in the limit becomes zero.

4.3. Quantum Mechanics Level: Zero-Dimensional Point Particles

Assume that the MA device is filled with an electron gas as the fluid. Under quantum theory, a subatomic particle like the electron is not a single point but rather exists in two positions at once, hence quantum superposition. What does this mean for the MA device? The existing literature in this area has been summarised above, and here some additional comments are made.

4.3.1. Superposition and Uncertainty

The quantum mechanics perspective is that the electron is in geometric superposition, *i.e.* simultaneously in two locations in space, or more precisely its existence is stochastically distributed around two locations. QM asserts that the location is fundamentally uncertain and driven only by a probability function, the wave function. This also means that the exact position of the electron is fundamentally unknowable. Obviously this will cause difficulty for the Agent.

4.3.2. Measurement

Measurement is a key part of the activities of the Agent. Empirical evidence, e.g. the Zeno effect, shows that measurement affects the system under examination and that the process of measurement does affect a system in superposition. However it is difficult to explain how the act of observation causes the wave-function to collapse and the system to take a specific value, which is the problem of contextual measurement. Also problematic is that QM explanations of the MA assume that particles are in a quantum (coherent) state, but this is not the empirically observed behaviour at the macroscopic scale. It is difficult to explain why and where the transition occurs between coherent and discoherent states. Consequently the QM explanations of the MA do not cover the full scale from fundamental to macroscopic.

4.3.3. Pre-Existing Properties or Not?

Another difficulty for the MA device is that apply quantum mechanics denies that particles have pre-existing values. Per the Heisenberg uncertainty principle, the position and velocity of the electron are not both simultaneously knowable to precision. So there is nothing definite for the Agent to work on, unless it expends energy making measurements that collapse the wave function. QM proposes that the intrinsic parameters of the electron, e.g. the frequency (hence energy), position, and velocity, do not exist until they are observed, hence that the act of measurement is what forces them to take specific values. In many empirical tests these problems are circumvented by using large ensembles of particles, some of which are measured sacrificially as representatives of the larger population. The resulting means and probability distributions for these ensembles are key input variables

in the quantum theory. However, this does not definitively address the behaviour of individual particles.

4.3.4. Quantum Mechanics at the MA Level

It is difficult to see how the Agent might operate at the quantum level. For the sorting process the agent needs to know the velocity of the electron, and for the gating function it needs to know its position. Quantum mechanics does not permit both these to be known.

Most of the quantum analyses of the MA device in the literature have made the unrealistic assumption that the working fluid is a coherent substance, *i.e.* a condensed or entangled state [31] [32]. This is not how real fluids operate at macroscopic scales, and not the thermodynamic regime Maxwell had in mind. Consequently there is no conclusive explanation of the MA device at the QM level. In summary:

From a quantum mechanics perspective the Agent cannot know with certainty the energy, position, and velocity of the objects, due to Heisenberg uncertainty. This would limit the efficacy of the agent, and may be sufficient to altogether prevent it operating.

4.4. Sub-Particle Level: Cordus Theory Applied to Maxwell's Agent

This section considers the level deeper than the 0-D particle of quantum theory, for which the Cordus theory is used. A brief summary of the theory is first provided to set the context.

The Cordus theory predicts a specific structure to matter. There is an *inner structure* comprising two *reactive-ends*, which are a small finite distance apart (span), and each behaves like a particle in its interaction with the external environment [39]. A *fibril* joins the reactive-ends and is a persistent and dynamic structure but does not interact with matter. It provides instantaneous connectivity and synchronicity between the two reactive-ends. There is also an *external structure* whereby the reactive-ends periodically energise at the de Broglie frequency, and in doing so emit *discrete forces* in one or more of three orthogonal directions into the external environment. These discrete forces functionally make up a flux line. As a whole this set of structures is called a *particule* where it is necessary to emphasise that this is not a 0-D point. See **Figure 4** for an example.

Electric charge is carried at 1/3 charge per discrete force, with the sign of the charge being determined by the direction of the discrete force. So the number and propagation direction of energised flux tubes determines the overall electric charge of the particule.

The stochastic nature of the QM superposition can be conceptually recovered, being understood to represent the energisation states of the two reactive ends. In QM the 0-D particle is in *both* places at once, and simultaneously in neither until observed. In the Cordus theory the particule oscillates its energised location between its two reactive ends. Superposition arises because the Cordus particule has two reactive-ends with a separation between them, and these energise in turn at a frequency. The act of observation forces the photon particule to collapse to one location.

4.4.1. Agent with Cordus Particules

Next, consider the MA from the perspective of the Cordus theory. There are several issues to consider.

Escape mechanisms

Each incoming electron has a velocity as a whole, but its location oscillates between two moving places. The gate will need to be large enough in section to accommodate the electron span. In addition, the Agent will need to measure the locations of both reactive-ends, so that it can keep the gate open for the necessary temporal window to capture both. Otherwise the electron may escape again by tunnelling (see below).

However this temporal window also means there is risk of escape by a previous captive while the gate is open. Hence the efficacy of the system is reduced. There is nothing in the formulation of the MA device that prevents backflow through the gate. Only if particles were classical 0D points would this temporal window be infinitesimally short. In summary:

For a working fluid comprising sub-microscopic particules, geometric superposition creates an ambiguity about the spatial location of the particule relative to the gate, which decreases the efficacy of the capture process.

4.4.2. Tunnelling

Superposition causes a further difficulty, in that at small scales it can be difficult to confine an electron. This is

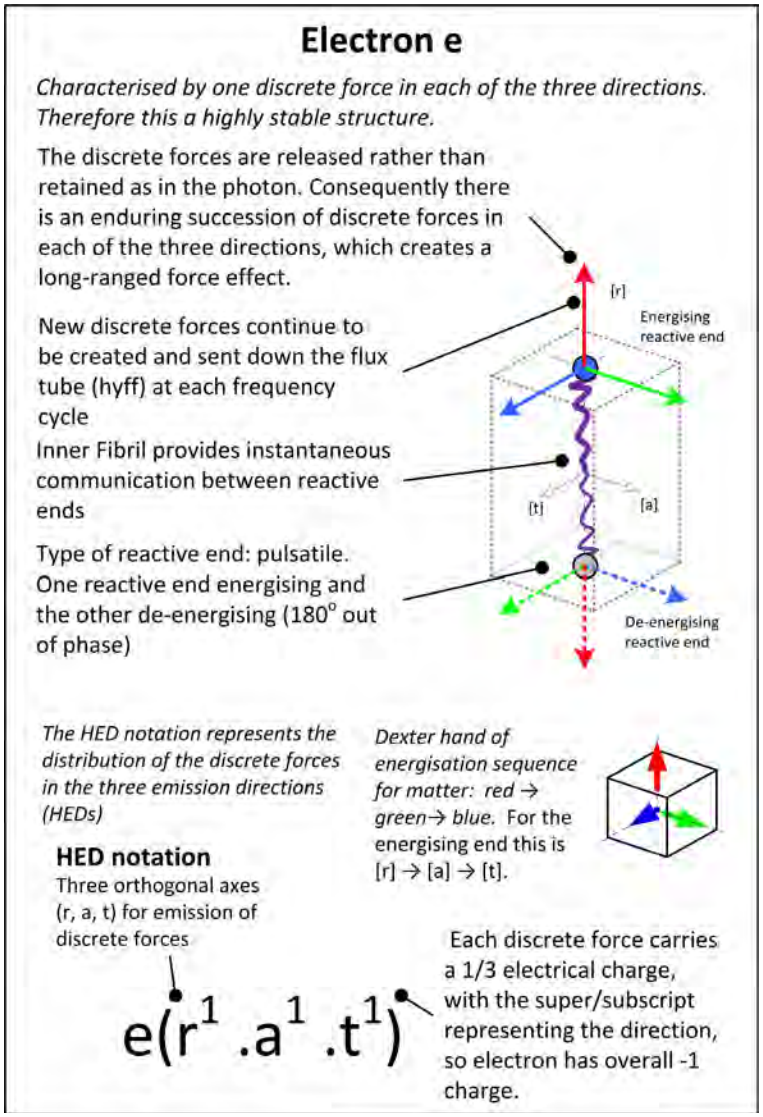

Figure 4. The representation of the electron's internal and external structures. It is proposed that the particle has three orthogonal discrete forces, energised in turn at each reactive end. Adapted from [40] with permission.

evident in the empirically observed effects of the Josephson junction where a superconducting current can flow across a narrow insulating gap, and quantum tunnelling where a particle crosses an energy gap that should otherwise not be possible. The present theory has an explanation for tunnelling, which is given for photons at [46].

The Cordus theory anticipates that tunnelling would occur in the gate of the MA. Consider an electron with two reactive-ends in vessel A, and an Agent comprising a thin layer of material. Now the *energised* reactive-end emits discrete forces that interact with those of the Agent materials (e.g. the insulator atoms), hence generating reactive forces that prevent the reactive-end from penetrating the material, thus the electron is instead reflected. However the *denergised* reactive-end has low reactivity and can be displaced into the bulk of the Agent material, *i.e.* beyond the surface plane. If the denergised reactive-end starts to reenergise inside the bulk, then it is ejected back into medium A. However, if the thickness of the bulk material comprising the Agent is thin, then the denergised reactive-end may move through the thin barrier and then safely reenergise inside vessel B. Then the other reactive-end may also travel through into vessel B at its next dormant cycle. Thus the particule as a whole can tunnel across the barrier. This is proposed as the explanation for the Josephson junction and quantum tunnelling. Unfortunately for the MA device, the electrons in vessel B can also tunnel back into A. So the MA de-

vice needs a thin gate to reduce its operational depth relative to the mean free path of the objects, but tunnelling reduces the efficiency of a thin insulator. Only if particles are 0-D points would this not be a problem.

4.4.3. Measurement at the Fundamental Scale

Consider the measurement process of the Agent. Take a situation where vessel A is filled with an electron gas, with the electron as defined in the Cordus theory. Now consider the measurement responsibilities of the Agent at this fundamental level. It has to determine the velocity of each object (electron) before deciding whether to admit it to B. How will it do this? One option is for the Agent to generate photons and bounce them off the objects. Generating photons involves an energy cost for the Agent. The smaller the objects being measured, or the faster their velocity, the higher the required energy of the photon to obtain the necessary spatial and temporal resolution. This will adversely affect the efficiency of the Agent.

Furthermore there is still the question of how the photon might affect the electron. Specifically the photon may be absorbed by the electron, thereby changing its energy. This will be significant at the level of electrons and other small particules, less so at the macroscopic level of tennis balls. The Agent will then be pumping vessel A, and a strict MA implementation cannot permit this active measurement.

Are there ways of detecting the objects without the cost and interference of emitting photons at them? The answer to this depends on the philosophical position of whether objects have values that pre-exist, whether locality applies, and how contextual measurement works.

4.4.4. Locality and Contextual Measurement

The conventional theories of physics, including quantum mechanics, expect locality to be preserved. This means that a 0-D point particle is expected to be only affected by the values of the fields (electrical, magnetic, gravitational, etc.) at the infinitesimally small location of the point, a related expectation is that a property of the particle cannot be changed unless an external field or force is made to apply at that point. In contrast the Cordus theory proposes that the principle of locality fails. This is because the Cordus particule has a span and there are zones around each reactive-end where the discrete forces interact with the discrete forces of other particules. Consequently the particule is affected by more than the fields at its nominal centre point, and thus the theory asserts a *Principle of Wider locality*. Confirmatory evidence for this is seen in the evanescent field of the photon, whereby the locus of the photon is affected by material properties beyond its nominal point location [39].

The next issue is about the conceptuality of measurement, and what happens when an observer measures a quantum system. From the perspective of the Cordus theory there are two main ways to measure a particle. One is to collapse it, as when a photon is stopped and absorbed in a detector. This collapse provides information on its location. The theory proposes that measuring or otherwise grounding one reactive-end causes the whole photon to collapse [39]. The second method of measurement is by remote interaction through fields or flux tubes of discrete forces. This does not destroy the particle under examination, nor arrest it, but the interaction between the probing discrete forces and the particle's own emission if discrete forces affects its re-energisation and hence properties of location and energy (frequency). This has been applied to give a Cordus explanation of refraction and reflection of light [39], and the wider phenomenon includes the Zeno effect and the pumping of laser cavities. This second type of measurement is therefore always contextual: it depends on how the measurement is made and how aggressive the probing discrete forces are relative to the particle under examination. However, and this is important, *any* externally imposed measurement interaction *will* change the particle under examination, it is only a matter of degree.

Applying this to the MA situation means that it is impossible to assay the velocity of an electron, or any other object, without affecting it in some way. Even passively observing the proximity of an electron involves interacting with its discrete forces, hence interfering with it. Consequently, as the objects in the MA device become smaller, so the measurement intrusion becomes worse, and it becomes increasingly difficult to determine where the object is and how fast it is moving. Its location may be determined by arresting it, which is no use to the MA case. Or its velocity may be determined, but then the dynamic nature of the re-energisation process makes it difficult to be sure about the location of the current reactive-end. In this way the Cordus theory also conceptually recovers the Heisenberg uncertainty principle.

4.4.5. Do Intrinsic Parameters Have Values Prior to Measurement?

As previously identified, quantum theory proposes that objects *do not* have values that exist before measurement.

In contrast the Cordus theory proposes that the electron does have specific values for all its parameters, that exist before the measurement takes place, but 1) they are dynamic and fast-changing (e.g. the position of the energising reactive-end can change so fast that it appears the particle is in two positions), 2) some of the parameters are coupled and cannot be measured simultaneously, and this is the uncertainty principle (e.g. the position and velocity of the electron are both determined by the progressive spatial position of the reactive-ends), 3) the act of measurement can interfere with the parameter and thereby change what is being measured (e.g. measurement of the frequency of a particle involves interacting with its discrete forces, hence affecting the emission thereof and thus affecting the frequency). In summary:

At the fundamental level, all measurement is contextual. It is impossible to assay the velocity of an object without affecting it in some way (*contextual measurement intrusion*). *This applies even to passive observation of the fields of an object.*

4.4.6. Passive Detection of the Energetic Object

So, no form of using photons to detect the incoming particules is acceptable at the fundamental level, if the objective is a thermodynamic extraction of energy. How about a less active form of measurement, like passively detecting the fields? Consider an Agent that waits passively and detects the electric fields of the approaching electrons, and assume that the sorting is by the energy (frequency) of the electron rather than velocity. Thus the Agent can wait until it detects a higher-than-average frequency, and then open the gate to admit that electron.

However, there are practical difficulties. There is the fundamental question of how the Agent would passively measure the field of an approaching electron. Assuming physical realism, it seems necessary that the Agent employ another charged particle to do this. This measurement particle could be another electron. The Agent would monitor the deflection of the measurement particle under the forces of the incoming particle, and respond accordingly. However this has further problems, as we shall see.

The next problem is that the Agent will need to determine the direction in which the electron is moving, since only electrons moving perpendicular to the wall, as opposed to tangential to it, are desired. Opening the gate to a tangential electron will not lead to capture, but may increase the chance of escapees from B. Determining the direction will need at least two measurements. Given the small mean path length in an equilibrated situation, this will be challenging: the measurement, decision-making, and gate-activation would need to be fast.

In an attempt to solve this, consider an improved trapdoor design of an Agent. Create a pore between vessels A and B, and block it with a molecule that includes a sensing electron. This sensor would move its position as it interacted with the fields of a sufficiently energetic incoming object, and this would cause the molecule as a whole to change shape and momentarily open the pore to let the energetic object through. Assume that the molecule could be designed so that it only hinged open for objects with velocity perpendicular to the wall. This design has the Agent simply responding opportunistically to energetic objects. It avoids all the memory issues of other MA proposals: the need to measure, record and erase data, and the energy cost thereof. Afterward the molecule of our hypothetical molecular Agent resets itself and repositions the sensor electron in readiness for another capture.

It might be thought that this restorative force could be elastic, e.g. mediated by bonds. Imagine a molecule that could be bent under the interaction with the incoming object, and then spring back into place when it had passed. We will also need to imagine that this molecule has some non-linear sensitivity such that it prevents back flow, for example that the sensor electron is the trigger rather than the gate itself, and is located in vessel A, hence insulated from B. It is like a one-way spring-loaded trapdoor that only lets through the energetic objects. We have to accept that our Agent may absorb some of the energy of the incoming object, but we can also anticipate that it would give the energy back to the object as it moved through the pore. Thus an Agent might appear not to require an energy source, as all its interactions would be elastic. However this is not so.

The measuring particle would need to be in a constrained location for deflection to be monitored, and would need a force to return it to the sensing position after a duty cycle. That resetting activity is problematic, because it causes hysteresis losses.

4.4.7. Hysteresis Losses

An elastic matter-based Agent using a charged particle (e.g. electron or proton) or even a neutron as the detector will have losses. This is because moving the sensing particle backwards and forwards involves acceleration, and it will emit a bremsstrahlung photon. Thus a hysteresis loss occurs. The same applies to the neutron, since it has

a magnetic moment, albeit smaller. Even a perfectly balanced neutral particle with zero magnetic moment will still, per general relativity, emit a gravitational wave and radiate energy when subject to acceleration [47]. Although this emitted energy will be miniscule, it is nonetheless another loss that must be recouped from the harvested particle. The Agent requires external energy to reset so that it can continue operating. The Agent could be contrived to take the necessary energy from the objects that it captures, but that would defeat the purpose. It seems inevitable that a realistic design of Agent will always suffer from bremsstrahlung hysteresis losses. The losses might be reduced by moving matter more slowly, but this corresponds to an Agent that works slower. A slower Agent suffers from other problems, most especially the worsening of its ability to measure and complete a capture before energetic particules transfer their energy via impact with other particules. The converse is that the faster the Agent operates, the more likely it is to make a successful capture, but the greater the hysteresis losses.

Consequently we conclude that:

It is not possible to create a matter-based Agent that is lossless, because bremsstrahlung hysteresis losses will always occur when matter is moved back and forth within the Agent.

4.4.8. A General Design of a Matter-Based Agent

So we identify that the MA device requires energy to operate, and therefore cannot be lossless. However, if the energy it could extract from Brownian motion was sufficiently large, and it extracted this energy continuously, then this would not be a problem. This requires an examination of Brownian motion.

4.5. Brownian Motion and Entropy per the Cordus Framework

4.5.1. Explanation of Entropy in Terms of Geometric Irreversibility

The Cordus theory can be applied to explain Brownian motion. This is relevant since Brownian motion is what the MA device seeks to harness. Consider a particle P in vessel A of the MA device. The logic is as follows.

Particules have two ends, and hence two locations at which they can be affected. Each reactive-end emits discrete forces out into the external environment, contributing to a mesh of discrete forces in space, which is the fabric [48]. All the other particules do the same. Correspondingly, any particule P receives discrete forces from all the particules (many N) in its accessible universe. In turn this fabric interferes with the emission of discrete forces for particule P. Due to the sizeable zone of influence provided by the *Principle of Wider Locality*, the particule P is affected by external fabric events in a zone outside the particule, including discrete forces in the fabric. These interfere with its own emissions, and therefore change its frequency. The interference also moves the location of the reactive-end in response to the imbalance between its own emitted discrete forces and the external discrete forces from the fabric. Since the fabric is discrete, it is also somewhat random in its composition. Consequently P will be buffeted by the fabric, and will be displaced one way and then the next. The movement of P means that at the next instant it is emitting discrete forces from a *different* location in the universe. Then the geometric *superposition* of the two reactive-ends means that disturbances at one reactive-end are communicated superluminally to the other, which then also engages with the fabric. This increases the complexity of the response of P to the fabric.

Consequently other remote particules N are also bumped into slightly different locations by the changed emissions of P. The overall effect is that all the particules move around. The vast number of particules in the accessible universe, plus the time delay between them (fields are assumed to propagate only at the speed of light), adds so much complexity to the system that it is practically impossible to return particule P and all the many other particules N to their original geometric positions and energy states. Consequently the system as a whole is irreversible.

This, it is proposed, is where the arrow of time arises [49], and entropy too. This is because any original energy (or temperature) differences between objects in the fluid A are eventually dispersed among all the objects, and the irreversibility prevents the original state from being recovered. There is a chain of causality whereby the whole universe affects the position of the reactive-ends of particule P, and as soon as P moves in response it starts to affect the whole universe in return. Thus the fluid in A becomes more thermodynamically homogenous, and energy becomes non-available for doing work. Hence entropy increases. In this context entropy represents all of the un-available energy, the disorder of the system, the number of ways the objects in A can be arranged, or the degree to which the system has deviated from the original geometric layout.

4.5.2. Brownian Motion

Then Brownian motion may be explained in the Cordus theory as arising from the jostling by the fabric of many small particules P. These particules then apply forces to larger clumps of matter, such as molecules and collections of molecules, which aggregate those forces in unpredictable ways. Hence Brownian motion becomes observable at a macroscopic level, and does not require quantum coherence at this level. Larger objects are exposed to the fabric perturbations as much as smaller ones, but the Brownian motions of larger object are reduced because of the effects of cancellation of forces across the relatively rigid body, the many small forces receives, and larger inertial mass. Brownian movement is therefore proposed to be a proxy variable for a deeper fabric perturbation effect.

Accepting this interpretation that Brownian motion results from the interplay of discrete forces at the fundamental level, and adding the complexity of superposition and wider locality, then this suggests a further impediment to the successful operation of the MA device: the future path of an object changes rapidly and randomly. It is impossible to predict by the Agent. This worsens for smaller objects. Also, the more compact the Agent, the worse things get for its own efficiency (as above). In summary:

The random motions of small objects observed as Brownian motion, derive from the aggregation of multiple even finer random forces from the fabric, such that the future path of an object is unpredictable after it has been measured. This means there is no value in the Agent making a measurement of the object's position and velocity: both these will change before it moves through the gate. The smaller the object the greater the perturbation hence the greater the Brownian velocity but also the greater the variability.

The exception is if the object is already at the gate, and springs it open without the agent having to do any prior measurement. This also requires the gate to be very thin, so that the capture can be effected before the randomness of Brownian motion changes the direction of the object. However in that case objects in vessel B will also be on the other side of the gate, and will escape or tunnel back to A. Such a device will not preserve a pressure or temperature differential: the two vessels will equilibrate. Even then the Agent will have hysteresis losses.

Thus the MA is predicted to be unable to extract work from Brownian motion. Thus in the end we find that the Maxwell Agent will not work at all at the fundamental level.

5. Discussion

5.1. Outcomes

This work provides several novel outcomes. The first is that it provides a comprehensive analysis of the Maxwell Agent apparatus, covering multiple levels from macroscopic to fundamental. The results predict that the MA device cannot be implemented as a perpetual motion device. It requires energy to operate. However it can in principle provide a one-time extraction of work for the expenditure of an initial energy. The analysis also shows that the MA device is primarily a sorting machine. It could in principle sort by attributes other than energy.

The argument is summarised as follows:

A practical implementation of a macroscopic MA device seems feasible, using large objects that are sparsely distributed. A macroscopic MA device permits, at best, a one-time extraction of energy. This is at the cost of input energy or parasitic losses, hence thermodynamic leverage. This would not be a perpetual energy device.

The primary function of a MA device is sorting and reducing disorder, i.e. a one-time separation of species by some attribute. The thermodynamic MA situation is merely a special case for sorting and reducing disorder, hence reduction of entropy.

Practical difficulties exist for the Agent when operating on a molecular fluid, in that thermalisation erases the velocity difference between objects, such that the residual Brownian motion has a short mean free path. The Agent needs time to wait for a fortuitous incoming energetic object. However that same time also permits more thermalisation between the objects. This requires the Agent to undertake frequent re-measurement activities, with associated energy cost. The perfect gas assumption is incompatible with the Agent as it reduces the interaction of the objects with the wall. The larger the objects, and the fewer, the less the thermalisation and the greater the thermodynamic leverage, but the longer the Agent must wait for a fortuitous alignment with the gate. As the objects become smaller in momenta and more numerous, so the thermodynamic leverage decreases, and in the limit becomes zero.

From a quantum mechanics perspective the Agent cannot know with certainty the energy, position, and veloc-

ity of the objects, due to Heisenberg uncertainty. This would limit the efficacy of the agent, and may be sufficient to altogether prevent it operating.

For a working fluid comprising sub-microscopic particules, geometric superposition creates an ambiguity about the spatial location of the particule relative to the gate, which decreases the efficacy of the capture process.

At the fundamental level, all measurement is contextual. It is impossible to assay the velocity of an object without affecting it in some way (contextual measurement intrusion). This applies even to passive observation of the fields of an object.

It is not possible to create a matter-based Agent that is lossless, because bremsstrahlung hysteresis losses will always occur when matter is moved back and forth within the Agent.

The random motions of small objects observed as Brownian motion, derive from the aggregation of multiple even finer random forces from the fabric, such that the future path of an object is unpredictable after it has been measured. This means there is no value in the Agent making a measurement of the object's position and velocity: both these will change before it moves through the gate. The smaller the object the greater the perturbation hence the greater the Brownian velocity but also the greater the variability.

The exception is if the object is already at the gate, and springs it open without the agent having to do any prior measurement. This also requires the gate to be very thin, so that the capture can be effected before the randomness of Brownian motion changes the direction of the object. However in that case objects in vessel B will also be on the other side of the gate, and will escape or tunnel back to A. Such a device will not preserve a pressure or temperature differential: the two vessels will equilibrate. Even then the Agent will have hysteresis losses.

The second novel contribution is that the paper shows that the NLHV solution of the Cordus theory can explain entropy and Brownian motion. The theory also provides physically natural explanations for superposition, entanglement, irreversibility, entropy, contextual measurement, coherence-discord transition, and tunnelling. The NLHV sector has otherwise not made significant contribution to these thermodynamic and related phenomena.

In this way we have offered a candidate explanation for the MA that is 1) based in physical realism and obviates the need for metaphysical mechanisms, and 2) covers the scale from the macroscopic to the quantum level and beyond. This is achieved with an original theory of physics. This theory conceptually recovers the continuum represented by conventional thermodynamics, and quantum behaviours. However it is not a derivation of quantum mechanics but rather a NLHV theory, and hence the complexity of the treatment provided here.

5.2. Implications for the Second Law of Thermodynamics

At the macroscopic level, the Second Law states that energy cannot be extracted from an equilibrated fluid, one with homogeneous pressure and velocity. Maxwell was questioning whether this still applied at the fundamental scale if there was some Agent to capture the particles with higher Brownian motion. The present analysis identifies that the Agent is primarily a sorting device and is energy-consuming, rather than purely a passive thermodynamic one-way device. Velocity is only one of the attributes that it might sort against. Whatever it sorts for, it always requires energy to operate, and this applies also to the thermodynamic situation. Depending on the application it might require more or less energy, and depending on the situation (object size, quantity, velocity) it might even give a once-off extraction of energy. However some energy consumption is inevitable even in the most passive designs conceivable, because of the need to move its matter-based working parts in space, hence low grade Bremsstrahlung emission and hysteresis losses. Consequently we dismiss the possibility that any physical Maxwell Agent could be a long-term perpetual energy device.

What about the extraction of energy from Brownian motion in an equilibrated fluid? The present analysis shows that the operating characteristics of the device become more compromised as the scale of the objects reduces from the macroscopic to the fundamental. The problems for the device are the necessity to use passive measurement (to avoid pumping the system) and the consequent difficulty of measuring the position and velocity of the objects. The latter issue is already problematic at the level of the perfect gas assumption, and becomes still more acute as the scale reduces further. When the situation is reduced to the scale at which Brownian motion is apparent, the analysis predicts that it is unlikely that even a once-off extraction of work will be possible.

Thus the present work finds in favour of the Second Law, by confirming that energy cannot be extracted from

an equilibrated fluid at either macroscopic or particule level.

There are potentially interesting implications for entropy. Maxwell's paradox is only secondarily a thermodynamic question: it is really a question about sorting and hence entropy. The present analysis shows that the concept of entropy applies at the bulk level, and can be reversed (at an energy cost) at the particle level. Thus we have shown, using the Cordus NLHV theory, that entropy is a group property, *i.e.* an attribute of the assembly of particules, not a characteristic of the individual particle. This is close to Maxwell's original expectations. This also recovers the conventional statistical interpretation, but from a different direction.

6. Conclusions

The problem posed by Maxwell is a profound question about the intersection of thermodynamics with fundamental physics. This analysis shows that the NLHV design predicts that even a perfect MA mechanism with perfectly elastic collisions between macroscopic balls has the following limitations:

1) There is no perpetual energy MA device at either the macroscopic level (perfectly elastic ball collisions), or the molecular level (perfect gas).

2) The MA device is primarily a sorting machine, and thermodynamic sorting is merely one of multiple applications.

3) It permits at best a one-time extraction of energy from a mixture of energetic species, but only at large geometric scales. At small scales the opportunity for escapees increases, and the losses increase.

These conclusions are in accord with conventional analyses based on statistical mechanics. Consequently the predictions are not necessarily novel when looked in isolation. Rather, the original contribution is recovering these findings from the perspective of a single particle in a NLHV solution. This is valuable because it provides a rational explanation for the thermodynamic effects based on physical realism at the level of fundamental physics, which is not achieved by purely statistical or quantum approaches. Furthermore the same NLHV Cordus theory successfully explains or recovers many other phenomena including wave particle duality, basic optical laws of refraction & reflection [39], pair production & annihilation [44] [50], stability and instability of nuclides (H to Ne) [43] [51], asymmetrical lepto- & baryogenesis [45], and the relativity of simultaneity (time dilation) [49]. The theory provides one coherent framework of explanation for all these phenomena. With the addition of the ability to explain aspects of thermodynamics at the fundamental level, the theory demonstrates resilience and validity.

The present work finds in favour of the second law, by confirming that energy cannot be extracted from an equilibrated fluid at either macroscopic or particule level, when applied over a longer time period. Further, entropy is a group property, not a characteristic of the individual particle. A MA is primarily a sorting device, and has the potential to change entropy, though with an energy cost.

Acknowledgements

The authors declare no funding sources external to their affiliations.

Author Contributions

All authors contributed to the creation of the underlying concept, development of the thermodynamic ideas, and editing of the paper. DP created the images and identified the hysteresis losses and Brownian motion.

Conflict of Interest Statement

The authors declare that there is no conflict of interests regarding the publication of this article. The research was conducted without personal financial benefit from any external funding body, nor did any such body influence the execution of the work or the decision to publish.

References

[1] Maxwell, J.C. (1891) Theory of Heat. Longmans, Green, and Co., London.

[2] Maruyama, K., Nori, F. and Vedral, V. (2009) *Reviews of Modern Physics*, **81**, 1-23. http://dx.doi.org/10.1103/RevModPhys.81.1

[3] Wang, Y.-Z. (1986) *Energy Conversion and Management*, **26**, 249-252. http://dx.doi.org/10.1016/0196-8904(86)90063-4

[4] Bannerman, S.T., Price, G.N., Viering, K. and Raizen, M.G. (2009) *New Journal of Physics*, **11**, 63044.

[5] Binnewies, T., Sterr, U., Helmcke, J. and Riehle, F. (2000) *Physical Review A—Atomic, Molecular, and Optical Physics*, **62**, 011601. http://dx.doi.org/10.1103/PhysRevA.62.011601

[6] Reinaudi, G. and Guery-Odelin, D. (2008) *Physical Review A—Atomic, Molecular, and Optical Physics*, **78**, 015401.

[7] Thorn, J.J., Schoene, E.A., Li, T. and Steck, D.A. (2008) *Physical Review Letters*, **100**, 240407. http://dx.doi.org/10.1103/PhysRevLett.100.240407

[8] Thorn, J.J., Schoene, E.A., Li, T. and Steck, D.A. (2009) *Physical Review A—Atomic, Molecular, and Optical Physics*, **79**, 063402.

[9] Liew, R., Zeegers, J.C.H., Kuerten, J.G.M. and Michalek, W.R. (2012) *Physical Review Letters*, **109**, 054503. http://dx.doi.org/10.1103/PhysRevLett.109.054503

[10] Eggers, J. (1999) *Physical Review Letters*, **83**, 5322-5325. http://dx.doi.org/10.1103/PhysRevLett.83.5322

[11] Isert, N., Maa, C.C. and Aegerter, C.M. (2009) *The European Physical Journal E*, **28**, 205-210. http://dx.doi.org/10.1140/epje/i2008-10403-7

[12] Chatterjee, M.N., Kay, E.R. and Leigh, D.A. (2006) *Journal of the American Chemical Society*, **128**, 4058-4073. http://dx.doi.org/10.1021/ja057664z

[13] Quan, H.T., Liu, Y.-X., Sun, C.P. and Nori, F. (2007) *Physical Review E—Statistical, Nonlinear, and Soft Matter Physics*, **76**, 031105. http://dx.doi.org/10.1103/PhysRevE.76.031105

[14] Vaikuntanathan, S. and Jarzynski, C. (2011) *Physical Review E—Statistical, Nonlinear, and Soft Matter Physics*, **83**, 061120. http://dx.doi.org/10.1103/PhysRevE.83.061120

[15] Jacobs, K. (2012) *Physical Review E—Statistical, Nonlinear, and Soft Matter Physics*, **86**, 040106. http://dx.doi.org/10.1103/PhysRevE.86.040106

[16] Moore, S.K. (2012) *IEEE Spectrum*, **49**, 14-16. http://dx.doi.org/10.1109/mspec.2012.6189562

[17] Aquino, G., Grigolini, P. and Scafetta, N. (2001) *Chaos, Solitons & Fractals*, **12**, 2023-2038. http://dx.doi.org/10.1016/S0960-0779(00)00162-4

[18] Hosoya, A., Maruyama, K. and Shikano, Y. (2011) *Physical Review E—Statistical, Nonlinear, and Soft Matter Physics*, **84**, 061117. http://dx.doi.org/10.1103/PhysRevE.84.061117

[19] Gyftopoulos, E.P. (2002) *Physica A: Statistical Mechanics and Its Applications*, **307**, 421-436. http://dx.doi.org/10.1016/S0378-4371(01)00631-8

[20] Gyftopoulos, E.P. (2002) *Physica A: Statistical Mechanics and Its Applications*, **307**, 405-420.

[21] Livorati, A.L.P., Loskutov, A. and Leonel, E.D. (2012) *Physica A: Statistical Mechanics and Its Applications*, **391**, 4756-4762. http://dx.doi.org/10.1016/j.physa.2012.05.002

[22] Zaslavsky, G.M. and Edelman, M. (1997) *Physical Review E—Statistical Physics, Plasmas, Fluids, and Related Interdisciplinary Topics*, **56**, 5310-5320. http://dx.doi.org/10.1103/physreve.56.5310

[23] Zheng, J., Zheng, X., Zhao, Y., Xie, Y., Yam, C., Chen, G., Jiang, Q. and Chwang, A.T. (2007) *Physical Review E—Statistical, Nonlinear, and Soft Matter Physics*, **75**, 041109. http://dx.doi.org/10.1103/PhysRevE.75.041109

[24] Dong, H., Xu, D.Z., Cai, C.Y. and Sun, C.P. (2011) *Physical Review E—Statistical, Nonlinear, and Soft Matter Physics*, **83**, 061108. http://dx.doi.org/10.1103/PhysRevE.83.061108

[25] Cai, C.Y., Dong, H. and Sun, C.P. (2012) *Physical Review E—Statistical, Nonlinear, and Soft Matter Physics*, **85**, 031114. http://dx.doi.org/10.1103/PhysRevE.85.031114

[26] Niven, R.K. (2006) *Physica A: Statistical Mechanics and Its Applications*, **365**, 142-149. http://dx.doi.org/10.1016/j.physa.2006.01.021

[27] Weiss, C. and Wilkens, M. (1997) *Optics Express*, **1**, 272-283. http://dx.doi.org/10.1364/OE.1.000272

[28] Kim, S.W., Sagawa, T., De Liberato, S. and Ueda, M. (2011) *Physical Review Letters*, **106**, 070401. http://dx.doi.org/10.1103/PhysRevLett.106.070401

[29] Erez, N. (2012) *Physica Scripta*, T**151**, 014028. http://dx.doi.org/10.1088/0031-8949/2012/t151/014028

[30] Pekola, J.P. and Hekking, F.W.J. (2007) *Physical Review Letters*, **98**, 210604. http://dx.doi.org/10.1103/PhysRevLett.98.210604

[31] Jennings, D. and Rudolph, T. (2010) *Physical Review E—Statistical, Nonlinear, and Soft Matter Physics*, **81**, 061130

http://dx.doi.org/10.1103/PhysRevE.81.061130

[32] Maruyama, K., Morikoshi, F. and Vedral, V. (2005) *Physical Review A—Atomic, Molecular, and Optical Physics*, **71**, 012108.

[33] Zurek, W.H. (2003) *Physical Review A—Atomic, Molecular, and Optical Physics*, **67**, 012320.

[34] Einstein, A., Podolsky, B. and Rosen, N. (1935) *Physical Review*, **47**, 777-780. http://dx.doi.org/10.1103/PhysRev.47.777

[35] Bell, J.S. (1964) *Physics*, **1**, 195-200.

[36] Leggett, A. (2003) *Foundations of Physics*, **33**, 1469-1493. http://dx.doi.org/10.1023/A:1026096313729

[37] De Broglie, L. (1925) *Annales de Physique*, **3**, 98-109. http://tel.archives-ouvertes.fr/docs/00/04/70/78/PDF/tel-00006807.pdf

[38] Bohm, D. and Bub, J. (1966) *Reviews of Modern Physics*, **38**, 453-469. http://dx.doi.org/10.1103/RevModPhys.38.453

[39] Pons, D.J., Pons, A.D., Pons, A.M. and Pons, A.J. (2012) *Physics Essays*, **25**, 132-140. http://dx.doi.org/10.4006/0836-1398-25.1.132

[40] Pons, D.J. (2015) *Applied Physics Research*, **7**, 14-26. http://dx.doi.org/10.5539/apr.v7n4p24

[41] Pons, D.J., Pons, A.D. and Pons, A.J. (2014) *Physics Essays*, **27**, 26-35. http://dx.doi.org/10.4006/0836-1398-27.1.26

[42] Pons, D.J., Pons, A.D. and Pons, A.J. (2014) *Applied Physics Research*, **6**, 50-63. http://dx.doi.org/10.5539/apr.v6n3p50

[43] Pons, D.J., Pons, A.D. and Pons, A.J. (2015) *Physics Research International*, **2015**, Article ID: 651361. http://dx.doi.org/10.1155/2015/651361

[44] Pons, D.J., Pons, A.D. and Pons, A.J. (2015) *Journal of Nuclear and Particle Physics*, **5**, 58-69.

[45] Pons, D.J., Pons, A.D. and Pons, A.J. (2014) *Journal of Modern Physics*, **5**, 1980-1994. http://www.scirp.org/Journal/PaperInformation.aspx?paperID=51921 http://dx.doi.org/10.4236/jmp.2014.517193

[46] Pons, D.J., Pons, A.D., Pons, A.M. and Pons, A.J. (2011) Cordus Conjecture: Part 1.2 Quo Vadis, Photon? http://vixra.org/abs/1104.0017

[47] Einstein, A. (1920) Relativity: The Special and General Theory. Holt, New York.

[48] Pons, D.J. and Pons, A.D. (2013) *The Open Astronomy Journal*, **6**, 77-89. http://dx.doi.org/10.2174/1874381101306010077

[49] Pons, D.J., Pons, A.D. and Pons, A.J. (2013) *Applied Physics Research*, **5**, 23-47. http://dx.doi.org/10.5539/apr.v5n6p23

[50] Pons, D.J., Pons, A.D. and Pons, A.J. (2014) *Applied Physics Research*, **6**, 28-46. http://dx.doi.org/10.5539/apr.v6n2p28

[51] Pons, D.J., Pons, A.D. and Pons, A.J. (2013) *Applied Physics Research*, **5**, 145-174. http://dx.doi.org/10.5539/apr.v5n6p145

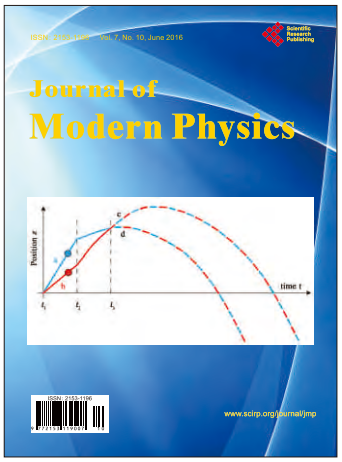

Call for Papers

Journal of Modern Physics

ISSN: 2153-1196 (Print) ISSN: 2153-120X (Online)
http://www.scirp.org/journal/jmp

Journal of Modern Physics **(JMP)** is an international journal dedicated to the latest advancement of modern physics. The goal of this journal is to provide a platform for scientists and academicians all over the world to promote, share, and discuss various new issues and developments in different areas of modern physics.

Editor-in-Chief

Prof. Yang-Hui He City University, UK

Executive Editor-in-Chief

Prof. Marko Markov Research International, Buffalo Office, USA

Subject Coverage

Journal of Modern Physics publishes original papers including but not limited to the following fields:

Biophysics and Medical Physics
Complex Systems Physics
Computational Physics
Condensed Matter Physics
Cosmology and Early Universe
Earth and Planetary Sciences
General Relativity
High Energy Astrophysics
High Energy/Accelerator Physics
Instrumentation and Measurement
Interdisciplinary Physics
Materials Sciences and Technology
Mathematical Physics
Mechanical Response of Solids and Structures
New Materials: Micro and Nano-Mechanics and Homogeneization
Non-Equilibrium Thermodynamics and Statistical Mechanics
Nuclear Science and Engineering
Optics
Physics of Nanostructures
Plasma Physics
Quantum Mechanical Developments
Quantum Theory
Relativistic Astrophysics
String Theory
Superconducting Physics
Theoretical High Energy Physics
Thermology

We are also interested in: 1) Short Reports—2-5 page papers where an author can either present an idea with theoretical background but has not yet completed the research needed for a complete paper or preliminary data; 2) Book Reviews—Comments and critiques.

Notes for Intending Authors

Submitted papers should not have been previously published nor be currently under consideration for publication elsewhere. Paper submission will be handled electronically through the website. All papers are refereed through a peer review process. For more details about the submissions, please access the website.

Website and E-Mail

http://www.scirp.org/journal/jmp **E-mail: jmp@scirp.org**

What is SCIRP?

Scientific Research Publishing (SCIRP) is one of the largest Open Access journal publishers. It is currently publishing more than 200 open access, online, peer-reviewed journals covering a wide range of academic disciplines. SCIRP serves the worldwide academic communities and contributes to the progress and application of science with its publication.

What is Open Access?

All original research papers published by SCIRP are made freely and permanently accessible online immediately upon publication. To be able to provide open access journals, SCIRP defrays operation costs from authors and subscription charges only for its printed version. Open access publishing allows an immediate, worldwide, barrier-free, open access to the full text of research papers, which is in the best interests of the scientific community.

- High visibility for maximum global exposure with open access publishing model
- Rigorous peer review of research papers
- Prompt faster publication with less cost
- Guaranteed targeted, multidisciplinary audience

Scientific Research Publishing

Website: http://www.scirp.org

Subscription: sub@scirp.org

Advertisement: service@scirp.org